Advances in
INORGANIC CHEMISTRY

EDITED BY

A. G. Sykes

Department of Chemistry
The University of Newcastle
Newcastle upon Tyne
United Kingdom

VOLUME 45

ACADEMIC PRESS
San Diego London Boston
New York Sydney Tokyo Toronto

Academic Press
a division of Harcourt Brace & Company
525 B Street, Suite 1900, San Diego, California 92101-4495, USA
http://www.apnet.com

Academic Press Limited
24-28 Oval Road, London NW1 7DX, UK
http://www.hbuk.co.uk/ap/

International Standard Book Number: 0-12-023645-1

PRINTED IN THE UNITED STATES OF AMERICA
97 98 99 00 01 02 QW 9 8 7 6 5 4 3 2 1

ADVANCES IN INORGANIC CHEMISTRY, VOL. 45

SYNTHESES, STRUCTURES, AND REACTIONS OF BINARY AND TERTIARY THIOMOLYBDATE COMPLEXES CONTAINING THE (O)Mo(S_x) AND (S)Mo(S_x) FUNCTIONAL GROUPS (x = 1, 2, 4)

DIMITRI COUCOUVANIS

Department of Chemistry, The University of Michigan, Ann Arbor, Michigan 48109

I. Introduction

Molybdenum is one of the most abundant elements on the planet [found as molybdenite (MoS_2) and wulfenite ($PbMoO_4$)], and in the oceans molybdenum is the most abundant of the redox-active transition elements (*1*). As a result, in the course of evolution molybdenum has been widely adopted by bacteria, plants, and animals as a metal of choice for the development of active centers in redox-active enzymes.

0898-8838/98 $25.00

In biological systems Mo is present as the Fe/Mo cofactor of the nitrogenase enzymes (*2*) and of the multitude of oxidoreductases (*3*). In the latter the common molybdopterin cofactor (*4*), in addition to a dithiolene functionalized pyranopterin (*5*) ligand (Fig. 1), contains terminal oxo ligands and in the case of xanthine oxidase both oxo and thio ligands. Some aspects of molybdenum sulfur chemistry discussed in this work may be relevant to the biosynthesis of the molybdopterin cofactor and the function of xanthine oxidase (*6*).

The importance of molybdenum sulfur compounds in nonbiological catalysis is exemplified by the hydrodesulfurization (HDS) reaction. This reaction is carried out under H_2 at high temperatures and pressures and is used for the removal of sulfur (as H_2S) from organosulfur compounds present in crude petroleum (*7*). The catalyst consists of "sulfided" molybdates supported on γ-Al_2O_3 and usually contains Co^{II} or Ni^{II} as promoter ions. It has been suggested (*8*) that HDS catalysis occurs at the edges rather than on the basal planes of the γ-Al_2O_3-supported MoS_2 crystallites, and the promotion effects of Co^{II} or Ni^{II} may occur at the same sites. The Mo atoms found at the edges of the

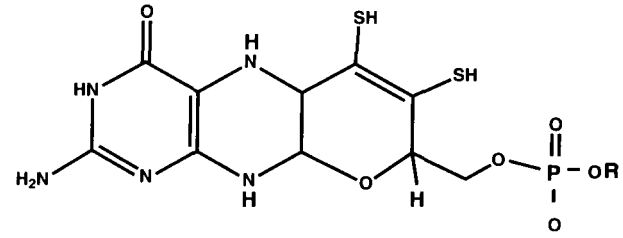

A

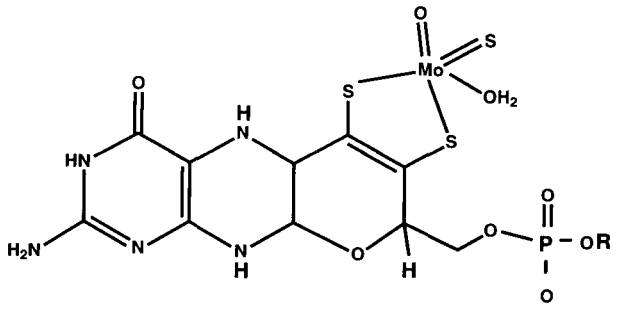

B

FIG. 1. (A) Molybdopyranopterin and (B) the molybdopyranopterin cofactor of the Mo oxidoreductases.

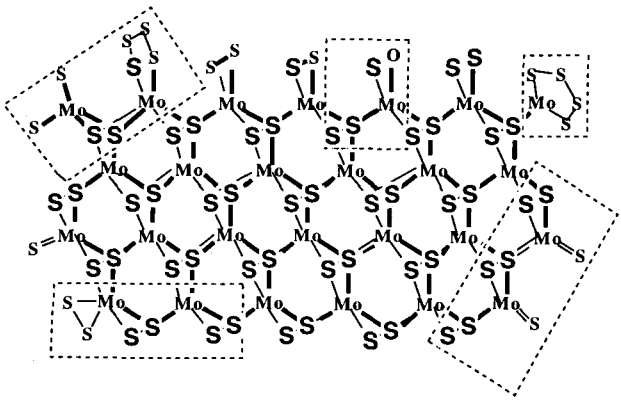

FIG. 2. Possible Mo/S and Mo/S/O groups at the edges of MoS_2. The outlined features have been observed in Mo/S and Mo/S/O complexes.

MoS_2 crystallites may be bound by any of several oxo, thio, or sulfido ligands (*8*) (Fig. 2) and these units may be directly or indirectly involved in the catalytic process.

A number of these "functional groups" (outlined in Fig. 2), often characterized by distinct reactivity properties, are known to exist in molybdothio anions that contain Mo in various formal oxidation states (Fig. 3). This review will concentrate on classes of Mo com-

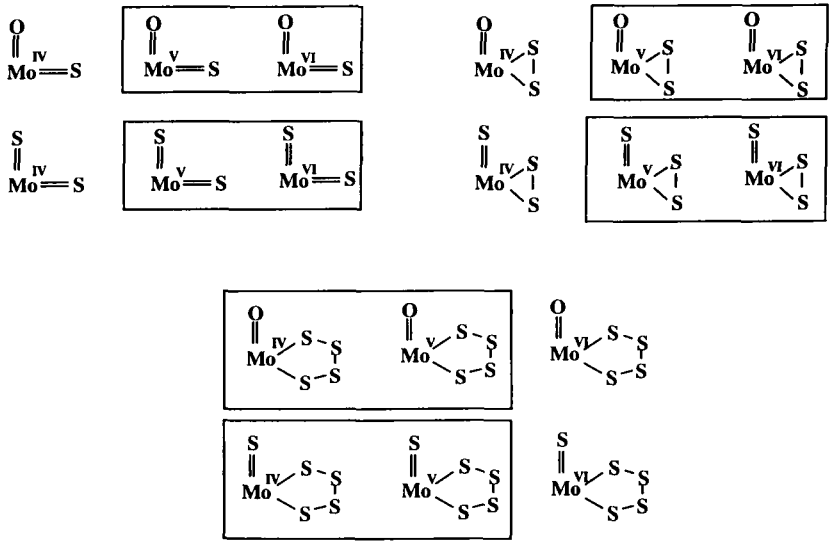

FIG. 3. Mo/S functional groups. The groups within boxes have been observed in crystallographically determined structures.

pounds that contain the chromophores shown in Fig. 3. These compounds possess as a common feature terminally bound S_x^{2-} ligands and include the tertiary $[MoS_xO_{4-x}]^{2-}$ anions, the binary $[(L)(Mo_2S_4)(L')]^{2-}$ series, and the tertiary $[(L)(Mo_2O_2S_2)(L')]^{2-}$ and $[(L)(Mo_2OS_3)(L')]^{2-}$ series (L, L' = S_x^{2-}, x = 1, 2, 4). Throughout this article the Mo_2S_4, $Mo_2O_2S_2$, and Mo_2OS_3 designations represent the *syn*-$[(=S)_2Mo_2(\mu\text{-}S)_2]^{2+}$, *syn*-$[(=O)_2Mo_2(\mu\text{-}S)_2]^{2+}$, and *syn*-$[(=S)(=O)Mo_2(\mu\text{-}S)_2]^{2+}$ cores, respectively, unless otherwise indicated. Similarly the (S_2) and (S_4) ligands are η^2-S_2^{2-} and η^2-S_4^{2-} coordinated to the Mo atoms and the (=E) ligands (E = S^{2-}, O^{2-}) are terminally coordinated chalcogenide dianions.

Of direct relevance to this work are various other reviews that cover the chemistry of Mo/S complexes (*9*, *10*), the S_x^{2-} anions (*11*), the S_2^{2-} ligand (*12*), and the sulfur-bridged molybdenum and tungsten compounds (*13*).

II. Mo/S Chemistry

A. General Considerations

The chemistry of molybdenum ions with sulfur ligands is unique when compared to other transition metal ions. The diversity in structural and reactivity characteristics of Mo/S complexes derives mainly from a close matching of the S *3p* and Mo *4d* orbital energies (*14*), which provide low-energy superexchange pathways for intramolecular electron transfer processes (*15*). The latter allow for sulfur ligand transformations concomitant with Mo valence state interconversions that span oxidation states III, IV, V, and VI. An example of this diversity is available in the remarkable set of electron-redistribution isomers of the triad of $[(Cp)(Mo_2S_4)(Cp)]$ complexes (*16*) that have been reported as distinct $(Cp)_2Mo_2^{III}(\mu\text{-}S_2)_2$ (*17*), $(Cp)_2Mo_2^{IV}(\mu\text{-}S_2)(\mu\text{-}S)_2$ (*18*), and *anti*-$[(Cp)(Mo_2S_4)(Cp)]$ (*19*) units (Fig. 4). These isomers are thermally (*20*) or photochemically (*21*) interconvertible. A theoretical analysis of $[(Me\text{-}Cp\text{–}Mo)_2(\mu\text{-}S_2)(\mu\text{-}S)_2]$ and its isomers explains how the central S_4 unit "traverses in many compounds a range in S–S bonding from ring to isolated S_2^{2-} bridges" (*22*).

At times, the ground states of electron-redistribution isomers of isoelectronic complexes are close enough in energy so that minor perturbations (crystal packing forces, solvent dielectrics, ion pairing) are sufficient to stabilize preferentially one isomer over another. A remarkable example of such an event is the existence, isolation, and structural characterization of the $[Mo_2^V(S_2)_6]^{2-}$ (*23*) and

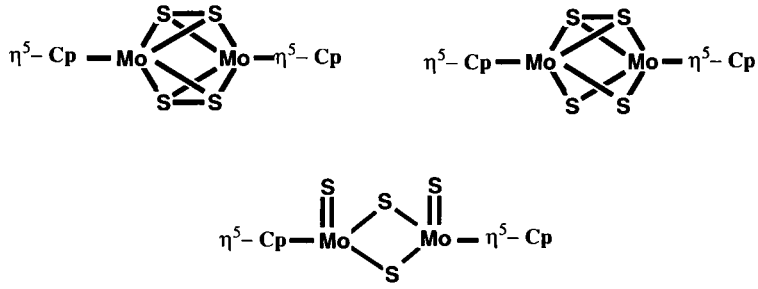

FIG. 4. Schematic representation of the three isomers of the [(Cp)(Mo_2S_4)(Cp)] complexes.

[(S_4)(Mo_2S_4(S_4)]$^{2-}$ (*24*) anions (Fig. 5). The former, isolated from aqueous solution as an NH_4^+ salt, transforms to the latter on dissolution in dimethylformamide and addition of R_4N^+ cations (*25*).

Numerous examples of the redox interplay between molybdenum and sulfur have been reported (*26–28*). The synthesis of the [$S{=}Mo^{IV}(S_4)_2$]$^{2-}$ anion (*24a*, *29*) from the reaction of [$Mo^{VI}S_4$]$^{2-}$ with elemental sulfur or organic trisulfides paradoxically involves the reduction of the Mo^{VI} ion under oxidizing conditions. This reaction is rationalized in terms of the internal oxidation of S_2^{2-} ligands (*vide*

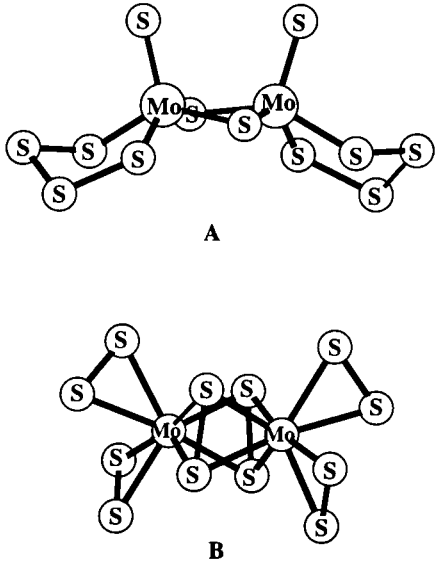

FIG. 5. Two [Mo_2S_{12}]$^{2-}$ isomers.

infra). The reactions of the VS_4^{3-} and MoS_4^{2-} anions with the oxidizing tetraalkylthiuram disulfides, or $(R_2Dtc)_2$, afford the $V_2^{IV}(\mu\text{-}S_2)_2(R_2Dtc)_4$ (*30–32*) and $Mo^V(S_2)(R_2Dtc)_3$ (*33*, *34*) dithiocarbamate complexes. Here also, the reduction of the metal is coupled to the oxidation of the S^{2-} ligands that form the S_2^{2-} disulfido groups. Other similar, internal redox, systems have been reported (*24c*, *35–36*). A kinetic study (*37*) of the reaction of MoS_4^{2-} with certain disulfides to form $[(S_2)(Mo_2S_4(S_2)]^{2-}$ has led to a mechanism based on the internal reduction of Mo^{VI} and a rate-determining step involving the formation of the $(L)_2Mo^{IV}(S_2)$ group from $(L)_2Mo^{VI}(S)_2$.

B. The Mo=S Bond

The chemistry of the Mo=S bond is intimately associated with synthetic aspects or reactivity characteristics for the vast majority of the Mo–S complexes reviewed in this work. In six-coordinate $S{=}Mo(L)_5$ and five-coordinate $S{=}Mo(L)_4$ complexes, the involvement of the molybdenum (d_{xz} and d_{yz}) orbitals in π bonding with the sulfur p orbitals orthogonal to the Mo–S σ bond results in essentially a triple Mo–S bond (Fig. 6).

In the $(L)_5Mo{=}S$ complexes competition of π donor ligands (trans to the S atom in the Mo=S bond) for the same Mo d orbitals results in a weakening of the Mo=S bond. In the $(L)_4Mo{=}S$ square pyramidal complexes a similar energy level scheme (Fig. 7B) applies (*38*), although it is proposed that the energy of the σ^* orbital is lowered in the pyramidal complexes (*39*). The Mo–L triple bonds are predominant for the IV, V, and VI oxidation states or the d^2, d^1, and d^0 electronic configurations that do not involve population of the strongly antibonding π^* orbital. An examination of the energy level diagram (Fig. 6) shows the ready accessibility of the σ^* and π^* orbitals and justifies the contention (*40*) that the photochemistry of these compounds promises to be an exciting area.

The energy level schemes for the $E{=}Mo(L)_3$ (C_{3v}) and $E{=}Mo(L)_4$ (C_{4v}) complexes are shown in Fig 7. In C_{3v} geometry the $d_{x^2-y^2}$ orbital is less antibonding and the bond order of the terminal (axial) ligand is reduced from being a triple bond. The energies of the a_1, b_1, e, and b_2 orbitals in $[MoOCl_4]^-$ have been calculated as 4.63, 3.66, 2.80, and 0.87 eV, respectively; they are above the Cl *3p* in-plane (a_2 and b_2) orbitals at −1.45 eV and the Cl *3p* out-of-plane (b_1, e, and a_1) orbitals at −2.14, −2.43, and −2.91 eV, respectively (*41*). Certain reactions of the trigonal pyramidal $E{=}Mo(L)_3$ complexes lead to square pyramidal

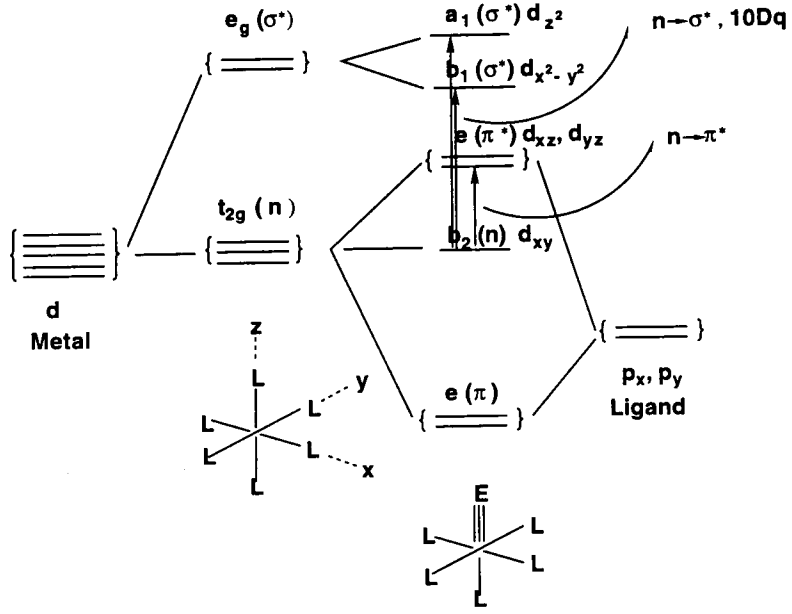

FIG. 6. Energy level schemes for the $Mo(L)_6$ and $E{=}Mo(L)_5$ complexes.

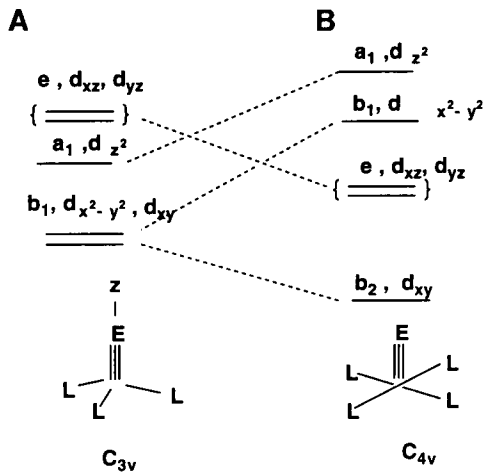

FIG. 7. Energy level schemes for the $E{=}Mo(L)_3$ and $E{=}Mo(L)_4$ complexes.

$E{=}Mo(L)_4$ complexes. The energetics of this transformation have profound effects on reactivity (see Section IV,B).

III. Binary Thiomolybdates and Tertiary Oxo/thiomolybdates

A. The $(MoS_xO_{4-x})^{2-}$ Anions

The reactions of oxomolybdates [$(MoO_4)^{2-}$ or $(Mo_7O_{24})^{6-}$] with H_2S or $(NH_4)_2S_x$ under basic conditions give thiomolybdate products that, depending on reaction times or conditions, contain Mo=S and Mo=O units in various combinations (*42*). The chemistry and spectroscopic properties of the tetrahedral $(MoS_nO_{4-n})^{2-}$ anions have been reviewed (*43–45*) and the structures of various thiomolybdates have been determined (*46*).

The kinetics of the interconversion of sulfido and $(MoO_nS_{4-n})^{2-}$ species in aqueous solution have been studied (*47*). The results indicate that crowding by the larger S^{2-} ligands at the reaction site makes associative substitution more difficult and results in slower rates as the S^{2-}/O^{2-} ratio increases.

Investigations of bonding in the $(MoO_nS_{4-n})^{2-}$ anions using ^{33}S and ^{17}O NMR spectroscopy have been reported (*48*, *49*). The monotonic deshielding observed in the ^{95}Mo NMR as oxygens are successively replaced by sulfur is explained by *ab initio* calculations (*49*) that show an increase in the electron density on the Mo atom as oxygen atoms are successively replaced by sulfur atoms. Theoretical studies of the bonding in the $(Mo_{4-n}S_n)^{2-}$ anions have been published (*50*). The solution chemistry of the $(MoS_4)^{2-}$ anion has been investigated (*51*) electrometrically and the formation of various thioanions, including $(Mo_2S_7)^{2-}$, was detected. A multitude of heterometallic complexes have been obtained whereby the thiomolybdate anions serve as ligands. The vast majority of these complexes are $(MoS_4)^{2-}$ derivatives. Various reviews have been published on these compounds (*23c*, *43*, *44*, *52*). The first reports of $\{M[MoS_4]_2\}^{2-}$ complexes (M = Ni, Fe, Co, Zn) and the use of the $(MoS_4)^{2-}$ anion as a ligand appeared in 1971 (*53*, *54*) and the structure of the $(Ph_4P)_2\{Ni[MoS_4]\}$ complex was subsequently determined (*55*) ($Mo-S_b$ = 2.23Å, Mo=S = 2.15 Å; Ni—Mo = 2.80 Å). The electrochemistry of the $\{M[MoS_4]_2\}^{2-}$ anions (M = Ni, Pd, Pt) shows (*56*) a $2e^-$ reversible reduction for the Ni complex and a $1e^-$ reduction for the Pt complex. The calculation of electronic structure for a wide range of $[M(MS_4)_2]^{2-}$ complexes (M = Mo, W) has been reported (*50b*).

In later years a great number of $(MoS_4)^{2-}$ complexes with iron were reported (Fig. 8). The syntheses of these compounds were inspired by

the Fe/Mo/S center in nitrogenase. Among them are included complexes such as $[L_2FeS_2MS_2]^{2-}$ [L = PhS^- (*57a,b*), Cl^- (*58*), PhO^- (*59*), NO^+ (*60a*); $L_2 = S_5^{2-}$ (*61*)], $[Cl_2FeS_2MS_2FeCl_2]^{2-}$ (*58a*), $[Fe(MoS_4)_2]^{3-}$ (*62*), $[(S_2)OMoS_2FeCl_2]^{2-}$ (*63*), and $[S_2MoS_2FeS_2Fe(S\text{-}p\text{-}C_6H_4Me)_2]^{3-}$ (*59*, *64*). The synthesis and structural characterization of the $[(PhS)_2FeS_2MoO_2]^{2-}$ complex were reported more recently (*57c*). The spectroscopic and structural properties of these complexes have been reviewed (*52*). An electron paramagnetic resonance (EPR) study of the reactions of $(MoS_4)^{2-}$ with Roussin's salts $Fe_2(SR)_2(NO)_4$ and

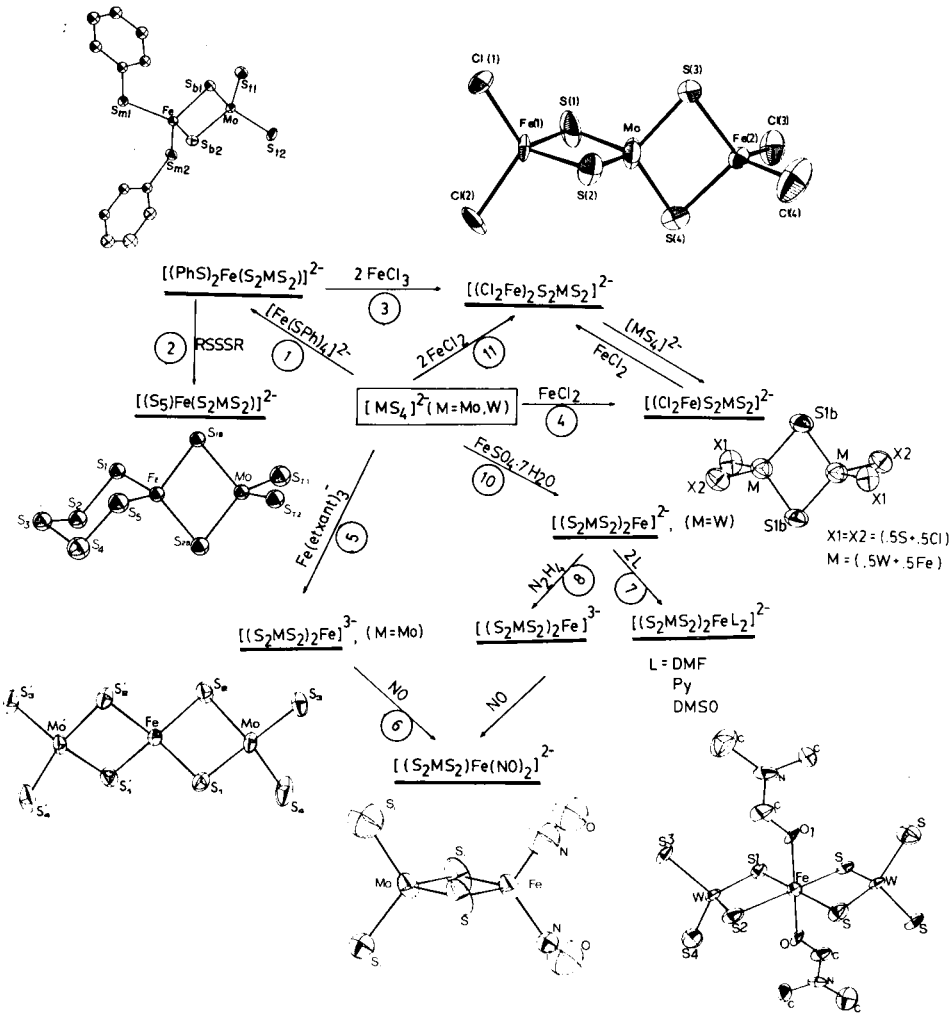

FIG. 8. The $[MoS_4]^{2-}$ anion as a ligand; Fe/MoS_4 complexes.

$[Fe_4S_3(NO)_7]^-$ has detected the formation of nitrosyl complexes such as $[Fe(NO)_2(S_2MoS_2)]^-$ and $[Fe(NO)(S_2MoS_2)_2]^{2-}$ (*60b*).

The use of the $(MoS_4)^{2-}$ anion as a ligand for $Mo(CO)_4$ led to the unusual $[(CO)_4MoS_2MoS_2]^{2-}$ and $\{[(CO)_4Mo]_2[MoS_4]\}^{2-}$ complexes (*65*) that contain two Mo atoms within the same molecule in two widely different oxidation states, 0 and VI. The trinuclear $W^{VI}(W^0)_2$ analog also has been obtained (*65b*).

The $[MoFe_3S_6(CO)_6]^{2-}$ complex (*66*) contains the $[(CO)_6Fe_2(\mu\text{-}S)_2]^{2-}$ "ligand" and could be described as a structural derivative of the $[Cl_2Fe(MoS_4)]^{2-}$ complex wherein the two Cl^- ligands have been replaced by the $[(CO)_6Fe_2(\mu\text{-}S)_2]^{2-}$ anion. The synthesis and structure of the $(MeCp)_2M(MoS_4)]$ complexes (M = Mo, W) have been reported (*67*). A variety of mixed-ligand heterometallic complexes with $(MoS_4)^{2-}$ as one of the coligands has been reported, including $(bipy)_2Mn(MoS_4)$, obtained (*68*) in a straightforward manner from MoS_4^{2-}, bipy, and Mn^{2+}; the Cu^I dimers (*69*) $LCu(MoS_4)CuL$ (L = 2,2-bipyridine, 1,10-phenanthroline); and polymeric $[(CuNCS)_4MS_4]^{2-}$ heterobimetallic clusters (*70*) of Cu^I with $(MoS_4)^{2-}$. A multitude of neutral $(MS_4)^{2-}/M'L$ complexes are known for M′ = a coinage metal, $L = CN^-$, Cl^-, or NCS^-. These complexes include $[WS_4(CuCN)_2]^{2-}$ (*71a,b*) and $[MoS_4(CuCl)_3]^{2-}$ and variants (*71c,f*). The reduction of Cu^{II} in aqueous solution by $(NH_4)_2MoS_4$ gives (*72a*) polymeric NH_4CuMoS_4. The linear trimetallic $(AuPEt_3)(S_2MoS_2)(AuPEt_3)$ complex contains a μ-$(MoS_4)^{2-}$ ligand and has been structurally characterized (*72b*). The synthesis of the $[(PhS)_2Mo(O)(MoS_4)]^{2-}$ anion is accomplished (*73*) in DMF solution by substitution of two of the thiophenolate ligands in the $[(PhS)_4Mo(O)]^-$ complex (*74*) by the $(MoS_4)^{2-}$ chelating ligand. An infrared (IR)–Raman study of the Cu^I–MoS_4 complexes has been reported (*75*) and redox-based interconversions (*76*) between $[(CuCN)(MoS_4)]^{2-}$ and $[(CuCN)_2(MoS_4)]^{2-}$ have been investigated.

Other trinuclear and tetranuclear univalent coinage metal derivatives of thiomolybdate and thiotungstate dianions include $[(O)MoS_3Cu_2(Py)_2(PPh_3)_2]$ (*77a*), $[(O)MoS_3Cu_3(NCS)_3]^{2-}$ (*77b,d*), $[(O)MoS_3Cu_3(\mu_3\text{-}Cl)_2(PPh_3)_3]$ (*77c*), and the "incomplete cubanes" $[(Edt)_2M_2S_4Cu(PPh_3)]^-$ (*77e*) (M = Mo, W). The silver analogues of the latter also have been reported (*77f*). The neutral cubane clusters $[(Edt)_2M_2S_4Cu_2(PPh_3)_2]$ (*77g*) are structural derivatives of the incomplete cubanes (see above) and contain an additional $[Cu(PPh_3)]^+$ unit (*77g*). The heterometallic $[MS_4(CuCl)_4)]^{2-}$ (M = Mo, W) complexes (*78*) contain a central μ_4-$(MS_4)^{2-}$ bridge that symmetrically binds four CuCl units. These dianions oligomerize and form interionic Cu_2Cl_2 rhombic

bridging units. The oligomerization process depends on the types of counterions that accompany the $[MS_4(CuCl)_4)]^{2-}$ anions.

B. Binary Thiomolybdates

1. *The $[S{=}Mo(S_4)_2]^{2-}$ Anion and the $[(S_x)(Mo_2S_4)(S_y)]^{2-}$ Series*

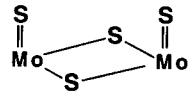

The $[Mo_2S_4]^{2+}$ unit

Explorations of the chemistry of the binary molybdenum sulfides started with initial reports on the synthesis and structural characterization of the $[(S_2)_2Mo(\mu\text{-}S_2)]_2^{2-}$ (*23*) (Fig. 5B) and the $[Mo_3S_{13}]^{2-}$ (Fig. 9) thioanions by Muller and co-workers (*23d–j*). Soon thereafter, the discovery and detailed characterization of new thiomolybdates such as $[S{=}Mo(S_4)_2]^{2-}$ (*24a*), $[(S_2)(Mo_2S_4)(S_2)]^{2-}$ (*35*, *79*), $[(S_4)(Mo_2S_4)(S_2)]^{2-}$ (*24*), and $[S{=}Mo(MoS_4)_2]^{2-}$ (*80*) revealed the remarkable complexity of the Mo/S system.

The reaction of $(Et_4N)_2(MoS_4)$ (*46*) with either elemental sulfur or organic trisulfides in CH_3CN solution affords (*24*) highly crystalline $[Et_4N]_2[S{=}Mo(S_4)_2]$. The $[S{=}Mo(S_4)_2]^{2-}$ anion also can be made from $(NH_4)_2S_3$ and $(NH_4)_2MoS_4$ in aqueous solution and crystallizes as an Et_4N^+ salt on addition of Et_4NCl. The formation of this interesting Mo^{IV} complex (Fig. 10) under oxidizing conditions has been discussed in terms of internal electron transfer (see Section II,A).

Crystalline $[Et_4N]_2[O{=}Mo(S_4)_2]$ is obtained by hydrolysis of $[Et_4N]_2[S{=}Mo(S_4)_2]$ in hot "wet" DMF. Attempts to exchange the Et_4N^+ cations in $[Et_4N]_2[S{=}Mo(S_4)_2]$ with Ph_4P^+ resulted in the isolation of Ph_4P^+ salts of the $[(S_4)(Mo_2S_4)(S_4)]^{2-}$ (Fig. 5A) and $[(S_2)(Mo_2S_4)(S_4)]^{2-}$ anions (*24*). The same anions also are isolated following addition of

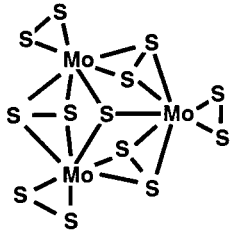

FIG. 9. Schematic representation of the $[Mo_3S_{13}]^{2-}$ anion.

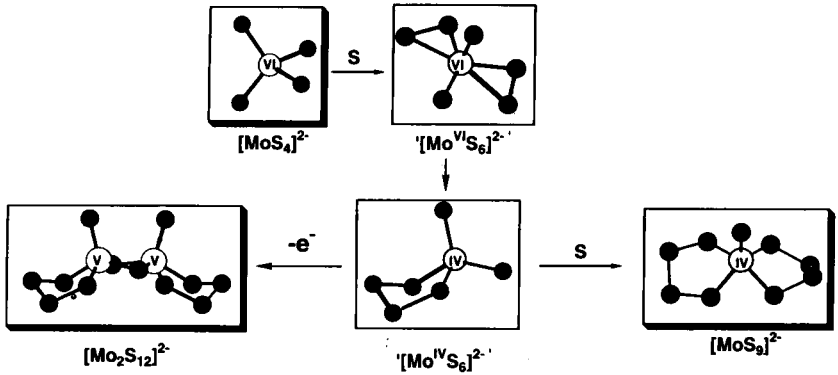

FIG. 10. Proposed pathway in the synthesis of the $[S{=}Mo(S_4)_2]^{2-}$ anion. (In this and in all subsequent figures the structures within solid-line frames have been plotted from crystallographically determined coordinates.)

Ph_4PCl to CH_3CN solutions of $(NH_4)_2[Mo_2(S_2)_6]$ (Fig. 5B). The $[(S_2)(Mo_2S_4)(S_2)]^{2-}$ anion was obtained by oxidation of $(NH_4)_2MoS_4$ with diphenyl disulfide or diselenide in DMF solution and was isolated as a $(Ph_4P)^+$ salt in 80% yield (*35*). These early observations in Mo/S chemistry revealed the rich chemistry of the system and led to proposals of complex equilibria between various thioanions.

Among the thioanions that were proposed to coexist in equilibria or to be possible intermediates in the formation of the $[S{=}Mo(S_4)_2]^{2-}$, $[(S_4)Mo(Mo_2S_4)Mo(S_2)]^{2-}$ (*24a,b*), and $[S{=}Mo(MoS_4)_2]^{2-}$ (*80*) complexes are the $[Mo_2S_7]^{2-}$ (*24a,b*, *79*) and $[(S)(Mo_2S_4)(S_4)]^{2-}$ (*24a*, *79*) anions. The former has been reported (*51*) to form in aqueous $(MoS_4)^{2-}$ solutions at pH ~5, and to exist as a ligand in the [Fe(Salen)]$_2(Mo_2S_7)$ complex (*81*), but had not been isolated in the solid state, whereas the latter, a possible precursor to $(Mo_2S_7)^{2-}$, was until then an unknown derivative of the $(Mo{=}S)^{2+}$ (*24a*) unit.

Subsequent studies of the reactivity of the known thiomolybdates (and particularly the $[(S_4)(Mo_2S_4)S_2)]^{2-}$ complex) with Ph_3P have resulted (*82*, *83*) in the systematic synthesis of the $[(S_x)(Mo_2S_4)(S_y)]^{2-}$ anions (Fig. 11; Table I).

A mixture of $[(S_4)(Mo_2S_4)(S_2)]^{2-}$ and $[(S_4)(Mo_2S_4)(S_4)]^{2-}$ (Fig. 11, structures 4A and 6A) and also $[(S_2)(Mo_2S_4)(S_2)]^{2-}$ (Fig. 11, structure 2B) is obtained by oxidation of the $[S{=}Mo(S_4)_2]^{2-}$ anion with diphenyl disulfide (*35*, *83*). The possibility of internal electron transfer processes, mediated by the S_x^{2-} ligands, often presents the choice of more

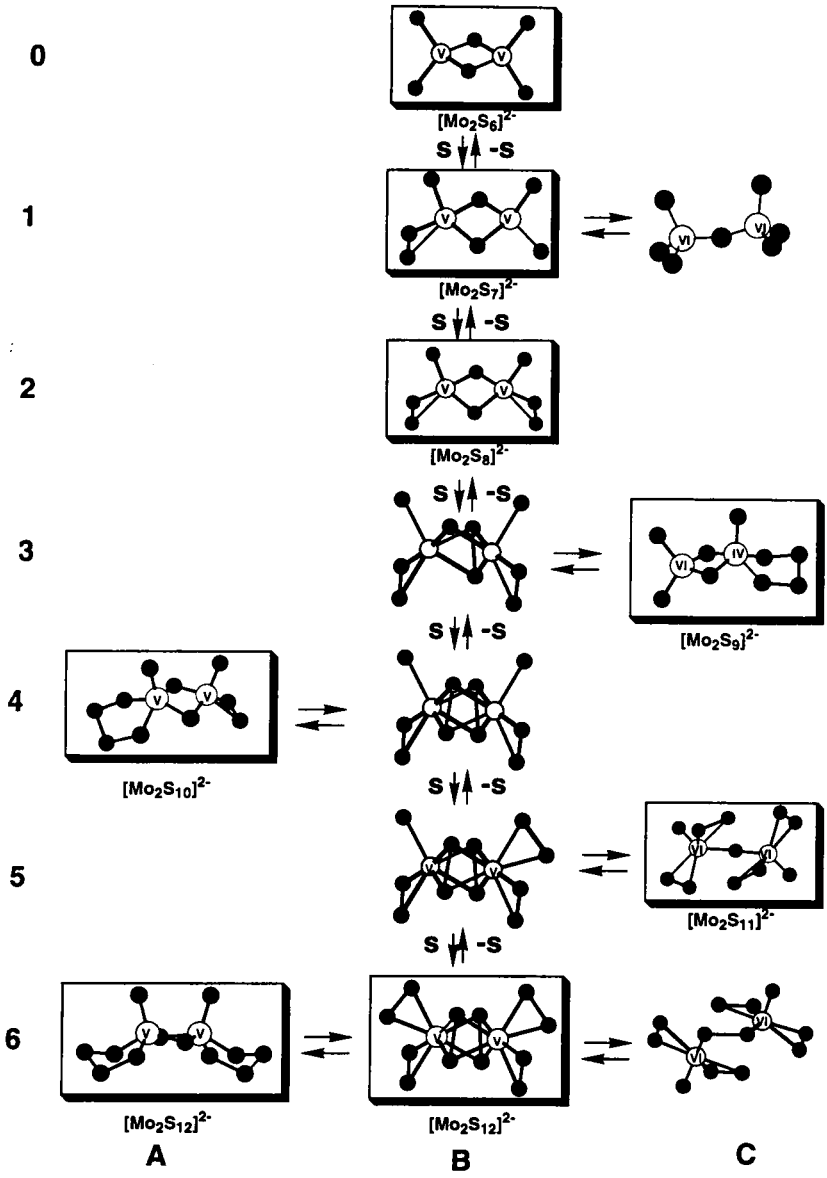

FIG. 11. The $[(S_x)(Mo_2S_4)(S_y)]^{2-}$ anions.

TABLE I

DISTANCES AND ANGLES IN BINARY Mo/S COMPLEXES AND SELECT DERIVATIVES THAT CONTAIN THE $[Mo_2S_4]^{2+}$ CORE[a]

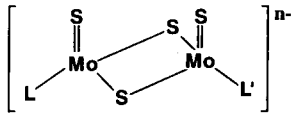

L	L'	n	Mo—Mo (Å)	Mo—S_b (Å)	Mo=S_t (Å)	Mo—L (Å)	Mo—L' (Å)	Mo—S—Mo (°)	S—Mo—S (°)	Reference
S^{2-}	S^{2-}	2	2.856(1)	2.301(1)	2.157	2.145	2.145	76.8(1)	103.2(1)	*82a,b*
S^{2-}	S_2^{2-}	2	2.848(2)	2.323 2.283[b]	2.103	2.174(3)	2.405	76.3(1)	101.3(1) 103.7(1)[e]	*82a,b*
S^{2-}	S_4^{2-}	2	2.859(1)	2.271(3)[c] 2.237(5)[c] 2.342(4)[d] 2.368(4)[d]	2.142(4)[c] 2.105(3)[d]	2.157(3)	2.387	76.6	105.2(1)[b] 99.0(1)[c]	*82a,b*
S_2^{2-}	S_2^{2-}	2	2.821(1)	2.310(4,2)	2.118	2.393(4,8)	2.393(4,8)	75.3	101.2	*35*
S_2^{2-}	S_4^{2-}	2	2.846(1)	2.342[c] 2.295[f]	2.118	2.432	2.412	75.70	102.0	*24a*
S_2^{2-}	S_4^{2-}	2	2.837(1)	2.341[c] 2.296[f]	2.110	2.395	2.406	75.5	102.0	*24b*
$(CS_3)^{2-}$	$(CS_3)^{2-}$	2	2.823(1)	2.300(7)	2.100(2)	2.433(8)	2.433(8)	75.6(1)	100.8(1)	*161a*
$(CS_4)^{2-}$	$(CS_4)^{2-}$	2	2.840(3)	2.316(5)	2.108(5)	2.412(5)[g] 2.391(4)[h]	2.413(5)[g] 2.391(4)[h]	75.6(1)	101.4(3)	*160, 161a*
$(Edt)^{2-}$	$(Edt)^{2-}$	2[i]	2.863(2)	2.319(4)	2.089(4) 2.112(3)	2.405(3)		76.22	99.84	*89b*
			2.855(1)	2.315(2)	2.103(2)	2.394(2)		76.2(1)	100.6(1)	*89c*
$(Edt)^{2-}$	$(Edt)^{2-}$	2[j]	2.878(2)	2.298(2) 2.344(2)	2.129(2)	2.400		76.62(7)	103.38(7)	*89b*
$[S=Mo(S_4)_2]^{2-}$		—	—	—	2.128(1)	2.331(1) 2.387(1)		—	—	*24a*

[a] In this and the rest of the tables that report crystallographic data the average values of chemically equivalent distances or angles are given. The number in parentheses represents the larger of the individual standard deviations or the standard deviation from the mean, $\sigma = [\sum_{i=1}^{N}(x_i - x)^2/N(N-1)]^{1/2}$. If only two values are available for a given distance or angle, the average value is reported without a standard deviation in parentheses.

[b] Involves the Mo bound to L = S.

[c] Bound to the Mo^{IV} ion.

[d] Bound to the Mo^{VI} ion.

[e] Bound to the $Mo(S_4)$ unit.

[f] Bound to the $Mo(S_2)$ unit.

[g] Bond with the C–S group of the ligand.

[h] Bond with the C–S–S group of the ligand.

[i] Syn isomer.

[j] Anti isomer.

than one structure for a given complex, and the structures formally described in Fig. 11 as 4B and 5B have been obtained in different isomeric forms (Fig. 11, structures 4A and 5C).

The $[(S_4)(Mo_2S_4)(S)]^{2-}$ anion (Fig. 11, structure 3C) can only be obtained by the BH_4^- reduction of the $[(S_4)(Mo_2S_4)(S_2)]^{2-}$ complex in DMF solution. A possible pathway for this reaction has been sug-

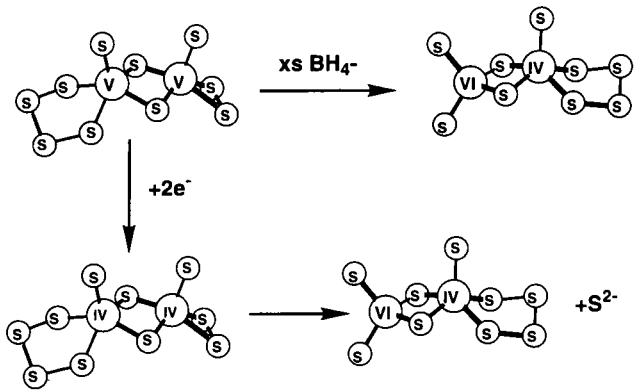

FIG. 12. The synthesis of the $[(S_4)(Mo_2S_4)(S)]^{2-}$ anion.

gested (*83*) (Fig. 12). The description of this complex as the valence-localized $[(S{=}Mo^{IV}(S_4)(Mo^{VI}S_4)]^{2-}$ ion is prompted by the asymmetric $[Mo_2S_4]^{2+}$ core (Table I) that shows two sets of Mo–μ-S bonds at 2.355 and 2.254 Å, respectively. Abstraction of two sulfur atoms from the S_4^{2-} ligand in this complex leads to the $[(S{=}Mo^{IV}(S_2)(Mo^{VI}S_4)]^{2-}$ ion (Fig. 11, structure 1B). A detectable structural asymmetry in this ion (Table I) suggests that a valence-localized form contributes somewhat to the description of its structure. The $[Mo^{VI}S_3)_2S]^{2-}$ form of this ion (Fig. 11, structure 1C) would be isostructural to that of the known $[Mo_2O_7]^{2-}$ anion (*84*). Attempts to obtain $[(Mo^{VI}S_3)_2S]^{2-}$ by the reaction of $[(Mo^{VI}O_3)_2O]^{2-}$ with $(Me_3Si)_2S$ have led to the monomeric $[(Mo^{VI}O_3OSiMe_3]^-$ complex (*85*).

The $\{[(S_2)_2Mo(\mu\text{-}S_2)]_2\}^{2-}$ anion [Fig. 5B; Mo–Mo, 2.826(2), 2.828(2) Å; S–S, 2.038(5)–2.056(5) Å] (*23*) is unique among the binuclear binary Mo/S complexes in that it contains the $Mo_2(\mu\text{-}S_2)_2$ rather than the $Mo_2(\mu\text{-}S)_2$ bridging unit. The complex is obtained as a black crystalline dihydrate by the reaction of $(NH_4)_2MoS_2O_2$ with $(NH_4)_2S_x$ (*23f*). The lability of this complex, which in the solid state exists as an NH_4^+ salt, already has been noted in its remarkable, cation-induced, transformation to the isomeric $[(S_4)(Mo_2S_4)(S_4)]^{2-}$ anion. The latter can be obtained from DMF solutions of $(NH_4)_2\{[(S_2)_2Mo(\mu\text{-}S_2)]_2\}$ on addition of Et_4NCl.

The $[Mo(\mu\text{-}S_2)_2Mo]^{6+}$ core in the $[X_4Mo(\mu\text{-}S_2)_2MoX_4]^{2-}$ anions (*86*) shows slightly longer Mo–Mo bonds and shorter S–S bonds [Mo–Mo, 2.857(1)–2.852(4) Å; S–S, 1.998(9)–1.969(9) Å] by comparison to $\{[(S_2)_2Mo(\mu\text{-}S_2)]_2\}^{2-}$. The former is obtained in very good yield from

$Mo(S_2)X_3$ ($X = Cl^-$, Br^-). The expected lability of the X^- ligands in this molecule should make it a good reagent for the synthesis of other complexes with the $Mo(\mu\text{-}S_2)_2Mo$ unit. The $[Mo(\mu\text{-}S_2)_2Mo]^{6+}$ core also is found in the solid-state structure of $[Cl_{4/2}Mo(\mu\text{-}S_2)_2MoCl_{4/2}]$ (*87*) and in the structure of the $\{(Et_2Dtc)_2[Mo(\mu\text{-}S_2)_2Mo](Et_2Dtc)_2\}^{2+}$ complex (*88*). The extraordinary H_2 activation chemistry associated with certain isomeric forms of the $[(Cp)(Mo_2S_4)(Cp)]$ complex has been studied in detail mainly by M. Rakowski-DuBois and co-workers (*19a*). This work poses the question whether other complexes that contain the $[Mo_2S_4]^{2+}$ core might not display similar reactivity.

Reduction of the S_2^{2-} ligands in $\{[(S_2)_2Mo(\mu\text{-}S_2)]_2\}^{2-}$ by an excess of other oxidizable sulfur ligands L ($L = Et_2Dtc^-$, PhS^-, Edt^{2-}) leads to generation of the $[Mo_2S_4]^{2+}$ core and concomitantly to $[(L)_n(Mo_2S_4)(L)_n]$ complexes (*89a*). Both the syn (*89b,c*) and *anti* (*89b*) isomers of the $[(Edt)(Mo_2S_4)(Edt)]^{2-}$ complex have been synthesized and structurally characterized. The bonding in these molecules has been examined through extended Hückel and Fenske–Hall calculations that show a greater Mo–Mo *4d* overlap for the syn isomer relative to the anti isomer and a greater relative stability of the syn isomer (*89d*). A compilation of characteristic infrared data and of electronic spectra for mainly binary sulfide complexes that contain the $[Mo_2S_4]^{2+}$ core can be found in Table II.

2. *Other Binary and Tertiary Group VI Chalcogenides M/E (M = W; E = S, Se, Te)*

A number of W/S complexes analogous and often isostructural to corresponding Mo/S complexes have been reported, including $(W_2S_{11})^{2-}$ (*90c*), $(W_2S_{12})^{2-}$ (*24c*), $[S{=}W(WS_4)_2]^{2-}$ (*90d*), $[(WS_4)(S)W(\mu\text{-}S)_2W(S)(S_2)]^{2-}$ (*90e*), and $[(WS_4)(S)W(\mu\text{-}S)_2W(S)(WS_4)]^{2-}$ (*90f*). The very interesting $[W(WS_4)_2]^{2-}$ anion contains a four-coordinate square, formally W^{II}, central ion bound by two tetrathiotungstate dianions (*90a,b*). A doubt has been raised concerning the identity of this unusual molecule (*90c*).

From the synthetic and crystallographic studies of W/Se chemistry (*91*) it has been revealed that certain aspects of this chemistry do not parallel those of W/S chemistry. This is particularly true for the degree of catenation found with the E_x^{2-} chalcogenide ligands. Thus the Se_3^{2-} ligand found in the $[(Se_3)(Se)W(\mu\text{-}Se)]_2^{2-}$ and $[(Se_3)(Se)W(\mu\text{-}Se)_2W(Se)(Se_2)]^{2-}$ complexes (*91*) has no counterpart in Mo/S or W/S chemistry. As a general rule, selenide chemistry appears more complex and the compounds are less stable.

TABLE II

CHARACTERISTIC ELECTRONIC AND INFRARED ABSORPTION SPECTROSCOPIC DATA OF BINARY Mo/S COMPLEXES AND SELECT DERIVATIVES THAT CONTAIN THE $[Mo_2S_4]^{2+}$ CORE

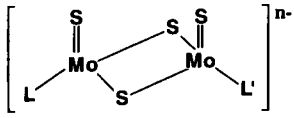

L	L'	Infrared absorption (cm^{-1})[a]	λ_{max} (nm: $\varepsilon \times 10^{-3}$)[b]	Reference
S^{2-}	S^{2-}	503(m); 475(m); 452(w)	290(26.0); 310(19.3); 362(sh); 454(9.9); 482(sh)	*82b*
S^{2-}	S_2^{2-}	504(m); 480(m); 454(w)	295(sh); 362(sh); 422(sh); 452(5.2); 560(2.4)	*82b*
S^{2-}	S_4^{2-}	506(m); 487(m); 456(w)	298(23.8); 350(sh); 422(7.0)	*82b*
S_2^{2-}	S_2^{2-}	512(sh); 453(w)	290(sh); 464(2.7); 574(3.3)	*82b*
S_4^{2-}	S_4^{2-}	523(s); 496(w); 439(m); 416(w); 348(w); 325(w); 315(w); 298(m)	—	*24c*
$(CS_3)^{2-}$	$(CS_3)^{2-}$	C=S, 982(s); Mo–S_b, 464(w)	344; 444(sh)	*161*
$(CS_4)^{2-}$	$(CS_4)^{2-}$	C=S, 1052(s); Mo–S_b, 460(w)	314(sh); 365(sh); 470(sh); 610(sh)	*161*
$[(S{=}Mo(S_4)_2]^2$		S=Mo, 525(s)	316(15.7); 340(sh); 405(sh); 470(sh)	*24a*

[a] In KBr disk.
[b] In DMF.

The $[(E)M_2E_4(E)]^{2-}$ series (Fig. 11, structure 0B), structurally described in terms of two edge-sharing ME_4 tetrahedra, are represented only by the $[Mo_2S_6]^{2-}$ (*82*) and $[W_2Se_6]^{2-}$ (*92*) ions. In the series $[E{=}M(Se_4)_2]^{2-}$ (M = Mo, W; E = S, Se, O), the anions $[Se{=}W(Se_4)_2]^{2-}$, $[Se{=}Mo(Se_4)_2]^{2-}$, $[S{=}W(Se_4)_2]^{2-}$, $[S{=}Mo(Se_4)_2]^{2-}$, $[O{=}W(Se_4)_2]^{2-}$, and $[O{=}Mo(Se_4)_2]^{2-}$ have been reported (*93*).

The Mo and W oxytellurides, $[O{=}Mo(Te_4)_2]^{2-}$ and $[O{=}W(Te_4)_2]^{2-}$, obtained from soluble polytellurides and high-valent metal chlorides, are known and their structures have been determined (*94*). These complexes have structures that are similar to those of the previously reported (*93*) sulfides (*24*) and selenides (*93*). Their ^{125}Te NMR spectra are consistent with their structures.

C. Tertiary Oxo/thiomolybdates

1. The $[(S_x)(Mo_2OS_3)(S_y)]^{2-}$ Series

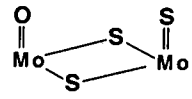

The $[Mo_2OS_3]^{2+}$ unit

Molybdothio anion dimers that contain both Mo=S and Mo=O units are rare and the small number of such complexes that have been reported, such as $[(\eta^2\text{-}S_2)Mo(=O)(\mu\text{-}S)_2Mo(=O)(\mu\text{-}S)_2Mo(=O)(=S)]^{2-}$ (*95*) and $[(S_2)Mo_2OS_3)(S_2)]^{2-}$ (*97*), have been obtained by serendipitous means.

Oxidation of the RS^- ligands in thiolate complexes by S_x^0 fragments [present in solutions of either dibenzyl trisulfide (*73d*) or elemental sulfur] generates S_x^{2-} anions that replace the thiolate complexes. This reaction has been used effectively (*98*) in the synthesis of $[M(S_x)_2]^{2-}$ complexes from $[M(SPh)_4]^{2-}$ thiolates (*99*) (M = Mn, Ni, Zn; x = 4, 5, or 6). A similar reaction has been employed for the synthesis of complexes that contain both Mo=S and Mo=O units within a central $[Mo_2OS_3]^{2+}$ core. These compounds were obtained by the oxidative removal of the coordinated PhS^- ligands from the $[(O=Mo(PhS)_2(MoS_4)]^{2-}$ anion (*73a,b,c*) (Fig. 13, structure 1A; Table III). The latter was made in DMF solution via the substitution of two of the thiophenolate ligands in the $[O=Mo(PhS)_4]^-$ complex (*74*) by the MoS_4^{2-} chelating liquid (Fig. 13).

The various $[(S_x)(Mo_2OS_3)(S_y)]^{2-}$ derivatives (Fig. 13) can be obtained in a rational manner by S addition reactions (*73a,b*) using elemental sulfur or sulfur abstraction reactions using Ph_3P. The $[(S_4)(Mo_2OS_3)(S_2)]^{2-}$ complex (Fig. 13, structure 1C) exists in two isomers with the S_2^{2-} ligand adjacent to either the Mo=S or the Mo=O groups. The reaction of a 50:50 mixture of these isomers with one-half equivalent of Ph_3P results in sulfur abstraction from the S_2 ligand adjacent to the Mo=S chromophore and gives exclusively one product (Fig. 13, structure 2C). A similar reaction of $[(S_2)(Mo_2OS_3)(S_2)]^{2-}$ (Fig. 13, structure 2A) with one equivalent of Ph_3P also results in sulfur abstraction from the S_2^{2-} ligand adjacent to the Mo=S unit (Fig. 13, structure 2B). This preference for sulfur abstraction has been attributed to a release of steric crowding, which is more pronounced around the $(\mu\text{-}S)_2(S)Mo(S_2)$ unit than the $(\mu\text{-}S)_2(O)Mo(S_2)$ unit (*73*). An alternate explanation is based on the

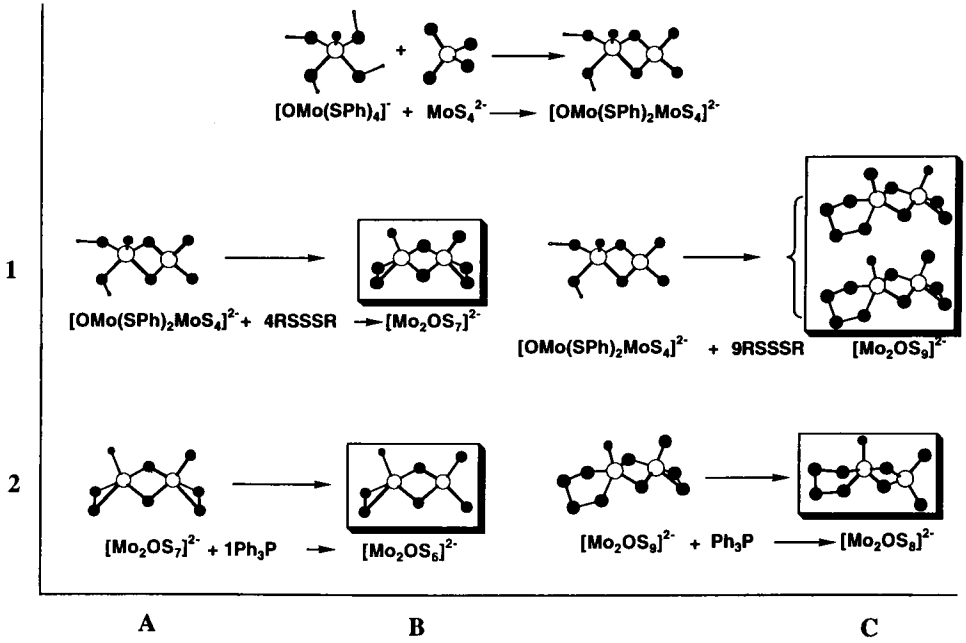

FIG. 13. The $[(S_x)(Mo_2OS_3)(S_y)]^{2-}$ complexes.

TABLE III

DISTANCES IN TERTIARY Mo/S/O COMPLEXES AND SELECT DERIVATIVES THAT CONTAIN THE $[Mo_2S_3O]^{2+}$ CORE[a]

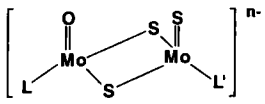

L'	L	n	Mo−Mo (Å)	Mo=S (Å)	Mo=O (Å)	O=Mo−S_b (Å)	S=Mo−S_b (Å)	O=Mo−L (Å)	S=Mo−L' (Å)	Reference
S^{2-}	S_2^{2-}	2	2.864(1)	2.132(3)	1.680(7)	2.370(3)	2.285(3)	2.406	2.175(3)	*73a,b*
						2.331(3)	2.320(3)			
S^{2-}	S_4^{2-}	2	2.888(3)	2.135(7)	1.67(1)	2.382(8)	2.262(7)	2.388	2.182(7)	*73a,b*
						2.365(6)	2.275(7)			
S_2^{2-}	S_2^{2-}	2	2.820(1)	2.055(2)	1.677(4)	2.326	2.319	2.399	2.387	*73a,b*
		2	2.832(1)	2.111(3)	1.759(9)	2.326	2.308	2.392	2.396	*23c*
S_2^{2-}	S_4^{2-}	2	2.850(1)	1.862(7)[b]	2.014(5)[b]	2.302[b]	2.350[b]	2.400[b]	2.412[b]	*73a,b*

[a] See footnote *a*, Table I.

[b] Subject to site occupation disorder.

TABLE IV

CHARACTERISTIC ELECTRONIC AND INFRARED ABSORPTION SPECTROSCOPIC DATA OF TERTIARY Mo/S/O COMPLEXES THAT CONTAIN THE $[Mo_2S_3O]^{2+}$ CORE[a]

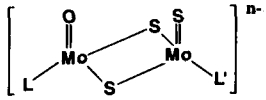

L′	L	n	Infrared absorption (cm^{-1})[b]	λ_{max} (nm; $\varepsilon \times 10^{-3}$)[c]
S^{2-}	S_2^{2-}	2	945(m); 503(m); 483(w); 461(w)	412; 476(sh)
S^{2-}	S_4^{2-}	2	944(m); 506(m); 489(m); 482(w)	408
S_2^{2-}	S_2^{2-}	2	938(m); 546(w); 354(w)	390; 470; 550(sh)
S_2^{2-}	S_4^{2-}	2	949(m); 932(m); 458(w); 354(w)	370; 430

[a] Data from Refs. *73a,b*.
[b] In CsI disk.
[c] In DMF.

argument that the $S_2 \rightarrow$ Mo charge transfer depletes more electron density from the antibonding π^* orbital of the S_2^{2-} ligand in the O=Mo−S_2 than in the S=Mo−S_2 unit and results in a stronger S–S bond in the former (*28a*). This latter argument is not supported by crystallographic data (Table II) that show a wide range in S–S distances instead of consistently longer S–S bonds in the (S_2)Mo(S) units. The electronic and infrared spectral data (Table IV) also are mainly inconclusive in this respect.

2. The $[O{=}Mo(S_4)]^{2-}$ Anion and the $[(S_x)(Mo_2O_2S_2)(S_y)]^{2-}$ Series

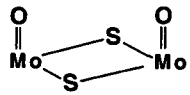

The $[Mo_2O_2S_2]^{2+}$ unit

Tertiary oxo/thiomolybdates that contain the $[Mo^V_2O_2S_2]^{2+}$ cores are very common and have been reported with a wide variety of terminal ligands. The binary complexes within the $[(S_x)(Mo_2O_2S_2)(S_y)]^{2-}$ series include $[(S_2)(Mo_2O_2S_2)(S_2)]^{2-}$ (*100*), $[(S_2)(Mo_2O_2S_2)(S_3O_2)]^{2-}$ (*101*), the $[(S_2)(Mo_2O_2S_2)(MoS_4)]^{2-}$ and $[(S_2)(Mo_2O_2S_2)(MoOS_3)]^{2-}$ anions (*102*) (which were isolated in a crystalline solid that contained virtually equimolar amounts of both of these trimetallic complexes), the monomeric $[(S)(Mo_2O_2S_2)(S_4)]^{2-}$ and its dimeric form

$\{[(S)(Mo_2O_2S_2)(S_4)]_2\}^{4-}$ (*103*), the $[(S_4)(Mo_2O_2S_2)(S_2)]^{2-}$ anion (*104*), and $[(S_4)(Mo_2O_2S_2)(S_4)]^{2-}$ (*97*).

A general approach that has been found effective in the systematic synthesis of most of the $[(S_x)(Mo_2O_2S_2)(S_y)]^{2-}$ complexes (Fig. 14; Tables V and VI) is based on the $[(S_2)(Mo_2O_2S_2)S_4)]^{2-}$ complex (Fig. 14, structure 3A). Sequential, stoichiometric S addition or S abstraction reactions to or from Fig. 14 (structure 3A) afford various derivatives with the $(Mo_2O_2S_2)^{2+}$ core intact (*105*). The synthesis of structure 3A is carried out by the reaction of $(NH_4)_6(Mo_7O_{24})\cdot 4H_2O$ with sulfur-enriched $(NH_4)_2S$ in water. The complex forms under aerobic conditions and is isolated as a Et_4N^+ salt after standing for 24 hr (*104*). In short reaction times but otherwise similar conditions this reaction affords in good yield the $[O{=}Mo(S_4)_2]^{2-}$ complex (*106*). The latter was obtained previously in low yield by the hydrolysis of the $[S{=}Mo(S_4)_2]^{2-}$ anion (*24a*). A probable pathway that leads to the $[O{=}Mo(S_4)_2]^{2-}$ and $[(S_2)(Mo_2O_2S_2)(S_4)]^{2-}$ complexes (Fig. 15) is based on an intramolecular redox process not unlike the one outlined for the synthesis of $[S{=}Mo(S_4)_2]^{2-}$ from $(MoS_4)^{2-}$ (Fig. 10).

3. *The Solvated $[Mo_2O_2S_2]^{2+}$ Core and Derivatives*

Stoichiometric reactions of the $[(S_4)(Mo_2O_2S_2)(S_2)]^{2-}$ complex with I_2 in DMF solution result in the sequential oxidation of the S_4^{2-} and S_2^{2-} ligands and formation of the neutral $[(DMF)_3(Mo_2O_2S_2)(S_2)]$ and the cationic $[(DMF)_3(Mo_2O_2S_2)(DMF)_3]^{2+}$ complexes (*104*) (Fig. 16, structures 2B and 1B; Table V). The latter, isolated as an I^- salt, is a 2:1 electrolyte soluble in both water and nonaqueous solvents. The structure of $[(DMF)_3(Mo_2O_2S_2)(S_2)]$ has been determined (*103*). The lability of the DMF ligands in both structures 2B and 1B (Fig. 16) makes these compounds excellent reagents for the synthesis of a great number of complexes that contain the $[Mo_2O_2S_2]^{2+}$ core. Representative derivatives of structure 2B (Fig. 16) are the $[(L)(Mo_2O_2S_2)(L')]^n$ complexes (*104*) with L = S_2^{2-}, L' = $[S_2C_2O_2]^{2-}$, CS_3^{2-}, $2Cl^-$ ($n = -2$); L = S_2^{2-}, L' = trithiacyclononane (TTN) (n = 0); or L = S_2^{2-}, L' = Cp (n = −1). All of these complexes (*105*) are expected to be well suited for the synthesis of "mixed-ligand" derivatives with ligands L other than S_2^{2-} using their $[(Cl)_2(Mo_2O_2S_2(L')]^n$ derivatives. The latter are obtained by the reaction of benzoyl chloride with the Mo-coordinated S_2^{2-} ligands. In these reactions the S_2^{2-} ligands are converted to the $(PhCOS)_2$ disulfide and are replaced by two Cl^- ions (*73b*, *113*). This reaction is clean and could also be useful in the synthesis of monothio aryl carboxylic acid derivatives.

The $[(S_2)(Mo_2O_2S_2)(Cp)]^-$ monoanion (Fig. 16, structure 2C, which

TABLE V

DISTANCES AND ANGLES IN TERTIARY Mo/S/O COMPLEXES AND SELECT DERIVATIVES THAT CONTAIN THE $[Mo_2O_2S_2]^{2+}$ CORE[a]

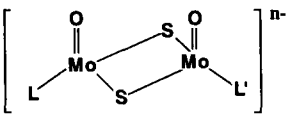

L	L'	n	Mo−Mo (Å)	M=O (Å)	(L)Mo−S_b (Å)	(L')−S_b (Å)	Mo−L (Å)	Mo−L' (Å)	M−S−M (°)	S−Mo−S (°)	Reference
$(DMF)_3$	S_2^{2-}	0	2.813(1)	1.686	2.317(3)		2.186(6) 2.212(6) 2.224(6)[b]	2.38	74.8	102.5	*103a*
S^{2-}	S_4^{2-}	2[c]	2.896(1)	1.692	2.277	2.372	2.167(3)	2.412	77.0	101.5	*103a*
S^{2-}	S_4^{2-}	4[d]	2.852(2) 3.554(2)[e]	1.664	2.324	2.350 2.420[f]	—	2.435	75.2	98.4 75.8[f]	*103a*
S_2^{2-}	S_2^{2-}	2	2.828(1) 2.825(2)	1.683 1.675	2.322 2.324		2.394 2.41(2)		75.0 74.9	102.1 101.8(2)	*100c* *100d*
S_2^{2-}	S_4^{2-}	2	2.829(1)	1.676	2.297(3) 2.316(3)	2.365(2) 2.353(3)	2.394	2.420	74.6	101.6(1) 98.5(1)	*83, 104*
S_2^{2-}	Cp^-	1	2.855(1)	1.673	2.310(4)		2.396	2.380(9)[g]	77.0	101.5	*103a*
S_4^{2-}	S_2^{2-}	2	2.853(3)	1.691	2.330		2.43(1)		75.5	101.5	*97a*
$(CS_3)^{2-}$	$(CS_4)^{2-}$	2	2.835(2)	1.678(9)	2.305(5)		2.433(6)	2.401(5)	75.4(2)	100.5(2)	*161*
Cp^-	$(SO_3)^{2-}$	1	2.838(2)	1.681(6)	2.308(3)		2.063(7)	2.38(2)	75.9(1)	101.9(1)	*113, 175*
Cp^-	$(S_2O_3)^{2-}$	1	2.850(2)	1.69(1)	2.296(3)		2.08(1)	2.40(4)	76.8(2)	101.2(2)	*113, 175*
Cp^-	$(SO_4)^{2-}$	1	2.831(1)	1.685(3)	2.303(2)		2.087(4)	2.374(7)	75.9(1)	101.8(1)	*113, 175*
$(S_2O_2)^{2-}$	$(S_2O_3)^{2-}$	2[h]	2.810(3)	1.65(2)	2.315(5)		—[h]	—[h]	74.7(2)	101.3(1)	*113*
S_2^{2-}	$(S_2O_3)^{2-}$	2	2.794(1)	1.678(9)	2.316(4)[i] 2.269(4)[j]		2.44	2.395(5)[k] 2.26(1)[l]	74.6(1)	103.5(2) —[m]	*113*
$(SO_4)^{2-}$	$(SO_4)^{2-}$	2	2.818(1)	1.675(5)	2.304(2)		2.08(1)	2.08(1)	75.5(1)	101.7(1)	*113*
$(DMF)_3$	$(SO_4)^{2-}$	0	2.823(1)	1.655(5)	2.300(2)		2.146(6) 2.189(6) 2.245(6)[n]	2.081)6)	75.6(1)	102.6(1)	*113*
$(SO_4)^{2-}$	$(SO_4)^{2-}$[o]	2	2.775(2)	1.638(7)	2.316(4) 2.278(7)		2.104(6)	2.09(2)	75.1(1)	101.9(1)	*174*

$(S_2O_3)^{2-}$	$(S_2O_3)^{2-}$	2[p]	2.686(1)	1.662	2.312	2.408(2)[q]	2.397(2)[q]	89.0(2)[s]	96.7(2)[u]	*113*
					1.916	2.099(5)[r]	2.074(5)[r]	71.0(1)[t]		
$(VDS)^{2-}$	$(VDS)^{2-}$	2	2.882(1)	1.676(6)	2.328	2.215(8)[v]		—	—	*169*
						2.382(3)[w]				
DMAD, DMAD		2								
—[x]			2.853(1)	1.675	2.331(3)	2.425(8)		75.5	100.9	*25*
—[y]			2.904(1)	1.684(2)	2.328	2.419		77.1(1)	100.9(1)	*25*
$[O=Mo(S_4)_2]^{2-}$		2	—	1685(7)	—	2.363(2)		—	—	—
						2.395(2)				
$(Edt)^{2-}$, $(Edt)^{2-}$		2	2.866(3)	1.659(3)	2.341(9)	2.412(9)		75.5(4)	100.5(4)	*89c*

[a] See footnote *a*, Table I.
[b] Trans to the Mo=O group.
[c] Dimeric Ph_4P^+ salt.
[d] Tetrameric $\{S_4(Mo_2S_2S_2)S]_2^{4-}$ Et_4N^+ salt.
[e] Interdimer Mo–Mo distance.
[f] Associated with the central Mo_2S_2 unit.
[g] Mo–C distances to the η^5-Cp carbon atoms.
[h] Positionally disordered L and L′.
[i] Trans to the $(S_2O_3)^{2-}$ S donor.
[j] Trans to the $(S_2O_3)^{2-}$ O donor.
[k] The $(S_2O_3)^{2-}$ S donor.
[l] The $(S_2O_3)^{2-}$ O donor.
[m] Intrabridge angle.
[n] Trans to the Mo=O group.
[o] From the $\{[(SO_4)(Mo_2O_2S_2)(SO_4)]_2^{2-}(\eta^4-SO_4)\}^{6-}$ tetramer.
[p] The central core in this complex is the mixed-ligand bridged $[Mo_2(O)_2(\mu-S)(\mu-O)]^{2+}$ unit.
[q] Mo–S.
[r] Mo–O.
[s] Mo–O–Mo.
[t] Mo–S–Mo.
[u] S–Mo–O angle.
[v] Mo–C bond.
[w] Mo–S bond.
[x] Syn isomer.
[y] Anti isomer.

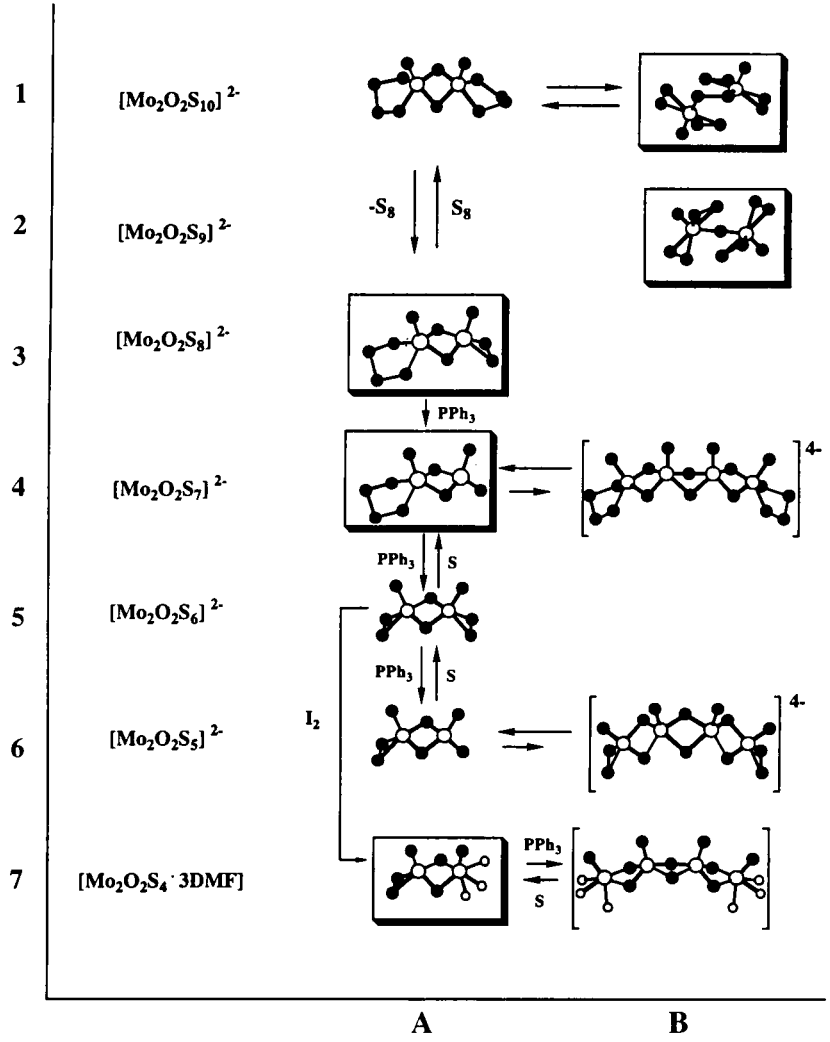

FIG. 14. The $[(S_x)(Mo_2O_2S_2)(S_y)]^{2-}$ complexes.

is readily available from structure 2B) and its derivatives have been used extensively in ^1H NMR studies of reactions of the $(S_x)Mo{=}O$ chromophore. The Cp^- ligand is a convenient spectroscopic "handle" and has been used as a "reporter" of the changes that accompany reactions of the $[(S_x)(Mo_2O_2S_2)(Cp)]^-$ complexes (*28b*) (*vide infra*).

The $[(DMF)_3(Mo_2O_2S_2)(DMF)_3]^{2+}$ complex (Fig. 16, structure 1B) also has been used effectively in the synthesis of a plethora of

TABLE VI

CHARACTERISTIC ELECTRONIC AND INFRARED ABSORPTION SPECTROSCOPIC DATA OF TERTIARY Mo/S/O COMPLEXES AND SELECT DERIVATIVES THAT CONTAIN THE $[Mo_2O_2S_2]^{2+}$ CORE

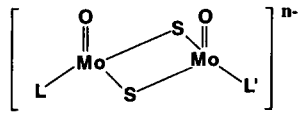

L'	n	Infrared absorption (cm^{-1})	κ_{max} (nm)	Reference
$(DMF)_3$, $(DMF)_3$	2+	Mo=O, 928(m), 947(s); Mo–S_b, 469(m)[a]	276; 286(br, sh); 358(sh)[b]	*104, 105*
$(DMF)_3$, S_2^{2-}	0	Mo=O, 948(s), 954(s), Mo–S_b, 469(m); Mo–S_a, 527(m)[a]	269(br, sh)[b]	*104, 105*
S^{2-}, S_4^{2-}[c]	2	Mo=O, 890(m), 943(m); Mo–S_b, 465(m); Mo–S_a, 494(m), 420(w)[a]	270; 365[b]	*104, 105*
S^{2-}, S_4^{2-}[f]	4	Mo=O, 933(s); Mo–S_b, 462(m); Mo–S_a, 410(w)	365; 270[b]	*103*
S_2^{2-}, Cp^-	1	Mo=O, 909(m), 948(s); Mo–S_b, 462(m); Mo–S_a, 527(m)[d]	270; 311[b]	*103*
S^{2-}, Cp^-	1	Mo=O, 903(s), 914(m), 930(s); Mo–S_b, 464(m)[a]	270; 320[b]	*103*
$(CS_3)^{2-}$, Cp^-	1	Mo=O, 911(m), 951(s); Mo–S_b, 466(m)[a]	270(sh); 298(sh); 313(sh)[b]	*103*
$(VDS)^{2-}$, Cp^-	1	Mo=O, 932(s), 950(m); Mo–S_b, 460(w); Mo–S_a, 526(s), 420(w)[a]	274(br); 296(sh); 360(sh); 467(sh)[b]	*103*
$(CS_3)^{2-}$, $(CS_4)^{2-}$	2	Mo=O, 953(s); Mo–S_b, 466(w)[a]	—	*103*
$(CS_3)^{2-}$, S_4^{2-}	2	Mo=O, 949(s); Mo–S_b, 468(w); Mo–S_a, 422(s)[d]	258; 310[b]	*103*
$(VDS)^{2-}$, $(VDS)^{2-}$	2[g]	Mo=O, 947; Mo–S_b, 473; S–S, 520[a]	—	*169*
$(VDS)^{2-}$, $(VDS)^{2-}$	2[g]	Mo=O, 940(s); Mo–S, 469(w), 420(VW), 382(w), 358(w), 331(w)[a]	—	*25*
$(DMDA)^{2-}$, $(DMDA)^{2-}$	2[h]	Mo=O, 942(m); Mo–S_b, 463(w)[a]	—	*25*
$(DMDA)^{2-}$, $(DMDA)^{2-}$	2[i]	Mo=O, 923(s); 911(w); Mo–S_b, 462(w)[a]	318; 380(sh)[e]	*25*
$(SO_3)^{2-}$, Cp^-	1	Mo=O, 962(s), 903(m); ν–SO_3^{2-}, 1166, 646, 571, 502[d]	—	*175*
$(S_2O_3)^{2-}$, Cp^-	1	Mo=O, 955(s), 915(m); ν–$S_2O_3^{2-}$, 1277, 1172, 1150, 662, 542; Mo–S_b, 483, 470[d]	—	*175*
$(SO_4)^{2-}$, $(SO_4)^{2-}$[j]	2	Mo=O, 960(s), 903(m); ν–SO_4^{2-}, 1280, 1157, 1114, 660, 618, 582[d]	—	*174*

[a] In KBr disk.
[b] In DMF.
[c] Ph_4P^+ salt dimer.
[d] In CsI disk.
[e] In CH_3CN solution.
[f] Et_4N^+ salt tetramer.
[g] The cis, syn isomer.
[h] Syn isomer.
[i] Anti isomer.
[j] From the $\{[(SO_4)(Mo_2O_2S_2)(SO_4)]_2^2$ $(\eta^4-SO_4)\}^{6-}$ tetramer.

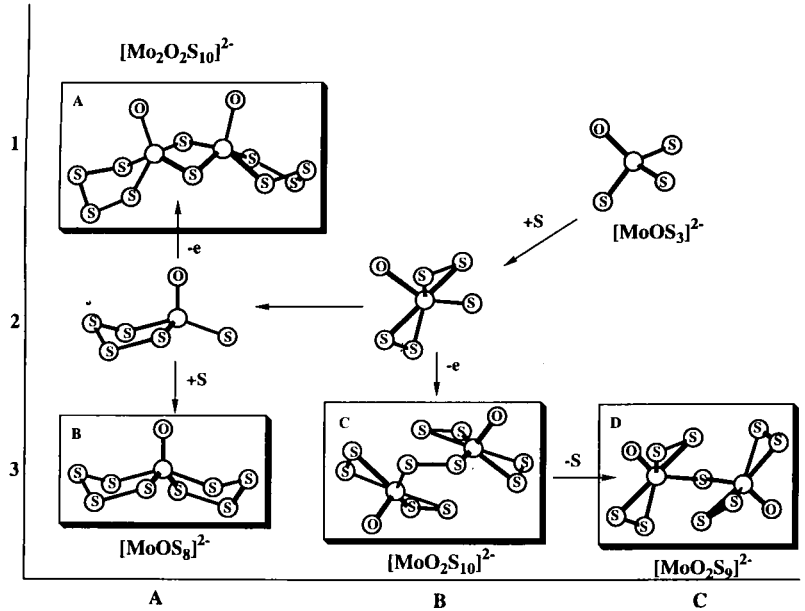

FIG. 15. Proposed pathways in the synthesis of the $[O{=}Mo(S_4)_2]^{2-}$ anion.

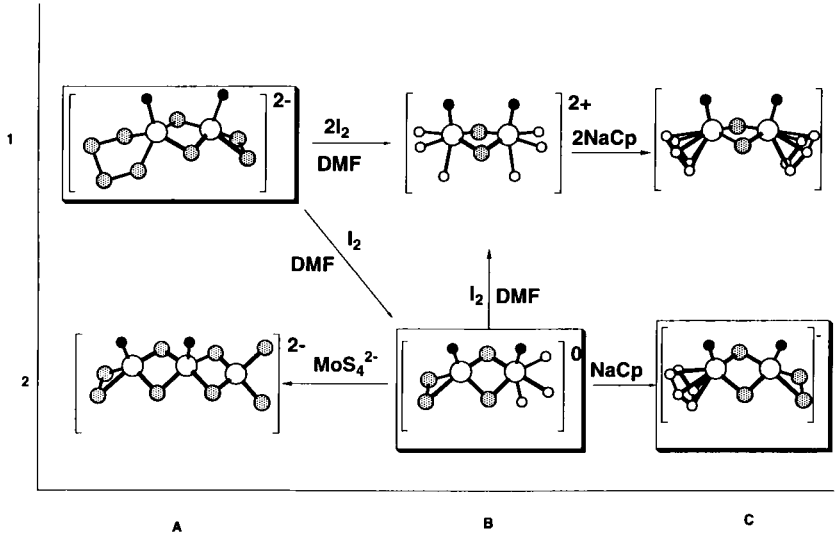

FIG. 16. The synthesis of the solvated $[Mo_2O_2S_2]^{2+}$ core and derivatives.

$[(L)(Mo_2O_2S_2)(L)]^n$ molecules (*105*) (Fig. 17). Of these, some have been reported previously, including L = $(NCS)_3$, n = −4 (*107*); L = EDTA, $n = -2$ (*108*); L = $S_2P(i\text{-}Pr)_2$, $n = 0$ (*109*); L = $n\text{-}Bu_2Dtc$, $n = 0$ (*110*); and L = Cp^-, $n = 0$ (*111*). The synthetic utility of structure 1B (Fig. 16) parallels that of the similarly water soluble $[(H_2O)_3(Mo_2O_2S_2)(H_2O)_3]^{2+}$ complex (*112*). The syntheses of the $[(H_2O)_3(Mo_2O_2S_2)(H_2O)_3]^{2+}$ complex by acidification of $Na_2[(Cys)(Mo_2O_2S_2)(Cys)]$ and various other $[(L)(Mo_2O_2S_2)(L)]^n$ complexes have been reported in detail (*112b*). The same synthetic procedure has been found successful for the synthesis of various $[(L)(Mo_2O_3S)(L)]^{2-}$ complexes from $Na_2[(Cys)(Mo_2O_3S)(Cys)]$ (*112b*). These complexes contain both $\mu\text{-}S^{2-}$ and $\mu\text{-}O^{2-}$ bridges (*112c–f*). A convenient, high-yield synthesis of the "mixed-bridge" $[Mo_2O_3S]^{2+}$ core has been reported by the reaction of $(Et_4N)_2[MoS_2O_2]$ with SO_2 in CH_3CN. This reaction affords the crystalline $(Et_4N)_2[(S_2O_3)(Mo_2O_3S)(S_2O_3)]$ complex. The lability of the $(S_2O_3)^{2-}$ ligands in this structurally characterized (*113*) molecule makes it an excellent reagent for the synthesis of other complexes with the $[Mo_2O_3S]^{2+}$ core. Selected features in the structures of the $[(L)(Mo_2O_2S_2)(L)]^n$ complexes are given in Table V and characteristic features of the electronic and infrared spectra of these complexes are included in Table VI.

4. The $[(S_2)_2Mo(O)]$ Structural Unit and Derivatives

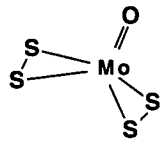

The $[O{=}Mo^{VI}(S_2)_2]$ unit

Oxidation of $[O{=}Mo^{IV}(S_4)_2]^{2-}$ with $[(Cp)_2Fe]^+$ affords the $\{[O{=}Mo^{VI}(S_2)_2]_2(\mu\text{-}S)\}^{2-}$ and $\{[O{=}Mo^{VI}(S_2)_2]_2(\mu\text{-}S_2)\}^{2-}$ complexes (*106*) (Fig. 18, structures 2A and 3B; Table VII). In the structures of these complexes (Table VII), the $\eta^2\text{-}S_2$ ligands and the μ-S ligands occupy the equatorial positions of the pentagonal pyramidal structure of the Mo^{VI} ion. The oxo ligand is located at the apical position and trans to a weakly interacting S_2 ligand from the second $[O{=}Mo^{VI}(S_2)_2]$ subunit.

The $[O{=}Mo^{VI}(S_2)_2]$ chromophore in these complexes is derived by internal electron transfer within the $[O{=}Mo^{IV}(S_4)]$ unit. As indicated previously, this process in reverse accounts for the synthesis of $[O{=}Mo^{IV}(S_4)]$ and the $[O{=}Mo^{IV}(S_4)_2]^{2-}$ anion from $(MoOS_3)^{2-}$ (Fig. 15). Indeed, it appears likely that, under certain circumstances, the $[O{=}Mo^{VI}(S_2)_2]$ and $[O{=}Mo^{IV}(S_4)]$ units may exist in equilibrium. This

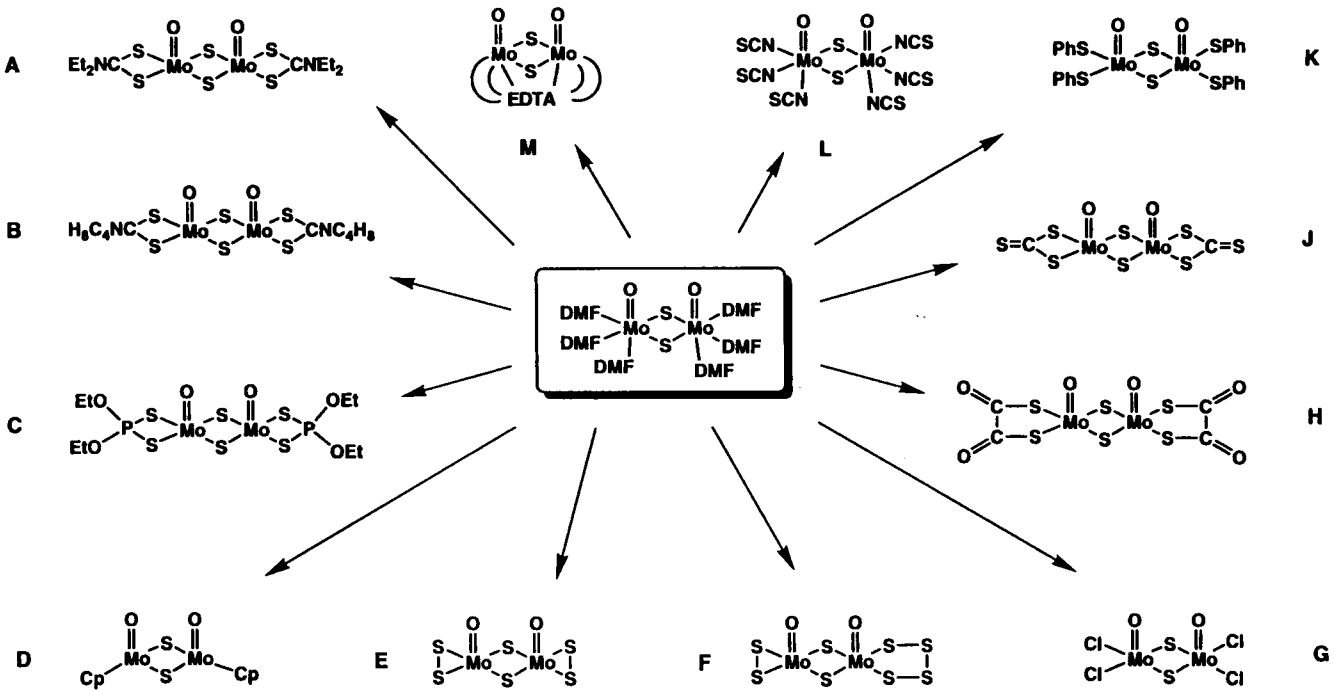

FIG. 17. The synthetic utility of the $[(DMF)_3(Mo_2O_2S_2)(DMF)_3]^{2+}$ complex.

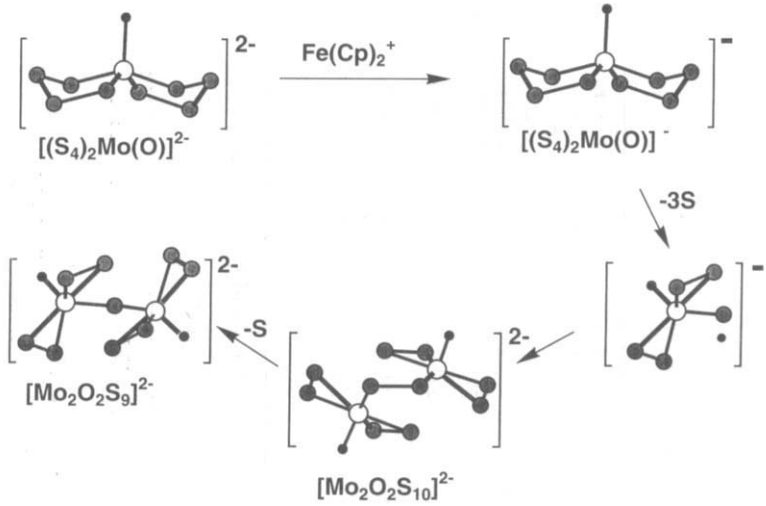

FIG. 18. A proposed pathway toward the synthesis of $\{[O{=}Mo^{VI}(S_2)_2]_2(\mu\text{-}S)\}^{2-}$.

type of equilibrium would be consequence of the close energy matching between the Mo *4d* orbitals and the sulfur *3p* orbitals and would account for the apparent similar energies between the pentagonal bipyramidal $[E{=}Mo^{VI}(S_2)_2L)]^n$ complexes and the square pyramidal $[E{=}Mo^{IV}(S_4)(L)]^n$ complexes (L = a bidentate chelating ligand). The pentagonal bipyramidal complexes with the $O{=}Mo^{VI}(S_2)_2$ structural unit are quite common. This is not the case for the square pyramidal complexes with the $O{=}Mo^{IV}(S_4)$ unit. With the exception of the $[E{=}Mo(S_4)_2]^{2-}$ and the $[(Cp)Mo(S_4)_2]^-$ (*116*) complexes, the only other square pyramidal complex of this structural type is the structurally characterized $[O{=}Mo^{IV}(S_4)(MNT)]^{2-}$ obtained by a substitution reaction between the $\{[O{=}Mo^{VI}(S_2)_2]_2Cl\}^-$ complex and Na_2MNT (*106b*). An interesting question can be raised whether, in solution, the $[O{=}Mo^{IV}(S_4)(Mo^{VI}S_4)]^{2-}$ and $[O{=}Mo^{IV}(S_4)(Mo^{VI}OS_3)]^{2-}$ complexes (Figs. 13 and 14, structures 2C and 4A, respectively) exist in equilibrium with their pentagonal bipyramidal, internal redox isomers, $[O{=}Mo^{VI}(S_2)_2(Mo^{VI}S_4)]^{2-}$ and $[O{=}Mo^{VI}(S_2)_2(Mo^{VI}OS_3)]^{2-}$, respectively. A spectroscopic handle that can differentiate between the two different isomers is not available in the rather uninformative infrared or electronic spectra (Table VIII).

A proposed pathway (*83*, *106*) for the oxidative coupling and formation of $\{[O{=}Mo^{VI}(S_2)_2]_2S\}^{2-}$ and $\{[O{=}Mo^{VI}(S_2)_2]_2S_2\}^{2-}$ has been suggested (Fig. 18). The removal of S^{2-} (as NiS) by the reaction of structure 2A (Fig. 19) with $NiCl_2$ affords the $\{[O{=}Mo^{VI}(S_2)_2]_2Cl\}^-$ complex

TABLE VII

DISTANCES IN TERTIARY Mo/S/O COMPLEXES AND SELECT DERIVATIVES THAT CONTAIN THE $[O=Mo(S_2)_2]$ UNIT[a]

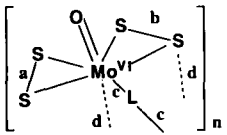

L	n	Mo−Mo (Å)	Mo=O (Å)	Mo−S (**a**) (Å)	Mo−S (**b**) (Å)	Mo−S(L′) (**d**) (Å)	Mo−L (**c**) (Å)	S−S (**a**) (Å)	S−S (**b**) (Å)	Reference
$\frac{1}{2}S$	2	3.606(1)	1.676(6)	2.37(2)	2.409(6)	2.856(3)	2.50(2)	2.028(8)	2.042(4)	*105*
$\frac{1}{2}SMe$	2	3.570(1)	1.672(6)	2.380(3)	2.420(5)	2.84(2)	2.526(3)	2.037(4)	2.046(4)	*105*
$\frac{1}{2}S$	4	3.606(1)	1.676(8)	2.386(4)	2.380(4)	2.919(9)	2.538(8)[b]	2.043(5)	2.051(5)	*105*
		3.561(1)			2.387(7)					
$\frac{1}{2}Cl$	2[c]	3.550(1)	1.654(10)	2.377(4)	2.379(3)	2.88(3)[d]	2.535(3)[b]	2.055(6)	2.038(5)	*105*
					2.392(4)					
$\frac{1}{2}S_7^{2-}$	2[e]	—	1.670(6)	2.390(8)	2.390(8)	2.490(8)[f]	2.472(4)[g]	2.038(5)	2.038(5)	*117a*
η^2-Monothiooxalate	1	—	1.70(4)	2.38(2)	2.38(2)	2.31(4)[h]	2.53(2)[i]	2.03(2)	2.03(2)	*119*
η^2-Bipy	1	—	1.690(10)	2.371(7)[j]	—	2.207(12)[l]	2.351(2)[m]	2.055(6)	—	*118a*
				2.431(7)[k]				2.038(6)		
$\frac{1}{2}S_2$	2[n]	4.108(1)	2.420(11)[o]	2.430(3)	2.420(3)	2.648(2)	2.523(3)	2.037(5)	2.026(4)	*115*

[a] See footnote *a*, Table I. Bold letters in parentheses correspond to letters in the structure at the top of this table, identifying the different types of S_2^{2-} bonding.
[b] Equatorially bound μ-η^2, η^1-disulfido ligand.
[c] This complex contains an η^1-Cl^- ligand bound to one of the Mo atoms and a μ-η^2, η^1-disulfido bridging ligand (see Fig. 19, structure 2C).
[d] Axially bound μ-η^2, η^1-disulfido ligand.
[e] $\{[O=Mo^{VI}(S_2)_2]_2(\mu_2\text{-}S_7)(\mu_2\text{-}H_2NNH_2)\}^{2-}$ anion.
[f] Mo–μ-H_2N–NH_2 bond.
[g] Bonds to the μ-S_7^{2-} ligand.
[h] Axially bound oxygen atom of the monothiooxalate ligand.
[i] Equatorially bound S atom of the monothiooxalate ligand.
[j] η^2-S_2 sulfur atoms neighboring the equatorial N atom and nearly trans to each other.
[k] η^2-S_2 sulfur atoms distant from the equatorial N atom.
[l] Axial Mo–N bond.
[m] Equatorial Mo–N bond.
[n] Instead of terminal O or S groups the complex contains Me_5-Cp ligands bound to the Mo atoms.
[o] Mo–C distances to the Me_5-Cp ligand.

TABLE VIII

CHARACTERISTIC ELECTRONIC AND INFRARED ABSORPTION SPECTROSCOPIC DATA OF TERTIARY MO/S/O COMPLEXES AND SELECT DERIVATIVES THAT CONTAIN THE $[O=Mo(S_2)_2]$ CORE

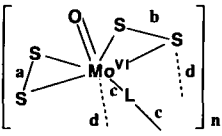

L	n	Infrared absorption (cm^{-1})	λ_{max} (nm; $\epsilon \times 10^{-3}$)	Reference
⅛S	2	Mo=O, 926(s), 528(m), 358(m), 352(m), 341(m)[a]	392(3.8); 432(4.0); 522(1.9)[b]	*105*
⅛SMe	2	Mo=O, 957(w), 939(vs), 927(vs); 545(m), 535(m), 358(m), 347(m)[a]	354(sh); 382(2.9); 436(3.0); 530(2.5)[b]	*105*
⅛S	4	Mo=O, 940(vs), 930(vs), 912(w), 534(m)[a]	338(10.4); 414(8.1); 510(7.9)[b]	*105*
⅛Cl	2	Mo=O, 949(s), 936(vs), 539(m), 378(m), 366(m), 297(m)[a]	350(3.0); 390(sh); 474(2.7); 530(sh)[b]	*105*
⅛S	2	Mo=S, 520(s), 530(s)[a]	360; 400; 485; 590[d]	*121*[c]
⅛S_7^{2-}	2	Mo=O, 925(vs), 532(s), 485(w, sh); 470(w), 344(s)[e]	248(25); 317(14.9); 452(4.0); 530(2.43)[d]	*117*[f]
Bipy	1	Mo=O, 930(s); S–S, 540(s), 370(m), 340(m)[e]	305(9.5); 330(3.9); 418(.25); 483(1.0); 565(1.0)[b]	*118a*
η^2-Monothiooxalate	1	Mo=O, 930(s); S–S, 530	—	*119*

[a] In CsI disk.
[b] In DMF.
[c] Data for the $\{[S=Mo^{VI}(S_2)_2]_2(\mu\text{-}S_2)\}^{2-}$ anion.
[d] In CH_3CN.
[e] In KBr disk.
[f] Data for the $\{[O=Mo^{VI}(S_2)_2]_2(\mu_2\text{-}S_7)(\mu_2\text{-}H_2NNH_2)\}^{2-}$ anion.

(Fig. 19, structure 2C). The μ-S ligand in structure 1A (Fig. 19) is unusually labile and is replaced by an η^2-S_2 ligand in a transformation that converts the $\{[(\eta^2\text{-}S_2)_2Mo(O)]_2(\mu\text{-}S)\}^{2-}$ complex, structure 1A, into $[O=Mo(\mu\text{-}\eta^2,\eta^1\text{-}S_2)(\eta^2\text{-}S_2)][O=Mo(\eta^2\text{-}S_2)_2(=S)]^{2-}$, structure 1C (Fig. 19). In this form the complex is probably oxidized to the structurally characterized $\{[O=Mo(\mu\text{-}\eta^2,\eta^1\text{-}S_2)(\eta^2\text{-}S_2)]O=Mo(\eta^2\text{-}S_2)_2(S)]\}_2^{2-}$ tetramer (Fig. 19, structure 3B). The ready dissociation of structure 2C to the $[O=Mo^{VI}(S_2)_2]$ and $[O=Mo^{VI}(S_2)_2(Cl)]^-$ fragments makes this complex ideally suited as a reagent for the synthesis of $(\eta^2\text{-}[O=Mo^{VI}(S_2)_2(L)]$ complexes in reactions with bidentate chelating ligands (L). These complexes usually have a seven-coordinate pentagonal bipyramidal structure. At times, certain ligands (such as MNT) promote internal redox, and the square pyramidal complexes, $[O=Mo^{IV}(S_4)(L)]$, are isolated (*106b*) rather than their pentagonal bipyramidal internal redox isomers.

The $(\eta^2\text{-}S_2)_2Mo(O)$ unit structurally resembles the oxo/peroxomolybdate units studied extensively by Stomberg and co-workers in

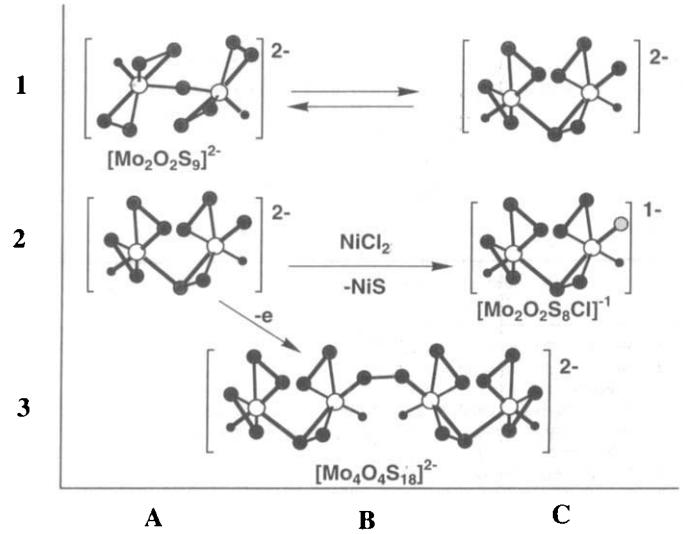

FIG. 19. Reactions of the $\{[O{=}Mo^{VI}(S_2)_2]_2(\mu\text{-}S)\}^{2-}$ complex.

complexes such as $[Mo_2O_3(O_2)_4(H_2O)_2]^{2-}$ (*114a*), $[Mo_3O_7(O_2)_4]^{4-} \cdot 2H_2O$ (*114b*), $[Mo_4O_{12}(O_2)_2]^{4-}$ (*114c*), $[Mo_5O_{10}(O_{28})^{6-} \cdot 5H_2O$ (*114d*), $[Mo_7O_{22}(O_2)_2]^{6-} \cdot 8H_2O$ (*114e*), and $[Mo_{10}O_{22}(O_2)_{12}]^{8-} \cdot 16H_2O$ (*114f*). Thus far the diversity in nuclearity apparent in the oxo/peroxomolybdate series has not been found with the oxo/disulfido complexes.

In the structure of $\{[O{=}Mo^{VI}(S_2)_2]_2(\mu\text{-}S)\}^{2-}$ a small amount of $\{[O{=}Mo^{VI}(S_2)_2]_2(\mu\text{-}S_2)\}^{2-}$ was found as a minor component at the same anion site. At a later date the $\{[O{=}Mo^{VI}(S_2)_2]_2(\mu\text{-}S)\}^{2-}$ was obtained apparently free of the disulfido minor component (*114g*). The $\{[(Cp^*)Mo^{VI}(S_2)_2]_2(\mu\text{-}S_2)\}$ complex (*115*) is very nearly isostructural to $\{[O{=}Mo^{VI}(S_2)_2]_2(\mu\text{-}S_2)\}^{2-}$, with the oxo ligands in the latter replaced by the Cp* groups in the former. A similar situation prevails with the $[(Cp)Mo(S_4)_2]^-$ and $[(Cp)Mo(Se_4)_2]^-$ complexes (*116*) that are isostructural and formally isoelectronic to $[S{=}Mo(S_4)_2]^{2-}$. In $[(Cp)Mo(S_4)_2]^-$ the Mo coordinated S_4^{2-} anion shows the unusual alternation in the S–S distances similar to the one previously found in the $[S{=}Mo(S_4)_2]^{2-}$ anion. It would be of interest to investigate the extent to which the Mo=S and Cp–Mo groups are interchangeable in thiomolybdate complexes and how their chemistry may show comparative reactivity.

In the $[O{=}Mo(S_2)_2](\mu\text{-}S_7)(\mu\text{-}NH_2NH_2)[O{=}Mo(S_2)_2]$ complex (*117*) the $O{=}Mo(S_2)_2$ units are bridged by a S_7^{2-} ligand and by a hydrazine molecule. The $\mu_2\text{-}S_7^{2-}$ ligand coordinates in the equatorial planes of

the pentagonal bipyramidal Mo^{VI} centers, satisfies the coordination requirements of the Mo^{VI} ions, and as a result the S_2^{2-} ligands are not used in the bridging mode. The bridging hydrazine N donor atoms are bound trans to the O=Mo groups at the rather long distances of 2.487(8) and 2.492(8) Å and occupy the positions occupied by the μ-η^2,η^1-S_2 ligands in structure 1A (Fig. 19).

A number of monomeric, pentagonal bipyramidal complexes of the type $[O{=}Mo(S_2)_2(L)$ have been reported. The complex with L = 2,2-bipyridyl (*118a*) is obtained from MoO_4^{2-} and aqueous S_x^{2-} in the presence of 2,2-bipyridyl. The corresponding W complex also is known and has been structurally characterized (*118b*). A similar complex with L = monothiooxalate $(C_2O_3S)^{2-}$ has been isolated (*119*) serendipitously by the reaction of $Cs_2[Mo_2O_4(C_2O_4)_2(H_2O)_2] \cdot 2H_2O$ with $Cs_2(S_2C_2O_2)$.

The tetrameric $(Nb_4Se_{22})^{6-}$ complex (*120*) is isostructural to the $\{[(O)Mo(\mu\text{-}\eta^2,\eta^1\text{-}S_2)(\eta^2\text{-}S_2)][(O)Mo(\eta^2\text{-}S_2)_2(S)]\}2^{2-}$, or $(Mo_4O_4S_{18})^{2-}$, tetramer (*105*) (Fig. 19, structure 3B). The $\{[(S_2)_2W(S)]_2(\mu\text{-}S)\}^{2-}$ and $[(S)W(\mu\text{-}\eta^2,\eta^1\text{-}S_2)(\eta^2\text{-}S_2)][(S)W(\eta^2\text{-}S_2)_2(SH)]^{2-}$ complexes, with structures similar to those shown in Fig. 19, have been synthesized and structurally characterized (*121a*). The $\{[O{=}W^{VI}(S_2)_2]_2(\mu\text{-}S)\}^{2-}$ complex is isostructural to the Mo analog (*121b*) and the $\{[S{=}Mo^{VI}(S_2)_2]_2(\mu\text{-}S_2)\}^{2-}$ complex has been synthesized and spectroscopically characterized (*121c*).

D. The $[E{=}Mo(MoS_4)_2]^{2-}$ Complexes (E = S, O) and Derivatives

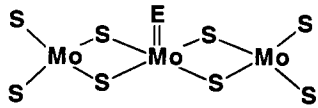

The $[E{=}Mo(MoS_4)_2]^{2-}$ Structural Unit

The pyramidal $[E{=}Mo(MoS_4)_2]^{2-}$ complexes (Tables IX and X) contain as a common structural feature the $(Mo^{IV}{=}S)^{2+}$ unit and are analogous to the $[E{=}Mo(S_4)_2]^{2-}$ complexes with $(MoS_4)^{2-}$ ligands replacing S_4^{2-} ligands. The $[S{=}Mo(MoS_4)_2]^{2-}$ complex and its structure were first reported in 1983 (*80c*). The anion was obtained by heating $(NH_4)_2MoS_4$ in DMF solution. The presence of moisture leads to hydrolysis and formation of the $[O{=}Mo(MoS_4)_2]^{2-}$ complex (*80c*). The synthesis and structure of the S=W analogue of the same compound had been reported earlier (*44*). The syntheses of $\{[(O{=}Mo(MoS_4)(Mo(O)(S)_2(S_2)\}^{2-}$ (*95a,b*) and $\{[(O{=}Mo(MoOS_3)(Mo(O)(S)_2(S_2)\}^{2-}$ (*95a*) have been reported. The former was obtained by stirring

TABLE IX

DISTANCES IN BINARY AND TERTIARY $[E=Mo(MS_4)_2]^{2-}$ COMPLEXES AND SELECT DERIVATIVES[a]

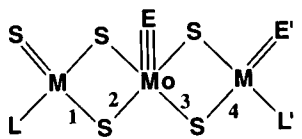

M	E	E′	L	L′	M−Mo (Å)	Mo=E (Å)	M=E′ (Å)	M=S (Å)	Mo−S_b (1) (Å)	Mo−S_b (2) (Å)	Mo−S_b (3) (Å)	Mo−S_b (4) (Å)	Mo−L′ (Å)	Reference
Mo	O	O	S	S_2^{2-}	3.030(1) 2.884(1)[b]	1.668(4)	1.691(4)	2.082(2)	2.231(2)	2.442(2)	2.363(2)	2.276(2)	2.391	*95b*
					3.047(1) 2.896(1)	1.654(5)	1.65(1)	2.144(3)	2.238(3)	2.458(2)	2.374(2)	2.287(3)	2.395	*95a*
Mo	S	S	S	S	2.953	2.086(4)	2.148(3)	2.145(4)	2.239	2.408	2.380	2.240	2.136(3)	*80a*
Mo	O	S	S	S	2.983	1.743(9)	2.132(5)	2.143(4)	—	2.411(5)		—	2.136	*80c*
W	O	S	S	S_2^{2-}	3.055(2)	1.64(1)	1.89(1)[c]	2.131	2.215(5)	2.435	2.335	2.275	2.374[d]	*96*
W[e]	O	O	S	S_2^{2-}	3.100(1) 2.899(1)[f]	1.671(8)	1.720(9)	2.139(3)	2.237	2.467	2.365	2.295	2.375	*96*

[a] See footnote *a*, Table I. Bold numbers in parentheses refer to numbers in the structure at the top of the table.

[b] Bound to the Mo coordinated by the S_2^{2-} ligand.

[c] The rather short distance and the high temperature factor of the E′ atom suggest that the site is partially occupied by oxygen and sulfur atoms.

[d] The M=L bond length is 2.140(5) Å.

[e] In this complex the metal bound to E′ is Mo.

[f] Mo–Mo distance.

TABLE X

CHARACTERISTIC ELECTRONIC AND INFRARED ABSORPTION SPECTROSCOPIC DATA OF BINARY AND TERTIARY $[E=Mo(MS_4)_2]^{2-}$ COMPLEXES AND SELECT DERIVATIVES

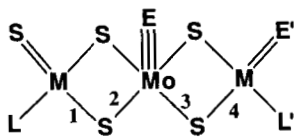

M	E	E′	L	L′	Infrared absorption (cm^{-1})	λ_{max} (nm; $\varepsilon \times 10^{-3}$)	Reference
Mo	O	O	S	S_2^{2-}	Mo=O, 962, 943, 910(sh), 905; Mo=S, 527(m), 508(s); Mo–S, 480(m)[a]	272(19.6); 320(sh, 11.6); 376(10.2); 442(8.8); 480(sh, 5.64)[b]	*95a*
					Mo=O, 963, 943; Mo=S, 516(m), 501(s), 425[a]	230(41.0); 270(18.3); 287(17.1); 315(15.4); 378(8.2); 442(12.8)[b]	*95b*
					Mo=O, 958, 943; Mo=S, 520(m), 500(s); Mo–S, 478(m)[a]	268; 282(sh); 312; 436; 480(sh)[b]	*105a*
Mo	S	S	S	S	Mo=S, 509(m), 489(m), 471(w), 453(sh, vw)[a]	311(26.4); 340(sh); 373(sh); 465(18.0)[b]	*80c*
					W=S,[c] 517(m), 500(s), 492(s), 479(s), 465(m), 434(w)[a]	241(37.7); 271(28.6); 285(sh); 325(sh); 392(21.7)[b,c]	
W[c]	O	O	S	S_2^{2-}	Mo=S, 509(m), 489(m), 471(w), 453(sh, vw)[a]	272(19.6); 320(sh, 11.6); 376(10.2); 442(8.8); 480(sh, 5.64)[b]	*96*

[a] In KBr disk.

[b] In CH_3CN solution.

[c] Data for the W derivative $W_3S_9^{2-}$.

$[Mo(O)_2(S)_2)]^{2-}$ in methanol at low temperatures (*95b*), acidifying solutions of $[Mo(O)(S)_3)]^{2-}$ (*95b*), or by the reaction of polyoxymolybdates with hexamethyldisilylthiane (*95a*). These two anions share the same lattice and in the crystal structure (*95a*) both molecules occupy the same site with approximately equal weight. The stepwise syntheses of linear trimetallic complexes of the type $[(S_2)(Mo_2O_2S_2)(MS_4)]^{2-}$ or $[(DMF)_3(Mo_2O_2S_2)(MS_4)]^{2-}$ are possible by reactions of the $[(DMF)_3(Mo_2O_2S_2)(DMF)_3]^{2+}$ cation or $[(S_2)(Mo_2O_2S_2)(DMF)_3]^{2+}$ with $(MS_4)^{2-}$ tetrathiometallate ligands (*96*, *105*). Further reaction of the $[(DMF)_3(Mo_2O_2S_2)(MS_4)]^{2-}$ complexes with the $(MS_4)^{2-}$ ligands affords the $\{[(O{=}Mo(MS_4)(Mo(S)_3(S_2)\}^{2-}$ complexes (*96*) rather than resulting in the anticipated $[(MS_4)(Mo_2O_2S_2)(MS_4)]^{2-}$ tetranuclear species, analogous to the known $[(WS_4)(W_2S_4)(WS_4)]^{2-}$ complex (*80a,b*). Apparently, the first step in these reactions is the formation of the linear tetranuclear complexes that dissociate to reactive dimeric $[(MS_4)(MoO)(S)]^-$ species. The structural data (Table IX) for this class of complexes consistently show long inner Mo–μ-S bonds by comparison to the shorter, outer, Mo–μ-S bonds. The data are suggestive of a central $E{=}Mo^{IV}$ unit bound by two Mo^{VI} thiomolybdate chelates to give a molecule with localized electronic structure and a Mo valence sequence of VI–IV–VI. There appears to be a tendency for delocalization to a VI–V–V system in situations wherein sulfur has been added to the terminal Mo^{VI} thioanions, as in the $\{[(O{=}Mo(MoS_4)(Mo(O)(S)_2(S_2)\}^{2-}$ and $\{[(O{=}Mo(MoOS_3)(Mo(O)(S)_2(S_2)\}^{2-}$ complexes (*95*, *96*).

E. The $[Mo_3S(S_2)_3]^{4+}$ Core and Derivatives

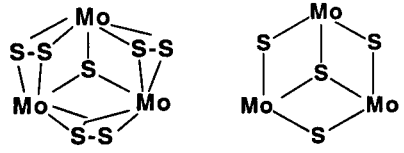

The $[Mo_3S(S_2)_3]^{4+}$ and $[Mo_3S(S)_3]^{4+}$ units

This class of clusters has been reviewed extensively by Shibahara (*13*) and consequently only a brief overview, designed to underscore the diversity in structure and reactivity, will be presented herein. The trinuclear $[(S_2)_3Mo_3S(S_2)_3]^{2-}$ complex anion (Fig. 9) contains three terminal S_2^{2-} ligands attached symmetrically to three Mo^{IV} ions triply bridged by a central μ_3-S^{2-} central ligand. This very interesting molecule, which has been proposed (*23k*) as a model for crystalline MoS_2,

is synthesized as an NH_4^+ salt hydrate in 26% yield by the reaction of $(NH_4)_6Mo_7O_{24}$ with $(NH_4)_2S_x$ (*23f*). The same reaction also produces $(NH_4)_2[(S_2)_2Mo(\mu\text{-}S_2)]_2$ in 40% yield.

The S_2^{2-} ligands in $[Mo_3S_{13}]^{2-}$ undergo sulfur abstraction by CN^- to give the $[Mo_3S_4]^{4+}$ core that can be isolated as the $[Mo_3S_4(CN)_9]^{5-}$ complex (*23h*, *122*, *123*) [Eq. (1)].

$$[Mo_3S_{13}]^{2-} + 12CN^- \rightarrow [Mo_3S_4(CN)_9]^{5-} + 3SCN^- + 3S_2^{2-} \quad (1)$$

A similar sulfur abstraction reaction from the core of $[Mo_3S_{13}]^{2-}$ has been reported [Eq. (2)].

$$[Mo_3S_{13}]^{2-} + 3edt^{2-} \rightarrow [Mo_3S_4(Edt)_3]^{2-} + S_x^{2-} \quad (2)$$

It is suggested (*124*) that in this reaction the RS^- ligand abstracts a sulfur atom from the coordinated S_2^{2-} ligand [Eq. (3)].

$$RS^- + S_2^{2-} \rightarrow RSS^- + S^{2-} \quad (3)$$

Electrochemical reduction of complexes that contain the $[Mo_3S(S_2)_3]^{4+}$ core in aqueous media have been reported and show that the reduction is not involving the Mo^{IV} ions. In the same study the synthesis of $[(L)_3Mo_3S(S)_3)^n$ complexes is reported (*125*). One of these complexes has been characterized structurally (L = 2-mercaptobenzoate dianion, $n = -2$). On reaction with excess HNTA the $[Mo_3S_{13}]^{2-}$ anion affords the $[Mo_3S_4(HNTA)_2(NTA)]^{3-}$ complex (*126a*). The structure of this complex has been determined. The Mo_3S_4 core also has been obtained by degradation of the $[Mo_4S_4]^{6+}$ core in $[Mo_4S_4(NCS)_{12}]^{6-}$ by a reaction with triazacyclononane, or [9]aneN$_3$, that gives (*126b*) $[Mo_3S_4([9]aneN_3)_3]^{4+}$. Another synthesis of a cluster that contains the Mo_3S_4 core involves coupling of $[(Cys)(Mo_2O_2S_2)(Cys)]^{2-}$ dimers that, through a Mo_4S_4-containing intermediate, proceed to afford the $Mo_3S_4^{4+}$ core (*127*).

In a series of very interesting papers Shibahara and co-workers reported on the reactions of the $[Mo_3S_4(H_2O)_9]^{4+}$ ion (*129–137*) with metals under acidic conditions. Heterometallic clusters that contain the Mo_3MS_4 cubane units were obtained with Fe (*131*, *132*), Co (*133*), Ni (*134*), Cu (*135*), Hg (*133*), Sn and Sn^{2+} ion (*136*), and In (*137*).

The mixed chalcogenido $Mo_3O_2S_2]^{4+}$, $[Mo_3O_3S]^{4+}$, and $[Mo_3OS_3]^{4+}$ cores also exist (*130*) in molecules such as $[Mo_3O_2S_2(NCS)_9]^{5-}$ (*138–140*), $[Mo_3O_3S(HNTA)_3]^{2-}$ (*141*), and $[Mo_3OS_3(Dtp)_4(CH_3CN)]$ (*142*).

The syntheses of the aqua ions of these clusters have been described in detail (*130*).

The reactivity of the $[Mo_3E_nS_{4-n}]$ core is under study and the $[(H_2O)_9Mo_3ES_3]^{4+}$ clusters have been reported to react with acetylene to give the $[(H_2O)_9Mo_3(\mu_2\text{-}E)(\mu\text{-}S)(\mu_3\text{-}S_2C_2H_2)]^{4+}$ complexes. The structure of one of these compounds (E = 0) has been determined (*143*). Complexes with mixed metal cores such as $[(H_2O)_9Mo_xW_{3-x}S_4]^{4+}$ have been reported (*144*) (x = 1, 2) (also $[(HNTA)_3Mo_xW_{3-x}S_4]^{2-}$). The $[Mo_3S_4(Cl)_3(Dmpe)_3]^+$ species has been synthesized and structurally characterized (*145*). The procedure employed in this synthesis gave the cluster directly by a reaction of $MoCl_3(THF)_3$ with NaSH in THF followed by addition of Dmpe.

New clusters with the Mo_3S_4 core and Et_3P, $Et_2HP{=}O$, and halide ligands have been synthesized (*146*) using the polymeric trimers $Mo_3S_7X_y$ (*147*). These compounds are considered excellent starting materials for the synthesis of complexes that contain the Mo_3S_4 core.

The synthesis (*128*, *148*) and characterization of the $[Mo_4S_4(H_2O)_{12}]^{4+}$ cubane has been described. The $[Mo_4S_4(CN)_{12}]^{8-}$ cluster contains the $[Mo_4S_4]^{4+}$ unit (*149*). The same unit in oxidized forms is found in $[Mo_4S_4(^iPr\text{-}Cp)_4]^{+,2+}$ (*150*) and also in $[Mo_4S_4(NO)_4(CN)_8]^{8-}$ (*151*). The synthesis (*152*) and solution chemistry (*153*) of the oxidized $[Mo_4S_4(H_2O)_{12}]^{5+}$ cluster have been reported. The structure of $Cs_3[Mo_4S_4(EDTA)_2]\cdot 28H_2O$ containing the oxidized $[Mo_4S_4]^{5+}$ (*154*) core and the structure of the $[Mo_4S_4]^{6+}$ core (*155*) have been determined.

IV. Reactions of Oxo/thiometallates. Functional Group Chemistry

A. Bonding and Characteristic Reactivity of the Mo–S_x Groups

In the rich chemistry of the $Mo(S)(S_x)$ and $Mo(O)(S_x)$ "functional groups" (Fig. 3; x = 1, 2, and 4), the nucleophilic character of the S_x^{2-} ligands plays an important role in reactions toward alkynes, heteroallenes, and SO_2. In tetrahedral Mo, thio and oxothio anions in the presence of a Mo=E "spectator" group (*vide infra*), adjacent to the site of attack by an electrophile, greatly facilitate electrophilic addition reactions. This applies not only to the $(L)_2Mo(E)_2$ units but also to the $(L)_2Mo(E)(S_2)$ complexes. In the latter the span of the S_2^{2-} ligand at ~2.0 Å is too small to accommodate two coordination sites, and the coordination geometry of the $(L)_2Mo(E)(S_2)$ unit can be described as pseudotetrahedral, with the centroid of the S_2^{2-} ligand occupying one

coordination site. In situations wherein both a Mo=O and a Mo–S_x ligand (x = 1, 2) are bound to the same tetrahedrally coordinated Mo atom, the Mo=O group serves as a spectator, and the site of reactivity without exception is the "softer" Mo–S_x chromophore. Apparently the strength of the Mo=O bond precludes the reactivity expected on the basis of the greater polarity of the Mo=O group.

An analysis of the structural and reactivity data available for the various $[(L)(Mo_2^{V}E_2S_2)(L')]^{n-}$ and $[E{=}Mo^{IV}(L)(L')]^{n-}$ thiomolybdate complexes (E = O^{2-} or S^{2-}, L, L' = O^{2-}, S^{2-}, S_2^{2-}, Cp^-, CS_4^{2-}, or S_4^{2-}) reveals trends that can be attributed to distal or proximal electronic effects associated with the axial (E) and equatorial (L, L') ligands. The chemistry of the Mo–η^2-S_4^{2-} group, in most cases, can be attributed to the presence of the Mo–η^2-S_2^{2-} group (*28b*) that emerges as the "activated" S_4^{2-} ligand dissociates S_2. Direct evidence for a Mo–η^2-S_4^{2-}/Mo–η^2-S_2^{2-} equilibrium has been obtained unequivocally by ^1H NMR spectroscopic studies in CH_3CN solutions of $[(Cp)(Mo_2^{V}O_2S_2)(S_2)]^-$ and elemental sulfur (*28b*) (*vide infra*). The activation of the coordinated S_4^{2-} ligand and the subsequent dissociation of S_2 seems to be a consequence of both distal and proximal electronic effects. In the $[(L)(Mo_2^{V}E_2S_2)(L')]^{n-}$ complexes, the π-donor ligands S_4^{2-} and Cp^- on one side of the dimeric complexes can affect the reactivity of the ligands on the opposite side of the $(Mo_2^{V}E_2S_2)^{2+}$ unit. This is illustrated in the ready dissociation of S_2 from the $[(S_4)(Mo_2E_2S_2)(S_4)]^{2-}$ and $[(S_4)(Mo_2E_2S_2)(Cp)]^-$ complexes (*28b*). Similarly, dissociation of CS_2 readily occurs in analogous complexes where the S_4^{2-} ligands have been replaced by CS_4^{2-} (*28a*) (*vide infra*). In contrast, no dissociation of S_2 is observed in solutions of the $[(S_4)(Mo_2E_2S_2)(S_2)]^{2-}$ complexes, where the η^2-S_2^{2-} ligand, a weaker π donor, is not affecting the distant S_4^{2-} ligand. The propagation of electronic effects across the length of these molecules could be rationalized in terms of extensive delocalization of electron density within the "out-of-plane" π system that involves the d_{xz} and d_{yz} orbitals on the Mo^{V} atoms and "out-of-plane" p orbitals on the sulfur ligands. As a consequence of these effects, conversion of an η^2-S_2^{2-} ligand in the $[(S_2)(Mo_2E_2S_2)(S_4)]^{2-}$ complexes to a dithiolene, vinyl disulfide, or CS_4^{2-} promotes the dissociation of S_2 from the distant η^2-S_4 ligand, with generation of another η^2-S_2^{2-} ligand that further reacts with electrophilic reagents.

Proximal effects also are important in activation of the coordinated η^2-S_4^{2-} and η^2-CS_4^{2-} ligands in the $[(L)(Mo_2E_2S_2)(L)]^{2-}$ complexes (L = CS_4^{2-}, S_4^{2-}). In general, η^2-S_4^{2-} ligands proximal to oxo-axial ligands do not dissociate S_2 readily and are less reactive than those

proximal to sulfido-axial ligands. The *p* orbitals of the axial E groups (E = O, S) overlap and form two π bonds with the Mo d_{xz} and d_{yz} orbitals, which also have the proper symmetry to *p* bond with the *3p* orbitals of the S donor atoms in equatorial L, L′ ligands. The strongly electron-withdrawing oxo group apparently is more effective than a terminal sulfido group in weakening the Mo–S (out of plane) π bonding and indirectly strengthens the $p\pi$–$p\pi$ interactions in the S/S bonds directly adjacent to the Mo–S bonds. Crystallographic data, available for the $[E{=}Mo(S_4)_2]^{2-}$ complexes, support the previous arguments regarding the effects of neighboring axial ligands (*vide infra*). The effects of $d\pi$–$p\pi$ Mo–S bonding in the $p\pi$–$p\pi$ interactions within the S–S bonds are evident in the S–S bond lengths of the Mo-coordinated S_4^{2-} ligands. A significant elongation of the S–S bonds directly adjacent to the Mo atom correlates directly with a shortening of the corresponding Mo–S bonds (Table XI) and suggests that bonding electrons from the S–S bond are transferred to Mo–S bonding orbitals.

TABLE XI

M–S AND S–S DISTANCES OF MO-COORDINATED S_4^{2-} LIGANDS

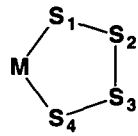

Compound[a]	S(1)–S(2) (Å)	S(2)–S(3) (Å)	S(3)–S(4) (Å)	M–S(1) (Å)	M–S(4) (Å)	Reference
$[Zn(S_4)_2]^{2-}$	2.045(4)	2.044(5)	2.062(5)	2.376(3)	2.331(3)	98
	2.034(5)	2.032(5)	2.056(5)	2.343(2)	2.354(3)	
$[Ni(S_4)_2]^{2-}$	2.073(2)	2.037(4)	2.073(2)	2.185(2)	2.185(2)	*98, 156*
$(Ph_3P)_2Pt(S_4)$	2.024(8)	2.022(10)	2.081(10)	2.360(6)	2.366(5)	*157*
$[(S_2)(Mo_2S_4)(S_4)]^{2-}$ [b]	2.093(4)	2.018(4)	2.053(3)	2.399(2)	2.427(2)	*24a*
$[(S_2)(Mo_2S_4)(S_4)]^{2-}$ [c]	2.019(5)	1.970(6)	2.115(5)	2.409(2)	2.403(3)	*24b*
$[S{=}Mo(S_4)_2]^{2-}$	2.107(1)	2.012(1)	2.166(1)	2.387(1)	2.331(1)	*24a*
$[O{=}Mo(S_4)_2]^{2-}$	2.120(3)	2.008(3)	2.159(3)	2.395(2)	2.363(2)	*24a*
$[(\eta^5\text{-Cp})_2Mo(S_4)]$	2.081(8)	2.018(9)	2.085(7)	—	—	*158*
$[(\eta^5\text{-Cp})_2W(S_4)]$	2.105(7)	2.016(8)	2.116(9)	—	—	*159*
$[(\eta^5\text{-Cp})Mo(S_4)_2]^-$	2.141(2)[d]	2.031(2)	2.061(2)	2.305(2)	2.446(2)	*116a*
	2.124(2)	2.022(2)	2.073(2)	2.336(2)	2.430(2)	

[a] The $[Zn(S_4)_2]^{2-}$ anion contains two crystallographically independent S_4^{2-} ligands.
[b] Ph_4P^+ salt; data for the S_4^{2-} ligand not subject to disorder.
[c] Ph_4As^+ salt; data for the S_4^{2-} major component in a disordered structure.
[d] The complex contains two crystallographically independent S_4^{2-} ligands.

The alternation of S–S bonds is not observed in the S_4^{2-} ligands of the tetrahedral $[Zn(S_4)_2]^{2-}$ complex that contains the d^{10} Zn^{II} ion. The transfer of bonding S–S electrons to Mo–S bonding orbitals also is apparent in the structural features of the Mo–CS_4 complexes (Table XII). Here again the Mo–S bond directly adjacent to the lengthened S–S bond of the CS_4^{2-} ligand always is shorter than the Mo–S bond with the thiolate sulfur of the ligand. Such differences in M–S bonding are not observed in the structure of the $[Ni(CS_4)_2]^{2-}$ complex (*98*).

Based on the previous discussion and the nature of the Mo–η^2-S_4 chromophore, the reactions of the thio- and oxo/thiometallates mainly involve the Mo=S and Mo–S_2 groups and include (Figs. 20 and 21) sulfur addition reactions, sulfur abstraction reactions, addition of electrophilic molecules such as CS_2 and DMA, Mo=S dimerization reactions, and abstraction of S^{2-} by thiophilic metal ions.

The addition of sulfur to terminal sulfido ligands very likely is the end result of electrophilic attack on the Mo^{n+}=S (n = 4, 5, 6) sulfur by the $S^+(S)_xS^-$ products of heterolytically cleaved S_8 molecules, and accounts for the synthesis of the $[E{=}Mo^{IV}(S_4)_2]^{2-}$ anions (*24a*) (E = S, O) and various members of the $[(S_x)(Mo_2^{V}S_4)(S_y)]^{2-}$ (*82*), $[(S_x)(Mo_2^{V}O_2S_2)(S_y)]^{2-}$ (*104*, *106*), and $[(S_x)(Mo_2^{V}OS_3)(S_y)]^{2-}$ (*73*) series (Figs. 11, 13, and 14).

In the $[(S_4)(Mo_2E_2S_2)(S_2)]^{2-}$ complexes, the easily polarizable η^2-S_2^{2-} ligands also react readily with nucleophiles such as trialkyl or triaryl phosphines and are more reactive than the η^2-S_4^{2-} ligands. The abstraction of S with Ph_3P, from the $(S_2)Mo{=}S$ and $(S_2)Mo{=}O$ units

TABLE XII

M–S AND S–S DISTANCES OF M-COORDINATED $(CS_4)^{2-}$ LIGANDS

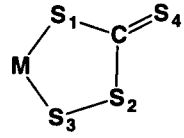

Compound	S(2)–S(3) (Å)	S(1)–C (Å)	S(2)–C (Å)	M–S(1) (Å)	M–S(3) (Å)	Reference
$[Ni(CS_4)_2]^{2-}$	2.064(2)	1.707(4)	1.711(5)	2.174(2)	2.165(2)	*98*
$[S{=}Mo(CS_4)_2]^{2-}$	2.102(5)	1.735(12)	1.719(12)	2.386(3)	2.320(3)	*160, 161*
(trans)[a]	2.100(5)	1.739(12)	1.709(12)	2.380(3)	2.333(3)	
$[S{=}Mo(CS_4)_2]^{2-}$	2.105(4)	1.756(10)	1.726(11)	2.376(3)	2.320(3)	*161*

[a] Contains two symmetry-independent $(CS_4)^{2-}$ ligands.

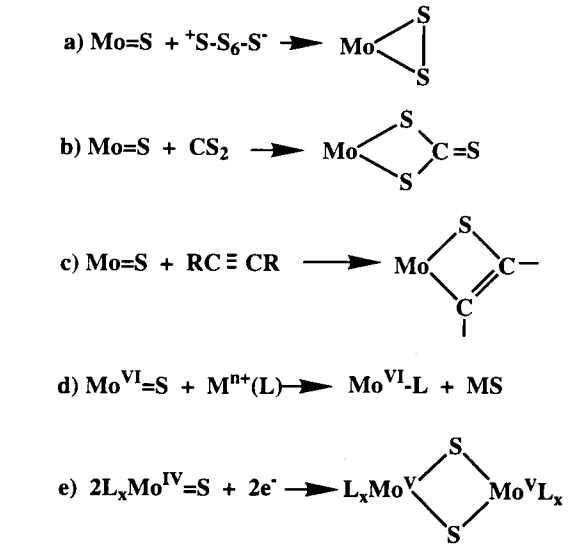

FIG. 20. Reactions of the Mo=S chromophore.

in these complexes, occurs at ambient temperature and results in the formation of the $[(E{=}Mo(S_4)(MoS_3E)]^{2-}$ complexes (*82*, *103*). The η^2-S_4^{2-} ligands do not react further with Ph_3P unless heated to 80°C for extended periods of time. With transition metal ions, the thiomolyb-

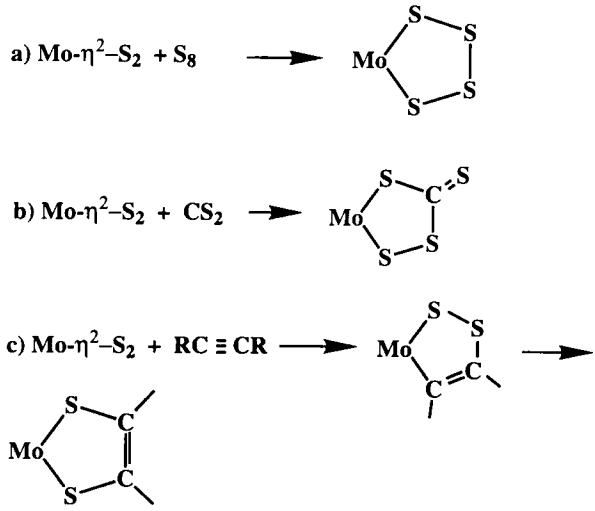

FIG. 21. Reactions of the Mo—η^2-S_2 chromophore.

denyl groups can serve either as electron pair donors or as a source of sulfide ions for the eventual formation of highly insoluble, thermodynamically stable, transition metal sulfides. The former course of reactivity is represented in the multitude of heterometallic complexes wherein the $(MoS_4)^{2-}$ anion serves as a ligand for transition metal ions (*52–54*). The irreversible removal of sulfide ions from Mo=S units by the formation of insoluble transition metal sulfides allows for the introduction of nonsulfur terminal ligands in the thiomolybdate ions by metathetical reactions. An example of this reaction is available in the synthesis of the $\{[O{=}Mo^{VI}(S_2)_2]_2X\}^-$ anions from the reaction of NiX_2 (X = Cl, I) with an isomeric form of the $\{[(\eta^2\text{-}S_2)_2Mo(O)]_2(\mu\text{-}S)\}^{2-}$ anion (*83*, *106*).

B. The Spectator Group Effect

The industrially important olefin metathesis reaction is a reaction that involves the simultaneous cleavage of two olefin double bonds followed by the formation of the alternate double bonds [Eq. (4)]:

$$C{=}C + C^*{=}{}^*C \rightarrow 2{}^*C{=}C. \tag{4}$$

At present it is accepted that the catalyst is a metal alkylidene complex that reacts with an olefin to form a metallacyclobutane intermediate (Fig. 22) that decomposes to give the product olefin (*162*). The metal alkylidene complex is formed from the $Mo(O)_2Cl_2$ catalyst and olefin with elimination of an organic carbonyl compound. In these reactions the Mo=O and $Mo{=}CH_2$ groups are proposed to be activated by the Mo=O spectator groups and as a result readily add an olefin. These additions result in a change in the coordination geometry of the Mo atoms from four-coordinate tetrahedral to five-coordinate square pyramidal. Associated with this change is a large negative free energy that is attributed mainly to the transformation of the bond order of the Mo=O spectator group from double to triple (*162*) (Fig. 22).

C. Addition of Electrophiles to the Mo–S_x Groups

1. Addition of CS_2; Trithio- and Perthiocarbonate Complexes

The generation of the perthiocarbonate anion, $(CS_4)^{2-}$, generally is accomplished by the addition of a polysulfide or disulfide dianion to CS_2. The associated counterions include Na^+, K^+, Cs^+, Sn^{2+}, and NH_4^+ (*15*). The $[M(CS_4)_2]^{2-}$ complexes can be generated in the

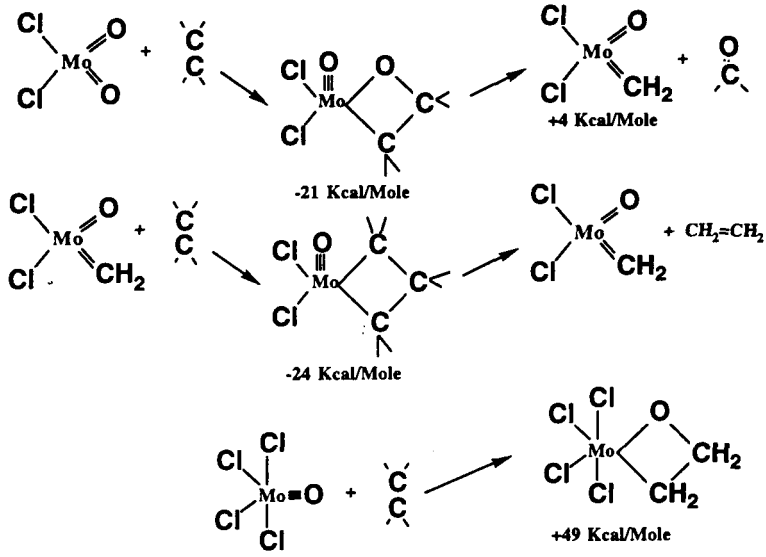

FIG. 22. A minimal mechanism for the olefin metathesis reaction (Data from Ref. *162a*).

$[M(CS_3)_2]^{2-}$ complexes (M = Ni, Pt) by either I_2 oxidation or sulfur addition reactions (*16*).

Addition of CS_2 to DMF solutions of $[Ph_4P]_2[S{=}Mo(\eta^2\text{-}S_4)_2]$ and $[Ph_4P]_2[(S_4)Mo_2S_4)(S_2)]^{2-}$ results in the formation of perthiocarbonate derivative complexes (*160*) (Fig. 23; Table XIII). The illustrated pathways are based on CS_2 addition mechanisms involving the Mo–η^2-S_2 units. It should be noted that addition to the Mo=S unit, followed by intramolecular S transfer, also is a possible pathway to $(CS_4)^{2-}$. Both cis and trans isomers of the $[S{=}Mo(\eta^2\text{-}CS_4)_2]^{2-}$ anion have been isolated (*161*). The $[O{=}Mo^{IV}(S_4)_2]^{2-}$ complex is unreactive toward CS_2 unless activated by Ph_3P (*73b*).

Presumably, Ph_3P "activation" involves the generation of reactive η^2-S_2 or Mo=S units from the Mo-coordinated η^2-S_4 ligands. These observations also suggest that the lack of reactivity of the $[O{=}Mo^{IV}(S_4)_2]^{2-}$ complex toward CS_2 is due either to the absence of a reactive Mo=S functional group or to the inability of the Mo–η^2-S_4 unit in $[O{=}Mo^{IV}(S_4)_2]^{2-}$ to dissociate S_2 and generate the reactive Mo–η^2-S_2 group.

The $[(CS_4)(Mo_2S_4)(CS_4)]^{2-}$ complex reversibly loses CS_2 to give the known $[(S_2)(Mo_2S_4)(S_2)]^{2-}$ complex (*35*, *79*). The $(CS_4)^{2-}$ ligands in both isomers of $[S{=}Mo(\eta^2\text{-}CS_4)_2]^{2-}$ (Fig. 23, structures 3A and 3B) also readily lose CS_2. One of these products has been spectroscopically

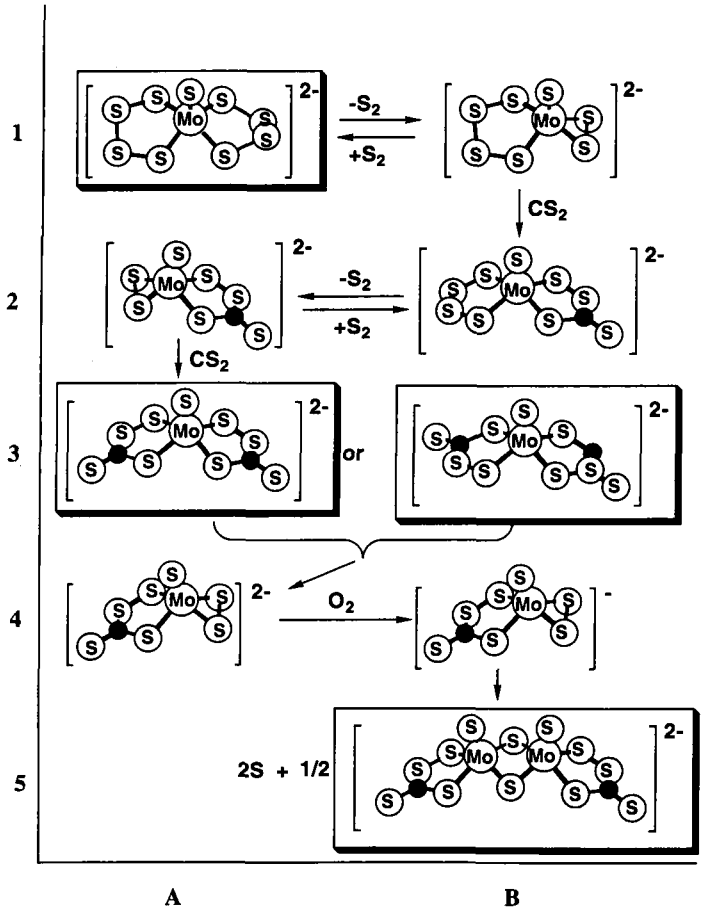

FIG. 23. Synthesis of Mo–thiocarbonate complexes.

examined and postulated to be the $[S{=}Mo(S_2)(CS_4)]^{2-}$ complex (Fig. 23, structure 4A) (*160b*). The formation of $[(CS_4)(Mo_2S_4)(CS_4)]^{2-}$ (Fig. 23, structure 5B) from $[S{=}Mo(\eta^2\text{-}CS_4)_2]^{2-}$ may be due to a solvent-assisted self-coupling reaction of the postulated $[S{=}Mo(S_2)(CS_4)]^{2-}$ intermediate followed by reductive S–S bond cleavage. The $[(\eta^2\text{-}CS_3)(Mo_2S_4)(\eta^2\text{-}CS_3)]^{2-}$ complex has been obtained by the reaction of CS_2 with $(Mo_2S_6)^{2-}$ or the reaction of Ph_3P with the $[(CS_4)(Mo_2S_4)(CS_4)]^{2-}$ anion (*161*). The same anion also can be obtained from $(MoS_4)^{2-}$ (*vide infra*).

The lack of reactivity of the remaining free Mo=S groups in the $(CS_3)^{2-}$ and $(CS_4)^{2-}$ complexes may be due to the stability of the Mo–S

TABLE XIII

CHARACTERISTIC ELECTRONIC AND INFRARED ABSORPTION SPECTROSCOPIC DATA OF BINARY AND TERTIARY $[(L)(Mo_2E_2(L')]^{2-}$ COMPLEXES[a]

Compound	Infrared absorption (cm^{-1})	λ_{max}
$[CS_4)(Mo_2S_4)(CS_4)]^{2-}$	C=S, 982; Mo–S_b, 464(2)[b]	314(sh); 365; 470(sh); 610(sh)[c]
$[CS_3)(Mo_2S_4)(CS_3)]^{2-}$	C=S, 1052; Mo–S_b, 460(w)[b]	344, 444(sh)[c]
$[CS_3)(Mo_2O_2S_2)(CS_4)]^{2-}$	C=S, 1054; Mo=O, 950(s), 982 (m); Mo–S_b, 460(w)[b]	374(sh); 460[c]
$[CS_3)(Mo_2O_2S_2)(S_4)]^{2-}$	C=S, 1058; Mo=O, 949(vs); Mo–S_b, 468(m)[b]	258(sh); 310(sh)[c]
$[CS_3)(Mo_2S_4)(S_2)]^{2-}$	C=S, 1051; Mo=O, 952(s); Mo–S_b, 479(2)[b]	330(sh); 380(sh), 460[c]
$[CS_3)(Mo_2O_2S_2)(CS_3)]^{2-}$	C=S, 1046; Mo=O, 947(s), 934; Mo–S_b, 470(w)[b]	450[c]

[a] E = S, O; L, L′ = $(CS_4)^{2-}$ or $(CS_3)^{2-}$, S_x^{2-}. Data from Ref. *161*.
[b] In KBr disk.
[c] In DMF.

triple bond in the stable $(CS_4)^{2-}$ and $(CS_3)^{2-}$ five-coordinate Mo^V complexes and/or the weak electrophilic character of CS_2. The reactions of $(MoS_4)^{2-}$ with CS_2 afford the $[(CS_3)(Mo_2S_4)(CS_3)]^{2-}$ complex, which has been structurally characterized (Table I). A pathway that leads to this compound has been suggested (*73b*) (Fig. 24). The same molecule has been obtained by addition of CS_2 to the $[(S)(Mo_2O_2S_2)(S)]^{2-}$ anion (*113*) (Table III).

The addition of CS_2 to the Mo=S and the (Mo–η^2-S_4-derived) Mo–η^2-S_2 functional groups (*28b*) in $[(S)(Mo_2O_2S_2)(S_4)]^{2-}$ [Eqs. (5–7)] also has been described and very likely is influenced by the spectator group effect (*162*).

$$[(S)(Mo_2O_2S_2)(S_4)]^{2-} + CS_2 \rightarrow [(CS_3)(Mo_2O_2S_2)(S_4)]^{2-} \quad (5)$$

$$[(CS_3)(Mo_2O_2S_2)(S_4)]^{2-} = [(CS_3)(Mo_2O_2S_2)(S_2)]^{2-} + \tfrac{2}{8}S_8 \quad (6)$$

$$[(CS_3)(Mo_2O_2S_2)(S_2)]^{2-} + CS_2 \rightarrow [(CS_3)(Mo_2O_2S_2)(CS_4)]^{2-} \quad (7)$$

The importance of this effect also is demonstrated by the synthesis of the $[(CS_3)(Mo_2O_2S_2)(S_4)]^{2-}$ complex (*161*) from $[(S)(Mo_2O_2S_2)(S_4)]^{2-}$ and one equivalent of CS_2. The synthesis and structure of the related $[(CS_3)(Mo_2O_2S_2)(S_2)]^{2-}$ complex (Fig. 25, structure 2A) have been reported (*161b*). The preferential reactivity of the four-coordinate

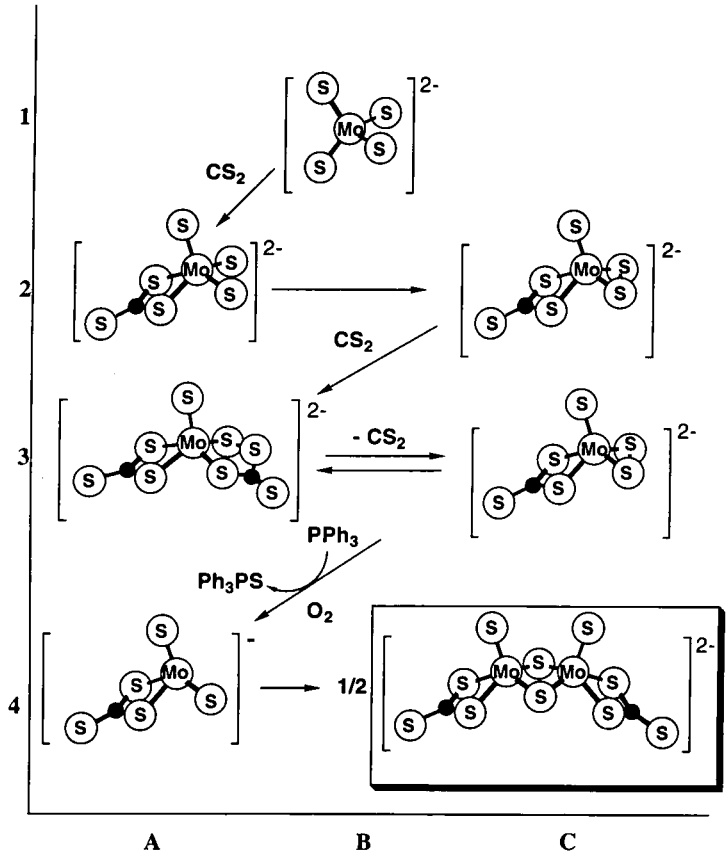

FIG. 24. The reaction of $(MoS_4)^{2-}$ with CS_2.

$(\mu\text{-}S)_2(O)Mo{=}S$ group relative to the five-coordinate $(\mu\text{-}S)_2(O)Mo{-}S_4$ group very likely has its origin in the different bond orders of the Mo=O chromophores in the two groups (Fig. 25).

The structures of various $(CS_4)^{2-}$ and $(CS_3)^{2-}$ complexes have been determined (Tables I and III). The vibrational infrared, ^{13}C NMR, and electronic spectra of the Mo–trithio- and perthiocarbonate complexes have been compiled in Table XIII. The energy of the C=S vibration of the coordinated $(CS_3)^{2-}$ ligands invariably is lower (~980 cm^{-1}) than that of the C=S vibration in the $(CS_4)^{2-}$ complexes (~1050 cm^{-1}) and can be used as a spectroscopic diagnostic criterion for the identification of the ligands with considerable confidence. An additional diagnostic indicator for the $(CS_3)^{2-}$ and $(CS_4)^{2-}$ ligands is the

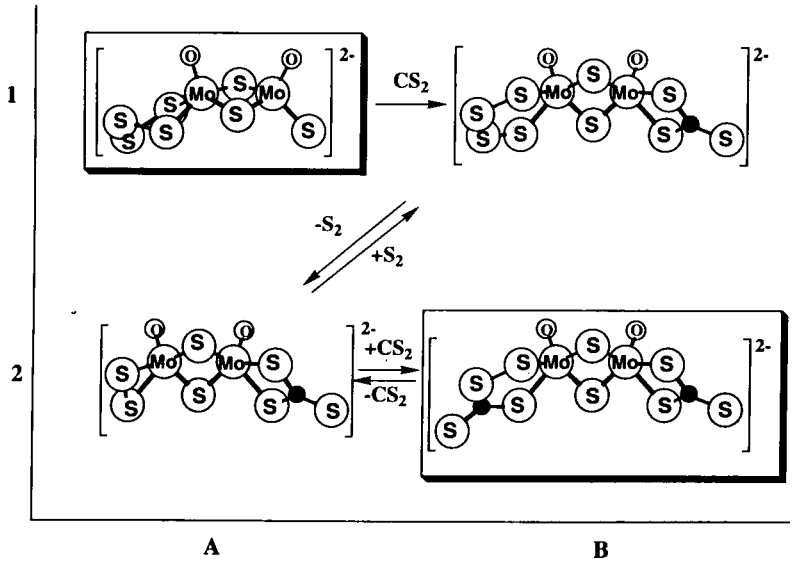

FIG. 25. CS_2 addition to the $[(S_x)(Mo_2O_2S_2)(S_y)]^{2-}$ complexes.

characteristic ^{13}C NMR resonance associated with each of the two ligands. Generally, this resonance is found near 246 ppm for the Mo-coordinated $(CS_4)^{2-}$ ligands and around 253 ppm for the Mo-coordinated $(CS_3)^{2-}$ ligands (*161*).

2. *Reactions of Activated Alkynes with the Mo–η^2-S_4^{2-}, Mo–η^2-S_2^{2-}, Mo=O, and Mo=S Functional Groups; Dithiolene Complexes*

The addition of alkynes to transition metal sulfide complexes is a well-known reaction and examples include the synthesis of $(R\text{-}Cp)_2Ti(DMAD)$ from $(R\text{-}Cp)_2TiS_5$ and DMA (*165a,b*), of $(R\text{-}Cp)V(DMAD)_2$ from $(R\text{-}Cp)_2V_2S_5$ and DMA (*165d*), of $(R\text{-}Cp)_2V_2(S)_2(DMAD)$ from $(R\text{-}Cp)_2V_2S_4$ and DMA (*165d*), of $(R_n\text{-}Cp)_2Mo_2(S_2C_2R_2)_2$ from $(R_n\text{-}Cp)_2Mo_2S_4$ and R_2C_2 (*19a*), of $Fe_2(DMAD)(CO)_6$ from $Fe_2S_2(CO)_6$ and DMA (*165e*), of $[Ni(DMAD)_2]^{2-}$ from $[Ni(S_4)_2]^{2-}$ and DMA (*98*), of $(Et\text{-}Me_4\text{-}Cp)_4Ru_2S_2C_2R_2$ from $(Et\text{-}Me_4\text{-}Cp)_4Ru_2S_4$ and R_2C_2 (*165f*), and of $[Fe(DMAD)_2)_2^{2-}$ from $[Fe_2S_{12}]^{2-}$ (*166*) and DMA (*167*). Reactions of dicarbomethoxy acetylene (DMA) with the binary and tertiary molybdenum sulfides also give dicarbomethoxy dithiolene (DMAD) complexes (Table XIV). A possible mechanism suggested for these reactions (*28a*) involves cycloaddition of the electrophilic alkyne to the coordinated S_x^{2-} chelate ligand. Precedence

TABLE XIV

DISTANCES AND ANGLES IN SELECTED DITHIOLENE Mo COMPLEXES[a]

Compound	Mo=S (Å)	Mo=S (Å)	C–S (Å)	S–Mo–S[b] (°)	S–Mo–S[c] (°)	S–Mo=O (°)	Reference
$[Mo(DMAD)_3^{2-}$	2.393(5)		1.74(2)	80.7(2)	82.9(10)	—	*25*
$[Mo_2(\mu\text{-}S)_2(DMAD)_4]^{2-}$[d]	2.383[e]		1.732[e]	80.1	84.1	—	*25*
	2.459[f]		1.697[f]				
$[O{=}Mo(DMAD)_2]^{2-}$	2.380(4)	1.686(6)	1.758(9)	83.1	84.8	108.9(5)	*25*
$[O{=}Mo(Bdt)_2]^{2-}$	2.388(2)	1.699(6)	1.767(6)	83.1(1)	85.8(1)	—	*171c*
	2.38(3)	1.665(5)	1.75(1)			107.5(6)	*170c*
$[O{=}Mo^{V}(Bdt)_2]^{-}$	2.377(1)	1.668(3)	1.763(4)	84.4(1)	84.6(1)	—	*171c*
$[O{=}Mo(Ph_3Si\text{-}Bdt)_2]^{2-}$	2.39(2)	1.677(4)	1.763(6)	—	—	108.6(14)	*170c*
$[O{=}Mo^{IV}(Tdt)_2]^{2-}$	2.388(5)	1.700(9)	1.77(1)	—	—	108.2(17)	*170c*
$[O)_2Mo^{VI}(MNT)_2]^{2-}$	2.42[g]	1.69(1)	1.77(1)	—	—	—	*171b*
	2.59[h]	1.73(1)					

[a] See footnote *a*, Table I.
[b] Intraligand.
[c] Interligand.
[d] Mo–Mo distance, 2.938(1) Å.
[e] Distances cis to a bridging sulfide.
[f] Distances trans to a bridging sulfide.
[g] Cis to an oxo ligand.
[h] Trans to an oxo ligand.

for this type of interaction can be found in the reactions of dithiolene complexes (*168*).

In the thiomolybdate complexes both the Mo–η^2-S_x and Mo=S groups are nucleophilic enough to undergo attack by dicarbomethoxy acetylene. When both are present within a molecule the Mo=S serves as the spectator group. This is apparent in the reaction of the $[S{=}Mo(S_4)_2]^{2-}$ anion with DMA (Fig. 26). It is proposed that the chromophores that first undergo nucleophilic attack are the Mo–S_2 groups that emerge as the Mo–η^2-S_4 units dissociate S_2. The vinyl disulfide complexes, $[S{=}Mo(VDS)_2]^{2-}$, that may form initially have not been detected but very likely are the species that undergo a sulfur-catalyzed isomerization reaction to give the corresponding dithiolenes, DMAD. On occasion the vinyl disulfide (VDS) formed by addition of DMA to the Mo–S_2 group can be isolated (*vide infra*). The question still remains whether S_x^{2-} ligands bound to metals other than Mo undergo $S_{x\text{-}2}$ dissociation. If this dissociation indeed takes place then alkyne addition to the M–S_2 unit and VDS formation may also occur with metals other than Mo. The DMA addition to the $(R\text{-}Cp)_2TiS_5$ complex that leads to $(R\text{-}Cp)_2Ti(DMAD)$ is reported to initially give a vinyl disulfide complex that eventually rearranges to the dithiolene (*165a*).

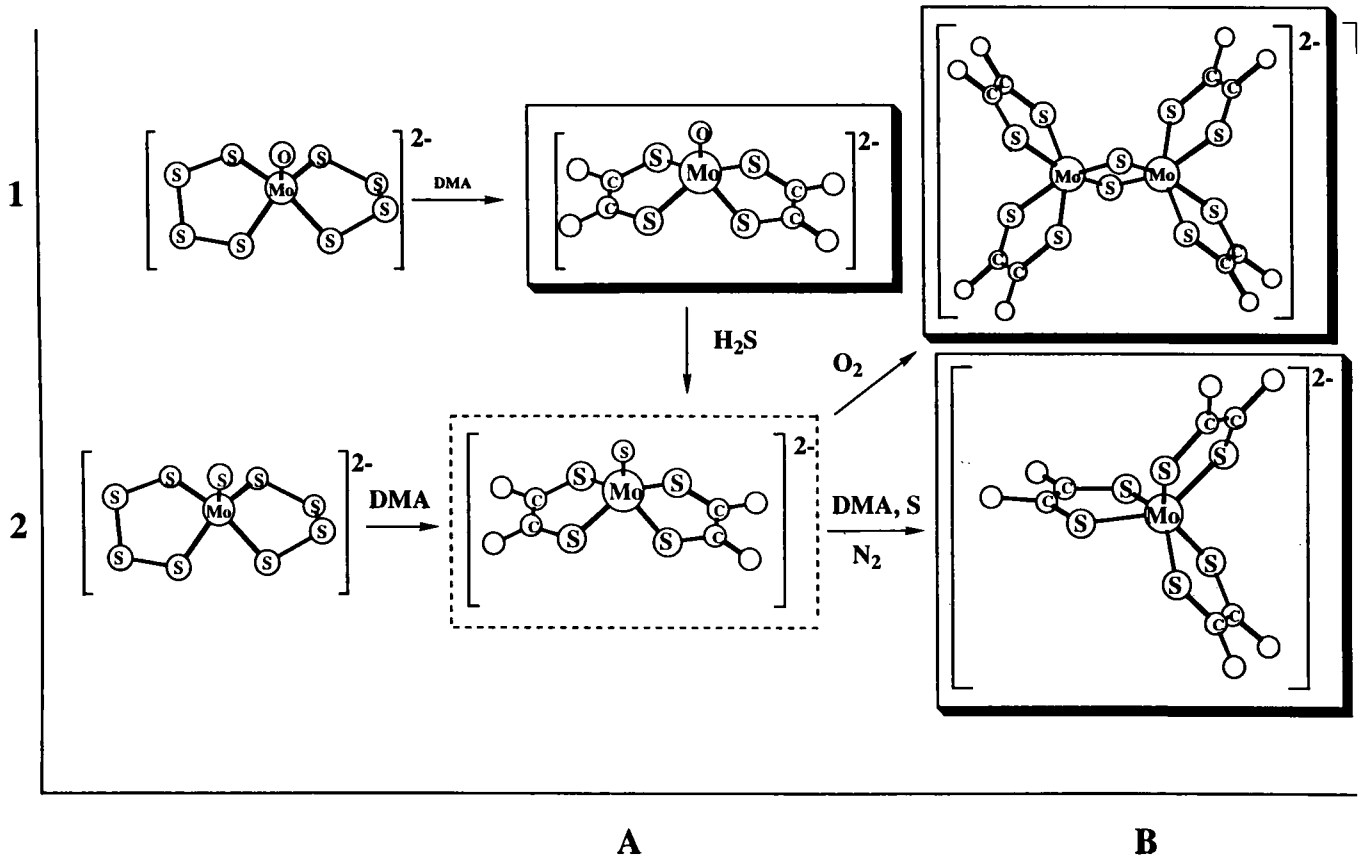

FIG. 26. Reactions of binary Mo/S complexes with DMA.

The reaction of the $[S{=}Mo(S_4)_2]^{2-}$ and $[(S_4)(Mo_2S_4)(S_2)]^{2-}$ complexes with DMA (Fig. 26) proceed until all S_x^{2-} ligands (with the exception of the μ-S^{2-} sulfido ligands) are converted into the DMAD ligands. The type of DMAD complex that forms depends on the synthetic conditions. The $[Mo^{IV}(DMAD)_3]^{2-}$ complex (Fig. 26, structure 2B; Table XIV) is the final product obtained when the reaction of $[S{=}Mo(S_4)_2]^{2-}$ with DMA is carried out under anaerobic conditions. In the presence of oxygen, the same reaction affords the oxidized $[(DMAD)_2Mo^{V}(\mu\text{-}S)_2Mo^{V}(DMAD)_2]^{2-}$ complex (*25*, *28b*) (Fig. 26, structure 1B). The same compound also has been obtained by the reaction of either $[(S_4)(Mo_2S_4)(S_2)]^{2-}$ or $[(S_2)(Mo_2S_4)(S_2)]^{2-}$ with DMA. It has been suggested (*28b*) that the dithiolene ligands form (1) as a result of S addition to the vinyl sulfide ligands initially obtained by addition of DMA to the Mo=S group or (2) by isomerization of the vinyl disulfides that form by addition of DMA to the $Mo{-}S_2$ group.

The reaction of oxo/thiomolybdates with DMA (Fig. 27) occurs exclusively with the $Mo{-}S_x$ group (x = 1, 2). Thus the $[O{=}Mo(S_4)_2]^{2-}$ anion affords the $[O{=}Mo(DMAD)_2]^{2-}$ complex (*25*, *28b*) (Fig. 26, structure 2A). In Fig. 27, the $[(S_2)(Mo_2O_2S_2)(S_2)]^{2-}$ complex, structure 3A, forms the bis-vinyl disulfide complex, $[(VDS)(Mo_2O_2S_2)(VDS)]^{2-}$, structure 3B, which has been characterized structurally (*169*).

Subsequently the isomerization of the vinyl disulfide ligand (in the Cp analogue of this complex) to dithiolene was recognized to occur by a process that was proposed to occur either thermally or via sulfur catalysis (*28b*) (Fig. 28). The $[(DMAD)(Mo_2O_2S_2)(DMAD)]^{2-}$ complex (Fig. 27, structure 2C), rather than $[(VDS)(Mo_2O_2S_2)(VDS)]^{2-}$, is isolated following the reaction of $[(S_2)(Mo_2O_2S_2)(S_4)]^{2-}$ with DMA. In this reaction the solution contains sufficient amounts of dissociated sulfur, which in turn catalyzes the rapid isomerization of the vinyl disulfide ligands that undoubtedly form initially.

The addition of CS_2 and DMA to the $[(L)(Mo_2O_2S_2)(S)]^{2-}$ complexes (L = S_4^{2-}, η^5-Cp; Figs. 29 and 30) demonstrates the exceptional reactivity of the Mo(O)(S) chromophore, which directly and exclusively involves the Mo=S unit activated by the neighboring spectator Mo=O group (*103*). Mechanistic pathways have been proposed, as shown in Fig. 29, for reactions of the $[(S_4)(Mo_2O_2S_2)(S)]^{2-}$ anion (structure 3B) that lead to the $[(CS_3)(Mo_2O_2S_2)(CS_4)]^{2-}$ or the $[(DMAD)(Mo_2O_2S_2)(DMAD)]^{2-}$ anions (structures 2A and 1C). In the absence of electrophiles structure 3B exists in equilibrium with the dimeric form $\{[(S_4)(Mo_2O_2S_2)(S)]_2\}^{4-}$, structure 5B, which has been isolated and characterized structurally as the Et_4N^+ salt (*103*). The lattice energy of the Ph_4P^+ salt of the same compound is sufficiently different to

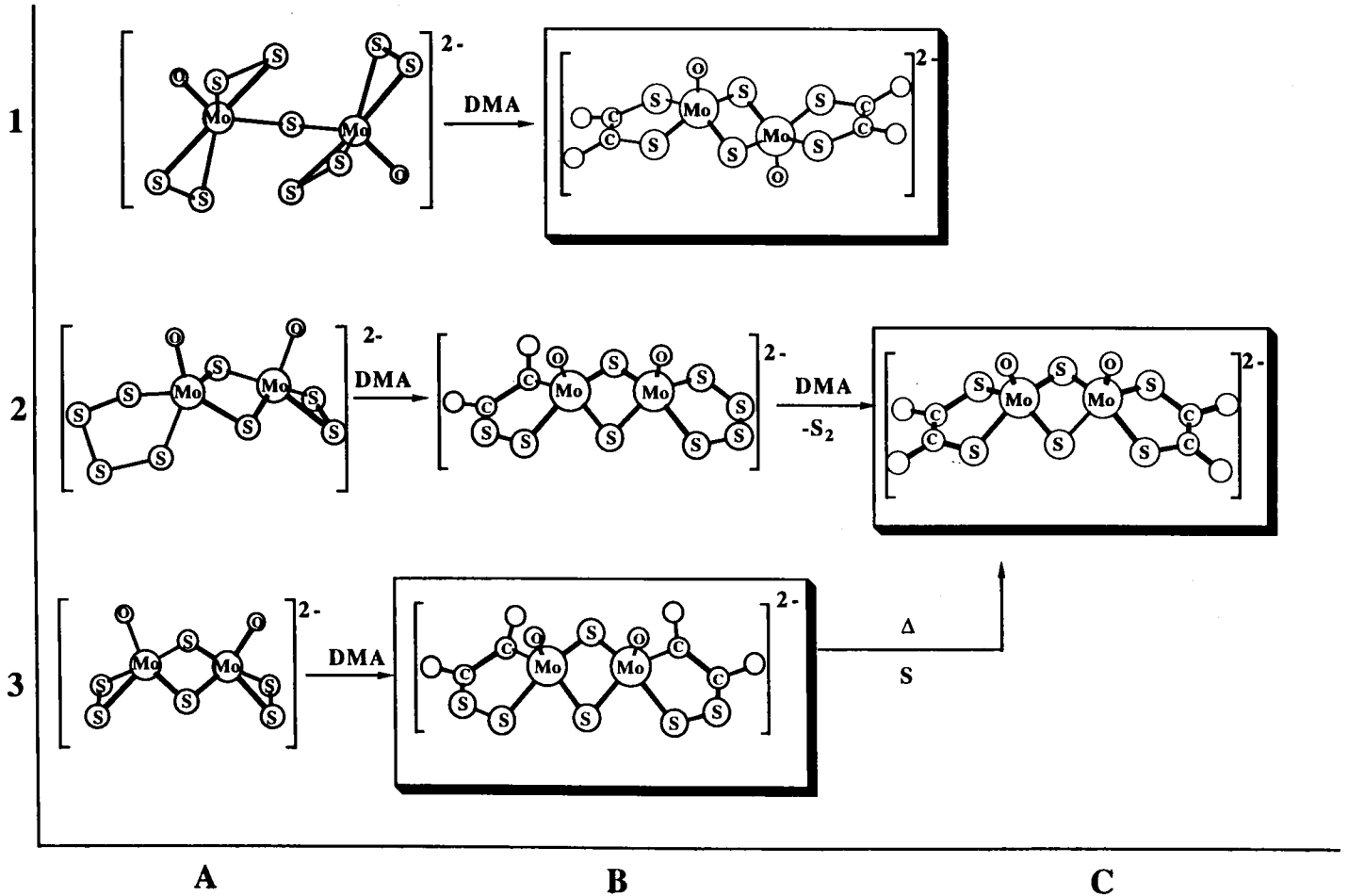

FIG. 27. Reactions of oxo/thiomolybdates with DMA.

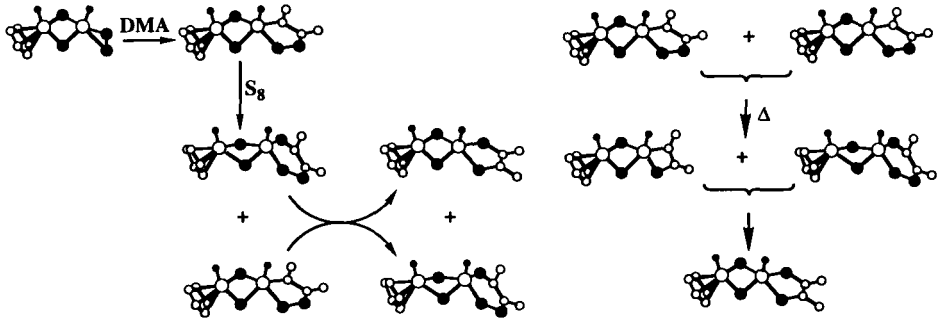

FIG. 28. Proposed mechanism for the sulfur-catalyzed and thermal isomerization of the coordinated vinyl disulfide ligand to 1,2-dithiolene.

stabilize the monomeric form of a compound (structure 3B) that also has been characterized structurally (*103*). The sequence of electrophile additions to structure 3B suggests a reactivity order: Mo=S > Mo–S_2 > Mo–S_4. Similar reactivity patterns have been reported for the $[(\eta^5\text{-Cp})(Mo_2O_2S_2)(S)]^-$ complex (Fig. 30). In the latter, addition of electrophiles such as CS_2 or DMA to the Mo–S_2 group leads to $(CS_4)^{2-}$ and $(VDS)^{2-}$ ligands, which eventually isomerize to dithiolenes. Proposed mechanisms for the thermally and sulfur-catalyzed isomerization reactions have been advanced (Fig. 28) on the basis of NMR data that show ^1H resonances assigned to vinyl sulfide, vinyl disulfide, and dithiolene complexes.

The sulfur-rich dithiolene persulfide ligand SDMAD in the structurally characterized $[(\eta^5\text{-Cp})_2Mo(SDMAD)]$ complex is obtained (*169b*) by the reaction of $(\eta^5\text{-Cp})_2MoS_4$ with DMA. This compound undergoes sulfur abstraction by Ph_3P to give the $[(\eta^5\text{-Cp})_2Mo(DMDA)]$ dithiolene complex. Its existence justifies earlier postulates (*28b*) of the possible involvement of a perthiolene intermediate in the vinyl disulfide-to-dithiolene isomerization process (Fig. 28). The lack of evidence for the formation of a vinyl disulfide ligand in the reactions of DMA with any of the $[(S_x)(Mo_2S_4)(S_y)]^{2-}$ complexes has been noted (*28b*). It is suggested that the exceptionally reactive Mo=S group initially affords a vinyl sulfide ligand that rapidly abstracts sulfur from the neighboring S_x^{2-} ligands to form the stable dithiolene.

Interest in the molybdenum oxidoreductases and recognition of the importance of the molybdopyranopterin cofactor (Fig. 1) in the active sites of these enzymes have led to the synthesis of $[(L)_2Mo^{IV}{=}O]^{2-}$ [L = MNT (*170a,b*), Bdt (*170c*, *171c*), Tdt (*170c*)], $[(L)_2Mo^{VI}(O)_2]^{2-}$ [L = Bdt (*171c*), MNT (*171b*, *170e*), Tdt (*170d,e*)], and $[(L)_2Mo^{V}(O)_2]^-$

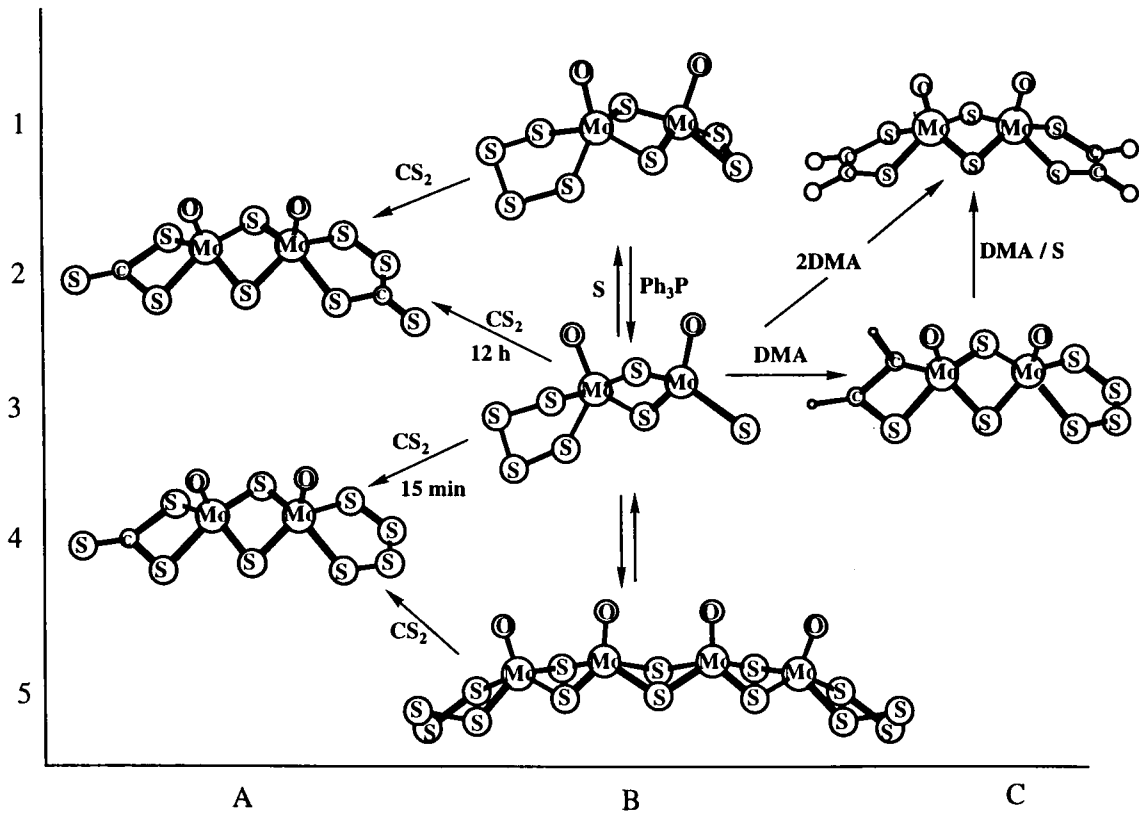

FIG. 29. The chemistry of the Mo(O)(S) unit in the $[(S_4)(Mo_2O_2S_2)(S)]^{2-}$ complex.

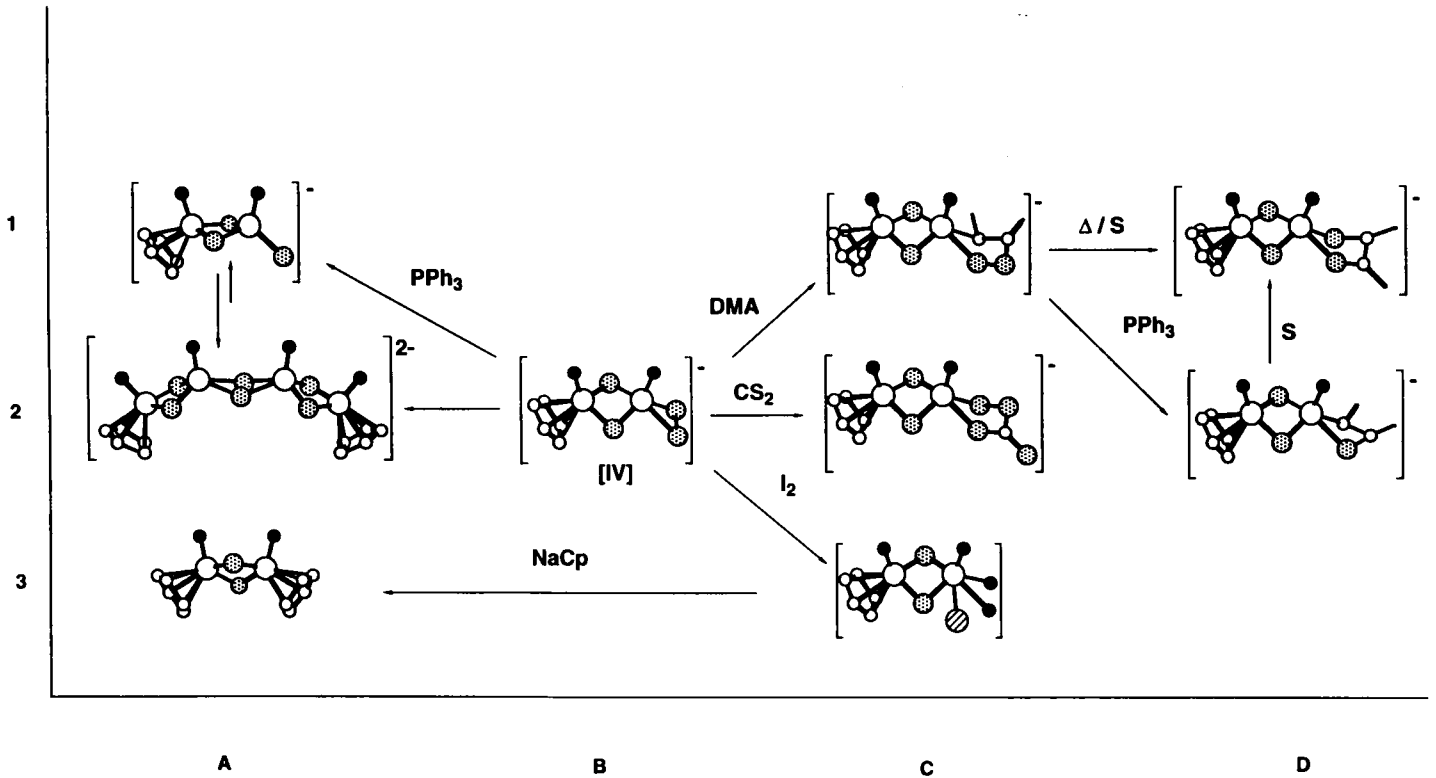

FIG. 30. The chemistry of the Mo(O)(S) unit in the $[(Cp)(Mo_2O_2S_2)(S)]^-$ complex.

complexes (Table XV) (*171c*), which together with analogous DMA complexes can be considered as partial structural analogues for the Mo oxidoreductase cofactor. The resonance Raman spectra of some of these molecules (*171d*) and particularly vibrations associated with the dithiolene functionality are similar to those observed in the molybdoenzymes and are thought to be associated with the dithiolene-functionalized pterin unit. Some of these complexes can be prepared (*173*) conveniently by the reaction of alkynes with the Mo–S_x chromophore (*172*). The $[(Bdt)_2Mo^{VI}(O)_2]^{2-}$ complex has been obtained by the reaction of Me_3NO with the $[O{=}Mo^{IV}(Bdt)_2]^{2-}$ complex (*170c*). The dioxo-Mo^{VI} dithiolene complexes serve as oxo-transfer agents (*171b*) and the $[Mo^{VI}(O)_2(MNT)_2]^{2-}$ complex has been reported to oxidize HSO_3^- to HSO_4^- as it is reduced to $[Mo^{IV}O(MNT)_2]^{2-}$. The reaction obeys saturation kinetics with $K_m = 0.010(1)\ M$ and a K_{obs} (at substrate saturation concentration) of 0.87(4) sec^{-1}. Similarly, the catalytic oxidation of benzoin by air or pyridine N-oxide has been reported with $[O{=}Mo(Bdt)_2]^{2-}$ used as a catalyst (*170g,h*).

TABLE XV

CHARACTERISTIC ELECTRONIC AND INFRARED ABSORPTION SPECTROSCOPIC DATA OF SELECTED DITHIOLENE Mo COMPLEXES

Compound	Infrared absorption (cm^{-1})	λ_{max}	Reference
$[Mo(DMAD)_3^{2-}$ [a]	C=O, 1730(br); C=O (DMF of solvation, 1710(s); C–O, 1200(s)[b]	356; 450(sh); 650[c]	*25, 160b*
$[Mo_2(\mu{-}S)_2(DMAD)_4]^{2-}$	C=O, 1730(br); C=O (DMF of solvation, 1710(s); C–O, 1200(s)[b]	380; 430(sh); 582; 680[c]	*25*
$[O{=}Mo(DMAD)_2]^{2-}$	Mo=O, 914(s); Mo–S, 388(w), 348(w)[b]	360; 460(sh); 550[c]	*25*
$[O{=}Mo^{V}(Bdt)_2]^-$	944[b]		*171c*
$[O{=}Mo^{IV}(pH_3Si{-}Bdt)_2]^{2-}$	Mo=O, 910; Mo–S, 365[b]	359(13.0); 445(1.3)[c]	*170c*
$[O{=}Mo^{IV}(Bdt)_2]^{2-}$	Mo=O, 905[b]	—	*171*
	Mo=O, 902; Mo–S, 356[b]	328(12.0); 385(0.98); 452(0.47)[c]	*170c*
$[(O)_2Mo^{VI}Bdt)_2]^{2-}$	Mo=O, 858, 829; Mo–S, 356, 322[b]	—	*170d*
$[(O{=}Mo^{IV}(Tdt)_2]^{2-}$	Mo=O, 905; Mo–S, 357[b]	331(11.0); 380(0.7); 454(0.37)[c]	*170c*
$[(O)_2Mo^{VI}(Tdt)_2]^{2-}$	Mo=O, 863, 835; Mo–S, 381, 358, 329, 318[b]	—	*170d*
$[(O)_2Mo^{VI}(MNT)_2]^{2-}$	Mo=O, 885, 851; Mo–S, 354, 330, 313; C=C, 1472[b]	—	*170a*
	Mo=O, 890, 855[b]	365(6.2); 425(6.9); 525(1.62)[c]	*171b*

[a] The cyclic voltammetry of the complex (obtained on a Pt electrode) shows two reversible waves at +0.020 and +0.420 V vs. Ag/AgCl in CH_3CN solution.

[b] In KBr disk.

[c] In CH_3CN solution.

A report of a new strategy for the synthesis of ene-1,2-dithiolate complexes has appeared (*173b*) [Eq. (8)]:

$$(L)_xM^n(S)_2 + R(C_2)R \rightarrow (L)_xM^{n-2}(\text{dithiolene}) \quad (8)$$

where $(L)_xM$ = $\{HB(Me_2pz)_3\}WX$. The reaction of $\{[O{=}Mo(\eta^2 \cdot S_2)_2]_2(\mu\text{-}S)\}^{2-}$ with DMA affords a mixture of products with infrared spectra (Table VIII) that suggest the presence of both the anti and syn isomers of $[(DMAD)(Mo_2O_2S_2)(DMAD)]^{2-}$. The structures of both of these isomers have been determined (*25*) (Table VI). The anti geometry is rarely found with the $(Mo_2O_2S_2)^{2+}$ unit. A change of the Mo oxidation state, from +6 in $\{[(\eta^2\text{-}S_2)_2Mo(O)]_2(\mu\text{-}S)\}^{2-}$ to +5 in the DMAD products, suggests that internal electron transfer has taken place with oxidation of a S_x^{2-} ligand to elemental sulfur.

3. *Addition of SO_2 to the Thiomolybdate Complexes*

The Mo–S_x bonds (x = 1, 2, 4) within the Mo(O)(S_x) units react readily with SO_2 to give various products that contain thiosulfite, thiosulfate, sulfite, or sulfate ligands (Tables V and VI). These reactions are best described as electrophilic additions to the Mo–S_x bond and in many instances may be subject to the effects of the spectator Mo=O group (see Section III,B).

The reaction of either $[(S_4)(Mo_2O_2S_2)(S_2)]^{2-}$ or $\{[(S_4)(Mo_2O_2S_2)(S)]_2\}^{4-}$ with SO_2 in CH_3CN solution at ambient temperature affords (Fig. 31), on standing for 12 hr, the $[(S_2O_3)$

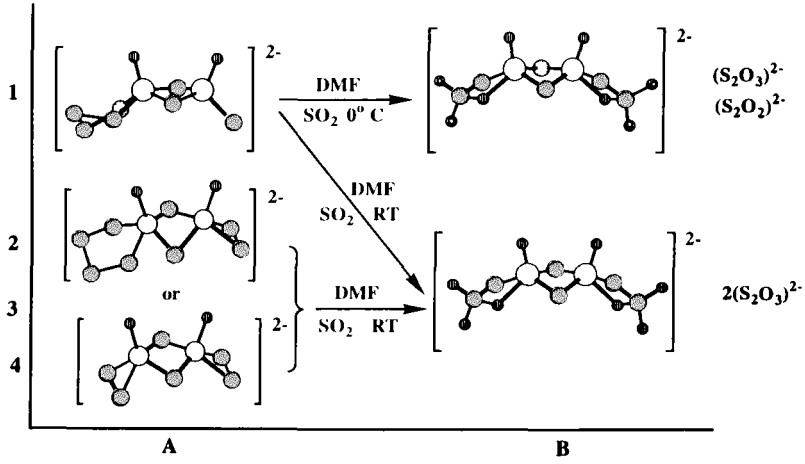

FIG. 31. Addition of SO_2 to tertiary thiomolybdate complexes.

$(Mo_2O_2S_2)(S_2O_3)]^{2-}$ complex (Fig. 31, structure 3B). The same reaction at 0°C results in the $[(S_2O_2)(Mo_2O_2S_2)(S_2O_3)]^{2-}$ complex, where the $S_2O_2^{2-}$ and $S_2O_3^{2-}$ ligands are disordered and distributed equally among the two ligand sites (Fig. 31, structure 1B). In shorter reaction times (~2 hr), at ambient temperature, the $[(S_4)(Mo_2O_2S_2)(S_2O_3)]^{2-}$ complex is obtained. The reaction in DMF solution for ~3 hr also affords the $[(S_2O_3)(Mo_2O_2S_2)(S_2O_3)]^{2-}$ complex (*113*).

At high temperature (~110°C), in DMF solution, the $[(DMF)_3(Mo_2O_2S_2)(SO_4)]^{2-}$ and $[(SO_4)(Mo_2O_2S_2)(SO_4)]^{2-}$ complexes form from reactions of SO_2 with $[[(S_4)(Mo_2O_2S_2)(S_2)]^{2-}$ or $\{[(S_4)(Mo_2O_2S_2)(S)]_2\}^{4-}$, respectively. The $[(DMF)_3(Mo_2O_2S_2)(SO_4)]^{2-}$ also is obtained by the stoichiometric reaction of $[(DMF)_3(Mo_2O_2S_2)(DMF)_3]^{2+}$ with $(Et_4N)_2SO_4$ in CH_3CN solution. The lability of the SO_4^{2-} ligands in these complexes makes them ideally suited for the synthesis of other complexes that contain the $(Mo_2O_2S_2)^{2+}$ core.

A series of interesting tetrameric molecules is isolated when some of the SO_2 reactions described above are carried out in the presence of the $(CH_3)_2NH_2^+$ cation (*113*, *174*). The $(Et_4N)_x((CH_3)_2NH_2)_{6-x}\{\{[SO_4][Mo_2O_2S_2][SO_4]\}_2\mu_4\text{-}SO_4\}^{6-}$ complexes (x = 1, 2, 3) (Fig. 32) contain a central μ_4-SO_4^{2-} ligand that is "trapped" by interdimer hydrogen bonds between the η^2-$(SO_4)^{2-}$ ligands and the $(CH_3)_2NH_2^+$ cations.

The reaction of SO_2 with the $[(Cp)(Mo_2O_2S_2)(S_2)]^-$ complex at 0°C in CH_3CN solution gives $[(Cp)(Mo_2O_2S_2)(SO_3)]^-$. At ambient temperature similar reactions between SO_2 and either $[(Cp)(Mo_2O_2S_2)(S_2)]^-$ or $[(Cp)(Mo_2O_2S_2)(S)]^-$ in CH_3CN solution afford $[(Cp)(Mo_2O_2S_2)(S_2O_3)]^-$. At higher temperatures (~100°C) similar reactions in DMF solution give $[(Cp)(Mo_2O_2S_2)(SO_4)]^-$. All three of these complexes have been structurally characterized (Fig. 33) and are shown to contain in the $[Mo_2O_2S_2]^{2-}$ core an η^5-Cp ligand and bidentate $(SO_3)^{2-}$, $(S_2O_3)^{2-}$, and $(SO_4)^{2-}$ ligands.

The reaction of $[(Cp)(Mo_2O_2S_2)(S)]^-$ with SO_2 was monitored by ^1H NMR spectroscopy in an SO_2-saturated CH_3CN-d_3 solution in a sealed NMR tube (*175*). A variety of $[(Cp)(Mo_2O_2S_2)(L)]^-$ products were identified over a period of time by the characteristic resonances of the Cp^- ligand protons. Definite assignments of the $(SO_3)^{2-}$, $(S_2O_3)^{2-}$, and $(SO_4)^{2-}$ products were made by comparison to the NMR resonances of isolated, structurally characterized, "authentic" samples. A correlation between the chemical shift and the sum of the Pauling electronegativities for the atoms in the $(S_xO_y)^{2-}$ ligands was used (*113*) to

FIG. 32. Two orientations of the structure of the $\{\{[SO_4][Mo_2O_2S_2][SO_4]\}_2\mu\text{-}SO_4\}^{6-}$.

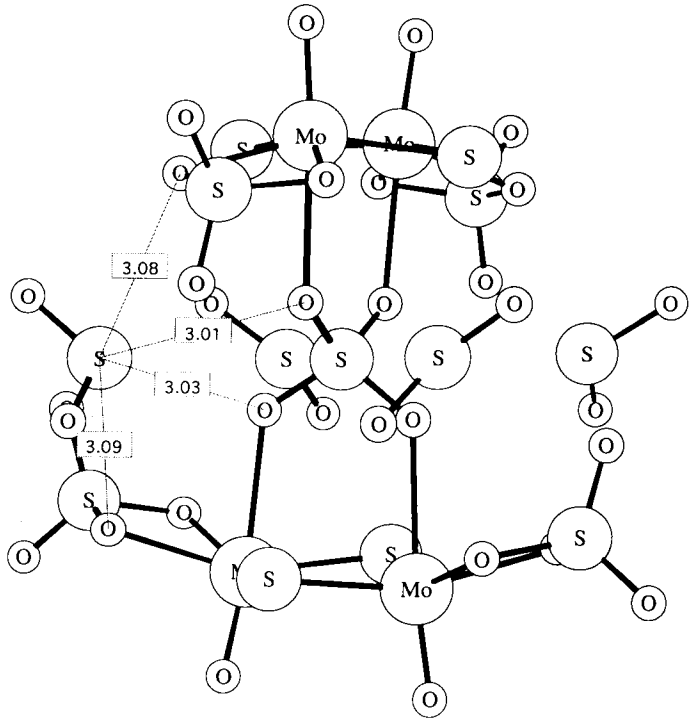
Mo
Mo
3.08
3.01
3.03
3.09
Mo

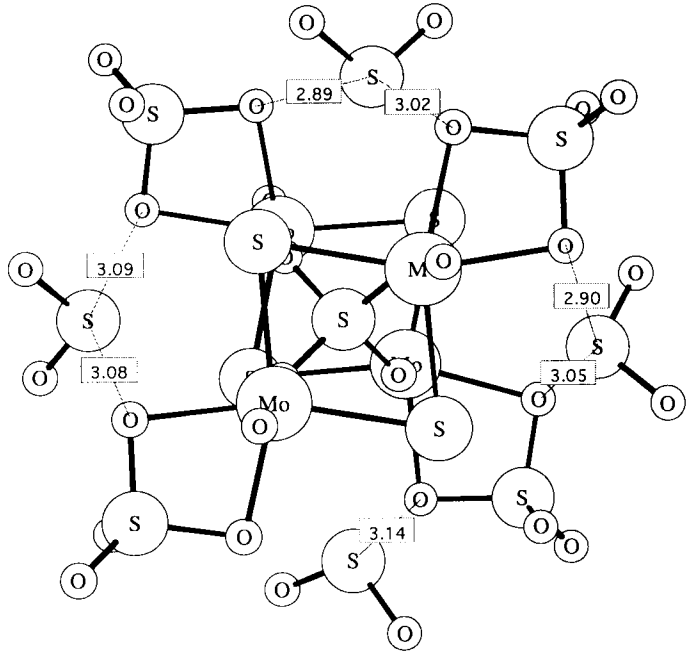
2.89
3.02
3.09
3.08
2.90
3.05
3.14

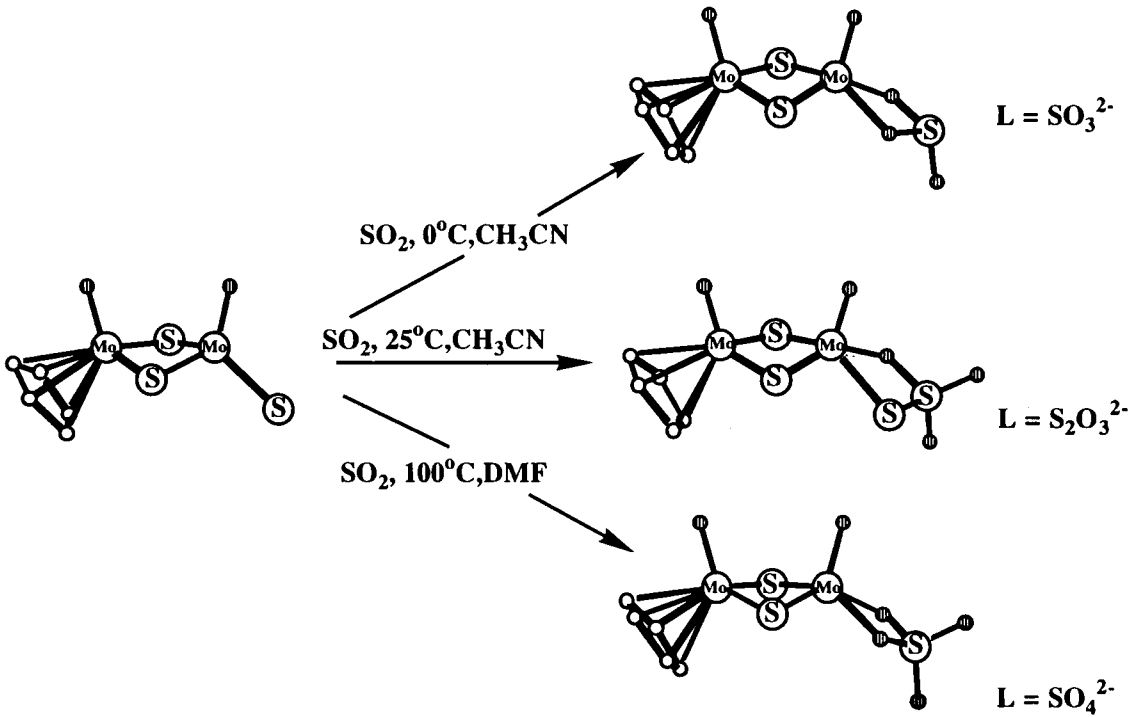

FIG. 33. Addition of SO_2 to the $[(Cp)(Mo_2O_2S_2)(S_x)]^-$ complexes (x = 1, 2).

assign resonances for complexes in solution with L = $(S_2O_2)^{2-}$ and $(S_2O)^{2-}$

D. Role of the Mo=S Group in the Active Site of Xanthine Oxidase

Reactivity studies of the $(O)Mo^{VI}(S)$ groups (*103*) in the oxo/thiomolybdate complexes clearly show the greater comparative reactivity of the $Mo^{VI}=S$ group relative to the $Mo^{VI}=O$ group. The results of these studies have led to the suggestion (*103*) that the Mo=S group may be a site of exceptional reactivity in the $(O)Mo^{VI}(S)$ chromophore in xanthine oxidase. The presence of the latter in the Mo cofactor has been suggested on the basis of analysis of Mo extended X-ray absorption fine structure (EXAFS) data (*176*). The data (for the reduced form of the cofactor) show that the first coordination sphere around the Mo atom contains the Mo(O)(S) unit (Fig. 34).

A modification of the first step in the proposed minimal mechanism (*177*) for the oxidation of xanthine to uric acid has been suggested (*103*). In this modification xanthine (RH) initially inserts into the $Mo^{VI}=S$ bond by an initial electrophilic attack by the Mo^{VI} at the C-8 position of xanthine. Subsequently the S atom accepts the C-8 proton to form $R\text{-}Mo^{VI}(O)SH$ (Fig. 35). Events that follow include (1) internal $2e^-$ reduction of the Mo and electrophilic attack by R^+ on the Mo=O group and (2) hydroxylation of the Mo^{IV} center to eventually form $RO\text{-}Mo^{IV}(O)SH$ (Fig. 35), as proposed in the original mechanism (*177*).

The reactivity of the Mo=S chromophore in the Mo center of xanthine oxidase also has been revealed in the reaction of this enzyme with bisulfite, which is a competitive inhibitor of xanthine oxidase (*178*). The $(HSO_3)^-$ inhibitor is a protector of the enzyme against cyanolysis and a 1:1 complex of the inhibitor and the enzyme has been isolated. The proposed mode of interaction involves the Mo=S group directly (Fig. 36). The suggestion that the interaction product very

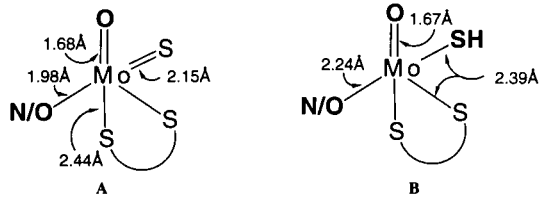

FIG. 34. The Mo coordination spheres in (A) the oxidized and (B) the reduced forms of xanthine oxidase as derived from EXAFS analyses (Data from Ref. *176*).

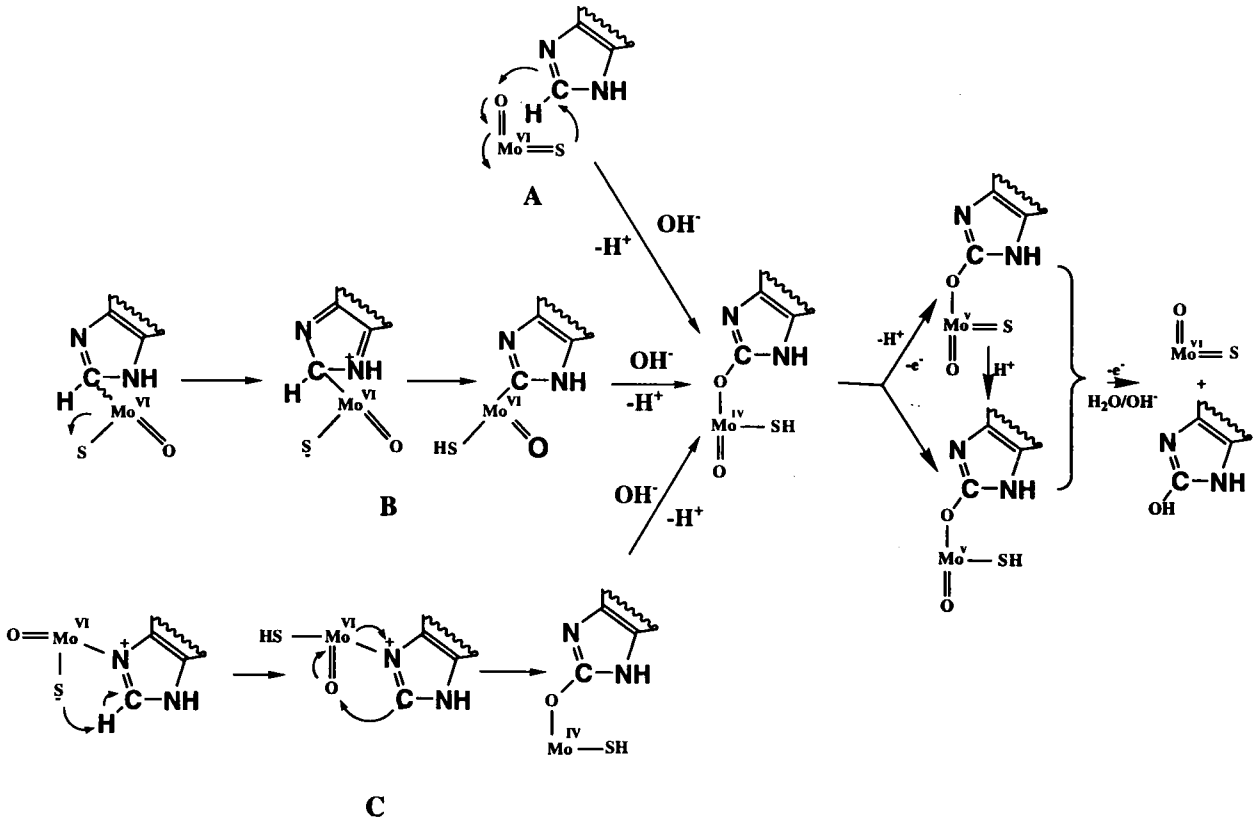

FIG. 35. Possible mechanisms for the action of xanthine oxidase (A, data from Ref. *177;* B, data from Ref. *103*).

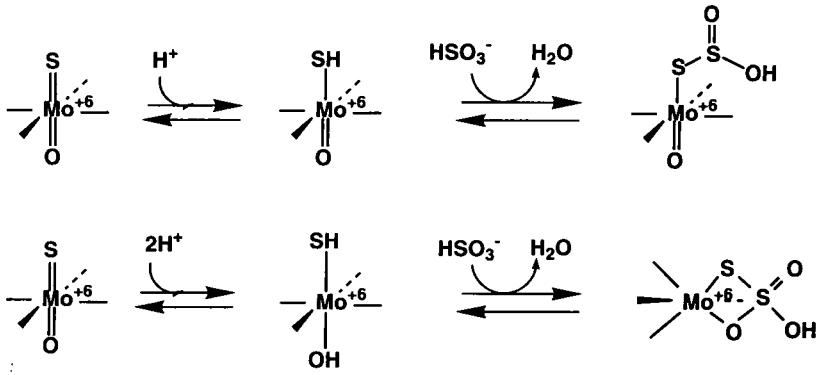

FIG. 36. Proposed mechanism of xanthine oxidase inhibition by $(HSO_3)^{2-}$ (Data from Ref. *178*).

likely contains an Mo-bound protonated thiosulfate ligand is supported by recent work with the $[(S)(Mo_2O_2S_2)(S_4)]^{2-}$ complex (*179*). The latter reacts with HSO_3^- and the isolated and structurally characterized product indeed contains a protonated thiosulfate ligand that presumably forms by insertion of the HSO_3^- anion into the Mo=S bond. The possible involvement of the Mo=S group in xanthine oxidase function also is suggested by recent ^{13}C electron and nuclear double resonance (ENDOR) studies (*180*). These studies show that the (^{13}C-labeled) formaldehyde-inhibited xanthine oxidase center has a carbon bound to the Mo atom at 1.9 Å. The proposed arrangement that places a C atom 1.9 Å from the Mo atom (Fig. 37A) is supported

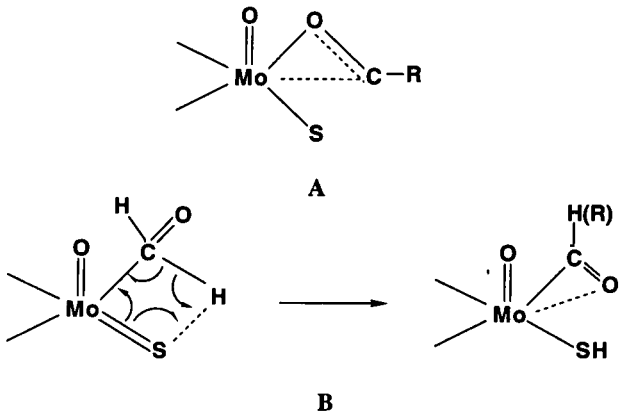

FIG. 37. Proposed modes of interaction of formaldehyde with the Mo cofactor in xanthine oxidase (A, after Ref. *180*).

by EXAFS studies (*181*) and could in fact be the result of a formaldehyde C–H bond addition to the active Mo=S group (Fig. 37B). It is quite clear that enough evidence exists that points to the involvement of the Mo=S group in xanthine oxidase function. Indeed, the reactivity patterns observed with model complexes that contain the Mo(O)(S) group suggest that the Mo=S is a site of preferential reactivity. Very recently ^{17}O and ^{13}C ENDOR measurements and kinetic studies (*182*) on xanthine oxidase have been interpreted in terms of the formal addition of xanthine across the Mo=S bond rather than involving the direct participation of the Mo=O group. These studies are in agreement with the mechanism proposed (*103*) earlier.

V. List of Abbreviations

HDS	Hydrodesulfurization
R_2Dtc	Dialkyldithiocarbamate
Cp	Cyclopentadienyl anion
Me-Cp	Methylcyclopentadienyl anion
Bdt	Benzenedithiolate dianion
PhS	Thiophenolate anion
Tdt	Toluenedithiolate anion
Bipy	2,2-Bipyridine
Phen	1,10-Phenanthroline
CH_3CN	Acetonitrile
Et_4N^+	Tetraethylammonium
DMF	Dimethylformamide
Ph_4P^+	Tetraphenylphosphonium
Ph_4As^+	Tetraphenylarsonium
H_2Salen	Salicylaldimine
NMR	Nuclear magnetic resonance
Ph_3P	Triphenylphosphine
TTN	Trithiacyclononane
^iPr	Isopropyl
^nBu	*n*-Butyl
H_4EDTA	Ethylenediaminetetraacetic acid
H_2Cys	Cysteine
Cp*	Pentamethylcyclopentadienyl anion
Edt	Ethanedithiolate dianion
H_3NTA	Nitrilotriacetic acid
THF	Tetrahydrofuran
DMA	Dicarbomethoxy acetylene
H_2DMAD	1,2-Dicarbomethoxy-2,2-ethylenedithiol

PEt_3	Triethyl phosphine
H_2VDS	1,2-Dicarbomethoxy vinyl disulfide
H_2MNT	1,2-Dicyanoethylene-1,2 ethylenedithiol
Dmpe	Dimethylphosphino ethane
PPh_3	Triphenylphosphine
H_2Dtp	Dithiophosphoric acid

ACKNOWLEDGMENTS

The author wishes to thank his co-workers who coauthored the publications referenced in this review. Without their contributions much of the Iowa and Michigan work reported in this review would not have been possible. The author also wishes to thank Professor Dieter Fenske, University of Karlsruhe, whose gracious hospitality provided the stimulating environment where this review was written. The entire research on Mo/S chemistry in the author's laboratories was made possible by the generous grant support that has been provided for nearly two decades by the National Science Foundation.

REFERENCES

1. (a) Cox, P. A. "The Elements"; Oxford University Press: New York, 1989; (b) Stiefel, E. I. In *Molybdenum Enzymes, Cofactors, and Model Systems;* ACS Symposium Series 535; Stiefel, E. I., and Coucouvanis, D. Newton, N. E., Eds.; 1993, 1–19.
2. (a) Burgess, B. *Chem. Rev.* **1990,** *90,* 1377; (b) Newton, W. E. In "Biological Nitrogen Fixation"; Stacey, G., Burris, R. H., and Evans, H. J., Eds.; Chapman and Hall: New York, 1992; p. 877; (c) Kim, J.; Rees, D. C. *Science* **1992,** *257,* 1677; (d) Kim, J.; Rees, D. C. *Nature* **1992,** *360,* 553; (e) Chan, M. K.; Kim, J.; Rees, D. C. *Science* **1993,** *260,* 792; (f) Bolin, J. T.; Ronco, A. E.; Morgan, T. V.; Mortenson, L. E.; Xuong, N. H. *Proc. Natl. Acad. Sci. U.S.A.* **1993,** *90,* 1078.
3. (a) *Molybdenum Enzymes, Cofactors, and Model Systems;* ACS Symposium Series 535; Stiefel, E. I., Coucouvanis, D., and W. E. Newton, Eds.; 1993; (b) "Molybdenum Enzymes, Metallic Ions Biology"; Spiro, T. G., Ed.; J. Wiley: New York, 1985; Vol. 7; (c) Enemark, J. H.; Young, C. G. *Adv. Inorg. Chem.* **1994,** *40,* 1.
4. (a) Rajagopalan, K. V. In "Biochemistry of the Elements"; Frieden, E., Ed.; Plenum Press: New York, 1984; p. 149. (b) Rajagopalan, K. V. *Adv. Enzymol. Relat. Areas Mol. Biol.* **1991,** *64,* 215. (c) Coughlan, M. P., Ed. "Molybdenum and Molybdenum-Containing Enzymes"; Pergamon: Oxford, 1980; (d) Newton, W. E.; Otsuka, S., Eds. "Molybdenum Chemistry of Biological Significance"; Plenum: New York, 1980; (e) Holm, R. H. *Coord. Chem. Rev.* **1990,** *100,* 183.
5. (a) Romao, M. J.; Archer, M.; Moura, I.; Moura, J. J. G.; LeGall, J.; Engh, R.; Schneider, M.; Hof, P.; Huber, R. *Science* **1995,** *270,* 1170; (b) Schindeling, H.; Kisker, C.; Hilton, J.; Rajagopalan, K. V.; Rees, D. C. *Science* **1996,** *272,* 1615; (c) Schneider, F.; Lowe, J.; Huber, R.; Schindeling, H.; Kisker, C.; Knablein, J. *J. Mol. Biol.* **1996,** *263,* 53; (d) Chan, M. K.; Mukund, S.; Kletzin, A.; Adams, M. W. W.; Rees, D. C. *Science* **1995,** *267,* 1463.
6. (a) Hille, R. In *Molybdenum Enzymes, Cofactors, and Model Systems;* ACS Symposium Series 535; Stiefel, E. I., Coucouvanis, D., and Newton, W. E., Eds.; **1993,** 22–37; (b) Bray, R. C. *Adv. Enzymol. Relat. Areas Mol. Biol.* **1980,** *51,* 107; (c)

Bray, R. C. *Rev. Biophys.* **1988,** *21,* 299; (d) See also Johnson, J. L., in Ref. *6a,* pp. 345, and Hille, R., and Massey, V., in Ref. 4b, p. 443.

7. (a) Massoth, F. E. *Adv. Catal.* **1978,** *27,* 265; (b) Topsoe, J.; Clausen, B. S. *Catal. Rev.-Sci. Eng.* **1984,** *26,* 395; (c) Weisser, O.; Landa, S. "Sulfide Catalysts: Their Properties and Applications"; Pergamon Press: London, 1973.
8. Stiefel, E. I.; Halbert, T. R.; Coyle, C. L.; Wei, L.; Pan, W.-H.; Ho, T. C.; Chianelli, R. R.; Daage, M. *Polyhedron* **1989,** *8,* 1625.
9. Stiefel, E. I. *Profr. Inorg. Chem.* **1977,** *22,* 1.
10. Sarkar, S.; Misra, S. B. S. *Coord. Chem. Rev.* **1984,** *59,* 239.
11. Mark Draganjac, M.; Rauchfuss, T. B. *Angew. Chem., Int. Ed. Engl.* **1985,** *24,* 742.
12. Muller, A.; Jaegermann, W.; Enemark, J. H. *Coord. Chem. Rev.* **1982,** *46,* 245.
13. Shibahara, T. *Coord. Chem. Rev.* **1993,** *123,* 73.
14. For the neutral free atoms, a compilation of Roothaan–Hartree–Fock atomic wavefunctions (E. Clementi and C. Roetti, *Atomic Data and Nuclear Data Tables* **1974,** *14,* #3–4) shows the sulfur *3p* orbitals with an energy of −0.43694 a.u. and the molybdenum *4d* (s^1d^5) with an energy of −0.34811 a.u. The localization of partial positive charge on the Mo and partial negative charge on the S is expected to bring these energies even closer together.
15. Carducci, M. D.; Brown, C.; Solomon, E. I.; Enemark, J. H. *J. Am. Chem. Soc.* **1994,** *116,* 11856.
16. Wachter, J. *J. Coord. Chem., Sect. B* **1987,** *15,* 219.
17. Beck, W.; Danzer, W.; Thiel, G. *Angew. Chem., Int. Ed. Engl.* **1973,** *12,* 582 [and later found to be anti-$(Cp)_2Mo_2^V(S)_2)(\mu\text{-}S)_2$ (Danzer, W.; Fehlhammer, W. P.; Liu, A. T.; Thiel, G.; Beck, W. *Chem. Ber.* **1982,** *115,* 682.]
18. (a) Rakowski DuBois, M.; DuBois, D. L.; VanDerveer, M. C.; Haltinwanger, R. C. I. *Inorg. Chem.* **1981,** *20,* 3064; (b) Brunner, H.; Meier, W.; Wachter, J.; Guggolz, E.; Zahn, T.; Ziegler, L. *Organometallics* **1982,** *1,* 1107.
19. (a) Allshouse, J.; Kaul, B. B.; Rakowski DuBois, M. *Organometallics* **1994,** *13,* 28; (b) Rakowski DuBois, M.; DuBois, D. L.; VanDerveer, M. C.; Haltinwanger, R. C. I. *Inorg. Chem.* **1981,** *20,* 3064.
20. Solutions of $[(Meg_5CpMo)_2(\mu\text{-}S)_2(\mu\text{-}S_2)]$ thermally convert into $[(Me_5CpMo(\mu\text{-}S)_2]_2$ at 100°C. Kubas, G. J.; Ryan, R. R. *J. Am. Chem. Soc.* **1985,** *107,* 6138.
21. The electron redistribution forms *anti*-$[(Me_5CpMo(\mu\text{-}S)(S)]_2$, $[(Me_5CpMo)_2(S)_2(\mu\text{-}S_2)]$ and $[(Me_5CpMo)_2(\mu\text{-}S_2)]$ are photochemically interconvertible when irradiated with visible light. Bruce, A. E.; Tyler, D. R. *Inorg. Chem.* **1984,** *23,* 3433.
22. Tremel, W.; Hoffman, R.; Jemmis, D. E. *Inorg. Chem.* **1989,** *28,* 1213.
23. (a) Müller, A.; Nolte, W. O.; Krebs, B. *Angew. Chem., Int. Ed. Engl.* **1978,** *17,* 279; (b) Müller, A.; Nolte, W. O.; Krebs, B. *Inorg. Chem.* **1980,** *19,* 2835; (c) Müller, A. *Polyhedron* **1986,** *5,* 323; (d) Müller, A.; Bhattacharrya, R. G.; Pfefferkorn, B. *Chem. Ber.* **1979,** *112,* 778; (e) Müller, A.; Bhattacharrya, R. G.; Eltzner, W.; Mohan, N.; Sarkar, S. *Chem. Uses Molybdenum, Proc. Int. Conf.* **1979,** *3,* 59; (f) Müller, A.; Krickemeyer, E. *Inorg. Synth.* **1990,** *27,* 47; (g) Müller, A.; Jaegerman, W. *Inorg. Chem.* **1979,** *18,* 2631; (h) Müller, A.; Reinsch, U. *Angew. Chem., Int. Ed. Engl.* **1980,** *19,* 72; (i) Müller, A.; Pohl, S.; Dartmann, M.; Cohen, J. P.; Bennett, J. M.; Kirchner, R. M.; *Z. Naturforsch. Teil B* **1979,** *34,* 434; (j) Diemann, E.; Müller, A.; Aymonino, P. J. *Z. Anorg. Allg. Chem.* **1981,** *479,* 191; (k) Müller, A.; Diemann, E. *Chimia* **1985,** *39,* 312.
24. (a) Draganjac, M.; Simhon, E.; Chan, L. T.; Kanatzidis, M.; Baenziger, N. C.; Coucouvanis, D. *Inorg. Chem.* **1982,** *21,* 3321; (b) Clegg, W.; Christou, G.; Garner,

C. D.; Sheldrick, G. M. *Inorg. Chem.* **1981,** *20,* 1562; (c) Cohen, S. A.; Stiefel, E. I. *Inorg. Chem.* **1985,** *24,* 4657.
25. Coucouvanis, D.; Hadjikyriacou, A.; Toupadakis, A.; Koo, S.-M.; Ileperuma, O.; Draganjac, M.; Salifoglou, A. *Inorg. Chem.* **1991,** *30,* 754.
26. Wedd, A. G. In "Sulfur, Its Significance for Chemistry, for the Geo-, Bio- and Cosmosphere and Technology"; Müller, A., and Krebs, B., Eds; Elsevier: Amsterdam, 1984; p. 181.
27. Young, C. G.; Kocaba, T. O.; Yan, X. F.; Tiekink, R. T.; Wei, L.; Murray III, H. H.; Coyle, C. L.; Stiefel, E. I. *Inorg. Chem.* **1994,** *33,* 6252.
28. (a) Coucouvanis, D.; Hadjikyriacou, A.; Draganjac, M.; Kanatzidis, M. G.; Ileperuma, O. *Polyhedron* **1986,** *5,* 349; (b) Coucouvanis, D.; Toupadakis, A.; Koo, S.-M.; Hadjikyriacou, A. *Polyhedron* **1989,** *8,* 1705.
29. Simhon, E. D.; Baenziger, N. C.; Kanatzidis, M.; Draganjac, M.; Coucouvanis, D. *J. Am. Chem. Soc.* **1981,** *103,* 1218.
30. Halbert, T. R.; Hutchings, L. L.; Rhodes, R.; Stiefel. E. I. *J. Am. Chem. Soc.* **1986,** *108,* 6437.
31. Yang, Y.; Huang, L.; Liu, Q.; Kang, B. *Acta Crystallogr., Sect. C* **1991,** *47,* 2085.
32. Tiekink, E. R. T.; Yan, X. F.; Young, C. G. *Austral. J. Chem. Soc.* **1992,** *45,* 897.
33. Pan, W.-H.; Halbert, T. R.; Hutchings, L. L.; Stiefel, E. I. *J. Chem. Soc., Chem. Commun.* **1985,** 927.
34. Harmer, M. A.; Halbert, T. R.; Pan, W.-H.; Coyle, C. L.; Cohen, S. A.; Stiefel, E. I. *Polyhedron* **1986,** *5,* 341.
35. Pan, W.-H.; Harmer, M. A.; Halbert, T. R.; Stiefel, E. I. *J. Am. Chem. Soc.* **1984,** *106,* 459.
36. Sarkar, S.; Ansari, *M. A. J. Chem. Soc., Chem. Commun.* **1986,** 324.
37. Coyle, C. L.; Harmer, M. A.; George, G. N.; Daage, M.; Stiefel, E. I. *Inorg. Chem.* **1990,** *29,* 14.
38. Mayer, J. M.; Nugent, W. A. "Metal-Ligand Multiple Bonds: The Chemistry of Transition Metal Complexes Containing Oxo, Nitrido, Imido, Alkylidene or Alkylidyne Ligands." Wiley Interscience: New York, 1988.
39. Dubois, D. L.; Hoffmann, R. *Nouv. J. Chim.* **1977,** *1,* 479.
40. Pourreau, D. B.; Groffroy, G. L. *Adv. Organomet. Chem.* **1985,** *24,* 249.
41. Deeth, R. J. *J. Chem. Soc., Dalton Trans.* **1991,** 1895.
42. Berzelius, J. J. *Poggendorffs Ann. Phys. Chem.* **1826,** *7,* 262; *ibid., 8,* 269.
43. Diemann, E.; Müller, A. *Coordination Chem. Rev.* **1973,** *10,* 79.
44. Müller, A.; Diemann, E.; Jostes, R.; Bogge, H. *Angew. Chem., Int. Ed. Engl.* **1981,** *20, 934.*
45. McDonald, J. W.; Friesen, G. D.; Rosenhein, L. D.; Newton, W. E. *Inorg. Chim. Acta* **1983,** *72,* 205.
46. (a) $[Et_4N]_2MoS_4$; Kanatzidis, M. G., Coucouvanis, D. *Acta Crystallogr.* **1983,** *C39,* 835; (b) $[NH_4]_2MoS_4$; Lapasset, J.; Chezeau, N.; Belougne, P. *Acta Crystallogr.* **1976,** *B32,* 3087; (c) $(Cs)_2MoOS_3$; Krebs, B.; Muller, A.; Kindler, E. *Z. Naturforsch.* **1970,** *B25,* 222.
47. Harmer, M. A.; Sykes, A. G. *Inorg. Chem.* **1980,** *19,* 2881.
48. Belton, P. S.; Cox, I. J.; Harris, R. K.; O'Connor, M. J. *Austral. J. Chem.* **1986,** *39,* 943.
49. Combariza, J. E.; Enemark, J. H.; Barfield, M.; Facelli, J. C. *J. Am. Chem. Soc.* **1989,** *111,* 7619.
50. (a) El-Issa, B. D.; Ali, A. A. M.; Zanati, H. *Inorg. Chem.* **1989,** *28,* 3297; (b) Jostes, R.; Muller, A. *J. Mol. Struct.* **1988,** *164,* 211.

51. Saxena, R. S.; Jain, M. C.; Mittal, M. I. *Austral. J. Chem.* **1968,** *21,* 91.
52. Coucouvanis, D. *Acc. Chem. Res.* **1981,** *14,* 201.
53. Müller, A.; Ahlborn, E.; Heinsen, H.-H. *Z. Anorg. Allg. Chem.* **1971,** *386,* 102.
54. Müller, A.; Diemann, E.; Heinsen, H. H. *Chem. Berichte* **1971,** *104,* 975.
55. Sotofte, I. *Acta Chem. Scand.* **1976,** *A30,* 157.
56. Callahan, K. P.; Pilliero, P. A. *J. Chem. Soc., Chem. Commun.* **1979,** 13.
57. (a) Coucouvanis; D.; Simhon, E. D.; Swenson, D.; Baenziger, N. C. *J. Chem. Soc., Chem. Commun.* **1979,** 361; (b) Tieckelmann, R. H.; Silvis, H. C.; Kent, T. A.; Huynh, B. H.; Waszczak, J. V.; Teo, B.-K.; Averill, B. A. *J. Am. Chem. Soc.* **1980,** *102,* 5550; (c) Cai, J.; Chen, C. *Jiegou Huaxue* **1991,** *10,* 93.
58. (a) Coucouvanis, D.; Baenziger, N. C.; Simhon, E. D.; Stremple, P.; Swenson, D.; Kostikas, A,; Simopoulos, A.; Petrouleas, V.; Papaefthymiou, V. *J. Am. Chem. Soc.* **1980,** *102,* 1732; (b) Coucouvanis, D.; Simhon, E. D.; Stremple, P.; Ryan, M.; Swenson, D.; Baenziger, N. C.; Simopoulos, A.; Papaefthymiou, V.; Kostikas, A.; Petrouleas, V. *Inorg. Chem.* **1984,** *23,* 741; (c) Muller, A.; Bogge, H.; Tolle, H.-G.; Jostes, R.; Schimanski, U.; Dartmann M, *Angew. Chem., Int. Ed. Engl.* **1980,** *8,* 654.
59. Silvis, H. C.; Averill, B. A. *Inorg. Chim. Acta* **1981,** *54,* L57.
60. (a) Coucouvanis, D.; Simhon, E. C.; Stremple, P.; Baenziger, N. C. *Inorg. Chim. Acta* **1981,** *53,* L135; (b) Butler, A. R.; Glidewell, C.; Johnson, I. L.; Walton, J. C. *Polyhedron* **1987,** *6,* 2085.
61. Coucouvanis, D.; Baenziger, N. C.; Simhon, E. D.; Stremple, P.; Swenson, D.; Kostikas, A.; Simopoulos, A.; Petrouleas, V.; Papaefthymiou, V. *J. Am. Chem. Soc.* **1980,** *102,* 1730.
62. (a) Coucouvanis, D.; Simhon, E. D.; Baenziger, N. C. *J. Am. Chem. Soc.* **1980,** *102,* 6644; (b) McDonald, J. W.; Friesen, G. D.; Newton, W. E. *Inorg. Chim. Acta* **1980,** *46,* L79; (c) Müller, A.; Hellmann, W.; Schneider, J.; Schimanski, U.; Demmer, U.; Trautwein, A.; Bender, V. *Inorg. Chim. Acta* **1982,** *65,* L41.
63. Miller, A.; Sarkar, S.; Bögge, H. R.; Jostes, R.; Trautwein, A.; Lauer, U. *Angew. Chem., Int. Ed. Engl.* **1983,** *22,* 561.
64. (a) Tieckelmann, R. H.; Averill, B. A. *Inorg. Chim. Acta* **1980,** *46,* L35; (b) Teo, B. K., Antonio, M. R.; Tieckelman, R. H.; Silvis, H. C.; Averill, B. A. *J. Am. Chem. Soc.* **1982,** *104,* 6126.
65. (a) Rosenhein, L. D.; McDonald, J. W. *Inorg. Chem.* **1987,** *26,* 3414; (b) Xiao, T.; Yu, P.; Zhuang, B. *Chin. Sci. Bull.* **1992,** *37,* 1669.
66. Kovacs, J. A.; Bashkin, J. K.; Holm, R. H. *Polyhedron* **1987,** *6,* 1445.
67. Daran, J.-C.; Prout, K.; Adam, G. J. S.; Green, M. L. H.; Sala-Pala, J. *J. Organomet. Chem.* **1977,** *C40,* 131.
68. Srinivasan, B. R.; Sarkar, S. *Inorg. Chem.* **1990,** *29,* 3898.
69. (a) Sarkar, S.; Mishra, S. B. S. *J. Indian Chem. Soc.* **1985,** *62,* 821; (b) Sarkar, S.; Mishra, S. B. S. *Indian J. Chem.* **1987,** *25A,* 871.
70. (a) Potvin, C.; Manoli, J. M.; Secheresse, F.; Marzak, S. *Inorg. Chim. Acta* **1987,** *124,* 9; (b) Manoli, J. M.; Potvin, C.; Secherese, F.; Marzak, S. *J. Chem. Soc., Chem. Commun.* **1986,** 1557; (c) Manoli, J. M.; Potvin, C.; Secherese, F.; Marzak, S. *Inorg. Chim. Acta* **1988,** 257; (d) Potvin, C.; Manoli, J. M.; Secheresse, F.; Marzak, S. *Inorg. Chem.* **1987,** *26,* 4370.
71. (a) Muller, A.; Dartman, M.; Romer, C.; Clegg, W.; Sheldrick, G. *Angew. Chem., Int. Ed. Engl.* **1981,** *20,* 1060; (b) Gheller, S. F.; Hambley, T. W.; Rodgers, J. R.; Brownlee, R. T. C.; O'Connors, M. J.; Snow, M. R.; Wedd, A. *Inorg. Chem.* **1984,** *23,* 2519; (c) Clegg, W.; Garner, C. D.; Nicholson, J. R. *Acta Crystallogr. Sect. C* **1983,** *39,* 552; (d) Manoli, J. M.; Potvin, C.; Secheresse, F. *J. Chem. Soc., Chem.*

Commun. **1982,** 1159; (e) Potvin, C.; Manoli, J. M.; Salis M.; Secheresse, F. *Inorg. Chim. Acta* **1984,** *83,* L19; (f) Secheresse, F.; Salis M.; Potvin, C.; Manoli, J. M. *Inorg. Chim. Acta* **1986,** *114,* L19.

72. (a) Binnie, W. P.; Redman, M. J.; Mallio, W. J. *Inorg. Chem.* **1970,** *9,* 1449; (b) Müller, A.; Menge R. *Z. Anorg. Allg. Chem.* **1972,** *393,* 259; (c) Kinsch, E. M.; Stephan, D. W. *Inorg. Chim. Acta* **1985,** *96,* L87.
73. (a) Coucouvanis, D.; Koo, S.-M. *Inorg. Chem.* **1989,** *28,* 5; (b) Koo, S.-M. Ph.D. thesis, University of Michigan, 1990; (c) Morris, N. L.; Jameson, G. B.; Pope, M. T. *Inorg. Chem.* **1985,** *24,* 3482; (d) Coucouvanis, D.; Swenson, D.; Stremple, P.; Baenziger, N. C. *J. Am. Chem. Soc.* **1979,** *101,* 3392.
74. (a) Boyd, I. W.; Dance, I. G.; Murray, K. S.; Wedd, A. G. *Austral. J. Chem.* **1978,** *31,* 279; (b) Bradbury, J. R.; MacKay, M. F.; Wedd, A. G.; *Austral. J. Chem.* **1978,** *31,* 2433.
75. Clark, R. J. H.; Joss, S.; Zvagulis, M.; Garner, C. D.; Nicholson, J. R. *J. Chem. Soc., Dalton Trans.* **1986,** 1595.
76. Kony, M.; Bond, A. M.; Wedd, A. G. *Inorg. Chem.* **1990,** *29,* 4521.
77. (a) Hou, H. W.; Xin, X. Q.; Huang, X. X.; Cai, J. H.; Kang, B. S. *Chin. Chem. Lett.* **1995,** *6,* 91; (b) Shi, S.; Ji, W.; Xie, W.; Chong, T. C.; Zeng, H. C.; Lang, J. P.; Xin, X. Q. *Mater. Chem. Phys.* **1995,** *39,* 298; (c) Shi, B.; Gao, F.; Shao, E.; Wei, G.; Jin, Z. *Jiegou Huaxue* **1992,** *11,* 235; (d) Lang, J.; Bao, S.; Zhu, H.; Xin, X.; Cai, J.; Weng, L.; Hu, Y.; Kang, B. *Gaodeng Xuexiao Xuaxue Xuebao* **1992,** *13,* 889; (e) Zhu, N.; Zheng, Y.; Wu, X. *Polyhedron* **1991,** *10,* 2743; (f) Zhu, N.; Wu, X.; Lu, J. *J. Chem. Soc., Chem. Commun.* **1991,** 235; (g) Zhu, N.; Zheng, Y.; Wu, X. *J. Chem. Soc., Chem. Commun.* **1990,** 780.
78. (a) Secherese, F.; Bernes, S.; Francis, R.; Jeannin, Y. *J. Chem. Soc., Dalton Trans.* **1991,** 2875; (b) Nicholson, J. R.; Flood, A. C.; Garner, C. D.; Clegg, W. *J. Chem. Soc., Chem. Commun.* **1983,** 1179.
79. Miller, K. F., Bruce, A. E., Corbin, J. L., Wherland, S., Stiefel, E. I. *J. Am. Chem. Soc.* **1980,** *102,* 5102.
80. (a) Secherese, F.; Defebure, J.; Daran, J. C.; Jeannin, Y. *Inorg. Chem.* **1982,** *21,* 1311; (b) Fedin, V. P.; Mironov, Y. V.; Sokolov, M. N.; Mizonov, Y. I.; Fedorov, V. E. *Inorg. Chim. Acta* **1989,** *163,* 65; (c) Pan, W. H.; Leonowicz, M. E.; Stiefel, E. I. *Inorg. Chem.* **1983,** *22,* 672; (d) Bernhole, J.; Stiefel, E. I. *Inorg. Chem.* **1985,** *24,* 1323; (e) Müller, A.; Hellman, W.; Romer, C.; Romer, M.; Bogge, H; Jostes, R.; Schimanski, U. *Inorg. Chim. Acta* **1984,** *L75,* 83; (f) Herberhold, M.; Xin, G.; Müller, A.; Penk, M. *Z. Naturforsch.* **1990,** *42b,* 25.
81. Mitchell, P. C. H.; Parker, D. A. *J. Chem. Soc., Dalton Trans.* **1976,** 1821.
82. (a) Coucouvanis, D.; Hadjikyriacou, A. I. *Inorg. Chem.* **1986,** *25,* 4317; (b) Hadjikyriacou, A. I.; Coucouvanis, D. *Inorg. Chem.* **1987,** *26,* 2400; (c) Hadjikyriacou, A. I.; Coucouvanis, D. *Inorg. Synth.* **1990,** *27,* 39.
83. Hadjikyriacou, A. I., Ph.D thesis, University of Michigan, 1988.
84. Day, V. W.; Fredrich, M. F.; Klemperer, W. G.; Shum, W. J. *Am. Chem. Soc.* **1977,** *99,* 6146.
85. Do, Y.; Simhon, E. D.; Holm, R. H. *Inorg. Chem.* **1985,** *24,* 1831.
86. Fenske, D.; Czeska, B.; Schumacher, C.; Schmidt, R. E.; Dehnicke, K. *Z. Anorg. Allg. Chem.* **1985,** *520,* 7.
87. Marcoll, J.; Rabenau, A.; Mootz, D.; Wunderlich, H. *Rev. Chim. Miner.* **1974,** *11,* 607.
88. Young, C. G.; Kocaba, T. O.; Yan, X. F.; Tiekink, R. T.; Wei, L.; Murray III, H. H.; Coyle, C. L.; Stiefel, E. I. *Inorg. Chem.* **1994,** *33,* 6252.

89. (a) Miller, K. F.; Bruce, A. E.; Corbin, J. L.; Wherland, S.; Stiefel, E. I. *J. Am. Chem. Soc.* **1980,** *102,* 5104; (b) Bunzey, G.; Enemark, J. H. *Inorg. Chem.* **1978,** *17,* 682; (c) Hsie, T.-C.; Gebreyes, K.; Zubieta, J. *Trans. Met. Chem.* **1985,** *10,* 81; (d) Chandler, T.; Lichtenberger, D. L.; Enemark, J. H. **1981,** *20,* 75.
90. (a) Makhyoun, M. A. *Polyhedron* **1988,** *7,* 2675; (b) Bhaduri, S.; Ibers, J. A. *Inorg. Chem.* **1986,** *25,* 3; (c) Chandrasekaran, J.; Ansari, M. A.; Sarcar, S. *Inorg. Chem.* **1988,** *27,* 3663; (d) Koniger-Ahlborn, E.; Muller, A. *Angew. Chem., Int. Ed. Engl.* **1975,** *14,* 573; (e) Stiefel, E. I. *Inorg. Chem.* **1983,** *22,* 672; (f) Müller, A.; Diemann, E.; Wienboker, U.; Bogge, H. *Inorg. Chem.* **1989,** *28,* 4046; (g) Secheresse, F.; Lefebvre, J.; Daran, J. C.; Jeannin, Y. *Inorg. Chim. Acta* **1980,** *45,* L45.
91. Wardle, R. W. M.; Bhaduri, S.; Chau, C.-N.; Ibers, J. A. *Inorg. Chem.* **1988,** *27,* 1747.
92. Lu, Y.-J.; Ansari, M. A.; Ibers, J. A. *Inorg. Chem.* **1989,** *28,* 4049.
93. Wardle, R. W. M.; Mahler, C. H.; Chau, C.-N.; Ibers, J. A. *Inorg. Chem.* **1988,** *27,* 2790.
94. Flomer, W. A.; Kolis, J. W. *Inorg. Chem.* **1989,** *28,* 2513.
95. (a) Do, Y.; Simhon, E. D.; Holm, R. H. *Inorg. Chem.* **1985,** *24,* 2827; (b) Xin, X.; Jin, G.; Wang, B.; Pope, M. *Inorg. Chem.* **1990,** *29,* 553.
96. Coucouvanis, D.; Patek, A. J.; Lane, J., Manuscript in preparation.
97. (a) Müller, A.; Romer, M.; Romer, C.; Reinsch-Vogel, Bogge, H.; Schimanski, U. *Monatsh. Chem.* **1985,** *116,* 711; (b) Xin, X.; Morris, N. L.; Jameson, G. B.; Pope, M. T. *Inorg. Chem.* **1985,** *24,* 3482.
98. Coucouvanis, D.; Patil, P. R.; Kanatzidis, M. G.; Detering, B.; Baenziger, N. C. *Inorg. Chem.* **1985,** *24,* 24.
99. Coucouvanis, D.; Murphy, C. N.; Simhon, E.; Stremple, P.; Draganjac, M. *Inorg. Synth.* **1982,** *21,* 23.
100. (a) Rittner, W.; Müller, A.; Neumann, A.; Bather, W.; Sharma, R. C. *Angew. Chem., Int. Ed. Engl.* **1979,** *18,* 530; (b) Zhang, Z. *Kexue Tongbao* **1985,** *30,* 764; (c) Clegg, W.; Sheldrick, G. M.; Garner, C. D.; Christou, G. *Acta Crystallogr.* **1980,** *B36,* 2784; (d) Clegg, W.; Mohan, N.; Muller, A.; Neumann, A.; Rittner, W.; Sheldrick, G. M. *Inorg. Chem.* **1980,** *19,* 2066.
101. Müller, A.; Reinsch-Vogell, U.; Krickemeyer, E.; Bogge, H. *Angew. Chem., Int. Ed. Engl.* **1982,** *21,* 796.
102. Do, Y.; Simhon, E. D.; Holm, R. H. *Inorg. Chem.* **1985,** *24,* 2827.
103. (a) Coucouvanis, D.; Toupadakis, A.; Lane, J. D.; Koo, S. M.; Kim, C. G.; Hadjikyriacou, A. *J. Am. Chem. Soc.* **1991,** *113,* 5271; (b) Coucouvanis, D.; Toupadakis, A.; Kim, C., To be published.
104. Coucouvanis D.; Toupadakis, A.; Hadjikyriacou, A. I. *Inorg. Chem.* **1988,** *27,* 3272.
105. Hadjikyriacou, A. I.; Coucouvanis, D. *Inorg. Chem.* **1989,** *28,* 2169.
106. (a) Toupadakis, A. Ph.D. thesis, University of Michigan, **1990**; (b) Coucouvanis, D.; Al-Ahmad, S., Manuscript in preparation.
107. Shibahara, T.; Kuroya, H.; Matsumoto, K.; Ooi, S. *Bull. Chem. Soc. Jpn.* **1983,** *56,* 2945.
108. Spivack, B.; Dori, Z. *J. Chem. Soc., Dalton Trans.* **1973,** 1173.
109. Atovmyan, L. O.; Tkachev, V. V.; Shchepinov, S. A. *Koord. Khim.* **1978,** *4,* 610.
110. Howlader, N. C.; Haight, Jr., G. P.; Hambley, T. W.; Snow, M. R.; Lawrance, G. A. *Inorg. Chem.* **1984,** *23,* 1811.
111. Tanner, L. D.; Haltiwanger, R. C.; Rakowski DuBois, M. *Inorg. Chem.* **1988,** *27,* 1741.
112. (a) Spivack, B.; Dori, Z. *J. Chem. Soc. Chem. Commun.* **1973,** 909; (b) Shibahara, T.; Akashi, H. *Inorg. Synth.* **1992,** *29,* 254; (c) Ott, V. R.; Swieter, D. S.; Schultz,

F. A. *Inorg. Chem.* **1977,** *16,* 2538; (d) Dirand-Colin, J.; Ricard, L.; Weiss, R. *Inorg. Chim. Acta* **1976,** *18,* L212; (e) Newton, W. E.; McDonald, J. W. *J. Less-Common Met.* **1977,** *54,* 51; (f) Goodgame, D. M. L.; Rollins, R. W.; Skapski, A. C. *Inorg. Chim. Acta* **1985,** *24,* L61.

113. Kim, C. G. Ph.D thesis, University of Michigan, 1993.
114. (a) Stomberg, R. *Acta Chem. Scand.* **1968,** *22,* 1076; (b) Trysberg, L.; Stomberg, R. *Acta Chem. Scand.* **1981,** *A35,* 823; (c) Stomberg, R.; Trysberg, L.; Larking, I. *Acta Chem. Scand.* **1970,** *24,* 2678; (d) Persdotter, I.; Trysberg, L.; Stomberg, R. *Acta Chem. Scand.* **1986,** *A40,* 1; (e) Stomberg, R. *Acta Chem. Scand.* **1969,** *22,* 2024; (f) Persdotter, I.; Trysberg, L.; Stomberg, R. *Acta Chem. Scand.* **1986,** *A40,* 83; (g) Wu, X.-T.; Lu, S.-F.; Zu, L.-Y; Wu, Q.-J.; Lu, J.-X. *Inorg. Chim. Acta* **1987,** *133,* 43.
115. Rakowski-DuBois, M.; DuBois, D. L.; VanDerveer, M. C.; Haltinwanger, R. C. *Inorg. Chem.* **1981,** *20,* 3064.
116. O'Neal, S. C.; Pennington, W. T.; Kolis, J. W. *Organometallics* **1989,** *8,* 2281.
117. (a) Du, S.; Zhu, N.; Wu, X.; Lu, J. *Inorg. Chem.* **1992,** *31,* 2847; (b) Zhu, N.; Du, S.; Wu, X.; Lu, J. *Angew. Chem., Int. Ed. Engl.* **1992,** *31,* 87.
118. (a) Chakrabarty, R.; Bhattacharya, S.; Pierpond, C. G.; Bhattacharya, R. *Inorg. Chem.* **1992,** *31,* 3573; (b) Simonnet-Jegat, C.; Jourdan, N.; Robert, F.; Bois, C.; Secheresse, F. *Inorg. Chim. Acta* **1994,** *216,* 201.
119. Mennemann, K.; Mattes, R. *Angew. Chem., Int. Ed. Engl.* **1977,** *16,* 260.
120. Schreiner, S.; Aleandri, L. E.; Kang, D.; Ibers, J. A. *Inorg. Chem.* **1989,** *28,* 392.
121. (a) Manoli, J. M.; Potvin, C.; Secherese, F. *Inorg. Chem.* **1987,** *26,* 340; (b) Manoli, J. M.; Potvin, C.; Secheresse, F. *Inorg. Chim. Acta* **1987,** *153,* 27; (c) Chandasekaran, J.; Ansari, M. A.; Sarkar, S. *Inorg. Chem.* **1988,** *27,* 3663.
122. Müller, A.; Bogge, H.; Schimanski, U.; Penk, M.; Nieradzik, K.; Dartmann, M.; Krickemeyer, E.; Schimanski, J.; Romer, C.; Dornfeld, H.; Wieboker, U.; Hellmann, W.; Zimmermann, M. *Monatsh. Chem.* **1989,** *120,* 367.
123. Müller, A.; Jostes, R.; Eltzner, W.; Nie, C.-S.; Diemann, E.; Bogge, H.; Zimmermann, M.; Dartmann, M.; Reinsch-Vogell, U.; Che, S.; Cyvin, S. J.; Cyvin, B. N. *Inorg. Chem.* **1985,** *24,* 2872.
124. Halbert T. R.; McGauley, K.; Pan, W.-H.; Czernuszewicz, R. S.; Stiefel, E. I. *J. Am. Chem. Soc.* **1984,** *106,* 1849.
125. Hegetschweiler, K. K. T.; Baeumle, M.; Rihs, G.; Schneider, W. *Inorg. Chem.* **1991,** *30,* 4342.
126. (a) Cotton, F. A.; LLusar, R.; Marler, D. O.; Schwotzer, W. *Inorg. Chim. Acta* **1985,** *102,* L25; (b) Cotton, F. A.; Dori, Z.; LLusar, R.; Schwotzer, W. *Inorg. Chem.* **1986,** *25,* 3654.
127. Kathirgamanathan, P.; Martinez, M.; Sykes, A. G. *J. Chem. Soc., Chem. Commun.* **1985,** 1437.
128. Cotton, F. A.; Dori, Z.; LLusar, R.; Schwotzer, W. *J. Am. Chem. Soc.* **1985,** *107,* 6734.
129. Shibahara, T.; Kuroya, H. *Polyhedron* **1986,** *5,* 357.
130. Shibahara, T.; Akashi, H. *Inorg. Synth.* **1992,** *29,* 260.
131. Shibahara, T.; Akashi, H.; Kuroya, H. *J. Am. Chem. Soc.* **1986,** *108,* 1342.
132. Katada, M.; Akashi, H.; Shibahara, T.; Sano, H. *J. Radioanal. Nucl. Chem. Lett.* **1990,** *145(2),* 143.
133. Shibahara, T.; Akashi, H.; Yamasaki, M.; Hashimoto, K. *Chem. Lett.* **1991,** 689.
134. Shibahara, T.; Yamasaki, M.; Akashi, H.; Katayama, T. *Inorg. Chem.* **1991,** *30,* 2693.

135. Shibahara, T.; Akashi, H.; Kuroya, H. *J. Am. Chem. Soc.* **1988,** *110,* 3313.
136. Akashi, H.; Shibahara, T. *Inorg. Chem.* **1989,** *28,* 2906.
137. Sakane, G.; Shibahara, T. *Inorg. Chem.* **1993,** *32,* 777.
138. Shibahara, T.; Yamada, T.; Kuroya, H.; Hills, E. F.; Kathirgamanathan, P.; Sykes, A. G. *Inorg. Chim. Acta* **1986,** *113,* L19.
139. Shibahara, T.; Akashi, H. *Inorg. Synth.* **1992,** *29,* 254.
140. Shibahara, T.; Yamasaki, M.; Sakane, G.; Minami, K.; Yabuki, T.; Ichimura, A. *Inorg. Chem.* **1992,** *31,* 640.
141. Shibahara, T.; Hattori, H.; Kuroya, H. *J. Am. Chem. Soc.* **1984,** *106,* 2710.
142. Yao, Y.; Akashi, H.; Sakane, G.; Shibahara, T.; Ohtaki, H. *Inorg. Chem.* **1995,** *34,* 42.
143. Shibahara, T.; Sakane, G.; Mochida, S. *J. Am. Chem. Soc.* **1993,** *115,* 10408.
144. Shibahara, T.; Yamasaki, M.; Watase, T.; Ichimura, A. *Inorg. Chem.* **1994,** *33,* 292.
145. Cotton, F. A.; LLusar, R. *Polyhedron* **1987,** *6,* 1741.
146. Cotton, F. A.; Kibala, P. A.; Miertschin, C. S. *Inorg. Chem.* **1991,** *30,* 548.
147. (a) Ferorov, V. Ye.; Mironov, Yu. V.; Kuz'mina, O. A.; Fedin, V. P. *Zh. Neorg. Khim* **1986,** *31,* 2476.; *Russ. J. Inorg. Chem. (Engl.)* **1986,** *31,* 1429; (b) Marcoll, J.; Rabenau, A.; Mootz, D.; Wunderlich, H. *Rev. Chem. Miner.* **1974,** *11,* 607.
148. (a) Shibahara, T.; Kuroya, H.; Matsumoto, K.; Ooi, S. *Inorg. Chim. Acta* **1986,** *116,* L25; (b) Sharp, C.; Sykes, A. G. *J. Chem. Soc., Dalton Trans.* **1988,** 2579.
149. Müller, A.; Eltzner, W.; Bogge, H.; Jostes, R. *Angew. Chem. Int. Ed. Engl.* **1982,** *21,* 795.
150. Bandy, J. A.; Davies, C. E.; Green, J. C.; Green, M. L. H.; Prout, K.; Rodgers, D. P. S. *J. Chem. Soc., Chem. Commun.* **1983,** 1395.
151. Müller, A.; Eltzner, W.; Clegg, W.; Sheldrick, G. M. *Angew. Chem. Int. Ed. Engl.* **1982,** *21,* 536.
152. Martinez, M.; Ooi, B.-L.; Sykes, A. G. *J. Am. Chem. Soc.* **1987,** *109,* 4615.
153. Ooi, B.-L.; Sharp, C.; Sykes, A. G. *J. Am. Chem. Soc.* **1989,** *111* 125.
154. Shibahara, T.; Kuroya, H.; Matsumoto, K.; Ooi, S. *J. Am. Chem. Soc.* **1984,** *106,* 789.
155. (a) Shibahara, T.; Kuroya, H.; Matsumoto, K.; Ooi, S. *Inorg. Chim. Acta* **1986,** *116,* L2; (b) Li, J.; Lang, J.; Xin, X.; Yu, K. *Gaodeng Xuexiao Xuaxue Xuebao* **1992,** *13,* 1173.
156. Müller, A.; Krickemeyer, E.; Bogge, H.; Clegg, W.; Sheldrick, G. M. *Angew. Chem., Int. Ed. Engl.* **1982,** *22,* 1006.
157. Dudis, D.; Fackler, J. P. *Inorg. Chem.* **1982,** *12,* 3578.
158. Block, H. D.; Allman, R. *Cryst. Struct. Commun.* **1975,** *4,* 53.
159. Davis, B. R.; Bernal, I.; Kopf, H. *Angew. Chem., Int. Ed. Engl.* **1971,** *10,* 921.
160. (a) Coucouvanis, D.; Draganjac, M. *J. Am. Chem. Soc.* **1982,** *104,* 6820; (b) Draganjac, M., Ph.D. thesis, University of Iowa, 1983.
161. (a) Coucouvanis, D.; Draganjac, M.; Koo, S.-M.; Toupadakis, A.; Hadjikyriacou, A. I. *Inorg. Chem.* **1992,** *31,* 1186; (b) Lin, Q.; Huang, L.; *Chin. Chem. Lett.* **1990,** *1,* 121.
162. (a) Rappe, A. K.; Goddard, W. A. III *J. Am. Chem. Soc.* **1980,** *102,* 5115; (b) Rappe, A. K.; Goddard, W. A. III *J. Am. Chem. Soc.* **1982,** *104,* 448.
163. Gattow, G.; Behrendt, W. "Topics in Sulfur Chemistry"; Greorg Thieme Publ.: Stuttgart, **1977;** Vol. 2, p. 173.
164. Coucouvanis, D.; Fackler, J. P. Jr. *J. Am. Chem. Soc.* **1967,** *89,* 1346.
165. (a) Giolando, D. M.; Rauchfuss, T. B.; Rheingold, A. L.; Wilson, S. R. *Organometallics* **1987,** *6,* 667; (b) Darkwa, J.; Giolando, D. M.; Jones-Murphy, C.; Rauchfuss,

T. B. *Inorg. Synth.* **1990,** *27,* 51; (c) Bolinger, C. M.; Rauchfuss, T. B.; Rheingold, A. L. *J. Am. Chem. Soc.* **1983,** *105,* 6321; (d) Muller, E. G.; Petersen, J. L.; Dahl, L. F. *J. Organomet. Chem.* **1976,** *111,* 91; (e) Seyferth, D.; Henderson, R. S. *J. Organomet. Chem.* **1979,** *182,* C39; (f) Rauchfuss, T. B.; Rogers, D. P. S.; Wilson, S. R. *Am. Chem. Soc.* **1986,** *108,* 3114.

166. Coucouvanis, D.; Swenson, D.; Stremple, P.; Baenziger, N. C. *J. Am. Chem. Soc.* **1979,** *101,* 3392.

167. Kanatzidis, M. G.; Coucouvanis, D. *Inorg. Chem.* **1984,** *23,* 403.

168. (a) Schrauzer, G. N.; Mayweg, V. P. *J. Am. Chem. Soc.* **1965,** *87,* 483; (b) Wing R. M.; Tustin, G. C.; Okamura, W. H. *J. Am. Chem. Soc.* **1970,** *92,* 1935.

169. (a) Halbert, T. R.; Pan, W.-H.; Stiefel, E. I. *J. Am. Chem. Soc.* **1983,** *105,* 5476; (b) Pilato, R. S.; Eriksen, K. A.; Greaney, M. A.; Stiefel, E. I.; Goswami, S.; Kilpatrick, L.; Spiro, T. G.; Taylor, E. C.; Rheingold, A. L. *J. Am. Chem. Soc.* **1991,** *113,* 9372.

170. (a) McCleverty, J. A.; Locke, J.; Ratcliff, B.; Wharton, E. *Inorg. Chim. Acta* **1969,** *3,* 283; (b) Stiefel, E. I.; Bennett, L. E.; Dori, Z.; Crawford, T. H.; Simon, C.; Gray, H. B. *Inorg. Chem.,* **1970,** *9,* 281; (c) Oku, H.; Ueyama, N.; Kondo, M.; Nakamura, A. *Inorg. Chem.* **1994,** *33,* 209; (d) Oku, H.; Ueyama, N.; Nakamura, A. *Inorg. Chem.* **1995,** *34,* 3667; (e) Oku, H.; Ueyama, N.; Nakamura, A.; Kai, Y.; Kanhisa, N. *Chem. Lett.* **1994,** 607; (f) Yoshinaga, N.; Ueyama, N.; Okamura, T.; Nakamura, A. *Chem. Lett.* **1990,** 1655; (g) Ueyama, N.; Kamabuchi, K.; Nakamura, A. *J. Chem. Soc., Dalton Trans.* **1985,** 635; (h) Ueyama, N.; Kamabuchi, K.; Nakamura, A. *J. Chem. Soc., Dalton Trans.* **1990,** 387.

171. (a) Ueyama, N.; Oku, H.; Nakamura, A. *J. Am. Chem. Soc.* **1992,** *114,* 7310; (b) Das, S. K.; Chandhuri, P. K.; Biswas, D.; Sarkar, S. *J. Am. Chem. Soc.* **1994,** *116,* 9061; (c) Boyde, S.; Ellis, S. R.; Garner, C. D.; Clegg, W. *J. Chem. Soc., Chem. Commun.* **1986,** 1541; (d) Subramanian, P.; Burgmayer, S.; Richards, S.; Szalai, V.; Spiro, T. G. *Inorg. Chem.* **1990,** *29,* 3849.

172. Bolinger, C. M.; Rauchfuss, T. B. *Inorg. Chem.* **1982,** *21,* 3947.

173. (a) Soricelli, C. L.; Szalai, V. A.; Burgmayer, S. J. N. *J. Am. Chem. Soc.* **1991,** *113,* 9877; (b) Eagle, A. A.; Harben, S. M.; Tiekink, E. R. T.; Young, C. G. *J. Am. Chem. Soc.* **1994,** *116,* 9749.

174. Kim, C. G.; Coucouvanis, D. *Inorg. Chem.* **1993,** *32,* 2232.

175. Kim, C. G.; Coucouvanis, D. *Inorg. Chem.* **1993,** *32,* 1881.

176. (a) Tullius, T. D.; Kurtz, D. M., Jr.; Conradson, S. D.; Hodgson, K. O. *J. Am. Chem. Soc.* **1979,** *101,* 2776; (b) Hille, R.; George, G. N.; Eidsness, M. K.; Cramer, S. P. *Inorg. Chem.* **1989,** *28,* 4018; (c) Turner, N. A.; Bray, R. C.; Diakun, G. P. *Biochem.* **1989,** *260,* 563.

177. Hille, R. In *Molybdenum Enzymes, Cofactors, and Model Systems;* ACS Symposium Series 535; Stiefel, E. I., Coucouvanis, D., and Newton, W. E., Eds.; 1993, 22–37.

178. Fish, K. M.; Massey, V.; Sands, R. H.; Dunham, W. R. *J. Biol. Chem.* **1990,** *265,* 19665.

179. Howes, B. D.; Bennett, B.; Bray, R. C.; Richards, R. L.; Lowe, D. J. *J. Am. Chem. Soc.* **1994,** *116,* 11624.

180. C. G. Kim and D. Coucouvanis, to be published.

181. Turner, N. A.; Bray, R. C.; Diakun, G. P. *Biochem. J.* **1989,** *260,* 563.

182. Howes, B. D., Bray, R. C.; Richards, R. L.; Turner, N. A.; Bennett, B.; Lowe, D. J. *Biochemistry* **1996,** *35,* 1432.

ADVANCES IN INORGANIC CHEMISTRY, VOL. 45

THE TRANSITION METAL ION CHEMISTRY OF LINKED MACROCYCLIC LIGANDS

LEONARD F. LINDOY

School of Chemistry, University of Sydney, Sydney NSW 2006, Australia

I. Introduction

In recent times there has been a trend toward the synthesis of larger molecular entities that are multicomponent in nature. One category of this type involves linked macrocyclic ligand ring systems. Macrocyclic systems often show unique complexation properties; for example, they usually give rise to very kinetically and thermodynamically stable complexes and hence retain their integrity under a variety of conditions (*1*). In this review the transition metal ion chemistry of linked macrocyclic ring systems will be discussed. Linked macrocyclic systems that are capable of binding simultaneously to two or more metal ions yield the prospect of generating unusual electronic, catalytic, and/or redox properties (associated with the proximity of the metal centers). Heterometallic complexes are also a possibility and if rigid spacers are employed then the distance between metal centers can be tuned. The latter may enable the selective control of electronic properties. Further, such complexes are of interest as potential models for charge transfer, electron transport, and other processes found in a number of metal-containing natural systems such as the active sites of particular di- or polynuclear proteins (*2*).

0898-8838/98 $25.00

Many covalently linked bis(macrocyclic) ligands incorporating synthetic rings have now been reported and a number of linked porphyrin systems are also known (*3*); however, compounds of this latter type are not discussed in this review. A monograph by Bradshaw *et al.* has comprehensively reviewed the synthetic procedures for obtaining aza-containing macrocyclic and bis(macrocyclic) ligands (*4*) and less emphasis is given to this aspect in the present discussion.

A range of bis(crown) and bis(azacrown) rings have also been synthesized but the metal ion chemistry of these species has largely involved the alkali and alkaline earth metals (*5*). As such, such systems fall outside of the scope of the present review.

Interest in linked macrocyclic ligands has increased very greatly by the finding that bis(cyclam) derivatives (*6*) [including nickel and zinc metal complex derivatives (*7*)], incorporating either alkyl or aromatic linking groups between the rings, are effective in inhibiting several strains of human immunodeficiency virus type 1 (HIV-1) and type 2 (HIV-2) with low levels of cytotoxicity. Interaction with the bis(macrocycle) species was shown to occur at an early stage in the HIV reproduction cycle.

II. Linked Aza Macrocyclic Ring Systems

A. Linked Triaza Ring Systems

Examples of linked cyclic amine systems have been known for a considerable time. For example, the synthesis of the bis-linked system (**1**; $n = 2$), consisting of two potentially tridentate macrocycles, was reported in 1977 (*8*). Potentiometric measurements have been employed to obtain the stability constants for the 1:1 complexes of this ligand system with Mn(II), Ni(II), Co(II), Zn(II), and Cd(II). All these metals are bound strongly, with the binding constants varying from a log K_{ML} value of 15.0 for the Mn(II) species to 21.5 for the Ni(II) species. Although the respective structures are not

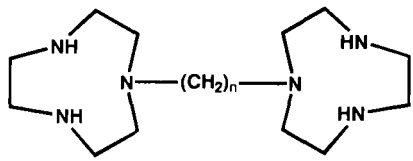

(1)

discussed by the authors, there seems little doubt that **1**(n = 2) acts as a sexadentate ligand toward each of these metals under the conditions employed. The flexibility of the ligand should allow coordination to a single metal, whereby all chelate rings will be five-membered.

Subsequent studies by Wieghardt *et al.* (*9*) were successful in using **1**(n = 2) to obtain dinuclear complexes in which the ligand occupied three facial coordination sites on each of two metal centers—a mode of coordination well documented to occur for the single ring analogue, 1,4,7-triazacyclononane (*10*). In the course of these studies, a range of stable mononuclear complexes of type $[ML]^{n+}$ [M = Cr(III), Mn(II), Fe(III), Co(III), Ni(II), Ni(III), Cu(II), and Zn(II)] were isolated as their bromide, hexafluorophosphate, or perchlorate derivatives. Spectrophotometric measurements were in accord with the adoption of a distorted octahedral geometry for each of the complex cations. An electrochemical study indicated that the Ni(III) species is a strong one-electron oxidant. The structure of low-spin $[FeL]Br_3 \cdot 4H_2O$ has since been shown to be monomeric (Fig. 1) (*11*).

Reaction of **1** with the metal carbonyls of chromium, molybdenum, and tungsten in dimethylformamide (DMF) gives air-stable, binuclear complexes of type $[(CO)_3MLM(CO)_3]$ (*9*). These proved to be useful starting species for generating (via oxidative decarbonylation reac-

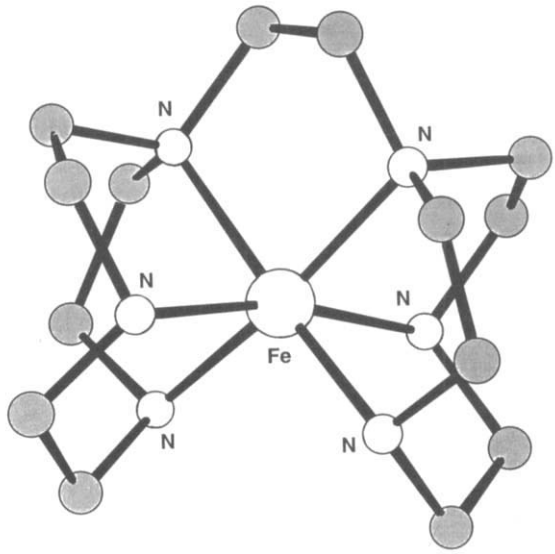

FIG. 1. The structure of the complex cation in $[FeL]Br_3 \cdot 4H_2O$.

tions) related binuclear species containing the metals in higher oxidation states. For example, $[CO]_3CrLCr(CO)_3$ reacts with bromine in chloroform to yield $[Br_3CrLCrBr_3]$. However, the related complexes $[Cl_3MLMCl_3]$ [M = Cr(III), Fe(III), and Co(III)] are generated on direct reaction of **2** with the corresponding metal chloride in a 1:2 (ligand:metal) ratio. The divalent metal species $[Cl_2CuLCuCl_2]$ and $[Cl_2MnLMnCl_2]$ were also prepared by direct means.

If $Mn(ClO_4)_2$ is reacted with **1** in alkaline solution in the presence of air, a black precipitate of the oligomeric oxo-bridged species, $[Mn_4(L)_2O_6](ClO_4)_4$, forms. This unusual (Mn(IV) species has been assigned an adamantane-like structure.

The synthesis of the related bis(macrocycle) incorporating a three-carbon bridge between the two 1,4,7-triazacyclononane rings has also been reported (*12*) as well as, in a separate study, an efficient procedure for incorporating longer linkages between the rings (*13*). The latter procedure is also applicable to the preparation of analogous linked 1,5,9-triazacyclododecane macrocyclic systems. Subsequently, Sessler *et al.* (*14*) published a further synthesis for the bis(1,4,7-triazacyclononane) derivative incorporating a four-methylene linkage between the nine-membered rings.

The formation of Cu(II) complexes with bis(1,4,7-triaza-1-cyclononyl) ligands incorporating tri- and tetramethylene bridging groups (*15*) has been investigated. Both ligands form stable 1:1 and 2:1 Cu(II) complexes. Potentiometric studies in aqueous media indicate that the 1:1 copper complex of the ligand incorporating a trimethylene bridge is more stable than its tetramethylene analogue (although the stabilities of these complexes differ by only 0.5 log K units); the reverse order applies for the 2:1 species (whose stabilities differ by 2.4 log units). Such behavior has been rationalized in terms of the relative ease of breaking a six- versus a seven-membered chelate ring in the respective monomeric 1:1 species, a process that must occur on formation of the dinuclear species.

The UV–vis spectra of the respective 1:1 and 2:1 complexes have been determined. Comparison of the spectra suggested that slightly

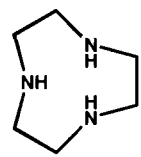

(2)

different coordination environments may be present in the 1:1 complexes whereas the 2:1 species clearly have similar environments.

Crystals of the Cu(II) chloride complexes of each ligand were obtained and were employed for X-ray diffraction studies. The structures of $[Cu_2LCl_4] \cdot 2H_2O$ (L = **1**; n = 3) and $[Cu_2LCl_4]$ (L = **1**; n = 4) are shown in Figs. 2 and 3, respectively. The Cu(II) ions in both complexes have five-coordinate geometries; two chloride ions and two secondary amine nitrogens occupy the base of a square pyramid that has the tertiary nitrogen in the apical position. The ligands adopt somewhat different conformations in each complex; the pair of chloride ions attached to the two Cu(II) are effectively syn for $Cu_2LCl_4 \cdot 2H_2O$ (L = **1**; n = 3) but anti for Cu_2LCl_4 (L = **1**; n = 4). The copper atoms are displaced 0.18 and 0.20 Å above the respective planes toward the axial amine groups. Related square pyramidal stereochemistries are found in the 1:1 Cu(II) chloride (*16*) and Cu(II) bromide complexes (*17*) of triazacyclononane. It is of interest that the Cu–Cu distances in $[Cu_2LCl_4] \cdot 2H_2O$ (L = **1**; n = 3) and $[Cu_2LCl_4]$ (L = **1**; n = 4) are 8.6 and 8.3 Å, respectively. Thus, for these systems the compound with the longer bridging chains shows, at least in the solid state, a shorter intramolecular metal–metal distance.

Linked complexes incorporating second-row transition ions have been prepared. In a comparative study, ruthenium complexes of mono- and dinuclear complexes of 1,4,7-triazacyclononane (**2**) and its ethane-linked derivative (**1**; n = 2) have been synthesized starting from $[Ru(DMSO)_4Cl_2]$ (where DMSO is dimethyl sulfoxide) (*18*). The resulting Ru(III) products are of type $[RuLCl_3]$ (L = **2**), $[Ru_2LCl_6]$ (L = **1**; n = 2), and $[Ru_2LBr_6]$ (L = **1**; n = 2). These products readily undergo hydrolytic conversion in aqueous sodium carboxylate or so-

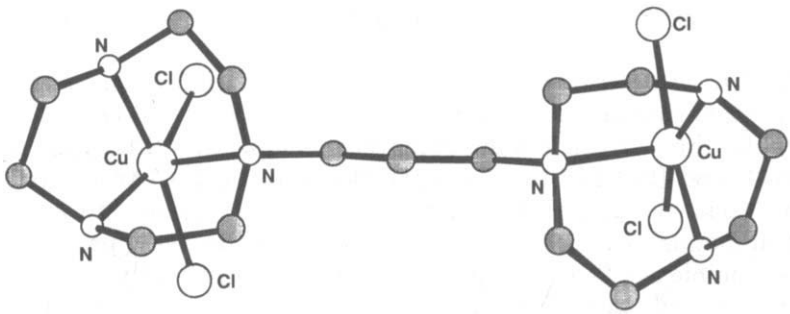

FIG. 2. The structure of $[Cu_2LCl_4]$ (L = **1**; n = 3).

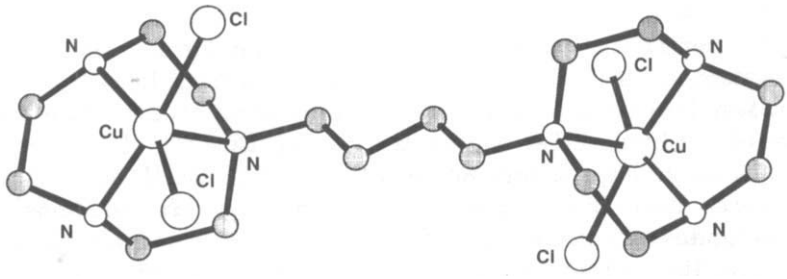

FIG. 3. The structure of $[Cu_2LCl_4]$ (L = **1**; n = **4**).

dium carbonate to hydroxo/oxo-bridged dinuclear species incorporating Ru(III) or Ru(III)/Ru(IV). In recent years the coordination chemistry of such oxo- or hydroxo-bridged dinuclear ruthenium species has been much studied. A motivation for this interest has been the discovery that in edge- and face-sharing dioctahedral compounds, the metal oxidation states can range between +2 and +5, and include mixed-valent species (*19*, *20*).

The formation of bridged dinucleating species of the above type can often be promoted by the use of a tridentate cyclic amine, such as **2**, as a "blocking group" for three facial sites on each metal ion; the process is further aided by the very considerable kinetic and thermodynamic stabilities of the macrocyclic species generated (*18*). The complexes $[Ru_2L(\mu\text{-}OH)_2(\mu\text{-}PhCO_2)][PF_6]_3$ (L = **1**; n = 2), $Ru_2L_2(\mu\text{-}OH)_2(\mu\text{-}CO_3)Br_2 \cdot 3.75H_2O$ (L = **2**), and $[Ru_2L)(\mu\text{-}O)_2(\mu\text{-}CO_3)]PF_6 \cdot 5H_2O$ (L = **1**; n = 2) have been isolated. The latter two have been investigated by X-ray diffraction and were shown to contain octahedral edge-sharing ruthenium units of types $Ru_2(\mu\text{-}OH)_2(\mu\text{-}CO_3)^{2+}$ and $Ru(\mu\text{-}O)_2(\mu\text{-}CO_3)^+$, respectively; the structure of $[Ru_2L(\mu\text{-}O)_2(\mu\text{-}CO_3)]^+$ (L = **1**; n = 2) is shown in Fig. 4. The Ru–Ru metal–metal distance in this latter cation is 2.469 Å. Binuclear Ru(IV) analogues of the above three complexes may be readily generated in solution using either chemical or electrochemical oxidation.

The linked tetra-N-methylated derivative (**3**) and its tri-N-methylated single-ring analogue (**4**) each react with $RhCl_3 \cdot 3H_2O$ in ethanol to yield the corresponding uncharged complexes: $[Rh_2Cl_6L] \cdot 2H_2O$ (L = **3**) and $[RhCl_3L]$ (L = **4**) (*21*). Because the 1,4,7-triazacyclononane backbone in both **3** and **4** will coordinate facially to an octahedral metal, structures in which this was the case were proposed for these complexes. If these species are then (individually) suspended in water and treated with sodium borohydride, followed by the addition of hexafluorophosphate anion, then red–brown crystals of

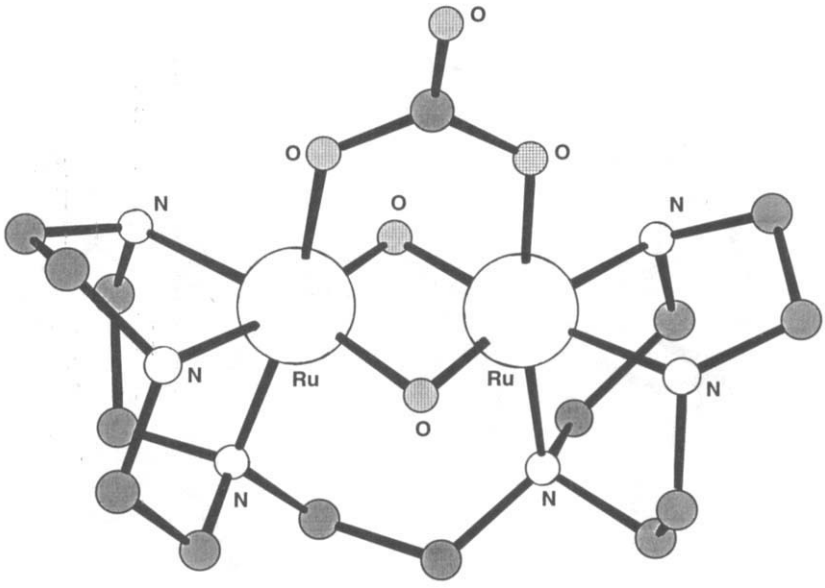

FIG. 4. The structure of $[Ru_2L(\mu\text{-}O)_2(\mu\text{-}CO_3)]^+$ (L = **1**; n = 2).

syn-$[Rh_2(H)_2(\mu\text{-}H)_2L](PF_6)_2$ (L = **4**) and *anti*-$[Rh_2(H)_2(\mu\text{-}H)_2L_2](PF_6)_2$ (L = **3**) form.

The X-ray structure of the latter complex (Fig. 5) shows that it contains a $[HRh(\mu\text{-}H)_2RhH]^+$ core. Both complexes may be considered classical rhodium hydride species, although they are of a less common variety in that the ancillary amine ligands are purely σ-donor in nature. The presence of the linkage in **3** is reflected in the ^1H NMR spectra of these complexes. At room temperature, the complex of **4** is fluctional whereas that of **3** is rigid.

The cyclic voltammograms for the above complexes each show a

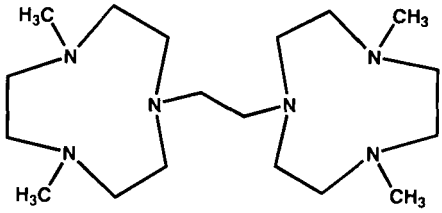

(3)

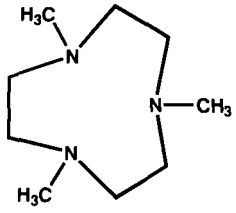

(4)

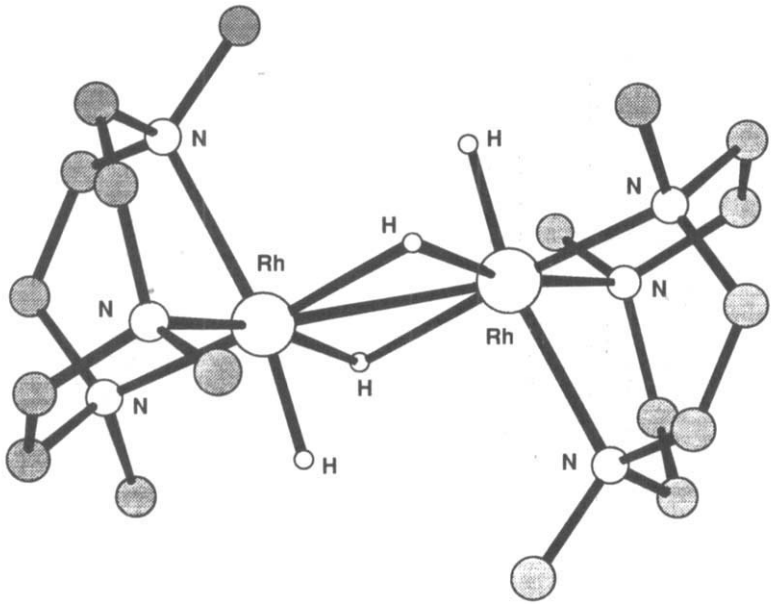

FIG. 5. The structure of *anti*-$[Rh_2(H)_2(\mu\text{-}H)_2L_2]^{2+}$ (L = **3**).

reversible one-electron transfer wave that was assigned to a one-electron reduction process. Thus in the case of **3** a mixed-valence Rh(II)/Rh(III) species is accessible electrochemically, although attempts to obtain such a complex in the solid state were unsuccessful.

The dinucleating pendant arm ligand (**5** in Fig. 6), incorporating 10 potential donor sites, has been synthesized and used to prepare the following complexes: $[Co_2(LH_4)(OH_2)_2](NO_3)_4 \cdot 5H_2O$, $[Ni_2(LH_4)(NCMe)_2](PF_6)_4 \cdot 4H_2O$, $[Zn_2(LH_4)(NO_3)_2](NO_3)_2$, and $[Cu_2(LH_2)](BPh_4)_2$ (where LH_4 = **5**) (*22*). The X-ray structures of each of these complexes have

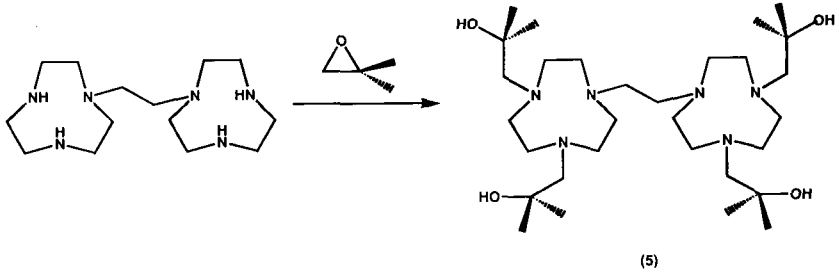

(5)

FIG. 6. Synthesis of a tetra alcohol pendant arm derivative.

been determined. All have anti (transoid) configurations except the Cu(II) species, which adopts a syn configuration and is accompanied by intramolecular hydrogen bonding. The structure of $[Co_2(LH_4)(OH_2)_2]^{4+}$ is shown in Fig. 7. Ligands such as **5** can be used to control the availability of vacant site(s) at a metal center by varying the number of pendant arms as well as the donicity of the cyclic core. In the present case, coordination to two octahedral metal ions will leave one vacant site at each metal center.

In the case of the Co(II) complex, the sixth coordination site on each metal is occupied by a water molecule. The stability toward oxidation of this complex is unusual because the Co(II) complex of the corresponding 1,4,7-triazacyclononane derivative, incorporating three pendant alcohol arms, readily oxidizes in air at neutral pH to form the corresponding Co(III) species (*23*).

The dark blue copper complex formed by reaction of Cu(II) acetate with **5** has the ligand bound in its doubly deprotonated form; protons have been lost from two of the pendant arm alcohol groups. This loss of an alcohol proton at each copper site is unusual in the complex of a divalent cation. This is particularly so in the present case because the complex was crystallized at neutral pH. Two O···H···O bridges are present between the two halves of the bound ligand dimer. Each copper site has a distorted square pyramidal coordination geometry.

The Wieghardt study discussed earlier (*9*) also encompassed the preparation of an acetato-bridged Fe(III) complex of **1**; (n = 2). Such

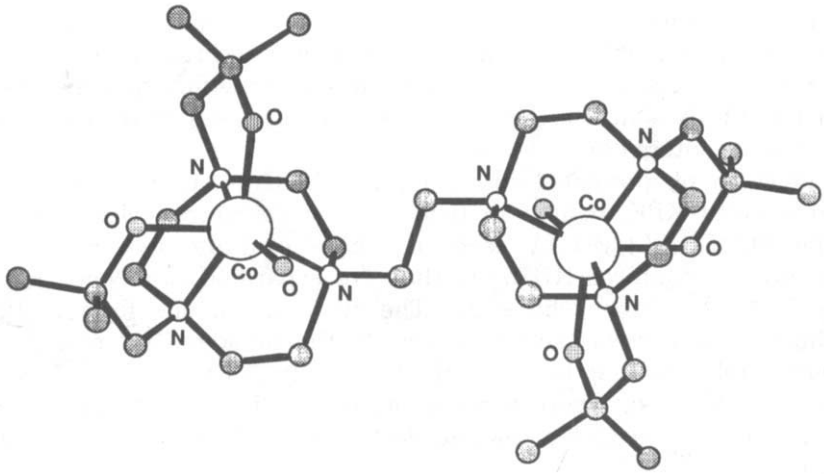

FIG. 7. The structure of $[Co_2(LH_4)(OH_2)]^{4+}$ (LH_4 = **5**).

species are of interest because oxo-bridged dinuclear Fe(III) cores occur at the active sites of a number of metalloproteins (including hemerythrin, ribonucleotide reductase, purple acid phosphatase, methane monooxygenase, and rubrerythrin).

The respiratory protein hemerythin (Hr) incorporates a triply bridged diiron core (*24*). In its deoxy form, two iron atoms are bridged by hydroxo and two carboxylate groups attached to the side chains of glutamate and aspartate residues, and five imidazole ligands cap the diiron core. This arrangement leaves one iron coordination site vacant for the binding of a dioxygen molecule. In oxyhemerythrin, dioxygen binds in the form of its hydroperoxide to the binuclear oxo-bridged Fe(III) core, which retains its bridging carboxylates and imidazole capping ligands.

It was postulated (*9*) that the use of **1**(n = 2) could result in stabilization of a hemerythrin model complex, incorporating a (μ-oxo)bis (μ-acetato)diiron(III) core. However, it was subsequently proposed (*25*) that this complex might be better formulated as a tetranuclear species. Based on this, it was suggested by Sessler *et al.* (*14*) that steric influences might favor the formation of a dinuclear species if the length of the link between the triaza rings was increased to four methylene groups. The preparation of the required ligand (**1**; n = 4) was carried out. However, this derivative was also found to yield an Fe(III) tetranuclear species, $[Fe_4O_2(acetato)_4L_2](PF_6)_4$ (L = **1**; n = 4), rather than stabilizing the required diiron core complex of the type present in hemerythrin. The structure of the tetranuclear species is shown in Fig. 8.

In an attempt to gain greater rigidity (and possibly, stability) of tetrameric complexes of the above type, it was decided to attempt the synthesis of the tetranuclear species in which the four acetates were replaced by two dicarboxylic acids of the required length to span adjacent iron centers (*26*).

Reaction of glutonic acid with $[Fe_2Cl_6L]$ (L = **1**; n = 4) in the presence of KPF_6 results in two forms of the tetranuclear species $\{[Fe_2O(C_5H_6O_4)_2L]_2\}(PF_6)_4$, each of which contains two (μ-oxo)bis (μ-carboxylato)diiron(III) cores that are separated from each other by 7.748 Å in the solid state. The structure of one form of this "dimer of dimers" is shown in Fig. 9; the arrangement present is very similar to that found in $[Fe_4O_2(acetato)_4L_2](PF_6)_4$ (L = **1**; n = 4). Despite this, electrochemical studies indicate that the former complex is more stable toward electrochemical reduction than the latter.

Based on the above results it appears that bis(macrocycle) ligands

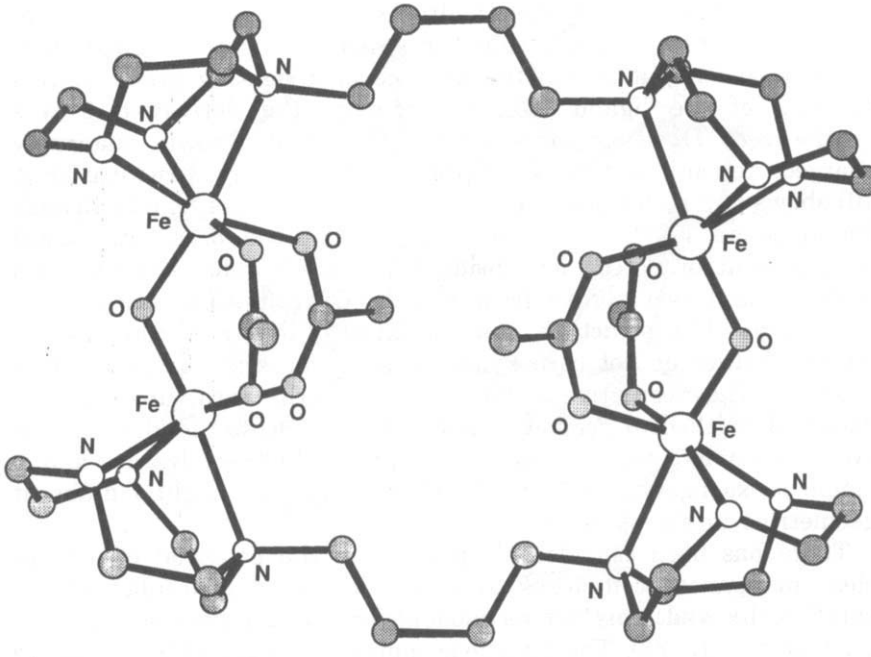

FIG. 8. The structure of $[Fe_4O_2(acetato)_4L_2](PF_6)_4$ (L = **1**; n = 2).

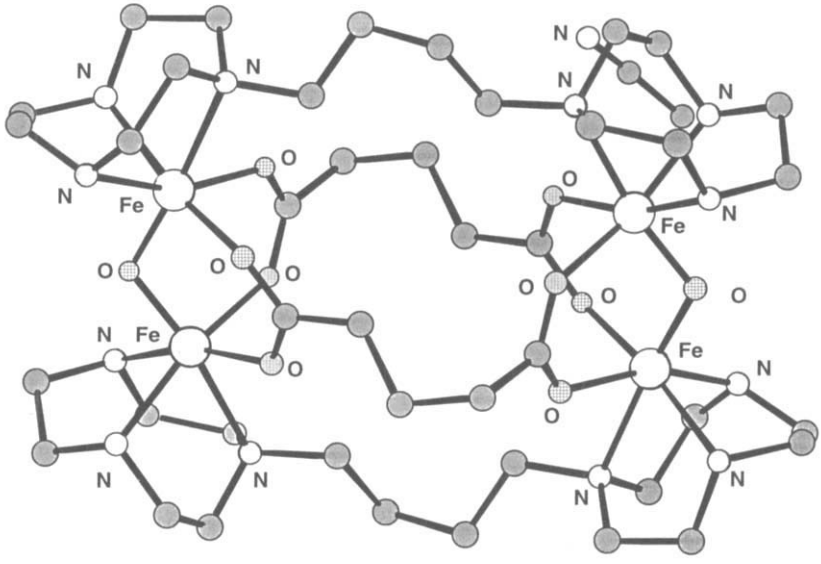

FIG. 9. The structure of one form of the cation $[Fe_2O(C_5H_6O_4)L]_2^{4+}$.

of type **1**, containing a flexible hydrocarbon linkage, tend to promote tetranuclear rather than dinuclear species. It was reasoned that, in part, this might reflect the absence of a ligating group in this bridging of the ligand (*26*). Accordingly, the derivative **6** was synthesized. However, once again, the yield was a quadruply charged, tetranuclear Fe(III) species whose X-ray structure (Fig. 10) shows two molecules of **6** acting as ditopic, heptadentate ligands bound to an Fe_4O_6 core. The core is composed of a tetrahedral arrangement of Fe(III) ions bridged by six oxygens (two oxo, two hydroxo, and two alkoxo from **6** (*27*). Overall, this core has an adamantane-like structure; it is of interest that a similar species forms whether or not carboxylate ions are present in the reaction mixture. The respective Fe(III) atoms in the structure adopt a distorted octahedral geometry made up of a facially binding triazacyclononone moiety, a μ-alkoxo group, a μ-hydroxo ligand, and a single μ-oxo ligand. The four N_3 rings adopt two slightly different geometries in the structure.

There has been considerable interest in the potential of polynuclear manganese complexes to oxidize water to molecular oxygen catalytically and thus act as models for the manganese center in photosystem II (*28*). The binuclear complex $[Mn_2L(\mu\text{-}OAc)_2]^{2+}$, where L = **7**, has been investigated using a number of techniques—including EPR, magnetic susceptibility measurements, and electrochemical measurements. The X-ray structure (Fig. 11) confirmed the presence of a mixed ("valence-trapped") Mn(II)/Mn(III) cation. Both manganese ions adopt a distorted octahedral coordination geometry, with each metal bound to the three nitrogens of one ring, a bridging phenoxy ion, and two oxygens from each of two bridging acetate groups. The adoption of this unusual geometry clearly reflects the inherent structural features of the bis(macrocyclic) ligand system (**7**). Electrochemical studies (in acetonitrile) indicated that the above mixed-valence species undergoes one-electron oxidation

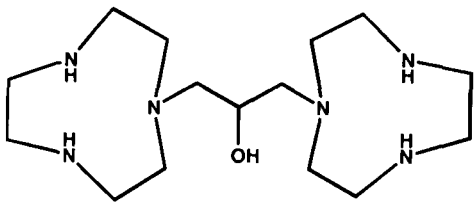

(6)

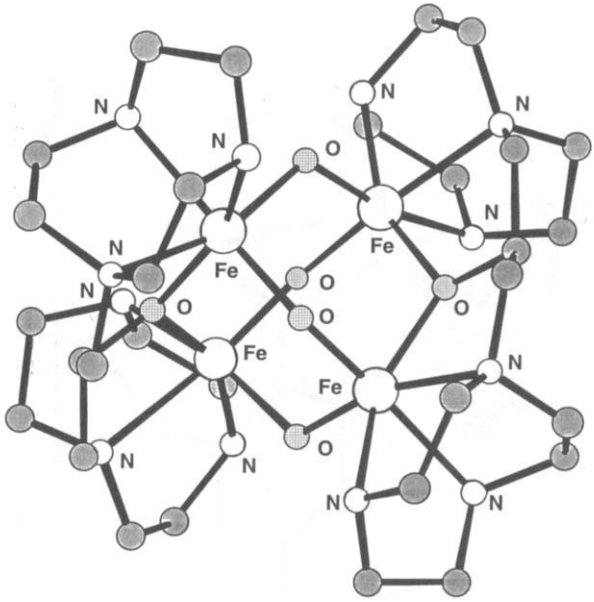

FIG. 10. The structure of tetranuclear Fe(III) complex of **6**.

as well as one-electron reduction to yield Mn(III)/Mn(III) and Mn(II)/Mn(II) species, respectively.

B. LINKED TETRAAZA AND HIGHER AZA RING SYSTEMS

A considerable number of linked tetraaza macrocyclic systems have now been reported. An early example, first isolated in low yield as its

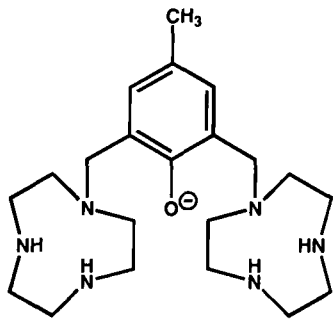

(7)

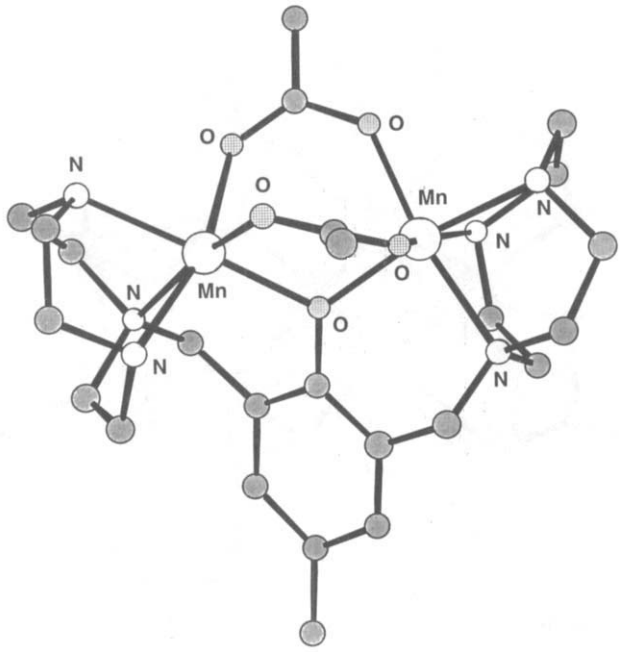

FIG. 11. The structure of $[Mn_2L(\mu\text{-acetato})_2^{2+}$.

di-Ni(II) iodide complex (**8**) (*29*), was formed by direct condensation of two molecules of the related monomeric nickel complex (**9**) (*30*).

The mechanism of formation of the dimer has been suggested to involve the combination of radicals generated at the γ position of the six-membered chelate ring derived from acetylacetone in **9** (*31*). That is, a one-electron oxidation of the monomeric complex takes place at the γ carbon followed by dimerization; further oxidation of the initial bridging C—C bond formed leads to formation of a C=C bond. The

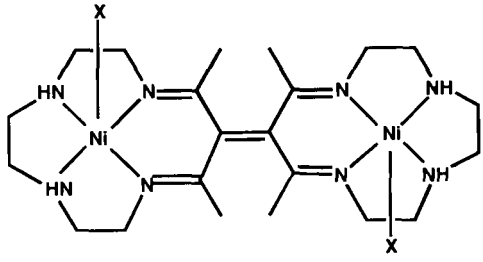

(8)

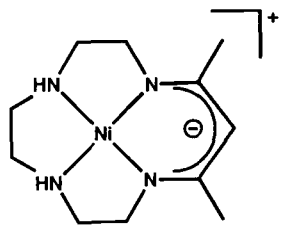

(9)

low yield obtained in the original preparation presumably reflects the occurrence of side reactions such as ligand dehydrogenation and/or oxidation. Indeed, reactions of this type have been documented for the oxidation of **9** with bromine (*32*).

An improved method for synthesizing the above dinuclear complex has been reported (*33*). Oxidation of **9** in deoxygenated acetonitrile using Fe(III) perchlorate gives the dinuclear species in approximately 70% yield. Cyclic voltametry on the starting Ni(II) monomeric complex, as well as on the corresponding Cu(II) complex, gave evidence for radical formation on oxidation. The crystal structure of the dinuclear Ni(II) complex, in which an acetonitrile ligand is coordinated to each nickel, has been determined. The configuration adopted by the ligand in this structure is quite similar to that found in the corresponding diiodide complex mentioned above (*29*). Steric interaction between the methyl substituents surrounding the double bond linkage joining the rings results in this link being quite strained. As a consequence, the respective double bonds in the dimer are almost completely localized.

A new family of bis(macrocyclic ligand) nickel complexes of type **10** has been synthesized (*34*). The procedure involved electrophillic substitution of **9** or its 14-membered analogue (*35*) at their respective γ carbons, using two difunctional electrophiles, terephthaloyl chloride or isophthaloyl chloride. This procedure was based on a previous study describing electrophillic attack by benzoyl chloride on the above starting complexes (*36*).

The visible spectra of each of the new (dinuclear) complexes confirmed the presence of a square planar coordination environment for the Ni(II) ions.

The related Fe(II) dinuclear complex of type **11** (L = acetonitrile) has been reported (*37*). This complex is generated by the reaction of 1,4,8,11-tetraazacyclotetradecane (cyclam) with $Fe(OH_2)_6(ClO_4)_2$ in

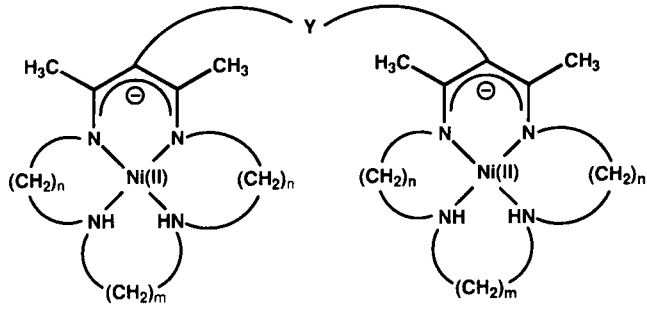

(10)

oxygenated acetonitrile. An X-ray study (Fig. 12) reveals that the iron atoms and the tetraimine moiety joining the two centers are essentially coplanar. The length of the C–C link between the rings is 1.41 Å; this corresponds to about 40% double bond character. Thus, unlike the complexes of **8**, delocalization of the double bond character occurs in this species.

The nature of the axial ligands in the low-spin complexes of types **11** and **12** has been shown to have a marked effect on the redox properties of the corresponding complexes (*38*). For example, for **12** (X = Cl), dioxygen removes an electron such that a valance-averaged, mixed-valence species with a charge of +5 is formed. However, for **11** (X = DMF), dioxygen attacks the C=C link to generate two doubly charged keto-β-diimine monomeric complexes. For X = CH_3CN in the presence of wet acetonitrile, oxidative dehydrogenation occurs to yield a new di-Fe(II) species with a charge of +4 incorporating two keto-β-diimine moieties, one at each end of the bis(macrocycle). Under other redox conditions, a number of other metal-containing products have

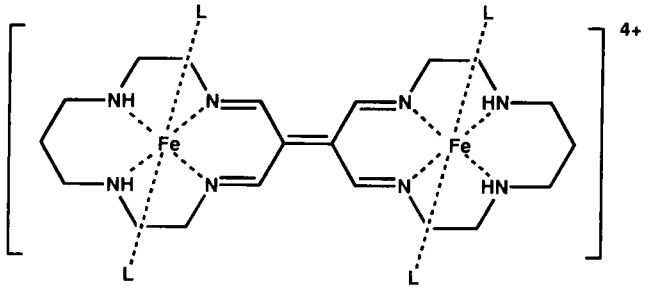

(11)

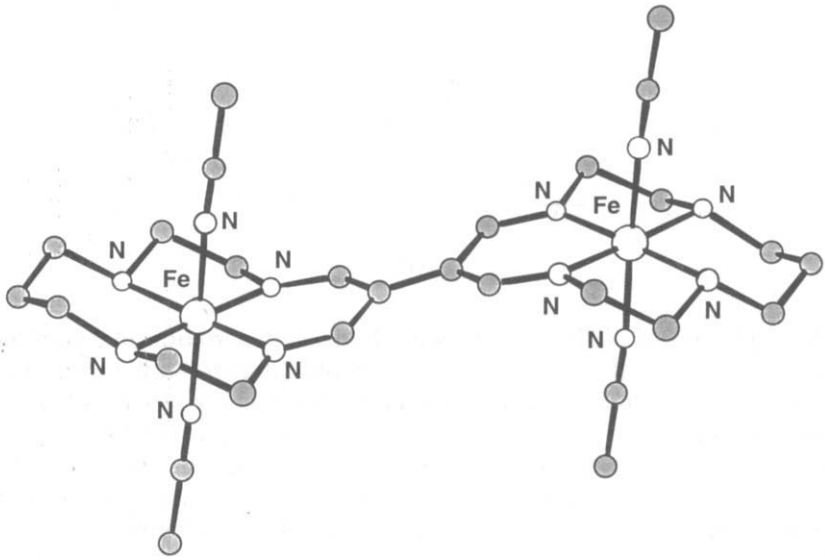

FIG. 12. The structure of the dinuclear Fe(II) complex of type **11**. Acetonitrile ligands occupy the axial coordination positions.

also been demonstrated to form. In a parallel study, the synthesis and properties of a ruthenium dinuclear mixed-valence complex has also been investigated (*39*).

McAuley and Xu (*40*) have investigated the formation and redox chemistry of the corresponding di-Ni(II) species (**13**). Although a number of previous studies have shown that the oxidation of the Ni(II) complex of cyclam produces corresponding Ni(III) species, under the conditions used in the present study the oxidation reaction was seen to proceed further. This dinuclear complex cation (**13**) results from

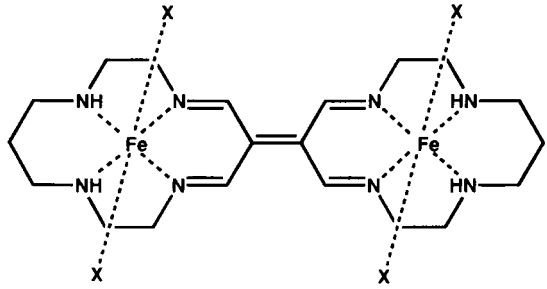

(12)

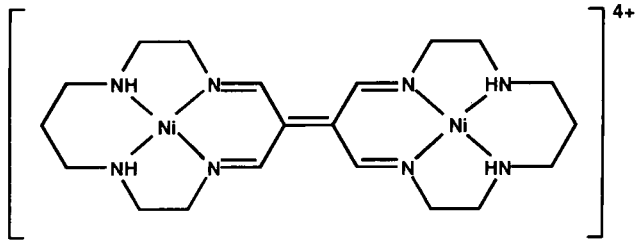

(13)

the oxidation of Ni(II) cyclam with hydrogen peroxide in acidic perchlorate media; it was isolated as its perchlorate salt. Once again, evidence for π-electron delocalization between the rings was obtained and the nature of the overall structure was confirmed by X-ray diffraction (Fig. 13). Each Ni(II) lies in the plane of its macrocyclic donors, with planarity being maintained across the carbon bridge framework. For this system, both chemical and electrochemical reduction were demonstrated to result in cleavage of the link between the macrocyclic rings, yielding a pair of mononuclear radical ions.

The Ni(II) complex of **14** is another system that has been shown to undergo dimerization on electrochemical oxidation (via π-cation radical formation). The dimerization process was found to be rapid in acetonitrile. The initial product (**15**) is readily deprotonated to yield **16** (*41*).

The versatility of this general procedure is further illustrated by the synthesis of the bis system (**17**) (*42*). This dinuclear complex was obtained by template condensation of the precursor complex, $[Ni_2L]$ {LH_4 = tetrakis[1-(3-methylisothiosemicarbazono)ethyl]-ethane}, with 3-ethoxyacrylaldehyde in DMF and followed by the usual oxidative coupling/deprotonation process. The X-ray structure of the diamag-

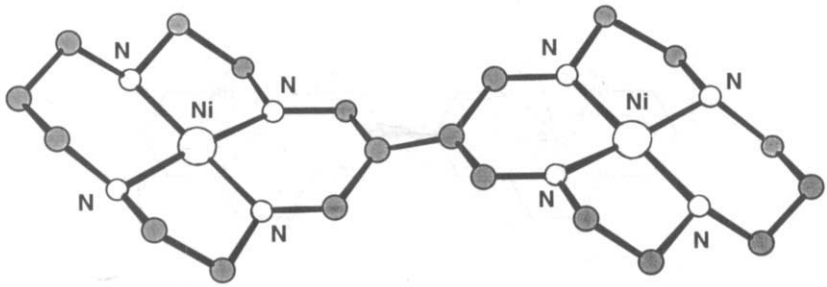

FIG. 13. The structure of the tetra cation **13**.

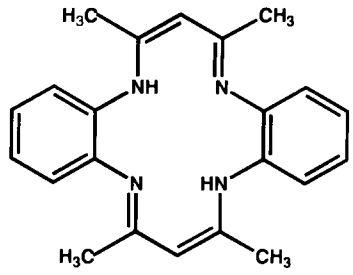
H3C
CH3
NH
N
N
HN
H3C
CH3

(14)

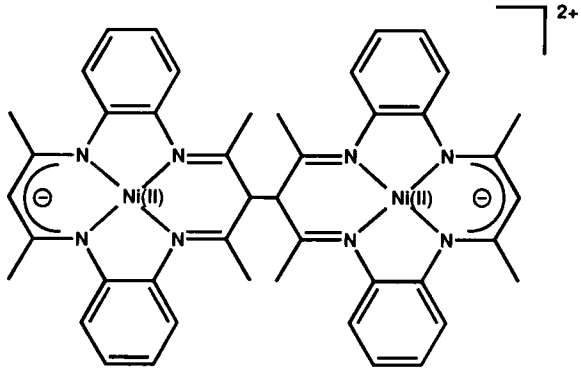
2+
N
N
Ni(II)
N
N
N
N
Ni(II)
N
N

(15)

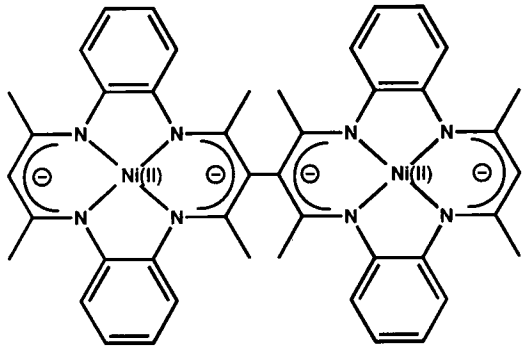
N
N
Ni(II)
N
N
N
N
Ni(II)
N
N

(16)

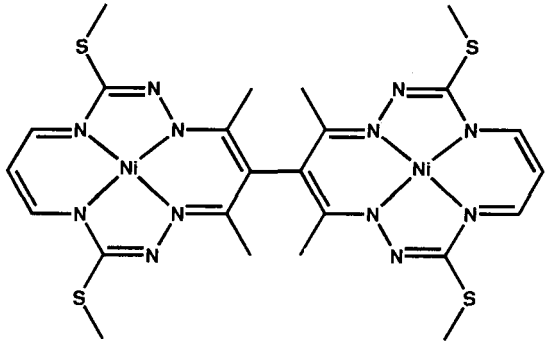

(17)

netic product (Fig. 14) has been obtained. Both macrocyclic components are equivalent and are orientated nearly perpendicular to each other (the dihedral angle between adjacent planes is 80.6°). The twist around the single C–C bonds largely reflects steric interactions between the appended methyl groups and effectively inhibits delocalization of the π systems between the rings.

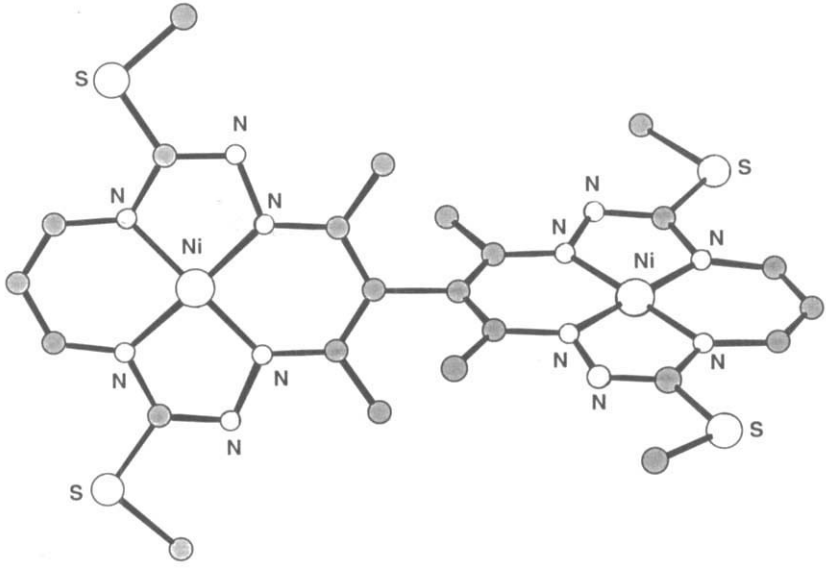

FIG. 14. The structure of **17**.

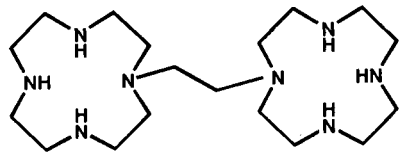

(18)

Ligand **18**, in which two 12-membered (cyclen) subunits are linked by a $-CH_2CH_2-$ bridge, yields a di-Cu(II) complex of type $[Cu_2L](ClO_4)_4$ (L = **18**) in which a weak ferromagnetic interaction between the Cu(II) sites is present (*43*).

There are a number of reports of studies involving dinucleating ligands incorporating linked subunits of the 14-membered ring, cyclam (or its derivatives). Linked systems based on cyclam are expected to yield complexes with d^n metals that show elevated kinetic and thermodynamic stabilities, because the latter are well-documented properties of the complexes of cyclam (*1*).

A small yield of the linked cyclam derivative (**19**) was identified as a minor product in the Ni(II) template synthesis of cyclam (*44*). It is noted that the two cyclam subunits are linked via carbons in their respective backbones; in general, this is expected to cause less perturbation of the coordination properties of the individual rings than would occur if the link was via nitrogen atoms in each ring. An X-ray structure of the nickel(II) perchlorate derivative, $[Ni_2L](ClO_4)_4$ (L = **19**), has been obtained. Each of the nickel ions in this complex is in a (low-spin) square planar environment, with both halves of the ligand adopting the low-energy trans III configuration (*45*).

Like $[Ni(cyclam)]^{2+}$, the above dinuclear nickel complex exists in aqueous solution as a mixture of low-spin, four-coordinated and high-spin, six-coordinated species, with the equilibrium between the two being dependent on the ionic strength. In the presence of excess per-

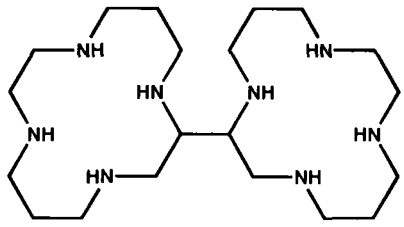

(19)

chlorate ion, the equilibrium is shifted toward the low-spin form. Thus, the presence of a direct linkage between individual cyclam rings in **19** does not appear to affect markedly this aspect of this ring's coordination behavior toward Ni(II).

The dimeric derivative of dioxocyclam (**20** in Fig. 15) has also been synthesized by means of a single-step reaction between the appropriate tetraester and linear tetraamine in a 1 : 2 molar ratio (*46*). This double-ring macrocycle complexes with two Cu(II) ions in aqueous solution, with the simultaneous release of four protons. EPR evidence indicates that the very stable di-Cu(II) complex exhibits weak metal–metal interaction. The Cu(II) ions were demonstrated to be readily oxidized to their trivalent state by means of two consecutive one-electron steps; the latter are separated by only approximately 100 mV. This is only slightly greater than the value of 36 mV expected from a purely statistical basis. Because many redox processes in organic and bioorganic chemistry involve two-electron single-step processes, the quasi-independent redox behavior of the two connected metal centers in the present system suggests that it may be considered as a potential two-electron redox reagent.

An investigation of the effect of ring size on ring-to-ring effects in dimetallic complexes of the above type has been carried out (*47*). The analogous bis(macrocyclic) ligand incorporating 13-membered subunits has been synthesized and its complexation behavior toward Cu(II) compared with that of the corresponding 14-membered ring species. A detailed potentiometric investigation of Cu(II) binding by both these ligand species has been performed. The incorporation of two Cu(II) ions into these bis(rings) involves three pH-controlled steps. In general, greater ring-to-ring effects are seen for the bis(13-membered system) and this was ascribed to the presence of less shielded electrostatic interactions between the metal centers in this case. In turn, this may indirectly reflect the lower coordination ability of the 13-membered subunit toward Cu(II) relative to the 14-membered analogue.

The neutral (fully deprotonated) di-Cu(II) complex of the bis(13-

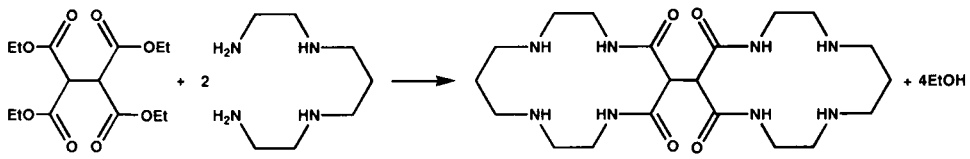

(20)

FIG. 15. The synthesis of a bis(dioxocyclam) derivative.

membered ring species) undergoes a reversible oxidation process via two one-electron steps; these are again separated by 100 mV, giving evidence for the presence of a small interaction between copper sites. As mentioned previously, similar behavior was observed for the bis(14-membered ring) system.

Reduction of **20** with diborane in bis(2-methoxyethyl)ether yields the bis(cyclam) derivative (**21**) (*48*). Addition of one equivalent of nickel(II) nitrate to an aqueous solution of **21** at pH 7, followed by one equivalent of copper(II) nitrate, is expected to result in a mixture of complexes in the proportion of 1:1:2 [di-Cu(II) complex: di-Ni(II) complex: Cu(II)/Ni(II) complex] (provided the two rings behave independently toward both metals). Separation of these three species was achieved by ion-exchange chromatography. Spectral and electrochemical investigations on the above binuclear complexes were undertaken. The visible spectra are very similar to those of the corresponding (mononuclear) cyclam complexes and, for example, the spectrum of the binuclear complex is virtually equal to the sum of the spectra of $[Cu(cyclam)]^{2+}$ and $[Ni(cyclam]^{2+}$. Despite this, electrochemical studies confirm the presence of a weak interaction between the coordinated metals in each dinuclear complex. This is manifested by a shift in the second oxidation potential [M(II) → M(III)] to a more positive value in each case.

The dinuclear species $[Ni_2L]^{4+}$ (L = **21**) has also been demonstrated to exist as an equilibrium mixture of yellow (low-spin) and blue (high-spin) forms in aqueous solution, further demonstrating the parallel between the metal-ion chemistry of the present binuclear species relative to that of cyclam.

The EPR spectra of $[Cu(cyclam)]^{2+}$ and $[CuNiL]^{4+}$ (L = **21**) in a water/DMF glass at ~120°C are almost identical, indicating that any interaction between the metals in the binuclear complex is not strong. Both spectra are typical of the presence of axial symmetry and show a $g_{\|}$ signal that is split into a quartet by the hyperfine coupling constant of the copper.

The relative electrocatalytic abilities of $[Ni(cyclam)]^{2+}$ and $[Ni_2L]^{4+}$

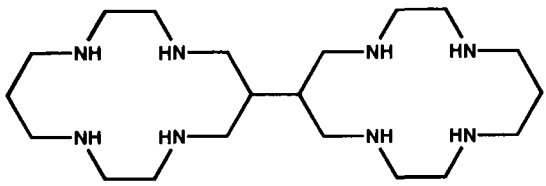

(21)

(L = **21**) toward CO_2 and H_2O reduction have been investigated (*49*). Because the latter complex possesses two metal sites, the prospect that these could bind two substrates simultaneously in such a manner that different reaction products might result {relative to the use of $[Ni(cyclam)]^{2+}$} was considered. In particular, for CO_2 activation, the possibility that the dinuclear species might favor a coupling reaction to yield a C_2 product provided a motivation for the study. Namely, it was thought feasible that the proposed sequence would involve the reduction of the nickel centers, leading to simultaneous reaction with two CO_2 molecules and formation of a C–C bond. However, on electroreduction, both the mononuclear and binuclear compounds were found to react similarly with CO_2 in aqueous media, yielding only a C_1 product (CO); no coupling reaction was observed with the binuclear complex. A feature of both systems is that they are exceptionally selective in reducing CO_2, i.e., no product other than CO is produced. On the other hand, the systems differ with regard to the electroreduction of water to produce hydrogen. The dinuclear species was found to be a much more efficient catalyst for this potentially important reaction than is $[Ni(cyclam)]^{2+}$.

The electrocatalytic capabilities of the above type of bis(macrocycle) have been the subject of further study (*50*). In this extension, the effect of replacing the 14-membered rings of **21** with 13-membered rings was investigated. The corresponding binucleating systems incorporating two 13-membered rings (**22**), as well as one 13- and one 14-membered ring (**23**), were synthesized using procedures related

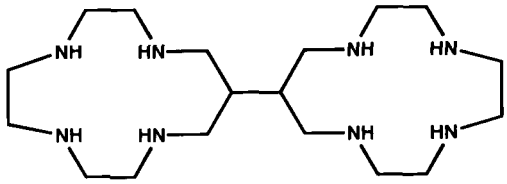

(22)

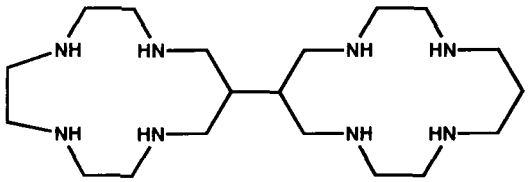

(23)

to that employed previously for the bis(cyclam) species (**21**) (*48*). The relative behavior of the di-Ni(II) complexes of each of the above bis(macrocycles), along with those of **21**, was then studied with regard to serving in electrocatalysis for hydrogen generation. Not surprisingly, the spectral and electrochemical properties of the dinickel complex of the mixed-ring-size ligand (**23**) seemed characteristic of both the 13- and 14-membered ring systems. Each dimetallic system was demonstrated to serve as an electrocatalyst for hydrogen production; the efficiency, at -1.5 V, for the respective dinuclear Ni(II) complexes followed in the ligand order of (14–14) > (13–14) ≫ (13–13). The efficiency thus drops as 13-membered rings replace 14-membered rings.

The related bis(macrocyclic ligand) Ni(II) complex (**24**), incorporating the meso–meso form of the ligand, has also been synthesized—this time from the corresponding monomeric Ni(II) complex (**9**) by again taking advantage of the reactivity of the γ-carbon position (*51*). Oxidative coupling was achieved with Fe(III) in acetonitrile and this was followed by reduction of the resulting imine-containing intermediate with sodium borohydride. The dinuclear Ni(II) species (**24**) formed is a significantly better catalyst for carbon dioxide reduction than is its corresponding mononuclear (single-ring) derivative (**25**). It is also superior to the corresponding bis(cyclam) species (**21**), even though the latter incorporates the same bis(macrocycle) skeleton (but without the methyl substituents).

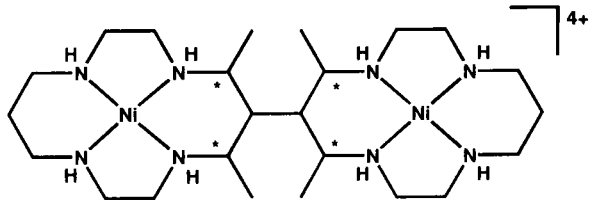

(24)

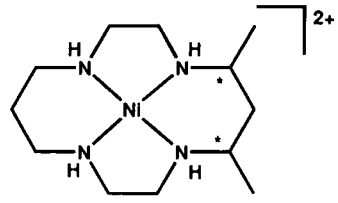

(25)

A complex of type $[Ni_2L](ClO_4)_4 \cdot 4H_2O$ has been isolated containing the xylyl-bridged biscyclam (**26**) (*52*). Under the conditions employed, cyclic voltammetry gave no evidence for any interaction between the bound nickel centers in this complex. However, in the presence of CO_2, electrocatalytic reduction of this species to CO appears to be promoted. The X-ray structure of the di-Ni(II) complex confirms that the metal sites are widely separated. Each cyclam ring is held in a stable trans III square planar arrangement with the nickel occupying the central cavity; no unusual bond distances or angles are present. The respective cyclam coordination planes are almost parallel and are orientated on opposite sides of the bridging xylyl group.

It is noted that the general procedure (involving the corresponding bi-dioxomacrocycle as precursor) has been employed for the synthesis of the pentaaza ligands of type **27** (*53*). In this study, protonated forms of **27** were demonstrated to form 1:1 complexes with a range of anions, including citrate^{3-}, AMP^{2-}, ATP^{4-}, HPO_4^{2-}, $[Fe(CN)_6]^{4-}$, and $[Fe(CN)_6]^{3-}$ anions.

A novel procedure for the production of bis(polyazamacrocycles) has recently been reported. Bis(chromium) alkoxycarbene complexes incorporating bridging alkoxy groups have been shown to undergo photochemical cycloaddition to protected imidazolines to yield protected bis(azapenams) (*54*). Deprotection, followed by acid treatment, leads to selective dimerization to produce bis(dioxocyclams) that are bridged at either end with 4-, 5-, 6-, or 12-atom α,ω-diol links. A representative example is given by **28**. These bis(oxocyclam) products were shown to form both mononuclear and dinuclear Ni(II) complexes. The structure of the 5-atom, doubly bridged complex of **28** has been confirmed by X-ray crystallography (Fig. 16).

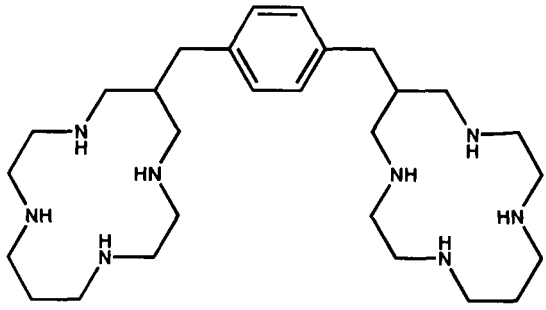

(26)

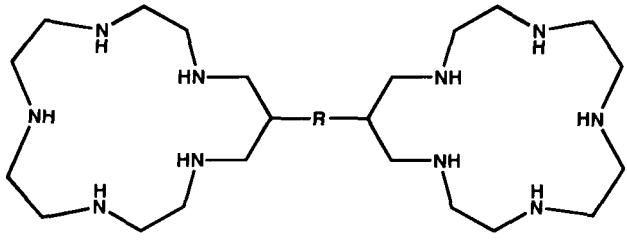

(27)

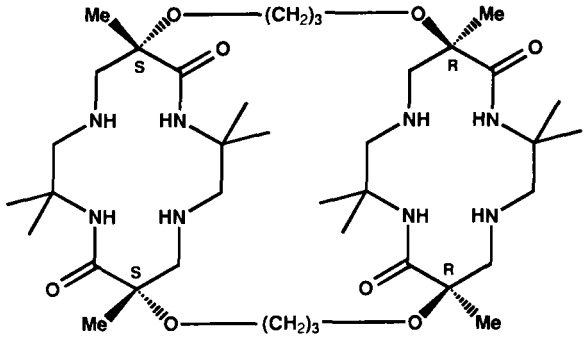

(28)

The characterization of a series of Cu(II) complexes of the binucleating bis(isocyclam) ligands of type **29**, in which a flexible linear polymethylene chain (n = 2–4) links a nitrogen of each macrocyclic ring, has been reported (*55*). These species were obtained by detosylation of the corresponding protected macrocycles (Fig. 17). The complexes are of type $Cu_2LX_4 \cdot xH_2O$ (where X = ClO_4 or NCS). The magnetic moments of all complexes are normal. Nevertheless, the hyperfine structure of the EPR spectra in frozen DMF clearly demonstrated the presence of magnetic coupling between the Cu(II) ions.

In an independent study, Kaden *et al.* (*56*) have also undertaken an

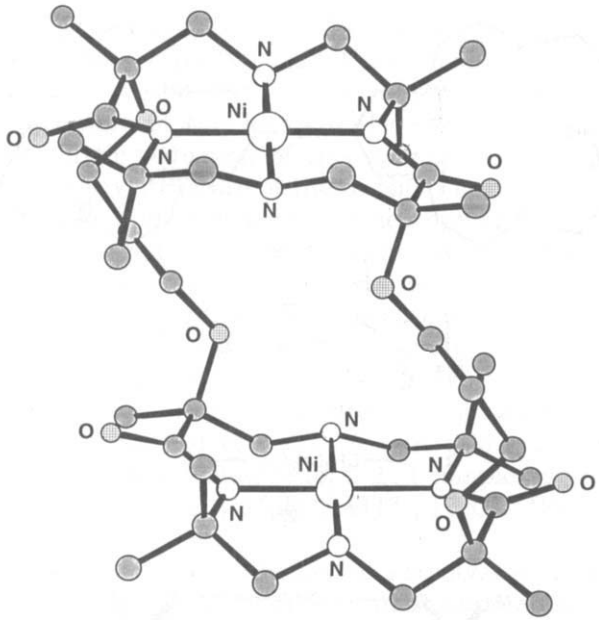

FIG. 16. The structure of the doubly bridged dinuclear Ni(II) complex **28**.

investigation of the complexation of both **29** (n = 2) and the related xylyl bridged species (**30**) toward Ni(II) and Cu(II). Both ligand species were demonstrated to yield complexes of type $[M_2L]^{4+}$. Spectrophotometric titration of **29** (n = 2) or **30** with Cu^{2+} at constant pH also confirmed the formation of binuclear species. The slopes of the respective titration plots remained constant between 0 and 2 equivalents of Cu(II), indicating that both copper sites give rise to analogous spectral properties; a sharp end point was observed at 2 equivalents of Cu(II) in each case. The visible spectra of the respective Ni(II) and Cu(II) complexes suggest that the metals in these derivatives are in square planar environments. EPR studies on the Cu(II) species con-

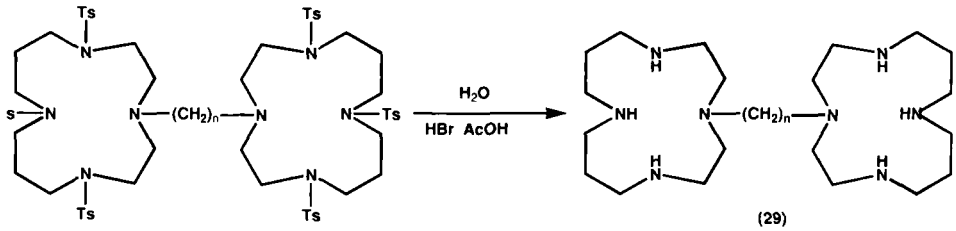

FIG. 17. The synthesis of linked isocyclam derivatives via detosylation of the tosylated precursors.

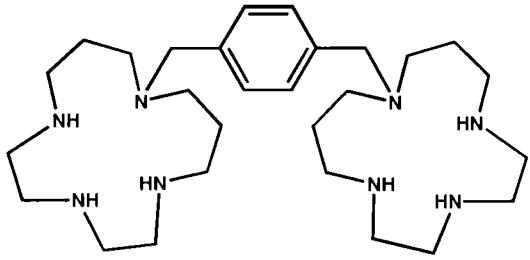

(30)

firmed the presence of an interaction between the metal centers, with the strength of interaction depending on the length of the bridge.

Cyclic voltammetry and differential pulse polarography have been used to investigate the redox properties of the di-Ni(II) species in acetonitrile. Effectively, a two-electron step was observed for the complex of **30**, whereas that of **29** (n = 2) yielded two clear one-electron steps. This is in accord with the occurrence of an interaction between the nickel sites for the latter system containing the shorter link between the isocyclams.

The X-ray structures of the dinickel perchlorate complexes of **29** (n = 2) and **30** have been determined (Figs. 18 and 19). A square planar coordination geometry for the Ni(II) in each complex was confirmed. For both complexes, the nickel atoms are separated by the greatest possible distance [7.05 Å in the complex of **29** (n = 2; 11.56 Å in the complex of **30**]. It is worth noting that the closely related

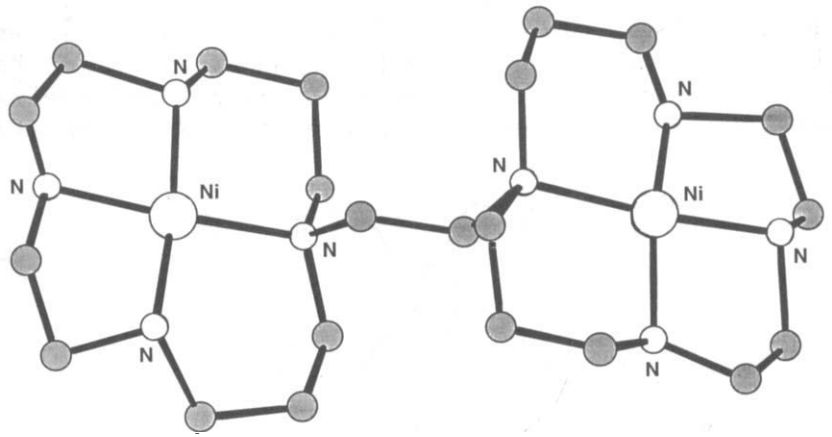

FIG. 18. The structure of the dinuclear Ni(II) complex of **29** (n = 2).

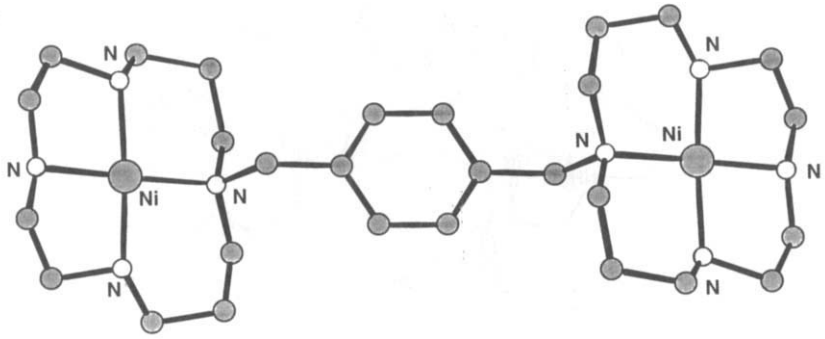

FIG. 19. The structure of the dinuclear Ni(II) complex of **30** (n = 2).

isomeric bis(isocyclam) derivative (**31**) has also been reported and demonstrated to yield a dinuclear Cu(II) complex on reaction with copper perchlorate in hot propanol (*57*).

The family of bis(cyclam macrocycles) represented by **32**, in which the cyclam subunits are linked through nitrogen atoms by $-(CH_2)_n-$ (n = 2–4), *m*-xylyl, or *p*-xylyl groups, has been synthesized (*58*). The di-Ni(II) and di-Cu(II) complexes of these bis(macrocycles) have been used in an investigation of the effects of mutual electrostatic interaction on the redox behavior of the respective metal centers.

The electrochemistry of the above systems once again involves a two-electron process, involving two reversible one-electron steps. The difference in potential between these steps is given by $\Delta E°$. This value is made up of a statistical component associated with a "valence scrambling" equilibrium as well as a component that reflects the electrostatic repulsion between the metal centers.

For the present series of complexes, because of the presence of extended bridges between the macrocycle subunits, it was assumed that any nonelectrostatic effect between metal centers is negligible. Accordingly the systems were treated in terms of a simple electrostatic

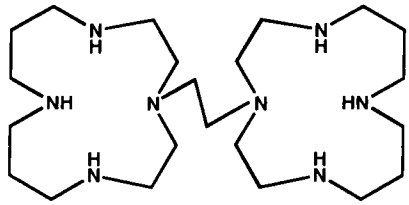

(31)

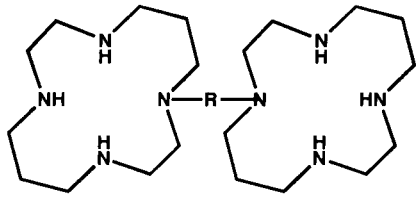

(32)

R = —CH_2CH_2—

—$CH_2CH_2CH_2$—

—$CH_2CH_2CH_2CH_2$—

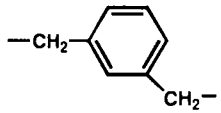

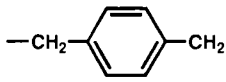

model. On this basis, the observed redox behavior is in accord with the electrostatic repulsion decreasing as the distance between metal sites increases.

An alternative synthesis for the *p*-xylyl-linked system of type **32**, employing a facile *de novo* procedure has been published (*59*). Interest in new syntheses for this compound was motivated by the report that this was the compound of choice for further development in the search for new anti-HIV compounds (*6*).

The bis(trimethylated cyclam) derivative (**33**) has been prepared in

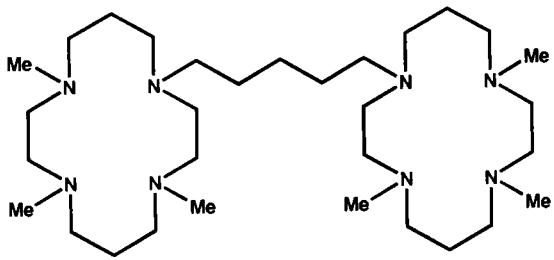

(33)

low yield by the reaction of glutaryl dichloride with two equivalents of the corresponding (parent) tri-N-methylated cyclam ring, followed by reduction of the diamide derivative produced with diborane in THF. Reaction of **33** with nickel perchlorate in ethanol yields a dinuclear species of the usual type, $[Ni_2L](ClO_4)_4$ (*60*). Urfer and Kaden (*61*) have described procedures for obtaining a number of mixed-ring bis(macrocycles), starting from tri-N-protected tetraaza rings and employing bromoacetyl bromide as the bridging reagent. The reaction sequence involves the use of the latter reagent to acylate the first tri-N-protected ring (at its nonprotected secondary nitrogen) followed by the employment of this acylated product for alkylation of a second triprotected tetraaza ring. The heteroditropic bis(macrocycle) is then obtained by diborane reduction of the amide moiety followed by deprotection. Structures **34–36** illustrate the range of products (including protected derivatives) obtained in this study, where R is tosyl, H, CH_3; R′ is H, CH_3; and X is $-CH_2CH_2$ or $-C(O)-CH_2CH_2-$ or C(O)C(O)−.

Both the symmetric and nonsymmetric bis(macrocyclic) ligands were titrated at constant pH with Cu(II) to confirm that two Cu(II) per ligand can be bound and, if so, to determine whether the complexation process involves two steps or one. For the symmetric sys-

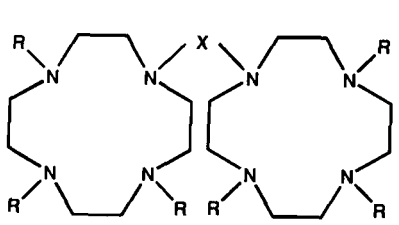

(34)

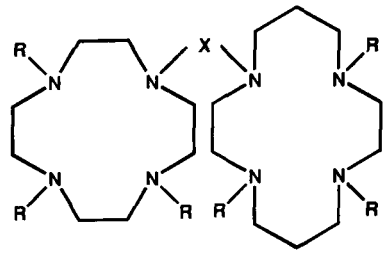

(35)

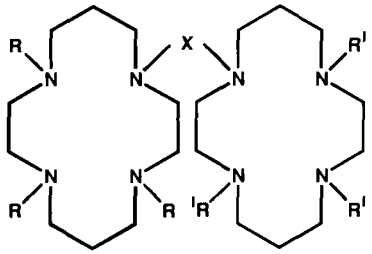

(36)

tems **34** (R = H, X = CH_2CH_2) and **36** (R = R′ = H, X = CH_2CH_2) there was a steady increase in absorption at 610 and 530 nm, respectively, until a sharp end point occurs at a 2:1 (metal:ligand) ratio. This is strong evidence that the respective binding sites are equivalent, or close to equivalent. Unexpectedly, the nonsymmetric system **35** (R = H, X = CH_2CH_2) also gave a similar result, suggesting that the differences in binding constant, as well as the ligand field strength of each site, are not sufficiently different to observe stepwise binding.

In contrast to the above observations, the ligand incorporating an unsubstituted cyclam bridged to a trimethyl-substituted cyclam undergoes selective metal-ion binding, with the first metal ion being incorporated into the unsubstituted cyclam site and the second being bound by the trimethyl ring derivative. Thus sequential addition of two metal ions in the correct proportions has been demonstrated to provide a means of preparing heterometallic complexes in some instances, without the subsequent need for chromatographic separation of such species from their dinucleating, single-metal analogues. Zn/Cu and Cu/Zn isomers with **36** (R = H, R′ = Me, X = CH_2CH_2) have been prepared.

As part of this study, it was shown that particular binuclear Ni(II) complexes yielded $E^{\circ}_{1/2}$ values that are shifted by 50–150 mV to more positive values relative to the values for the corresponding mononuclear complexes, in agreement with the results from previous studies. This shift may be rationalized in terms of the additional positive charge on the dinuclear complex, resulting in the oxidation of Ni(II) to Ni(III) being less favored. A similar reasoning may be used to explain the 90–100 mV separating the values for the homodinuclear nickel complex of the symmetrical ligand (**36**; R = R′ = H, X = CH_2CH_2). As expected, the related dinuclear Ni(II) complex of the unsymmetrical system (**35**; R = H, X = CH_2CH_2) gave a much greater separation.

The EPR spectra of the dinuclear Cu(II) complex of **36** (R = H, R′ = CH_3, X = CH_2CH_2) have been obtained and, as for related systems of this type studied previously (see earlier), the presence of a weak interaction between the Cu(II) ions was again clearly indicated.

In the context of HIV drug research, the syntheses of a range of other N,N′-linked bis(macrocycles), many obtained in small yields, have been described recently (*6*).

Recent reports also describe the use of *tert*-butyloxycarbonyl (Boc) protecting groups in the preparation of a number of bis(polyazamacrocyclic) ligands of general type **37** (*62*, *63*). As discussed above, a

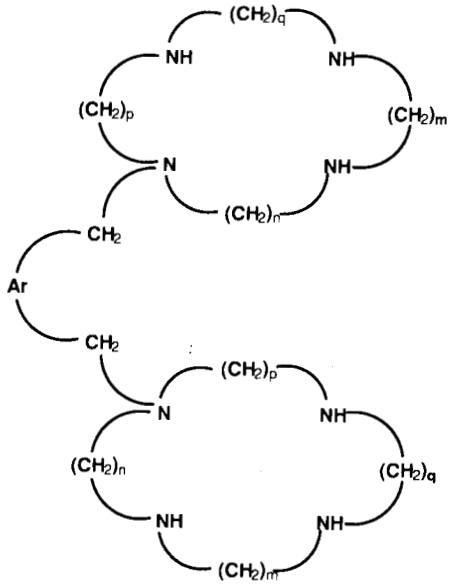

(37)

preferred method for linking two tetraaza macrocyclic units is to start from the corresponding triprotected tetraaza species and condense this with a difunctional electrophile. Frequently tosyl groups have been employed as protecting groups for secondary amines, but the detosylation procedure has often proved not straightforward and its success can depend on the nature of the species involved. In general, the removal of Boc protecting groups tends to be more facile, requiring gentler conditions than is necessary for the detosylation reaction. As a result, there is less chance of unwanted side products being generated.

Using a trial-and-error procedure, it was found that 2.4 equivalents of Boc_2O yielded optimum yields of the corresponding triprotected derivatives when reacted with the tetraaza macrocycles, cyclen (12-membered), cyclam (14-membered), and the corresponding symmetrical 16-membered macrocycle. These partially protected products were then reacted with an aromatic "spacer" group, namely, dibromo *o*-, *m*-, or *p*-xylyl or anthracenyl derivatives. The Boc groups were removed by treatment of the resulting linked systems with 6 *M* HCl for 1 hr. A number of such *o*-xylyl and anthracenyl derivatives were also obtained by reaction of phthaloyl dichloride or anthracene-1,8-dicarbonyl dichloride with the protected macrocycles. In these cases reduc-

tion of the intermediate diamides was carried out using diborane in THF. Deprotection of the secondary amines by acid treatment then yielded the required products in near 60% yield.

In an attempt to obtain close-linked bis(macrocycles) related to the systems just discussed, McAuley *et al.* (*64*) were successful in synthesizing the spiro-linked derivatives **38** and **39** in which an sp^3 carbon atom is common to both macrocyclic rings. Although the number of such spiro-linked systems remains small, examples of both open-chain (*65*) and other macrocyclic systems (*66–70*) incorporating such a linkage are known. When the shared atom is an sp^3 carbon then the resulting tetrahedral arrangement will dispose the respective macrocyclic rings to adopt a mutually orthogonal alignment. Unlike most linked systems, free rotation around the linkage joining the macrocyclic subunits is thus not possible for such systems.

Once again, the di-Ni(II) complexes of the bis(cyclam) system **40** exhibits the characteristic robustness that is a feature of $[Ni(cyclam)]^{2+}$ (*71*). The X-ray structure of the dinuclear Ni(II) complex has been determined (Fig. 20). Nickel atoms fully occupy each of the cyclam cavities in a low-strain coordination arrangement; each ring adopts the low-energy trans III form found for $[Ni(cyclam)]^{2+}$. An interesting feature of the solid-state structure is that the angle between the rings is not 90°, but rather 84°. The resulting reduction in orthogonality between the d_z^2 orbitals may increase the prospect

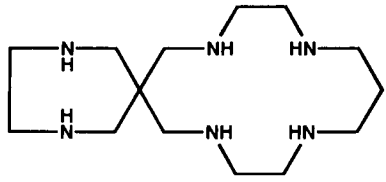

(38)

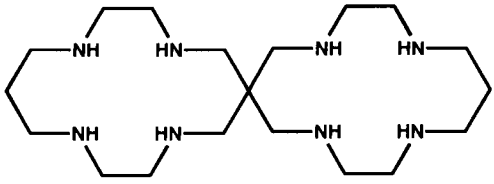

(39)

of communication between the metal sites. As expected, the above dinuclear Ni(II) complex is readily oxidized (both chemically and electrochemically) to the corresponding [Ni(III)–Ni(III)] species; attempts to isolate the intermediate [Ni(II)–Ni(III)] species were unsuccessful.

The dinucleating bis(dimethylcyclam) ligand **40** has been synthesized and its complexes with Ni(II) and Zn(II) isolated (*72*). The employment of an *ortho*-dihalo-xylyl group for condensation with two molecules of **9**, by the usual electrophilic attack mechanism, followed by sodium borohydride reduction, gives an arrangement in which the macrocyclic rings are oriented face to face. The resulting complex, $[Ni_2(\mu\text{-}Br)Br_2L]Br \cdot H_2O$ (L = **40**), was obtained in 60–70% yield. Treatment of this species with sodium cyanide in water/ethanol results in demetalation to yield the free bis(macrocycle). Treatment of this metal-free species with Zn(II) perchlorate, followed by slow crystallization of the resulting product over several weeks, gave the carbonato-bridged species **41**. The structures of the dinucleating ligand in the above di-Ni(II) complex and in **41** are very similar, with the cyclam rings adopting stable trans III arrangements in each case. The two methyl substituents on each ring are orientated equatorially with respect to the corresponding chair-form chelate ring. In contrast, the xylylene group is arranged axially; it is this orientation of the *ortho*-xylylene moiety that directs the adoption of a face-to-face configuration. The structure of a chloro-bridged complex of **40**, related to the bromo derivative mentioned above, has also been reported (*73*).

Based on a related procedure for synthesizing single-ring complexes (*74*), template condensation of $[Ni(2,3,2\text{-tet})]^{2+}$ (2,3,2-tet = 1,9-

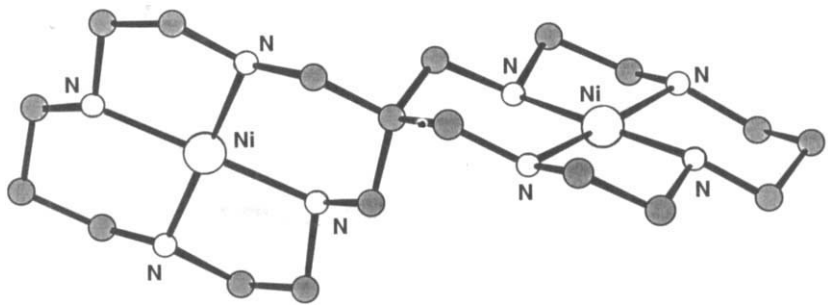

FIG. 20. The structure of the di-Ni(II) complex of a spiro-linked bis(cyclam) derivative (**39**).

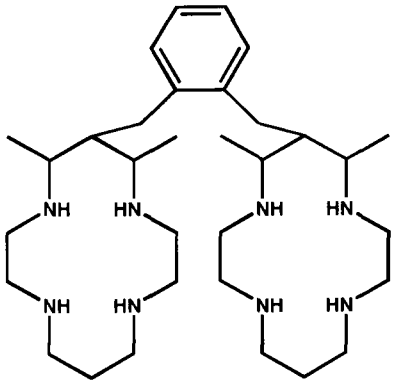

(40)

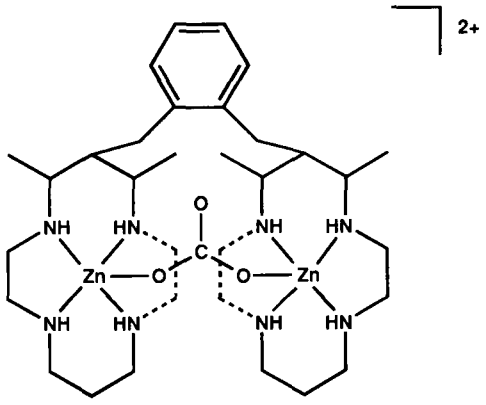

(41)

diamino-3,7-diazanonane) with formaldehyde and aliphatic diamines was demonstrated to yield bis(pentaaza-macrocyclic) complexes of type **42** (n = 2–5) in a one-pot reaction (*75*, *76*). The new ligand systems have their macrocyclic subunits linked by polymethylene chains of various length via noncoordinating, bridge-head nitrogens in each ring.

The electrochemical and spectral data for the dinuclear Ni(II) complexes were found to be very similar to those of the corresponding mononuclear species (**43**). The visible spectrum of each complex indicated the presence of low-spin, square planar Ni(II). Interestingly,

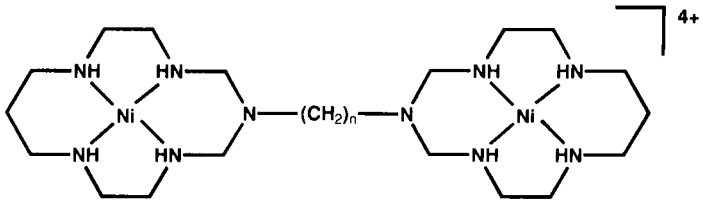

(42)

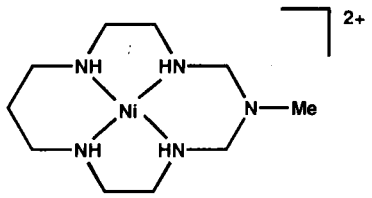

(43)

these complexes are quite stable to pH over the range 2–12. The voltammograms for the individual complexes contain single anodic and cathodic peaks that are separated by ~100 mV. The number of methylene groups linking the rings has almost no effect on the respective $E_{1/2}$ values; this provides strong evidence for the absence of interaction between the metal sites.

Oxidation of the above complexes to the corresponding Ni(III) species was found to occur readily using either chemical or electrochemical means (under acidic conditions). EPR spectral data for the bis(macrocyclic) Ni(III) complexes are very similar and confirm the presence of a d^7 electronic configuration in which the metal is in a tetragonally distorted environment.

Rate data for the oxidation of the respective Ni(II) complexes to their Ni(III) analogues have been obtained. The formation of the latter was observed to be first order in Ni(II) and oxidant ($S_2O_8^{=}$ or H_2O_2), with the rate constants being several times greater for the dinuclear complexes than for the single-ring analogue.

The analogous series of Cu(II) complexes have also been prepared by a procedure similar to that for the Ni(II) species starting from the 1:1 Cu(II) complex of 2,3,2-tet.

In other studies, a related *in situ* procedure has been employed to produce a di-Cu(II), bis(macrocyclic ligand) system linked by an ethylene bridge through noncoordinating N atoms (77). The ligand in this

case incorporates a 1,3-diazacyclohexane ring in each macrocyclic subunit.

An *in situ* procedure involving condensation of the appropriate open-chain, spiro-linked amine with nitromethane and formaldehyde in water in the presence of copper perchlorate has been employed to obtain the dinuclear Cu(II) perchlorate complex of **44** (*78*). The visible spectrum of this complex is very similar to that of its mononuclear analogue. In solution, the metal in each complex was assigned a tetragonally distorted octahedral environment in which axial solvation completes the coordination sphere. As with other complexes of this general type, the addition of dilute acid did not affect the spectrum of this species.

Electrochemical studies, related to those discussed previously, gave clear evidence for the presence of interaction between the metal sites. A detailed investigation of the EPR spectrum of this complex has been undertaken, enabling structural parameters to be deduced.

An extension of the template reaction mentioned above [involving condensation of the Cu(II) complex of a tetradentate amine with formaldehyde and a nitroalkane] was employed to prepare the Cu(II) complexes of the series of bis(tetraaza macrocyclic) ligands given by **45** (*79*). Reduction of the nitro groups in these species with Zn/HCl produced the corresponding metal-free bis(pendant amino) derivatives (**46**).

EPR studies gave no evidence for interaction between the Cu(II) centers in the bis(nitro) derivative incorporating 14-membered macrocyclic rings when the latter are joined by an ethylene bridge. In accordance with this, molecular mechanics calculations coupled with simulated EPR data suggested that this complex will adopt a "stretched" arrangement in solution. The absence of interaction in this complex contrasts with the behavior of the related di-Cu(II) complex corresponding to **43**; (n = 2) for which a weak interaction was demonstrated to be present (*76*). For this latter species the calculations suggest that it exists largely in a face-to-face configuration in solution.

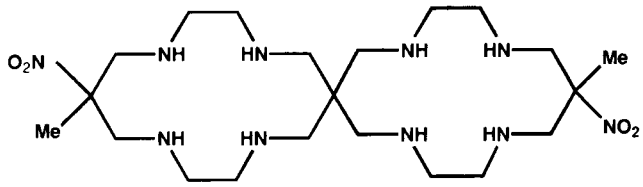

(44)

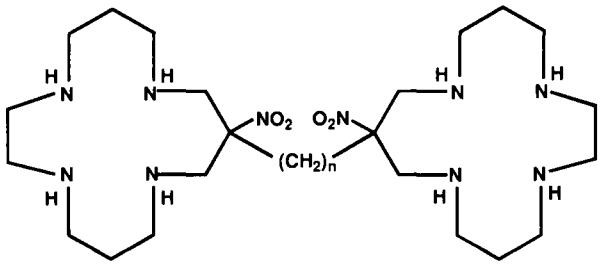

(45)

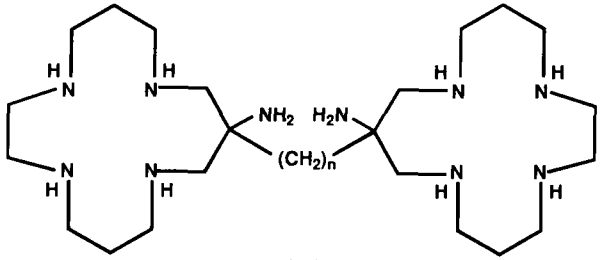

(46)

Co(II), Ni(II), and Cu(II) binuclear complexes of the dilinked species (**47**), incorporating 13-membered macrocycle subunits, have been reported (*80*). The X-ray structure of one such product, $[Cu_2(Tos)L](ClO_4)_2 \cdot 4H_2O$ (where Tos is the tosylate anion and L = **47** has been determined (Fig. 21). This complex has a distorted square pyramidal coordination geometry; four nitrogen donors coordinate in the basal plane with a tosylato oxygen occupying the axial site. The basal nitrogens deviate from their mean plane by ±0.12 Å. Each of the macrocycles adopts a dish-shaped arrangement, with the Cu(II) coordinating on the outer side of the dish. This complex reacts with F^-, Cl^-, Br^-,

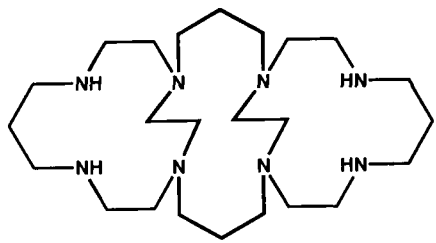

(47)

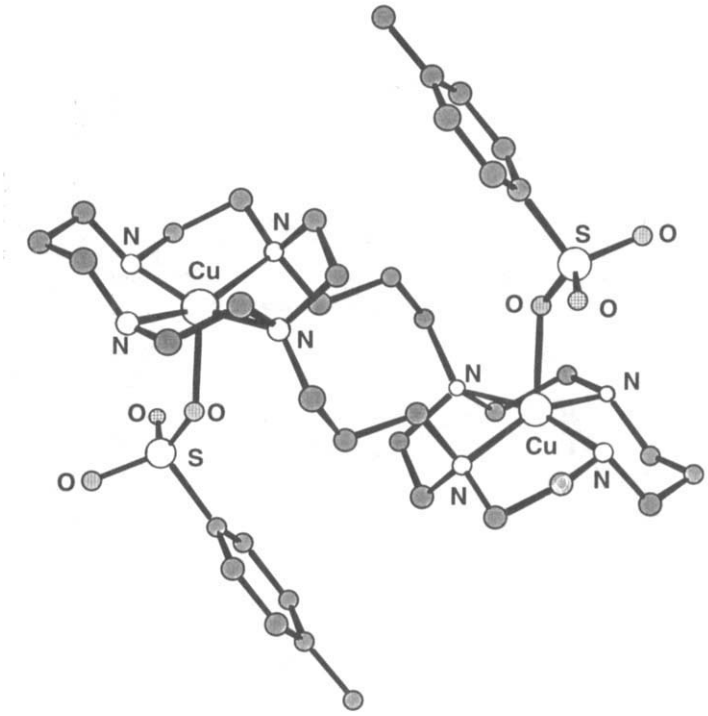

FIG. 21. The structure of $[Cu_2(Tos)L]^+$ (Tos = tosylate anion, L = **47**).

I^-, and N_3^- in aqueous solution to form a range of anion-bridged complexes of type $[Cu_2XL](ClO_4)_3 \cdot xH_2O$ (X = halide). All these have magnetic moments that fall in the normal range. The Ni(II) complex, $[Ni_2L](ClO_4)_4$, is essentially diamagnetic and each nickel was assigned a square planar coordination geometry.

The di-Co(II) species, $[Co_2OHL](ClO_4)_3$, rapidly binds CO_2 in aqueous solution to yield $[Co_2CO_3L](ClO_4)_2 \cdot 3H_2O$. An X-ray diffraction study of this product revealed that each Co(II) ion has a distorted octahedral geometry made up of four nitrogens from **47** and two oxygens from the carbonate anion (Fig. 22).

A variety of linked, Schiff base macrocyclic ligands and their metal complexes have been isolated. An early ligand of this type is given by **48** (*81*). Reaction of the free ligand with Ni(II) or Cu(II) acetate yields the corresponding dimetallic complexes. In contrast, the nickel(II) complexes of type **49** were obtained by means of a Schiff base condensation *in situ* in which the required amine and dialdehyde reagents were reacted in hot DMF in the presence of nickel acetate (*82*).

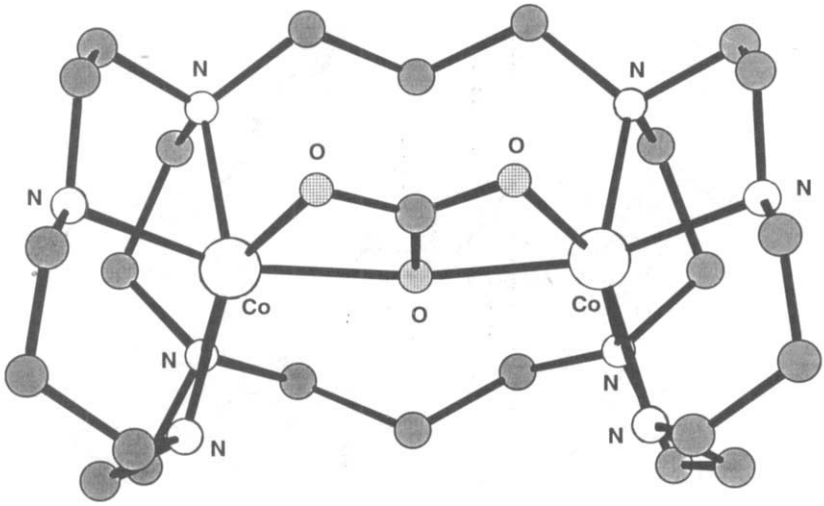

FIG. 22. The structure of $[Co_2CO_3L]_2$ (L = **47**).

The *in situ* Schiff base condensation of 2,6-diacetylpyridine with *N,N,N',N'*-tetrakis(3-aminopropyl)-1,2-diaminoethane in the presence of copper(II) chloride was demonstrated to yield the dinuclear cation **50** (n = 2; R = CH_3) as its perchlorate salt (*83*). The corresponding single-ring, mononuclear copper(II) complex **51** (R = CH_3) had been reported previously (*84*). Both this and the dinuclear species yield similar visible spectra, suggesting that similar copper coordination

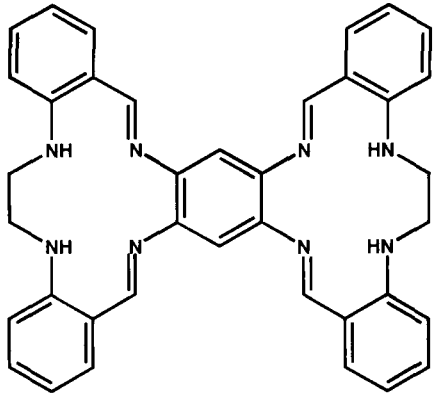

(48)

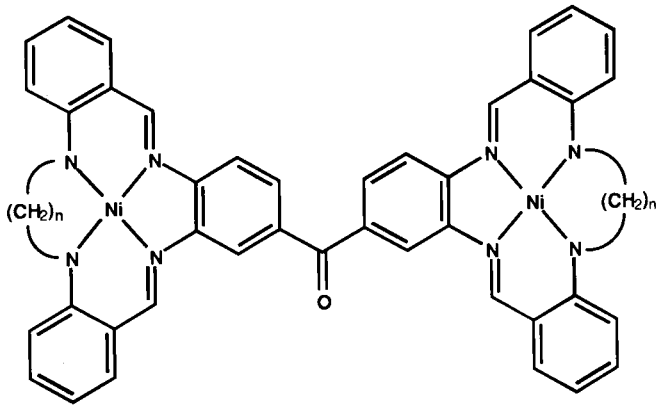

(49)

environments are present in each complex. For the dinuclear species, variable-temperature magnetic studies indicated that some antiferromagnetic interaction occurs between the Cu(II) sites; Curie–Weiss behavior was observed over the temperature range 290–87 K, with θ =

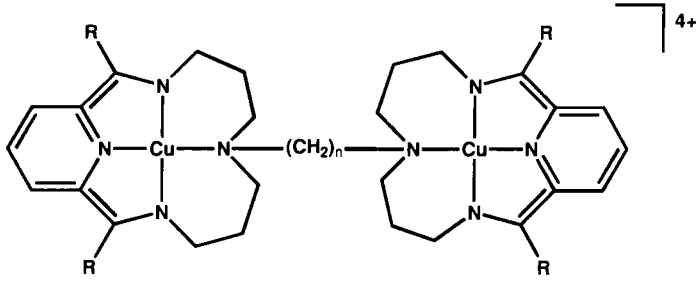

(50)

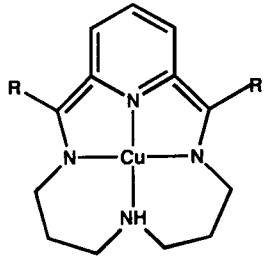

(51)

−14 K. ESR studies (DMF glass) gave clear evidence for interaction between the sites, particularly when the spectrum was compared with the similar spectrum of the above mononuclear species. The coupling of two ^{63}Cu nuclei ($I = \frac{3}{2}$) is expected to give rise to two sets of seven hyperfine lines whose separation ($A_{\parallel}$) is one-half of that for the hyperfine lines in the spectrum of the corresponding mononuclear complex. This situation is closely approximated by the present system.

In an extension of the above study (*85*), Cu(II) complexes of ligands of type **50** incorporating from three to six methylene groups linking the macrocyclic subunits have been prepared. Two dinuclear Ni(II) complexes were also isolated. The properties of the copper complexes were found to be generally similar to those discussed above for the parent complex. Nevertheless, as the link between the macrocyclic rings becomes longer, the respective negative Weiss constants decrease, suggesting that the already weak antiferromagnetic interaction present in the parent complex decreases further along the series. Heterobinuclear [Ni(II)/Cu(II)] complexes of the above ligand series (n = 2–6) have been prepared by *in situ* condensation in the presence of a mixture of these metals (*86*). A mixture of Cu(II)/Cu(II), Cu(II)/Ni(II), and Ni(II)/Ni(II) species was obtained, but the individual complexes were able to be separated by chromatography using an SP-Sephadex C-25 ion-exchange column.

An X-ray diffraction study of the di-Ni(II) complex **50** (n = 4; R = CH_3) shows that it adopts an open configuration in the solid state, in which the macrocyclic subunits are widely spaced (*87*). The X-ray structures of two Cu(II) complexes of this ligand have also been determined (*88*). $[Cu_2(H_2O)_2L](ClO_4)_4 \cdot 4H_2O$ also adopts an open structure in which the copper sites are widely separated. In contrast, $[Cu_2Cl_2L](ClO_4)_2 \cdot H_2O$ crystallizes in a closed configuration in which the tetramethylene chain is folded such that the two macrocyclic subunits face each other. In part, the difference between the structures of these complexes appears to reflect the reduced electrostatic repulsion between the copper centers when the latter are each bound to a chloro ligand, rather than to an uncharged water ligand, as occurs in $[Cu_2(H_2O)_2L]^{4+}$.

The square planar/octahedral equilibrium commonly observed for the Ni(II) complexes of tetraaza ligands in aqueous solutions has once again been shown to occur for the Cu(II)/Ni(II) and Ni(II)/Ni(II) systems (*89*). The equilibria for both systems show the usual dependence on temperature, with the percentage of square planar form increasing as the temperature is increased. It was found that the position of the equilibrium was also dependent on the length of the polymethylene

bridge—shortening the bridge had an effect similar to lowering the temperature—for both the homo- and heterobinuclear species. That is, formation of the octahedral form is favored as the bridge is shortened.

A parallel study of the Ni(II)/Ni(II) complexes of related reduced forms of the above ligand series (namely, of type **52**) in aqueous solution has been carried out (*90*). Once again, as the length of the methylene chain between the macrocyclic subunits decreases, the proportion of octahedral over square planar complex present increases.

A heterobinuclear [Cu(II)/Ni(II)] complex of **52** ($n = 3$) has been isolated {after chromatographic separation from the corresponding [Cu(II)/Cu(II)] and [Ni(II)/Ni(II)] products also formed} following reaction of a mixture of both metals with this dinucleating ligand (*91*). It has been possible to reduce the Cu(II) selectively in the hetereobinuclear complex by electrolysis (at −0.6 V), using a mercury pool as working electrode. After loss from the macrocyclic cavity, the Cu(O) generated presumably forms an amalgam with the mercury. From the resulting solution the complex of **52** ($n = 3$), containing one Ni(II), was isolated. Addition of one equivalent of Cu(II) to a solution of this product was shown to regenerate the original heterodinuclear species.

The above study has been extended to encompass the synthesis of a new system incorporating differentially substituted macrocyclic subunits (*92*). Starting from the mononuclear Ni(II) complex of **52** ($n = 3$) described above, it proved possible to obtain a selective Michael addition reaction between acrylonitrile and the secondary amine groups of the vacant macrocyclic ring. Reaction of the product with Ni(II) yielded the nonsymmetrical complex **53**. Based on comparative visible spectral studies, one nickel atom in this complex was assigned a four-coordinate geometry; the second appears to be five-coordinate.

In wide ranging studies, Bush *et al.* (*93, 94*) have investigated an extended series of binuclear complexes of type **54** incorporating di-linked tetraimine macrocyclic subunits. These systems adopt face-to-

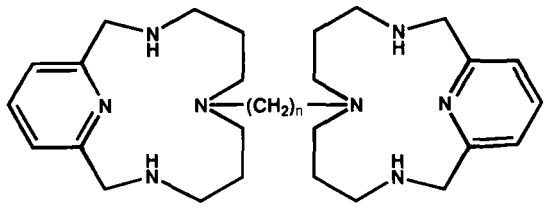

(52)

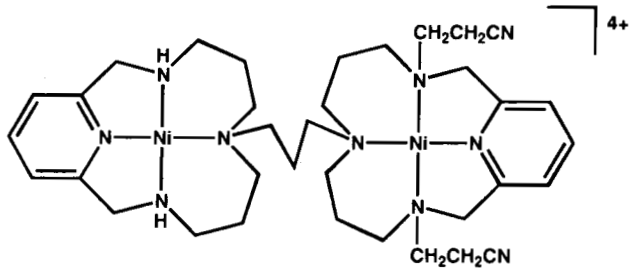

(53)

face orientations, although the rings may be displaced somewhat with respect to each other in some complexes. These systems incorporate large flexible cavities between the macrocycle rings, which can be varied in size by changing the nature of the linking (—R^1—) groups. For example, in one study dinuclear Ni(II) complexes were prepared in which R^1 varied over the range: $-N(CH_3)(CH_2)_2N(CH_3)-$, $-NH(CH_2)_2NH-$, $-NH(CH_2)_3NH-$, $-NH(CH_2)_5NH-$, $-N(CH_2CH_2)_2N-$, and $-NHCH_2C_6H_4CH_2NH-$ (*94*). Dinuclear Co(II) and Fe(II) complexes of such cofacial dimers have been investigated as dioxygen binders and, for example, particular Fe(II) species are excellent reversible dioxygen carriers. The dinuclear complexes of the above metals also exhibit a range of interesting redox properties that have

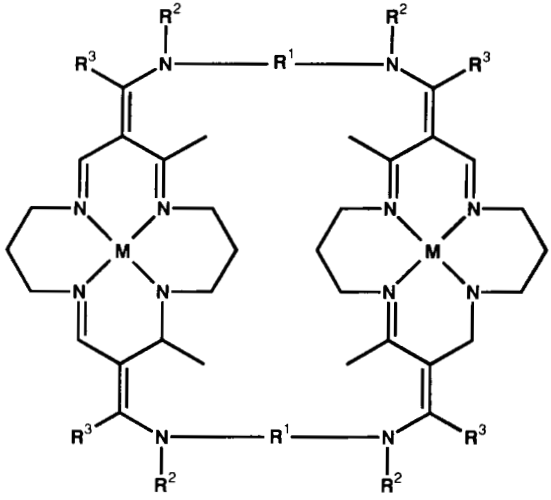

(54)

been studied in detail. The chemistry of these interesting and well-studied systems has been reviewed elsewhere (*95*) and will not be discussed further here.

III. Concluding Remarks

Synthetic routes for compounds of the type discussed in this review have been developed over the past 25 years or so. Interest in this area has stemmed, in part, from the intellectual and practical challenge arising from design and synthesis aspects, but also because particular compounds might provide models for dimetallic protein centers found in biology. However, as often happens interest in such compounds has been engendered by a recently discovered medical relevance—namely, that some compounds are active against HIV. In this context, it is likely that there will be an acceleration of new chemistry in the area. It is hoped that the present review will be helpful in this enterprise.

Acknowledgments

The author thanks the Australian Research Council for support and I. M. Atkinson and J. Kim for technical assistance in the preparation of this review.

References

1. Lindoy, L. F., "*Chemistry of Macrocyclic Ligand Complexes*"; Cambridge University Press: London, 1989.
2. Guerriero, P.; Vigato, P. A.; Fenton, D. E.; Hellier, P. C. *Acta Chem. Scand.* **1992,** *46,* 1025; Vigato, P. A.; Tamburini, S.; Fenton, D. E. *Coord. Chem. Rev.* **1990,** *106,* 25; Fenton, D. E.; Okawa, H. *J. Chem. Soc., Dalton Trans.* **1993,** 1349; "*Perspectives on Bioinorganic Chemistry*"; Hay, R. W., Dilworth J. R., and Nolan, K. B., Eds.; JAI Press: USA, 1993; Vol. 2, pp. 81–138.
3. Collman, J. P.; Wagenknecht, P. S.; Hutchison, J. E. *Angew. Chem., Int. Ed. Engl.* **1994,** *33,* 1537.
4. Bradshaw, J. S.; Krakowiak, K. E.; Izatt, R. M. "*Aza-Crown Macrocycles*"; John Wiley & Sons: New York, 1993; Vol. 51.
5. Hiraoka, M., Ed. "*Crown Ethers and Analogous Compounds,* Studies in Organic Chemistry"; Elsevier: Amsterdam, 1992; Vol. 45, p. 335; Bradshaw, J. S.; Izatt, R. M.; Yan, Z. *Chem. Rev.* **1994,** *94,* 939.
6. De Clercq, E.; Yamamoto, N.; Pauwels, R.; Baba, M.; Schols, D.; Nakashima, H.; Balzarini, J.; Debyser, Z.; Murrer, B. A.; Schwartz, D.; Thornton, D.; Bridger, G.;

Fricker, S.; Henson, G.; Abrams, M.; Picker, D. *Proc. Natl. Acad. Sci. U.S.A.*, **1992,** *89,* 5286; Bridger, G. J.; Skerlj, R. T.; Thornton, D.; Padmanabhan, S.; Martellucc, S. A.; Henson, G. W.; Abrams, M. J.; Yamamoto, N.; De Vreese, K.; Pauwels, R.; De Clercq, E. *J. Med. Chem.* **1995,** *38,* 366

7. Inouye, Y.; Kanomori, T.; Yoshida, T.; Bu, X.; Shinoya, M.; Koike, T.; Kimura, E. *Biol. Pharm. Bull.* **1994,** *17,* 243; Inouye, Y.; Kanamori, T.; Sugiyama, M.; Yoshida, T.; Koika, T.; Shioaoya, M.; Enomoto, K.; Suchiro, K.; Kimura, E. *Antiviral Chem. Chemother.* **1995,** *6,* 337.
8. Tanaka, N.; Kobayashi; Y., Takamoto, S. *Chem. Letts.* **1977,** 107.
9. Wieghardt, K.; Tolksdorf, I., Herrmann, W. *Inorg. Chem.* **1985,** *24,* 1230.
10. Chaudhuri, P.; Wieghardt, K. *Prog. Inorg. Chem.* **1987,** *35,* 329.
11. Geilenkirchen, A. Wieghardt, K.; Nuber, B.; Weiss, J. *Z. Naturforsch.* **1989,** *44B,* 1333.
12. Martin, A. E.; Ford, T. M.; Bulkowski, J. E.; *J. Org. Chem.* **1982,** *47,* 412.
13. Weisman, G. R.; Vachon, D. J.; Johnson, V. B.; Gronbeck, D. A. *J. Chem. Soc., Chem. Commun.* **1987,** 886.
14. Sessler, J. L.; Sibert, J. W.; Lynch, V. *Inorg. Chem.* **1990,** *29,* 4143.
15. Zhang, X.; Hsieh, W.-Y.; Margulis, T. N.; Zompa, L. J. *Inorg. Chem.* **1995,** *34,* 2883.
16. Schwindinger, W.; Fawcett, T.; Lalancette, R.; Potenza, J.; Schugar, H. *Inorg. Chem.* **1980,** *19,* 1379.
17. Bereman, R.; Churchill, M.; Schaber, P.; Winkler, M. *Inorg. Chem.* **1979,** *18,* 3122.
18. Geilenkirchen, A.; Neubold, P.; Schneider, R.; Wieghardt, K.; Flörke, U.; Haupt, H.-J.; Nuber, B. *J. Chem. Soc., Dalton Trans.* **1994,** 457.
19. Wieghardt, K.; Herrmann, W.; Koppen, M.; Jibril, I.; Huttner, G. *Z. Naturforsch. Teil B* **1984,** *39,* 1335; Neubold, P.; Della Bedova, B. S. P. C.; Wieghardt, K.; Nuber, B.; Weiss, J. *Angew. Chem., Int. Ed. Engl.* **1989,** *28,* 763.
20. Wieghardt, K.; Herrmann, W.; Koppen, M.; Jibril, I.; Huttner, G. *Z. Inorg. Chem.* **1990,** *29,* 3355.
21. Hanke, D.; Wieghardt, K.; Nuber, B.; Lu, R.-S.; McMullan, R. K.; Koetzle, T. F.; Bau, R. *Inorg. Chem.* **1993,** *32,* 4300.
22. Blake, A. J.; Donlevy, T. M.; England, P. A.; Fallis, I. A.; Parsons, S.; Ross, S. A.; Schröder, M. *J. Chem. Soc., Chem. Commun.* **1994,** 1981.
23. Belal, A. A.; Farrugia, L. J.; Peacock, R. D.; Robb, J. J. *J. Chem. Soc., Dalton Trans.* **1989,** 931; Belal, A. A.; Chaudhuri, P.; Fallis, I.; Farrugia, L. J.; Hartung, R.; Macdonald, N. M.; Nuber, B.; Peacock, R. D.; Weiss, J.; Wieghardt, K. *Inorg. Chem.* **1991,** *30,* 4397; Fallis, I.; Farrugia, L. J.; Macdonald, N. M.; Peacock, R. D. *Inorg. Chem.* **1993,** *32,* 779; Fallis, I.; Farrugia, L. J.; Macdonald, N. M.; Peacock, R. D. *J. Chem. Soc., Dalton Trans.* **1993,** 2759.
24. Vincent, J. B.; Oliver-Lilley, G. L.; Averill, B. A. *Chem. Rev.* **1990,** *90,* 1447; Que, L.; Scarrow, R. C. *In "Metal Clusters in Proteins"*; Que, L., Ed.; ACS Symposium Series 372, American Chemical Society: Washington, D.C., 1988; pp. 152–178; Lippard, S. J. *Angew. Chem., Int. Ed. Engl.* **1988,** *27,* 344; Wilkins, R. G.; Harrington, P. C. *Adv. Inorg. Biochem.* **1983,** *5,* 51; Klotz, I. M.; Kurtz, D. M. *Acc. Chem. Res.* **1984,** *17,* 16.
25. Toftlund, H.; Murray, K. S.; Zwack, P. R.; Taylor, L. F.; Anderson, O. P. *J. Chem. Soc., Chem. Commun.* **1986,** 191.
26. Sessler, J. L.; Sibert, J. W.; Lynch, V.; Markert, J. T., Wooten, C. L. *Inorg. Chem.* **1993,** *32,* 621.
27. Sessler, J. L.; Sibert, J. W.; Burrell, A. K.; Lynch, V.; Markert, J. T.; Wooten, C. L. *Inorg. Chem.* **1993,** *32,* 4277.

28. Chang, H.-R.; Diril, H.; Nilges, M. J.; Zhang, X.; Potenza, J. A.; Schugar, H. J.; Hendrickson, D. N.; Isied, S. S. *J. Am. Chem. Soc.* **1988,** *110,* 625; Diril, H.; Chang, H.-R.; Nilges, M. J.; Zhang, X.; Potenza, J. A.; Schugar, H. J.; Isied, S. S.; Hendrickson, D. N. *J. Am. Chem. Soc.* **1989,** *111,* 5102.
29. Cunningham, J. A.; Sievers, R. E. *J. Am. Chem. Soc.* **1973,** *95,* 7183.
30. Cummings, S. C.; Sievers, R. E. *J. Am. Chem. Soc.* **1970,** *92,* 215; Cummings, S.; Sievers, R. E. *Inorg. Chem.* **1970,** *9,* 1131.
31. Endicott, J. F.; Durham, B. "Coordination Chemistry of Macrocyclic Compounds"; Melson, G. A., Ed.; Plenum Press: New York, 1979; Chap. 6.
32. Hipp, C. J.; Lindoy, L. F.; Busch, D. H. *Inorg. Chem.* **1972,** *11,* 1988.
33. Mochizuki, K.; Toriumi, K.; Ito, T. *Bull. Chem. Soc., Jpn.,* **1984,** *57,* 881.
34. Matsumoto, N.; Hirano, A.; Ohyoshi, A. *Bull. Chem. Soc., Jpn.* **1983,** *56,* 891.
35. Martin, J. G.; Cummings, S. C. *Inorg. Chem.* **1973,** *12,* 1477.
36. Matsumoto, N.; Wakizaka, K.; Ohyoshi, A. *Bull. Chem. Soc., Jpn.* **1982,** *55,* 3165; Matsumoto, N.; Ohyoshi, A. *Bull. Chem. Soc., Jpn.* **1983,** *56,* 134.
37. Mountford, H. S.; Spreer, L. O.; Otvos, J. W.; Calvin, M.; Brewer, K. J.; Richter, M.; Scott, B. *Inorg. Chem.* **1992,** *31,* 717.
38. Zhou, J.; Li, A.; Lange, C.; Allan, C. B.; Spreer, L. O.; Otvos, J. W.; Calvin, M. *Inorg. Chim. Acta* **1996,** *246,* 241; Mountford, H. S.; MacQueen, D. B.; Li, A.; Otvos, J. W.; Calvin, M.; Frankel, R. B.; Spreer, L. O. *Inorg. Chem.* **1994,** *33,* 1748; Spreer, L. O.; Li, A.; MacQueen, D. B.; Allan, C. B.; Otvos, J. W.; Calvin, M.; Frankel, R. B.; Papaefthymiou, G. C. *Inorg. Chem.* **1994,** *33,* 1753.
39. Spreer, L. O.; Allan, C. B.; MacQueen, D. B.; Otvos, J. W.; Calvin, M. *J. Am. Chem. Soc.* **1994,** *116,* 2187.
40. McAuley, A.; Xu, C. *Inorg. Chem.* **1992,** *31,* 5549.
41. McElroy, F. C.; Dabrowiak, J. C. *J. Am. Chem. Soc.* **1976,** *98,* 7112.
42. Arion, V. B.; Gerbeleu, N. V.; Levitsky, V. G.; Simonov, Y. A.; Dvorkin, A. A.; Bourosh, P. N. *J. Chem. Soc., Dalton Trans.* **1994,** 1913.
43. Ciampolini, M.; Micheloni, M.; Nardi, N.; Vizza, F.; Buttafava, A.; Fabbrizzi, L.; Perotti, A. *J. Chem. Soc., Chem. Commun.* **1984,** 998.
44. Barefield, E. K.; Chueng, D.; Van Derveer, D. G. *J. Chem. Soc., Chem. Commun.* **1981,** 302.
45. Bosnich, B.; Poon, C. K.; Tobe, M. L. *Inorg. Chem.* **1965,** *4,* 1102; Adam, K. R.; Antolovich, M.; Brigden, L. G.; Lindoy, L. F. *J. Am. Chem. Soc.* **1991,** *113,* 3346.
46. Buttafava, A.; Fabbrizzi, L.; Perotti, A.; and Seghi, B. *J. Chem. Soc., Chem. Commun.* **1982,** 1166; Fabbrizzi, L.; Forlini, F.; Perotti, A.; Seghi, B. *Inorg. Chem.* **1984,** *23,* 807.
47. Buttafava, A.; Fabbrizzi, L.; Perotti, A.; Poggi, A.; Seghi, B. *Inorg. Chem.* **1984,** *23,* 3917.
48. Fabbrizzi, L.; Montagna, L.; Poggi, A.; Kaden, T. A.; Siegfried, L. C. *Inorg. Chem.* **1986,** *25,* 2672; Fabbrizzi, L.; Montagna, L.; Poggi, A.; Kaden, T. A.; Siegfield, L. C. *J. Chem. Soc., Dalton Trans.* **1987,** 2631.
49. Collin, J.-P.; Jouaiti, A.; Sauvage, J.-P. *Inorg. Chem.* **1988,** *27,* 1986.
50. Mochizuki, K.; Gotoh, H.; Suwabe, M.; Sakakibara, T. *Bull. Chem. Soc. Jpn.* **1991,** *64,* 1750.
51. Mochizuki, K.; Manaka, S.; Takeda, I.; Kondo, T. *Inorg. Chem.* **1996,** *35,* 5132.
52. Kido, H.; Takada, M.; Suwabe, M.; Yamaguchi, T.; Ito, T. *Inorg. Chim. Acta* **1995,** *228,* 133.
53. Kimura, E.; Yatsunami, A.; Watanabe, A.; Machida, R.; Koike, T.; Fukioka, H.; Kuramoto, Y.; Sumomogi, M.; Kinimitsu, K.; Yamashita, A. *Biochem. Biophys. Acta*

1983, *745,* 37; Kimura, E.; Kuramoto, Y.; Koike, T.; Fujioka, H.; Kodama, M., *J. Org. Chem.* **1990,** *55,* 42.
54. Dumas, S.; Lastra, E.; Hegedus, L. S. *J. Am. Chem. Soc.* **1995,** *117,* 3368.
55. Murase, I.; Ueno, S.; Kida, S. *Inorg. Chim. Acta* **1986,** *111,* 57.
56. Schneider, R.; Riesen, A.; Kaden, T. A. *Helv. Chim. Acta* **1985,** *68,* 53.
57. Garcia-Espaňa, E.; Micheloni, M.; Paoletti, P.; Biani, A. *Gazzetta Chim. Ital.* **1985,** *115,* 399.
58. Ciampolini, M.; Fabbrizzi, L.; Perotti, A.; Poggi, A.; Seghi, B.; Zanobini, F. *Inorg. Chem.* **1987,** *26,* 3527.
59. Xu, D.; Mattner, P. G.; Prasad, K.; Repic, O.; Blacklock, T. J. *Tetrahedron Lett.* **1996,** *37,* 5301.
60. Barefield, E. K.; Foster, K. A.; Freeman, G. M.; Hodges, K. D. *Inorg. Chem.* **1986,** *25,* 4663.
61. Urfer, A.; Kaden, T. A. *Helv. Chim. Acta* **1994,** *77,* 23.
62. Boitrel, B.; Andrioletti, B.; Lachkar, M.; Guilard, R. *Tetrahedron Lett.* **1995,** *36,* 4995.
63. Brandès, S.; Gros, C.; Denat, F.; Pullumbi, P.; Guilard, R. *Bull. Soc. Chim. Fr.* **1996,** *133,* 65.
64. McAuley, A.; Beveridge, K.; Subramanian, S.; Whitcombe, T. W. *Can. J. Chem.* **1989,** *67,* 1657.
65. Oehmke, R. W.; Bailar, J. C. *J. Inorg. Nucl. Chem.* **1965,** *27,* 2199; Phillip, A. T. *Aust. J. Chem.* **1986,** *21,* 2301; Gahan, L. R.; Hart, K. E.; Kennard, C. H. L.; Kingston, M. A.; Smith, G.; Mak, T. C. W. *Inorg. Chim. Acta* **1986,** *116,* 5; Dunlevy, T. M.; Gahan, L. R.; Hambley, T. W.; Hanson, G. R.; Markiewicz, A.; Murray, K. S.; Swann, I. L.; Pickering, S. R. *Aust. J. Chem.* **1990,** *43,* 1407.
66. Weber, E. *Angew. Chem., Int. Ed. Engl.* **1979,** *18,* 219.
67. Czugler, M.; Weber, E. *J. Chem. Soc., Chem. Commun.* **1981,** 472.
68. Weber, E. *J. Org. Chem.* **1982,** *47,* 3478.
69. Bouquant, J.; Delville, A.; Grandjean, J.; Laszlo, P. *J. Am. Chem. Soc.* **1982,** *104,* 686.
70. Ouchi, M.; Inoue, Y.; Sakamoto, H.; Yamahira, A.; Yoshinaga, M.; Hakushi, T. *J. Org. Chem.* **1983,** *48,* 3168.
71. McAuley, A.; Subramanian, S.; Whitcombe, T. W. *J. Chem. Soc., Chem. Commun.* **1987,** 539.
72. Kajiwara, T.; Yamaguchi, T.; Kido, H.; Kawabata, S.; Kuroda, R.; Ito, T. *Inorg. Chem.* **1993,** *32,* 4990.
73. Kajiwara, T.; Yamaguchi, T.; Oshio, H.; Ito, T. *Bull. Chem. Soc., Jpn.* **1994,** *67,* 2130.
74. Suh, M. P.; Kang, S. G. *Inorg. Chem.* **1988,** *27,* 2544.
75. Rosokha, S. V.; Lampeka, Y. D.; *J. Chem. Soc., Chem. Commun.,* **1991,** 1077.
76. Rosokha, S. V.; Lampeka, Y. D.; Maloshtan, I. M. *J. Chem. Soc., Dalton Trans.* **1993,** 631.
77. Kang, S.-G. Ryu, K.; Jung, S.-K.; Kim, C.-S. *Bull. Korean Chem. Soc.* **1996,** *17,* 331.
78. Bernhardt, P. V.; Comba, P.; Gahan, L. R., and Lawrance, G. A.; *Aust. J. Chem.* **1990,** *43,* 2035.
79. Comba, P.; Hilfenhaus, P. *J. Chem. Soc., Dalton Trans.* **1995,** 3269.
80. Murase, I.; Vučković, G.; Kodera, M.; Harada, H.; Matsumoto, N.; Kida, S. *Inorg. Chem.* **1991,** *30,* 728.
81. Black, D. St. C.; Vanderzalm, C. H. B.; Wong, L. C. H. *Aust. J. Chem.* **1979,** *32,* 2303.

82. Fleischer, E. B.; Sklar, L.; Kendall-Torry, A.; Tasker, P. A.; Taylor, F. B. *Inorg. Nucl. Chem. Lett.* **1973,** *9,* 1061.
83. Murase, I.; Hamada, K.; Kida, S.; *Inorg. Chim. Acta* **1981,** *54,* L171.
84. Lindoy, L. F.; Tokel, N. E.; Anderson, L. B.; Busch, D. H. *J. Coord. Chem.* **1971,** *1,* 7.
85. Murase, I.; Hamada, K.; Ueno, S.; Kida, S. *Synth. React. Inorg. Met.-Org. Chem.* **1983,** *13,* 191.
86. Mochizuki, K.; Endoh, Y. *Bull. Chem. Soc., Jpn.* **1989,** *62,* 936.
87. Foster, K. A.; Brown, D. R.; Timken, M. D.; Van Derveer, D. G.; Belford, R. L.; Barefield, E. K. *J. Coord. Chem.* **1988,** *19,* 123.
88. Mochizuki, K.; Miyashita, S. *Chem. Lett.* **1996,** 899.
89. Mochizuki, K.; Iijima, A.; Endoh, Y.; Ikeda, Y. *Bull. Chem. Soc., Jpn.* **1990,** *63,* 565.
90. Mochizuki, K.; Ikeda, Y. *Bull. Chem. Soc., Jpn.* **1990,** *63,* 1587.
91. Mochizuki, K.; Tsutsumi, M.; Yamaji, Y.; *Inorg. Chim. Acta* **1992,** *191,* 35.
92. Mochizuki, K.; Lu, H. Y.; Suzuki, Y. *Inorg. Chim. Acta* **1993,** *204,* 267.
93. Busch, D. H. *Pure Appl. Chem.* **1980,** *52,* 2477; Busch, D. H.; Jackels, S. C.; Callahan, R. C.; Grzybowski, J. J.; Zimmer, L. L.; Kojima, M.; Olszanski, D. J.; Schammel, W. P.; Stevens, J. C.; Holter, K. A.; Mocak, J. *Inorg. Chem.* **1981,** *20,* 2834; Busch, D. H.; Christoph, G. G.; Zimmer, L. L.; Jackels, S. C.; Grzybowski, J. J., Callahan, R. W.; Kojima, M.; Holter, K. A.; Mocak, J., Herron, N.; Chavan, M. Y.; Schammel, W. P. *J. Am. Chem. Soc.* **1981,** *103,* 5107; Herron, N.; Schammel, W. P.; Jackels, S. C.; Grzybowski, J. J.; Zimmer, L. L.; Busch, D. H. *Inorg. Chem.* **1983,** *22,* 1433; Herron, N.; Schammel, W. P.; Jackels, S. C., Grzybowski, J. J.; Zimmer, L. L.; Busch, D. H. *Inorg. Chem.* **1983,** *22,* 1433; Hoshino, N.; Jircitano, A.; Busch, D. H. *Inorg. Chem.* **1988,** *27,* 2292.
94. Hoshino, N.; Goldsby, K. A.; Busch, D. H. *Inorg. Chem.* **1986,** *25,* 3000.
95. Busch, D. H.; Cairns, C. *Prog. Macrocyclic Chem.* **1987,** *3,* 1; Busch, D. H.; Alcock, N. W. *Chem. Rev.* **1994,** *94,* 585.

STRUCTURE AND PROPERTIES OF COPPER–ZINC SUPEROXIDE DISMUTASES

IVANO BERTINI,* STEFANO MANGANI,† AND MARIA SILVIA VIEZZOLI*

*Department of Chemistry, University of Florence, 50121 Florence, Italy
†Department of Chemistry, University of Siena, 53400 Siena, Italy

0898-8838/98 $25.00

I. The Need for Superoxide Dismutase

Following discovery of the superoxide dismutase[1] (SOD) enzymes by Keilin and Mann (*1*), and their ability to catalyze the dismutation of the superoxide radical anion (O_2^-) in laboratory experiments (*2*), discussion has taken place over the intervening years as to whether such enzymes do catalyze O_2^- dismutation *in vivo*, and whether there is a need for a complex enzyme to accelerate a reaction that is already very fast. This is not the place to address these points, but the current feeling is that the answer to both questions is in the affirmative.

The superoxide radical anion is physiologically produced in controlled amounts in animals and plants from the one-electron reduction of dioxygen occurring in several metabolic pathways (*3–5*). Under pathological conditions, large amounts of superoxide and related active oxygen species are released (*6*, *7*). Thus, a twofold aspect of superoxide effects on living organisms emerges from the available experimental data. First, excess of O_2^- should be eliminated to avoid the formation of radicals and toxic species such as OH and singlet oxygen, which are characterized by very high reactivity; second, O_2^- appears also to be involved in useful processes for the organism, for example, the cell killing effect of tumor necrosis factor and the antibacterial effect of myeloperoxidases (*7*, *8*). The actual role of superoxide dismutase enzymes in living organisms needs to be reconsidered in view of this wider framework. The overall disproportionation reaction, which is catalyzed by SODs, is shown in Eq. (1):

$$2O_2^- + 2H^+ \rightarrow O_2 + H_2O_2. \quad (1)$$

[1] The enzyme residue sequence numbering used throughout the text is that of human Cu_2Zn_2 superoxide dismutase, unless otherwise stated explicitly at the beginning of the section.

Although the stoichiometry of the reaction is correct, it must be taken with the caveat that the reactions that are actually occurring are those of Eqs. (2) and (3):

$$HO_2 + O_2^- \rightarrow O_2 + HO_2^- \tag{2}$$

and/or

$$2HO_2 \rightarrow O_2 + H_2O_2. \tag{3}$$

The direct reaction of superoxide with itself does not play, in practice, a role in the dismutation (see Section IX,A). It is recalled here that the pK_a of HO_2 is 4.8. Hydrogen peroxide is then subject to a further disproportionation by catalases to yield water and dioxygen or it is used as a substrate in reactions of peroxidases. In fact, O_2^- is often produced when a living organism needs H_2O_2 as an oxidant. Reactions such as Eq. (4),

$$NAD(P)H + 2O_2 \rightarrow 2O_2^- + NAD(P)^+ + H^+, \tag{4}$$

are known to be catalyzed by the respiratory burst oxidase in order to produce H_2O_2. Hydrogen peroxide is needed, for example, by horseradish peroxidase to oxidize phenols, by ligninase to attack lignin, by myeloperoxidases to form ClO^-, etc.

In photosynthesis, secondary pathways for electron transfer actually lead to superoxide production (*9–12*), the thylakoid-bound Cu_2Zn_2SOD catalyzing the O_2^- dismutation. Because the chloroplasts lack catalase, the excess H_2O_2 is a substrate for ascorbate peroxidases to produce dehydroascorbate, which is further re-reduced by NADPH via the glutathione–glutathione reductase pathway (*12*).

If we now believe that SOD catalyzes reaction (1), we should be aware that any metal having two oxidation states with a reduction potential between that of the O_2/O_2^- (−0.33 V vs. NHE, pH 7, P_{O_2} = 0.101 MPa)[2] and O_2^-/H_2O_2 (+0.89 V vs. NHE, pH 7) redox couples can catalyze the dismutation according to Eqs. (5) and (6):

$$M^{n+} + O_2^- \rightarrow M^{(n-1)+} + O_2 \tag{5}$$

$$M^{(n-1)+} + O_2^- + 2H^+ \rightarrow M^{n+} + H_2O_2. \tag{6}$$

[2] If unit activity is used for the standard state of O_2, instead of unit pressure, the reduction potential must be adjusted by +0.17 V.

However, the concentration of free transition-metal ions in living organisms is very low because such ions are complexed or precipitated at physiological pH.

From all the above considerations it would appear that, in order to protect species from toxic effects of superoxide release in tissues, living organisms need an efficient catalyst for superoxide dismutation, and that SOD accomplishes this task with maximum efficiency. In this respect, recent experiments have demonstrated that SOD-deficient bacteria and yeast mutants are highly sensitive to dioxygen (*13*, *14*), suggesting that SOD activity is important for aerobial cell growth. Furthermore, evidence has been provided that, in *Drosophila melanogaster,* Cu_2Zn_2SOD may protect against ionizing radiation and may even give increased longevity in combination with catalase (*15*, *16*). In humans, motor neuron degenerative diseases are in some cases associated with genetic mutations leading to cytosolic SOD of reduced activity (*17*, *18*), or of altered peroxidase-like activity (*19*, *20*).

Besides the O_2^- production by stimulated immune system cells (such as macrophages and neutrophils exposed to oxidative burst during the inflammatory process) (*21–25a*), the steady release of O_2^- over time intervals has been observed in human fibroblasts in response to cytokines such as interleukin-1α and tumor necrosis factor-α (*25*). This suggests that continuous O_2^- production may have a role in the regulation of inflammatory processes (*7*). Consequently, the role of superoxide dismutases in such compartments may be that of ensuring O_2^- homeostasis rather than its scavenging.

The physiological processing of O_2^- is performed by three different metalloenzymes: Fe, Mn, and Cu–Zn SOD. Recently, a protein having superoxide activity, containing nickel, has been isolated from *Streptomices grisens* (*25b*). The Cu–Zn SOD enzyme, which we are dealing with here, is found in eukaryotes and in bacteria (*25a*). The enzyme maintains an intracellular level of O_2^- at 10^{-12}–10^{-11} *M* (*26*). A common isoenzyme is isolated from red blood cells and is a dimer of 32,000 MW, like cytoplasmic and most of the periplasmic Cu_2Zn_2 SODs. On the other hand, chloroplastic and extracellular enzymes are tetrameric. A natural monomeric species has been isolated from the periplasmic space of an *Escherichia coli* strain. This CuZnSOD displays a catalytic activity comparable to that of bovine SOD, but is highly sensitive to proteases (*27*).

A comparison of sequences of different Cu_2Zn_2SODs (Fig. 1) shows that 23 amino acids are invariant, and that most of them are residues close to or part of the active site. Some are at the dimer interface and some are a part of the conserved "Greek key" β-barrel supersecondary

structure (*28*). At the active site, besides those amino acids coordinating the copper and zinc ions, there are other invariant residues, such as Arg-143, involved in substrate guidance and recognition, and Asp-124, which helps to orientate correctly copper and zinc ligands by hydrogen bonding to His-46 (Cu ligand) and His-71 (Zn ligand). There are also five glycines that, because of their small size, contribute to maintaining the structure of the active site (see Section II). Pro-66 is another conserved residue close to the active site; due to its rigid stereochemical constraints, it contributes to stabilizing the conformation of the zinc loop (see Section II).

At the dimer interface Gly-51 and Gly-114 are invariant residues that form hydrogen bonds with the nonconserved residue at position 151; Cys-57 and Cys-146 form a disulfide bridge stabilizing a region of the protein structure involved in monomer/monomer contact (see Section II). Four invariant residues, two Gly (16 and 147), one Phe (45), and one Leu (106) seem to contribute to maintaining the stable Greek key β-barrel fold (see Section II).

Even if sequence invariance occurs for residues connected with the active site or with the dimeric nature of the protein, it has been demonstrated through site-directed mutagenesis that invariance does not necessarily prove that a residue is essential for activity (*28*).

The dimeric enzyme is very stable (*29*, *30*). Copper and zinc play a relevant role in stabilizing the structure (*31*). To unfold human SOD requires 6 *M* guanidinium chloride, whereas 3.5 *M* concentration unfolds the metal-depleted form. Unfolding measurements on SOD using variable concentrations of the denaturing agents guanidinium chloride and urea indicate the presence of a concentration-dependent monomer $\rightleftharpoons$ dimer equilibrium (*32*, *33*); 8 *M* urea causes dissociation of bovine SOD into active subunits (*34*, *35*). The possible monomer $\rightleftharpoons$ dimer equilibrium *in vivo* is an intriguing issue (*33*). It is noteworthy that an isoenzyme of rice SOD and an isoenzyme from *E. coli* were isolated as an active monomer (*27*, *36*).

FIG. 1. Multiple alignment of amino acid sequences of 38 Cu–Zn SODs: The amino acid numbering scheme of bovine SOD, used as a reference, is at the top of the figure. Alignment positions in β-strand conformation in the bovine structure are included in shaded boxes. Residues involved in subunit contacts in the dimeric form of bovine SOD are indicated by black boxes placed above the bovine sequence. The amino acids forming the upper rim of the electrostatic channel are denoted by empty boxes. Reprinted with permission from Ref. *347*.

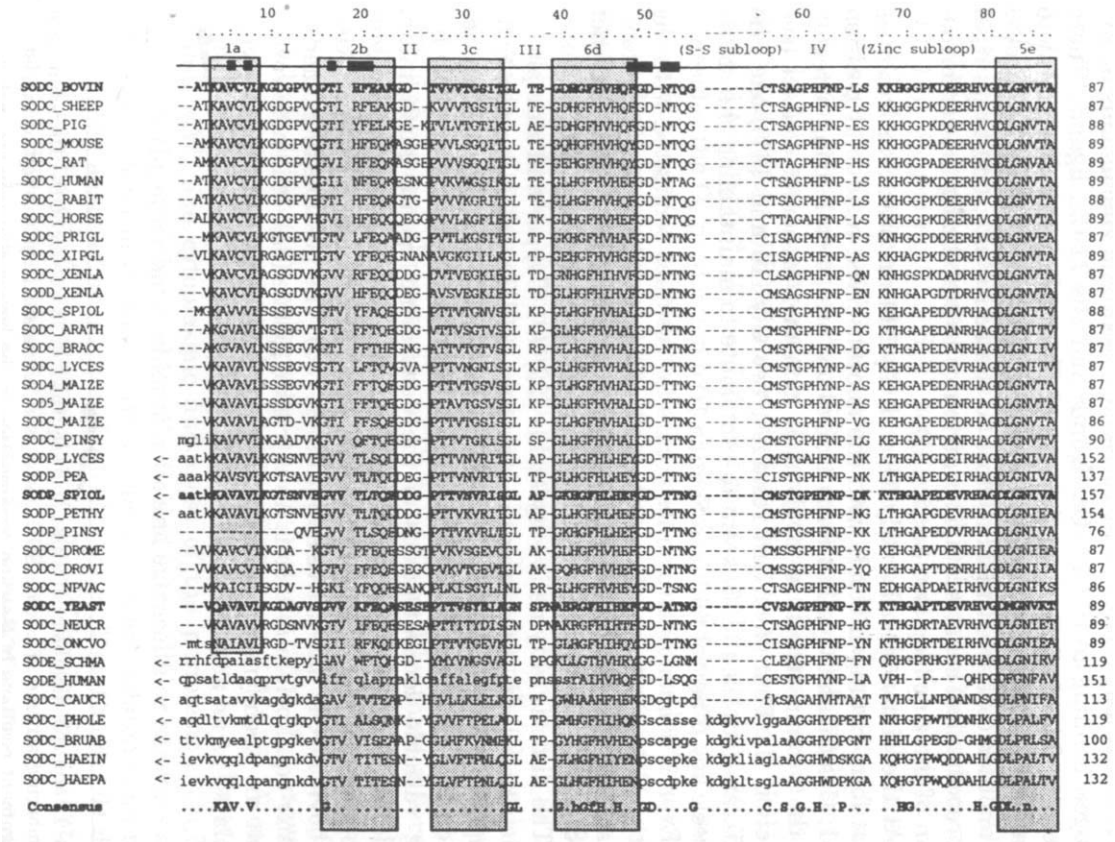
10
20
30
40
50
60
70
80
1a
I
2b
II
3c
III
6d
(S-S subloop)
IV
(Zinc subloop)
5e
SODC_BOVIN
SODC_SHEEP
SODC_PIG
SODC_MOUSE
SODC_RAT
SODC_HUMAN
SODC_RABIT
SODC_HORSE
SODC_PRIGL
SODC_XIPGL
SODC_XENLA
SODD_XENLA
SODC_SPIOL
SODC_ARATH
SODC_BRAOC
SODC_LYCES
SOD4_MAIZE
SOD5_MAIZE
SODC_MAIZE
SODC_PINSY
SODP_LYCES
SODP_PEA
SODP_SPIOL
SODP_PETHY
SODP_PINSY
SODC_DROME
SODC_DROVI
SODC_NPVAC
SODC_YEAST
SODC_NEUCR
SODC_ONCVO
SODE_SCHMA
SODE_HUMAN
SODC_CAUCR
SODC_PHOLE
SODC_BRUAB
SODC_HAEIN
SODC_HAEPA
Consensus

FIG. 1.

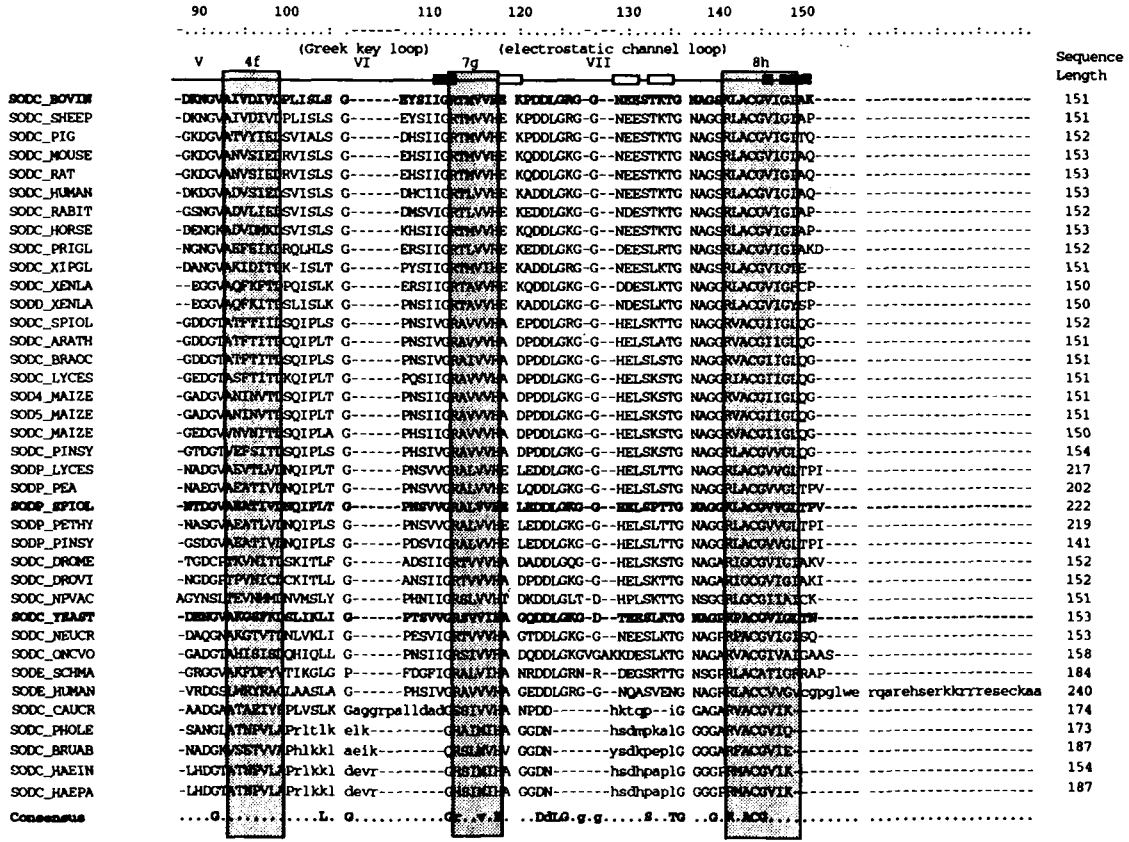

FIG. 1. Continued.

II. The Crystal Structures of Dimeric Copper–Zinc Superoxide Dismutases

Accurate three-dimensional structures of proteins by single-crystal X-ray diffraction experiments provide a powerful aid in the interpretation of information from other techniques, leading to a deeper understanding of the chemistry and the biological function of the molecules. The X-ray crystal structure determination of Cu_2Zn_2SOD[3] represents a fundamental step toward a thorough knowledge of the enzyme.

It must be recognized that precise information about the local structure of metal centers in different phases (solution, glassy or frozen solutions, amorphous) has also been provided by spectroscopic techniques such as nuclear magnetic resonance, X-ray absorption spectroscopy, and electron–nuclear double resonance on native, reduced, or metal-substituted SOD derivatives.

A. Bovine Cu_2Zn_2SOD

1. The Overall Structure

The first X-ray studies on a Cu_2Zn_2SOD were performed by the Richardson group over the decade 1972–1982 on the enzyme from bovine erythrocytes (*37–40*) and resulted in a structure refined at 2.0 Å resolution (*41a*). The Cu_2Zn_2SOD dimers from bovine erythrocytes are made of two subunits of identical amino acid composition, each containing 151 residues. The crystal structure has revealed that the two monomers are related by an almost exact, noncrystallographic twofold axis. The monomers show extensive contact mediated by hydrophobic and hydrophilic interactions that involve about 9% of the total monomer surface (*41a*) (see Section II,A,5).

The main features of the SOD monomer fold are a characteristic eight-stranded β-barrel and three long loops of nonorganized secondary structure. The β-barrel is made of eight antiparallel β-strands connected by seven turns and loops in the Greek key β-barrel motif (*41a*). Figure 2 shows a side view (a) and a top view (b) of the enzyme ribbon diagram with the traditional numbering used for bovine Cu_2Zn_2SOD (*41a*). The turn and loop numbering follows that introduced by Getzoff *et al.* (*28*). The strands are numbered consecutively starting from the N terminus and proceeding clockwise around the barrel. The turns and loops connecting the eight β-strands are indicated by ro-

[3] Within this section the enzyme residue numbering will follow that of the sequence of each structurally determined SOD; hence, residues having the same role in the enzyme may differ in their numbering.

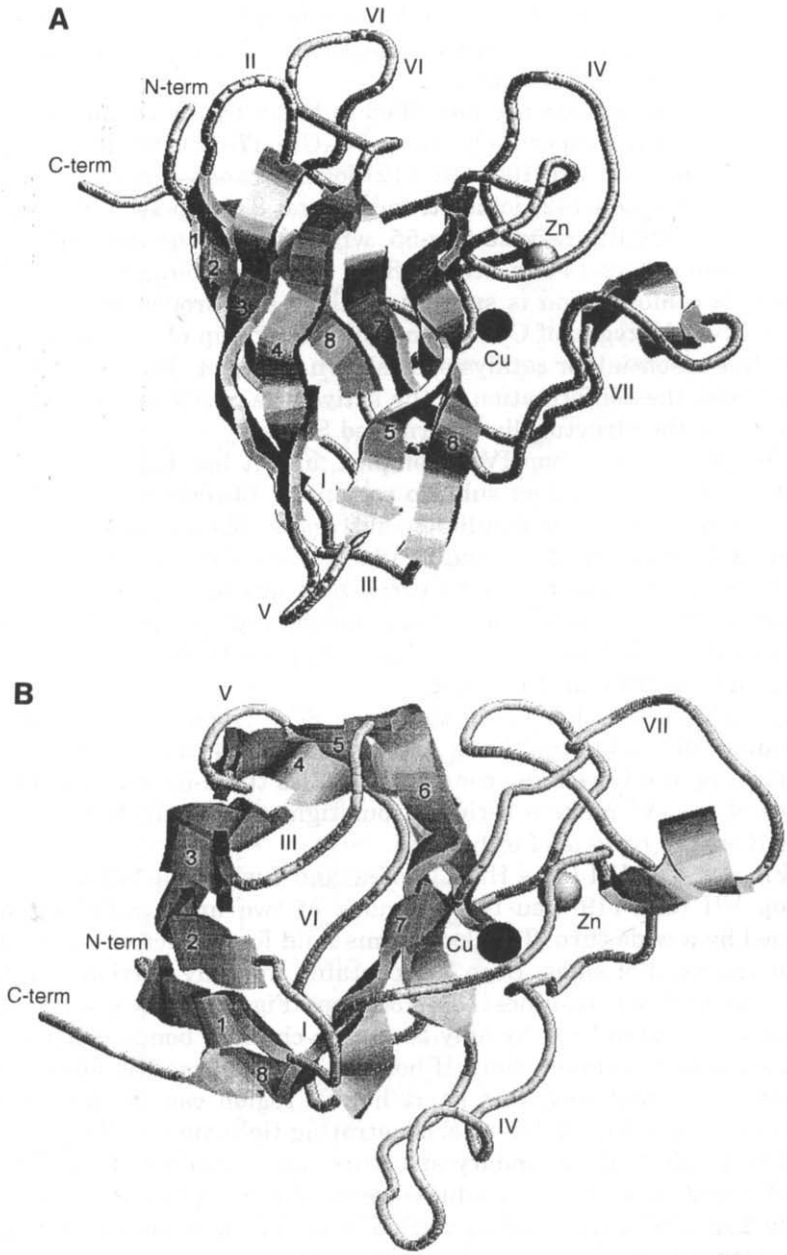

FIG. 2. Ribbon diagram of the Cu_2Zn_2SOD monomer showing the secondary structures of the enzyme and the arrangement of the eight strands in the Greek-key barrel fold. (the β strands and loops are numbered following the conventions established in Refs. *28* and *41*). The metal ions are represented as spheres of arbitrary radius. (A) Side view; (B) top view highlighting the β-barrel and the active site location.

man numerals that follow the order in which they occur in the amino acid sequence. Figure 3 shows the amino acid sequence and topology of a bovine Cu_2Zn_2SOD subunit.

The three long loops are identified in Fig. 2 by the roman numerals IV, VI, and VII, respectively. Loop IV (Gln-47–Leu-82) joins strands 6 and 5, loop VI (Pro-100–Gly-112) joins strands 4 and 7, and loop VII (Glu-119–Leu-142) joins strands 7 and 8. Loop IV is the longest loop and hosts the residue Cys-55, which makes the disulfide bridge with residue Cys-144 in strand 8. It must be pointed out that the disulfide conformation is such as to allow a hydrogen bond between the carbonyl oxygen of Cys-55 and the NH_2 group of residue Arg-141, which is essential for catalysis, as shown in Fig. 4. The disulfide bond influences the conformation of the active site cavity and is conserved among all the structurally determined SODs.

The structure of loop IV is complex, and it has been described as composed of two distinct subloop regions: a 14-residue loop (Gln-47–Pro-60) containing the disulfide bond, and a 22-residue loop (His-61–Leu-82) bearing the Zn-ligand residues (*41a*). The first subloop region contains a series of five tight turns that are linked by three main-chain hydrogen bonds. The second subloop region starts from His-61 and contains four more turns. This region hosts the Zn binding site and includes all four Zn ligands.

Loop VI is the shortest of the three SOD loops and it is made by residues 100 to 112 and links Asp-99 of strand 4 to Arg-113 of strand 7, forming the Greek key connection across the β-barrel. The 13 residues of loop VI make a series of four tight turns, which also involve one β-strand residue of either end.

Finally, loop VII links His-118 of strand 7 with Ala-143 of strand 8. Loop VII (Glu-119–Leu-142) is made of two antiparallel stretches joined by a wide turn. This loop forms a lid for the active site with its two antiparallel sides. Loop VII contains the only portion of α-helix present in SOD (residues 131–136) (see Fig. 2). It is a six-residue-long α-helix stabilized by only two main-chain H bonds, whereas the six side-chain to main-chain H bonds distort it from the ideal conformation. Alternatively, this short helical region can be described as formed by a series of five interpenetrating tight turns (*41a*).

The Cu_2Zn_2SOD secondary structure has a marked β-character in that about 62% of the residues are in the β conformation whereas only 26% are in the α conformation. Most of the latter are located in the loop regions and only six residues build the α-helix in loop VII. About 70 residues are involved in the eight-stranded β-barrel.

The eight β-strands forming the walls of the β-barrel display an overall right-handed twist. Strands 1,2 and 5,4 are joined by five-

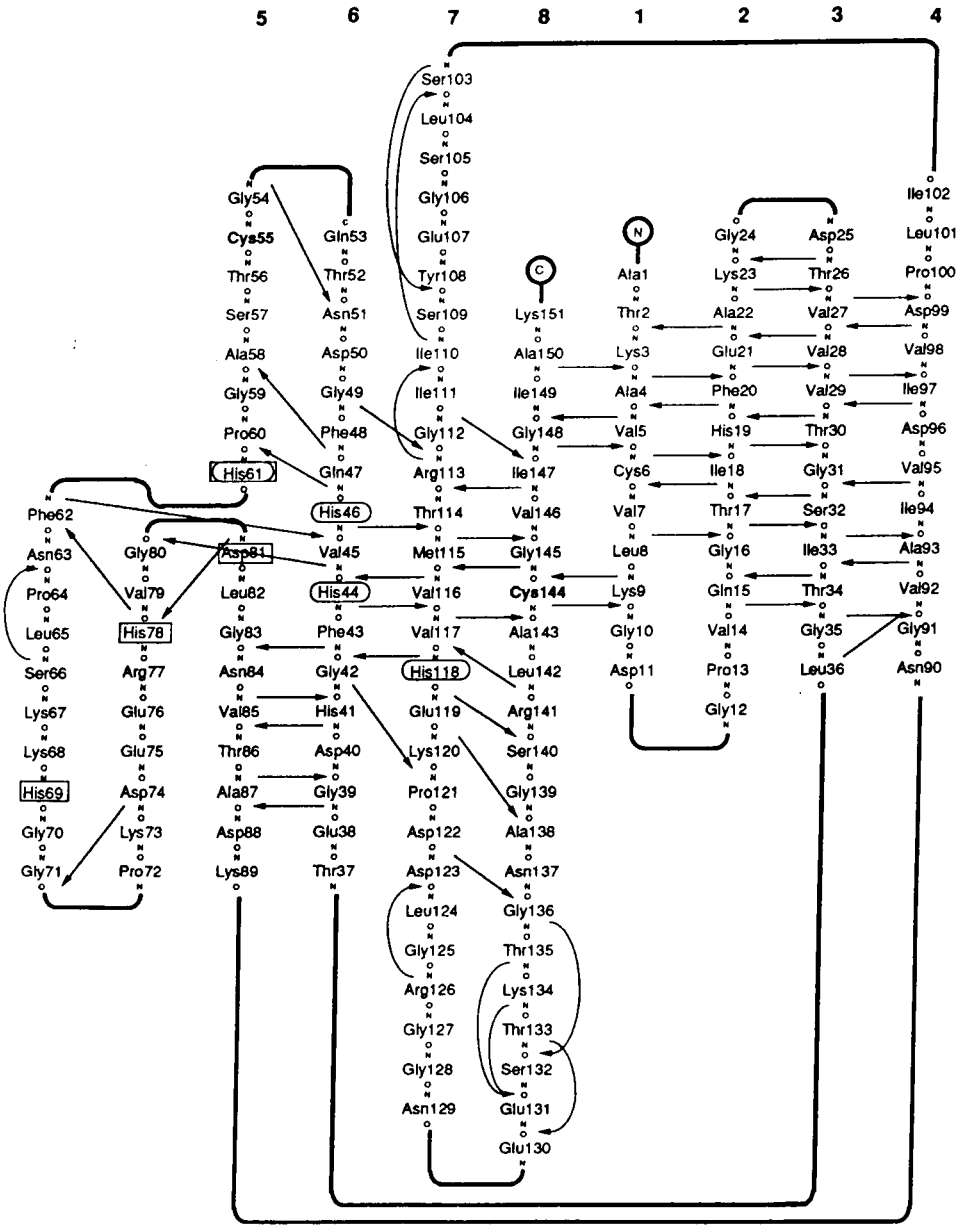

FIG. 3. Amino acid sequence of bovine SOD and its topology. Main-chain to main-chain hydrogen bonds are represented by arrows. Residues coordinating the copper ion are marked with oval boxes; residues coordinating the zinc ion are marked with rectangular boxes. Cys-55 and Cys-144, which form the disulfide bridge, are in bold type. The conventional β-strand numbering is shown at the top of the figure. Reprinted with permission from Ref. *48*.

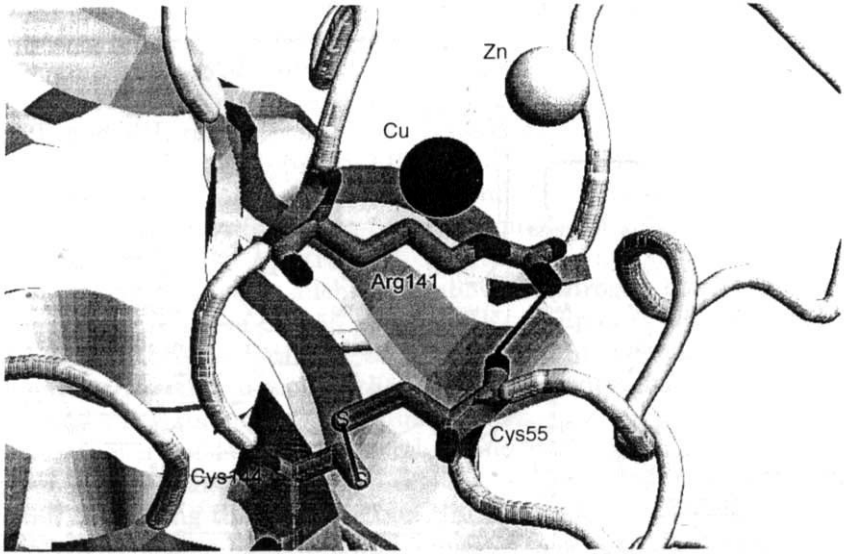

FIG. 4. View of the disulfide bridge between Cys-55 and Cys-144. The H bond linking the Cys-55 carbonyl oxygen with the guanidinium group of Arg-141 is also shown.

residue turns, whereas strands 2,3 are joined by a type II'[4] tight turn in a hairpin connection. Strand 3 links the nonadjacent strand 6 across the barrel in a Greek key topology and, as already mentioned, the other β-strand links are made by the three main loops.

Apart from the β-strands, the second major element of secondary structure in SOD is constituted by the tight turns that are made by four amino acid residues and that may contain a hydrogen bond between the carbonyl oxygen of the *n*th residue and the amide proton of the *n*th + 3 residue. The 56 residues are involved in such tight turns, and only one of them joins two adjacent β-strands while the remaining 17 occur in loop regions. Out of the 18 four-residue tight turns, 12 are of type I, two of type I', two of type II', and one of type II, and one of type IV. The category of five-residue turns is present in SOD with the two turns Gly-10–Val-14 and Asp-88–Val-92.

2. *Refinement Technique*

This crystal structure has been refined using the Hendrickson–Konnert restrained refinement technique (*42*, *43*), which minimizes the sum of weighted squares of the differences between the observed

[4] The nomenclature of the secondary structure follows the categories defined by Lewis *et al.* (*41b*).

and calculated structure factors and stereochemical parameters. The weights used were the inverse of the parameter variance. Noncrystallographic symmetry restraints were used between selected atoms of the four different subunits, which were selected as clearly equivalent atoms. In the active site the only imidazole ring of His-61 was refined unrestrained whereas the remaining metal-to-ligand bond lengths and angles were refined restrained. The structure has been refined to an R factor of 0.255 for the 4392 atoms of the model against the 16,245 reflections between 7.0- and 2.0-Å spacings. The model has been completed by adding the active site water molecules and further refined to an R factor of 0.193 against a selected subset of data containing 15,253 reflections between 4.0- and 2.0-Å spacings (*28*, *44*). The second model also contained hydrogen atoms added to one monomer in calculated positions.

3. The Active Site Cavity

The active site cavity is built outside the β-barrel, between loops IV and VII, and consists of a crevice about 15 Å deep and 12 Å long that narrows to about 3 Å in the proximity of the copper, making it perfectly suited to host the small cylindrical superoxide substrate. The copper has a solvent-exposed surface of only 5.2 Å^2, and the zinc is completely buried in the protein (*44*). The rim of the cavity is a highly conserved region in different Cu_2Zn_2SODs. It hosts charged residues that give rise to an electric field (*45*, *46*). The electrostatic gradient generated by the positive and negative charges present in the cavity is thought to be responsible for the steering of the superoxide anion toward the active site (*vide infra*). The side chains of Glu-130, Glu-131, Lys-134, and Thr-135 are on one side of the cavity, and on the opposite side the catalytically important Arg-141 side chain lies at about 6 Å from the copper. The side chains of Glu-119 and Lys-120 complete the edge of the opening. The cavity crevice extends from Thr-135 toward the zinc binding site. Figure 5 shows the cavity with the residues that are important in determining the shape and the strength of the electrostatic field (*45*).

The cavity hosts a chain of water molecules that are found in almost invariant positions in every crystal structure. This network extends from the water molecule coordinated to copper in two opposite directions and links that water molecule with the bulk solvent. The coordinate set deposited within the Protein Data Bank (*47*) (PDB code 2SOD) contains only the copper-bound water molecule; Fig. 6 shows, as an example, the water molecule chain observed in the reduced form of the bovine erythrocyte Cu_2Zn_2SOD structure (PDB code 1SXA) (*48*).

Usually these waters are well ordered and may indicate the path-

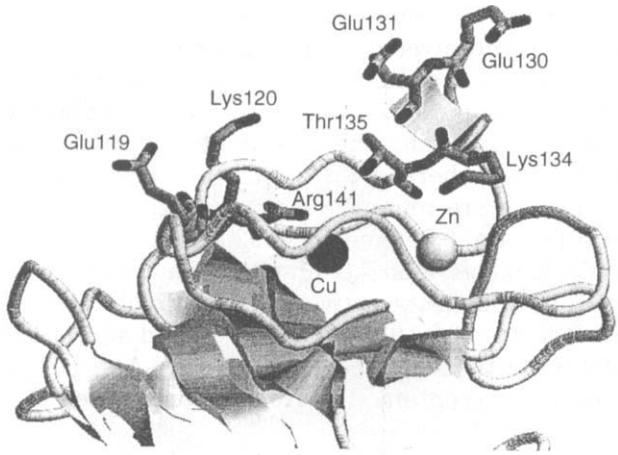

FIG. 5. Ribbon diagram of the enzyme showing the active site cavity. The residues considered important for activity are represented in full as sticks. The zinc and copper ions are represented as spheres of arbitrary radius.

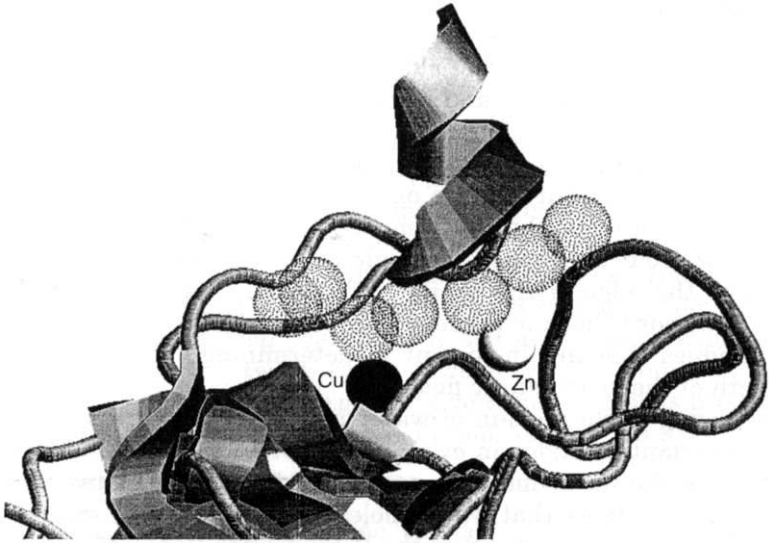

FIG. 6. The water structure in the active site of bovine SOD as obtained from the crystal structure of the reduced enzyme at pH 7.5 (1SXA). The water molecules are represented as spheres of radius corresponding to the van der Waals radius of the oxygen atom, superimposed on the ribbon diagram of the enzyme.

way of substrate diffusion into the active site. Furthermore, the water chain may provide an efficient relay system to deliver into the active site the protons needed by the reacting substrate. They may thus play an essential role in the catalytic mechanism (*48*, *49*). The function of water molecules in enzyme active sites has been reviewed (*50*, *51*) and it is a very attractive and active subject of investigation that can take advantage of the enormous amount of information contained in the crystal structure data collected in the PDB database.

4. The Active Site

Each monomer hosts an active site where one Cu(II) ion and one Zn(II) ion are bound. The active site is located between loops IV and VII on the external surface of the β-barrel, in front of β-strands 5, 6, and 7 (Fig. 2). The copper ligand residues are all located on the β-barrel except for His-61, which belongs to loop IV like the other zinc ligand residues.

The catalytic center is the copper ion, which is coordinated by four histidines (His-44, His-46, His-61, and His-118) and by a weakly bound water molecule in a geometry sometimes described as a distorted square pyramid (square planar) and sometimes as a distorted flattened tetrahedron (Fig. 7).

In any case, the Cu(II) site deviates markedly from an ideal coordination geometry. The water molecule occupies the apical position toward the opening of the cavity. The zinc ion is bound to three histidines (His-61, His-69, and His-78) and to an aspartate residue (Asp-81) in an al-

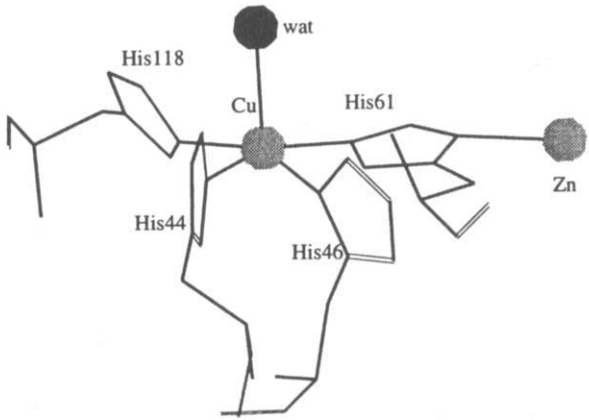

FIG. 7. Sketch of the copper coordination polyhedron obtained from the 2SOD crystal structure. The copper and zinc atoms and the water molecule are represented by spheres of arbitrary radius.

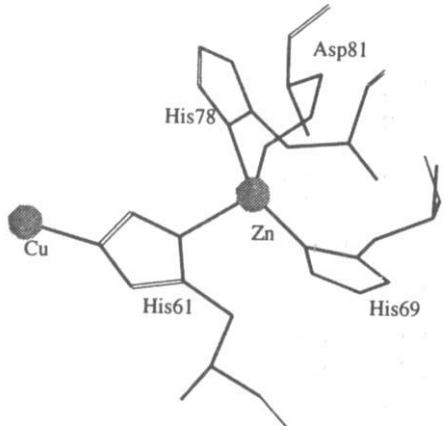

FIG. 8. Sketch of the zinc coordination polyhedron obtained from the 2SOD crystal structure. Copper and zinc are represented by spheres of arbitrary radius.

most regular tetrahedral geometry (Fig. 8). For a long time the zinc ion was believed to play merely a structural role in the enzyme; indeed it may be replaced by several other metals [Co(II), Cu(II), Cd(II), Hg(II)] with only a minor loss in activity with respect to native enzyme.

In this monoclinic form (space group $C2$) of the bovine Cu_2Zn_2SOD there are four independent subunits: no significant differences have been found in the metal site geometries of the four subunits. Figure

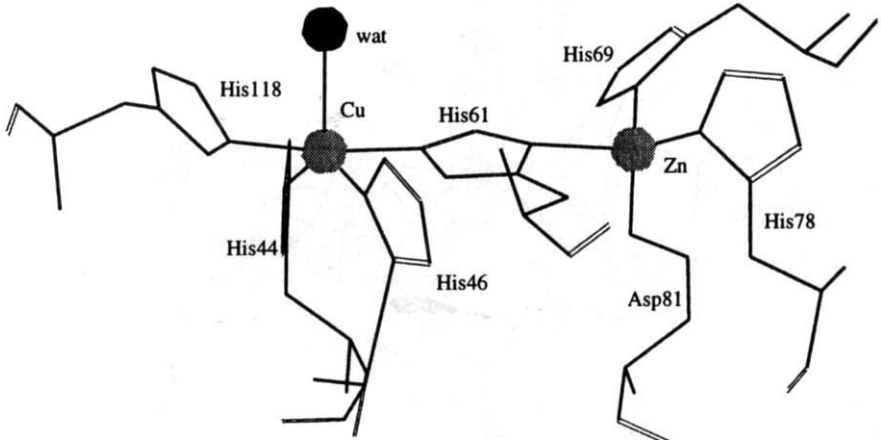

FIG. 9. Overall view of the metal coordination in the active site obtained from the 2SOD crystal structure. The metals and the water interacting with copper are represented by spheres of arbitrary radius.

9 shows an overall view of the metal coordination as determined in the 1982 crystal structure.

The unique feature of this metal site is that one of the histidines, His-61 in the bovine enzyme sequence, provides an imidazolate ligand to the two metals, bridging zinc and copper by binding them through the Nδ1 and Nε2 atoms of its pentaatomic ring, respectively. Such coordination brings the two cations to a distance of about 6.5 Å. Spectroscopic data have suggested that the imidazolate bridge is stable over the whole pH range where SOD activity is invariant (pH 5.0–9.5) (*52*). Indeed, the bridge has been observed unbroken in crystals of Cu_2Zn_2SOD obtained in the pH range 5.0–7.5 (*vide infra*). Imidazolate bridges between two metal ions are common in small molecule complexes, but this is the only case so far that such a ligand has been found in a protein. Studies on model compounds have shown that the binding of a metal ion to a histidine imidazole nitrogen can lower the pK_a of the other NH group by several pH units (*53*). The metal ion binding to histidine thus promotes the substitution of the free NH proton by a second metal ion so to cause an apparent reduction of the pK_{a2} of the histidine imidazole ring from 14.4 to below 5.0, a step of about 10 pH units.

It is important to point out that the shape of the active site cavity and the disposition of the copper ligands are such that the only access to the copper coordination is from the opening of the cavity, where a fifth coordination position is available for the substrate or the inhibitors. Indeed, in the crystal structures, every exogenous ligand is found bound to such position, which is usually associated with weaker bonding to the square planar cupric ion. Only the strongest ligands, such as azide and cyanide, are able to make a close approach to Cu(II) by causing the loosening of the Cu(II)–His-46 bond (see Section II,J). These structural aspects of the active site have obvious mechanistic implications that will be discussed in Section IX.

The orientation of the metal ligands is determined by a series of hydrogen bonds forming a complex network. All the potential H-bonding atoms of the seven groups acting as metal ligands are involved in hydrogen bonding with other protein atoms. Exceptions are provided by two of them, and these are exposed to the solvent: the His-61 peptide NH group, which is H-bonded to a water molecule in the active site channel, and the His-69 carbonyl oxygen, which is H-bonded to a water molecule external to that channel.

The zinc coordination bonds involve only the zinc-binding region of loop IV, and the residues that are H-bonded to Zn ligands are also located mainly in that region of the monomer (Asn-63, Lys-67, Lys-68, Arg-77, His-78, and Asp-81) or in loop VII (Asp-122 and Thr-133).

The Cu ligands instead join strands 6 and 7 with loop IV. The residues that are H-bonded to the Cu ligands involve β-strands 6 (His-41, Gly-42) and 7 (Thr-114, Val-116) as well as loop VII (Asp-122, Gly-139) and both regions of loop IV (Gly-59 in the disulfide region, Asn-63 in the zinc binding region).

Tainer *et al.* (*41a*) argue that the larger number of different structural elements brought together by the Cu binding network with respect to the Zn network may account for the larger effect of Cu site occupancy on the thermal stability of the enzyme. Indeed it has been shown that removal of the copper ion causes a greater lowering of the thermal denaturation temperature of the enzyme than does removal of the zinc ion (*54*). For a long time it has been noted that the involvement of residues from multiple structural elements and the wide separation in the amino acid sequence of metal ligands are characteristic of catalytic sites as opposed to structural or storage sites (*55*).

In all four independent monomers present in the asymmetric unit of the Cu_2Zn_2SOD monoclinic structure, there is a second bridge between Cu and Zn. This is made by the H bonds that link the Zn ligand His-69 with the Cu ligand His-44 through the fully deprotonated carboxyl group of Asp-122. This group is completely buried and inaccessible to the solvent and forms short, strong, charged H bonds with the above histidine residues, whose electron density is very well defined in all subunits. Residue Asp-122 is invariant in SOD sequences, and helps to properly orientate the Cu and Zn ligands. Tainer *et al.* (*41a*) have suggested that the H bonds between Asp-122, His-44, and His-69 may have a role in determining the reduction potential of the Cu(II) ion.

Table I reports the crystal structures of Cu_2Zn_2SOD enzymes so far determined and deposited with the Brookhaven Protein Data Bank (*47*). It should be noticed that Cu_2Zn_2SOD has the ability to crystallize in different space groups depending on the crystallization conditions. This suggests that the protein has the ability to make different intermolecular contacts with different groups depending on the pH and the medium used for crystallization. The variability of Cu_2Zn_2SOD crystal forms provides a unique opportunity to analyze and rationalize the factors influencing its crystal packing, and this has not yet been exploited.

The SOD dimer has been described as generated by the action of a dyad axis on one of the monomers. The two monomers are very similar, but an analysis of the coordinates deposited with the PDB shows that there are significant deviations from the binary symmetry involving the main polypeptide chain and also the active sites (obvi-

TABLE I

PUBLISHED CRYSTAL STRUCTURES OF Cu_2Zn_2SODs (EC 1.15.1.1)[a]

Source: Bovine erythrocytes (*41*)
PBD code, 2SOD; space group, *C*2; $Z = 4$
Cell: $a = 93.65$, $b = 90.33$, $c = 71.65$, $\beta = 95.1$
Asymmetric unit content: two dimers
Max. resolution, 2.0 Å; completeness, NR; R_m, NR; R, 0.255

Source: Human erythrocyte, recombinant, expressed in yeast (*S. cerevisiae*) (*63*)
PDB code; 1SOS; space group, $C222_1$; $Z = 8$
Cell: $a = 205.2$, $b = 167.0$, $c = 145.5$
Asymmetric unit content: five dimers
Max, resolution, 2.5 Å; completeness, 81.5%; R_m, NR; R, 0.210

Source: Human erythrocyte, recombinant, expressed in yeast (*S. cerevisiae*) (*18*)
PDB code, 1SPD; space group, $P6_3$; $Z = 6$
Cell: $a = b = 113.5$, $c = 71.5$
Asymmetric unit content: one dimer
Max. resolution, 2.4 Å; completeness, 89.8%; R_m, NR; R, 0.224

Source: *Xenopus laevis,* expressed in *E. coli* (*49*)
PDB code, 1XSO; space group, $P2_12_12_1$; $Z = 4$
Cell: $a = 73.33$, $b = 68.86$, $c = 59.73$
Asymmetric unit content: one dimer
Max. resolution, 1.5 Å; completeness, 98.8%; R_m, 0.078; R, 0.104

Source: Yeast (*S. cerevisiae*), 277 K (*74*, *75*)
PDB code, 1SDY; space group, $P2_12_12$; $Z = 4$
Cell: $a = 105.3$, $b = 143.0$, $c = 62.1$
Asymmetric unit content: two dimers
Max. resolution, 2.5 Å; completeness, 98.2%; R_m, 0.06; R, 0.158

Source: Spinach leaves (*72*)
PDB code, 1SRD; space group, *C*2; $Z = 4$
Cell: $a = 166.27$, $b = 45.97$, $c = 85.68$, $\beta = 99.38$
Asymmetric unit content: two dimers
Max. resolution, 2.0 Å; completeness, NR; R_m, 0.048; R, 0.249

Source: Yeast (*S. cerevisiae*) reduced, 93 K (*56*)
PDB code, 1JCV; space group, *R*32; $Z = 12$
Cell: $a = 118.39$, $b = 118.39$, $c = 73.50$
Asymmetric unit content: one monomer
Max. resolution, 1.55 Å; completeness, 86.7%; R_m, 0.092; R, 0.190

Source: Yeast (*S. cerevisiae*), reduced (*56*)
PDB code, 1JCW; space group, *R*32; $Z = 12$
Cell: $a = 119.28$, $b = 119.28$, $c = 75.05$
Asymmetric unit content: one monomer
Max. resolution, 1.7 Å; completeness, 82.3%; R_m, 0.099; R, 0.186

Source: Yeast (*Candida albicans*), reduced (*56*)
PDB code, 1YSO; space group, *R*32; $Z = 12$
Cell: $a = 119.33$, $b = 119.33$, $c = 75.19$
Asymmetric unit content: one monomer
Max. resolution; 1.73 Å; completeness, 92.4%; R_m, 0.063; R, 0.182

Source: Bovine erythrocytes, reduced, 277 K (*48*, *82*)
PDB code, 1SXA; space group, $P2_12_12_1$; $Z = 4$
Cell: $a = 47.89$, $b = 51.14$, $c = 148.15$
Asymmetric unit content: one dimer
Max. resolution, 1.9 Å; completeness, 90.5%; R_m, 0.073; R, 0.166

Source: Bovine erythrocytes, reduced, 277 K (*48*, *82*)
PDB code, 1SXB; space group, $P2_12_12_1$; $Z = 4$
Cell: $a = 47.71$, $b = 50.98$, $c = 147.82$
Asymmetric unit content: one dimer
Max. resolution, 2.0 Å; completeness, 98.0%; R_m, 0.076; R, 0.152

Source: Bovine erythrocytes, reduced, 277 K (*48*)
PDB code, 1SXC; space group, $P2_12_12_1$; $Z = 4$
Cell: $a = 47.89$, $b = 51.14$, $c = 148.15$
Asymmetric unit content: one dimer
Max. resolution, 1.9 Å; completeness, 97.0%; R_m, 0.100; R, 0.156

Source: Bovine erythrocyte mutant Cys-6Ala, 277 K (*80*)
PDB code, 3SOD; space group, *C*2; $Z = 4$
Cell: $a = 92.5$, $b = 89.4$, $c = 70.5$, $\beta = 95.7$
Asymmetric unit content: two dimers
Max. resolution, 2.1 Å; completeness, 82.0%; R_m, 0.099; R, 0.190

Source: Bovine erythrocytes, zinc substituted by cobalt, 277 K (*76*)
PDB code, 1COB; space group, $P2_12_12_1$; $Z = 4$
Cell: $a = 51.0$, $b = 147.6$, $c = 47.5$
Asymmetric unit content: one dimer
Max. resolution, 2.0 Å; completeness, 75.2%; R_m, 0.068; R, 0.176

Source: Bovine erythrocytes nitrated at Tyr-108 (*79*)
PDB code, 1SDA; space group, *C*2; $Z = 4$
Cell: $a = 93.65$, $b = 90.33$, $c = 71.65$, $\beta = 95.1$
Asymmetric unit content: two dimers
Max. resolution, 2.5 Å; completeness, 89.0%; R_m, 0.033; R, 0.187

Source: *Xenopus laevis,* native, complex with cyanide, 98 K (*87*)
PDB code, 1XSO; space group, $P2_12_12_1$; $Z = 4$
Cell: $a = 72.15$, $b = 68.10$, $c = 57.57$
Asymmetric unit content: one dimer
Max. resolution, 1.7 Å; completeness, 85.9%; R_m, 0.051; R, 0.172

(*Continues*)

TABLE I (*Continued*)

Source: Bovine erythrocytes, reduced, complex with azide, 277 K[b]
PDB code, 1SXZ; space group, $C222_1$; $Z = 8$
Cell: $a = 104.6$, $b = 197.5$, $c = 50.8$
Asymmetric unit content: one dimer
Max. resolution, 2.0 Å; completeness, 87.8%; R_m, 0.074; R, 0.165

Source: Bovine erythrocytes, reduced, complex with thiocyanide, 277 K[b]
PDB code, 1SXS; space group, $C222_1$; $Z = 8$
Cell: $a = 104.6$, $b = 197.5$, $c = 50.8$
Asymmetric unit content: one dimer
Max. resolution, 2.0 Å; completeness, 96.9%; R_m, 0.076; R, 0.175

Source: Bovine erythrocytes, native, complex with azide, 277 K (*90*)
PDB code, not in PDB; space group, $P2_12_12_1$; $Z = 4$
Cell: $a = 50.99$, $b = 147.63$, $c = 47.53$
Asymmetric unit content: one dimer
Max. resolution, 2.1 Å; completeness, 96.6%; R_m, 0.083; R, 0.166

[a] Cell dimensions are in angstroms, cell angles are in degrees. The crystal structures have been determined at room temperature if not stated explicitly. NR, Not reported. $R_m = \Sigma|I_i - \langle I\rangle|/\Sigma\langle I\rangle$, where I_i is an individual intensity measurement, and $\langle I\rangle$ is the average intensity for this reflections; the sum is over all reflections. R is a conventional crystallographic agreement factor. PDB, Protein Data Bank.
[b] From Ref. *83b*.

ously the amino acid side chains respect less the dyadic symmetry). Table II lists the intradimer root-mean-square (RMS) deviations, relative to the Cα atoms of the Cu_2Zn_2SOD main chain. It can be seen that the average RMS deviation of Cα ranges between 0.25 and 1.13 Å with maximum deviations up to 5.1 Å. By considering that the reported error on the atomic positions from the crystallographic analysis is at most 0.20–0.25 Å, it may be concluded that the structure of Cu_2Zn_2SOD is far from being related by a dyad axis, and any discussion about the symmetry is in most cases only a rough approximation.

In only one case the Cu_2Zn_2SOD dimer has been observed to lie on a crystallographic twofold axis. This occurs in the three structures of Cu_2Zn_2SOD from yeast and fungii, which have been crystallized in the trigonal space group $R32$ (*56*) (see Section II,I,3). The single crystals were obtained from ammonium sulfate and sodium chloride at pH 7.5. Three different structure determinations were carried out both at room temperature and at 93 K. The crystal asymmetric unit consists of only one monomer because the dimer lies on the special positions of point symmetry two.

The differences observed in Cu_2Zn_2SOD crystal structures are indicative of flexibility (i.e., the ability to adopt slightly different conformations depending on the crystallization conditions), which is mainly due to extensive loop structure.

The main features of Cu_2Zn_2SOD so far described, namely the β-barrel, the disulfide bridge, and the metal ligands, are conserved among the different structurally determined dimers. Inspection of the

TABLE II

ROOT-MEAN-SQUARE DEVIATIONS AND MINIMUM AND MAXIMUM DISPLACEMENT[a]

Structure	RMSD (Å)	Min	Max
1COB	0.335	0.251	1.687
1SDA	0.398(OY)	0.299	2.425
	0.360(BG)	0.286	1.614
1SDY	0.672	0.348	5.113
2SOD	0.833(OY)	0.597	3.963
	0.737(BG)	0.522	2.458
1SOS	0.346(AF)	0.296	1.041
	0.325(BG)	0.290	0.758
	0.254(CH)	0.231	0.948
	0.425(DI)	0.348	2.051
	0.376(EJ)	0.324	1.667
1SPD	1.130	0.939	4.337
1SRD	0.299(AB)	0.264	0.885
	0.316(CD)	0.291	0.677
1SXA	0.294	0.251	1.340
1SXB	0.293	0.217	1.289
1XSO	0.359	0.216	2.911

[a] From the best fit of backbone Cα atoms of the SOD chain within the dimeric structures. The letters in parentheses are the monomer chain identification used in the Brookhaven Protein Data Bank (PDB) files. Coordinates are from the crystal structures released in the PDB (*47*). In cases in which the crystal structure consists of more than one dimer in the asymmetric unit, the corresponding values are reported and the naming of the monomers constituting the dimer couple follows the naming reported in the PDB. The calculations have been performed with the CCP4 suite of programs for protein crystallography (*341*).

structures reveals that the main differences in folding are located in the loops and turns connecting the eight β-barrel strands.

5. *The Cu_2Zn_2SOD Quaternary Structure: The Monomer / Monomer Interface*

The contact surface between the monomers (Fig. 10) comprises the N terminus and β-strand 1 (residues 1–7), the C terminus and β-strand 8 (residues 146–151), and the two loop regions between residues 47–52 in loop IV and 100–112 in loop IV (the Greek key loop).

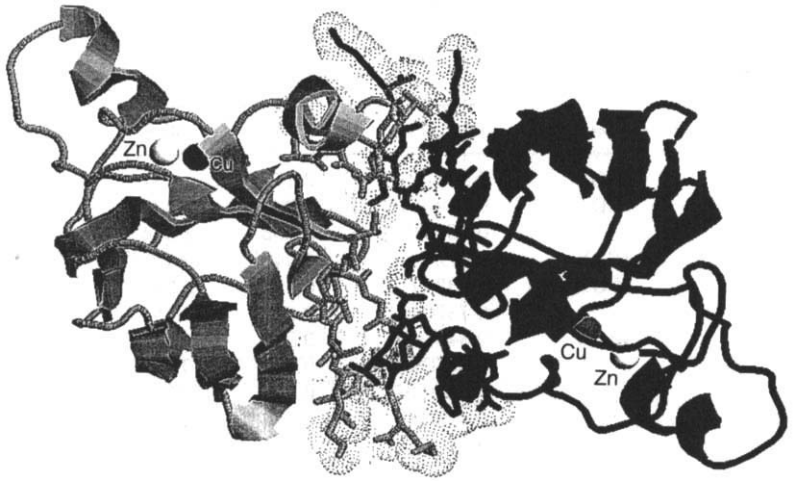

FIG. 10. The monomer/monomer interface in the 2SOD dimer represented as the dotted Connolly surface (*348*, *349*) of the residues facing the two monomers, which are represented in full as sticks superimposed on the ribbon diagram of the enzyme.

The extension of the contact region explains the high stability of the dimer to thermal and chemical denaturation. The enzyme is stable up to 353 K and remains active in 4% sodium dodecyl sulfate and in 8 *M* urea (*31*, *57–59*).

Highly optimized hydrophobic interactions can be observed across the monomer–monomer interface between residues related by the noncrystallographic twofold axis, e.g., the conserved residues Ile-111 and Val-146. Hydrophobic packing also involves Ala-4 with Leu-106 from the other monomeric unit. Mutations of residues in the interface region can lead to disruption of the quaternary structure, resulting in the formation of stable SOD monomers. Replacement of the human enzyme's two interface residues Phe-50 and Gly-51 with Glu has resulted in a stable, soluble SOD monomer that is almost devoid of catalytic activity (*60*).

Formation of natural mutants of the corresponding interface residues of human Cu_2Zn_2SOD in familial amyotrophic lateral sclerosis (FALS) has been demonstrated (*18*).

B. HUMAN Cu_2Zn_2SOD

Human Cu_2Zn_2SOD has been expressed in yeast (*61*, *62*) and its crystal structure determined at 2.5 Å resolution (*63*). The crystals belong to the $C222_1$ space group and contain five SOD dimers in the

asymmetric unit. The five dimers form honeycomb-like layers in the *ab* crystal plane. The layers are stacked so as to leave in the crystal lattice open channels that contain solvent (>68% by weight). The human enzyme contains 153 residues. The insertion of two residues in the bovine enzyme has little effect on the structure except for the loop where the insertion takes place, at position 25. The overall tertiary structure and the active site are conserved. The authors note a feature that was overlooked in the bovine enzyme analysis, namely, that the short six-residue helix present in SOD is oriented so as to stabilize, and be stabilized by, the Zn^{2+} cation in a favorable dipole–charge interaction. The zinc binding seems to contribute to the appropriate conformation of the electrostatically important residues Glu-132, Glu-133, and Lys-136, which are conserved throughout the sequences and are thought to be involved in substrate recognition (*45*, *64*).

The crystal structure of wild-type human SOD has also been determined, (space group $P6_3$) and refined to 2.4 Å resolution (see Table I) (*18*).

C. *Xenopus laevis* Cu_2Zn_2SOD

The South African frog *Xenopus laevis* has the peculiarity of having duplicated genes in its genome. Consequently, two isoenzymes of Cu_2Zn_2SOD with different amino acid sequences have been identified (*65*). The two isoenzymes X-SODa and X-SODb, are characterized by different thermal stabilities (*66*). The existence of two different *a* and *b* monomers gives rise, on association in the dimer, to three different isoenzymes of *aa*, *ab*, and *bb* composition, having different stabilities. The most stable X-SODb homodimer has been expressed in *E. coli* (*67*) and subjected to crystallographic analysis (*68*). It crystallyzes in the orthorhombic space group $P2_12_12_1$ (see Table I) with one dimer in the asymmetric unit. The monomer contains 150 amino acid residues, and shares a high degree of homology (>50%) with other known SODs. The crystals provided a complete data set (98.8%) to 1.49 Å resolution when X-rays from a synchrotron source were used. The structure has been refined to a very low final crystallographic *R* factor of 0.104 for all 49,209 reflections by using simulated-annealing and energy minimization techniques, followed by restrained least-squares refinement and finally by anisotropic refinement of all nonhydrogen atoms. The nonpolar H atoms have been introduced at calculated positions after the restrained refinement, converging to an *R* factor of 0.145. During the following anisotropic refinement of the nonhydrogen atoms in which the restraints on the metal–ligand distances were released, the *R* factor dropped to the final value of 0.104. The re-

sulting model has a very good geometry with small deviations from ideality. The anisotropic refinement satisfies the Hamilton test (*69*), which ensures that the data have not been overfitted, but the authors do not comment about improvement of the model obtained after anisotropic refinement, with respect to the model obtained from the more conventional restrained least-squares refinement at $R = 0.145$.

The X-SODb has the same overall tertiary and quaternary structure of all Cu_2Zn_2SODs reviewed so far, resulting in quite low values of 0.726 and 1.170 Å for the RMS deviations of the Cα atoms in the bovine and yeast enzymes, respectively. The SOD fold shows once again its robustness. Indeed, the several amino acid substitutions and the insertion in the bovine enzyme are absorbed well by the structure, the only substantially different part of it being the turn between residues 89 and 92, where a one-residue deletion occurs with respect to the bovine enzyme. It is of particular interest that the 10 substitutions of Pro and Gly residues in X-SODb and bovine SOD do not result in any evident changes in backbone conformations.

Site 149 of the X-SODb sequence is occupied by a Tyr residue, which is rather uncommon in SODs. The structure reveals that this tyrosine is involved in two intermolecular contacts related by the noncrystallographic twofold axis between the two monomers. The residues interacting with Tyr-149 are Phe-62 of the same subunit and Arg-113 of the other subunit. It is proposed that the increased thermostability of the XSODb homodimer with respect to the other possible dimers built with the *a* isoenzyme is due to these two interactions.

The active site structure is similar to the other metal sites in Cu_2Zn_2SODs, the only noticeable difference being the accurate observation of a shorter Cu(II)–water distance of 2.26 and 2.48 Å in the A and B subunits, respectively. In this site the noncovalent interactions responsible for the orientations of the ligands forming the metal binding site are conserved.

Once again a well-defined network of hydrogen-bonded water molecules is observed extending from the active site in two opposite directions spanning the cavity openings, reinforcing the proposal of an active role of the water in the enzyme mechanism (see Section IX).

D. Spinach Cu_2Zn_2SOD

SODS are present in plants, and Cu_2Zn_2SOD has been obtained from spinach leaves (*70*). Its amino acid sequence shares 55% homology with the bovine enzyme (*71*). The monomer contains 154 amino acids, three more than the bovine enzyme.

The structure has been determined at 2.0 Å resolution using a data

set obtained by merging data collected on a four-circle diffractometer from 25 different crystals (*72*). The crystals belong to the space group *C*2, the same as bovine SOD, but have a different unit cell (see Table I). The overall structure of this plant SOD is very similar to that of bovine erythrocyte SOD. However, the RMS deviation obtained from the best fit of the spinach and bovine SOD Cα and metal atoms (except for the three N-terminal residues) is 1.10 Å. Nevertheless, the topology of the two structures is identical. The metal ligands and functionally important residues Asp-124, Thr-137, Gly-141, and Arg-143 are conserved. A relevant difference between the bovine and spinach enzymes is that the copper-bound water molecule has not been detected in the latter structure. The authors do not report the completeness of the data, nor the figures relative to the quality of the data set used for refinement. This makes it difficult to compare and discuss confidently the observed small differences with the bovine enzyme active site model.

A major structural difference with respect to the bovine enzyme is found in the N-terminal region, where the spinach SOD has the insertion of an Asp residue in a turn at position 26. The turn is then enlarged and has a different conformation. Furthermore, the peptide NH group of Asp-25 is hydrogen bonded to the carbonyl oxygen of Ala-1; this H-bond is not present in bovine SOD and is responsible for a different extended conformation of the N-terminal region in the spinach enzyme. The H bond from Ala-1 to Asp-25 connects the Glu-24–Asp-26 turn region with the N terminus, causing a rigid, stable conformation of this part of the molecule. A second difference is found in the region near Val-33 and Ala-97 in the β-barrel. Val-33 is located in strand 3 and Ala-97 in strand 6, but they are adjacent in the tertiary structure, though they are far apart in the sequence. The corresponding residues in bovine SOD are Gly-31 and Val-95. The side chain of Val-33 in spinach SOD occupies the same spatial position of the Val-95 side chain in bovine SOD. The double exchange of a bulky residue with a small residue, and of a small residue with a bulky one, has no effect on the β-barrel, and maintains its structure unchanged. This finding brings forward the interesting observation that the same stabilization effect on the β-barrel structure, by side-chain interactions, has been achieved in different ways in the spinach and bovine enzymes, through concerted mutations allowing for the exchange of the complementary side chain of residues that may be far apart in the sequence.

E. Yeast Cu_2Zn_2SOD

Yeast SOD has been obtained and crystallized from the yeast *S. cerevisiae* (*73*). It has the same dimeric structure as the bovine and

spinach enzymes. Each subunit has 153 amino acids and shares a 55% homology with the bovine enzyme. Yeast SOD crystallizes in the space group $P2_12_12$ with a cell containing two dimers per asymmetric unit (see Table I). The structure has been solved by the molecular replacement technique using a bovine SOD monomer as a starting model. The refinement has been carried out in two stages. In the first one consecutive molecular dynamics and conventional restrained least-squares refinement led to a crystallographic R factor of 0.22 for the data between 6.0 and 2.5 Å (*74*). Subsequently, the structure was further refined to $R = 0.158$ by completing the model with the introduction of 516 water molecules (*75*).

The overall β-barrel and loop structure of Cu_2Zn_2SOD is maintained, despite an overall RMS deviation of 0.977 Å between the α-carbons of yeast and bovine SOD. The largest differences between the two structures occur at two insertion sites (residues 23–25 and 35–38) in loops II (2, 3) and III (3, 6), and at the interface between the two dimers (residues 127 and 128). The structure of the active site appears to be conserved in the bovine enzyme, with only minor differences in the overall geometry.

F. Bovine Cu_2Co_2SOD

Cobalt(II) has been used as a chromophoric probe to replace the spectroscopically and magnetically silent zinc(II), hence allowing the accumulation of a wealth of information on the system (see Section VIII). Furthermore, Cu_2Co_2SOD displays full enzymatic activity. Its crystal structure has been determined at 2.0 Å resolution (*76*). The crystals of Cu_2Co_2SOD belong to the space group $P2_12_12_1$ (see Table I), and despite the use of synchrotron radiation as the X-ray source, provide a 75.2% complete data set between 10.0 and 2.0 Å. The refinement has been carried out with a mix of molecular dynamics and conventional restrained least-squares methods, resulting in a model of almost ideal geometry and a final crystallographic R factor of 0.176. Again, the overall fold of SOD is preserved with only minor differences occurring in the loop regions. Despite the metal substitution, the active site structure shows small differences with respect to the native enzyme. The cobalt substitution does not perturb the active site. A water molecule has been clearly observed bound to Cu(II) at 2.38 Å, from which a network of H-bonded water molecules originates. The authors of the paper (*76*) note that most of the waters lie in the same positions as in the yeast enzyme, and propose that they help to stabilize the protein tertiary structure and may even have a role in catalysis.

G. Peroxynitrite-Modified Cu_2Zn_2SOD

The recent discovery that nitric oxide (NO) is a signaling molecule ubiquitous in tissue has raised the question that one of the pathways contributing to superoxide toxicity *in vivo* might be the formation of the highly reactive peroxynitrite anion ($ONOO^-$) produced by spontaneous reaction of NO with superoxide (*77*). It has been shown that peroxynitrite is a substrate of SOD (*78*). The interaction of SOD with peroxynitrite leads to a permanent modification of the enzyme at Tyr-108. The structural determination of the peroxynitrite-modified Cu_2Zn_2SOD has been conducted on monoclinic crystals (*79*). The structure confirms that peroxynitrite permanently modifies the Tyr-108 side chain with formation of 3-nitrotyrosine. The modification does not alter active site residues and the enzyme remains fully active.

H. Mutants of Cu_2Zn_2SOD

1. The Cys-6Ala Mutant of Bovine Cu_2Zn_2SOD

The crystal structure of the Cys-6Ala mutant of bovine SOD has been determined as part of a study aimed at investigating the role of this cysteine on the thermostability of Cu_2Zn_2SOD, and in an effort to understand and control the stability of the protein (*80*). The structure of the native enzyme shows that Cys-6 is buried in the β-barrel, where it makes hydrophobic interactions with neighboring chains. However, on heating it appears to form irreversible aggregates that prevent refolding. It appears that thermal inactivation occurs at a temperature lower than the melting temperature. The thermal scanning calorimetry profile of the mutant is consistent with either a two-step denaturation process or with the presence of two different species having different thermal stabilities (*80*). The mutation to Ala has proved effective in decreasing the rate of irreversible thermal denaturation, when incubated at 70°C for 180 min, despite causing the lowering of the melting temperature of the two putative components of the mutant enzyme with respect to the native enzyme. The crystal structure of the mutant has provided evidence for a concerted movement of the β-strand residues near the mutation site with respect to the native enzyme.

The authors propose that the observed shifts allow the enzyme to compensate for the energetic cost of the mutation by improving the packing and stereochemistry of the mutant molecule (*80*).

2. *The Cys-6Ala, Cys-111Ser Double Mutant of Recombinant Human Cu_2Zn_2SOD*

The double mutant Cys-6Ala, Cys-111Ser of human SOD gives crystals isomorphous with those of human SOD ($C222_1$) (see Section II,B). Alanine and serine are residues naturally occurring in other SODs at these positions. The double mutant is more stable than each of the single mutants to irreversible thermal denaturation, and all of them are more stable than the native enzyme, probably because of the removal of the reactive thiol groups.

The crystal structure shows that Ser-111 stabilizes the loop where it resides (the Greek key loop) by forming two H bonds with the carbonyl oxygen and the amide nitrogen of residues 106 and 113, respectively. In the wild-type human SOD crystal structure, Cys-111 is found to be involved in these H bonds in only 2 of the 10 independent subunits. The authors conclude that such intraloop side-chain to main-chain hydrogen bonds can thermodynamically stabilize the enzyme and, together with the zinc helix-dipole motif (see Section II,B), may provide a hint on how to modify the activity and the stability of human SOD and other β-barrel proteins.

I. Reduced Cu_2Zn_2SODs

One of the outstanding issues concerning the SOD mechanism involves the structure of the reduced enzyme. This point has been addressed by several authors attempting to provide a structural basis for Cu(I) as the catalytic species in SOD.

The first report of a reduced SOD structure was made in a preliminary announcement of the observation of a break in the histidinato bridge between copper and zinc, from studies on a reduced monoclinic form of bovine SOD (*81*). However, a full report has yet to appear in the literature, and the coordinates of the structure have not yet been released in the PDB.

1. *Reduced Bovine Cu_2Zn_2SOD at pH 7.5*

A second study reports two independent structural determinations on crystals obtained under anaerobic conditions from solutions of the reduced enzyme (*48*, *82*) at pH 7.5. The crystals are isomorphous with those of Cu_2Co_2SOD (*76*). In order to check the reproducibility of the experiment, two independent data sets were collected at

a synchrotron source on crystals from different batches. A third data set was obtained by merging the two experimental data sets so as to obtain a higher quality data set and hence a better final model. The refinement has been performed on all the three data sets. The metal centers were left unrestrained throughout all the refinement cycles. The final R factors were 0.166, 0.153, and 0.156 for the two independent and for the merged data sets, respectively. The reduced state of the copper in the crystals was proved by electron paramagnetic resonance (EPR) spectroscopy which shows no evidence of a Cu(II) signal in the crystal used for data collection nor in those from the same crystallization batch. The refinement procedure has provided a quite accurate model of the enzyme at 1.9 Å resolution in which, contrary to expectations, the copper coordination appears conserved with respect to the native oxidized form of the enzyme. Indeed, His-61 is found bridging copper and zinc in both subunits of the two independent structures. Only an overall increase in the Cu–ligand bond lengths has been observed. It should be noted that the difference in Cu–N bond length between Cu(II) and Cu(I) coordination compounds having the same coordination number is much less than 0.1 Å as observed in Schiff base, *N*-alkylpyrazole, phenantrolines, and tertiary amine copper complexes (*83a*). Only in chelating dioximes is a lengthening of 0.16 Å found on going from Cu(II) to Cu(I) (*83a*), which is about the estimated standard deviation in bond lengths found for the above SOD structures.

Apart from the His-61 bridge, the two structures reveal significant differences in the coordination geometry of the copper sites in the two subunits (A and B). In the A subunit the copper geometry can be described as a flattened tetrahedron with the water molecule interacting only weakly with it at 3.0 Å. In the B subunit the Cu(I) coordination is better respresented by a trigonal bipyramid having as the basal plane His-44, His-46, and the water molecule (at ~2.5 Å), with His-61 and His-118 in the axial positions.

A covalent modification of the Glu-119 side chain has been observed in this structure. An unexpected electron density of approximately 10 e^- has been found extending from one of the Glu-119 carboxylate oxygen atoms and could not be unambiguously assigned. The authors report that a similar density was also observed in the crystal structure of the oxidized enzyme so as to exclude a modification due to the dithionite used for reduction of the enzyme. The proximity of the modification to the active site suggests that it may affect the catalytic mechanism (*48*).

2. *Reduced Bovine Cu_2Zn_2SOD at pH 5.0*

The same research group has reported that crystal structure, at 2.0 Å resolution, of the reduced bovine enzyme obtained from crystals grown at pH 5.0 (*83b*). The crystals belong to the orthorhombic space group $C222_1$ with cell dimensions $a = 104.6$, $b = 197.5$, and $c = 50.8$ Å. This crystal form is characterized by a high solvent content, estimated at 73% from a $V_m = 4.5$ Å^3/Da. The packing of the Cu_2Zn_2SOD dimers is such that one of the two subunits makes very few intermolecular contacts with respect to the other in the crystal lattice. In other words, one subunit has a solution-like environment, being surrounded almost completely by water. This is reflected in an almost double average temperature factor for all the atoms of that subunit with respect to the other, indicating a larger mobility of the molecule.

The crystal structure shows a marked difference in the copper environments in the two monomers. In one of the subunits two electron density maxima are observed riding the cuprous ion in place of the usual density expected for the weakly bound water molecule. This is a two-center density that can be modeled with two water molecules at full occupancy, each being at coordinating distance from the metal ion, resulting in the unusual geometry shown in Fig. 11. The electron density could not be unambiguously interpreted because it can be modeled as well by a disulfide anion at about half occupancy. Such an anion may have been originated from the dithionite used for copper reduction.

On the contrary, the copper site in the solution-like subunit does

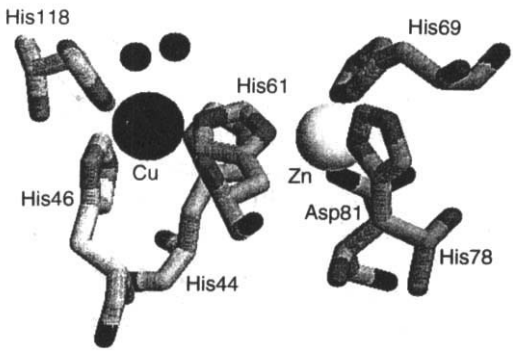

FIG. 11. The "anomalous" copper coordination sphere found in the crystal structure of reduced bovine Cu_2^I Zn_2SOD at pH 5.0. The metals and the two unknown atoms at bonding distance from Cu(I) are represented as spheres of arbitrary radius. The metal ligands are represented in full as sticks.

not show anything similar. Moreover, in this subunit the bridging ligand, His-61, is found disordered and away from the cuprous ion. It cannot be modeled properly because the electron density corresponding to the ring Nε2 nitrogen is missing. It appears to have moved away from the metal at about 3.0 Å. The metal appears to be disordered over two positions.

This finding indicates a possible detachment of the bridging His-61 in the structure and seems to confirm the flexibility of the copper site and its ability to shift between two different coordination geometries. The His-61 detachment from Cu(I) may be facilitated by the low pH, which favors protonation of the His-61 Nε2.

3. *The Reduced Yeast Cu_2Zn_2SOD at pH 7.7*

Three high-resolution tridimensional structures of a new crystal form of yeast Cu_2Zn_2SOD have been reported (*56*). Two independent determinations were conducted at room temperature and the third one at −180°C. The crystals belong to the rhombohedral space group *R*32 (see Table I). In this crystal form the SOD dimer sits on an exact crystallographic dyad axis so that the independent part of the molecule is made up by only one monomer. It is the first time that exact twofold symmetry has been observed for a dimeric SOD molecule. The crystals diffract to a limit of 1.70 and 1.73 Å at room temperature and to 1.55 Å at cryogenic temperature. However, in the last resolution shells the observed data cover between 41 and 55% of the theoretically possible reflections. The structures have been solved by molecular replacement, using as a starting model the yeast Cu_2Zn_2SOD previously reported or the A1A2 dimer of human Cu_2Zn_2SOD adequately modified to represent the primary structure of yeast SOD. The structures have been refined without stereochemical restraints for the active site atoms to *R* factors of 0.186 and 0.182 for the two room-temperature structures and 0.190 for the low-temperature structures.

All three structures show the unexpected result that the copper ion has shifted its position by about 1.0 Å with respect to the orthorhombic yeast SOD structure, leaving the bridging His-63 at 3.16 and 2.93 Å in the two independent room-temperature structures, respectively. The correctness of the copper position has been checked by using an anomalous scattering difference Fourier map (*84*). The movement of the metal also involves His-120 (opposite to His-63), which maintains the usual coordination distance from the copper. The result is that the copper ion appears to be tricoordinate by His-44, His-46, and His-120, and His-63 no longer bridges it with zinc. The authors conclude that despite the absence of any reductant in the

crystallization medium, the coordination of the copper in the three structures is indicative of its reduction to Cu(I), which displays such coordination in small molecule compounds.

The authors support this conclusion by showing the EPR spectra of a crystal compared with that of the original protein solution used for crystallization, with that of the same crystal dissolved in an equal volume of buffer and with the same solution 12 hr after the exposure to oxygen. All the spectra show the characteristic Cu(II) EPR lines but with intensities steadily decreasing from the crystallization solution to the crystal, thus indicating a decreasing amount of Cu(II) ions in the different systems.

The above observations deserve a comment about stereochemistry of the yeast SOD active site (which may hold also for the reduced bovine SOD at pH 5.0). The copper–His-63 Nε2 distances observed in the structures are in the range 2.93–3.16 Å, which is longer than the sum of the covalent radii of Cu (in either +2 or +1 oxidation state) and N. However, these distances still appear to indicate close contacts between the copper and the nitrogen. It is difficult to give a proper estimate for the contact distance of a Cu(I) or Cu(II) ion in coordination compounds. In small molecule complexes the intermolecular distances involving mononuclear copper ions are always large because the metals are buried in the ligand matrix. In the cubic $Fm3m$ lattice of metallic copper the second shell of copper atoms is at a distance of 3.61 Å. A safe estimate of the Cu contact distance in its lower oxidation state may hence be taken at about 1.8 Å. Becuase the van der Waals (vdW) radius of nitrogen is 1.55 Å (*85*), the reported positions of copper and His-63 Nε2 are closer than the sum of their contact radii, indicating that there are short contacts between the copper and His-63 in each of the three structures. Furthermore, if a proton (vdW radius = 1.2 Å) is built on the Nε2 of His-63, it points toward copper at a distance of about 2.7 Å, still making close contact with it.

The copper reduction and the following disruption of the Cu–His-62 bridge seem to occur on crystallization. However, analysis of the crystal intermolecular contacts shows there are only few strong protein–protein contacts (not water mediated), mainly occurring in the C-terminal region and in loop IV just before the disulfide bridge (residues 49–52). The latter, even if placed quite far from the metal site, may have an influence on it because they are located in the loop supporting the crucial His-63 ligand. On the other hand, the superposition of the reduced and oxidized yeast SOD structures shows that His-63 has remained in the same place and that detachment is caused by the copper movement.

The structural information available on the reduced state of Cu_2Zn_2 SOD provides a view of the copper site as a very flexible system, where the Cu(I) ion can shift between three- and four-coordination with a water molecule weakly interacting with it, giving rise to 4 + 1 coordination. The latter coordination is commonly observed in small molecule complexes [a recent example is provided by Lee *et al.* (*86*)]. It is noteworthy to point out that a concerted movement of the metal and of some of the ligands seems responsible for the coordination changes observed in the reduced yeast SOD and bovine SOD structures. In the case of yeast SOD it appears that reduction of the copper ion occurs on cyrstallization and that crystal packing does not play a role in the process. On the contrary, in the bovine SOD example, pH and the solution-like environment of one of the subunits seem to be responsible for the probable detachment of the His-61 from Cu(I).

J. Inorganic Anion Complexes of Cu_2Zn_2SOD

The structures of Cu_2Zn_2SOD complexes with small inorganic anions have been determined at different copper oxidation states.

1. *The Crystal Structure of the Cyanide Adduct of Cu_2Zn_2SOD from Xenopus laevis*

The crystal structure of cyanide-inhibited Cu_2Zn_2SOD from *X. laevis* has been determined at 98 K and refined at 1.7 Å to an *R* factor of 0.17 (*87*). Formation of the complex does not affect the overall structure of the protein. In both subunits the cyanide anion is found to be bound to Cu(II) through its C atom at about 2.2 Å. It interacts electrostatically with Arg-141 at 3.3 Å, pointing directly to it with its free end. On binding of the inhibitor the His-46 ligand moves 2.6–2.7 Å from copper, changing the metal coordination polyhedron into a distorted square pyramid. His-46 is at the apex and the cyanide is on the basal plane, confirming what was previously proposed after NMR experiments on Cu_2Co_2SOD (*88*, *89*).

2. *The Crystal Structure of the Azide Complex of Bovine Cu_2Zn_2SOD*

The azide complex crystals have been grown at pH 6.5 in the space group $P2_12_12_1$; the azide complex was prepared by soaking the crystals in a precipitant solution containing 1 *M* NaN_3. The data at 2.1 Å resolution have been refined to an *R* factor of 0.166 (*90*).

The competitive inhibitor azide makes strong coordination bonds of 1.97 and 2.18 Å, respectively, with the Cu(II) ion in the two subunits. Azide replaces the water molecule in the metal coordination and

makes an electrostatic interaction with the positively charged guanidinium group of the Arg-141 residue at a distance of about 3.6 Å. The binding of azide perturbs the copper coordination sphere by causing a shift of about 0.7–0.4 Å of the Cu(II) position with respect to the native enzyme, as is supported by spectroscopic studies (see Section VIII). The movement of copper is accompanied by that of His-118.

As in the cyanide complex, the His-46 coordination distance is lengthened by about 0.4 Å on average. The resulting copper coordination polyhedron is a distorted square pyramid with His-46 at the apical position and azide on the basal plane, paralleling the behavior observed in the cyanide complex. The above results allow rationalization of the previous spectroscopic data (*89*). The zinc coordination is left unaltered.

3. *The Crystal Structures of Azide and Thiocyanate Complexes of Reduced Bovine Cu_2Zn_2SOD*

The structures of the adducts of the competitive inhibitor azide and of the inhibitor thiocyanate with the reduced enzyme have been determined using the $C222_1$ crystal form obtained at pH 5.0 (*83b*). In both structures the inhibitors are found bound to Cu(I), replacing the water molecule(s) close to the metal site. However, their distances from Cu(I) are longer than those found in the oxidized enzyme, being in the range 2.7–2.9 Å. The coordination sphere of Cu(I) is left essentially unaltered by the interaction, as is that of Zn(II). In this case the anions extend in the cavity, having an electrostatic interaction with Arg-141 at 3.1–3.2 Å from its guanidinium group, stronger than in the oxidized enzyme. The thiocyanate anion appears to be bound to copper through the nitrogen atom.

The different behavior with respect to the oxidized enzyme reflects the different preference of Cu(II) and Cu(I) cations for five-coordination. Cu(I) prefers four-coordination, and the interaction with the negatively charged anions looks merely electrostatic, the two ends of the anions being almost equidistant from the two positively charged groups present in the cavity, namely Cu(I) and Arg-141.

The mechanistic implications of the observed anion binding modes in the two oxidation states of the enzyme are discussed in Section IX.

III. Activity

A. Activity Measurements

The ability of an enzyme to perform its function is appropriately measured by enzymatic activity, which follows the Michaelis–Menten

kinetics, i.e. by the parameters obtained using the Michaelis-Menten equation. If reference is made to the Michaelis–Menten reaction scheme [Eq. (7)],

$$E + S \underset{k_{-1}}{\overset{k_1}{\rightleftharpoons}} ES \overset{k_2}{\rightarrow} E + P, \tag{7}$$

saturation of the enzyme E, with the complete transformation into the enzyme–substrate complex ES, is never obtained for SOD (except in one case; see later) because the transformation of ES into free E and the product P is very fast and the amount of substrate is in general small. The rate constants k_1, k_{-1}, and k_2 are defined for single steps. The kinetics can be fitted to Eq. (8),

$$v = k_{cat}[E][S]/(K_m + [S]), \tag{8}$$

where v is the velocity, k_{cat} is the catalytic constant (or turnover number), and K_m is the Michaelis–Menten constant [$K_m = k_1/(k_{-1} + k_2)$]. With a low concentration of substrate (i.e., $[S] \ll K_m$), the velocity $v = k_{cat}[E][S]/K_m$ is referred to as a nonsaturating condition.

Superoxide can be generated by pulse radiolysis of aqueous solutions containing O_2 (*52*, *91–94*). The necessary irradiation is achieved with pulses of high-energy electrons (2–5 MeV), generated by a Van der Graaf linear accelerator. The irradiation also generates some radicals, i.e., OH radicals and H radicals are also formed. Formate, used as buffer (1–10 m*M*), converts all these radicals to superoxide according to reactions (9–11):

$$OH + HCO_2^- \rightarrow H_2O + CO_2^-, \tag{9}$$

$$H + HCO_2^- \rightarrow H_2 + CO_2^-, \tag{10}$$

$$CO_2^- + O_2 \rightarrow O_2^- + CO_2. \tag{11}$$

With formate and O_2 concentrations kept constant, it is possible to calibrate O_2^- concentrations by changing energy and pulse time. The oxygen aqueous solution containing formate is pulsed to generate O_2^- in the presence of varying amounts of enzyme. The decay of O_2^- is monitored spectrophotometrically at 245 nm (the maximum of absorbance of superoxide) as a function of the enzyme concentration, pH, and ionic strength. In the absence of enzyme the spontaneous

disappearance of O_2^- is a second-order process ($O_2^- + HO_2 \rightarrow O_2 + HO_2^-$) whose rate constant at pH 7.5 is $8.5 \times 10^7\ M^{-1}\ sec^{-1}$ (*93*). When superoxide dismutase is added to the solution the kinetics of the decay changes from a second-order process to a pseudo-first-order mechanism with respect to both the enzyme and the substrate concentrations (*92*, *93*). If the dose of O_2^- is constant, the rate of decay is proportional to the enzyme concentration. The rate constant, k_{cat}/K_m, for the bovine enzyme was determined to be $2.3 \times 10^9\ M^{-1}\ sec^{-1}$ at pH 7.0 and 25°C (*52*). Similar values were found for human SOD expressed in yeast and in *E. coli* (*95*, *96*) (Table III). There are no indications of saturation at the highest O_2^- concentration, and the measured rate constant is near the diffusion control. This method, besides the advantage of a direct determination of the catalytic constant, yields very high superoxide concentrations and is highly sensitive. Furthermore, it has been shown that the rate constants for the reduction of O_2^- by the reduced enzyme and for the oxidation of O_2^- by the oxidized enzyme are the same (*97*, *98*). By lowering the temperature to 5.5°C and raising the initial O_2^- concentration to about 5 m*M* (possible using a stopped flow apparatus), Fee and co-workers were able to saturate the enzyme and to determine the Michaelis–Menten parameters, K_m, and turnover number or k_{cat} (*99*). At pH 9.3, in H_2O, the turnover number is $0.9 \times 10^6\ sec^{-1}$ and K_m is $3.5 \times 10^{-3}\ M$. The saturative behavior is more pronounced in D_2O and decreases in the presence of acid, at variance with what happens in nonsaturating conditions when no isotopic effects are observed. These results suggest that, only in saturative conditions, proton transfer is rate limiting. In nonsaturating conditions the observed rate constant is probably determined by the rate of approach of O_2^- to the copper center [k_1 of reaction (7)]. Such a rate is controlled by the rate of substrate diffusion.

The polarographic method, another technique to measure the decay of superoxide, does not require special and expensive apparatus such as a Van der Graaf generator. A dropping mercury electrode works both as a source of superoxide and as a detector of superoxide dismutation products (*100*). The electroreduction of O_2 in aqueous solution can be a monoelectronic process that produces O_2^- ($O_2 + e^- \rightarrow O_2^-$) or a bielectronic process, with reduction to H_2O_2. The latter happens in the presence of protons: $O_2 + 2e^- + 2H^+ \rightarrow H_2O_2$.

The polarographic curves for the two processes are indicated in Fig. 12. Hydrophobic surfactants such as triphenylphosphinoxide (TPO) are used to cover the electrode surface and prevent proton transfer from occurring on the electrode surface. At pH 9.5 only the reduction of oxygen to superoxide is observable, whereas at lower pH two elec-

TABLE III

ACTIVITY OF SODs FROM DIFFERENT SOURCES AND OF SOME MUTANTS

Source	Activity	pH	$I(M)$	Ref.
Bovine SOD (erythrocyte)	3300 U/mg[a]	7.8	—	*2*
	$2.3 \times 10^9\ M^{-1}\ \text{sec}^{-1}$[b]	7.0	—	*52*
	$3.9 \times 10^9\ M^{-1}\ \text{sec}^{-1}$[b]	7.5	0.02	*128*
	$1.7 \times 10^9\ M^{-1}\ \text{sec}^{-1}$[b]	8.0	0.16	*118*
	32,180 U/mg[c]	7.4	—	*109*
Human SOD (erythrocyte)	3500 U/mg[a]	7.8	—	*103*
	6900 U/mg[a]	—	—	*61*
	120,500 U/mg[d]	—	—	*146*
Human SOD (*E. coli* cytoplasm)	7500 U/mg[a]	—	—	*61*
Human SOD (yeast)	6570 U/mg[a]	7.8	—	*104*
	$2.3 \times 10^9\ M^{-1}\ \text{sec}^{-1}$[b]	7.0	0.01	*95*
	$1.65 \times 10^9\ M^{-1}\ \text{sec}^{-1}$[b]	7.0	0.01	*342*
	$1.75 \times 10^9\ M^{-1}\ \text{sec}^{-1}$[e]	8.5	0.16	p.c.[f]
Human SOD (*E. coli*)	$2.3 \times 10^9\ M^{-1}\ \text{sec}^{-1}$[b]	7.0	0.01	*64*
Human SOD (*E. coli*)	$1.32 \times 10^9\ M^{-1}\ \text{sec}^{-1}$[e]	8.5	0.16	p.c.[f]
Human SOD (*E. coli*)	19,000 U/mg[c]	7.4	—	*119*
Ox SOD	$3.8 \times 10^9\ M^{-1}\ \text{sec}^{-1}$[b]	8.0	0.02	*116*
Pig SOD	$3.2 \times 10^9\ M^{-1}\ \text{sec}^{-1}$[b]	8.0	0.02	*116*
Sheep SOD	$3.3 \times 10^9\ M^{-1}\ \text{sec}^{-1}$[b]	8.0	0.02	*116*
Yeast SOD	$3.4 \times 10^9\ M^{-1}\ \text{sec}^{-1}$[b]	8.0	0.02	*116*
Extracellular human SOD	116,000 U/mg[d]	—	—	*146*
Extracellular recombinant human SOD	116,000 U/mg[d]	—	—	*146*
Shark (*Prionace glauca*) SOD	$3.75 \times 10^9\ M^{-1}\ \text{sec}^{-1}$[b]	7.5	0.02	*128, 343*
Bacillus abortus SOD (*E. coli*)	3800 U/mg[a]	7.8	—	*152*
Xenopus laevis SOD	$3.7 \times 10^9\ M^{-1}\ \text{sec}^{-1}$[b]	8.0	0.02	*329*
	$1.3 \times 10^9\ M^{-1}\ \text{sec}^{-1}$[b]	8.0	0.145	*329*
Thr-137IleHSOD (yeast)[g]	$1.20 \times 10^9\ M^{-1}\ \text{sec}^{-1}$[b]	7.0	—	*342*
Thr-137SerHSOD (yeast)	$1.25 \times 10^9\ M^{-1}\ \text{sec}^{-1}$[b]	7.0	—	*342*
Thr-137AlaHSOD (yeast)	$1.19 \times 10^9\ M^{-1}\ \text{sec}^{-1}$[b]	7.0	—	*342*
Thr-137ArgHSOD (yeast)	$1.04 \times 10^9\ M^{-1}\ \text{sec}^{-1}$[e]	8.5	—	p.c.[f]
Arg-143LysHSOD (yeast)	2840 U/g[a]	7.8	—	*104*
	$9.9 \times 10^8\ M^{-1}\ \text{sec}^{-1}$[b]	7.0	0.01	*95*
Arg-143IleHSOD (yeast)	708 U/mg[a]	7.8	—	*104*
	$1.8 \times 10^8\ M^{-1}\ \text{sec}^{-1}$[b]	7.0	0.01	*95*
Arg-143AlaHSOD (yeast)	$1.7 \times 10^8\ M^{-1}\ \text{sec}^{-1}$[b]	7.0	0.01	*95*
Arg-143GluHSOD (*E. coli*)	$3.5 \times 10^7\ M^{-1}\ \text{sec}^{-1}$[b]	7.0	0.01	*95*
Arg-143AspHSOD (*E. coli*)	$3.5 \times 10^7\ M^{-1}\ \text{sec}^{-1}$[b]	7.0	0.01	*95*
Cu_2E_2HSOD (*E. coli*)	$7.0 \times 10^8\ M^{-1}\ \text{sec}^{-1}$[b]	7.0	—	*96*
Asp-124AsnCu_2E_2HSOD (*E. coli*)	$5.2 \times 10^8\ M^{-1}\ \text{sec}^{-1}$[b]	7.0	—	*96*
Asp-124GlyCu_2E_2HSOD (*E. coli*)	$1.8 \times 10^8\ M^{-1}\ \text{sec}^{-1}$[b]	7.0	—	*96*
Glu-133GlnHSOD (*E. coli*)	$6.8 \times 10^9\ M^{-1}\ \text{sec}^{-1}$[b]	7.0	0.01	*64, 141*
Glu-132GlnHSOD (*E. coli*)	$4.2 \times 10^9\ M^{-1}\ \text{sec}^{-1}$[b]	7.0	0.01	*64, 141*
Glu-133Gln, Glu-132GlnHSOD	$7.0 \times 10^9\ M^{-1}\ \text{sec}^{-1}$[b]	7.0	0.01	*64, 141*

(*Continues*)

TABLE III (*Continued*)

Source	Activity	pH	$I(M)$	Ref.
Glu-133Lys, Glu-132GlnHSOD	$4.2 \times 10^9\ M^{-1}\ sec^{-1}$[b]	7.0	0.01	*64, 141*
Lys-120Leu *X. laevis* SOD	$2.1 \times 10^9\ M^{-1}\ sec^{-1}$[b]	8.0	0.02	*329*
	$1.0 \times 10^9\ M^{-1}\ sec^{-1}$[b]	8.0	0.145	*329*
Lys-134Thr *X. laevis* SOD	$2.1 \times 10^9\ M^{-1}\ sec^{-1}$[b]	8.0	0.02	*329*
	$1.0 \times 10^9\ M^{-1}\ sec^{-1}$[b]	8.0	0.145	*329*
Lys-120Leu, Lys-134Thr *X- laevis* SOD	$1.1 \times 10^9\ M^{-1}\ sec^{-1}$[b]	8.0	0.02	*329*
	$0.7 \times 10^9\ M^{-1}\ sec^{-1}$[b]	8.0	0.14	*329*
Glu-131Gln *X. laevis* SOD	$6.5 \times 10^9\ M^{-1}\ sec^{-1}$[b]	7.5	0.02	*175*
Asp-130Gln *X. laevis* SOD	$3.7 \times 10^9\ M^{-1}\ sec^{-1}$[b]	7.5	0.02	*175*
Lys-136ArgHSOD (*E. coli*)	30,400 U/mg[c]	7.4	—	*119*
Lys-136AlaHSOD (*E. coli*)	15,200 U/mg[c]	7.4	—	*119*
Lys-136GlnHSOD (*E. coli*)	22,800 U/mg[c]	7.4	—	*119*
His-63Ala yeast SOD (*E. coli*)	0.4% wild type[h]	—	—	*149*
His-63CysHSOD (*E. coli*)	<1% wild type[e]	7.4	0.16	*179*
	$3.8 \times 10^6\ M^{-1}\ sec^{-1}$[e]	8.5	0.02	*179*
Phe-50Glu, Gly-51GluHSOD	10 ± 5% wild type[a]	7.8	0.16	*60*
	$2.0 \times 10^7\ M^{-1}\ sec^{-1}$[e]	8.5	0.16	p.c.[f]
Phe-50Glu, Gly-51Glu, Glu-133GlnHSOD	$8.6 \times 10^7\ M^{-1}\ sec^{-1}$[e]	8.5	0.16	p.c.[f]

[a] Activity determined using the xanthine oxidase method (*2*).
[b] Activity determined using pulse radiolysis (*52, 91, 92, 112*).
[c] Activity determined using Paoletti's method (*108–110*).
[d] Activity determined using Marklund's method (*344*).
[e] Activity determined using the polarographic method (*100, 101*).
[f] p.c., Personal communication from Prof. E. Argese (University of Venice).
[g] HSOD, Human SOD.
[h] Activity determined by monitoring the autooxidation of 6-hydroxydopamine (*345*).

trons are transferred to O_2, leading to H_2O_2. The addition of superoxide dismutase converts part of O_2^- to O_2, increasing the limiting currents. The difference in the limiting currents measured in the absence and in the presence of SOD are related to the rate constant of SOD (*101*). In order to overcome the limitation of pH, connected to the bielectronic process, it was demonstrated that the use of a dropping mercury electrode with short drop time (s.d.t.m.e.) (0.1 sec versus 1–2 sec) allows minimization of the contribution of the reaction that leads to H_2O_2 (*101*). In such a way activity measurements are possible down to physiological pH and the method becomes competitive with the pulse radiolysis method.

These direct assays provide immediate answers about the rate of dismutation of superoxide by SOD. Activity assays performed on the same sample with different direct methods (i.e., pulse radiolysis and polarography) in most cases give similar dismutation rate constants

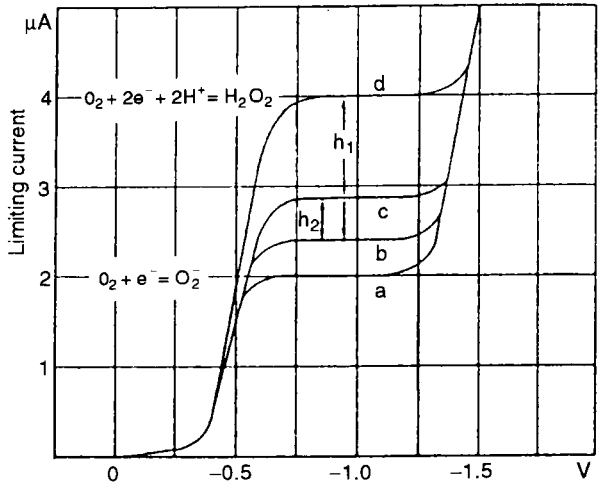

FIG. 12. Polarographic determination of oxygen and its derivatives. The cell current is plotted versus the potential for reduction of O_2^-. (a) pH 12.5, triphenylphosphinoxide (TPO) 0.9 m*M*; (b) pH 9.9, TPO 0.9 m*M*; (c) pH 9.9, TPO 0.9 m*M*, SOD 1.5×10^{-9} *M*; (d) pH 9.9, TPO 0.9 m*M*, SOD 1.5×10^{-7} *M*. The value of limiting current at −1.0 V is proportional to the concentration of O_2 in solution. Reprinted with permission from Ref. *100*.

(see Table III); some low-activity SOD mutants (in particular, monomeric mutants), however, show discrepancies for the two direct assays, discrepancies that we still do not understand (*102*).

In order to monitor SOD activity routinely, assays that require only instrumentation typical of a chemical or biochemical laboratory were set up. The assays consist of a reaction mixture that generates superoxide anion and a coupled redox reaction that scavenges the superoxide ion. The latter reaction is usually followed spectrophotometrically. The addition of superoxide dismutase destroys superoxide and inhibits the coupled reaction. The specific activity of the enzyme is determined on the basis of the amount of protein required to slow down to 50% the first-order coupled reaction, i.e., one enzymatic unit is the amount of protein that reduces the rate to 50% and the specific activity corresponds to the number of units per milligram of protein.

Following the method of McCord and Fridovich (*2*), the superoxide ion is generated through the oxidation of xanthine by oxygen, a reaction catalyzed by xanthine oxidase as shown in Fig. 13. O_2^- then reacts with oxidized cytochrome *c* and it is transformed into O_2. The disappearance of superoxide is monitored spectrophotometrically through the increase of the absorption band at 550 nm, as a consequence of

FIG. 13. Reaction between oxygen and xanthine, in the presence of the enzyme xanthine oxidase.

the reduction of oxidized cytochrome *c*. Superoxide dismutase, by successfully competing with cytochrome *c* for the oxidation of the superoxide ion, inhibits the reduction of oxidized cytochrome *c*. Activity values of 3300 and 3500 U/mg (*2*, *103*) were measured for the bovine and human enzymes, respectively, (Table III), corresponding to a kinetic rate constant of $2.3 \times 10^9\ M^{-1}\ sec^{-1}$, even though values of 6900 and 6600 U/mg have also been reported in literature (*104*). Such discrepancies were partially attributed to the different method for measuring protein concentration and to differences in homogeneity of the samples (*104*). Meaningful results are obtained when the activity of an isoenzyme or of a mutant is expressed relative to that of an isoenzyme taken as reference. However, the assay can be contaminated by the presence of other cytochrome *c* reducing agents (such as glutathione), or by impurities of superoxide dismutase in cytochrome *c*. Furthermore, the presence of anions that specifically bind to a residue in the SOD active cavity can inhibit the activity. This effect was first observed with phosphate, and Fridovich argued that the inhibitory power of the phosphate anion was an ionic strength effect (*105*); it was later proposed that phosphate interacts with Arg-143, a residue that is quite relevant for the attraction of superoxide in the cavity (*106*, *107*).

A relatively recent indirect assay was set up by Paoletti (*108*). The assay consists of a sequence of reactions that generate superoxide from molecular oxygen in the presence of EDTA, manganese(II) chloride, and mercaptoethanol (*108–110*). The reactions are monitored by following the oxidation of NAD(P)H by superoxide radicals through a decrease of absorbance at 340 nm, which corresponds to the maximum absorbance of NAD(P)H. The addition of SOD (scavenging superoxide) inhibits nucleotide oxidation (Fig. 14). At variance with the previous assays, whereby cytochrome *c* is reduced by superoxide, this method relies on the oxidation of NAD(P)H and, in theory, makes the detection less susceptible to aspecific reduction by common cellular components. The assay is very sensitive to the EDTA/Mn^{2+} ratio and to the mercaptoethanol concentration, both of which affect nucleotide

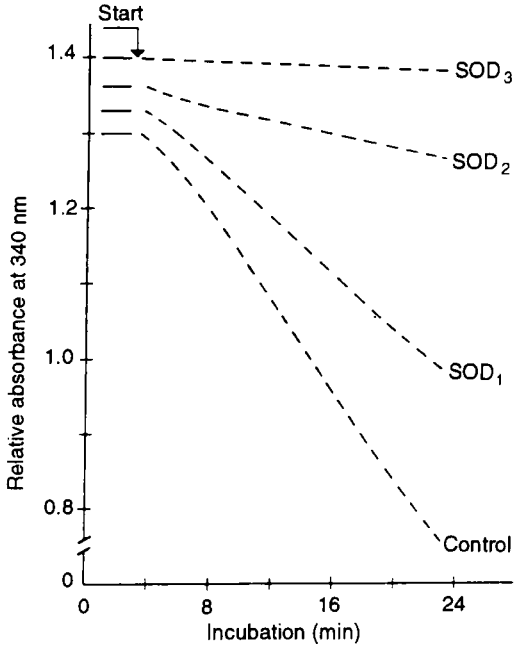

FIG. 14. Effect of superoxide dismutase on the rate of NADH oxidation. Decreases in absorbance are measured at 340 nm. Four assays are performed simultaneously in the absence (control) and in the presence of different amounts of SOD. Reprinted with permission from Ref. *108*. Copyright 1986, Academic Press.

oxidation rates (*109*). Therefore the presence of chelators, of endogenous Mn^{2+}, or of free thiols might alter the calibration curve.

The nitroblue tetrazolium assay (*111*) is another indirect method that is used especially for detecting SOD activity on gel electrophoresis. Superoxide radicals are generated by xanthine/xanthine oxidase or by the photoreduction of flavins (typically riboflavin), which oxidize H_2O to O_2^-. The gel on which SOD samples have been loaded is then stained with nitroblue tetrazolium chloride. This reagent is reduced by superoxide to the blue-colored formazan. SOD competes with nitroblue tetrazolium and produces colorless zones on the blue gels. This method, which is highly specific toward superoxide dismutase, is limited by its low reliability with respect to quantitative determinations.

The results obtained by indirect assay are hardly comparable, because the specific activity values are based on different types of reactions to induce the dismutation of superoxide. The results have different meanings, and only relative comparisons among different samples

can be made. Furthermore, indirect assays, which can be set up at a specific pH and buffer concentration, are not sufficiently versatile for SOD activity as a function of pH and ionic strength.

Activity measurements are made at low concentrations of SOD (typically micromolar). On the other hand, there is a concentration dependence equilibrium between monomeric and dimeric species. It has been suggested that bovine SOD at 25°C, pH 7.8, is only 50% in the dimeric form at a concentration 0.3–0.4 g/liter without any loss of activity (*33*).

All these assays can also be used to determine the activity of MnSOD and FeSOD. It should be noted that the nitroblue tetrazolium assay (*111*) allows differentiation of MnSOD, FeSOD, and Cu_2Zn_2 SOD. Indeed, these enzymes have different molecular weights and they run at different rates on acrylamide gel. In a mixture of the three proteins it is possible to resolve three spots representing Mn, Cu_2Zn_2, and FeSOD.

B. pH Dependence of Activity

In the pH range 5–9, activity is not influenced by pH. However, when pH exceeds 9, activity steeply decreases (*52*, *112*, *113*) (Fig. 15). This behavior cannot be ascribed to denaturation because NMR studies indicate no denaturation up to pH 12.5 (*114*). The rate constant curve versus pH shows an inflection at high pH, and for the human

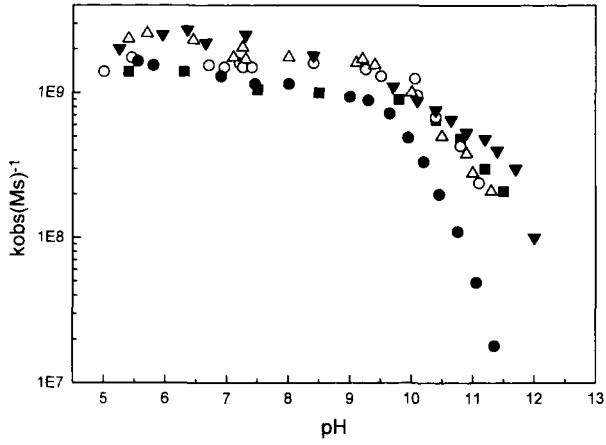

Fig. 15. Rate constant versus pH for bovine SOD (■), yeast SOD (○), mutant Cys-6Ala, Cys-111Ser of human SOD expressed in yeast (△), Thr-137Ile SOD (●), and Lys-136Ala SOD (▼).

enzyme an apparent pK_a of 10.7 ± 0.1 was calculated (*115*). This loss of activity at high pH has been matter of debate and many hypotheses have been proposed, including deprotonation of some residues belonging to the active site channel, such as Lys-136 (*116*, *117*) and Lys-122 (*117*, *118*), deprotonation of His-63 (*119*), which does not bridge the metal ions in the reduced species, and ionization of the water molecule, which is close to the copper ion (*119*). Mutations have shown that the lysines cannot be uniquely responsible for the drop in activity. By studying the Ile-137 mutant, which has the lowest apparent pK_a (*112*), it seems that the drop in activity is not related to changes involving the metal coordination sphere, but instead is related to changes in the electrostatic potential due to a deprotonation process (which could be represented by an OH^- group approaching copper) (*120*).

C. Ionic Strength Dependence of Activity

In wide-type Cu_2Zn_2SOD the activity decreases with ionic strength (*105*, *121*). Indeed, when ionic strength is increased from 0 to 150 m*M* (physiological ionic strength), the rate decreases by 30% (Fig. 16). This can be explained by taking into account two factors that moderate SOD activity: the overall negative charge of the dimeric protein

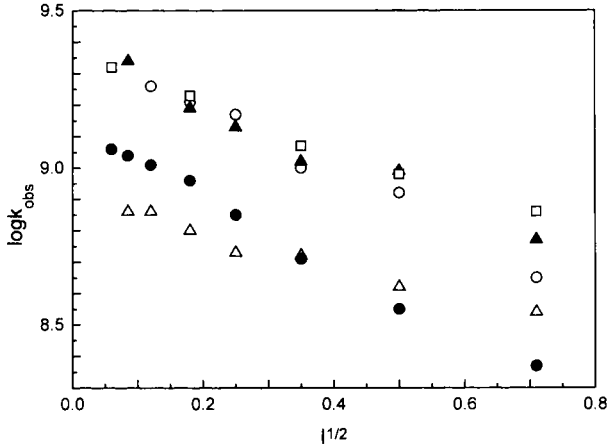

FIG. 16. Effect of ionic strength on dismutation rate of O_2^- by superoxide dismutase as measured experimentally by pulse radiolysis at pH 8. Ionic strengths were adjusted using NaCl. ○, Bovine SOD; ▲, human SOD expressed in yeast; □, mutant Cys-6Ala, Cys-111Ser of human SOD expressed in yeast; ●, Thr-137Ile SOD; △, Arg-143Lys.

(−4, at pH 7) and the positive active center. The former property determines a repulsive barrier for the negative superoxide; this repulsion is compensated by the electrostatic field generated by the positive copper and zinc ions and by the positively charged residues in the active site channel (*122*, *123*). In the presence of salt, the repulsive barrier is reduced; however there is a more substantial decrease in the positive target area. The combination of these effects yields, in wild-type SOD and also in most of the mutants, a decrease in activity as the ionic strength increases.

In the case of mutants such as the monomeric Phe-50Glu, Gly-51Glu, which has an overall charge of −4 (versus −2 of the wild-type SOD subunit), the activity is reduced to 10% and it is ionic strength independent. It is possible that the enhanced negative electric field strength of the monomeric mutant increases the repulsive barrier, causing a drastic decrease of activity. An increase in ionic strength reduces both the repulsive barrier and the steering effect of the positively charged residues of the active site, which apparently compensate each other. This produces catalytic rates that are ionic strength independent (*124*). Other monomeric mutants with the same charge density as the native protein, e.g., Phe-50Glu, Gly-51Glu, Val-148Lys, Ile-151Lys SOD (total charge, −2), show a dependence on the ionic strength qualitatively similar to wild-type SOD (*102*).

D. Computational Studies on Copper–Zinc SOD

Cu_2Zn_2SOD has been the subject of several theoretical studies aimed at predicting its structural and functional properties. The calculations performed to describe the catalytic process or to quantitate the experimental rates were essentially focused on the interaction and binding of the substrate. As discussed before, in nonsaturating conditions the diffusion of the substrate in the active site is the rate-limiting step of the catalytic process. This process is strongly determined by electrostatic forces due to the nature of the substrate. Consequently, electrostatic field calculations and Brownian dynamics simulations (*64*, *122*, *123*, *125–128*) have been extensively applied to SOD. On the contrary, no extensive studies are available for characterizing the subsequent steps, in which the electron transfer process occurs. Some preliminary calculations have been reported (*129*) whereby the energy for the process of transferring one electron from O_2^- to copper has been evaluated within a density functional approach.

Electrostatic calculations produced maps of the electrostatic forces in the active channel and enabled evaluation of the contribution of

each charged residue in the interaction with the substrate. Brownian dynamics calculations have been made for superoxide in order to estimate the rates of substrate–enzyme encounters for wild-type SOD and for the mutants (*130*). The results, compared with the experimental data on the mutants, pointed out that several residues make a large electrostatic contribution to the first step of the catalytic process, i.e., the binding of substrate. In a few cases the results disagree with the experimental data, indicating that other factors affect the reaction. The discrepancies have been rationalized, through molecular dynamics (MD) calculations, in terms of structural changes at the active site (see later).

Electrostatic field calculations have been also enabled rationalization of the dependence of catalytic rates on ionic strength (*122*, *126*, *131*). Due to the negative charges of SOD and the substrate, and to the diffusion-limited kinetidc rates, a positive dependence of catalytic rates on ionic strength would be expected, but the opposite is observed. This has been rationalized (*122*, *126*, *130–138*) taking into account that the diffusion of the charged substrate to the active site of SOD is determined by two competing effects: one is the repulsion between two species of the same charge, i.e., the substrate and the enzyme, after nonproductive collisions, and the other is the steering effect produced by the positive electrostatic field in the active site channel and at its entrance. The overall rate for the catalytic process, which is determined by the diffusion of the substrate, is the balance between these two effects, where the second is the dominant one. The first effect, which decreases the rates of collisions, is positively affected by an increase in ionic strength as the latter reduces the overall protein charge. The second effect, i.e., the steering of the substrate due to the positive charges of the channel, negatively affects the catalytic rates with increasing ionic strength because the attraction of the substrate would be reduced. Because the second effect in wild-type SOD is larger, an increase in ionic strength would reduce the productive collision rates and, for this enzyme, the catalytic rates.

Molecular dynamics studies have been particularly successful in rationalizing and predicting properties of SOD and its mutants (*139*, *140*). The different catalytic properties of the active site mutants have been interpreted as a result of structural and dynamic changes at the active site channel.

The overall protein structure and, in particular, the metal coordination sites and the active channel are quite stable when they are relaxed through MD calculations in the presence of explicit water. A striking result is the capability of these calculations to reproduce the

solvation properties of the metal sites and of the active channel. As will be discussed (see also Section VIII), the water molecule close to the copper ion is not coordinated to it and does not contribute to its ligand field. Consequently, in these calculations it was simply placed at its crystallographic position without any link to the protein by assigning it the force field parameters of the bulk water. During the MD trajectory on wild-type SOD and on all the mutants characterized by nuclear magnetic relaxation dispersion measurements (see Section VI) but Thr-137Ile, this water molecule maintains its position close to copper, as experimentally observed, despite the absence of any constraints. This indicates that the field produced at the active site by the residues of the channel is capable of maintaining the water molecule in its equilibrium position (*140*).

In the case of the Thr-137Ile mutant the same water molecule moves, after a few picoseconds of simulation, far from the metal site, and no other water molecule substitutes for it (Fig. 17). No other water molecules are present within 5 Å from copper, as is indeed observed experimentally (*112*). Replacing a hydrophilic residue with a hydrophobic residue at the active site destabilizes the structural

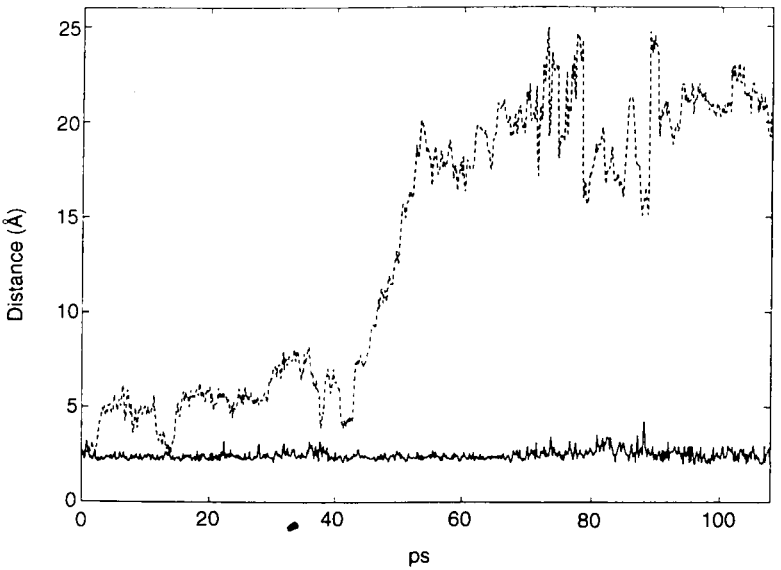

FIG. 17. Distance between copper and the oxygen of the closest water molecule to copper in wild-type SOD (solid line) and in Thr-137Ile SOD (dashed line) as a function of the simulation time. From Ref. *140;* Banci, L.; Carloni, P.; Orioli, P. L. *Proteins: Struct. Funct. Genet.* **1994** *18,* 216. Copyright © 1994 Wiley-Liss, Inc. Reprinted by permission of Wiley-Liss, Inc., a subsidiary of John Wiley & Sons, Inc.

water molecule and allows it to leave the cavity (*140*). This is a quite relevant result of these MD calculations, which are able to reproduce even fine details of the structural properties.

As expected on a pure electrostatic basis, neutralization of a negative residue in the channel would produce an increase in the catalytic rates, as has been indeed observed (*64*, *141*). The charge reversal from a negative to a positive residue is expected to produce an even larger increase in activity (*125*, *126*), but this does not occur (*64*, *141*). By analyzing the structural properties of the active channel in these mutants, as obtained by MD calculations, a large rearrangement of the electrostatic loop in the Glu-133Lys mutant has been observed. This could change the local electrostatic field, which could therefore not be enhanced by the charge reversal (*140*).

In addition to structural properties, the enzymatic activity is also modulated by the dynamic properties of the reaction site and of the channel. Mutation on Arg-143 produces, together with a decrease of the local positive field, a decrease of the flexibility of the bottleneck at the end of the active channel for the access to the copper site. The narrowest section of the active channel decreases in size on going from wild-type SOD to Arg-143Ile, to Arg-143Glu (*139*). Figure 18 shows the fluctuations of the distance between the residues at positions 143 and 137, which are the two groups determining the narrowest section of the active channel in SOD. This trend parallels closely the decrease in enzymatic activity observed for these mutants. The reduced size and mobility of the channel decrease the efficiency of the diffusion of the substrate in the channel, thus decreasing the number of encounters and therefore the enzymatic efficiency.

IV. Molecular Biology and Chemical Modifications

A. Expression Methods

Human SOD was one of the first types of Cu_2Zn_2SOD to be cloned and then expressed in different microorganisms. The human SOD gene was first isolated and sequenced. The wild-type human SOD proteins initiate with a methionine, which is then removed, followed by acetylation of the adjacent alanine to obtain the mature protein. In order to obtain a high transcription level of Cu_2Zn_2SOD in *E. coli*, the gene was cloned in a plasmid (ptac5) (Fig. 19) containing the *tac*1 promoter and transformed in an *E. coli* strain such as D1210 (*61*). Out of 500 colonies, 25 were able to produce SOD as 5% or more of the total soluble cell protein. Even if the activity of this recombinant

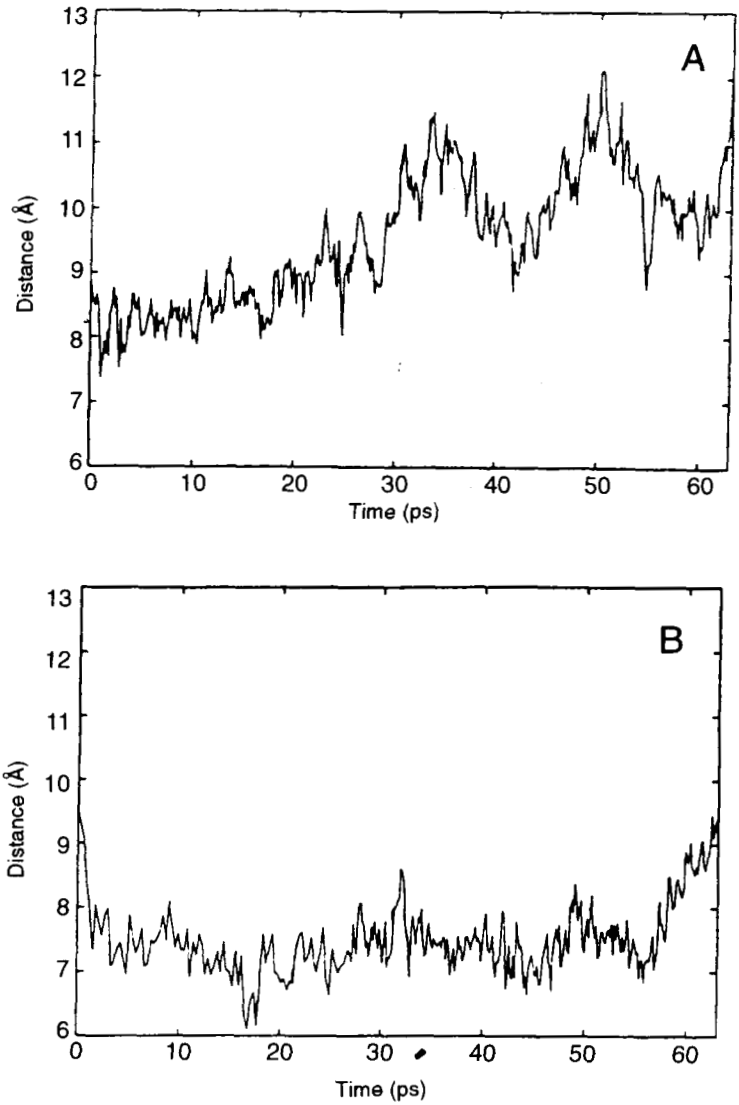

FIG. 18. Fluctuations of the distance between (A) Cζ Arg-143 and Cβ Thr-137 in wild-type SOD and (B) Cδ Glu-143 and Cβ Thr-137 in Arg-143Glu SOD. Reprinted with permission from Banci, L.; Carloni, P.; LaPenna, G.; Orioli, P. L. *J. Am. Chem. Soc.* **1992,** *114,* 6994. Copyright 1992 American Chemical Society.

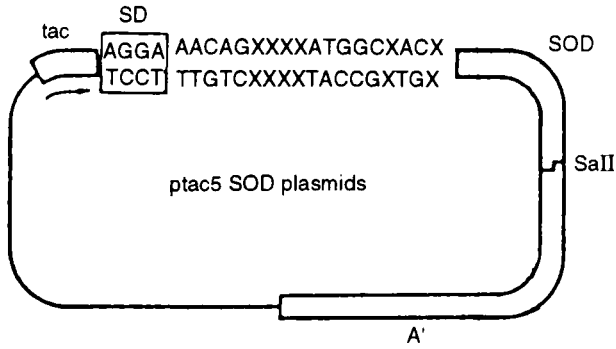

FIG. 19. Scheme of the ptac5 SOD plasmid, with the *tac*I promoter, the Shine–Dalgarmo sequence (SD), and the ATG-flanking sequence, with randomized positions, indicated by X, which contain all four bases. Reprinted from Ref. *61, Nucleic Acids Research,* **1985,** *13,* 2017, by permission of Oxford University Press.

protein is similar to that of purified human erythrocyte Cu_2Zn_2SOD (see Table III), the protein is not perfectly identical to the human protein because *E. coli* cells are unable to acetylate the exposed alanine. For this reason the expression of human SOD in yeast was also investigated. Human SOD was expressed in yeast using the yeast glyceraldehyde phosphate dehydrogenase promoter (*62*). The protein has a normal specific activity and it is indistinguishable from the human erythrocyte Cu_2Zn_2SOD.

Human SOD was also expressed in the periplasmic space of *E. coli* using a secretion vector that allows the protein to be accumulated in the periplasmic space. In 1988 the HSOD gene was cloned in a secretion vector pIN-III:OmpA (*142*) On induction of gene expression the protein was produced at a level of 10% of total cellular protein and was recovered through osmotic shock as the major component of the periplasmic fraction. Although the N-terminal alanine is not acetylated, it is practically indistinguishable from the acetylated form (see Table III).

Another periplasmic expression system (the plasmid pPHSOD1Iq) was constructed by Hallewell *et al.* (*64*); the plasmid contains a synthetic human SOD gene (*143*), joined to the leader sequence of *Photobacterium leiognathi* Cu_2Zn_2SOD (*144*), and the *lacIq* gene (*145*) in a pBR322 derivative containing the *tac*1 promoter (*61*). The synthetic SOD gene contains the Cys-6Ala, Cys-111Ser mutations, which are relevant for protein thermostability (*143*). In human SOD, Cys-6 and Cys-111 are the only free cysteines, the former buried and located adjacent to the dimer interface with the side chain pointed toward the interior of the β-barrel, whereas the latter is close to the dimer

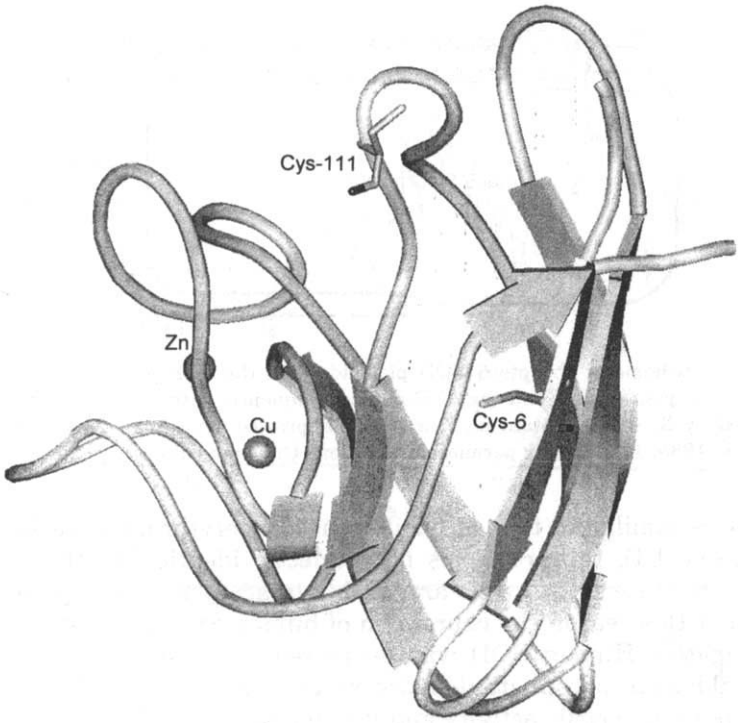

FIG. 20. Structure of human SOD indicating the position of the residues Cys-6 and Cys-111 (from Ref. *63*).

contact region but with its side chain pointed outward into the solvent (Fig. 20). Two mechanisms seem to be responsible for thermal inactivation of the cysteine-containing native enzyme: (1) hydrolysis of the backbone as happens for every cysteine-containing protein, and (2) incorrect formation of intermolecular disulfide bridges. Removal of Cys-6 and Cys-111 was demonstrated to increase protein thermostability (*143*).

Extracellular human SOD (EC-SOD), a tetrameric copper–zinc glycoprotein that is present in plasma, lymph, and synovial fluid, was expressed in Chinese hamster ovary cells (*146*, *147*). From cultures of these cells, recombinant EC-SOD was isolated in high yield with respect to native EC-SOD. Recombinant and native EC-SODs were compared and their properties were shown to be very similar (Table III).

Besides human SOD, other types of SOD were expressed in organisms different from those of the native species. Yeast SOD from *S. cerevisiae* was expressed in *E. coli* using the T7 RNA polymerase expression system (*148–150*). Cu_2Zn_2SOD from *X. laevis* was overex-

pressed from plasmid pKB under control of the *trc* promoter in *E. coli* (*151*). In *E. coli,* Cu_2Zn_2SOD from *Brucella abortus* was also expressed (*152*). The SOD gene was cloned in a pET3c vector containing the *T7* promoter. A leader sequence that directs secretion into the periplasmic space was also incorporated. The above plasmid was then inserted in the *E. coli* BL21 (DE3) strain, which carries the *T7* polymerase gene (*152*).

B. Chemical Modifications

Before the advent of biotechnology, in order to clarify the role of various amino acid residues in Cu_2Zn_2SOD, the first technique employed was chemical modification of specific residues.

Several α,β-diketones (phenylglyoxal, butanedione, and cyclohexanedione) inactivate the enzyme (the residual activity never exceeds 20%), interacting with and modifying one arginine/subunit (*153*). The inactivation, in the case of the bovine enzyme, is accompanied by some changes in the visible absorption spectrum of copper and by a small loss of copper, which, however, does not account for the inactivation and the spectral changes. Analysis of fragments obtained through treatment with CNBr demonstrated that the modified residue is Arg-143, whose presence was soon recognized to be very important for catalytic activity (*153*). In the case of the yeast enzyme the inactivation is complete and is not accompanied by any loss of copper(II) (*154*). Modification of the arginine residue affects the anion binding properties of the protein, lowering the affinity for CN^-, N_3^-, NCS^-, and CNO^-. The reduced affinity constants for these anions may be the result of modification of the copper coordination geometry or of neutralization of a positive charge in the active site, or both (*155*). Comparison of the rates of inactivation among Cu_2Zn_2SODs from different species indicate that bacterial enzymes are inactivated more rapidly by phenylglyoxal than are eukaryotic SODs (*156*).

Treatment of Cu_2Zn_2SOD with succinic anhydride led to full derivatization of all the lysine residues, indicating that all the lysines are accessible (*157*). The derivative has an increased negative charge that is reflected by a 10-fold decrease of activity, although the coordination geometry of the active site is not affected by succinylation (*157*). It was also proposed that this treatment might weaken the interactions between the two subunits (*157*). The lysine charge can also be neutralized through carbamylation and acetylation with a consequent decrease in activity and anion affinity (*105*, *158*).

The effect of chemical modifications on Arg-143 and lysines was also investigated for the reduced enzyme. It was observed that the

reduced, modified enzyme has a lower affinity for chloride than the reduced, untreated SOD, indicating that electrostatic interactions between positively charged groups and the substrate are present in the reduced state of the protein and play an important role in the catalytic mechanism (*159*) (see Sections II,A,J and IX,B).

Carboxylated polyethylenglycol (PEG, MW 5000) interacts with SOD through covalent binding with the protein amino groups (*160*, *161*) at the enzyme surface, resulting in a polymeric form with a molecular weight of 120,000 (*162*, *163*). This is confirmed by the line broadening of the ^1H NMR spectrum of the Cu_2Co_2 derivative (*163*). The structure of the active site geometry seems to be unaffected by PEG treatment, whereas the activity is reduced to 75%, and the affinity for N_3^- to 50%, with respect to the untreated enzyme. These results indicate that the lower activity must be ascribed to a decrease in the channeling of the O_2^- ion toward the active site, as a consequence of neutralization of positive charges.

Excess of hydrogen peroxide, one of the products of superoxide dismutation, at alkaline pH reduces copper(II) and inactivates the protein (*52*, *98*, *164*, *165*). Inactivation seems to be accompanied by changes in the visible and EPR spectra (*98*, *166*, *167*). The intensity of the EPR spectrum decreases with H_2O_2 concentration and with time, but it does not disappear completely (*167*). Kinetic studies in dilute solution indicated that inactivation is a first-order process with respect to enzyme and reagent (*98*). The effect of H_2O_2 was proposed to be related to the modification of the amino acid composition and to the destruction of one of the histidine ligands (*98*, *166*). The ^1H NMR investigation of the H_2O_2-treated Cu_2Co_2SOD derivative clearly shows that the coordinated residues are maintained, although there is evidence of some flexibility of the donor groups. Furthermore, His-48 (a copper-coordinated residue) is affected by the modification caused by H_2O_2 as far as its position with respect to the metal ion is concerned (*168*). Recent studies have provided evidence that treatment with H_2O_2 causes oxidation of histidine residues and that His-120 is selectively oxidized on the Cε1 atom and converted to 2-oxo-histidine (*169*).

The interaction of SOD with peroxynitrite has been investigated. Peroxynitrite is produced by the reaction between nitric oxide and superoxide, whose concentration increases in pathological conditions such as ischemia. It has been found that peroxynitrite is also a substrate for SOD and that the catalytic action of the enzyme permanently modifies Tyr-110 and converts it into 3-nitrotyrosine (*78*). The X-ray structure of the peroxynitrite-modified SOD has also been solved (see Section II,G).

C. The Mutants

From the very beginning of the investigation of superoxide dismutase it was noted that bovine SOD has an overall −4 charge and an isoelectric point at pH 5.2 (*170*). The protein should thus repel the anionic substrate. However, there is a positive charge on the surface of the active cavity and where the metal ion sits, which exerts a stronger and positive effect in guiding the substrate within the cavity. The ionic strength smoothens both effects with the result that it causes a decrease in activity, because the focused attraction has a larger effect on the enzyme activity than the overall repulsion (*122*).

The first mutation, according to this reasoning, was at position 143, where an Arg residue is strategically located (Fig. 21). When it is substituted with a Lys, which is still positive but has a different spatial location, the protein loses some of its activity. At pH 5 the latter is reduced to 10% when an Ile is present, and drops to 4% when there is a negative charge such as Glu or an Asp (Table III) (*95*, *104*). The pH dependence of the activity for these mutants is quite unique. Indeed, whereas wild-type SOD and most SOD mutants exhibit a constant rate in the pH range 5–9, with a drop at higher pH, the Arg-143Glu, the Arg-143Asp, and the Arg-143Lys mutants show drops at lower pH values, due to the deprotonation of the residue. This demonstrates that the presence of Arg at position 143 is crucial in keeping a stable positive charge up to pH 10 (*95*). The decrease in local positive charge on going from wild-type SOD to Arg-143Ile, to Arg-143Asp (or Glu) has a strong effect on the dependence of the catalytic rate on

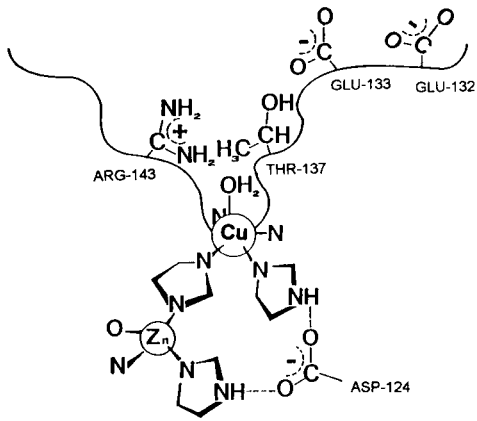

FIG. 21. Schematic drawing of the catalytic cavity of SOD.

ionic strength. Indeed, whereas the wild-type protein is greatly affected by ionic strength, the mutants, with negative residues at position 143, are almost unaffected by the increase in ionic strength (*95*). The ^1H NMR spectra of the Cu_2Co_2 derivative (see later) show that the ligands are not affected by these mutations. Interestingly, the affinity of N_3^- for the copper follows a pattern similar to that of activity. Because the dismutation of O_2^- by SOD is a very fast process and no saturation is observed at room temperature (see Section III) (*99*, *171*), the rate-limiting process of the catalytic rate of Cu_2Zn_2SOD is the binding of O_2^- to the active site. Therefore, whereas the activity is determined by k_{on} of O_2^- the affinity of N_3^- depends on the ratio k_{on}/k_{off}. If k_{off} is just determined by the barrier of the Cu–N bond breaking and is constant, then it is also reasonable that the patterns of k_{on} of O_2^- and the affinity constants of N_3^- are often similar.

If the Thr-137 residue is mutated the effects are also relatively large. The Thr-137Ile makes the cavity quite hydrophobic. Nuclear magnetic relaxation disperson studies (see Section VI) show that the semicoordinated water is now not present. Molecular dynamics calculations on the mutants have shown a high mobility of the water molecule close to the copper ion (see Section III,D). A rearrangement of the active site channel observed in this mutant is responsible for pushing out the water molecule and seems to produce a different electrostatic field with respect to wild-type SOD just on the coordination sphere of copper, but not to affect seriously its surroundings (*140*). Through spectroscopic investigation it was observed that the copper chromophore is more tetragonal than in wild-type SOD, with His-48 more firmly bound to copper in a more symmetrical environment (*112*) (see Table IV). A different effect on the hydrophilicity of the cavity is observed when Thr-137 is substituted by Ser or Ala: in the former case the hydrophilic residue stabilizes the water molecule more than in wild-type SOD, and in the latter case the small Ala, despite its hydrophobicity, slightly reduces the presence of water (*115*). The activity is not affected at all by the different stability of the water molecule close to copper (*115*). The Thr-137Arg mutant has a sizable activity but smaller than that of wild-type SOD (Table III), which, at low ionic strength, extrapolates at the same value of wild-type SOD. On the other hand, the affinity for anions such as azide is 20 times higher than is seen in wild-type SOD (*172*). A reasonable hypothesis for this behavior, confirmed by MD calculations (*112*), is that substitution of Thr-137 with Arg dramatically affects the loop formed by the side chains of Lys-136, Glu-132, and Glu-133, a loop that is implicated in electrostatic guidance of superoxide (Fig. 22). (*45*). In the case

TABLE IV

EPR PARAMETERS AND Hδ1 HIS-48 CHEMICAL SHIFTS OF THE Cu_2Co_2 DERIVATIVES FOR SOME Cu_2Zn_2SODs, SOME OF THEIR ADDUCTS WITH ANIONS, AND SOME OF THEIR MUTANTS[a]

Source[b]	$g_\parallel$	g	$A_\parallel$ (10^{-4} cm^{-1})	δ (ppm) Hδ1 His-48	Ref.
BSOD	2.26	2.07	143	34.5[c]	*207, 218, 242*
YSOB	2.26	2.08	141	34.1[d]	*243*
HSOD	2.26	2.07	140		*103*
HSOD (yeast)	2.28	2.09	145	34.6[d]	*346*
AS-HSOD (yeast)	2.28	2.09	142	34.6[d]	*346*
AS-HSOD (*E. coli*)	2.26	2.09	138	35.0[c]	*208*
BSOD + F^-	2.26	2.06	143	31.3[e]	*89*
BSOD + NCS^-	2.25	2.06	148	27.7[e]	*89*
BSOD + NCO^-	2.26	2.05	158	19.8[e]	*89*
BSOD + N_3^-	2.21	2.05	157	15.9[e]	*89*
BSOD + CN^-	2.21	2.06	188	13.0[e]	*89*
BSOD + HS^-	2.21	2.03	180	—	*278*
Cu_2E_2BSOD	2.27	2.04	148	—	*207, 243*
Cu_2E_2BSOD + N_3^-	2.24	2.06	164	—	*244*
Cu_2E_2BSOD + CN^-	—	2.06	181	—	*244*
Cu_2Hg_2BSOD	2.26	2.05	141	—	*243*
Cu_2Cd_2BSOD	2.26	2.05	138	—	*243*
Thr-137IleHSOD	2.25	2.04	162	38.6[d]	*89*
Thr-137AlaHSOD	2.26	2.07	140	36.3[c]	*115*
Thr-137SerHSOD	2.26	2.07	140	34.5[c]	*115*
Thr-137ArgHSOD	2.26	2.06	141	38.3[c]	*172*
Arg-143IleHSOD	2.26	2.08	137	34.6[d]	*270, 342*
Arg-143GluHSOD	2.28	2.09	148	36.2[d]	*270, 342*
His-80CysYSOD	2.26	—	139	—	*176*
His-46CysYSOD	2.23	—	151	—	*178*
His-120CysYSOD	2.27	2.05	175	—	*178*

[a] The data were collected between pH 5.0 and 7.5; in this range no spectroscopic changes are observed for the species cited. In rhombic systems $g_\parallel$ represents the reading at zero intensity on the left side of $g_x + g_y$.

[b] BSOD, Bovine SOD from erythrocytes; YSOD, yeast SOD; HSOD, human SOD; AS-HSOD, human SOD with the following modifications: Cys-6Ala, Cys-111Ser.

[c] Measured at 300 K.

[d] Measured at 303 K.

[e] Measured at room temperature.

of the Thr-137Arg mutant these residues are much further from the copper ion and point toward the surface of the protein, breaking the hydrogen bonding network that stabilizes the active channel (*112*, *172*).

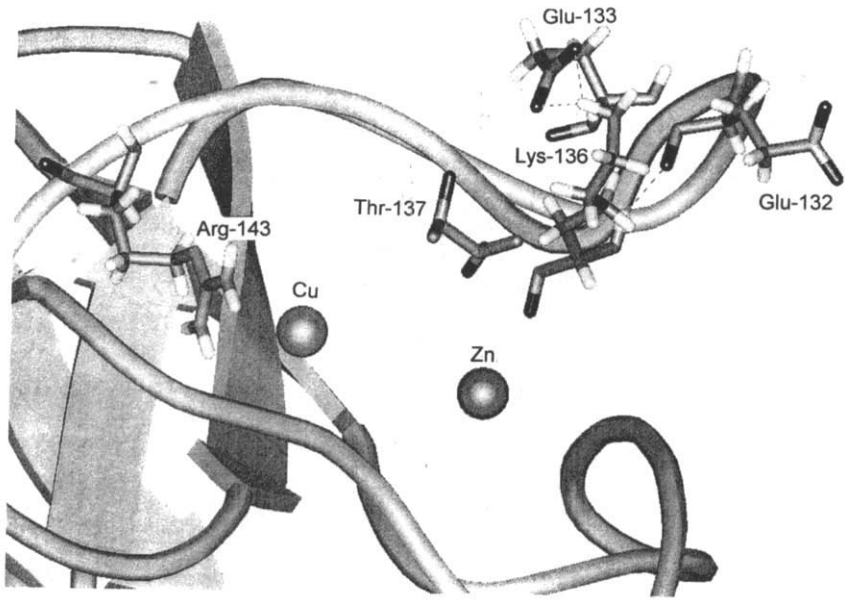

FIG. 22. The active site channel of human SOD with the hydrogen bond network among side chains of Glu-132, Glu-133, Lys-136, and Thr-137.

Asp-124 is responsible for a long-range bridge between the copper domain and the zinc domain, connecting, through hydrogen bonds, His-46 and His-71. Substitution of the residue with Asn, Gly, or Gln produces mutants that do not bind zinc. The mutants are stable at high pH whereas in the native zinc-deprived enzyme the copper ion, at high pH, moves to the zinc site to form a 50% dicopper derivative (*173*). The zinc-free Asn-124Asp mutant, at low pH (5–6), has about the same activity as wild-type SOD (Table III), and allows determination of the activity of a Cu_2E_2SOD derivative at high pH (Fig. 23) (*96*).

Through site-directed mutagenesis it was possible to design and obtain mutants that are significantly more active than the native protein (*174*). The substitution of the negative Glu-133 and/or Glu-132 with Gln, which gives rise to an increase in local positive charge while maintaining the orienting network, produces a two- to threefold more active protein (Fig. 24 and Table III). The decrease of activity on increase of ionic strength is stronger than for the native protein. These two effects corroborate the important role played by electrostatic interactions. However, electrostatic effects alone are insufficient to explain the activity behavior of SOD: the Glu-133Lys, Glu-132Gln mutant, which has a further increase in local positive charge, is less

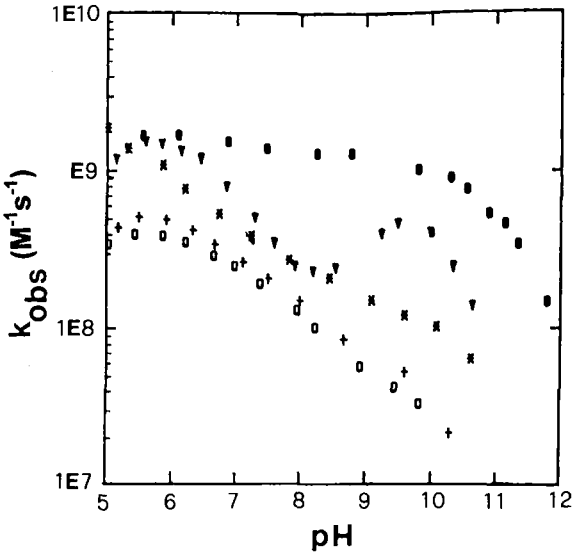

FIG. 23. Rate constant versus pH of Cu_2Zn_2 human SOD (●), Cu_2E_2 human SOD (▼), Cu_2E_2 Asp-124Asn SOD (★), Cu_2E_2 Asp-124Gly SOD (○), and Cu_2E_2 Asp-124Asn, Asp-125Asn SOD (+). Reprinted from Ref. *96*.

active than the Glu-133Gln, Glu-132Gln mutant, showing that the positive charge of Lys can disrupt the orienting network (*64*, *141*).

A similar enhancement of catalytic rate was observed with the Glu-131Gln mutant of *X. laevis* Cu_2Zn_2SOD, which corresponds to the Glu-133Gln of the human isoenzyme. However, the Asp-130Gln mutant differs from the corresponding mutant of the human enzyme: the mutant from *X. laevis* has a catalytic rate comparable to that of the native enzyme, indicating that some residues occupying the same position in the sequence of SODs from different organism might have a different role (*175*).

The role of Lys-136 is still a matter of debate. Its deprotonation has been related to the loss of activity observed at high pH (*116*). However, in the case of the human isoenzyme, the spectroscopic characterization, as a function of pH, of three mutants on this position (Arg-136, Ala-136, Gln-136), show the same pK_a values (within experimental error) as the native protein, both for the reduced and oxidized forms of the enzyme. These data ruled out Lys-136 as being responsible for the spectroscopically observed high-pH pK_a values (*119*). The activity of the Lys-136Gln and Lys-136Ala mutants at neutral pH is similar to that in the wild-type protein, whereas the Lys-136Arg de-

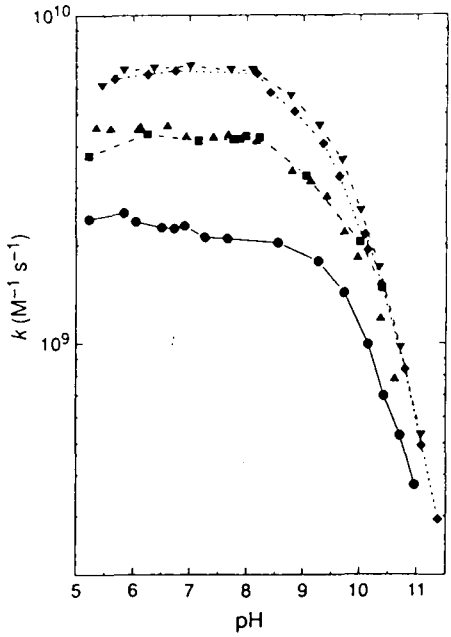

FIG. 24. Rate constant versus pH, at ionic strength = 0.01 *M*, for human SOD (●) and for the mutants Glu-132Gln, Glu-133Gln SOD (▼), Glu-133Gln SOD (◆), Glu-132Gln, Glu-133Lys SOD (■), and Glu-132Gln SOD (▲). Reprinted with permission from *Nature*; Getzoff, E. D.; Cabelli, D. E.; Fisher, C. L.; Parge, H. E.; Viezzoli, M. S.; Banci, L.; Hallewell, R. A.; **1992,** *358,* 347. Copyright 1992 Macmillan Magazines Limited.

rivative shows an increase of 1.5 times (Table III) (*119*). Activity profiles obtained through pulse radiolysis techniques on the same mutants indicate that the pK_a is essentially maintained, therefore Lys-136 does not seem to affect the activity profile (D. E. Cabelli, personal communication).

The role of the lysines of the active site channel, Lys-120 and Lys-134 (which correspond to positions 122 and 136 of the human isoenzyme) was investigated for the enzyme isolated from *X. laevis*. It was demonstrated that these lysines contribute to the steering of the superoxide anion toward the copper ion (*175*). Indeed, the activity of mutants at positions 120 and 134 is 60–65% with respect to wild type (*117, 175*). Furthermore, the pH dependence of the activity was investigated and the best fit of the experimental data was obtained with two pK_a values, $pK_1 = 9.3$ and $pK_2 = 11.3$, in the wild-type enzyme (*117*). The authors propose that pK_1 is mainly governed by Lys-120

and Lys-134 (*117*), even if the differences in pK_1 values for wild types and mutants are within experimental error.

In an attempt to redesign the metal binding site of SOD in order to convert it to a type 1 copper center, some mutants of yeast SOD, in which histidyl ligands in the metal sites were replaced by cysteines, were prepared (*150*, *176–178*). The mutant obtained substituting His-80 with Cys in the zinc site, and then replacing zinc(II) with copper(II), shows spectroscopic features typical of type 1 copper, as far as electronic, magnetic circular dichroism (MCD), electron paramagnetic resonance (EPR), and Raman spectra are concerned (*150*, *176*, *177*). On the other hand, when the newly introduced cysteine ligands bind copper(II) in its site, as in the case of His-46Cys and His-120Cys analogues, the properties of type 1 centers are not observed. Investigations on model complexes and on naturally occurring type 1 copper proteins have demonstrated that an essential feature is the presence of a trigonal N_2S site, whereas type 2 copper proteins tend toward tetragonal rather than trigonal geometries. Apparently the geometry around the metal, which is determined by the protein, is a determining factor as far as the type of copper is concerned. An interesting difference between His-46Cys and His-120Cys mutants is that the imidazolate bridge between copper and zinc remains intact in the His-46Cys mutant but is not present in the copper–cysteinate His-120Cys mutant (*177*, *178*).

In order to investigate the role of the imidazolate (His-63) that bridges copper and zinc ions, mutants on residue 63 have been prepared and characterized. The substitution of alanine in place of the bridging histidine ligand, in yeast SOD, perturbs the metal binding properties of the protein. The mutant His-63Ala shows significant changes in the geometry of the zinc site with respect to wild-type SOD, the pH independence of the spectral properties up to pH 12, typical of wild-type protein, is not maintained, and a pK_a of 9.3 was observed. In addition the activity of the His-63Ala mutant is pH dependent and, at physiological pH, is 250-fold less than that of wild type (*149*) (Table III).

The His-63Cys mutant seems to have the Cys bound to zinc, thus leaving copper(II) coordinated to three histidines and to solvent. Two water molecules have been proposed to interact with copper. Now water is regularly coordinated. The enzyme has no activity (Table III), although the reduction potential is still in the correct range to function. It has been proposed that a water bound to copper causes a decrease in the activity because the electron transfer has to occur through a water molecule rather than directly (*179*).

If we look at the interface of the dimer, a hydrophobic patch is noted that is responsible of the existence of the dimeric entity (Fig. 10). As mentioned in Section II, transformation of two neutral groups of the human isoenzyme (Phe-50 and Gly-51) into negative charged residues (two Glus) produces a monomeric species (*60*). This is checked through gel filtration experiments and through ^{1}H NMR of both the reduced derivative species and the oxidized paramagnetic CuCo derivative. The line width of the NMR signals is fully and unequivocally consistent with monomeric species. The ^{1}H NMR spectra show that the ligand assignment is similar to that of wild-type SOD and that the geometry of the chromophore is closest to that of the Ile-137 mutant (Table IV) (*60*). The enzyme is only 10% active (Table III) and its catalytic rate is not dependent on ionic strength. The reduction in activity has been ascribed to some structural changes in the active site channel, changes that may indirectly derive from the solvation of the newly exposed dimer interface or to its distortion (*60*). As far as the behavior with ionic strength is concerned, we should take into account that in this mutant the net protein charge is -4 (vs. -2 of the wild-type SOD subunit). As a consequence, the protein–substrate repulsion is higher than for wild-type SOD, which balances the steering effect of the positively charged residue in the active site channel. An increase in ionic strength, which reduces both electrostatic effects, seems to produce compensating effects in this case, thus producing catalytic rates that are ionic strength independent.

With the goal of increasing the catalytic activity a monomeric mutant (Phe-50Glu, Gly-51Glu), in which the negative Glu-133 is neutralized, was prepared. The mutant, Phe-50Glu, Gly-51Glu, Glu-133Gln, has an enhanced catalytic rate, and in contrast to Phe-50Glu, Gly-51Glu is ionic strength dependent. In this case the net protein charge is -3, compared to -4 of the Phe-50Glu, Gly-51Glu mutant, the protein–substrate repulsion is decreased, and the increased salt concentration again causes a decrease in catalytic rate (*124*).

V. Metal Substitutions

At low pH values SOD tends to lose the metal ions (*180*) and below pH 3 it exists almost entirely in a random coil form (*181*). Either the native metal ions or combinations of various metal ions can be readded to apoSOD at high pH to form a variety of metal-substituted SODs, which have been the subject of extensive physical measurements. ApoSOD is prepared by dialysis versus EDTA solution at pH

3.8 (*2*) or 1,10-phenathroline at pH 3.2 for 24 hr, at room temperature (*182*). In order to reobtain the holoenzyme or metal-substituted derivatives the pH is increased. The holoSOD was reconstituted from apoSOD for the first time in 1974 (*183*). A scheme to obtain metal-substituted derivatives is shown in Fig. 25.

It appears that Cu_2Zn_2SOD (and also Cu_2Cu_2SOD and Cu_2Co_2SOD) loses the metal at the zinc site between pH 4.5 and 3.0, and indeed all the spectral data indicate the formation of Cu_2E_2SOD[5] (*184*). The metal is rapidly rebound when the pH is raised. It is also suggested that a protein conformational change is involved rather than a simple competition between metal ions on one side and protons on the other. At pH below 4, the copper binding site is the only strong binding site. At pH 3.6, 95% of zinc is removed by dialysis, versus only 5% of copper (*180*). Below pH 3, copper is also lost from the protein (*184*). E_2Zn_2SOD can be obtained by reacting reduced SOD with CN^-, at pH 6 (Fig. 25).

For spectroscopic determinations of the amounts of protein material it should be noted that SOD absorbs, in the UV region, with a maximum at 265 nm. Different extinction coefficients were found for various isoenzymes, as a consequence of the different primary sequence. For example, ε_{max} is 15,900 M^{-1} cm^{-1}, for the human enzyme, and 10,300 M^{-1} cm^{-1} for the bovine enzyme (*2*, *103*). In the visible region of the electronic spectrum the holoenzyme has an absorption maximum at 680 nm [ε = 300 M^{-1} cm^{-1} (2)]. The Cu_2E_2 enzyme has a typical absorption with λ_{max} at 700 nm, at pH 6 (*183*). The two metal binding sites in SOD are largely determined by the tertiary structure of the protein, so that a number of M_2N_2SOD derivatives can be prepared (Fig. 25) with coordination properties similar to those seen for $Cu^{II}_2Zn^{II}_2SOD$ and $Cu^{I}_2Zn^{II}_2SOD$.

At the copper site there may be Ni^{2+}. This is obtained after addition of nickel at pH 7.5 to E_2N_2SODs that are obtained by adding the metal ion N to E_2E_2SOD at pH 6 (*185*) (Fig. 25). Nickel(II) is a reasonable probe for copper(II) because both tend, whenever possible, to give rise to square planar coordination geometries (*186*). Nickel(II) is five-coordinated, with a water molecule probably coordinated. When there is cobalt(II) in the copper site, the coordination number is again five, as in the case of nickel(II). However, when phosphate is present, it binds Arg-143 and cobalt. The latter would be displaced from its original place, causing detachment from the bridging histidine. Cobalt(II) is

[5] M indicates the metal ion in the copper site, N is the metal ion in the zinc site, and E means "empty."

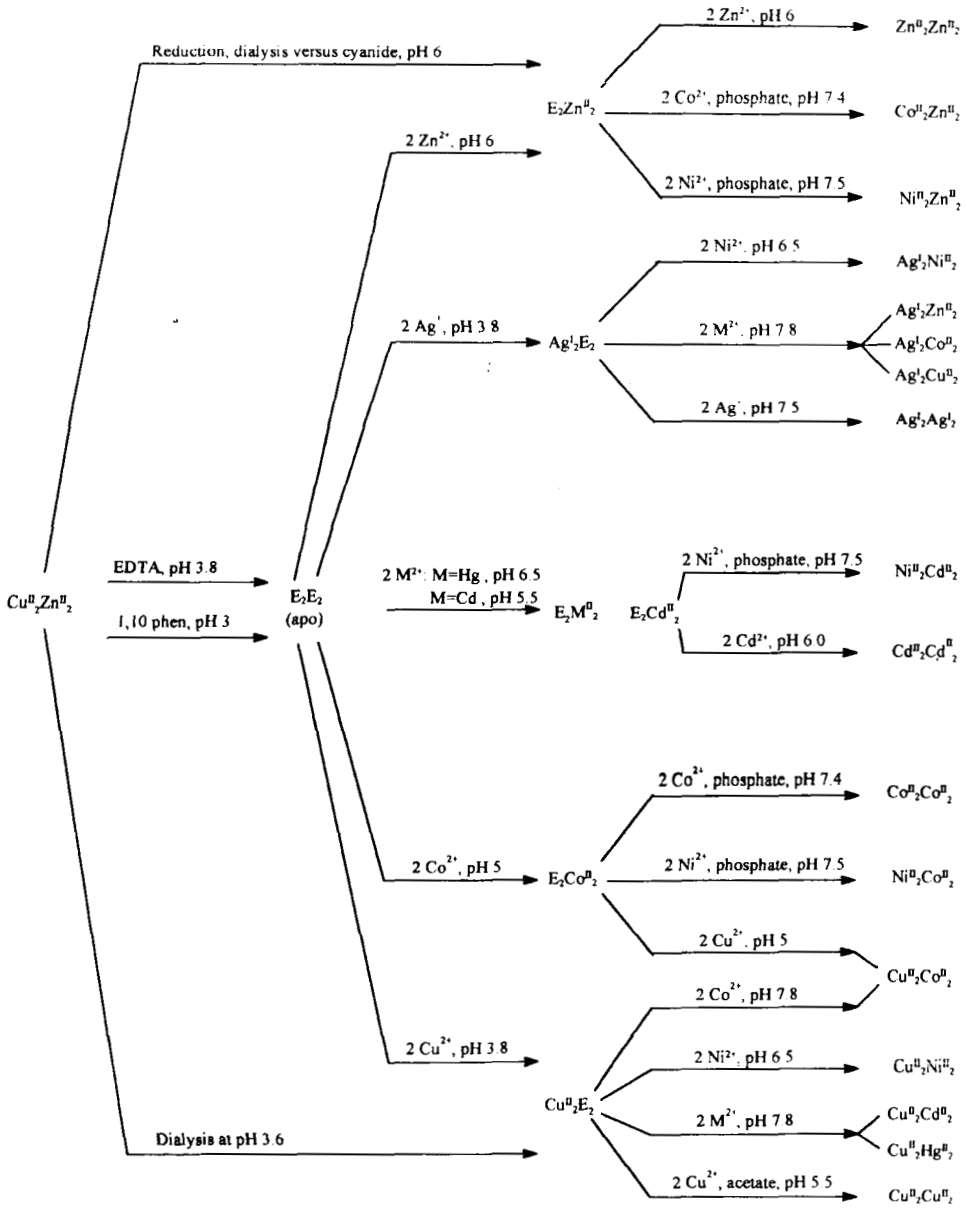

FIG. 25. Metal substitution procedures for Cu_2Zn_2SOD: E_2Co_2 (*289*); Cu_2Co_2 (*189, 350*); Cu_2Ni_2 (*258*); Cu_2Cu_2 (*252*); Cu_2Hg_2 (*243*); Cu_2Cd_2 (*243*); Cu_2E_2 (*243, 350*); Ag_2Zn_2 (*188*); Ag_2Co_2 (*188, 244*); Ag_2Ni_2 (*258*); Ag_2Cu_2 (*188*); Ag_2Ag_2 (*188*); Ag_2E_2 (*188*); Zn_2Zn_2 (*251, 351*); Ni_2Zn_2 (*185*); Ni_2Co_2 (*185*); Ni_2Cd_2 (*185*); Co_2Zn_2 (*185, 259*); Co_2Co_2 (*185, 259*); Cd_2Cd_2 (*197*).

tetrahedral with the three His nitrogens and a phosphate ion. Only above pH 10 is the bridge reestablished (*187*).

Ag^+ is a good probe for reduced copper, and has high affinity for the copper site. It may bind to the zinc site but only in the absence of other metal ions (*188*). When two Ag^+ and Cu^{2+} ions are present, only Ag_2Cu_2SOD is obtained, independently of the order of addition of the metal ions (*188*). The presence of Zn^{2+} in the zinc site increases the affinity of Ag^+, and thus it is proposed that zinc stabilizes the reduced enzyme. The only difference between Ag^+ and Cu^+ is that at high pH His-63 bridges Ag^+ and the metal at the zinc site, whereas Cu^+ remains coordinated to three His residues at every pH.

There may be a variety of metal ions in the zinc site (Fig. 25). The most important substitution (for spectroscopic studies) is that of zinc by cobalt (*189*). The coordination chemistry of cobalt is similar to that of zinc and the derivative is quite similar to the native enzyme. The affinity of zinc and other metal ions (*173*, *190*) for the zinc site at pH > 7.5 increases when copper(II) is bound to SOD. It seems that copper organizes the zinc site. Indeed, Cu_2E_2 transforms into Cu_2Cu_2 and E_2E_2SOD at pH higher than 7 (*173*).

For the E_2Co_2SOD derivative, a pH-dependent Co^{2+} migration from the zinc site to the empty copper site was observed, forming subunits containing Co^{2+} in both metal binding sites. The presence of phosphate was observed to facilitate the cobalt migration process, presumably due to the fact that the anion causes an enhancement of Co^{2+} binding to the copper site (*191*). Every time there is migration from E_2N_2SOD or M_2E_2SOD to MNSOD and EESOD, the problem remains of whether the M-His63-N moiety is randomly distributed or whether there is cooperativity within the dimeric unit of SOD.

An anticooperative behavior within the same subunit was proposed when copper binds E_2Co_2SOD at acidic pH (5.5). When the zinc site is partially occupied by cobalt, copper ions preferentially bind the subunits lacking cobalt. This can be explained by taking into account that the binding of copper to a site where the bridging His is already bound to cobalt requires a second deprotonation (*192*). An asymmetric behavior of the two subunits has been also proposed (*193*, *194*), but this hypothesis was shown to be wrong by Valentine *et al.* (*195*).

Cd^{2+} has been added either at the copper site or at the zinc site (*196*, *197*). Its properties have been investigated by perturbed angular correlation (PAC) studies and by ^{113}Cd NMR. The PAC coordination number may be higher than that usually proposed or found (*198*, *199*).

Differential scanning calorimetry has been used to compare the thermally induced unfolding of native SOD and apoSOD. The results

clearly demonstrate that metal ions play a significant role in enhancing the thermal stability of SOD (*31*). Some apparent affinity constant measurements are available for copper(II) and apoSOD (*200, 201*). The rate constant of metal release has been studied at low pH values (*182*).

The stability of the MNSOD derivative (indicated as such for this purpose) can be derived as follows: The first metal ion binds EESOD according to Eq. (12) with an apparent equilibrium constant K_M:

$$M + EESOD \rightleftharpoons MESOD. \tag{12}$$

The second metal ion binds according to Eq. (13) with apparent equilibrium constant K_N:

$$MESOD + N \rightleftharpoons MNSOD. \tag{13}$$

The overall stability is given by Eq. (14):

$$S_{MN} = \log K_M + \log K_N. \tag{14}$$

Table V gives the S_{MN} values that have been reported for several real and hypothetical derivatives of SOD at pH 6.25 (*188*). The data are instructive and show that the native enzyme is the most stable form.

From the early investigation of SOD (*202*) it was recognized that apoSOD was more labile toward a variety of inactivating stresses than was the holoenzyme. Addition of Cu^{2+}, besides restoring the ac-

TABLE V

RELATIVE SOLUTION STABILITIES OF METAL-SUBSTITUTED DERIVATIVES OF SOD AT pH 6.25[a]

M, N (in M_2N_2SOD)	$S_{M,N}$	M, N (in M_2N_2SOD)	$S_{M,N}$
Cu, Zn	24.9	Zn, Zn	18.15
Cu, Cu	24.5	Zn, Cu[b]	18.0
Ag, Zn	23.1	Ag, Ag	17.05
Ag, Cu	21.3	Zn, Ag[b]	14.15
Cu, Ag[b]	20.65		

[a] Reprinted with permission from Roe, J. A.; Peoples, R.; Scholler, D. M.; Valentine, J. S. *J. Am. Chem. Soc.* **1990,** *112,* 1538. Copyright 1990 American Chemical Society.

[b] Theoretical values: these species have not been observed.

tivity, enhanced the thermostability of the enzyme. Such stability further increases on addition of metal ions to the zinc site.

VI. Water in the Active Site Cavity

X-Ray crystallography has always shown the presence of water in the active cavity. Often, one molecule is about 2.2–3.0 Å from copper and another is a little farther (see Section II) (*41*, *44*, *63*, *75*).

Extended X-ray absorption fine structure (EXAFS) studies in aqueous solutions have shown that a water molecule in wild-type bovine SOD is 2.5 Å (Cu–O distance) from the metal (*203*). From ^{1}H NMR studies the same distance is proposed (see later). Ligand field calculations have shown that the water molecule essentially does not affect the energy levels (*89*, *204*).

The interaction of water with the paramagnetic copper(II) ion of oxidized SOD has been monitored through nuclear magnetic relaxation dispersion (NMRD) (*114*, *205–208*). The interaction of water protons with the unpaired electron of copper(II) causes an enhancement on the proton NMR relaxation. Usually the water proton T_1^{-1} measurements are performed at proton Larmor frequencies between 0.01 and 50 MHz. The profiles are of the type shown in Fig. 26. In a simplified model of the electron–nucleus coupling in macromolecules the T_1^{-1} enhancements are inversely proportional to the sixth power of

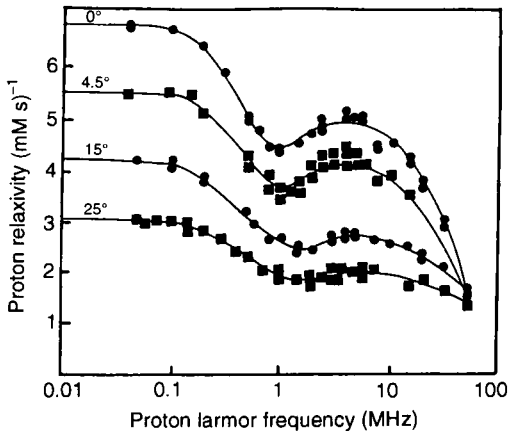

FIG. 26. ^{1}H T_1^{-1} values, as a function of the proton Larmor frequency for Cu_2Zn_2SOD at different temperatures (*205*). The lines are best-fit curves obtained with the inclusion of the effect of hyperfine coupling with the metal nucleus (*212*) (from Ref. *295*).

the average proton–copper distance and depend on the external magnetic field with an equation (*209*) of the type

$$T_1^{-1} \propto a\tau_s/(1 + \omega_s^2\tau_s^2) + b\tau_s/(1 + \omega_I^2\tau_s^2), \quad (15)$$

where ω_s and ω_I provide the energy of the split Zeeman levels for the electron and the nucleus, respectively, τ_s is the electron relaxation time, and a and b are constants containing the copper–proton distance. The drop of T_1^{-1} values at high field depends on the electronic relaxation time. If such time is the same, the T_1^{-1} values before the high-field decrease are proportional to the number of exchangeable protons sensing the unpaired electrons and to the reciprocal sixth power of the proton–copper distances. In general, a single water molecule is assumed to be responsible for the T_1^{-1} enhancement, so that analysis of the plots provides a copper–water distance.

The theory necessary for the analysis was developed in the 1980s (*207*, *210–213*) and a general computer program is now available (*214*). The program requires, besides the water proton T_1^{-1} values, the hyperfine coupling constants relative to the coupling between the copper nucleus and the unpaired electron. The program then provides the electronic relaxation times, the water–copper distance, and the angle between the copper–proton and the molecular z axis. In Table VI such values are reported for the native bovine SOD, human SOD, some mutants, and some adducts with inhibitors. The water–proton distance for bovine SOD is the same as proposed from EXAFS studies in aqueous solution (*203*).

In Fig. 27 the water ^1H T_1^{-1} profiles of Cu_2Zn_2SOD and of its Thr-137Ser, Thr-137Ala, and Thr-137Ile mutants are reported. The Ser derivative appears to have a water molecule closer to the metal ion (*115*, *208*, *215*). The Ala-137 derivative, as a consequence of the hydrophobicity of this residue, has a water molecule at a distance slightly longer than wild-type SOD (*115*, *208*, *215*). The NMRD profile of the Thr-137Ile mutant suggests that there is no water closer to copper(II) in the cavity, as there is in wild-type SOD, probably because of the bulkiness of the residue and the hydrophobicity of the cavity (*112*, *115*). As discussed in Section III,D, molecular dynamics simulations are capable of reproducing the presence of water in wild type SOD and its absence in the Ile mutant (*140*). The Thr-137Ile mutant is largely active (Table III), indicating that copper-bound water is not important for catalysis.

In the His-63Cys mutant (see Section IV,C) copper(II) is coordinated to three histidines and to solvent. Two water molecules have

TABLE VI

BEST-FIT PARAMETERS FOR THE WATER PROTON NMRD DATA ON Cu_2Zn_2SOD, SOME MUTANTS, AND SOME INHIBITOR DERIVATIVES

System[a]	τ_s (nsec)	r_{Cu-H} (Å)[b]	θ (deg)[c]	$A_\parallel$ (10^4 cm^{-1})	Ref.
BSOD	2.8	3.4	19	143	*207*
HSOD (yeast)	2.2	3.5	20	145	*208*
Cu_2E_2BSOD	3.6	3.2	24	148	*207*
Cu_2Cu_2BSOD	4.2	3.4	29	143	*207*
Arg-143GluHSOD	2.5	3.4	22	148	*208*
Arg-143IleHSOD	2.5	3.8	15	137	*208*
Thr-137AlaHSOD	1.5	3.7	—	140	*115*
Thr-137SerHSOD	2.1	3.2	—	140	*115*
Thr-137IleHSOD	3.8	4.7	20	162	*115*
His-63CysHSOD	1.5	2.8[d]	—	142	*179*
His-63CysHSOD + N_3^-	1.5	2.8	—	123	*179*
BSOD + 0.5 *M* P_i	3.2	3.3	36	143	*219*
BSOD + 0.5 *M* NCO^-	3.2	3.9	32	158	*219*
BSOD + 0.5 *M* NCS^-	2.3	3.6	19	—	*219*
BSOD + 2.0 *M* NCS^-	3.1	3.9	13	148	*219*
BSOD + 0.1 *M* N_3^-	3.9	4.8	37	157	*219*
BSOD + 2.0 *M* CN^-	7.7	5.2	53	188	*219*

[a] Abbreviations: BSOD, bovine SOD from erythrocytes; HSOD, human SOD.

[b] Calculated by assuming a single water molecule interacting with Cu^{2+} in the copper site with its protons equidistant from the ion.

[c] θ is the angle between the r_{Cu-H} direction and the unique axis of the hyperfine tensor for the interaction of a Cu^{2+} ion with its nucleus.

[d] Calculated by assuming two water molecules interacting with Cu^{2+}.

been proposed to be coordinated to copper on the basis of NMRD measurements. One of the water molecules is removed on azide binding (*179*).

Despite the indication that the water molecule close to copper in the native enzyme and in the mutants, not involving the metal ligands, has no effect on activity, it has some fine effects on some spectroscopic parameters. This appears true when the low-field water proton T_1^{-1} values are reported together with the values of $A_\parallel$ (between the copper ion and its unpaired electron) (see Tables IV and Table VI). In turn, large values of $A_\parallel$ are taken to indicate a deviation of the CuN_4 chromophore toward planarity (*216*). It has also been suggested that this is achieved through a displacement of copper. Of course, the effects described in Table VI are the results of fine structural changes sometimes not observable as optical transitions.

The water proton relaxivity of the native enzyme was found to in-

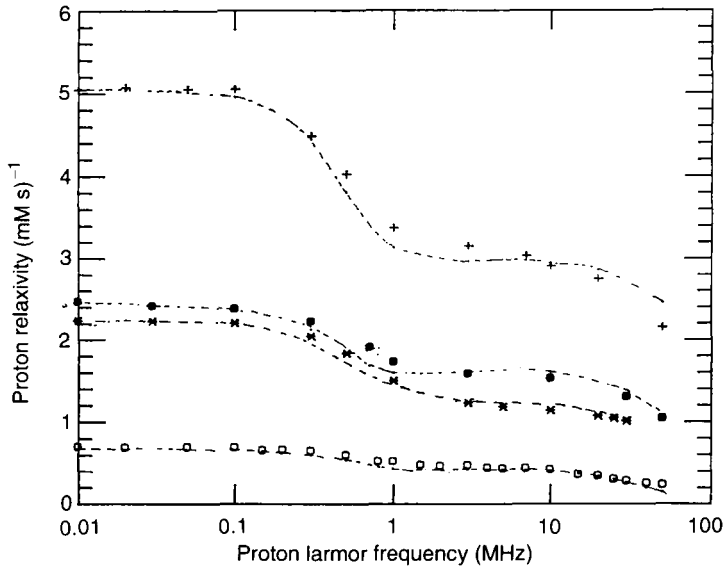

FIG. 27. ^1H T_1^{-1} values, at 298 K, as a function of the proton Larmor frequency for Cu_2Zn_2SOD (●), Thr-137Ser SOD (+), Thr-137AlaSOD (★), and Thr-137Ile SOD (○). T_1^{-1} values are subtracted from the bulk solvent and diamagnetic contribution and normalized to 1 m*M* copper concentration. Dashed lines are the best fits of the experimental data. Reprinted with permission from Banci, L.; Bertini, I.; Cabelli, D.; Hallewell, R. A.; Luchinat, C.; Viezzoli, M. S. *Inorg. Chem.* **1990,** *29,* 2398. Copyright 1990 American Chemical Society.

crease with pH, with a pK_a of 11.5 (*114*). A deprotonation of the water molecule interacting with copper was taken as explanation of this effect: indeed, the hydroxide proton was believed to experience a higher relaxation rate, with respect to water protons, as a consequence of a shorter Cu–H distance (*114*). Boden *et al.* suggested that the above behavior can be explained taking into account that, at high pH, an OH^- binds the copper ion, likely displacing a coordinated histidine (*206*). This hypothesis was partly confirmed by ^{17}O NMR studies of $H_2{}^{17}O$ solutions of bovine Cu_2Zn_2SOD: the large increase in T_{2p}^{-1} values, which is observed from neutral to alkaline pH, can be explained only by the addition of a hydroxide anion interacting with Cu^{2+} (*217*). The ^1H NMR spectra of the Cu_2Co_2SOD Ile-137 mutant show that all histidines are coordinated even at high pH (*120*).

The interaction of water with the copper ion in the presence of some anions that bind copper was monitored through NMRD (Fig. 28). In the case of N_3^- and CN^-, the water molecule is moved far away from

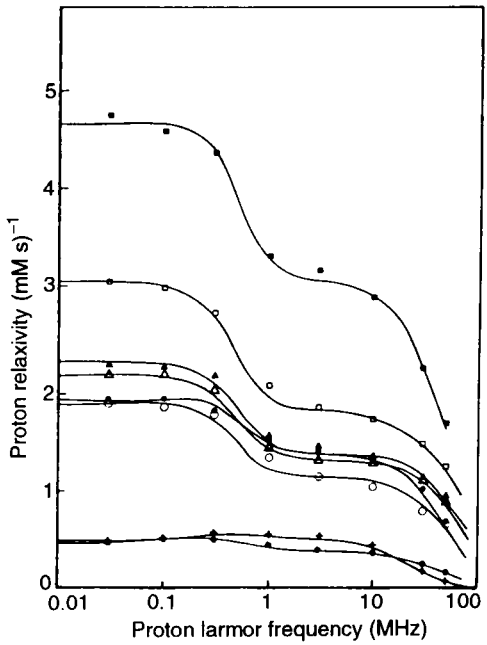

FIG. 28. ^1H T_1^{-1} values, at 298 K, as a function of the proton Larmor frequency for Cu_2Zn_2SOD solutions at pH 5.5 in the presence of 0.5 *M* $H_2PO_4^-$ (■), 0.5 *M* NCS^- (▲), 1.0 *M* NCS^- (△), 2.0 *M* NCS^- (○), 0.5 *M* NCO^- (●), a slight stoichiometric excess of CN^- (+), and 0.1 *M* N_3^- (★). The best-fit parameters are reported in Table VIII. Reprinted with permission from Bertini, I.; Banci, L.; Brown III, R. D.; Koenig, S. H.; Luchinat, C. *Inorg. Chem.* **1988,** *27,* 951. Copyright 1988 American Chemical Society.

the chromophore (*218*, *219*). In the case of NCO^-, there is a closer water molecule. In the presence of 0.5, 1.0, and 2.0 *M* NCS^-, which has a very low affinity constant, the water proton relaxivity decreases from the starting value toward those of NCO^-, with the largest effect between 0 and 0.5 *M* NCS^- (*219*). Phosphate, which was proposed to bind Arg-143 and not copper (Cu–P distance = 5 Å) (*106*), dramatically increases the relaxivity, probably because the acidic phosphate protons interact with the water molecule, increasing the number of exchangeable protons feeling the paramagnetic center (*219*).

Cu_2E_2SOD shows a more planar structure than the native enzyme. The profile for Cu_2E_2SOD has a higher relaxivity, attributable to a shortened Cu^{2+}–proton distance (*207*, *220*). The effect of N_3^- and NCS^- on Cu_2E_2SOD is similar to that observed on the native enzyme for the same anions (*220*). It is interesting to note that the T_1^{-1} values decrease down to about one-half by adding copper(II) until Cu_2Cu_2SOD

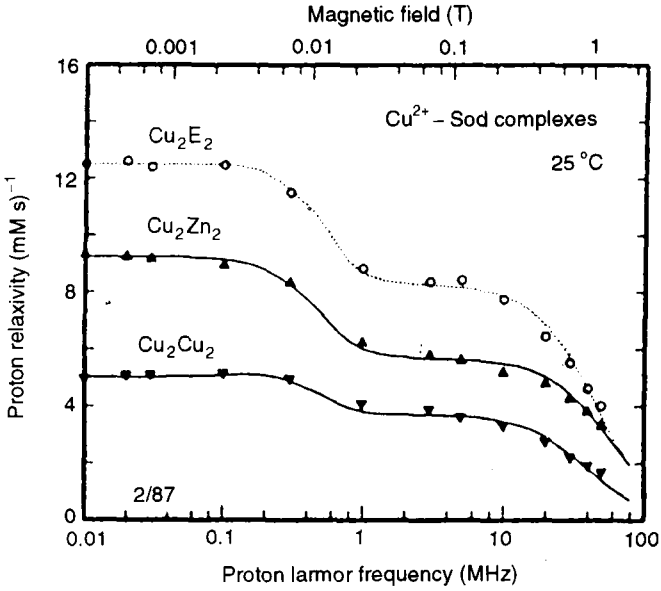

FIG. 29. ^1H T_1^{-1} values, at 298 K, as a function of the proton Larmor frequency for Cu_2Zn_2SOD, Cu_2E_2SOD, and Cu_2Cu_2SOD. T_1^{-1} values are subtracted from the bulk solvent and diamagnetic contribution and normalized to 1 mM copper concentration. Reprinted with permission from Banci, L.; Bertini, I.; Luchinat, C.; Monnanni, R.; Scozzafava, A. *Inorg. Chem.* **1988,** *27,* 107. Copyright 1988 American Chemical Society.

is formed (Fig. 29). The decrease in T_1^{-1} values is the result of magnetic coupling between the two metal ions whereas the electron relaxation values and copper–water distances are essentially not changed.

VII. Redox Properties

A. Reduction Potentials

Determination of the reduction potential of proteins is important when they perform redox reactions. Because SOD is a dismutase, its redox potential should be intermediate between that of the two semireactions [Eqs. (16) and (17)]:

$$O_2 + e^- \rightarrow O_2^- , \tag{16}$$

where $E^\circ = -0.33$ V vs. NHE (pH 7, $P_{O_2} = 0.101$ MPa), and

$$O_2 + 2H^+ + 2e^- \rightarrow H_2O_2, \tag{17}$$

where $E^\circ = 0.89$ V vs. NHE (pH 7).

Various values of reduction potentials for Cu_2Zn_2SOD are available, from 120 to 420 mV around neutrality. Values of 403 (*221*), 350 (*222*), 280 (*222*), and 400 mV (*223*) versus NHE at pH 7.0 and 120 mV at pH 7.5 (*224*) are reported in the literature. The variability of the values is largely due to the slow electron exchange rate, which is typical of nonelectron transfer proteins, especially if of large size. This reflects the experimental difficulties in such measurements. This aspect has been discussed in classical papers (*225*, *226*). If titrations are performed, the reactant should not interact with the protein by altering its potential. Potentiometric measurements, i.e., those methods based on the measurements of the reduction potential of systems containing various ratios of oxidized and reduced forms at equilibrium, need a redox partner that interacts weakly with the protein and reaches equilibrium fast. The latter condition is critical. Generally, the mediators that are used are capable of exchanging electrons with the protein and the partner. Direct methods, e.g., voltammetry, are very dependent on the protein–electrode interaction, which in turn depends on the applied potential and on the cleanliness of the electrode surface. Sometimes a promoter that is preferentially absorbed on the electrode is used. The hydrophilic nature of the promoter film prevents protein denaturation.

An extensive investigation of SODs and mutants has been performed by Luchinat *et al.* (*227*). The absolute values were later questioned by Hagen *et al.* (*224*). Still, the Luchinat investigation is the only one that allows comparison of the redox potentials among isoenzymes and mutants that have been treated with the same type of approach.

A typical cyclic voltammogram is shown in Fig. 30 for 10^{-3} *M* human SOD. 1,2-Bis(4-pyridyl)ethene has been used as a promoter. The working electrode was a gold electrode. The E° value has been taken as $E^\circ = (E_1 + E_2)/2$, where E_1 and E_2 are the anodic and cathodic peak potentials. The values are reported in Table VII. In 1973 Fee and Di Corleto (*223*) noted that the reduction of copper(II) is accompanied by the uptake of a proton from the medium. The reaction therefore is

$$\mathrm{ECu(II)} + e^- + \mathrm{H^+} \rightleftharpoons \mathrm{HECu(I)}. \tag{18}$$

The pH dependence of E° for human SOD is shown in Fig. 31. E° linearly decreases with increasing pH from 5 to 9. The slope is 55 mV/pH. The whole curve can be fitted with Eq. (19),

$$E^\circ = E^\circ_{\mathrm{lim}} + 2.3RT/F \log(1 + [\mathrm{H^+}]/K_a), \tag{19}$$

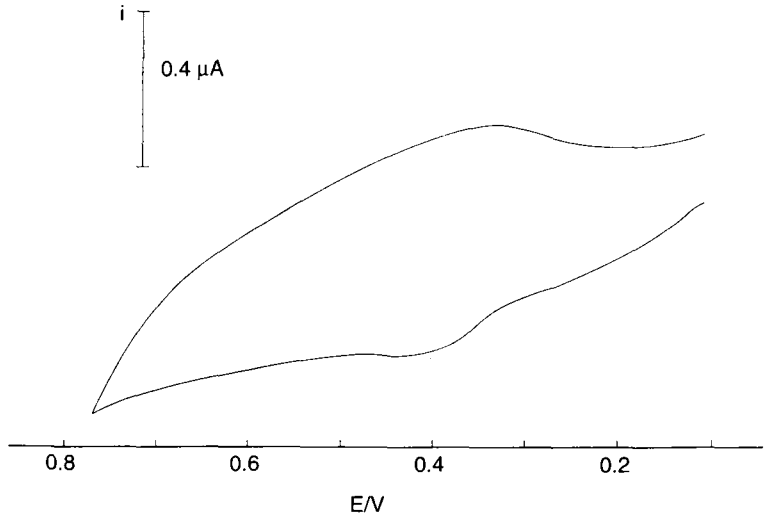

FIG. 30. Cyclic voltammogram of 10^{-3} *M* human SOD in the presence of 10^{-4} *M* 1,2-bis(4-pyridyl)ethene as a promoter and 0.1 *M* $NaClO_4$ as base electrolyte. Conditions: scan rate, 200 mV sec^{-1}, pH 7.42, 298 K. Reprinted with permission from Azab, H. A.; Banci, L.; Borsari, M.; Luchinat, C.; Sola, M.; Viezzoli, M. S. *Inorg. Chem.* **1992,** *31,* 4649. Copyright 1992 American Chemical Society.

where E°_{lim} is the high pH value (280 mV) and K_a is the constant of the single acid–base equilibrium. Its value is found to be 8.9 ± 0.6. The authors have discussed the meaning of this value in the light of the debate (*228*) on the deviation of pK_a obtained from electrochemical measurements with respect to the thermodynamic value. They concluded that this value could be consistent with that of 10.8 found from NMR measurements for the deprotonation of His-63, as shown in Fig. 32 (*227*). In this experiment the shift of the His-63 Hε1 proton is taken as a sensor of the protonation of His-63, according to the equilibria shown in Fig. 33.

The E° of the mutants so far investigated are lower than that of wild-type SOD (Table VII). Furthermore, substitution of Lys-136 has no effect on the pH dependence of E°, thus showing that its deprotonation is not involved in the pH dependence of E°. The Asp-124Asn mutation (see Section IV), which leads to a decrease in the affinity of the zinc site for metal ions and thus remains as Cu_2E_2SOD at every pH, has an E° value close to E_{lim} and is pH independent. The E° values for Cu_2E_2SOD, which undergoes the reaction given by Eq. (20),

$$2\,Cu_2E_2SOD \xrightarrow{pH} Cu_2Cu_2SOD + \text{apoenzyme}, \qquad (20)$$

TABLE VII

ELECTROCHEMICAL POTENTIALS FOR SOME ISOENZYMES AND AS-HUMAN SOD MUTANTS[a]

Derivative[b]	pH	$E°$ (V)	Ref.
BSOD	7.4	0.32	*227*
BSOD	7.0	0.40	*221*
BSOD	7.5	0.12	*334*
BSOD	7.0	0.28	*222*
BSOD	7.0	0.35	*222*
HSOD	7.4	0.36	*227*
AS-HSOD	7.4	0.37	*227*
Thr-137AlaHSOD	7.05	0.35(0.40)[c]	*227*
Thr-137SerHSOD	6.92	0.38(0.41)	*227*
Lys-136AlaHSOD	7.04	0.35(0.40)	*227*
Lys-136GlnHSOD	7.01	0.29(0.40)	*227*
Glu-133GlnHSOD	7.37	0.33(0.38)	*227*
Glu-132Gln, Glu-133GlnHSOD	7.45	0.30(0.37)	*227*
Cu_2E_2 AS-HSOD	5.11	0.28(0.51)	*227*
Cu_2E_2 AS-HSOD	7.50	0.25(0.37)	*227*
Cu_2E_2 AS-HSOD	9.15	0.23(0.30)	*227*
Cu_2E_2 AS-HSOD	10.55	0.22(0.29)	*227*
Cu_2E_2 Asp-124AsnHSOD	5.42	0.31(0.49)	*227*
Cu_2E_2 Asp-124AsnHSOD	7.21	0.30(0.39)	*227*
Cu_2E_2 Asp-124AsnHSOD	8.88	0.31(0.31)	*227*
Cu_2E_2 Asp-124AsnHSOD	10.45	0.29(0.29)	*227*

[a] AS-human SOD, Human SOD with the mutations Cys-6Ala, Cys-111Ser (see Section IV,A).

[b] BSOD, Bovine SOD from erythrocytes; HSOD, human SOD.

[c] The corresponding $E°$ values for human SOD-AS, obtained by interpolation from Fig. 31, are given in parentheses.

with a pK_a around 8, are similar to those of the Asp-124Asn mutant with the exception of a further decrease between pH 7 and 8, when migration starts to occur.

CN^- and N_3^- dramatically alter the $E°$ values (Table VIII). The measurement on the former derivative is performed at high pH. However, the low value is consistent with potentiometric measurements performed with methyl viologen (*222*) and with spectrophotometric titrations with $[Fe(CN)_6]^{4-}$ (*229*). With both anions, the oxidized form is so highly stabilized that SOD is no longer able to disproportionate O_2^- from the thermodynamic point of view.

As expected, Cu_2Co_2SOD behaves similarly to the native enzyme (Table VIII) (*227*).

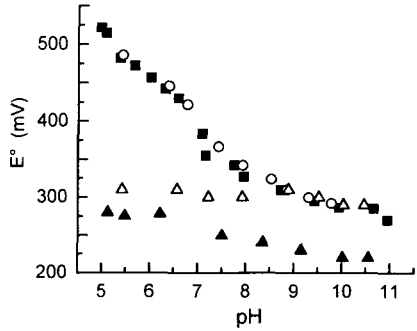

FIG. 31. The pH dependence of the redox potential for human SOD (■), human SOD-AS (○), Cu_2E_2 human SOD (△), and Cu_2E_2Asp-124Asn human SOD (▲). Reprinted with permission from Azab, H. A.; Banci, L.; Borsari, M.; Luchinat, C.; Sola, M.; Viezzoli, M. S. *Inorg. Chem.* **1992,** *31,* 4649. Copyright 1992 American Chemical Society.

B. ELECTRON TRANSFER BETWEEN $[Fe(CN)_6]^{4-}$ AND CU_2Zn_2SOD

The reduction potential of $[Fe(CN)_6]^{3-}$ is known (0.358 V) and that of SOD decreases with increasing pH. Therefore, the reaction given

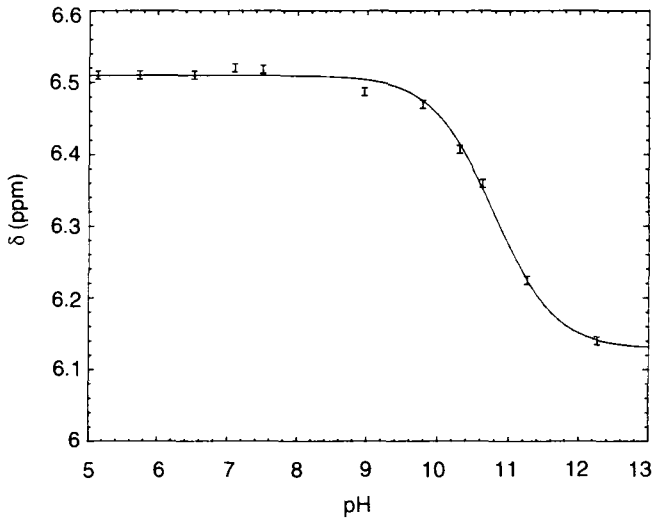

FIG. 32. Plot of the ^1H NMR chemical shift (600 MHz, 300 K) versus pH of the Hε1 of His-63 in reduced Cu_2Zn_2SOD. Reprinted with permission from Azab, H. A.; Banci, L.; Borsari, M.; Luchinat, C.; Sola, M.; Viezzoli, M. S. *Inorg. Chem.* **1992,** *31,* 4649. Copyright 1992 American Chemical Society.

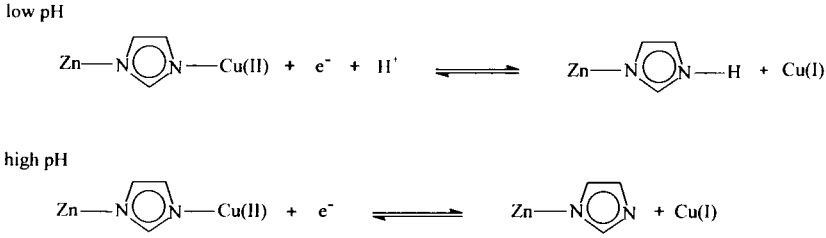

FIG. 33. Scheme of the deprotonation equilibria of the bridging His-63.

by Eq. (21)

$$ECu^{2+} + [Fe(CN)_6]^{4-} \underset{k_{-1obs}}{\overset{k_{1obs}}{\rightleftharpoons}} ECu^{+} + [Fe(CN)_6]^{3-} \qquad (21)$$

proceeds completely to the right in the pH range 5–7.2, starting with only the reactants (ECu^{2+} is the oxidized enzyme). The reaction is an overall second-order reaction and its rate is described by Eq. (22) (*229*):

$$d[ECu^{+}]/dt = k_{obs}[ECu^{2+}] = k_{1obs}[Fe(CN)_6]^{4-}[ECu^{2+}], \qquad (22)$$

where k_{obs} is the pseudo-first-order rate constant and k_{1obs} is the second-order rate constant for the reduction of ECu^{2+} by $[Fe(CN)_6]^{4-}$.

The reaction can be easily followed by monitoring, at 420 nm, the appearance of a band typical of $[Fe(CN)_6]^{3-}$. In Fig. 34 the linear relationship between k_{obs} and the concentration of the $[Fe(CN)_6]^{4-}$ is shown. The values of k_{-1obs} have also been obtained by measuring the rate of reaching the chemical equilibrium of the above reaction under

TABLE VIII

ELECTROCHEMICAL POTENTIALS FOR Cu_2Co_2 BOVINE SOD AND SOME ADDUCTS OF BOVINE SOD WITH ANIONS[a]

Derivative[b]	pH	$E°$ (V)
Cu_2Co_2BSOD	7.20	0.34(0.32)[c]
BSOD + N_3^-	7.32	−0.22(0.31)
BSOD + CN^-	10.18	−0.59(0.25)

[a] Reprinted with permission from Azab, H. A.; Banci, L.; Borsari, M.; Luchinat, C.; Sola, M.; Viezzoli, M. S. *Inorg. Chem.* **1992,** *31,* 4649. Copyright 1992 American Chemical Society.

[b] BSOD, Bovine SOD from erythrocytes.

[c] The corresponding $E°$ values for bovine SOD, obtained by interpolation, are given in parentheses.

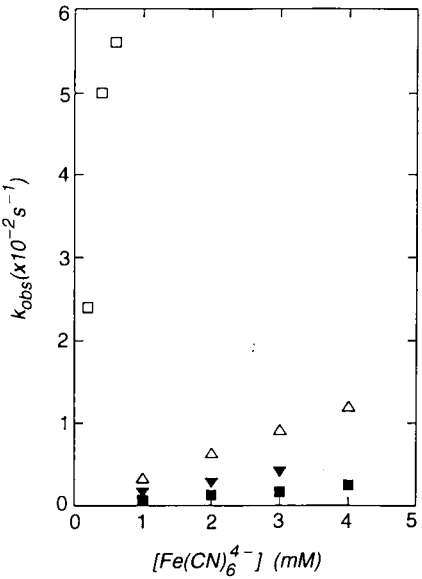

FIG. 34. Relationship between k_{obs} and concentration of $[Fe(CN)_6]^{4-}$ for human SOD (△) and some mutants: Glu-133Gln (□), Lys-136Gln (■), and Thr-137Ser (▽). Reprinted with permission from Bertini, I.; Hiromi, K.; Hirose, J.; Sola, M.; Viezzoli, M. S. *Inorg. Chem.* **1993,** *32,* 1106. Copyright 1993 American Chemical Society.

certain conditions. It has also been verified that the apparent equilibrium constant K is given by

$$K = k_{1obs}/k_{-1obs}. \tag{23}$$

The values of the three constants are reported in Fig. 35. It appears that k_{1obs} increases with increasing pH above pH 6, providing the pH dependence of K (*223*).

It is possible that, as for the substrate, the rate of approach determines k_{1obs} because the following step, electron transfer, may be quite fast. The approach of the anion may be regulated by the charge in the active cavity. Indeed, the kinetic values (Table IX) indicate a dramatic decrease when the positive Arg-143 is substituted by an Ile and a dramatic increase is observed when the negative Glu-133 residue is neutralized. The change in activity (Table IX) is qualitatively parallel, but not quantitatively, probably on account of the different charges of the two anions (i.e., $[Fe(CN)_6]^{4-}$ and O_2^-), which magnify the effect of the electrostatic charges in the active cavity in the case of $[Fe(CN)_6]^{4-}$ (*230*).

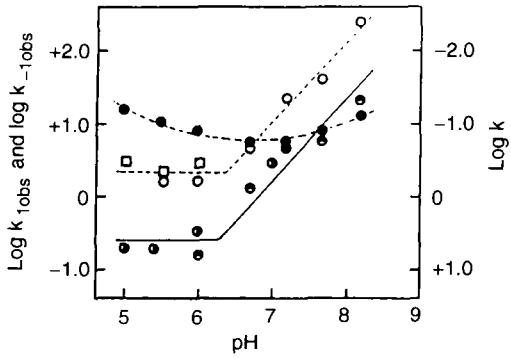

FIG. 35. The pH dependence of k_{1obs}, k_{-1obs}, and K: k_{1obs} (●) and k_{-1obs} (○) were directly obtained by kinetics; k_{-1obs} (□) was indirectly obtained by k_{1obs}/K; the apparent equilibrium constant K (◑) was obtained by the equilibrium method of Fee *et al.* (*223*); the apparent equilibrium constant K (◓) was obtained by the kinetic method. Reprinted with permission from Ozaki, S.; Hirose, J.; Kidani, Y. *Inorg. Chem.* **1988,** *27,* 3746. Copyright 1988 American Chemical Society.

A temperature dependence of the reduction potential allowed the calculation of the thermodynamic parameters (*221*): $\Delta G^{\circ\prime} = -9.31$ kcal/mol, $\Delta H^{\circ\prime} = -21.4$ kcal/mol, and $\Delta S^{\circ\prime} = -25.1$ eu (pH 7.0, I = 0.1 M) (*221*). The large negative $\Delta H^{\circ\prime}$ is attributed to strong Cu(I)–Im bonds and to the protonation of the bridging Im. It is proposed that

TABLE IX

REDUCTION RATE CONSTANTS AND ACTIVITIES FOR O_2^- DISMUTATION OF HUMAN SOD AND SOME OF ITS MUTANTS WITH $[Fe(CN)_6]^{4-}$[a]

Derivative	k_{1obs} (M^{-1} sec^{-1})	Activity (%)
Human SOD	2.88	100
Arg-143IleHSOD	0.018	11[b]
Thr-137SerHSOD	1.44	70[c]
Glu-133GlnHSOD	108	222[d]
Lys-136GlnHSOD	0.63	65[e]
Asp-124AsnHSOD	No reduction	81[f]

[a] Reprinted with permission from Bertini, I.; Hirami, K.; Hirose, J.; Sola, M.: Viezzoli, M. S. *Inorg. Chem.* **1993,** *32,* 1106. Copyright 1993 American Chemical Society.

[b] From Ref. *104.*

[c] From Ref. *115.*

[d] From Ref. *64.*

[e] From Ref. *119.*

[f] From Ref. *96.*

zinc(II) binding at the zinc site stabilizes a protein configuration at the copper site that is particularly favorable for Cu(I) binding. The negative entropy implies an increase in order on breaking the His-63 bridge. This may be not surprising if it is considered that the latter has not much freedom, that the proton comes from the solvent, and that water is indeed not bound to copper(II). The changes in the thermodynamic parameters account for the high reorganization energy associated with electron transfer; such reorganization energy makes SOD a poor electron transfer carrier.

VIII. The Spectroscopic Properties of Metal Ions

Spectroscopy is used to study metalloproteins whose X-ray structure is available in order to obtain further information on fine effects that generally escape detection with X-ray analysis or to provide additional evidence about electronic structure, dynamics, and reactivity. In the absence of X-ray analysis, spectroscopy becomes a challenge and represents a means to figure out structural information. In the case of SOD spectroscopic investigations have been very numerous because (1) metal substitution provides a unique wealth of derivatives and (2) the structural data were few until 1982, when the first structure became available and the scientific community was eagerly expecting the structure of other derivatives. It was not until after 1992, however, that several groups started producing X-ray structures. Therefore, most of the spectroscopic data preceded pertinent X-ray analysis, and now it may be useful to revisit the early work. A thorough review on the spectroscopic properties of SOD up to 1990 is available in the literature (*231*).

It may be appropriate to comment about the rigidity of the donor groups in SOD. In M_2N_2SOD, the geometry of the ligands of M is fixed by the protein frame and there is only a minor effect of the metal ion, which, however, may have preference for a certain stereochemistry. Therefore M^{2+} is generally bound to four His and sometimes to a water molecule. N^{2+} is bound to three His and an Asp. The possibility that the Asp behaves as bidentate with some metal ions has been mentioned (*232*) but never proved. Anions bind M^{2+} and, depending on the donor strength, may displace copper from the original position and loosen a metal–His bond. When M = M^+, His-63 is not bridging (*233*) except in one crystalline form (*82*) (see Section II,I).

A. Copper(II) in Native Protein

The copper(II) ion as a d^9 ion has a d–d spectrum, often with a single broad band that contains several transitions. The electronic

spectrum is reported in Fig. 36 (*2, 234–239*). The maximum at 14,700 cm^{-1} is responsible for the green color of the protein. There are other transitions in the UV region. The CD spectrum of the human enzyme shows a better resolution with bands at 13,300, 16,700, 22,400, 29,600, and 33,000 cm^{-1} (Fig. 37) (*204*). The first two bands belong to *d–d* transitions. A further weak positive CD band has been proposed by Valentine *et al.* to be present at 18,800 cm^{-1}, which would again be a *d–d* transition (*239*). The weak band at 22,400 cm^{-1} has been assigned to the lowest ligand metal charge transfer (LMCT) band. This band disappears whenever the bridge is removed and then is reasonably assigned to the bridging His to copper charge transfer (CT) (*239*). The last two bands are LMCT (*239*). This assignment is supported by model complexes having tetragonal Cu–imidazole and Cu–imidazolate compounds (*240, 241*). The spectra are essentially pH independent in the range pH 4–10. At pH below 4 the bridge is broken on the side facing zinc (*181*). What happens at high pH values will be discussed together with the role of anions (see later).

The EPR spectrum is rhombic at every temperature from 77 K to room temperature (*218, 242–244*) (Fig. 38). The $A_{\parallel}$ of the bovine enzyme is 141×10^{-4} cm^{-1}. The A_x and A_y values are obtained by simulating the spectra and are 35×10^{-4} and 52×10^{-4} cm^{-1}, respectively (*245*). The EPR spectra are shown in Fig. 38. In Table IV the relevant

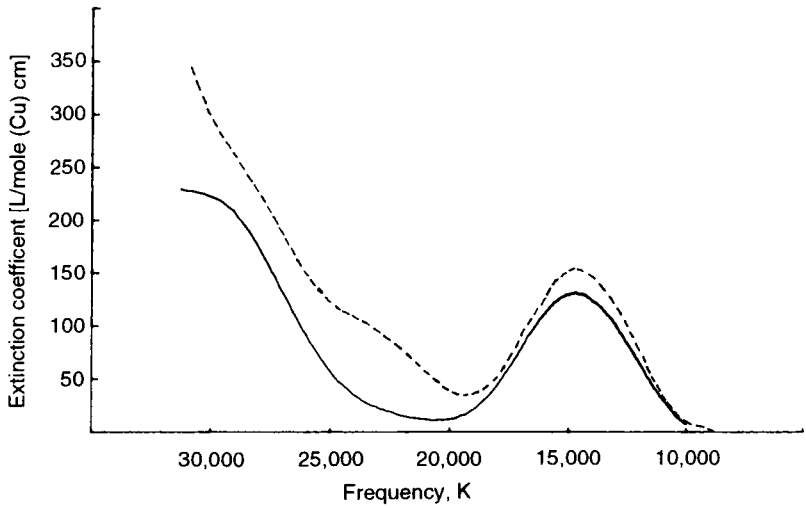

FIG. 36. Visible and near-IR absorption spectrum of $Cu_2^{II}Zn_2^{II}$ bovine SOD (---) and $Cu_2^{II}E_2$ bovine SOD (—) at pH 6.1. Reprinted with permission from Pantoliano, M. W.; Valentine, J. S.; Nafie, L. A. *J. Am. Chem. Soc.* **1982,** *104,* 6310. Copyright 1982 American Chemical Society.

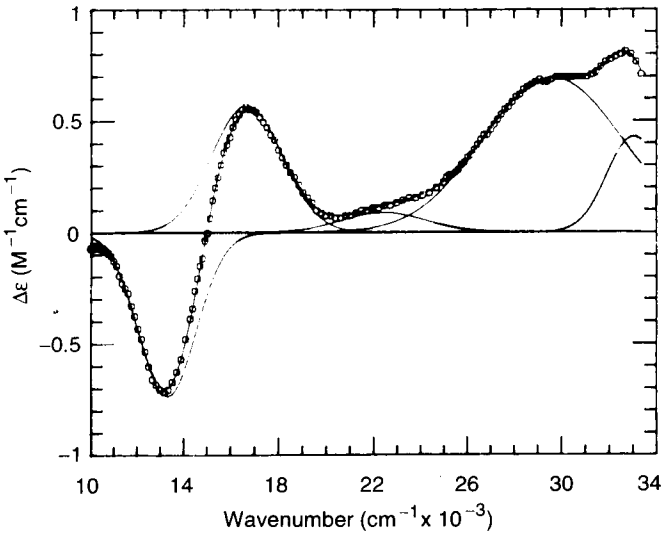

FIG. 37. Visible and near-IR circular dichroism spectrum of $Cu_2^{II}Zn_2^{II}$ human SOD with the individual Gaussian lines in the fitting of the experimental data. Reprinted with permission from Ref. *204*.

EPR data are reported for a series of isoenzymes, mutants, and anion derivatives. Single-crystal studies have led to two possible orientations of the g tensor (*245*). The d–d transitions, g values, and g orientations have been reproduced through an angular overlap model (*204*). The best fitting of the electronic transitions was achieved with nitrogen ligand parameters $e_\sigma^N = 7600\ cm^{-1}$, $e_\pi^N = 1000\ cm^{-1}$, and the water parameter $e_\sigma^O = 0\ cm^{-1}$. With the same parameters the computed g values are $g_x = 2.03$, $g_y = 2.08$, and $g_z = 2.28$, which fit quite well with the data obtained from single-crystal studies ($g_x = 2.03$, g_y

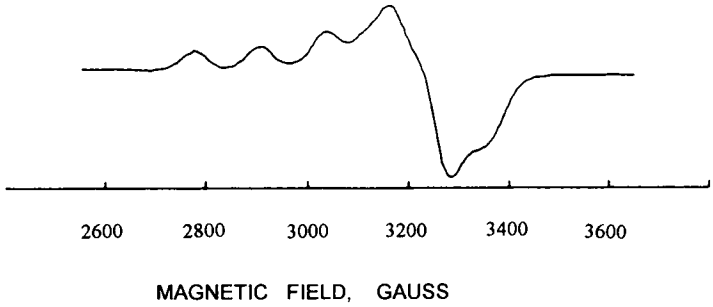

FIG. 38. EPR spectrum of $Cu_2^{II}Zn_2^{II}$ bovine SOD at pH 5.6 (303 K). Reprinted with permission from Pantoliano, M. W.; Valentine, J. S.; Mammone, R. J.; Scholler, D. M. *J. Am. Chem. Soc.* **1982,** *104,* 1717. Copyright 1982 American Chemical Society.

= 2.09, g_z = 2.26) (*245*). It appears that the water molecule does not contribute to the ligand field splitting. This is in agreement with the model that requires a free approach site for O_2^- (*246*).

Through electron spin echo spectroscopy, a splitting of the low-field lines was observed, arising from the interaction of copper(II) with the remote ^{14}N atoms of the coordinated imidazoles. This splitting, which disappears at low pH, was attributed to the presence of a divalent metal linked by an imidazolate bridge (*247*).

Electron and nuclear double resonance (ENDOR) studies at 5 K have led to the assignment of all protons of histidines bound to copper (*248*, *249*) and to the factorization of the coupling constants into a dipolar and an isotropic part. This has been possible through irradiation of a frozen sample at different g values. Figure 39 shows ENDOR spectra of bovine Cu_2Zn_2SOD, obtained at five working points of the

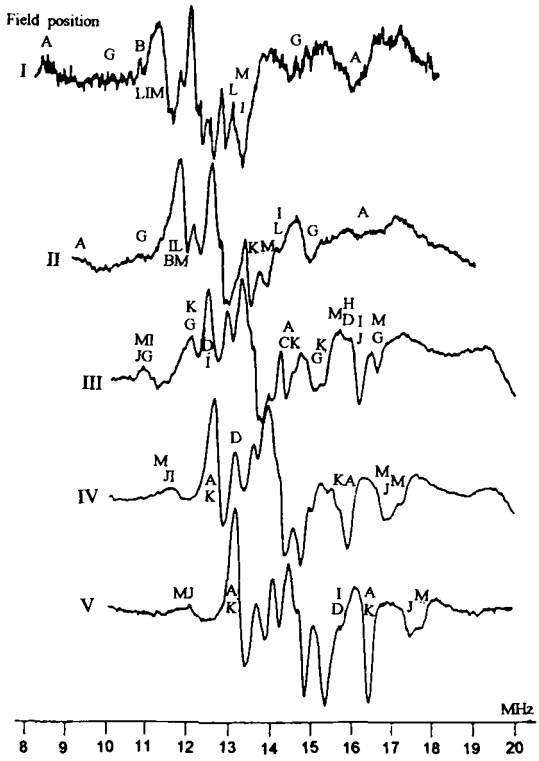

FIG. 39. ENDOR spectra of bovine SOD obtained at the five working points across the EPR spectrum. The letters indicate assigned resonances (see Table X). Reprinted with permission from Reinhard, H.; Kappl, R.; Hutterman, J.; Viezzoli, M. S. *J. Phys. Chem.* **1994,** *98,* 8806. Copyright 1994 American Chemical Society.

EPR spectrum. In Table X the assignment of some resonances is reported together with the isotropic hyperfine coupling constants. In all cases but three, the values are the same as those calculated from NMR contact shifts of the Cu_2Co_2 derivative at room temperature (see Section VIII,M). It is possible that these discrepancies may derive from slight geometrical distortions of the copper–histidine system at low temperature. The ^{14}N and ^{15}N hyperfine parameters of the coordinated nitrogens are also available, with the quadrupolar splitting of the former (*249*). Coupling with the distal nitrogens was observed through electron spin echo envelope modulation (ESEEM) of the ^{15}N enriched protein (*250*), though not specifically assigned.

^1H NMR experiments cannot be performed in this protein if interest is focused on the copper ligands, because the large electronic relaxation times broaden the lines beyond detection in a sphere about 6 Å from copper. Actually, the disappearance of histidine signals from reduced to oxidized state allowed the first proposal to be made about the coordinated His (*251*).

TABLE X

ISOTROPIC COUPLING CONSTANTS OF THE HISTIDINE PROTON SIGNALS IN THE ENDOR SPECTRA OF BOVINE SOD[a]

Protons[b]	Line assignment	a_{iso} (MHz)[c]
Hβ1 (His-44)	A	0.6118(0.350)
Hβ2 (His-44)	B	0.6118
Hδ2 (His-44)	C	0.8132
Hε1 (His-44)	D	0.4788
Hε2 (His-44)	E	1.0450
Hδ1 (His-46)	F	1.6492
Hδ2 (His-46)	G	0.6954
Hε1 (His-46)	H	1.2844
Hδ2 (His-61)	I	0.8740
Hε1 (His-61)	J	0.8740(1.440)
Hδ1 (His-118)	K	1.8810
Hδ2 (His-118)	L	0.6498
Hε1 (His-118)	M	1.2198(1.900)

[a] Reprinted with permission from Reinhard, H.; Kappl, R.; Huttermann, J.; Viezzoli, M. S. *J. Phys. Chem.* **1994,** *98,* 8806. Copyright 1994 American Chemical Society.

[b] His numbering follows the bovine SOD sequence.

[c] Isotropic coupling constants are in agreement with those obtained from the NMR contact shifts within experimental error except for three coupling constants, for which the corresponding values from the NMR contact shifts are given in parentheses for comparison.

The ^1H nuclear magnetic relaxation dispersion is discussed in Section VI.

B. Copper(II) in the Cu_2E_2 Enzyme

The electronic spectra show a small shift toward the high frequencies with respect to the native state (Fig. 36) (*239*, *243*). A similar shift is observed in the CD spectrum at low pH for the d–d transitions (*239*). Furthermore the weak band at 22,400 cm^{-1}, assigned to the lowest LMCT band (*239*), disappears because of the absence of the imidazolate bridge. In the EPR spectrum the $A_\parallel$ values is somewhat larger ($A_\parallel = 148 \times 10^{-4}$ cm^{-1}) than that in the native protein (Table IV) (*184*, *243*). It seems that the removal of the constraint due to the bridge relaxes the coordination sphere, providing a more tetragonal environment. This is more evident at low pH than at neutral pH. As a result of this minor rearrangement, according to NMRD measurements, the water close to copper is moved further away (see Section VI). Electron spin echo spectra of Cu_2E_2SOD show lines of 0.7, 1.5, and 4 MHz, which resemble the spectra of a model compound containing an imidazole ligand [Cu(II)–diethylenetriamine–imidazole] (*247*).

At pH > 7, Cu_2E_2SOD transforms into Cu_2Cu_2SOD and apoSOD (see Section V) (*173*).

C. Copper(II) with Other Metal Ions in the Zinc Site

Several copper derivatives have been prepared with Cu, Co, Ni, Cd, and Hg in the zinc site. The Cu_2Cu_2SOD shows magnetic exchange coupling effects between the two metal ions through the histidinato bridge. In a classical experiment copper(II) was added to apoprotein at pH 5.5 and the titration was followed by EPR. At the beginning the EPR of copper in the copper site developed and eventually the spectrum of the Cu–Cu dimer appeared, with simultaneous disappearance of the EPR spectrum of the monomer (Fig. 40). If the hamiltonian is written as

$$H = J\hat{S}_1 \cdot \hat{S}_2, \tag{22}$$

and the EPR parameters are explained with $J = 26$ cm^{-1} and the $S' = 0$ ground state (*252*). Such a J value has been obtained through the temperature dependence of the intensity of the EPR signal, which depends on the population of the excited $S' = 1$ level (*252*). The spectrum, which was first reported in 1973 (*253*), was subsequently shown to be due to the Cu–Cu moiety (*173*, *252*). The hyperfine values are about one-half of the monomeric species, as expected (*252*, *254*). The

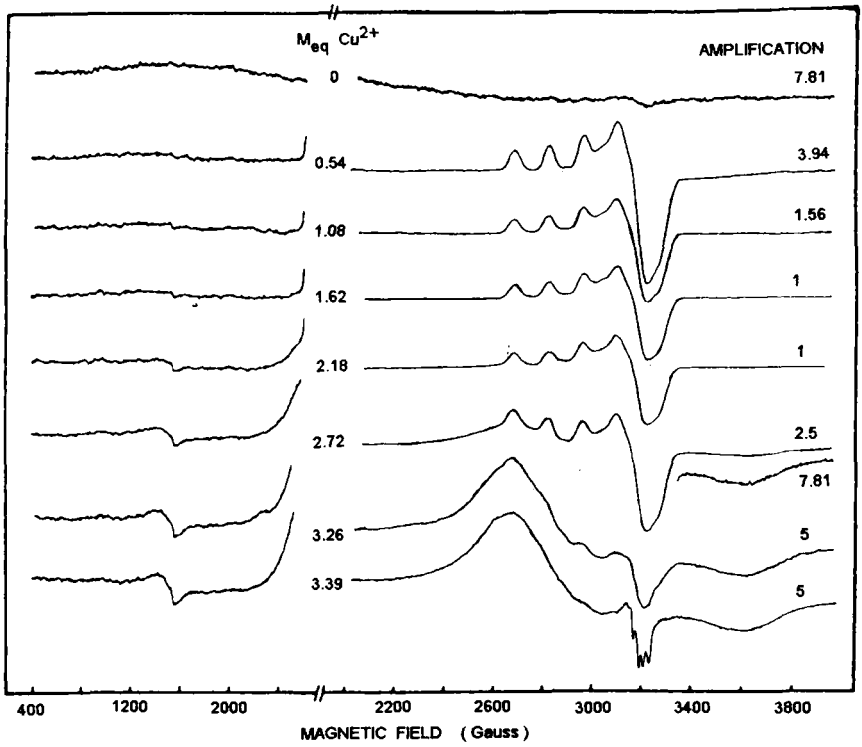

FIG. 40. EPR titration of apoSOD with Cu^{2+}. The spectra were recorded near 1090 K. Reprinted from *Biochim. Biophys. Acta,* Vol. 400; Fee, J. A.; Briggs, R. G.; p. 439, Copyright 1975, with kind permission of Elsevier Science–NL, Sara Burgerhartstraat 25, 1055 KV Amsterdam, The Netherlands.

interaction between the ground state of one copper and the excited levels of the other has been proposed to be significant with respect to the energy separation between $S' = 0$ and $S' = 1$ (*255*). In the lyophylized state the imidazole bridge is broken and the EPR of the two copper sites appears (*256*). This shows that some tension is experienced by the copper site. The visible absorption spectrum shows a very broad band with a maximum at 12,500 cm^{-1} (*173, 243*).

Copper(II) also experiences magnetic exchange coupling with cobalt(II) and nickel(II) when they occupy the zinc site. In the former case J has been estimated to be 17 cm^{-1} (*257*). The electronic spectra of copper(II) are barely affected by the presence of cobalt(II) or nickel(II) instead of zinc(II) (*243, 258*). The same holds when cadmium and mercury are in the zinc site (*243*).

D. Nickel(II) in the Copper Site

The electronic spectrum of Ni^{2+} in Ni_2N_2SOD is shown in Fig. 41 (*185*). It shows absorptions at 14,815 and 25,600 cm^{-1} with molar extinction coefficients of 14 and 85 M^{-1} cm^{-1} per subunit, respectively. The low intensity indicates the d–d nature of these transitions. The former band is attributed to the highest $^3F \rightarrow {}^3F$ transition and its value has been sensibly attributed to five-coordination. It is proposed, as in the case of cobalt, that the coordination donors are four His nitrogens (*185*). Although not clearly stated, it is probable that a water oxygen is the fifth ligand. The ^1H NMR spectra are well resolved, as shown in Fig. 42. The signals A, B, and G, which are due to exchangeable protons, are assigned to the three NH protons of the coordinated His and signal H is assigned to the metalike proton of His-46 (*185*).

E. Cobalt(II) in the Copper Site

If cobalt(II) is added to E_2N_2SOD, in the presence of acetate buffer, a five-coordinated complex is obtained (*259*) with four His nitrogens and a water oxygen as donors. Consistently, the electronic spectrum has a low absorbance (Fig. 43) (*259*) and the ^1H NMR spectrum gives sharp and well-spread signals (*260*) as a result of fast electronic relaxation times and large magnetic anisotropy (Fig. 44). The EPR spectra (Fig. 45) can be recorded at liquid helium as long as N is a diamag-

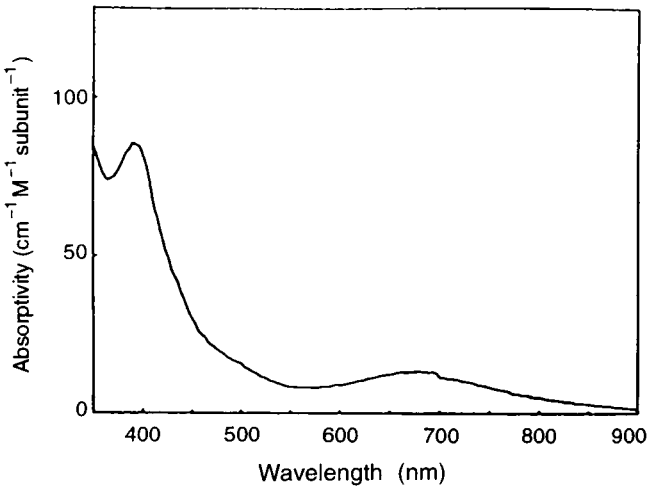

FIG. 41. Electronic spectrum of Ni_2Zn_2SOD in 50 mM phosphate buffer, pH 7.5. Reprinted from Ming, L. J.; Valentine, J. S. *J. Am. Chem. Soc.* **1990,** *112,* 6374. Copyright 1990 American Chemical Society.

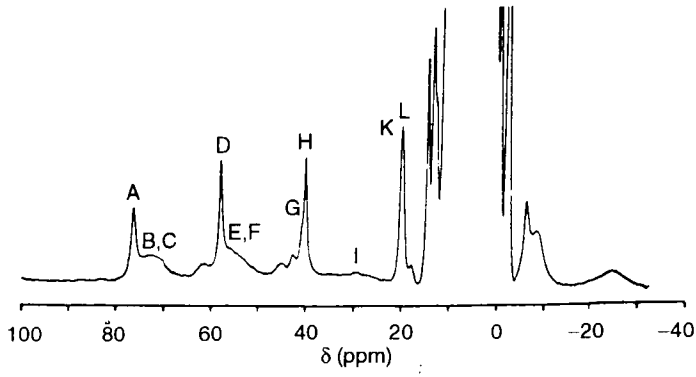

FIG. 42. The 200-MHz ^{1}H NMR spectrum of Ni_2Zn_2SOD in 50 m*M* phosphate buffer, pH 7.5. Reprinted from Ming, L. J.; Valentine, J. S. *J. Am. Chem. Soc.* **1990,** *112,* 6374. Copyright 1990 American Chemical Society.

netic metal (i.e., Zn^{2+}, Cd^{2+}) (*259*). The interaction of N_3^- with Co_2Zn_2-SOD was studied in the presence and in the absence of phosphate: EPR, NMR, and optical titrations demonstrated that different adducts are obtained depending on the presence of phosphate, at variance with what happens with CN^-, indicating a different mechanism of binding for different anions (*261*). If N is paramagnetic, magnetic exchange coupling occurs between cobalt(II) and N. On magnetic coupling, the total spin is either zero or an even number, and no EPR spectra are detected under the usual conditions. In Co_2Co_2SOD, the magnetic coupling and the fast electronic relaxation rates of five-coordinated cobalt induce fast electron relaxation in tetrahedral cobalt (i.e., that at the zinc site), and the NMR signals of the latter (Fig. 46a) are much sharper than in M_2Co_2SOD with M diamagnetic (*187, 191, 260*). The chemical shifts of the signal of tetrahedral cobalt are

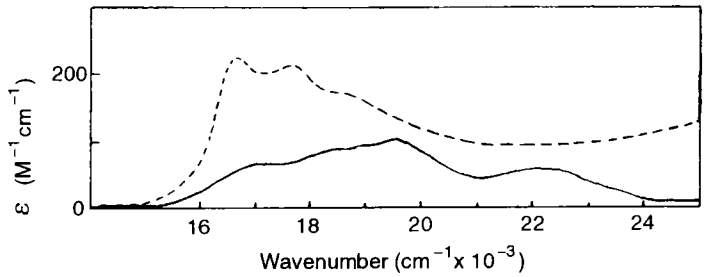

FIG. 43. Electronic spectra in the visible region of Co_2Zn_2SOD in the absence of phosphate (—) and Co_2Zn_2SOD in the presence of phosphate (---). Adapted with permission from Banci, L.; Bertini, I.; Luchinat, C.; Monnani, R.; Scozzafava, A. *Inorg. Chem.* **1987,** *26,* 153. Copyright 1987 American Chemical Society. Also adapted from Ref. *260.*

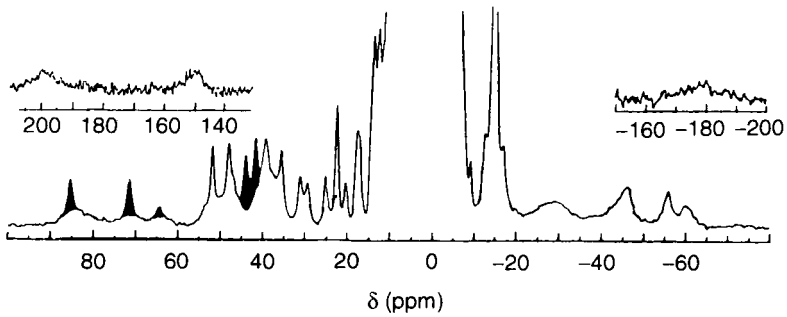

FIG. 44. The 90-MHz ^1H NMR spectrum of Co_2Co_2SOD. The filled signals belong to exchangeable protons. Reprinted with permission from Ref. *260*.

different depending on whether there is or is not a five-coordinated cobalt(II) at the copper site. In fact, the latter cobalt causes some pseudocontact shifts on the signals of the tetrahedral cobalt domain.

When cobalt(II) is added to E_2N_2SOD in phosphate buffer, an absorption spectrum typical of tetrahedral cobalt is displayed (Fig. 43). The EPR spectrum of cobalt(II) can be observed at liquid helium when N is diamagnetic (*259*) (Fig. 45a). It is suggested (*187*) that phosphate bridges the Arg-143 and the cobalt ion, thus moving the latter toward the outside of the cavity and breaking the imidazolate bridge (Fig. 47). The ^1H NMR spectra are typical of tetrahedral species, with little spreading of the signals and large line width (Fig. 46b) (*187*). At pH values greater than 10 the bridge is reestablished (*191*).

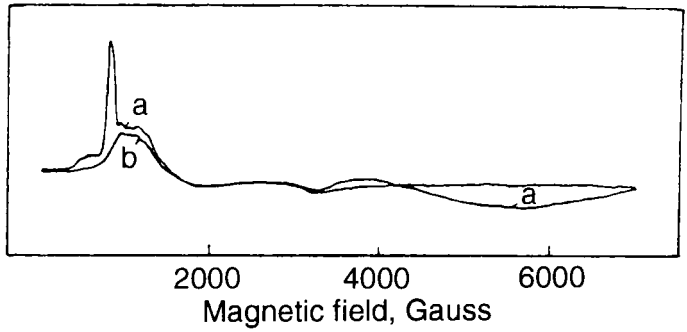

FIG. 45. EPR spectra of (a) Co_2Zn_2SOD in the presence of phosphate and (b) Co_2Zn_2-SOD in the absence of phosphate. Spectra are recorded at 10 K, pH 7.4. Reprinted from *FEBS Letters*, vol. 166. Calabrese, L.; Cocco, D.; Desideri, A.; p. 142. Copyright 1979 with kind permission of Elsevier Science–NL, Sara Burgerhartstraat 25, 1055 KV Amsterdam, The Netherlands.

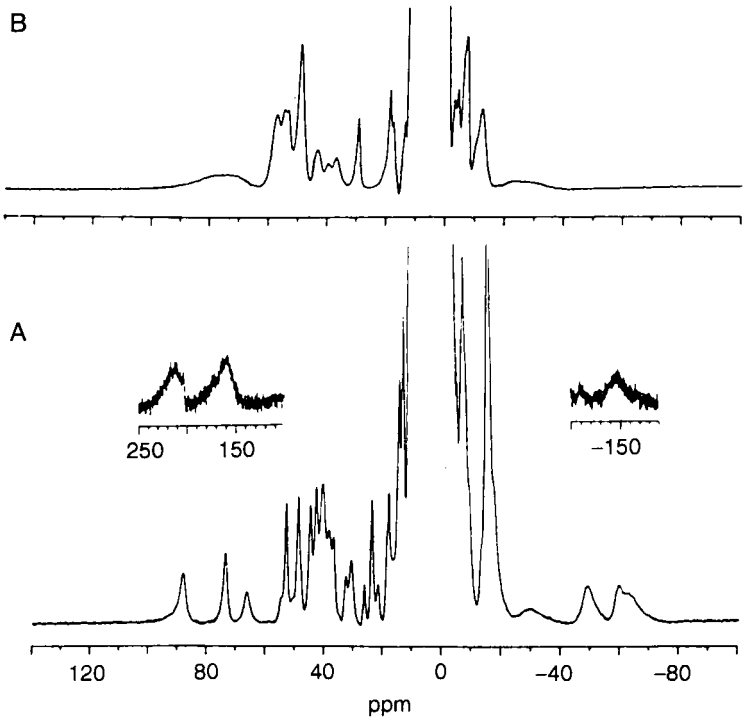

FIG. 46. The 200-MHz ^1H NMR spectra of Co_2Co_2SOD in the absence of phosphate (a) and in the presence of phosphate (b). Reprinted with permission from Ming, L. J.; Valentine, J. S. *J. Am. Chem. Soc.* **1990,** *112,* 4256. Copyright 1990 American Chemical Society.

F. ANION DERIVATIVES

Do anions bind copper(II) or other metal ions at the copper site? This was an important question before the appearance of pertinent X-ray data, because O_2^- is an anion. In the presence of N_3^-, SOD displays a CT at 28,200 cm^{-1} (*164*, *262*), which shows the N_3^- binds copper(II). By looking at the CD spectra (Fig. 48) it appears that CN^- and NCO^- also bind copper(II) because the spectra indeed change, even if no CT

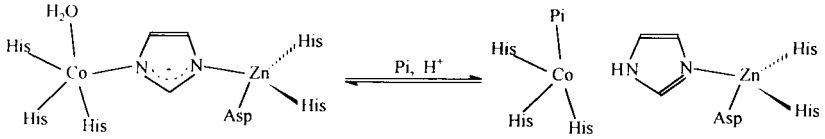

FIG. 47. Schematic representation of the breaking of the imidazolate bridge in Co_2Zn_2SOD in the presence of phosphate.

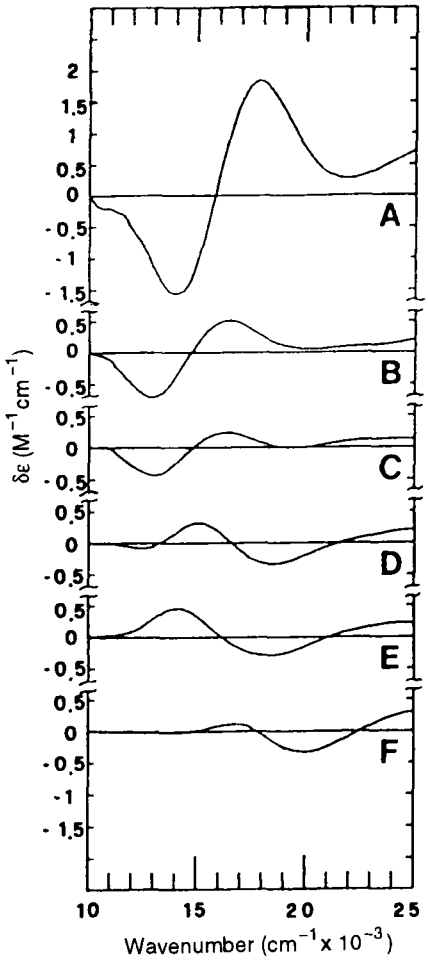

FIG. 48. Circular dichroism spectra of Cu_2Zn_2SOD (B) and of its derivative with thiocyanate (C), cyanate (D), azide (E), and cyanide (F). The CD spectrum of the Ile-137 mutant (A) is also shown. Reprinted with permission from Banci, L.: Bencini, A.; Bertini, I.; Luchinat, C.; Piccioli, M. *Inorg. Chem.* **1990,** *29,* 4867. Copyright 1990 American Chemical Society.

band are observed. The most well-studied anions are N_3^- and CN^-. The latter binds quantitatively and tends to reduce copper(II). The affinity of N_3^- for SOD is small and depends on the conditions. Spectrophotometric titrations provide an affinity constant of 138 ± 4 M^{-1} at pH 5.6 (*262*).

CN^- (*263*), N_3^- (*264*), and F^- (*264*) are competitive inhibitors. NCO^- and NCS^- have not been reported to be inhibitors (*229, 264, 265*). The EPR spectra show that CN^- and N_3^- provide an essentially tetragonal

structure, which contrasts with the rhombic structure of the native enzyme (*245*, *266*, *267*) (Table IV). It has been suggested that the three His plus the anion give rise to a tetragonal structure, which may have the fourth His as a fifth ligand more or less loosely bound. The binding of CN^- to copper was also proved by infrared (IR) and Raman spectroscopy: a band at 2137 cm^{-1} was attributed to the stretching frequency of the bound cyanide (*268*). The ^1H NMR spectrum of the copper–cobalt derivatives with different anions indicates that the protons of His-48 experience hyperfine coupling with the unpaired electron to a different extent. In the case of the CN^- derivative, negligible hyperfine coupling with the electrons of the copper ion is observed (Table IV) (*88*, *89*). The nuclear Overhauser effect (NOE) data with and without N_3^- show that the position of His-48 does not change appreciably within the protein framework (*89*). How then can the detachment of His-48 be reconciled with the NOE data? Movement of the copper ion satisfies the new requirements (*89*). This has been confirmed by X-ray studies (*90*, *269*). The water molecule close to copper is removed by CN^- and N_3^- (see Section VI). The X-ray data also show that the anions bind copper and interact with Arg-143. The affinity of anions for the enzyme decreases if Arg-143 is substituted through site-directed mutagenesis (*270*) or if the enzyme is treated with glyoxal, which reacts with the Arg residue (*163*). ^{14}N and ^{15}N NMR studies on the binding of N_3^- have provided copper–nitrogen hyperfine values that are consistent with an equatorial binding of the anion (*271*).

Ligands such as NCO^-, NCS^-, and F^- have also been extensively investigated and the interpretation of the data is rather intriguing. It has been proposed that their ability to move copper(II), as previously discussed, decreases in the order $NCO^- > NCS^- > F^-$. The electronic spectra of F^- and NCS^- are very similar to those of the native enzyme (Fig. 48). The same trend is observed in the chemical shifts of His-48 protons, in the case of the copper–cobalt derivative (Table IV).

The addition of NCO^- to a water solution of Cu_2Zn_2SOD causes a change in the electronic spectrum (*272*), the maximum of the absorption shifting from 14,700 to 15,100 cm^{-1}. The EPR spectra become more axial (*218*) (Table IV), whereas the ^1H T_1^{-1} values of water protons are only slightly affected (*267*). The binding of NCO^- to copper without displacing the water molecule is consistent with ^{13}C and ^{14}N NMR spectra (*267*). An affinity constant of $51 \pm 1\ M^{-1}$ was measured by CD spectroscopy (*262*).

NCS^- gives rise to a LMCT at 28,200 cm^{-1}, which shows direct binding (*273*). This is consistent with ^{13}C, ^{14}N, and ^{15}N NMR data (*266*, *267*). An affinity constant of $22 \pm 3\ M^{-1}$ has been measured at $I = 0.2$ M, pH 7.0. Under the same conditions the affinity constant of N_3^- is

88 ± 2 M^{-1} (*273*). However, it is proposed (*267*, *273*) that there is more than one binding site, as the apparent affinity constant decreases with increasing concentrations of NCS^-. The temperature dependence of the constant shows that the binding of NCS^- is entropy driven whereas it is disfavored from the enthalpic point of view. The thermodynamic parameters of NCS^- and N_3^- binding are reported in Table XI together with the analogous values of the diethylentriamine–copper complex (*273*).

Even the behavior of F^- is quite complex. ^{19}F NMR measurements show that F^- interacts with copper(II) (*274*, *275*). However, the electronic structure is hardly affected, as shown by the electronic and EPR spectra (*267*, *274*). F^- does not affect the relaxivity of water and has little effect on the NMR of Cu_2Co_2SOD (*275*).

These anions, which bind weakly to the metal ion, may have comparable affinity for the charged groups in the cavity. The binding at these groups affects the affinity of the anion for the metal ion, thus providing a spectral behavior difficult to understand in any detail. This holds also for phosphate, which reduces the affinity of Cu_2Zn_2 SOD for azide and cyanide (*107*). Phosphate was shown to interact with bovine Cu_2Zn_2SOD, but no changes in the electronic and EPR spectra were observed (*107*, *164*, *259*, *265*). The interaction of phosphate has been investigated through the paramagnetic effects caused by Cu(II) ions on the ^{31}P phosphate resonance. The ^{31}P NMR signal of phosphate shows a paramagnetic contribution to T_1^{-1} that is consistent with its binding at a site about 5 Å from the copper, whereas the contribution to T_2^{-1} is too large. At pH 6.3 two binding sites were observed, one at a distance >7 Å and another at approximately 5 Å from the copper. The latter could be the guanidinium group of Arg-143, located 5 Å from the copper (*106*). The idea of two binding

TABLE XI

THERMODYNAMIC PARAMETERS FOR LIGAND SUBSTITUTION REACTIONS IN SOD AND ONE MODEL SYSTEM[a]

Reaction[b]	K_{eq} (M^{-1})	$\Delta H°$ (kJ/mol)	$\Delta S°$ [J/(mol K)]	$\Delta G°$ (kJ/mol)
SOD + N_3^-	88 ± 2	−4.0 ± 1.0	28 ± 2	−11.0 ± 1.0
SOD + SCN^-	22 ± 3	11.7 ± 1.2	64 ± 4	−7.4 ± 2.4
$Cu(dien)^{2+}$ + N_3^-	75 ± 2	−10.6 ± 0.7	−2 ± 2	−10.0 ± 1.0
$Cu(dien)^{2+}$ + SCN^-	36 ± 2	−9.5 ± 1.0	−3 ± 3	−8.6 ± 1.0

[a] Reprinted with permission from Dooley, D. M.; McGuirl, M. A. *Inorg. Chem.* **1986**, *25*, 1261. Copyright 1986 American Chemical Society.

[b] dien, Diethylentriammine (1,4,7-triazaheptane).

sites could account for all these results (including T_2^{-1}) if the exchange of one site with bulk phosphate were relatively slow.

The overall model of anion binding is also consistent with the high-pH form of the enzyme. At pH > 10 the ^1H NMRD values increase (*114*), thus showing that at least a proton becomes closer to copper, and the ^{17}O relaxation values also increase (*217*). This behavior is followed best for the Ile-137 mutant, which is stable at high pH values (*120*). A hypothesis is that OH^- binds copper in a way similar to the other anions (*120*). Indeed, some signals of the ^1H NMR spectrum of the Cu_2Co_2 derivative, at high pH, experience variations in shift similar to those observed on addition of anions (*120*, *262*).

ENDOR studies on some anion adducts of SOD are available at low temperature. Hyperfine interactions of ^1H and ^{14}N with the Cu(II) site have been measured (*248*, *276*). From these data it appears that at 4.2 K CN^- loosens the coupling with His-48, whereas little change occurs on N_3^- binding (*248*). ESEEM spectra of ^{15}N SOD with cyanide (*250*) indicate that the inhibitor substitutes one of the histidines with the larger hyperfine constant (His-46 or His-48), producing a square planar configuration with the other three histidines.

Binding of formate to Cu_2Zn_2 and Cu_2Co_2SOD has been investigated by NMR spectroscopy. Formate belongs to a class of anions (such as chloride, acetate, and phosphate) that do not coordinate to copper. The formate binding occurs via hydrogen bonding of the carboxylate ion to the NHs of the side chain of Arg-143, without displacement of the water molecule (*277*).

Hydrogen sulfide (HS^-) is reported to bind copper(II), without inhibiting the enzyme. The visible and EPR spectra are strongly affected by HS^- binding, as with other anions (Table IV); however, the activity is slightly enhanced. A hypothesis of this behavior is that the HS^- ligand may improve the access of O_2^- to the catalytic site, displacing a water molecule (*278*).

Tetramer vanadate is also reported to bind SOD (*279*). It is proposed, on the basis of site-directed mutagenesis, that it binds to two lysines (positions 122 and 136) with an affinity constant of 2×10^7 M^{-1}, which is higher than that of CN^- (2×10^6 M^{-1}) (*107*). The affinity is drastically reduced when Arg-143 is mutated (*279*).

The interaction of Cu_2E_2SOD with azide produces effects on the EPR parameters similar to those observed for the native Cu_2Zn_2SOD (Table X) (*244*). Nevertheless, the binding of N_3^- to the copper ion was monitored in Cu_2E_2SOD (*244*) through ^{14}N electron spin echo spectroscopy. No appreciable effect was detected in the echo envelope spectrum with addition of ^{15}N azide, nor with ^{15}N cyanide, indicating that the binding of these anions to the Cu_2E_2 derivative does not alter the

magnetic coupling of the metal ion to ^{14}N of the ligated imidazoles (*247*). The interaction of Cu_2E_2SOD with azide and thiocyanate has been investigated through water ^1H NMR relaxation measurements (see Section VI) (*220*).

G. Other Metals at the Zinc Site

Zn^{2+} is not a great spectroscopic probe! However, because its d^{10} configuration ensures diamagnetism, it has been investigated by ^1H NMR (*280–282*).

1. Cobalt at the Site of Zinc

The visible absorption spectrum of E_2Co_2SOD (E = empty), with cobalt(II) in the zinc site, has an absorption maximum at 583 nm and an extinction coefficient of 370 M^{-1} cm^{-1} (Fig. 49). The CD spectrum possesses two negative bands at 585 and 530 nm. The EPR spectrum is observable below 100 K and shows $g_\perp = 4$ and $g_\parallel = 2.16$ (*189*). The ^1H NMR spectrum shows seven signals in the region between 35 and 55 ppm and two signals upfield that should belong to the residues (three His and one Asp) coordinated to cobalt(II) (Fig. 50a). The assignment of the spectrum, first proposed in 1985 (*262*), was completed through the investigation of the derivative, which was selectively deuterated at the Cε1 position of the imidazole rings (*283*).

The $Cu_2^ICo_2^{II}$ derivative is obtained through reduction of $Cu_2^{II}Co_2^{II}$ SOD. The electronic spectrum of this species shows a shift of the cobalt absorption maximum to a shorter wavelength (from 598 to 588), which renders the spectrum very similar to that of E_2Co_2SOD (Fig.

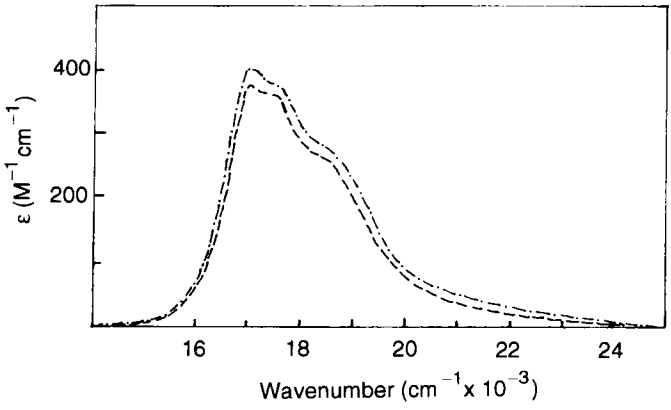

FIG. 49. Electronic absorption spectra of E_2Co_2SOD (-·-) and $Cu_2^ICo_2SOD$ (---). Reprinted with permission from Ref. *260*.

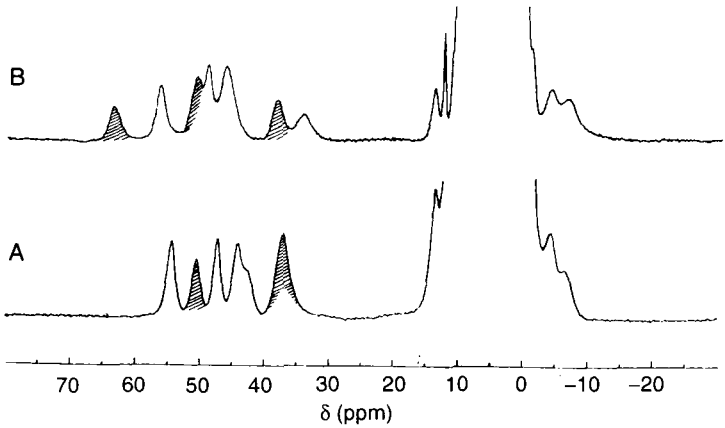

FIG. 50. The 300-MHz ^{1}H NMR spectra of (A) E_2Co_2SOD and (B) Cu^I_2 Co_2SOD. The shaded signals belong to exchangeable protons. Reprinted with permission from Ref. *168*.

49) (*284*, *285*). This result was related to the breaking of the imidazole bridge on reduction (*284*, *285*). It was later confirmed by the ^{1}H NMR spectrum of the same derivative, which clearly shows the presence of three exchangeable NH′ protons belonging to His-71, His-80, and His-63 (Fig. 50b). Therefore, His-63 is regularly coordinated to the Co(II) but no longer to Cu(I) (*233*). An extensive assignment of the resonances belonging to the residues coordinated to the metal ions and to some residues near the copper(I) ion was obtained (*286*). The dipolar shift induced by cobalt(II), on signals not belonging to cobalt-coordinated residues, was determined and used to determine the orientation of the magnetic susceptibility tensor (*286*). Evidence for breaking of the imidazolate bridge on reduction of copper was also given in the crystalline state through polarized absorption spectra (*287*).

The $Ag^I_2Co^{II}_2$ derivative has electronic and ^{1}H NMR spectra similar to the $Cu^I_2Co^{II}_2$ derivative. Also in this case, the presence of three solvent-exchangeable signals is strong evidence that His-63 is not a bridging ligand (*191*).

2. *Nickel at the Site of Zinc*

The electronic spectra of the nickel chromophore at the zinc site in the compounds Ag_2Ni_2 and $Cu^I_2Ni_2SOD$ are shown in Fig. 51. The band at 750 nm is the highest $F \rightarrow F$ transition and is on the high side of the energy range for pseudotetrahedral compounds (*258*). Distortions and ligand strength may account for it. Evidence of a possible bidentate binding of Asp-83 has been proposed by EXAFS (*232*).

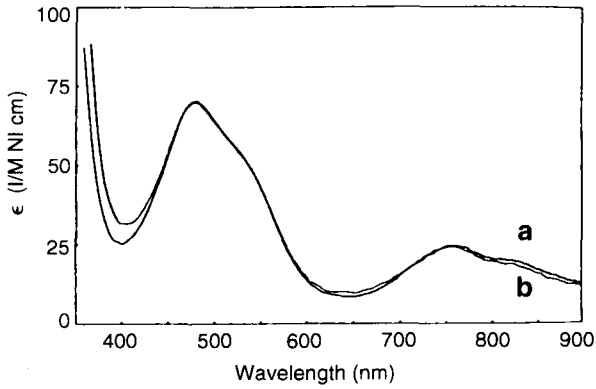

FIG. 51. Electronic absorption spectra of (a) $Cu_2^{I}Ni_2^{II}SOD$ and (b) Ag_2Ni_2SOD. Reprinted with permission from Ming, L. J.; Valentine, J. S. *J. Am. Chem. Soc.* **1987,** *109,* 4426. Copyright 1987 American Chemical Society.

The ^1H NMR spectra of the two derivatives show a number of isotropically shifted signals, in both the upfield and downfield regions, very similar to each other, indicating similar metal binding environments in both derivatives. Because Ag^+ and Cu^+ are diamagnetic, the isotropically shifted signals have been assigned to protons of the three His and one Asp residue coordinated to Ni^{2+}. The presence of three solvent-exchangeable signals, which account for three histidine NH, indicates that, in these derivatives, the His-63 bridging ligand is detached from the copper site and protonated (*258*, *288*).

3. *Copper at the Site of Zinc*

The two derivatives $Ag_2^{I}Cu_2^{II}$ and $Cu_2^{I}Cu_2^{II}SOD$ [the latter obtained through semireduction of $Cu_2^{II}Cu_2^{II}SOD$] show quite similar visible absorption and EPR spectra (*244*, *252*). The spectra are characteristic of Cu(II) in the zinc site without interference from paramagnetic ions in the copper site. The hyperfine coupling constant of 105×10^{-4} cm^{-1} is typical of copper(II) tetrahedral complexes (*244*, *252*). Experiments based on linear electric field effect (LEFE) in pulsed EPR also support the conclusion that Cu(II) in the zinc site retains the pseudotetrahedral coordination geometry. Furthermore, ENDOR and ESEEM experiments on $Ag_2^{I}Cu_2^{II}SOD$ pointed out that Cu(II) forms inequivalent bonds to the three coordinated imidazoles (*289*).

H. CADMIUM AT BOTH COPPER AND ZINC SITES

^{113}Cd NMR is a very sensitive tool to identify coordination number and donor atoms (*290*). ^{113}Cd NMR experiments on cadmium at the

copper (*197*) and zinc site (*196*) indicate (1) that the two subunits are identical and (2) that the coordination at the zinc site is similar in the case of E_2Cd_2SOD and $Cu_2^{II}Cd_2SOD$ (*196*, *197*). The chemical shifts are ≅320 ppm for Cd at the zinc site and 185 ppm for Cd at the copper site. For the former case there are two earlier reports (*291*, *292*). One of them agrees with the above values (*291*). It was also noted that the observed shift is much lower than that predicted on the basis of a simple additive model (*293*).

Experiments based on perturbed angular correlation (PAC) of γ rays, performed on the Cu_2Cd_2SOD derivative, demonstrated that His-63 bridges the two metal sites (*199*, *294*).

I. ^{1}H NMR Spectra of Cu_2Co_2 and Cu_2Ni_2SOD

The magnetic coupling between copper(II) and cobalt(II), or copper(II) and nickel(II), is responsible for the fast electronic relaxation times of copper(II), which become similar to those of the cobalt(II) or nickel(II) ions (*295*, *296*). As a consequence, ^{1}H NMR spectra can be performed as for any cobalt(II) or nickel(II) protein. This is absolutely a peculiarity as far as the NMR of copper(II) proteins is concerned. The spectra are shown in Fig. 52 (*262*, *288*). N_3^-, if added, is in fast exchange with the bulk anion and thus the signals can be followed on increasing addition of the anion. It appears that a set of protons

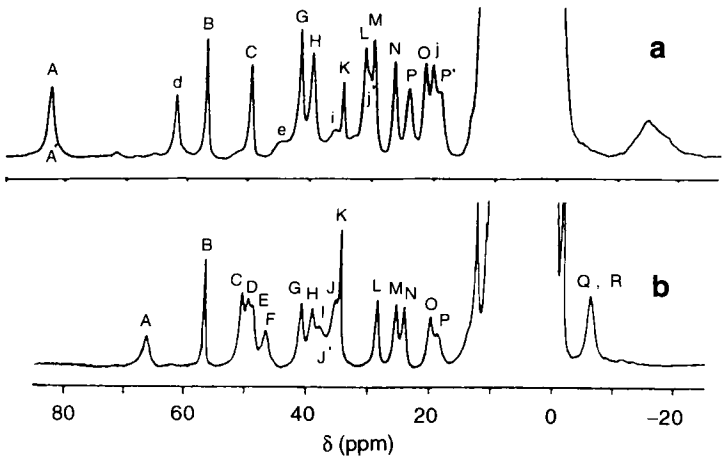

FIG. 52. The 300-MHz ^{1}H NMR spectra of (a) $Cu_2^{II}Ni_2^{II}SOD$ and (b) $Cu_2^{II}Co_2^{II}SOD$ at pH 6.5. Reprinted with permission from Ming, L. J.; Banci, L.; Luchinat, C.; Bertini, I.; Valentine, J. S. *Inorg. Chem.* **1988,** *27,* 4458. Copyright 1988 American Chemical Society.

corresponding to a His decreases its coupling with the unpaired electron of copper(II). When these studies were done it became historically important to be successful with the assignment. These systems were used to pioneer the procedure for the assignment of proton signals in paramagnetic molecules. A definitive assignment of the Cu_2Co_2 derivative was achieved through 1D NOE measurements (*297*) first and then confirmed through 2D NOESY spectroscopy (*298*, *299*) (Table XII). Rotilio *et al.* first misassigned the spectra (*300*) but eventually confirmed the above assignment (*301*).

A polyethyleneglycol (PEG) derivative, with large molecular weight, was investigated and a sizable Curie relaxation was observed (*163*).

The ^1H NMR spectra of the Cu_2Co_2SOD anion derivatives indicate that the protons of His-48 experience hyperfine coupling with the unpaired electrons to different extents: the hyperfine shifts decrease in the following order: $F^- > NCS^- > NCO^- > N_3^- > CN^-$ (Table IV) (*89*). ^1H NOE experiments on the Cu_2Co_2 adduct with N_3^- show that the interproton distances involving the histidines coordinated to copper(II) are similar to those measured in the absence of azide. All these results account for an increase of the copper–nitrogen (His-48) distance as a consequence of a movement of the copper ion (*89*). The decrease in hyperfine shifts of the His-48 protons can be taken as a qualitative estimate of the above movement. The Thr-137Ile mutant has the largest His-48 hyperfine shifts, which are indicative of a strongest Cu–His-48 bond (Table IV).

The assignment of the Cu_2Ni_2SOD ^1H NMR spectra was another significant achievement (*288*, *302*). It should be noted that tetrahedral nickel(II) has shorter electronic relaxation times than does tetrahedral cobalt(II), and consequently the ^1H NMR spectra are sharper in the former case.

J. ^1H NMR Spectra of the Reduced Enzyme

Because the reduced enzyme is diamagnetic, it was studied using NMR from the early days of application of this technique to biological systems (*251*, *280*, *303*, *304*). The recent results allow a complete assignment of the His protons bound to both copper(I) and zinc(II) (Table XIII). It appears that the bridge is broken on copper reduction. Indeed, an NH proton signal at 12.44 ppm could be assigned to the HNε2 of His-63 (Table XIII). This finding is consistent with the pH dependence of the reduction potential, which requires a proton together with the reducing electron (see Section VII,A). It is also consistent with the ^1H NMR spectrum of cobalt(II) in $Cu_2^ICo_2^{II}SOD$, which is

TABLE XII

ASSIGNMENT OF ^1H NMR SIGNALS OF METAL-COORDINATED RESIDUES IN Cu_2Co_2SOD[a]

Shift (ppm)	Assignment
67.4	His-63 Hδ2
57.0	His-120 HNδ1
50.3	His-46 HNε2
49.6	His-71 Hδ2
49.0	His-80 Hδ2
46.7	His-80 HNε2
41.0	His-46 Hδ2
39.5	His-120 Hε1
38.7	Asp-83 Hβ1
37.0	Asp-83 Hβ2
35.6	His-71 HNε2
34.7	His-48 HNδ1
28.4	His-48 Hδ2
25.7	His-46 Hε1
24.3	His-120 Hδ2
19.8	His-48 Hε1
18.7	His-46 Hβ1
−6.2	His-71 Hβ2
−6.2	His-46 Hβ2
12.30	His-48 Hβ2
11.21	His-120 Hβ2
8.44	His-120 NH[b]
6.40	His-48 Hβ1
4.43	His-120 Hα
3.73	His-48 Hα
3.13	His-120 Hβ1
1.23	Ala-140 β-CH_3
0.56	Val-118 γ_1-CH_3
−0.28	Arg-143 H-γ_1
−1.51	Val-118 γ_1-CH_3

[a] At 298 K, pH 5.5.

[b] Tentatively assigned on the basis of a single dipolar connectivity.

sensitive to the bridging/terminal character of His-63 (see Section VIII,G,1).

Several NMR studies indicate that there is binding of anions to the reduced species (*159*, *282*, *305*, *306*). However, the most significant information comes from X-ray studies (*83b*) (see Section II,J,3).

TABLE XIII

PROPOSED ASSIGNMENT OF HISTIDINE–IMIDAZOLE PROTONS OF HUMAN $Cu_2^{I}Zn_2^{II}$ SOD[a]

	ppm			
Residue	Hε1	Hδ2	HNδ1	HNε2
His-43[b]	8.64	7.14	12.9	14.07
His-80	8.57	6.86	—	12.70
His-110[b]	8.54	—[c]	—[d]	—[d]
His-48	8.52	—[c]	12.54	—
His-120	8.29	6.64	—[d]	—
His-71	7.78	6.82	—	15.40
His-46	6.78	7.11	—	13.42
His-63	6.57	6.05	—	12.44

[a] At 300 K, pH 5.5.
[b] His not associated with the active site.
[c] Not assigned.
[d] Not observed.

Monomeric species are now available with only 153 amino acid residues (*60*, *102*, *124*). A fully ^{13}C- and ^{15}N-labeled sample has been prepared and should lead to the solution structure. At the moment the full backbone assignment is available (unpublished results from this lab).

IX. Mechanistic Aspects of Cu_2Zn_2SOD

A. NONCATALYZED DISPROPORTIONATION OF O_2^-

The superoxide anion is produced in living cells of aerobic organisms mostly as an unwanted by-product of oxidative metabolism (*307*). The intrinsic toxicity of superoxide has been the subject of a passionate debate in past years (*308–310*). It seems that O_2^- toxic effects are not due to direct interaction of the O_2^- species with biological substrates, but rather to the likely products of chemical reactions involving superoxide.

Thermodynamic and chemical data support this point of view. The radical character of O_2^- can be estimated from the $H-OO^-$ bond energy. This amounts to the relatively small value of 301 kJ, indicating that the superoxide anion has a limited radical character (*311*). Indeed, the O_2^- anion is not able to produce homolytic cleavage of even

the weakest C—H bond present in the allylic carbons of linoleic acid (≈311 kJ) (*311*). On the contrary, its conjugate acid, HOO·, can break C—H bonds, because the radical character of HOO· is given by the bond energy of the H—OOH bond, which is ≈344 kJ.

Extensive reviews of the chemical properties of the superoxide anion are in Sawyer and Valentine (*308*) and in Sawyer (*311*).

Besides the effects of the HO_2 radical, the indirect toxicity of superoxide may also be due to the fact that superoxide may originate hydroxyl radicals through reaction (23) or even singlet oxygen through reactions (23) and (24) (*312*, *313*):

$$O_2^- + H_2O_2 + H^+ \rightarrow O_2 + H_2O + OH\cdot \tag{23}$$

where $k_{23} < 10^{-4}\ M^{-1}\ \text{sec}^{-1}$ (*312*, *314*), and

$$O_2^- + HO_2 + H^+ \rightarrow O_2 + H_2O_2 \tag{24}$$

where $k_{24} \approx 1 \times 10^8\ M^{-1}\ \text{sec}^{-1}$ (*308*, *315*).

The generation of singlet oxygen ($^1\Delta O_2$ or $^1\Sigma_g O_2$) in reactions (23) and (24) has been proposed on the basis of thermodynamic calculations (*313*), but direct experimental evidence is lacking.

The O_2^- disproportionation equilibria

$$2O_2^- + 2H^+ \overset{K_{25}}{\rightleftharpoons} H_2O_2 + O_2 \tag{25}$$

$$2O_2^- + H_2O \overset{K_{26}}{\rightleftharpoons} HO_2^- + O_2 + OH^- \tag{26}$$

are shifted to the right: at pH 7.0 $K_{25} = 4 \times 10^{20}$ and even at pH 14 $K_{26} = 9.1 \times 10^8$ (*311*). Because of this proton-driven equilibrium, and not for its intrinsic Brønsted base properties ($pK_b = 9.2$), O_2^- can be seen as a strong Brønsted base able to abstract protons from very weak acids (up to $pK_a > 23$) to form HO_2. In other words, the addition of O_2^- to aqueous solutions results in the quantitative formation of the strong bases HO_2^- and OH^-.

The maximum rate of O_2^- disproportionation occurs at pH = pK_a of the HO_2 weak acid and decreases with increasing pH. At pH 4.8 $k > 10^8\ M^{-1}\ \text{sec}^{-1}$. Thus O_2^- reacts with protic substrates to yield products that are consistent with an apparent one-electron oxidation of the substrate and the production of H_2O_2. However, it has been shown that there is not direct one-electron transfer to O_2^-. The process consists instead of the abstraction of a proton from the substrate:

$$HA + O_2^- \rightarrow A^- + HO_2 \tag{27}$$

in weak acids and in water; $k_{27} = 10^4$–10^{-3} M^{-1} sec^{-1}, depending on pH (*308*). In strong acids reaction (27) is extremely rapid.

Only after the protonation step [Eq. (27)] the reaction

$$HO_2 + O_2^- + H^+ \rightarrow H_2O_2 + O_2 \tag{28}$$

or

$$HO_2 + HO_2 \rightarrow H_2O_2 + O_2 \tag{29}$$

may occur; k_{28} and $k_{29} > 10^7$ M^{-1} sec^{-1}.

It has been proposed that the actual oxidant of the A^- substrate is the newly formed oxygen, as indicated by the quantitative yields of the nonoxidized substrate when O_2 from dismutation is continuously purged from the reaction vessel (*311*, *313*).

The direct reaction of O_2^- with H_2O_2 to give OH · radicals [Eq. (23)] is unlikely ($k < 10^{-4}$ M^{-1} sec^{-1}) (*314*), but complexes of redox-active metal ions such as Fe(III) may catalyze the reaction (*312*):

$$Fe(III)L + O_2^- \rightarrow Fe(II)L + O_2 \tag{30}$$

and then

$$Fe(II)L + H_2O_2 \rightarrow Fe(III)L + OH\cdot + OH^-. \tag{31}$$

On the other hand, the peroxidation reaction

$$M(II) + O_2^- \rightarrow M(III)\text{–}O_2^{2-} \tag{32}$$

may also occur. The latter reaction has been proposed to explain the unique *in vivo* toxicity of superoxide (*316*).

Whatever the actual reagents might be, it has been shown that O_2^- can oxidize sulfite and initiate a free-radical chain reaction, or oxidize iron-containing clusters present in enzymes, such as aconitase and fumarases, freeing Fe(II), which in turn initiates a Fenton-like chemistry by interacting with hydrogen peroxide (*317*). Fe(II) release from transferrin has also been observed following O_2^- secretion by stimulated human neutrophils (*318*).

B. Some Pertinent Facts about Cu_2Zn_2SOD Catalysis

Studies on Cu_2Zn_2SOD performed over the past 25 years have produced an enormous amount of information on the system. Nevertheless, several aspects of the mechanism of action of Cu_2Zn_2SOD toward O_2^- dismutation are still unclear. In this section we will summarize the facts that have been ascertained about Cu_2Zn_2SOD chemistry and with which any mechanistic proposal should be consistent.

1. Superoxide spontaneously disproportionates in water to dioxygen and hydrogen peroxide. As discussed in Section I, the uncatalyzed reaction is pH dependent and has a maximum rate at a pH equal to the pK_a of the $HO_2 \rightleftharpoons O_2^- + H^+$ equilibrium; namely, when $[O_2^-] = [HO_2]$ ($K_a = 1.6 \times 10^{-5}$ M, pKa = 4.8) (*315*, *319*) this means that the reaction given by Eq. (2)

$$O_2^- + HO_2 \rightarrow O_2 + HO_2^-$$

is fast, and even at pH 7.5 its rate constant k is equal to 8.5×10^7 M^{-1} sec^{-1}, compared to $k = 10^2$ M^{-1} sec^{-1} for the disproportionation among O_2^- radicals ($O_2^- + O_2^-$) (*97*, *320*).

2. Cu_2Zn_2SOD catalyzes the O_2^- dismutation to dioxygen and hydrogen peroxide in a first-order reaction with respect to both the enzyme and substrate and with a pseudo-second-order rate constant of about 2×10^9 M^{-1} sec^{-1}. The same catalytic efficiency is observed for copper in both +2 and +1 oxidation states (*52*, *91*, *97*). At steady state, the blue color of Cu_2Zn_2SOD is bleached by about 30% on reaction with O_2^- generated by pulse radiolysis. The bleaching is independent of the enzyme concentration and does not alter the superoxide disproportionation rate (*91*, *321*). The reduced $Cu_2^IZn_2SOD$ is not readily reoxidized by air oxygen at room temperature (*223*), but hydrogen peroxide oxidizes it. These observations suggest that the superoxide dismutation in Cu_2Zn_2SOD proceeds by a cyclic oxidation and reduction of the copper ion by two successive O_2^- molecules, as shown in the following scheme:

$$ECu(II) + O_2^- \rightarrow ECu(I) + O_2$$

$$ECu(I) + O_2^- + 2H^+ \rightarrow ECu(II) + H_2O_2.$$

3. Copper is essential for catalysis; removal of Cu(II) or its replacement with other metals results in the complete loss of catalytic activity (*2*) with the exception of Ag(I), for which catalytic activity up to

about 5% of the native enzyme has been claimed (*244*). On the contrary, the Zn(II) ion can be replaced by Co(II), Cu(II), or Cd(II), or by an empty site with none or limited loss of activity (*173*, *183*, *252*, *322*).

4. The dismutase reaction is reversible (*323*). Indeed, Cu_2Zn_2SOD is reduced by H_2O_2 (*98*, *164*, *321*). However, the fast Cu(II) reduction is followed by a slow irreversible inactivation of the enzyme, which has been attributed to a Fenton-like chemistry involving Cu(I) and H_2O_2 (*324*).

5. There are conflicting reports about the substrate K_m values. Evidence of a first-order rate-limiting step was provided by a polarographic method resulting in a K_m value of 0.5 m*M* (*263*). However, kinetics measured using the stopped-flow method do not show saturative behavior at 25°C and indicate that $K_m > 5$ m*M* (*325*). By lowering the temperature to 5.5°C at pH 9.3 and with an initial O_2^- concentration of ≈ 5 m*M*, Fee and Bull were able to observe saturative behavior in Cu_2Zn_2SOD (*99*) and to measure a K_m value of 3.5 m*M*.

6. Studies conducted in nonsaturating substrate conditions ($K_m \gg [O_2^-]$) show that the rate of catalyzed superoxide dismutation is independent of pH in the range 5.0–9.5 (*52*, *91*, *118*) even though the isoelectric point of Cu_2Zn_2SOD around 5 suggests a pH-dependent activity. This fact, together with the observation that the reaction is not slowed down if performed in D_2O (pH 10.0) (*99*, *324*), indicates that, under such conditions, proton transfer is not a rate-limiting step. It is worth noting that in the pH range 5.0–9.5 the EPR and visible spectra of the enzyme are also invariant, indicating that the copper site is unperturbed by the pH change. On the contrary, in the pH range 9.0–12.0 a reversible decrease of Cu_2Zn_2SOD activity is observed with concomitant changes in the chromophore (*114*, *120*, *206*). It has been proposed that the rate-limiting step is the diffusive approach of O_2^- to copper (*231*).

7. In nonsaturating conditions the rate-limiting step is the apparent binding of the substrate to copper (*99*). This means that the encounter rate of the superoxide with the enzyme is slower than the electron transfer process. The Marcus theory of electron transfer predicts that fast processes, such as that observed in SOD, occur only when the distance between the components of the redox couple is of the order of few angstrøms (*326*). Hence, the observation that in Cu_2Zn_2SOD the electron transfer is not the rate-limiting step implies that the superoxide substrate must dock close to the copper ion before the electron transfer and the consequent copper reduction occur. However, the theory does not require that a $Cu–O_2^-$ coordination bond should actually be formed, because the electron jump in a vacuum

could work as well. Under saturating conditions ($K_m \ll [O_2^-]$) (at 5.5°C and pH 9.3) a first-order rate constant of $k_{cat} = 1 \times 10^6$ sec^{-1} and $K_m = 3.5 \times 10^{-3}$ M were measured (*99*). A solvent isotope effect was also observed and k_{cat} was increased by the presence of the general acid ND_4^+. This suggests that water is the actual proton donor and that the proton transfer is the rate-limiting step in these conditions.

8. The rate of O_2^- dismutation is affected by the ionic strength of the medium (*105*, *118*, *327*). For instance, between pH 7 and 8 the activity of bovine Cu_2Zn_2SOD diminishes by about 70% on passing from ionic strength $I = 0.02$ M to $I = 0.25$ M (*118*). These results have been confirmed for the human enzyme. Interestingly, the ionic changes at pH 8.0 have a small effect on the neutral and acidic human SOD mutants of the Arg-143 residue, which possess the lesser activity (*95*). Above pH 12.0 the effect of solute activity vanishes. This observation implies the presence of electrostatic control of the access of superoxide to the active site (*vide infra*).

9. A wealth of information has been gathered from both theoretical and experimental studies about the role of the active site cavity residues in the electrostatic guidance of superoxide toward the copper center (*45*, *122*). The essential role played by the conserved Arg-143 residue (Arg-141 in the bovine SOD sequence) in catalysis has been demonstrated (*95*, *270*). The positively charged guanidinium group of this residue is located at about 6 Å from the copper, providing the final docking site for the superoxide anion. Substitution of Arg-143 by site-directed mutagenesis with negatively charged (Asp, Glu), neutral (Ile, Ala), or even positively charged (Lys) residues always results in loss of activity (*95*, *104*), paralleling the results of chemical modification studies (*153*, *154*, *328*). However, it must be stressed that, in any case, mutated Cu_2Zn_2SODs do have activities that are still high in absolute value, indicating that the role of Arg-143 is relevant, but not essential for catalysis. A much smaller effect is observed when the mutations affect the residues located at the rim of the cavity. Reductions of activity between 80 and 40% have been reported, depending on the ionic strength and on the type of enzyme when the residues Lys-120 and Glu-130 (Asp-130 in *Xenopus laevis* SOD) have been subjected to single or double substitutions by neutral amino acids (*175*, *329*) (see Section IV).

10. Each monomer seems to function independently, as shown by coupling native subunits with other native or chemically modified subunits (*330*). However, the separated monomers are much less active. The human SOD monomer obtained by site-directed mutagenesis of two dimer interface residues (Phe-50 and Gly-51) shows de-

creased activity (5–10% of the wild-type enzyme) (*60*). The X-ray crystal structures of Cu_2Zn_2SOD show small but significative differences occurring in the active sites in different subunits of the same SOD molecule in both copper oxidation states, which, however, may be averaged in solution (see Section II).

11. Electrochemical studies have shown a linear dependence of Cu_2Zn_2SOD reduction potential on pH between pH 5.0 and about 8.5. The slope of 0.059 V/pH indicates the uptake of one proton by the enzyme on copper reduction (*223*, *227*) (see Section VII).

12. NMR measurements on reduced bovine and human $Cu_2^IZn_2SOD$ have shown the appearance of a new proton signal in the histidine NH region on copper reduction (*233*). A new hyperfine-shifted exchangeable proton has been observed in $Cu_2^ICo_2SOD$ on copper reduction (*331*). Measurements of proton NOEs and the assignment of their chemical shifts have allowed the determination of interproton distances, which are consistent with the protonation of His-63 (*82*). Together with the EXAFS studies (*203*), NMR has provided the most direct evidence of the detachment and protonation of the bridging histidine on copper reduction (*233*, *331*).

13. A shift to higher frequencies of the absorption maximum in the visible spectrum of the Cu_2Co_2SOD is observed on copper reduction. This blue shift is analogous to that shown by the cobalt-substituted SOD with an empty Cu site. This observation has been interpreted as proof of the protonation of the bridging histidine on copper reduction (*284*).

14. Almost normal activity has been determined for the zinc-depleted enzyme (Cu_2E_2SOD; E = empty) (*332*), indicating that the presence of the histidine bridge is not essential for catalysis.

C. Mechanism of Action of Cu_2Zn_2SOD

Different mechanistic hypotheses that have been proposed for Cu_2Zn_2SOD are consistent with the main experimental evidence obtained for the enzyme so far. However, no hypothesis is able to satisfactorily explain all of the reported observations.

Early proposals (*52*, *171*, *333*) were based on the redox titration experiments and were centered on the alternate protonation and deprotonation of the bridging histidine, concomitant with the reduction and reoxidation of copper by two superoxide molecules consecutively accessing the active site (Fig. 53). This mechanism has been updated in the light of the crystal structure determination of bovine Cu_2Zn_2-SOD (*41*, *44*), as illustrated in Fig. 54.

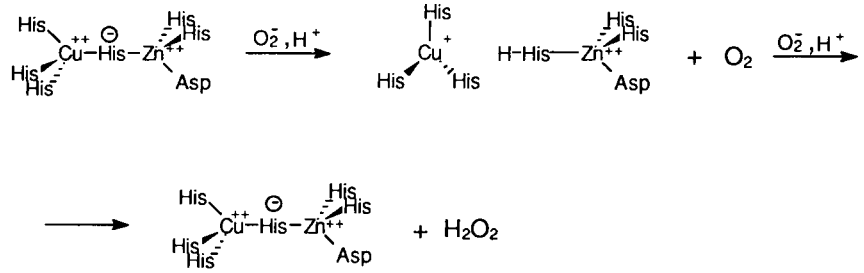

FIG. 53. Presumed scheme of the superoxide dismutation reaction by Cu_2Zn_2SOD prior to elucidation of the 2SOD crystal structure. Arg-141 is not involved in the mechanism.

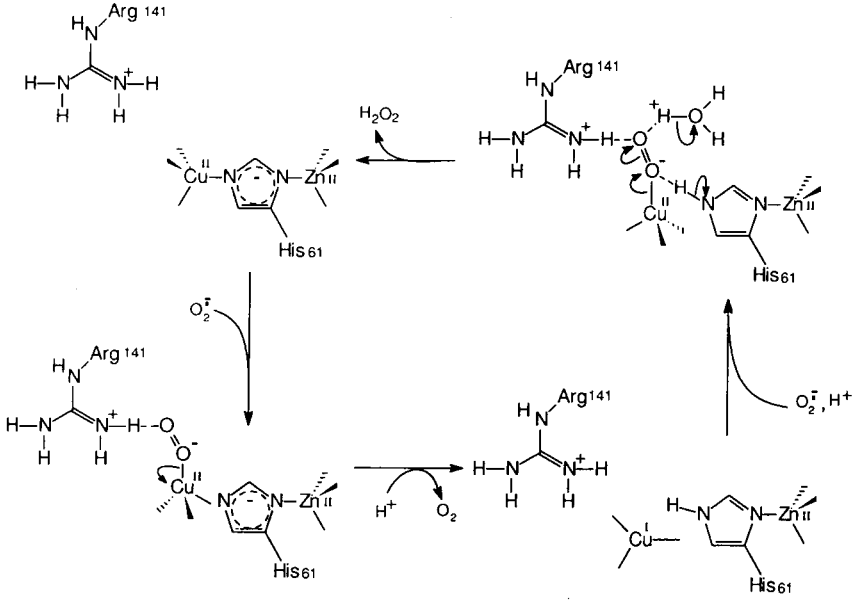

FIG. 54. Scheme of the reaction mechanism of Cu_2Zn_2SOD proposed by Tainer *et al.* (*44*) following the bovine enzyme numbering. The first substrate molecule replaces the axial water molecule and binds to Cu(II), being stabilized by the H bond with Arg-141. In the second step O_2^- reduces copper to Cu(I), with breaking of the His-61 bridge, and leaves as O_2. The Nε2 of His-61 is protonated. The zinc coordination becomes more tetrahedral. In the third step a second O_2^- molecule binds to Cu(I), positioning one of its O atoms at H-bond distance from the HNε2 of His-61 and the other at H-bond distance from the guanidinium group of Arg-141. Electron transfer from Cu(I) and proton transfer from His-61 form Cu-hydroperoxide, which leaves as hydrogen peroxide after receiving a second proton from a water molecule present in the active site.

This proposal highlights the role of Arg-143 in assisting substrate docking. Such behavior is suggested by the finding in the Cu_2Zn_2SOD crystal structure of a "ghost" superoxide molecule constituted by the copper-bound water molecule and by a second water molecule hydrogen bonded to the guanidinium group of Arg-143. The ghost substrate is oriented in such a way as to form a Cu—O—O angle of 120°, as expected for the bound O_2^- anion (*44*). Another feature of this mechanism is that zinc does not play a mere structural role but, helping to keep the copper site distorted, causes an increase of the reduction potential of Cu(II), thus favoring the reduction step. Furthermore, by coordination to the protonated His-63, it helps to position the proton in the proper orientation for H bonding and possible subsequent transfer to peroxide.

The work of Fee and Bull (*99*) points out that the speed of imidazolate bridge breaking and reforming is too low to allow such a process to occur between two successive O_2^- arrivals to the SOD active site. The postulated large rearrangement of the copper coordination during the catalytic cycle is not compatible with the extremely high reaction rates observed.

If we consider the energetics of the process, by taking into account the experimentally measured redox potentials of the Cu^{2+}/Cu^+ and O_2/O_2^- couples (see Section VII), it is possible to estimate that the energy associated with the electron transferred from O_2^- to Cu^{2+} is at most about 54 kJ mol^{-1}.

This is the value of a medium-strength hydrogen bond, and it seems unlikely that this amount of energy introduced into the system by the one-electron reduction causes the breaking and forming of the Cu–N and N–H bonds. However, for a system composed of many particles, such as an enzyme molecule, energy fluctuations of that size are possible and different conformational states may become available. It cannot be excluded that the introduction into the system of a moderate amount of energy like that associated with the above electron transfer can cause a transition toward a state wherein the His-63 bridge is broken and protonated.

The recently determined X-ray crystal structure of the yeast Cu_2Zn_2SOD, in which His-63 is no longer bound to copper (see Section II), shows that the side chain of this residue has moved away from copper toward the opening of the cavity (*334*), in agreement with NMR and MD analysis (*82*, *233*, *331*). If we take this structure as a model for the $Cu_2^IZn_2SOD$ with the bridge broken we can assume that His-63 has its Nε2 nitrogen protonated. In such a case the proton is positioned between the copper and the cavity opening and reduces the

already small solvent-exposed surface of the catalytic copper. It seems likely then that, instead of binding to copper, the O_2^- molecule may hit the histidine N–H moiety and form HO_2. Eventually the electron jumps from copper, originating the HO_2^- product, and the histidine bridge is reformed. The driving force is provided by the reduction of O_2^- to H_2O_2, which compensates the energy spent to reoxidize copper to Cu(II), and by the restoration of the original structure.

A different mechanism, in which the bridge between copper and zinc is not broken and the protons needed by the reaction are provided by the bulk solvent, has been proposed from theoretical calculations (*246*, *335*, *336*). In this mechanism a superoxide molecule forms a complex with Cu(II) thanks to the stabilizing effect of Arg-143. This stable intermediate can oxidize a second superoxide molecule by an outer-sphere electron transfer originating an $E–Cu^I–O_2^-$ complex (E = enzyme), which is subject to proton transfer from the solvent followed by electron transfer from copper, giving rise to $E–Cu^{II}–O_2H^-$. The hydroperoxide anion readily dissociates from the latter complex, leaving the metal in the oxidized state (*246*, *335*).

Alternatively the reduction step may be bypassed, directly obtaining the hydroperoxide complex (*336*). The two mechanisms are summarized in Fig. 55.

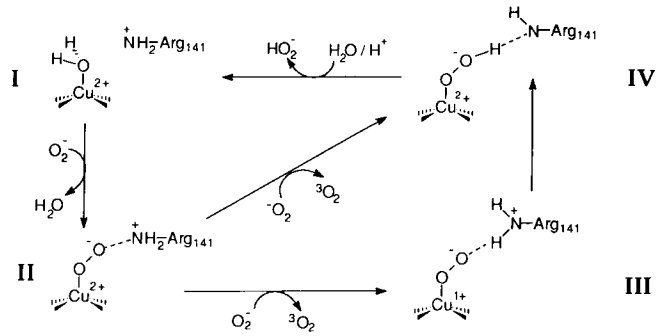

FIG. 55. Reaction scheme of superoxide dismutation following the bovine enzyme numbering. The first O_2^- molecule binds to Cu(II) and is stabilized by the H bond to Arg-141. A second superoxide molecule then approaches the active site and, by an outer-sphere electron transfer via the Cu-bound first O_2^- molecule, reduces the copper to Cu(I) (*44*) (step III). Alternatively, O_2^- directly reduces superoxide to peroxide (*336*) (step IV), leaving as dioxygen. Note that the Cu(I)–superoxide and Cu(II)–peroxide complexes are resonant forms of the same molecular arrangement. The newly formed peroxide is protonated by Arg-141 and leaves as HO_2^-. Arg-141 receives a proton from the solvent, restoring the active enzyme (I). These reaction proposals do not require the breaking and reforming of the Cu–His-61 bridge.

The possibility that the above mechanisms are operative has been supported by crystallographic evidence of the stability of the His-63 bridge in the reduced enzyme and in its complexes with anions (see Section II).

Most of the conflicting experimental evidence can be reconciled if we admit that the two mechanisms may both be operative but under different conditions. In low-substrate concentration conditions, such as those occurring *in vivo*, the traditional mechanism, whereby the proton donor is the protonated His-63 detached from zinc, may be accepted because of the slower turnover rates. On the contrary, under saturating conditions characterized by extremely high turnover rates, the second, outer-sphere, mechanism appears to be more competitive (*82*).

Interestingly, the kinetic results of an earlier study about the catalytic properties of Cu–histidine complexes toward superoxide disproportionation have been interpreted by two alternative mechanisms similar to those described above (*337*). The $[CuHis_2H]^{3+}$ complex was found to be the catalytically active species, with a $k_{cat} = 3.4 \times 10^8\ M^{-1}$ sec^{-1} independent of pH in the range 2–7.

Additional work has shown that a yeast Cu_2Zn_2SOD mutant, in which the bridging histidine has been replaced by a noncoordinating alanine, displays a pH-dependent activity and spectroscopy (*149*). Further studies on the zinc-depleted enzyme show that Cu_2E_2SOD (E = empty) has a pH-dependent dismutase activity toward superoxide (*334*). Such pH-dependent properties have been attributed to the possibility that the mutant and the apo forms have a hydroxyl group strongly bound to copper in place of the usual water molecule (see Section II). In fact, both the His-63AlaSOD mutant and Cu_2E_2SOD show a pK_a of 9.1, typical of copper-bound water in small molecule complexes and proteins. This behavior contrasts with that of Cu_2Zn_2-SOD, which has an abnormally high pK_a (>10.0). These findings are easily explained by considering that the presence of the imidazolate bridge between the metals forces the water and the resulting hydroxyl group to be only loosely bound to copper. Such interpretation is supported by X-ray crystallography and NMR data on the anion complexes of Cu_2Zn_2SOD (*88*, *90*, *269*). The strong ligands cyanide and azide are found closely bound to Cu(II), causing the Cu–His-48 bond to lengthen by about 0.5 Å (see Section II). On the contrary, in the analogous azide complex of reduced $Cu_2^IZn_2SOD$ with the intact bridge, the anion is found at about 3.0 Å from the Cu(I) ion (see Section II).

From the above findings, coupled with the demonstration that in Cu_2E_2SOD the second step of the catalytic process (the reoxidation of

copper by a second O_2^- molecule) is responsible for the observed pH dependence, Valentine *et al.* propose that such pH dependence of the catalytic rate is caused by the slow product release from the reoxidized copper (*334*). When the bridging histidine is absent, the newly formed peroxide/hydrogen peroxide will occupy the available equatorial position in the Cu(II) coordination sphere, resulting in a stronger bond and hence in a worse leaving group. The intact imidazolate bridge plays, in this proposal, an active role by preventing the peroxide to form a too stable bond with copper, thereby acting as a good leaving group.

D. Comparison with MnSOD and FeSOD Mechanisms

Mononuclear SODs contain manganese or iron in their active sites. MnSOD is found in prokaryotes and in mitochondria of higher organisms, whereas FeSOD is present in plants and prokaryotes. The X-ray crystal structures of the oxidized and reduced native enzymes and of the respective azide-inhibited forms have been reported (*338*, *339*). The metal ions are in both cases five-coordinate by three histidines, an aspartate, and a solvent/hydroxide molecule in a trigonal bipyramidal geometry. The active sites of both FeSOD and MnSOD appear to be quite similar and the oxidation states of the metals during catalysis are in both cases +2 and +3. The crystal structures of the "cambialistic" SOD from *Propionibacterium shermanii*, equally active with both iron or manganese in the active site, have been reported (*340*), showing again the same active site structure. These similarities are reflected in the proposed unified mechanism shown in Fig. 56.

The superoxide substrate is supposed to bind the oxidized metal, increasing its coordination number to six. On releasing the product O_2, the bound hydroxyl is protonated, forming a coordinated water molecule. A second superoxide molecule then approaches the catalytic center and binds to the reduced metal. The superoxide is reduced by the metal and protonated by the water, forming the second product, hydroperoxide, which finally leaves the active site, restoring the original catalytic center.

It can be seen that the above mechanism shares similarities with the Cu_2Zn_2SOD mechanism. However, the catalytic rates of FeSODs and MnSODs are two orders of magnitude smaller than that of Cu_2Zn_2SOD and dramatically pH dependent. The main differences are that the superoxide molecule increases, on binding, the metal coordination number to six and that the role of the Cu_2Zn_2SOD histidine

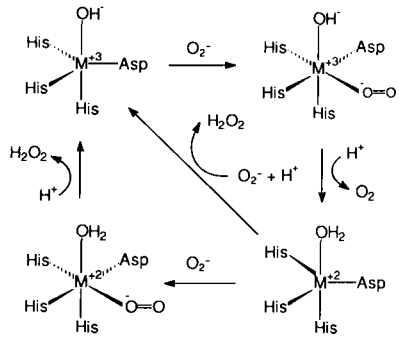

FIG. 56. Reaction scheme proposed for the superoxide dismutation by FeSODs and MnSODs. The first O_2^- molecule binds to the oxidized metal, increasing its coordination number to six. The reduction step follows, in which the metal coordination goes back to five on leaving the dioxygen molecule. A second O_2^- molecule then binds to the reduced metal, oxidizes it back to M(III), becomes protonated, and leaves as hydrogen peroxide.

bridge is here played by the water/hydroxide molecule. The binding mode of the substrate has been proposed on the basis of the structures of the azide-bound forms. A point to be clarified is that the hydroperoxide product does not appear to be a good leaving group due to its affinity toward the trivalent metal ion, thus leading to enzyme inhibition. Furthermore, in the case of FeSOD, it has been shown that exogenous ligands do not bind to the reduced enzyme. This brings support to an outer-sphere mechanism for O_2^- reduction.

X. Concluding Remarks

The very large amount of data currently available on the Cu_2Zn_2 SOD enzyme has enabled a deep understanding of its function and to the rationalization of most aspects of its chemistry and biochemistry. Different techniques have allowed the enzyme to be probed in all its aspects, from the finest details of the active site electronic structure to the overall description of its molecular assembly. The theoretical work has further completed and linked most aspects of this information. However, some parts of the picture are still fuzzy. There are aspects that in our opinion need further study:

1. The details of the electron and proton transfer and the role of the histidinato bridge during catalysis require elucidation to provide yet deeper insights.

2. The role of the quaternary structure in maintaining an active conformation of the enzyme and its dependence from the primary structure should be further analyzed in light of the information coming from the studies on active and inactive monomeric Cu_2Zn_2SODs.
3. The role of electrostatics in the guidance of superoxide to the active site has still to be completely rationalized.

With respect to the above last two points, X-ray and NMR methods should provide the structural information necessary to understand the function of single amino acids and may also provide the basis to correlate the differences in primary structure with the activity and function of the enzyme.

Once again, as always occurs in science, we have here an example of how the process of gaining basic knowledge on a system never ends. As we proceed to obtain a deeper understanding, more new questions arise and unexpected and intriguing aspects appear.

ACKNOWLEDGMENTS

We thank C. Luchinat and J. S. Valentine for carefully reading the manuscript. We are grateful to L. Banci, M. Borsari, K. Djinovic, B. Meier, and P. L. Orioli for valuable suggestions and helpful discussions. We are also grateful to M. Benvenuti for editorial work.

NOTE ADDED IN PROOF: The first crystallographic determination of a Cu_2Zn_2SOD from a prokaryotic organism has just appeared in the literature. This refers to the structure of Cu_2Zn_2SOD from the symbiont bacterium *Photobacterium leiognathi.* The structure has been determined at 1.9 Å resolution and refined to $R = 0.193$ (*75b*). This prokaryotic SOD presents several interesting original features. Actually, with eukaryotic SODs it shares the eight-stranded Greek-key β-barrel fold and a similar active site with the copper and zinc ions coordinated by the same type of residues in the same geometry. Furthermore, *P. leiognathi* Cu_2Zn_2SOD, like eukaryotic Cu_2Zn_2SODs, displays a homodimeric structure in which monomers are related by a noncrystallographic twofold axis. However, the similarities stop there, as the homodimer is formed by the interaction of two monomers through β-strands diametrically opposite those forming the monomer–monomer interface in the eukaryotic enzymes. The dimer interface is larger than that of the bovine SOD molecule and it involves mainly side chain contacts. The authors suggest that independent evolution has achieved a completely different mutual arrangement of the SOD monomers to obtain the same result. A further dramatic difference is found in the structure and in the residues forming the active site channel. Bovine SOD residues Glu-130, Glu-131, and Lys-134, which are responsible for the long-range guidance of the substrate, are missing in *P. leiognathi* SOD, which requires adopting a completely different strategy for attraction of superoxide into the active site.

This is realized by the insertion in the disulfide loop of a 8-residue loop containing the residues Lys-57, Asp-58, and Lys-60, which are indicated as the major candidates for providing the long-range guidance for the substrate, since they originate a positive electrostatic potential and are located in such a way as to be separated by the same distance in the dimer as the corresponding bovine SOD residues.

The results of *P. leiognathi* SOD structural determination and the consequent analysis strongly support the existence of a primordial SOD precursor that has evolved divergently to form the two distinct classes of prokaryotic and eukaryotic Cu_2Zn_2SODs in contrast with the previous proposal of gene transfer from the Leiognathid fish as the origin for *P. leiognathi* (*75c*).

References

1. Mann, T.; Keilin, D. *Proc. R. Soc. London* **1938,** *126,* 303.
2. McCord, J. M.; Fridovich, I. *J. Biol. Chem.* **1969,** *244,* 6049.
3. Davies, K. J. *Biochem. Soc. Symp.* **1995,** *61,* 1.
4. Halliwell, B. *Nutr. Rev.* **1994,** *52,* 253.
5. Richter, C.; Gogvadze, V.; Laffranchi, R.; Schlapbach, R.; Schweizer, M.; Suter, M.; Walter, P.; Yaffee, M. *Biochim. Biophys. Acta* **1995,** *1271,* 67.
6. Balentine, J. D. In "Pathology of Oxygen Toxicity"; Academic Press: New York, 1982; p. 359.
7. Meier, B.; Radeke, H. H.; Selle, S.; Younes, M.; Sies, H.; Resch, K.; Habermehl, G. G. *Biochem. J.* **1989,** *263,* 539.
8. McCord, J. M. *New Engl. J. Med.* **1985,** *312,* 159.
9. Foyer, C. H.; Hall, D. O. In "Chemical and Biochemical Aspects of Superoxide and Superoxide Dismutase"; Bannister, J. V., and Hill, H. A. O., Eds.; Elsevier/North-Holland: New York, Amsterdam, Oxford, 1980; pp. 380–389.
10. Elstner, E. F. In "Chemical and Biochemical Aspects of Superoxide and Superoxide Dismutase"; Bannister, J. V., and Hill, H. A. Q., Eds.; Elsevier/North-Holland: New York, Amsterdam, Oxford, 1980; pp. 390–401.
11. Allen, J. F. In "Superoxide and Superoxide Dismutases"; Michelson, A. M., McCord, J. M., and Fridovich, I., Eds.; Academic Press: New York, 1977; pp. 417–436.
12. Halliwell, B. *Prog. Biophys. Mol. Biol.* **1978,** *33,* 1.
13. Bilinski, T.; Kravwiec, Z.; Liczmanski, A.; Litwinska, J. *Biochem. Biophys. Res. Commun.* **1985,** *130,* 533.
14. Carlioz, A.; Touati, D. *EMBO J.* **1986,** *5,* 623.
15. Peng, T. X.; Moya, A.; Ayala, F. J. *Proc. Natl. Acad. Sci. U.S.A.* **1986,** *83,* 684.
16. Philips, J. P. S.; Campbell, D.; Michaud, M.; Charbonneau, M.; Hilliker, A. J. *Proc. Natl. Acad. Sci. U.S.A.* **1989,** *86,* 2761.
17. Bracco, F.; Scarpa, M.; Rigo, A.; Battistin, L. *Proc. Soc. Exp. Biol. Med.* **1991,** *196,* 36.
18. Deng, H.-X.; Hentati, A.; Tainer, J. A.; Lqbal, Z.; Cyabyab, A.; Hang, W.-Y.; Getzoff, E. D.; Hu, P.; Herzfeldt, B.; Roos, R. P.; Warner, C.; Deng, G.; Soriano, E.; Smyth, C.; Parge, H. E.; Ahmed, A.; Roses, A. D.; Hallewell, R. A.; Pericak-Vance, M. A.; Siddique, T. *Science* **1993,** *261,* 1047.
19. McCord, J. M.; Gurney, M. E. *Science* **1994,** *266,* 1586.
20. Wiedau-Pazos, M.; Goto, J. J.; Rabizadeh, S.; Gralla, E. B.; Roe, J. A.; Lee, M. K.; Valentine, J. S.; Bredesen, D. E. *Science* **1996,** *271,* 515.

21. Clark, I. A.; Chaudiri, G.; Cowden, W. B. *UCLA Symp. Mol. Cell. Biol., New Ser.* **1988,** *82,* 53.
22. Ferrante, A.; Mades, M.; Bates, E. J. D.; Goh, D. H. B.; Beard, L. J. *Immunology* **1988,** *63,* 507.
23. Klempner, M. S.; Dinarello, W. R.; Henderson, W. R.; Gallin, J. I. *J. Clin. Invest.* **1979,** *64,* 996.
24. Tsujimoto, M.; Yokota, S.; Vilcek, J.; Weissmann, G. *Biochem. Biophys. Res. Commun.* **1986,** *137,* 1094.
25. (a) Meier, B.; Redeke, H. H.; Selle, S.; Younes, M.; Sies, H.; Resch, H.; Hebermehl, G. G. *Biochem. J.* **1989,** *263,* 539; Stallings, W. C.; Pattridge, K. A.; Strong, R. K.; Ludwig, M. L.; Yamakura, F.; Isobe, T.; Steinman, H. M. In "Patterson and Patterson"; Gluşker, J. P., Patterson, B. K., and Rossi, M., Eds.; Pergamon Press: Oxford, 1987; pp. 505–513. (b) Youn, H.-D.; Youn, H.; Lee, J.-W.; Yim, Y.-I.; Lee, J. K.; Hah, Y. C.; Kang, S.-O. *Arch. Bioch. Biophys.* **1996,** *334,* 341.
26. Tyler, D. *Biochem. J.* **1975,** *147,* 493.
27. Battistoni, A.; Rotilio, G. *FEBS Lett.* **1995,** *374,* 199.
28. Getzoff, E. D.; Tainer, J. A.; Stempien, M. M.; Bell, G. I.; Hallewell, R. A. *Proteins: Struct. Funct. Genet.* **1989,** *5,* 322.
29. Pace, C. N. *Methods Enzymol.* **1986,** *131,* 266.
30. Biliaderis, C. G.; Weselake, R. J.; Petkau, A.; Friesen, A. D. *Biochem. J.* **1987,** *248,* 981.
31. Roe, J.; Butler, A.; Sholler, D.; Valentine, J.; Marky, L.; Breslauer, K. *Biochemistry* **1988,** *27,* 950.
32. Mei, G.; Rosato, N.; Silva, N.; Rusch, R.; Gratton, E.; Savini, I.; Finazzi-Agrò, A. *Biochemistry* **1992,** *31,* 7224.
33. Inouye, K.; Osaki, A.; Tonomura, B. *J. Biochem.* **1994,** *115,* 507.
34. Marmocchi, F.; Venardi, G.; Bossa, F.; Rigo, A.; Rotilio, G. *FEBS Lett.* **1978,** *94,* 109.
35. Bannister, J. V.; Anastasi, A.; Bannister, W. H. *Biochem. Biophys. Res. Commun.* **1978,** *81,* 469.
36. Kanematsu, S.; Asada, K. *Plant Cell Physiol.* **1989,** *30,* 381.
37. Richardson, D. C.; Bier, C. J.; Richardson, J. S. *J. Biol. Chem.* **1972,** *247,* 6368.
38. Thomas, K. A.; Rubin, B. H.; Bier, C. J.; Richardson, J. S.; Richardson, D. C. *J. Biol. Chem.* **1974,** *249,* 5677.
39. Richardson, D. C.; Thomas, K. A.; Richardson, J. S. *Biochem. Biophys. Res. Commun.* **1975,** *63,* 986.
40. Richardson, J. S.; Thomas, K. A.; Rubin, B. H.; Richardson, D. C. *Proc. Natl. Acad. Sci. U.S.A.* **1975,** *72,* 1349.
41. (a) Tainer, J. A.; Getzoff, E. D.; Beem, K. M.; Richardson, J. S.; Richardson, D. C. *J. Mol. Biol.* **1982,** *160,* 181; (b) Lewis, P. N.; Momany, F. A.; Sheraga, H. A. *Biochim. Biophys. Acta* **1973,** *303,* 211.
42. Hendrickson, A.; Konnert, J. A. "Biomolecular Structure, Function, Conformation and Evolution"; Pergamon Press: Oxford, 1980; pp. 43–57.
43. Hendrickson, W. A.; Konnert, J. H. In "Computing in Crystallography"; Diamond, R., Ramaseshan, S., and Venkatesan, K., Eds.; Indian Academy of Sciences: Bangalore, 1980; pp. 1–23.
44. Tainer, J. A.; Getzoff, E. D.; Richardson, J. S.; Richardson, D. C. *Nature* **1983,** *306,* 284.
45. Getzoff, E. D.; Tainer, J. A.; Weiner, P. K.; Kollman, P. A.; Richardson, J. S.; Richardson, D. C. *Nature* **1983,** *306,* 287.

46. Desideri, A.; Falconi, M.; Polticelli, F.; Bolognesi, M.; Djinovic, K.; Rotilio, G. *J. Mol. Biol.* **1992,** *223,* 337.
47. Bernstein, F. C.; Koetzle, T. F.; Williams, G. J. B.; Meyer, Jr., E. F. Rodgers, J. R.; Kennard, O.; Shimanouchi, T.; Tasumi, M. *J. Mol. Biol.* **1977,** *112,* 535.
48. Rypniewski, W. R.; Mangani, S.; Bruni, B.; Orioli, P. L.; Casati, M.; Wilson, K. S. *J. Mol. Biol.* **1995,** *251,* 282.
49. Djinovic, C. K.; Battistoni, A.; Carrì, M.; Polticelli, F.; Desideri, A.; Rotilio, G.; Coda, A.; Wilson, K.; Bolognesi, M. *Acta Crystallogr.* **1996,** *D52,* 176.
50. Meyer, E. F. *Protein Sci.* **1992,** *1,* 1543.
51. Levitt, M.; Park, B. H. *Structure* **1993,** *1,* 223.
52. Klug, D.; Rabani, J.; Fridovich, I. *J. Biol. Chem.* **1972,** *247,* 4839.
53. Sundberg, R. J.; Martin, B. R. *Chem. Rev.* **1074,** *74,* 471.
54. Forma, H. J.; Fridovich, I. *J. Biol. Chem.* **1973,** *248,* 2645.
55. Lipscomb, W. N. In "Methods for Determining Metal Ion Environments in Proteins: Structure and Function of Metalloproteins"; Darnall, D., and Wilkins, R., Eds.; Elsevier North-Holland: New York; 1980; pp. 265–302.
56. Ogihara, N. L.; Parge, H. E.; Hart, J. P.; Weiss, M. S.; Goto, J. J.; Crane, B. R.; Tsang, J.; Slater, K.; Roe, J. A.; Valentine, J. *Biochemistry* **1996,** *35,* 2316.
57. Lepock, J. R.; Arnold, L. D.; Torrie, B. H.; Andrews, B.; Kruuv, J. *Arch. Biochem. Biophys.* **1985,** *241,* 243.
58. Forman, H.; Fridovich, I. *J. Biol. Chem.* **1973,** *248,* 2645.
59. Malinowski, D.; Fridovich, I. *Biochemistry* **1979,** *18,* 5055.
60. Bertini, I.; Piccioli, M.; Viezzoli, M. S.; Chiu, C. Y.; Mullenbach, G. T. *Eur. J. Biophys.* **1994,** *23,* 167.
61. Hallewell, R. A.; Masiarz, F. R.; Najarian, R. C.; Puma, J. P.; Quiroga, M. R.; Randolph, A.; Sanchez-Pescador, R.; Scandella, C.; Smith, B.; Steimer, K. S.; Mullenbach, G. T. *Nucleic Acids Res.* **1985,** *13,* 2017.
62. Hallewell, R. A.; Mills, R.; Tekamp-Olson, P.; Blacher, R.; Rosenberg, S.; Otting, F.; Masiarz, F. R.; Scandella, C. *Biotechnology* **1987,** *5,* 363.
63. Parge, H. E.; Hallewell, R. A.; Tainer, J. *Proc. Natl. Acad. Sci. U.S.A.* **1992,** *89,* 6109.
64. Getzoff, E. D.; Cabelli, D. E.; Fisher, C. L.; Parge, H. E.; Viezzoli, M. S.; Banci, L.; Hallewell, R. A. *Nature* **1992,** *358,* 347.
65. Schininà, M. E.; Barra, D.; Bossa, F.; Calabrese, L.; Montesaro, L.; Carrì, M. T.; Mariottini, P.; Amaldi, F.; Rotilio, G. *Arch Biochem. Biophys.* **1989,** *272,* 507.
66. Capo, C. R.; Polticelli, F.; Calabrese, L.; Schininà, M. E.; Carrì, M. T.; Rotilio, G. *Biochem. Biophys. Res. Commun.* **1990,** *173,* 1186.
67. Battistoni, A.; Carrì, M. T.; Mazzetti, P.; Rotilio, G. *Biochem. Biophys. Res. Commun.* **1992,** *186,* 1339.
68. Desideri, A.; Falconi, M.; Polticelli, F.; Bolognesi, M.; Djinovic, K.; Rotilio, G. *J. Mol. Biol.* **1992,** *223,* 337.
69. Hamilton, W. C. *Acta Crystallogr.* **1965,** *18,* 502.
70. Asada, K.; Urano, M.; Takahashi, M. *Eur. J. Biochem.* **1973,** *36,* 257.
71. Kitagawa, Y.; Tsunasawa, S.; Tanaka, N.; Katsube, Y.; Sakiyama, F.; Asada, K. *J. Biochem.* **1986,** *99,* 1289.
72. Kitagawa, Y.; Tanaka, N.; Hata, Y.; Kusonoki, M.; Lee, G.; Katsube, Y.; Asada, K.; Alibara, S.; Morita, Y. *J. Biochem.* **1991,** *109,* 447.
73. Frigerio, F.; Falconi, M.; Gatti, G.; Bolognesi, M.; Desideri, A.; Marmocchi, F.; Rotilio, G. *Biochem. Biophys. Res. Commun.* **1989,** *160*(2), 677.

74. Djinovic, K.; Gatti, G.; Coda, A.; Antolini, L.; Pelosi, G.; Desideri, A.; Falconti, M.; Marmocchi, F.; Rotilio, G.; Bolognesi, M. *Acta Crystallogr.* **1991,** B47, 918.
75. (a) Djinovic, K.; Gatti, G.; Coda, A.; Antolini, L.; Pelosi, G.; Desideri, A.; Falconi, M.; Marmocchi, F.; Rotilio, G.; Bolognesi, M. *J. Mol. Biol.* **1992,** *225,* 791. (b) Bourne, Y.; Redford, S. M.; Steinman, H. M.; Lepock, J. R.; Tainer, J. A.; Getzoff, E. D. *Proc. Natl. Acad. Sci. U.S.A.* **1996,** *93,* 12774. (c) Martin, J. P.; Fridovich, I. *J. Biol. Chem.* **1981,** *256,* 6080.
76. Djinovic, K.; Coda, A.; Antilini, L.; Pelosi, G.; Desideri, A.; Falconi, M.; Rotilio, G.; Bolognesi, M. *J. Mol. Biol.* **1992,** *226,* 227.
77. Beckman, J.; Beckman, T.; Chen, J.; Marshall, P.; Freeman, B. *Proc. Natl. Acad. Sci. U.S.A.* **1990,** *87,* 1621.
78. Ischiropoûlos, H.; Zhu, L.; Chen, J.; Tsai, M.; Martin, J. C.; Smith, C. D.; Beckman, J. S. *Arch. Biochem. Biophys.* **1992,** *298,* 431.
79. Smith, C. D.; Carson, M.; van der Woerd, M.; Chen, J.; Ischiropoulos, H.; Beckman, J. S. *Arch. Biochem. Biophys.* **1992,** *299,* 350.
80. McRee, D. E.; Redford, S. M.; Getzoff, E. D.; Lepock, J. R.; Hallewell, R. A.; Tainer, J. A. *J. Biol. Chem.* **1990,** *265,* 14234.
81. Roberts, V. A.; Fisher, C. L.; Redford, S. M.; McRee, D. E.; Parge, H. E.; Getzoff, E. D.; Tainer, J. A. *Free Radical Res. Commun.* **1990,** *12–13,* 269.
82. Banci, L.; Bertini, I.; Bruni, B.; Carloni, P.; Luchinat, C.; Mangani, S.; Orioli, P. L.; Piccioli, M.; Rypniewski, W.; Wilson, K. *Biochem. Biophys. Res. Commun.* **1994,** *202,* 1088.
83. (a) Orpen, G.; Brammer, L.; Allen, F. H.; Kennard, O.; Watson, D. G. *J. Chem. Soc., Dalton Trans.* **1989,** S1; (b) unpublished results from our laboratory.
84. Stragsm G.; Kraut, J. *J. Mol. Biol.* **1968,** *35,* 503.
85. Bondi, A. *J. Phys. Chem.* **1964,** *68,* 441.
86. Lee, D.-H.; Nei, N.; Huntly, N. N.; Tyeklier, Z.; Kerlin, K. D.; Kaderli, S.; Jung, B.; Zuberbühler, A. D. *J. Am. Chem. Soc.* **1995,** *117,* 12498.
87. Djinovic Carugo, K.; Battistoni, A.; Carri, M. T.; Polticelli, F.; Desideri, A.; Rotilio, G.; Coda, A.; Bolognesi, M. *FEBS Lett.* **1994,** *349,* 93.
88. Banci, L.; Bertini, I.; Buchinat, C.; Scozzafava, A. *J. Biol. Chem.* **1989,** *264,* 9742.
89. Banci, L.; Bencini, A.; Bertini, I.; Luchinat, C.; Piccioli, M. *Inorg. Chem.* **1990,** *29,* 4867.
90. Djinovic, K.; Polticelli, F.; Desideri, A.; Rotilio, G.; Wilson, K.; Bolognesi, M. *J. Mol. Biol.* **1994,** *240,* 179.
91. Rotilio, G.; Bray, R. C.; Fielden, E. M. *Biochim. Biophys Acta* **1972,** *268,* 605.
92. Cabelli, D. E.; Bielski, B. H. *J. Phys. Chem.* **1983,** *87,* 1809.
93. Bielski, B. H. J.; Cabelli, D. E.; Arudi, R. L.; Ross, A. B. *J. Phys. Chem. Ref. Data* **1985,** *14,* 1041.
94. Salmon, G. A.; Sykes, A. G. *Methods Enzymol.* **1993,** *227,* 522.
95. Fisher, C. L.; Cabelli, D. E.; Tainer, J. A.; Hallewell, R. A.; Getzoff, E. D. *Proteins: Struct. Funct. Genet.* **1994,** *19,* 24.
96. Banci, L.; Bertini, I.; Cabelli, D. E.; Hallewell, R. A.; Tung, J. W.; Viezzoli, M. S. *Eur. J. Biochem.* **1991,** *196,* 123.
97. Klug-Roth, D.; Fridovich, I.; Rabani, J. *J. Am. Chem. Soc.* **1973,** *95,* 2786.
98. Bray, R. C.; Clocke, S. A.; Fielden, E. M.; Roberts, P. B.; Rotilio, G.; Calabrese, L. *Biochem. J.* **1974,** *139,* 43.
99. Fee, J. A.; Bull, C. *J. Biol. Chem.* **1986,** *261,* 13000.
100. Rigo, A.; Viglino, P.; Rotilio, G. *Anal. Biochem.* **1975,** *68,* 1.

101. Argese, E.; Orsega, E.; De Carli, B.; Scarpa, M.; Rigo, A. *Bioelectrochem. Bioenerg.* **1984,** *13,* 385.
102. Banci, L.; Bertini, I.; Viezzoli, M. S.; Argese, E.; Orsega, E.; Chin, C. Y.; Mullenbach, G. T. *JBIC,* **1997,** *2,* 295.
103. Briggs, R. G.; Fee, J. A. *Biochim. Biophys. Acta* **1978,** *537,* 86.
104. Beyer, Jr., W. F.; Fridovich, I.; Mullenbach, G. T.; Hallewell, R. A. *J. Biol. Chem.* **1987,** *262,* 11182.
105. Cudd, A.; Fridovich, I. *J. Biol. Chem.* **1982,** *257,* 11443.
106. Mota De Freitas, D.; Luchinat, C.; Banci, L.; Bertini, I.; Valentine, J. S. *Inorg. Chem.* **1987,** *26,* 2788.
107. Mota De Freitas, D.; Valentine, J. S. *Biochemistry* **1984,** *23,* 2079.
108. Paoletti, F.; Aldinucci, D.; Mocali, A.; Caparrini, A. *Anal. Biochem.* **1986,** *154,* 536.
109. Paoletti, F.; Mocali, A. *Methods Enzymol.* **1990,** *186,* 209.
110. Paoletti, F.; Mocali, A.; Aldinucci, D. *Chem. Biol. Interactions* **1990,** *76,* 3.
111. Beauchamp, C.; Fridovich, I. *Anal. Biochem.* **1971,** *44,* 276.
112. Bertini, I.; Banci, L.; Luchinat, C.; Bielski, B. H. J.; Cabelli, D.; Mullenbach, G. T.; Hallewell, R. A. *J. Am. Chem. Soc.* **1989,** *111,* 714.
113. Argese, E.; Rigo, A.; Viglino, P.; Orsega, E.; Marmocchi, F.; Cocco, D.; Rotilio, G. *Biochim. Biphys. Acta* **1984,** *787, 205.*
114. Terenzi, M.; Rigo, A.; Franconi, C.; Mondovi, B.; Calabrese, L.; Rotilio, G. *Biochim. Biophys. Acta* **1974,** *351,* 230.
115. Banci, L.; Bertini, I.; Cabelli, D.; Hallewell, R. A.; Luchinat, C.; Viezzoli, M. S. *Inorg. Chem.* **1990,** *29,* 2398.
116. O'Neill, P.; Davies, S.; Fielden, E. M.; Calabrese, L.; Capo, C.; Marmocchi, F.; Natoli, G.; Rotilio, G. *Biochem. J.* **1988,** *251,* 41.
117. Polticelli, F.; O'Neill, P.; Costanzo, S.; Lania, A.; Rotilio, G.; Desideri, A. *Arch. Biochem. Biophys.* **1995,** *321,* 123.
118. Argese, E.; Viglino, P.; Rotilio, G.; Scarpa, M.; Rigo, A. *Biochemistry* **1987,** *26,* 3224.
119. Banci, L.; Bertini, I.; Luchinat, C.; Viezzoli, M. S. *Inorg. Chem.* **1993,** *32,* 1403.
120. Banci, L.; Bertini, I.; Turano, P. *Eur. Biophys. J.* **1991,** *19,* 141.
121. Rigo, A.; Viglino, P., Rotilio, G.; Tomat, R. *FEBS Lett.* **1995,** *50,* 86.
122. Klapper, I.; Hagstrom, R.; Fine, R.; Sharp, K.; Honig, B. *Proteins: Struct. Funct. Genet.* **1986,** *1,* 47.
123. Sharp, K.; Fine, R.; Honig, B. *Science* **1987,** *236,* 1460.
124. Banci, L.; Bertini, I.; Chiu, C. Y.; Mullenbach, G. T.; Viezzoli, M. S. *Eur. J. Biochem.* **1995,** *234,* 855.
125. Sines, J. J.; Allison, S. A.; McCammon, J. A. *Biochemistry* **1990,** *29,* 9403.
126. Sines, J. J.; McCammon, J. A.; Allison, S. A. *J. Comp. Chem.* **1992,** *13,* 66.
127. Falconi, M.; Rotilio, G.; Desideri, A. *Proteins: Struct. Funct. Genet.* **1991,** *10,* 149.
128. Polticelli, F.; Falconi, M.; O'Neill, P.; Petruzelli, R.; Galtieri, A.; Lania, A.; Calabrese, L.; Rotilio, G.; Desideri, A. *Arch. Biochem. Biophys.* **1994,** *312,* 22.
129. Carloni, P.; Blochl, P. E.; Parrinello, M. *J. Phys. Chem.* **1995,** *99,* 1338.
130. Luty, B. A.; El Amrani, S.; McCammon, J. A. *J. Am. Chem. Soc.* **1993,** *115,* 11874.
131. Koppenol, W. H. In "Oxygen and Oxoradicals in Chemistry and Biology"; Rodgers, M. A. J., and Powers, E. L., Eds.; Academic Press: New York, 1981; pp. 671–674.
132. Shen, J.; Wong, C. F.; Subrasmaniam, S.; Albright, T. A.; McCammon, J. A. *J. Comp. Chem.* **1990,** *11,* 346.
133. Allison, S. A.; McCammon, J. A. *J. Chem. Phys.* **1985,** *89,* 1072.
134. Bacquet, R. J.; McCammon, J. A.; Allison, S. A. *J. Phys. Chem.* **1988;** *92,* 7134.

135. Shen, J.; McCammon, J. A. *Chem. Phys.* **1991,** *158,* 191.
136. Shen, J.; Subramanian, S.; Wong, C. F.; McCammon, J. A. *Biopolymers* **1989,** *28, 2085.*
137. Shen, J.; McCammon, J. A. *J. Comp. Chem.* **1986,** *7,* 346.
138. Davis, M. E.; McCammon, J. A. *Chem. Rev.* **1990,** *90,* 509.
139. Banci, L.; Carloni, P.; La Penna, G.; Orioli, P. L. *J. Am. Chem. Soc.* **1992,** *114,* 6994.
140. Banci, L.; Carloni, P.; Orioli, P. L. *Proteins: Struct. Funct. Genet.* **1994,** *18,* 216.
141. Banci, L.; Cabelli, D. E.; Getzoff, E. D.; Hallewell, R. A.; Viezzoli, M. S. *J. Inorg. Biochem.* **1993,** *50,* 89.
142. Takahara, M.; Sagai, H.; Inouye, S.; Inouye, M. *Biotechnology* **1988,** *6,* 195.
143. Hallewell, R. A.; Laria, I.; Tabrizi, A.; Carlin, G.; Getzoff, E. D.; Tainer, J. A.; Cousens, L. S.; Mullenbach, G. T. *J. Biol. Chem.* **1989,** *264,* 5260.
144. Steinman, H. *J. Biol. Chem.* **1987,** *262,* 1882.
145. Buechel, D. E.; Gronenborn, B.; Mueller-Hill, B. *Nature* **1980,** *283,* 541.
146. Tibell, L.; Hjalmarsson, K.; Edlund, T.; Skogman, G.; Engstrom, A.; Aasa, R.; Markland, S. In "Oxy-Radicals in Molecular Biology and Pathology"; Cerutti, P. A., Fridovich, I., and McCord, J. M., Eds.; Liss: New York, 1988; pp. 233–245.
147. Tibell, L.; Hjalmarsson, K.; Edlund, T.; Skogman, G.; Engstrom, A.; Marklund, S. L. *Proc. Natl. Acad. Sci. U.S.A.* **1987,** *84,* 6634.
148. Studier, F. W.; Rosenberg, A. H.; Dunn, J. J.; Dubendorff, J. W. *Methods Enzymol.* **1990,** *185,* 66.
149. Graden, J. A.; Ellerby, L. M.; Roe, J. A.; Valentine, J. S. *J. Am. Chem. Soc.* **1994,** *116,* 9743.
150. Lu, Y.; Gralla, E. B.; Roe, J. A.; Valentine, J. S. *J. Am. Chem. Soc.* **1992,** *114,* 3560.
151. Battistoni, A.; Carri, M. T.; Mazzetti, A. P.; Rotilio, G. *Biochem. Biophys. Res. Commun.* **1992,** *186,* 1339.
152. Chen, Y.-L.; Park, S.; Thornburg, R. W.; Tabatabai, L. B.; Kintanar, A. *Biochemistry* **1995,** *34,* 12265.
153. Malinowski, D. P.; Fridovich, I. *Biochemistry* **1979,** *18,* 5909.
154. Borders, Jr., C. L.; Johansen, J. T. *Biochem. Biophys. Res. Commun.* **1980,** *96,* 1071.
155. Bermingham-McDonough, O.; Mota De Freitas, D.; Kunamoto, A.; Saunders, J. E.; Blech, D. M.; Borders, C. L.; Valentine, J. S. *Biochem. Biophys. Res. Commun.* **1982,** *108,* 1376.
156. Borders, C. L.; Fridovich, I. *Arch. Biochem. Biophys.* **1985,** *241,* 472.
157. Marmocchi, F.; Mavelli, I.; Rigo, A.; Stevanato, R.; Bossa, F.; Rotilio, G. *Biochemistry* **1982,** *21,* 2853.
158. Cocco, D.; Rossi, L.; Barra, D.; Bossa, F.; Rotilio, G. *FEBS Lett.* **1982,** *150, 303.*
159. Mota De Freitas, D.; Ming, L. J.; Ramasamy, R.; Valentine, J. S. *Inorg. Chem.* **1990,** *29,* 3512.
160. Boccu', E.; Velo, G. P.; Veronese, F. M. *Pharmacol. Res. Comm.* **1982,** *14,* 113.
161. Conforti, A.; Franco, L.; Milanino, R.; Velo, G. P.; Boccu', E.; Largajolli, R.; Schiavon, O.; Veronese, F. M. *Pharmacol. Res. Comm.* **1987,** *19,* 287.
162. Veronese, F. M.; Caliceti, P.; Pastorino, A.; Schiavon, O.; Sartore, L.; Banci, L.; Monsu Scolaro, L. *J. Control. Rel.* **1989,** *10,* 145.
163. Banci, L.; Bertini, I.; Caliceti, P.; Monsu' Scolaro, L.; Schiavon, O.; Veronese, F. M. *J. Inorg. Biochem.* **1990,** *39,* 149.
164. Rotilio, G.; Morpurgo, L.; Giovagnoli, L.; Calabrese, L.; Mondovi, B. *Biochemistry* **1972,** *11,* 2187.

165. Fielden, E. M.; Roberts, P. B.; Bray, R. C.; Rotilio, G. *Biochem. Soc. Trans.* **1973,** *1,* 52.
166. Fuchs, H. J. R.; Borders, Jr., C. L. *Biochem. Biophys. Res. Commun.* **1983,** *116,* 1107.
167. Rotilio, G.; Morpurgo, L.; Calabrese, L.; Mondovi, B. *Biochim. Biophys. Acta* **1973,** *302, 229.*
168. Bertini, I.; Luchinat, C.; Viezzoli, M. S.; Wang, Y. *Arch. Biochem. Biophys.* **1989,** *269,* 586.
169. Uchida, K.; Kawakishi, S. *J. Biol. Chem.* **1994,** *269,* 2405.
170. Bannister, J. V.; Bannister, W. H.; Wood, W. *Eur. J. Biochem.* **1971,** *18,* 178.
171. Fielden, E. M.; Roberts, P. B.; Bray, R. C.; Lowe, D. J.; Mautner, G. N.; Rotilio, G.; Calabrese, L. *Biochem. J.* **1974,** *139,* 49.
172. Banci, L.; Bertini, I.; Bauer, D.; Hallewell, R. A.; Viezzoli, M. S. *Biochemistry* **1993,** *32,* 4384.
173. Valentine, J. S.; Pantoliano, M. W.; McDonnell, P. J.; Burger, A. R.; Lippard, S. J. *Proc. Natl. Acad. Sci. U.S.A.* **1979,** *76,* 4245.
174. Scozzofava, A.; Viezzoli, M. S. *Mol. Chem. Neuropath.* **1993,** *19,* 193.
175. Polticelli, F.; Bottaro, G.; Battistoni, A.; Carri, M. T.; Djinovic, K.; Bolognesi, M.; O'Neill, P.; Rotilio, G.; Desideri, A. *Biochemistry* **1995,** *34,* 6043.
176. Lu, Y.; LaCroix, L. B.; Lowery, M. D.; Solomon, E. I.; Bender, C. J.; Peisach, J.; Roe, J. A.; Gralla, E. B.; Valentine, J. S. *J. Am. Chem. Soc.* **1993,** *115,* 5907.
177. Lu, Y.; Roe, J. A.; Gralla, E. B.; Valentine, J. S. In "Bioinorganic Chemistry of Copper"; Karlin, K. D., Ed.; Chapman & Hall: New York, 1993; p. 64.
178. Lu, Y.; Roe, J. A.; Bender, C. J.; Peisach, J.; Banci, L.; Bertini, I.; Gralla, E. B.; Valentine, J. S. *Inorg. Chem.* **1996,** *35,* 1692.
179. Banci, L.; Bertini, I.; Borsari, M.; Viezzoli, M. S.; Hallewell, R. A. *Eur. J. Biochem.* **1995,** *232,* 220.
180. Pantoliano, M. W.; McDonnel, P. J.; Valentine, J. S. *J. Am. Chem. Soc.* ***1979,*** *101,* 6454.
181. Fee, J. A.; Phillips, W. D. *Biochim. Biophys. Acta* **1975,** *412,* 26.
182. Dunbar, J. C.; Johansen, J. T.; Uchida, T. *Carlsberg Res. Commun.* **1982,** *47,* 163.
183. Beem, K. M.; Rich, P.; Rajagopalan, K. V. *J. Biol. Chem.* **1974,** *249,* 4229.
184. Pantoliano, M. W.; Valentine, J. S.; Mammone, R. J.; Scholler, D. M. *J. Am. Chem. Soc.* **1982,** *104,* 1717.
185. Ming, L. J.; Valentine, J. S. *J. Am. Chem. Soc.* **1990,** *112,* 6374.
186. Cotton, F. A.; Wilkinson, G. "Advanced Inorganic Chemistry"; Wiley: New York, 1990.
187. Banci, L.; Bertini, I.; Luchinat, C.; Monnanni, R.; Scozzafava, A. *Inorg. Chem.* **1987,** *26,* 153.
188. Roe, J. A.; Peoples, R.; Scholler, D. M.; Valentine, J. S. *J. Am. Chem. Soc.* **1990,** *112,* 1538.
189. Fee, J. A. *J. Biol. Chem.* **1973,** *248,* 4229.
190. Hirose, J.; Iwatsuka, K.; Kidani, Y. *Biochem. Biophys. Res. Commun.* **1981,** *98,* 58.
191. Ming, L. J.; Valentine, J. S. *J. Am. Chem. Soc.* **1990,** *112,* 4256.
192. Viezzoli, M. S.; Wang, Y. *Inorg. Chim. Acta* **1988,** *153,* 189.
193. Dunbar, J. C.; Holmquist, B.; Johansen, J. T. *Biochemistry* **1984,** *23,* 4324.
194. Dunbar, J. C.; Holmquist, B.; Johansen, J. T. *Biochemistry* **1984,** *23,* 4330.
195. Ming, L. J.; Banci, L.; Luchinat, C.; Bertini, I.; Valentine, J. S. *Inorg. Chem.* **1988,** *27,* 728.
196. Bailey, D. B.; Ellis, P. D.; Fee, J. A. *Biochemistry* **1980,** *19,* 591.

197. Kofod, P.; Bauer, R.; Danielsen, E.; Larsen, E.; Bjerrum, M. J. *Eur. J. Biochem.* **1991,** *198,* 607.
198. Bauer, R.; Demeter, I.; Hasemann, V.; Johansen, J. T. *Biochem. Biophys. Res. Commun.* **1980,** *94,* 1296.
199. Bjerrum, M. J.; Kofod, P.; Bauer, R.; Danielsen, E. In "Proc. 5th Conf. Superoxide and Superoxide Dismutase"; Czapski, G., Ed.; Jerusalem, 1989.
200. Hirose, J.; Iwatzuka, K.; Kidani, Y. *Biochem. Biophys. Res. Commun.* **1981,** *98,* 58.
201. Hirose, J.; Yamada, M.; Hayakawa, C.; Nagao, H.; Noji, M.; Kidani, Y. *Biochem. Int.* **1984,** *8,* 401.
202. Forman, H. J.; Fridovich, I. *J. Biol. Chem.* **1973,** *248,* 2645.
203. Blackburn, N. J.; Hasnain, S. S.; Binsted, N.; Diakun, G. P.; Garner, C. D.; Knowles, P. F. *Biochem. J.* **1984,** *219,* 985.
204. Banci, L.; Bencini, A.; Bertini, I.; Luchinat, C.; Viezzoli, M. S. *Gazz. Chim. Ital.* **1990,** *120,* 179.
205. Gaber, B. P.; Brown III, R. D.; Koenig, S. H.; Fee, J. A. *Biochim. Biophys. Acta* **1972,** *271,* 1.
206. Boden, N.; Holmes, M. C.; Knowles, P. F. *Biochem. J.* **1979,** *177,* 303.
207. Bertini, I.; Banci, L.; Brown III, R. D.; Koenig, S. H.; Luchinat, C. *Inorg. Chem.* **1988,** *27,* 951.
208. Banci, L.; Bertini, I.; Hallewell, R. A.; Luchinat, C.; Viezzoli, M. S. *Eur. J. Biochem.* **1989,** *184,* 125.
209. Solomon, I. *Phys. Rev.* **1955,** *99,* 559.
210. Bertini, I.; Luchinat, C.; Mancini, M.; Spina, G. In "Magneto-Structural Correlations in Exchange-Coupled Systems"; Gatteschi, D., Kahn, O., and Willett, R. D., Eds.; Reidel Publishing Company: Dordrecht, 1985; pp. 421–461.
211. Bertini, I.; Lanini, G.; Luchinat, C.; Mancini, M.; Spina, G. *J. Magn. Reson.* **1985,** *63,* 56.
212. Bertini, I.; Briganti, F.; Luchinat, C.; Mancini, M.; Spina, G. *J. Magn. Reson.* **1985,** *63,* 41.
213. Koenig, S. H.; Brown III, R. D. In "Metal Ions in Biological Systems, Vol. 21"; Sigel, H., Ed.; Marcel Dekker: New York, 1987; p. 239.
214. Bertini, I.; Galas, O.; Luchinat, C.; Parigi, G. *J. Magn. Reson.* **1995,** *113,* 151.
215. Bertini, I.; Luchinat, C.; Banci, L.; Viezzoli, M. S. *Biol. Met.* **1990,** *3,* 146.
216. Bertini, I.; Scozzafava, A. In "Metal Ions in Biological Systems"; Sigel, H., Ed.; Marcel Dekker: New York and Basel, 1981; pp. 31–74.
217. Bertini, I.; Luchinat, C.; Messori, L. *Biochem. Biophys. Res. Commun.* **1981,** *101,* 577.
218. Fee, J. A.; Gaber, B. P. *J. Biol. Chem.* **1972,** *247,* 60.
219. Banci, L.; Bertini, I.; Luchinat, C.; Monnanni, R.; Scozzafava, A. *Inorg. Chem.* **1988,** *27,* 107.
220. Bertini, I.; Luchinat, C.; Monnanni, R.; Scozzafava, A.; Borghi, E. *Inorg. Chim. Acta* **1984,** *91,* 109.
221. St. Clair, C. S.; Gray, H. B.; Valentine, J. S. *Inorg. Chem.* **1992,** *31,* 925.
222. Lawrence, G. D.; Sawyer, D. T. *Biochemistry* **1979,** *18,* 3045.
223. Fee, J. A.; DiCorleto, P. E. *Biochemistry* **1973,** *12,* 4893.
224. Verhagen, M. F. J. M.; Meussen, E. T. M.; Hagen, W. R. *Biochim. Biophys. Acta* **1995,** *1244,* 99.
225. Armstrong, F. A. *Struct. Bonding* **1990,** *72,* 137.
226. Berg, H. In "Comprehensive Treatise of Electrochemistry"; Srinivasan, S., Chiz-

madzhev, Y. A., Bockris, J. O'M., Conway, B. E., and Yeager, E., Eds.; Plenum: New York, 1985; p. 190.
227. Azab, H. A.; Banci, L.; Borsari, M.; Luchinat, C.; Sola, M.; Viezzoli, M. S. *Inorg. Chem.* **1992,** *31,* 4649.
228. Zuman, P. In "The Elucidation of Organic Electrode Processes"; Academic Press: New York, 1969; p. 176.
229. Ozaki, S.; Hirose, J.; Kidani, Y. *Inorg. Chem.* **1988,** *27,* 3746.
230. Bertini, I.; Hiromi, K.; Hirose, J.; Sola, M.; Viezzoli, M. S. *Inorg. Chem.* **1993,** *32,* 1106.
231. Bertini, I.; Banci, L.; Luchinat, C.; Piccioli, M. *Coord. Chem. Rev.* **1990,** *100,* 67.
232. Mangani, S.; Orioli, P. L.; Carloni, P. *Inorg. Chim. Acta* **1994,** *216,* 121.
233. Bertini, I.; Luchinat, C.; Monnanni, R. *J. Am. Chem. Soc.* **1985,** *107,* 2178.
234. Solomon, E. I.; Hare, J. W.; Dooley, D. M.; Dawson, J. H.; Stephens, P. J.; Gray, H. B. *J. Am. Chem. Soc.* **1980,** *102,* 168.
235. Dawson, J. H.; Dooley, D. M.; Clark, R.; Stephens, P. J.; Gray, H. B. *J. Am. Chem. Soc.* **1979,** *101,* 5046.
236. Dooley, D. M.; Rawlings, J.; Dawson, J. H.; Stephens, P. J.; Andreasson, L.-E.; Malmstrom, B. G.; Gray, H. B. *J. Am. Chem. Soc.* **1979,** *101,* 5038.
237. Rosenberg, R. C.; Root, C. A.; Bernstein, P. K.; Gray, H. B. *J. Am. Chem. Soc.* **1975,** *97,* 2092.
238. Solomon, E. I.; Hare, J. W.; Gray, H. B. *Proc. Natl. Acad. Sci. U.S.A.* **1976,** *97,* 2092.
239. Pantoliano, M. W.; Valentine, J. S.; Nafie, L. A. *J. Am. Chem. Soc.* **1982,** *104,* 6310.
240. Fawcett, T. G.; Bernarducci, E. E.; Krogh-Jespersen, K.; Schugar, H. J. *J. Am. Chem. Soc.* **1980,** *102,* 1686.
241. Bernarducci, E.; Schwindinger, W. F.; Hughey, J. L.; Krogh-Jespersen, K.; Schugar, H. J. *J. Am. Chem. Soc.* **1981,** *103,* 1686.
242. Rotilio, G.; Calabrese, L.; Bossa, F.; Barra, D.; Finazzi Agro', A.; Mondovì, B. *Biochemistry* **1972,** *11,* 2182.
243. Beem, K. M.; Rich, W. E.; Rajagopalan, K. V. *J. Biol. Chem.* **1974,** *249,* 7298.
244. Beem, K. M.; Richardson, D. C.; Rajagopalan, K. V. *Biochemistry* **1977,** *16,* 1930.
245. Liebermann, R. A.; Sands, R. H.; Fee, J. A. *J. Biol. Chem.* **1982,** *257,* 336.
246. Osman, R.; Basch, H. *J. Am. Chem. Soc.* **1984,** *106,* 5710.
247. Fee, J. A.; Peisach, J.; Mims, W. B. *J. Biol. Chem.* **1981,** *256,* 1910.
248. Huettermann, J.; Kappl, R.; Banci, L.; Bertini, I. *Biochim. Biophys. Acta* **1988,** *956,* 173.
249. Reinhard, H.; Kappl, R.; Huttermann, J.; Viezzoli, M. S. *J. Phys. Chem.* **1994,** *98,* 8806.
250. Dykanov, S.; Felli, I. C.; Viezzoli, M. S.; Spoyalov, A.; Huttermann, J. *FEBS Lett.* **1994,** *345,* 55.
251. Lippard, S. J.; Burger, A. R.; Ugurbil, K.; Pantoliano, M. W.; Valentine, J. S. *Biochemistry* **1977,** *16,* 1136.
252. Fee, J. A.; Briggs, R. G. *Biochim. Biophys. Acta* **1975,** *400,* 439.
253. Fee, J. A. *Biochim. Biophys. Acta* **1973,** *295,* 107.
254. Bencini, A.; Gatteschi, D. In "Transition Metal Chemistry"; Melson, G. A., and Figgis, B. N., Eds.; Marcel Dekker: New York and Basel, 1982; pp. 1–178.
255. Bencini, A.; Gatteschi, D. "Electron Paramagnetic Resonance of Exchange-Coupled Systems"; Springer-Verlag: Berlin and New York, 1990.
256. Strothkamp, K. G.; Lippard, S. J. *J. Am. Chem. Soc.* **1982,** *104,* 852.
257. Morgenstern-Badarau, I.; Cocco, D.; Desideri, A.; Rotilio, G.; Jordanov, J.; Dupre', N. *J. Am. Chem. Soc.* **1986,** *108,* 300.

258. Ming, L. J.; Valentine, J. S. *J. Am. Chem. Soc.* **1987,** *109,* 4426.
259. Calabrese, L.; Cocco, D.; Desideri, A. *FEBS Lett.* **1979,** *106,* 142.
260. Banci, L.; Bertini, I.; Luchinat, C.; Monnanni, R.; Scozzafava, A.; Salvato, B. *Gazz. Chim. Ital.* **1986,** *116,* 51.
261. Desideri, A.; Paci, M.; Capo, C.; Calabrese, L.; Rotilio, G. *J. Inorg. Biochem.* **1988,** *33,* 277.
262. Bertini, I.; Lanini, G.; Luchinat, C.; Messori, L.; Monnanni, R.; Scozzafava, A. *J. Am. Chem. Soc.* **1985,** *107,* 4391.
263. Rigo, A.; Viglino, P.; Rotilio, G. *Biochem. Biophys. Res. Commun.* **1975,** *63,* 1013.
264. Rigo, A.; Stevanato, R.; Viglino, P.; Rotilio, G. *Biochem. Biophys. Res. Commun.* **1977,** *79,* 776.
265. Strothkamp, K. G.; Lippard, S. J. *Biochemistry* **1981,** *20,* 7488.
266. Bertini, I.; Luchinat, C.; Scozzafava, A. *J. Am. Chem. Soc.* **1980,** *102,* 7349.
267. Bertini, I.; Borghi, E.; Luchinat, C.; Scozzafava, A. *J. Am. Chem. Soc.* **1981,** *103,* 7779.
268. Han, J.; Blackburn, N. J.; Loehr, T. M. *Inorg. Chem.* **1992,** *31,* 3223.
269. Djinovic, K.; Battistoni, A.; Carri, M. T.; Polticelli, F.; Desideri, A.; Rotilio, G.; Coda, A.; Bolognesi, M. *FEBS Lett.* **1994,** *349,* 93.
270. Banci, L.; Bertini, I.; Luchinat, C.; Hallewell, R. A. *J. Am. Chem. Soc.* **1988,** *110,* 3629.
271. Bertini, I.; Luchinat, C.; Macinai, R.; Piccioli, M.; Scozzafava, A.; Viezzoli, M. S. *J. Magn. Reson. Ser. B* **1994,** *B104,* 95.
272. Morpurgo, L.; Giovagnoli, C.; Rotilio, G. *Biochim. Biophys. Acta* **1973,** *322,* 204.
273. Dooley, D. M.; McGuirl, M. A. *Inorg. Chem.* **1986,** *25,* 1261.
274. Viglino, P.; Rigo, A.; Stevanato, R.; Ranieri, G. A.; Rotilio, G.; Calabrese, L. *J. Magn. Reson.* **1979,** *34,* 265.
275. Banci, L.; Bertini, I.; Luchinat, C.; Scozzafava, A.; Turano, P. *Inorg. Chem.* **1989,** *28,* 2377.
276. Van Camp, H. L.; Sands, R. H.; Fee, J. A. *Biochim. Biophys. Acta* **1982,** *704,* 75.
277. Sette, M.; Paci, M.; Desideri, A.; Rotilio, G. *Biochemistry* **1992,** *31,* 12410.
278. Searcy, D. G.; Whitehead, J. P.; Maroney, M. J. *Arch. Biochem. Biophys.* **1995,** *318,* 251.
279. Wittenkeller, L.; Abraha, A.; Ramasamy, R.; Mota De Freitas, D.; Theisen, L. A.; Crans, D. C. *J. Am. Chem. Soc.* **1991,** *113,* 7872.
280. Cass, A. E. G.; Hill, H. A. O.; Smith, B. E.; Bannister, J. V.; Bannister, W. H. *Biochemistry* **1977,** *16,* 3061.
281. Cass, A. E. G.; Hill, H. A. O.; Smith, B. E.; Bannister, J. V.; Bannister, W. H. *Biochem. J.* **1977,** *165,* 587.
282. Cass, A. E. G.; Hill, H. A. O.; Hasemann, V.; Johansen, J. T. *Carlsberg Res. Commun.* **1978,** *43,* 439.
283. Banci, L.; Bertini, I.; Luchinat, C.; Viezzoli, M. S. *Inorg. Chem.* **1990,** *29,* 1438.
284. McAdam, M. E.; Fielden, E. M.; Lavelle, F.; Calabrese, L.; Cocco, D.; Rotilio, G. *Biochem. J.* **1977,** *167,* 271.
285. Moss, T. H.; Fee, J. A. *Biochem. Biophys. Res. Commun.* **1975,** *66,* 799.
286. Bertini, I.; Luchinat, C.; Piccioli, M.; Vicens Oliver, M.; Viezzoli, M. S. *Eur. Biophys. J.* **1991,** *20,* 269.
287. Merli, A.; Rossi, G.; Djinovic, K.; Bolognesi, M.; Desideri, A.; Rotilio, G. *Biochem. Biophys. Res. Commun.* **1995,** *210,* 1040.
288. Ming, L. J.; Banci, L.; Luchinat, C.; Bertini, I.; Valentine, J. S. *Inorg. Chem.* **1988,** *27,* 4458.

289. Gurbiel, R. J.; Peoples, R.; Doan, P. E.; Cliine, J. F.; McCracken, J.; Peisach, J.; Hoffman, B. M.; Valentine, J. S. *Inorg. Chem.* **1993,** *32,* 1813.

290. Bertini, I.; Luchinat, C. In "Bioinorganic Chemistry"; Bertini, I., Gray, H. B., Lippard, S. J., and Valentine, J. S., Eds.; University Science Books: Mill Valley, 1994; pp. 37–106.

291. Bailey, D. B.; Ellis, P. D.; Fee, J. A. *Biochemistry* **1980,** *19,* 591.

292. Armitage, I. M.; Uiterkamp, A. J. M. S.; Chlebowski, J. F.; Coleman, J. E. *J. Magn. Reson.* **1978,** *29,* 375.

293. Summers, M. F.; van Rijn, J.; Reedijk, J.; Marzilli, L. G. *J. Am. Chem. Soc.* **1986,** *108,* 4254.

294. Bauer, R.; Demeter, I.; Hasemann, V.; Johansen, J. T. *Biochem. Biophys. Res. Commun.* **1980,** *94,* 1296.

295. Bertini, I.; Luchinat, C. "NMR of Paramagnetic Molecules in Biological Systems"; Benjamin/Cummings: Menlo Park, CA, 1986.

296. Banci, L.; Bertini, I.; Luchinat, C.; Scozzafava, A. *J. Am. Chem. Soc.* **1987,** *109,* 2328.

297. Banci, L.; Bertini, I.; Luchinat, C.; Piccioli, M.; Scozzafava, A.; Turano, P. *Inorg. Chem.* **1989,** *28,* 4650.

298. Banci, L.; Bertini, I.; Luchinat, C.; Piccioli, M.; Scozzafava, A. *Gazz. Chim. Ital.* **1993,** *123,* 95.

299. Bertini, I.; Piccioli, M.; Scozzafava, A.; Viezzoli, M. S. *Magn. Reson. Chem.* **1993,** *31,* S17.

300. Paci, M.; Desideri, A.; Sette, M.; Falconi, M.; Rotilio, G. *FEBS Lett.* **1990,** *261,* 231.

301. Sette, M.; Paci, M.; Desideri, A.; Rotilio, G. *Eur. J. Biochem.* **1993,** *213,* 391.

302. Bertini, I.; Luchinat, C.; Ming, L. J.; Piccioli, M.; Sola, M.; Valentine, J. S. *Inorg. Chem.* **1992,** *31,* 4433.

303. Burger, A. R.; Lippard, S. J.; Pantoliano, M. W.; Valentine, J. S. *Biochemistry* **1980,** *19,* 4139.

304. Hill, H. A. O.; Lee, W. K.; Bannister, J. V.; Bannister, W. H. *Biochem. J.* **1980,** *185,* 245.

305. Fee, J. A.; Ward, R. L. *Biochem. Biophys. Res. Commun.* **1976,** *71,* 427.

306. Valentine, J. S.; Pantoliano, M. W. In "Copper Proteins"; Spiro, T. G., Ed.; Wiley: New York, 1981; pp. 291.

307. Fridovich, I. *Adv. Enzymol. Relat. Areas Mol. Biol.* **1986,** *58,* 61.

308. Sawyer, D.; Valentine, J. *Acc. Chem. Res.* **1981,** *14,* 393.

309. Sawyer, D.; Valentine, J. *Acc. Chem. Res.* **1982,** *15,* 200.

310. Sawyer, D. *Phys. Chem.* **1989,** *93,* 7977.

311. Sawyer, D. In "Oxygen Chemistry"; Oxford University Press: New York, Oxford, 1991; pp. 160–187.

312. Koppenol, W.; Butler, J. *FEBS Lett.* **1977,** *83,* 1.

313. Koppenol, W. *Nature* **1976,** *262,* 420.

314. Rigo, A.; Stevanato, R.; Finazzi-Agrò, A.; Rotilio, G. *FEBS Lett.* **1977,** *80,* 130.

315. Behar, D.; Czapski,G.; Rabani, J.; Dorfman, L.; Schwarz, H. *J. Phys. Chem.* **1970,** *74,* 3209.

316. Czapski, G.; Goldstein, S.; Mmeyerstein, D. *Free Radical Res. Commun.* **1987,** *4,* 241.

317. Fridovich, I. *Annu. Rev. Biochem.* **1995,** *64,* 97.

318. Brieland, K. J.; Fantone, J. C. *Arch. Biochem. Biophys.* **1991,** *284,* 78.

319. Rabani, J.; Nielsen, S. *J. Phys. Chem.* **1969,** *73,* 3736.

320. Bielski, B.; Cabelli, D. *J. Radiat. Biol.* **1991,** *59,* 291.

321. Klug, D.; Fridovich, I.; Rabani, J. *J. Am. Chem. Soc.* **1973,** *95,* 2786.
322. Calabrese, L.; Rotilio, G.; Mondovì, B. *Biochim. Biophys. Acta* **1972,** *263,* 827.
323. Hodgson, E.; Fridovich, I. *Biochem. Biophys. Res. Commun.* **1973,** *54,* 270.
324. Hodgson, E. K.; Fridovich, I. *Biochemistry* **1975,** *14,* 5294.
325. Bull, C.; Fee, J. A. *J. Am. Chem. Soc.* **1985,** *107,* 3295.
326. Marcus, R. *J. Chem. Phys.* **1965,** *43,* 2654.
327. Cudd, A.; Fridovich, I. *FEBS Lett.* **1982,** *144,* 181.
328. Borders, C. L. J.; Saunders, J. E.; Blech, D. M.; Fridovich, I. *Biochem. J.* **1985,** *230,* 771.
329. Polticelli, F.; Battistoni, A.; Bottaro, G.; Carri, M. T.; O'Neill, P.; Desideri, A.; Rotilio, G. *FEBS Lett.* **1994,** *352,* 76.
330. Malinowski, D.; Fridovich, I. *Biochemistry* **1979,** *18,* 237.
331. Bertini, I.; Capozzi, F.; Luchinat, C.; Piccioli, M.; Viezzoli, M. S. *Eur. J. Biochem.* **1991,** *197,* 691.
332. Pantoliano, M. W.; Valentine, J. S.; Burger, A. R.; Lippard, S. J. *J. Inorg. Biochem.* **1982,** *17,* 325.
333. Fridovich, I.; Hodgson, E. K. *Biochemistry* **1975,** *14,* 5299.
334. Ellerby, M. L.; Cabelli, D. E.; Graden, J. A.; Valentine, J. S. *J. Am. Chem. Soc* **1996,** *118,* 6556.
335. Osman, R. In "Superoxide and Superoxide Dismutase in Chemistry, Biology and Medicine"; Rotilio, G., Ed.; Elsevier: New York, 1996; pp. 141–144.
336. Rosi, M.; Sgamellotti, A.; Tarantelli, F.; Bertini, I.; Luchinat, C. *Inorg. Chem.* **1986,** *25,* 1005.
337. Weinstein, J.; Bielski, B. *J. Am. Chem. Soc.* **1980,** *102,* 4916.
338. Stallings, W. C.; Powers, T. B.; Pattridge, K. A.; Fee, J. A.; Ludwig, M. L. *Proc. Natl. Acad. Sci. U.S.A.* **1983,** *80,* 3884.
339. Lah, M. S.; Dixon, M.; Pattridge, K. A.; Stallings, W. C.; Fee, J. A.; Ludwig, M. L. *Biochemistry* **1995,** *34,* 1646.
340. Schmidt, M.; Meier, B.; Parak, F. *JBIC* **1996,** *1,* 532.
341. Collaborative Computational Project, *Acta Crystallogr.* **1994,** *D50,* 760.
342. Banci, L.; Bertini, I.; Cabelli, D. E.; Hallewell, R. A.; Luchinat, C.; Viezzoli, M. S. *Free Radical Res. Commun.* **1991,** *12–13,* 239.
343. Calabrese, L.; Polticelli, F.; Galtieri, A.; Barra, D.; Schinina', E.; Bossa, F. *FEBS Lett.* **1989,** *250,* 49.
344. Marklund, S. *J. Biol. Chem.* **1976,** *251,* 7504.
345. Heikkila, R. E. In "CRC Handbook of Methods for Oxygen Radical Research"; Greenwald, R. A., Ed.; CRC Press: Boca Raton, Florida, 1985; pp. 233–235.
346. Bertini, I.; Banci, L.; Luchinat, C.; Hallewell, R. A. In "Annals of the New York Academy of Sciences; Blanch, H. W., and Klibanov, A. M., Eds.; New York Academy of Science: New York, 1988; pp. 37–52.
347. Bordo, D.; Djinovic, K.; Bolognesi, M. *J. Mol. Biol.* **1994,** *238,* 366.
348. Connolly, M. *J. Appl. Crystallogr.* **1983,** *16,* 548.
349. Connolly, M. *Science* **1983,** *221,* 709.
350. Rotilio, G.; Gray, J. C.; Fielden, E. M. *Biochim. Biophys. Acta* **1972,** *268,* 147.
351. Cass, A. E. G.; Hill, H. A. O.; Bannister, J. V.; Bannister, W. H. *Biochem. J.* **1979,** *177,* 477.
352. Vega, A. J.; Fiat, D. *Mol. Phys.* **1976,** *31,* 347.
353. Calabrese, L.; Cocco, D.; Desideri, A. *FEBS Lett.* **1979,** *106,* 142.
354. Rosi, M.; Sgamellotti, A.; Tarantelli, F.; Bertini, I.; Luchinat, C. *Inorg. Chim. Acta* **1985,** *107,* L21.

ADVANCES IN INORGANIC CHEMISTRY, VOL. 45

DNA AND RNA CLEAVAGE BY METAL COMPLEXES

GENEVIÈVE PRATVIEL, JEAN BERNADOU, and BERNARD MEUNIER

Laboratoire de Chimie de Coordination du CNRS, 31077 Toulouse Cedex, France

I. Introduction

The reason why Nature chose phosphate esters to serve as nucleotide linkages in the genetic material DNA may relate to the high stability of the phosphate ester with respect to hydrolysis and to its negative charge, which reduces the rate of nucleophilic attack on the DNA backbone (*1*). Because efficient hydrolysis of these phosphodiester linkers is necessary in DNA repair, and at many different stages of transcription and translation, enzymes are involved in catalyzing the hydrolysis of P–O bonds of the DNA phosphate backbone. These hydrolytic enzymes are in fact metalloenzymes with metal ions present at the active site, as will be discussed in Section III. Published structures of nucleases have allowed the positions of these ions (cal-

0898-8838/98 $25.00

cium, zinc, or magnesium) to be determined with respect to the phosphate residue, in order to better understand their role. It will be seen in Section III that modeling of these hydrolytic enzymes is very challenging for synthetic chemists and that considerable progress will have to be made before it is possible to create artificial nucleases capable of competing with natural ones. The time scale of evolution allows a continuous recycling process to improve the design of enzymes able to catalyze the hydrolysis of the P–O bonds of DNA phosphodiesters. Chemists have been working in this area for only 20 years! Despite the fact that more than 2400 site-specific restriction enzymes representing 188 different sequence specificities have been discovered (*2*), there is still a need for artificial endonucleases that are able to cleave DNA and RNA at specific sites.

On the other hand, as will be described in Section II, bio(in)organic chemists and biochemists have been more successful in understanding the mechanism of action of bleomycin, an antitumoral antibiotic able to cleave DNA by using three cofactors: iron, dioxygen, and an electron source (for early reviews, see Refs. *3–7*). This naturally occurring molecule is the paradigm of many metal-containing cleaving reagents synthesized during the past 15 years, whereby oxidative degradation of DNA and RNA is due to high-valent metal species or reactive oxygen entities produced at the metal center. These new DNA and RNA cleavers might have a future as antitumoral or antiviral agents if they can be used to create irreversible damage to the DNA present in cancer cells or to retroviral DNA integrated within infected cells.

II. Oxidative DNA and RNA Cleavage Mediated by Transition Metal Complexes

A. Bleomycin

Bleomycins (BLMs) are a family of glycopeptide antitumoral antibiotics produced by *Streptomyces verticillus*. The structure of the two major components (BLMs A_2 and B_2) is depicted in Fig. 1. The five nitrogen atoms of BLM indicated in Fig. 1 are able to chelate strongly several metal cations, e.g., iron, manganese, cobalt, copper, or zinc. Many gram-negative and gram-positive bacteria are resistant to BLM because of their capacity to produce a protein able to sequester this antibiotic. The crystal structure of a BLM-resistant protein has been determined, and a BLM–protein binding model proposed (*8*). The metal center of bound metallo-BLM is buried within the protein

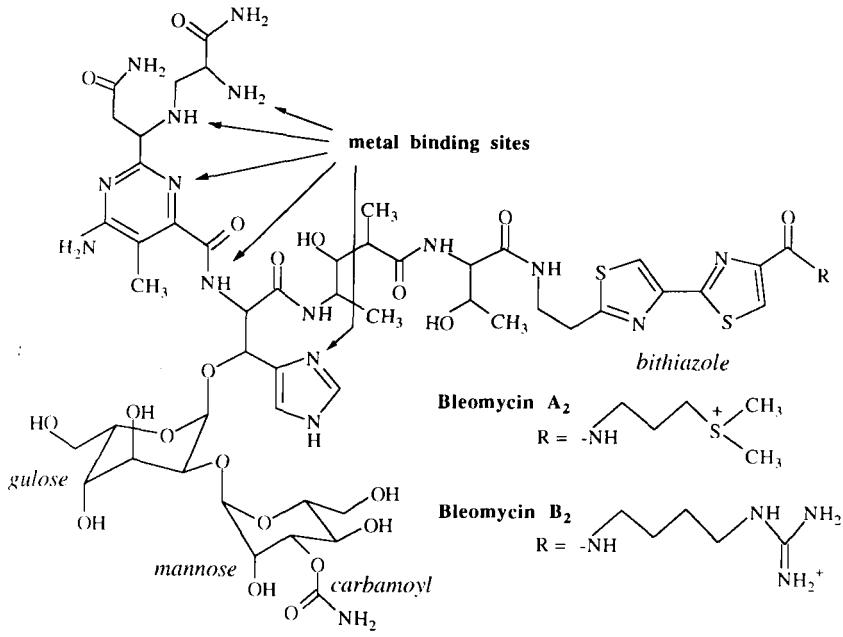

FIG. 1. Structures of bleomycin A_2 and B_2.

dimer, making unaccessible the sixth coordination site for oxygen activation (see below for the mechanism of action of bleomycin).

This potent anticancer drug is now widely used in chemotherapy in association with several other drugs (e.g., vinblastine, methotrexate, carboplatine, ifosfamide, or etoposide) in the treatment of Hodgkin's disease (*9*), of head and neck cancers (*10*, *11*), of disseminated germ cell tumors (*12*), and of poor-prognosis epidemic Kaposi's sarcoma (*13*) (for previous articles on the clinical use of BLM, see references listed in Refs. *9–13*).

One of the unique features of BLM is its lack of significant hepatic, renal, and bone marrow toxicities, undesired effects of many anticancer drugs. Two drawbacks are the tumor resistance and the BLM-induced pulmonary toxicity. Both effects are related to the level of BLM hydrolase, a protease that binds to DNA and inactivates BLM by hydrolyzing the β-alanine carboxamide moiety (*14*, *15*). Cells with high levels of BLM hydrolase are resistant to bleomycin, whereas lungs are sensitive to BLM-induced tissue injuries because of low levels of this enzyme. The structure of this protease, which binds DNA and is conserved from bacteria to humans, has been solved (*16*).

The cytoxicity of BLM toward cancer cells is oxygen dependent and

related to its ability to induce single- and double-stranded DNA breaks. Cell penetration limits the cytotoxicity of this DNA cleaver (*17*). By electropermeabilization, it has been shown that BLM is highly cytotoxic. After BLM internalization, cell apoptosis is observed and is probably due to the direct internucleosomal cleavage of chromatin (*18*).

Early studies on the mechanism of DNA cleavage by metallobleomycins have been reported in well-organized review articles (*3–7*), so here the focus is on advances in (1) the syntheses of BLM and structures of BLM complexes, (2) the interactions of BLM with DNA, (3) the nature of "activated" BLM, (4) the mechanism of DNA (and RNA) cleavage, and (5) BLM models.

1. Structures and Syntheses of Bleomycin Derivatives

As depicted in Fig. 1, the structure of BLM can be regarded as the association of three different domains: (1) a bithiazole unit with a positively charged lateral chain mainly responsible for DNA binding, (2) a metal-chelating system involving the pyrimidine, β-aminoalanine, and β-hydroxyimidazole residues [this proposal is confirmed by the determination of the three-dimensional structure of a Cu^{II}–BLM analogue (*19*); a sixth coordination site is vacant and available for the interaction with molecular oxygen in the case of the Fe^{II}–BLM complex], and (3) a disaccharide moiety containing a gulose and a carbamoylated mannose.

The total synthesis of BLM A_2 and related compounds has been achieved by Boger and co-workers (*20*). The approach developed by these authors also included the synthesis of 2-*O*-(3-*O*-carbamoyl-α-D-mannopyranosyl)-L-gulopyranose and its incorporation into a total synthesis of BLM structural analogues (*21*). The chemical synthesis of this disaccharide was also achieved by Kobayashi and Oshitari (*22*).

2. Interactions of Bleomycin with Metal Ions and DNA

The common factor of all bleomycins is their high capacity to bind metal ions strongly. The Cu^{II}–BLM complex is slightly more stable than the corresponding Fe^{III} analogue, Log K_{aff} being 18.1 and 16.0, respectively (*6*). In blood, BLM rapidly forms a copper complex that is thought to be involved in cellular uptake. ^{14}C-Labeled copper–BLM–A_2 is poorly internalized within KB_3 cells, but, surprisingly, the accumulation of the deglyco derivative within cell nuclei was higher than for BLM (*23*). This result is controversial with the classical idea that sugar residues of antitumoral agents are present to facilitate cell penetration.

Several recent investigations indicate that BLM binds to DNA not only by the bithiazole moiety but also by the metal binding domain and the disaccharide entity, which are also involved in the overall DNA binding and recognition process. Without bithiazole, BLM is unable to bind to DNA (*24*) and it is reasonable to assume that the two other structural factors (the metal-binding domain and the disaccharide) are involved in the fine tuning of sequence-specific BLM–DNA interactions. The important role of the bithiazole in DNA binding and cleavage efficiency has been confirmed by using analogues containing modified bithiazoles (*25*). BLM-bithiazole behaves as a (partial) intercalating agent, because Cu^{II}–BLM unwinds DNA. Bailly and Waring found that the 2-amino group of guanine plays an important role in the recognition of DNA by BLM (*26*), in agreement with nuclear magnetic resonance (NMR) studies on Zn–BLM and Co–BLM incubated with the oligodeoxyribonucleotides (ODNs) $d(CGCTAGCG)_2$ and $d(CCAGGCCTGG)_2$, respectively (*27*, *28*). These two latter studies confirmed that the metal-binding domain of BLM is folded and interacts with the minor groove of double-stranded DNA. In the Zn–BLM–oligonucleotide complex, the metal center is only 3.3 Å away from the closest deoxyribose C-4′–H. If we assume a 1.7 ± 0.1 Å metal–oxygen distance for a putative metal–oxo species, the oxygen atom of the oxo group will be 1.6 ± 0.3 Å from the abstracted hydrogen atom, depending on the metal–oxygen–hydrogen angle, very close to the expected oxygen atom distance in the transition state of the removal of H · at a 4′ position of a deoxyribose unit.

The recognition of B-DNA by BLM is enantiospecific because BLM is unable to cleave the nonnatural L-$d(CGCGCG)_2$ duplex, whereas the nature D oligomer is efficiently cleaved (*29*).

3. *Nature of "Activated Bleomycin"*

The oxidative degradation of DNA by BLM involves abstraction of the hydrogen atom at the 4′ positions of deoxyribose units (see Section II,A,4 for details on DNA cleavage) by a transient species, the so-called activated BLM resulting from activation of the Fe–BLM by two reducing equivalents in the presence of molecular oxygen (*3*, *4*, *30*). This drug–iron–oxygen complex is kinetically competent to initiate the attack on DNA (*31*). The DNA cleavage pattern is not in favor of diffusible HO · species as H atom abstracting agents, so "activated bleomycin" is a metal-centered oxygen-containing complex.

It has been hypothesized that activated BLM is a high-valent iron–oxo complex generated by a reductive activation of molecular oxygen reminiscent to that observed in cytochrome *P*-450 monooxygenases

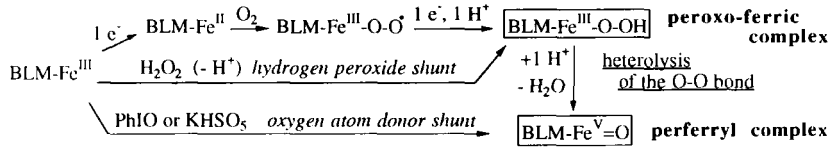

FIG. 2. Different routes for the generation of "activated bleomycin." The formal oxidation state (V) of the bleomycin–iron–oxo species (perferryl complex) is two oxidant equivalents above BLM–Fe^{III}, but one oxidant equivalent might be located on the ligand, as in Compound I of peroxidases, with an $iron^{IV}$–oxo–ligand radical cation structure.

(*30*, *32*) (see Fig. 2). Such a hypothesis (see the peroxide shunt in Fig. 2) has been supported by using single-oxygen atom donors, iodosylbenzene or potassium monopersulfate, as cofactors in DNA cleavage or olefin epoxidations catalyzed by iron– or manganese–bleomycin (*33–35*; and see Ref. *36* for a review of oxygen donors in metalloporphyrin-catalyzed oxygenations). The precursor of such high-valent iron–oxo species is the hydroperoxo complex BLM–Fe^{III}–OOH as depicted in Fig. 2. This intermediate, prepared from Fe^{III}–BLM and hydrogen peroxide, has been recently characterized by electrospray mass spectrometry (*37*). The d^5 BLM–Fe^{III}–OOH, prepared by reacting H_2O_2 with a dual syringe pump interfaced with the electrospray source, exhibits a peak at $m/z = 751$ (with $z = 2^+$). This peak shifts at 753 with $H_2{}^{18}O_2$. The electron spin resonance (ESR) spectrum of activated BLM with characteristic g values at 2.26, 2.17, and 1.94 was assigned to the low-spin d^5 BLM–Fe^{III}–OOH complex (*30*, *38*). The stability of BLM–Fe^{III}–OOH, and the slow scission of the peroxidic O–O bond to generate a perferryl species as in cytochrome *P*-450 or metalloporphyrin models, might be due to the weak electron transfer from the metal and its ligands to the antibonding orbital of the O–O bond to promote the heterolytic cleavage (porphyrin ligands and proximal ligands of heme proteins are better electron reservoirs than are BLM ligands), and not the reverse as stated by Mascharak *et al.* (*38*) (see Fig. 3).

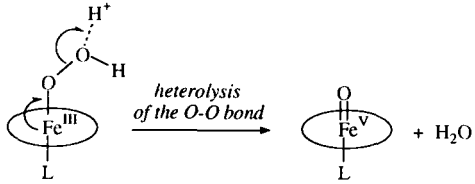

FIG. 3. Push–pull mechanism for the heterolysis of the O–O bond of an iron–peroxo complex. The oval indicates an electron-rich ligand, such as a porphyrin; L is a heme-proximal ligand (cysteine or histidine).

From oxygen isotope studies, Burger *et al.* reported that activated BLM formation is at least 10-fold faster than its decay (*39*). No significant amount of superoxide or peroxide is released during the decomposition of activated BLM. The decay of BLM–Fe^{III}–OOH to a highly reactive iron–oxo as the proximate DNA-attacking species cannot be excluded (*39*).

4. Mechanism of DNA (and RNA) Cleavage

Recent studies with *Euglena gracilis* and human leukemia HL-60 cells have assessed the need for intracellular iron for cellular DNA damage and cell growth inhibition by BLM (*40*). Growth inhibition and both single- and double-strand DNA breaks were substantially reduced in iron-deficient cells. In iron-deficient HL-60 cells, metal-free BLM and Cu–BLM are mainly inactive as cellular DNA cleavers. The earlier findings that free BLM, Zn–BLM, or Cu–BLM had the same cytotoxic activity as Fe–BLM can now be explained by their conversion into Fe–BLM inside host cells (*40*).

Several studies with DNA fragments have shown that the most frequent cleavage sites are at G-pyrimidine sequences. Frequency of cleavage decreases as follows: 5′-GC ~ GT > GA ⩾ GG (*41*, *42*). Breaks are also observed at 5′-AT sites in DNA fragments having AT-rich sequences. DNA cleavage is efficiently performed by BLM in the presence of iron(III) ions and hydrogen peroxide or in the presence of iron(III) ions, molecular oxygen, and a reducing agent. DNA strand scission is accompanied by the simultaneous release of free bases, base propenal derivatives **A**, 3′-phosphoglycolates **B**, 5′-phosphate ends **C**, and alkali-labile 4′-hydroxylated abasic sites **D** revealed by hydrazine (Fig. 4) (*3*, *4*, *43*, *44*). As demonstrated by deuterium isotope effects H-4′ abstraction is the rate-determining step (*45*). The k_H/k_D value ranges from 2 to 7 depending on structural changes on BLM derivatives (*46*). Then the radical at 4′ can react according to three different pathways: (1) with molecular oxygen (the so-called oxygen-dependent route) to generate an unstable hydroperoxide at 4′, which breaks down via a Criegee-type rearrangement to the corresponding base propenal, 3′-phosphoglycolate, and 5′-phosphate derivatives, (2) with the coordinated OH group of BLM–Fe^{IV}–OH via an oxygen rebound mechanism to give the 4′-hydroxylated site **E**, or (3) with BLM–Fe^{IV}–OH via an electron transfer to produce an intermediate cation **F**, which reacts with water to give **E**. Experiments with ^{18}O-labeled water indicate that this latter pathway is the main route to produce **E** (*47a*).

Recent kinetic data on DNA strand scission initiated by BLM indicate that strand cleavage precedes deoxyribose 3′-phosphate bond

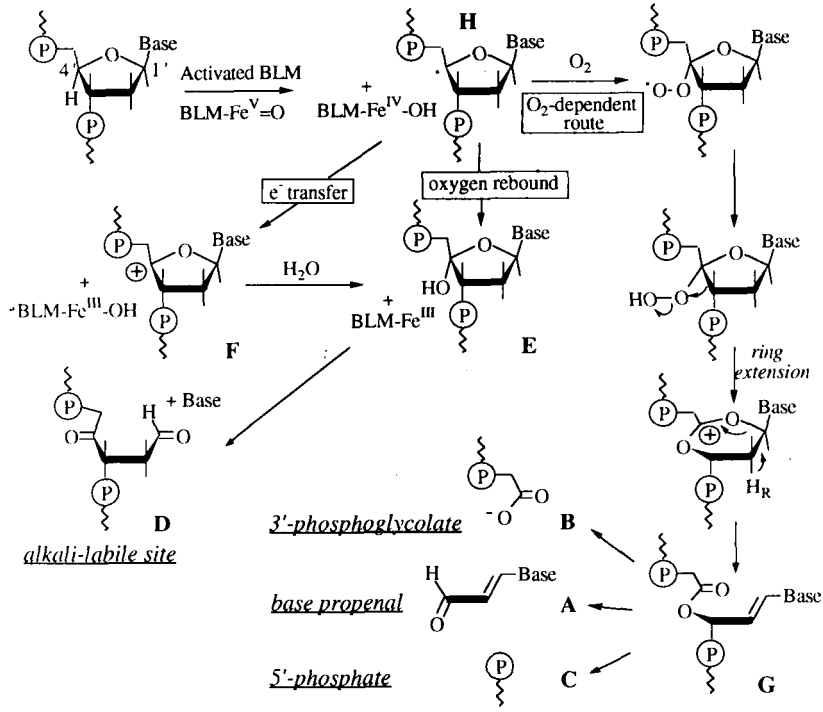

FIG. 4. Mechanism of the oxidative DNA cleavage by activated iron–bleomycin.

cleavage (*47b*). Strand scission occurs with a $t_{1/2}$ = 4.1 ± 0.5 min at 4°C, faster than base propenal ($t_{1/2}$ = 6.7 ± 0.3 min) or the 5′-phosphate end ($t_{1/2}$ = 7.4 ± 0.8 min) formation. So the common precursor **G** of products **A**, **B**, and **C** is decomposed via the cleavage of the C-3′–O bond to generate first the 3′-phosphoglycolate and consequently the DNA strand scission. The intermediate radical **H** resulting from H atom abstraction by activated BLM has been generated by photolysis of a single-stranded oligonucleotide modified with a photoactivatable substituent at 4′ (*48*, *49*). Giese *et al.* (*48*, *49*) proposed a mechanism involving the release of the 5′-phosphate directly from intermediate **H**. This proposal seems to be in contradiction with the kinetic data obtained by Burger *et al.* (*39*) (see above).

H-1′ abstraction by Fe–BLM from ODN duplexes containing a ribonucleotide unit was evidenced (*50*), but degradation of DNA–RNA hybrids by BLM involves C-4′ rather than C-1′ chemistry (*51*); the DNA strand of this heteroduplex is preferentially cleaved (*52*).

Double-strand breaks induced by BLM result from two single-

strand breaks generated on each strand by the same bleomycin molecule acting as catalyst (*53*, *54a*). The essential factor establishing the ratio of single-strand to double-strand cleavage at a specific site is related to the efficiency by which Fe–BLM can be reactivated. The specific cleavage of a DNA triple helix by iron–bleomycin has also been observed (*54b*). The strongest damage is located at the 5′ duplex–triplex junction.

It can also be noted that BLM-dependent damage to bases is a minor side reaction (*55*). Thus 7,8-dihydro-8-oxodeoxyguanosine, the predominant tautomer of 8-OH-dG, is formed in calf thymus DNA treated with BLM (*56*).

In spite of early reports that RNA is not degraded by BLM (*57*), additional studies indicate Fe–BLM-mediated degradation of certain RNA substrates, notably transfer RNAs, tRNA precursor transcripts, and HIV-1 reverse transcriptase mRNA (*6*, *58*). The RNA cleavage is much more selective than DNA cleavage. *Bacillus subtilis* $tRNA^{His}$ precursor was cleaved at U35 and the corresponding "tDNA" was also cleaved at the corresponding T35 site by BLM at low concentration (*59*). Keck and Hecht have found that metal-free BLM is able to mediate the sequence-specific hydrolysis of yeast $tRNA^{Phe}$ at Py–Pu sites not involving modified bases (*60*). The fact that RNA might constitute a therapeutically relevant target for BLM is now an open question.

5. *Bleomycin Models and Conjugates*

Sawai *et al.* (*61*) reported that enantiomeric models containing a D- or L-histidine entity exhibited a DNA cleaving activity in a chiral discrimination manner. Using a 4-substituted pyridine and two histidine residues, Sugiura *et al.* (*62*) have shown that the oxygen activation efficiency of the corresponding iron complexes increased with electron-donating substituents (methoxy and dimethylamino groups).

Mascharak *et al.* (*63*) have prepared a structural BLM model PMAH containing pyrimidine, imidazole, and primary and secondary amine building blocks. The $iron^{II}$–PMAH complex was studied by X-ray absorption, magnetic circular dichroism, and resonance Raman spectroscopy (*63*). This Fe–BLM model exhibits a five-coordinate, square pyramidal geometry in the solid state and a distorted octahedral geometry in solution with a solvent molecule at the sixth position. Similar spectral features have been found for Fe^{II}–BLM. This PMAH–Fe^{II} complex binds O_2 to generate PMAH–Fe^{III}–OOH, a low-spin hydroperoxo–iron(III) complex (*64*) able to promote the lipid peroxidation as BLM (*65*).

Lown *et al.* (*66*) have prepared functional models of bleomycin com-

posed of a metal-complexing motif similar to PMAH (with a pyridine instead of a pyrimidine) and an oligo-*N*-methylpyrrole peptide as DNA-binding entity. The DNA cleavage activity increases with the number of *N*-methylpyrrole units, but sequence selectivity studies on restriction fragments indicate that the models with lexitropsin-type vectors cleave DNA at AT-rich DNA sequences, as expected for minor-groove binders.

Bleomycin can be covalently attached to oligonucleotides or DNA binding proteins (*67–69*). A BLM–oligonucleotide conjugate cleaves DNA at GT sequences located near the junction site of the conjugate with its target (*67*, *68a*). A catalytic site-specific cleavage of a DNA target by a short oligonucleotide linked to BLM has also been reported by the same research group (*68b*). Up to three catalytic cycles have been obtained. The iron-binding motif of BLM (pyrimidoblamic acid β-hydroxy-L-histidine) linked to the terminal amine of the DNA binding domain of Hin recombinase interacts with DNA at the expected Hin binding sites (*69*). The corresponding iron complex cleaves DNA in the presence of dithiothreitol. Analysis of the cleavage pattern suggests that this site-specific DNA is mediated by a localized diffusible species, in contrast with BLM, which proceeds via nondiffusible species.

B. Copper Complexes

1. Bis(1,10-phenanthroline)copper

The complex $Cu^{I}(phen)_2$ **1** [see Fig. 5; another commonly used abbreviation is $Cu^{I}(oP)_2$] was the first to be recognized as an efficient chemical nuclease by Sigman *et al.* (*70–72*). The oxygen-dependent DNA cleavage activity of $Cu^{I}(phen)_2$ was the cause of the inhibition of *Escherichia coli* DNA polymerase I activity in the presence of a chelating agent, a thiol, and traces of copper salts (*70*). To generate these single-strand DNA breaks, two modes of activation can be used: hydrogen peroxide or molecular oxygen in the presence of a reducing agent (a thiol or ascorbic acid) (*73–75*). The active species responsible for DNA cleavage is still a matter of debate. A popular view is to consider that $Cu^{I}(phen)_2$ [or $Cu^{II}(phen)_2$ before being reduced] freely diffuses along double-stranded DNA, binds to DNA (see below for details on nucleic acid interactions), and then reacts with hydrogen peroxide to cleave DNA. Some reports indicate that freely diffusible hydroxyl radicals are not responsible for DNA strand scission (*73*, *76*), but others mention that the DNA-damaging species can diffuse over

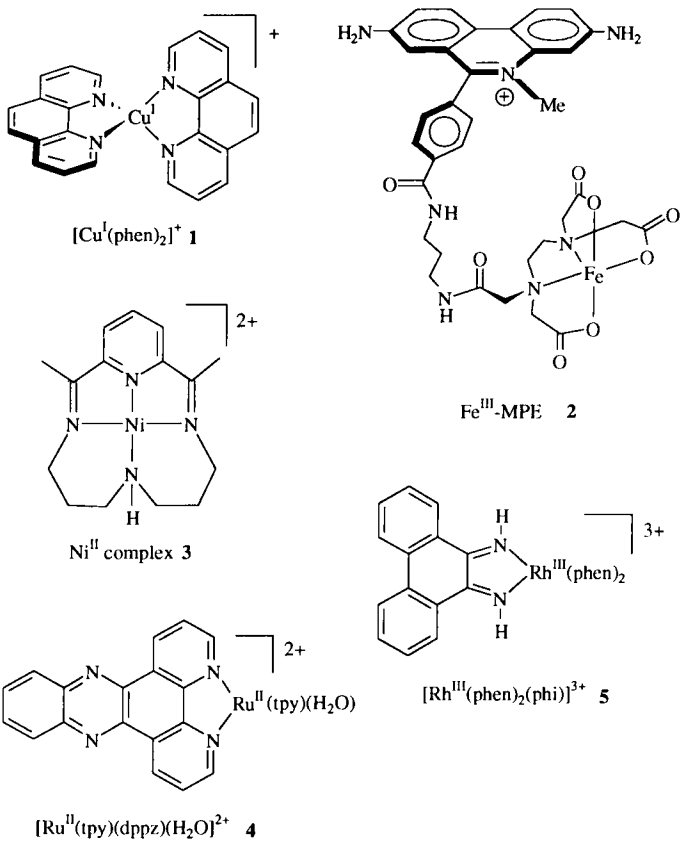

FIG. 5. Structures of the metal complexes **1**–**5** having an oxidative nuclease activity.

a limited range from the binding site of **1** (*77*). The damage to DNA bases by Cu^{I}(phen)$_2$/H$_2$O$_2$ is typical of those induced by HO·, suggesting that a minor reaction pathway involves free hydroxyl radicals (*78*). However, the nondiffusible active copper-centered species responsible for single-strand (ss) breaks is probably a coordinated hydroxo complex Cu^{II}–OH (or Cu^{III}–OH ?) rather than a copper–oxo species Cu^{III}=O (see Ref. *79* for a discussion by Mayer on the nonexistence of copper–oxo species, due to the filling of antibonding molecular orbitals by the too *d*-electron-rich metal–oxo complexes).

The pattern of DNA cleavage by activated Cu^{I}(phen)$_2$ is consistent with its binding in the minor groove of a right-handed double helix (*80*). Initial observation of the inhibition of cleavage by intercalators suggests that Cu^{I}(phen)$_2$ interacts with double-stranded (ds) DNA via

an intercalation mode (*73*). However, the observed cleavage specificity is related to a predominant preference for binding at 5′-TAT triplets, which is more suggestive of a minor groove binder behavior than that of an intercalator, for which GC preferences are expected (*81*). The $Cu^{I}(phen)_2$ is precluded from full intercalation by its tetrahedral geometry, but a model involving the partial intercalation of one phenanthroline ligand is also plausible (*82*). Z-DNA having a deep narrow minor groove is completely resistant to degradation by **1** (*74*). As expected for a minor-groove binder, C–H bonds at C-1′ and C-4′ of deoxyriboses, two sugar C–H bonds accessible from the minor groove, are the main targets of activated $Cu^{I}(phen)_2$ (*71*). Using 5′-^{32}P-labeled ds dodecamers, Sigman *et al.* (*70*) have shown that 3′-phosphoglycolates resulting from a C-4′ chemistry are minor DNA degradation products compared to those generated by a C-1′ chemistry, which represents 80–90% of the DNA damage (Fig. 6). After oxidation of the C–H bond at 1′, releasing the attached base, the first β-elimination liberates a 5′-phosphate end (the single-strand break event) and a damaged sugar residue still attached at the 3′ end of the DNA strand. The 5-methylene-2(5*H*)-furanone (5-MF) is released from its precursor by a thermal step (90°C for 1 min) or a piperidine treatment necessary to facilitate the second β-elimination (*83*). The released 3′-phosphomonoester termini were the potent inhibitors of *E. coli* DNA polymerase I activity as revealed by the nuclease activity of $Cu^{I}(phen)_2$, as mentioned above.

By itself, $Cu^{I}(phen)_2$ is an efficient chemical tool to probe small conformational changes of DNA. Comparison of the digestion patterns

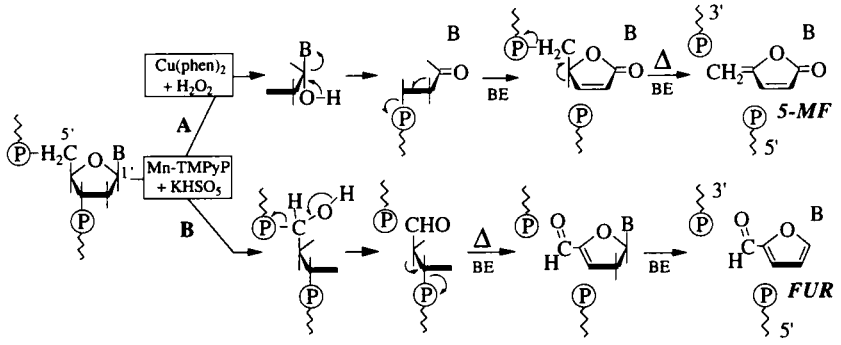

FIG. 6. Mechanism for the cleavage of DNA or DNA models after hydroxylation of C–H bonds on the 1′ and 5′ positions of deoxyribose by $Cu(phen)_2/H_2O_2$ (route A) or Mn–TMPyP/$KHSO_5$ (routes A and B) (Δ = thermal step, B = base, BE = β elimination).

generated by DNase I and $Cu^{I}(phen)_2$ of different variants of the *lac* operon control region provided information on DNA conformational variability in a region of biochemical function (*84*). Because of its size and its high reactivity, $Cu^{I}(phen)_2$ provides data complementary to that of DNase I. $Cu^{I}(phen)_2$ was also used to study the conformational changes in transcriptionally active complexes between RNA polymerase and promotor regions (*85*, *86*). The footprinting properties of $Cu^{I}(phen)_2$ were also useful to study RNA–protein complexes, in particular the interaction of TAT peptides with HIV *tar* RNA (*87*).

2. *Copper–Phenanthroline Conjugates*

This aspect has been recently reviewed by Sigman (*88*). The nuclease activity of copper–phenanthroline can be targeted by attachment of one modified 1,10-phenanthroline ligand to the 5′ end of oligodeoxyribonucleotides complementary to ss DNA (*89–91*) or RNA sequences (*92*). The phenanthroline can also be linked through N-2 of a deoxyguanosine residue (*93*). These modified phenanthroline ligands can also be tethered to oligo-α-deoxyribonucleotides resistant to nucleases (*94*) or to triple-helix-forming oligonucleotides in order to target the nuclease activity of the copper complex toward a double-stranded DNA sequence (*90*, *95*, *96*) (for a recent review on triple helices and the "antigene" strategy, see Ref. *97*). Different RNA molecules bearing uridine bases modified by a phenanthroline ligand were also used to achieve the oxidative sequence-specific cleavage of ss or ds DNA (*98*). All these conjugates contain only one phenanthroline ligand, so the coordination sphere of the chelated copper ion is probably completed by unknown extra ligands (water molecules, basic sites of DNA, or an excess of the conjugated molecule ?).

The nuclease activity of the copper–phenanthroline complex can also be directed at specific sites with DNA-binding proteins (trp, CAP, Cro, Fis, etc.) in order to study the interactions of these DNA-binding proteins with their DNA targets or to isolate long DNA fragments for sequencing, cloning, or chromosomal mapping (*99–105*). Conjugates with a minor-groove binder such as Hoechst 33258 or different peptides have also been prepared (*106*).

C. Iron Complexes

1. *Iron–EDTA*

Even without the ethylenediaminetetraacetate (EDTA) ligand, iron(II) salts are able to bind to DNA and to catalyze the formation of

hydroxyl radicals within the DNA from H_2O_2 via the well-known Fenton reaction (*107–109*), and to generate DNA damage, which can be repaired when cells are exposed to low hydrogen peroxide concentrations (*110*) (for additional information on oxidative DNA-damaging processes, see Ref. *111*).

When Fe^{II} is chelated by EDTA, its direct interaction with DNA is precluded because Fe^{II}–EDTA present as $[Fe^{II}–EDTA]^{2-}$ is a negatively charged complex, making difficult an electrostatic interaction with DNA (for the X-ray structure of the corresponding Fe^{III}–EDTA–aqua complex and a recent review on metal(III)–EDTA complexes, see Refs. *112* and *113*, respectively). This absence of direct contact of Fe–EDTA with DNA is now an advantage when using the Fe^{II}–EDTA/H_2O_2 system to generate the HO · radical in the close vicinity of DNA without or with very little sequence specificity. This hydroxyl radical footprinting method has been extensively developed by Tullius and co-workers to study DNA conformations and to map DNA–protein contacts (*114–118*). For example, a 150-base pair DNA sequence directly upstream of the thymidine kinase gene of herpes simplex virus I was found to have a helicity of 10.5 base pairs per turn, typical of a B conformation, when the DNA fragment was bound to crystalline calcium phosphate and cleaved by HO · radicals generated by Fe^{II}–EDTA/H_2O_2 (*114*). The DNase I footprinting method cannot be applied in such a case. In addition, Fe^{II}–EDTA catalyzes the scission of ss and ds DNA and RNA with the same reactivity, which simplifies the interpretation of experimental data from studies on DNA and RNA conformations (*119*).

The identity of the DNA-oxidizing species produced in the Fe^{II}–EDTA/H_2O_2 system has been an issue of debate. The presence of a weakly bound water molecule on Fe–EDTA (*112*) allows the possibility to create an oxo ligand at this position when the iron complex is oxidized by hydrogen peroxide (for the possible generation of iron–oxo species by activation of iron salts by hydrogen peroxide, see Ref. *120*). Comparison of DNA cleavage patterns generated by γ-radiolysis or by Fe^{II}–EDTA/H_2O_2 confirmed that hydroxyl radicals are responsible for DNA strand scission under the conditions used by Tullius *et al.* (*121*). The Fe^{II}–EDTA catalyzes production of HO · radicals from H_2O_2 in the presence of ascorbate, which reduces Fe^{III}–EDTA back to the Fe^{II} state according to Eqs. (1) and (2):

$$[Fe^{II}–EDTA]^{2-} + H_2O_2 \rightarrow [Fe^{III}–EDTA]^{-} + HO^{-} + HO\cdot; \quad (1)$$

$$[Fe^{III}–EDTA]^{-} + \text{ascorbate} \rightarrow [Fe^{II}–EDTA]^{2-}. \quad (2)$$

The neutral hydroxyl radicals react at a diffusion-controlled rate with bases and also with C–H bonds of deoxyriboses, leading to DNA breaks with 5′- and 3′-phosphate termini (*122*).

2. *Iron-Methidiumpropyl–EDTA*

In a pioneering work, Dervan designed a bleomycin model by attaching EDTA to an activated ester of *p*-carboxymethidium via a 1,3-diaminopropane linker (*123*). Methidiumpropyl–EDTA (MPE) is a bifunctional molecule able to interact with ds DNA by intercalation and to chelate iron(II) strongly (see Fig. 5 for the structure of Fe^{III}–MPE **2**). MPE in the presence of iron^{II}, molecular oxygen, and a reducing agent, usually dithiothreitol (DTT), cleaves a supercoiled plasmid DNA at low concentrations (10^{-8} *M*), comparable to that used with bleomycin (*123*). The postulated mechanism of DNA cleavage involves the reaction of the chelated Fe(II) with O_2 to give Fe(III) and $O_2^{\cdot-}$ [Eq. (3)]. Superoxide anions in protic media quickly disproportionate to hydrogen peroxide and dioxygen [Eq. (4)]. The H_2O_2 produced then reacts with Fe^{II}–MPE to generate HO · radicals via a Fenton reaction [Eq. (5)]:

$$Fe^{II}\text{–MPE} + O_2 \rightarrow Fe^{III}\text{–MPE} + O_2^{\cdot-}; \tag{3}$$

$$2O_2^{\cdot-} + 2H^+ \rightarrow H_2O_2 + O_2; \tag{4}$$

$$Fe^{II}\text{–MPE} + H_2O_2 \rightarrow Fe^{III}\text{–MPE} + HO^- + HO\cdot; \tag{5}$$

$$Fe^{III}\text{–MPE} + \text{reductant} \rightarrow Fe^{II}\text{–MPE}. \tag{6}$$

The presence of a reducing agent in the reaction mixture regenerates the active Fe^{II}–MPE form, making possible the catalytic production of hydroxyl radicals [Eq. (6)]. Consequently, only low concentrations of iron salts are required to efficiently cleave DNA (*123–125*). Superoxide dismutase, by depleting the medium of free superoxide anion, and catalase, by disproportionating hydrogen peroxide to water and dioxygen, are both able to inhibit DNA breaks mediated by Fe^{II}–MPE.

The DNA-binding affinities of metallo-MPE were obtained with inert metal ions. The affinity constants of Ni^{II}–MPE and Mg^{II}–MPE are 2.4×10^4 and 1.5×10^5 M^{-1}, respectively, similar to the affinity constant of ethidium bromide (*125*). As expected for an intercalator, Mg^{II}–MPE unwinds DNA (11 ± 3° per bound molecule), and the binding site size is two base pairs.

The products of DNA cleavage by **2** are the free nucleobases and

5′-phosphate termini, with equal proportions of 3′-phosphate and 3′-phosphoglycolate ends (*125*), suggesting that deoxyriboses are degraded by hydroxyl radicals via H atom abstraction at C-4′, C-1′, and C-3′. A C-4′ chemistry explains the release of nucleobases and the formation of 5′-phosphate and 3′-phosphoglycolate termini, but base propenals were not detected. The 3′-phosphate ends might be produced by a C-1′ chemistry. A C-3′ chemistry has also been proposed (*7*).

Fe^{II}–MPE cleaves ds DNA in a relatively poor sequence-specific manner, which is not unexpected because the methidium entity is an intercalator of low overall base specificity. The only specificity known for this DNA cleaver is a slight preference for GC-rich regions. Sequence specificity is lower than that obtained with DNase I, making Fe^{II}–MPE useful in footprinting experiments (for a discussion on the different merits of DNase I, Fe^{II}–EDTA, and Fe^{II}–MPE in footprinting studies, see Refs. *84* and *115*). The Dervan reagent has been used to determine the location, the size, and the relative importance of binding sites of small DNA-binding molecules on native DNA (*126*, *127*) or proteins on restriction fragments (*128*, *129*), and to study RNA (*130*, *131*), chromatin (*132–134*), and ribosome (*130*) structures.

3. *Iron–EDTA Conjugates with Oligonucleotides, Peptides, or Proteins*

The Fe–EDTA moiety has been successfully attached to various sequence-specific DNA-binding molecules such as antibiotics, polypeptides, oligonucleotides, or proteins to provide new classes of "DNA affinity cleavers." This strategy allows the design of artificial restriction enzymes with defined target sequences and binding site sizes (*135*). Accordingly, hybrid molecules have been prepared by tethering EDTA to distamycin (*136–138*), netropsin derivatives (*135*, *139*), oligopeptides (*140–142*), or oligonucleotides. Such Fe–EDTA–oligonucleotide conjugates can be targeted for cleaving (1) single-stranded DNA or RNA (so-called modified antisense oligonucleotides) (*143–147*) or (2) double-stranded DNA by triple helix formation (*148–155*). As a demonstration of this latter strategy, a large genomic DNA fragment of 340-kilobase pairs of the chromosome III of *Saccharomyces cerevisiae* was cleaved on both strands at the correct location by a 20-mer having two Fe–EDTA motifs attached at both the 5′ and 3′ ends, and was able to recognize the triple-helix site inserted within this large genomic DNA (*153*).

More recently, $tRNA^{Phe}$ has been modified with an Fe–EDTA motif attached at U47 and analysis of the autocleavage products of this

modified RNA provided a visualization of the RNA tertiary structure (*156*). By attaching EDTA to a cysteine residue of a protein, introduced by site-directed mutagenesis at different positions, mapping of its different conformations has been possible. This has been done with staphylococcal nuclease (*157*). The global structure of the protein was not modified by the presence of the Fe–EDTA entity. The Fe–EDTA was linked at the Cys-31 of ribosomal protein S4 and used to explore the 16S rRNA structure by hydroxyl radical probing (*158*). It can also be tethered to a macrocycle such as sapphyrin (*159*). 2,6-Dicarboxypyridine and *N,N*-bis(2-picolyl)amine have been used as iron chelators and tethered to oligonucleotides to cleave DNA in a sequence-specific manner (*160*).

D. Chromium, Manganese, Cobalt, Nickel, Ruthenium, Rhodium, Platinum, and Uranium Complexes

Besides copper and iron complexes, many other metal complexes are able to cleave DNA. The corresponding results will be presented in this Section, except when the ligand is a porphyrin (see Section II,E for DNA cleavage by metalloporphyrins). Complexes are classified by increasing atomic number of the metal center [for a previous review article, more focused on DNA probing by metal complexes rather than on DNA cleavage, see Pyle and Barton (*161*)].

1. Chromium Complexes

Little is known about DNA damage by Cr(III) complexes, even though these compounds are considered to be responsible for chromium mutagenicity. The $[Cr^{III}(phen)_2Cl_2]^+$ and $[Cr^{III}(bpy)_2Cl_2]^+$ complexes are both mutagenic and able to cleave a supercoiled plasmid DNA via ss breaks, whereas $[Cr^{III}(CN)_6]^{3-}$ is not mutagenic and is inefficient as a DNA cleaver (*162*).

2. Manganese Complexes

Outside of the category of manganese porphyrins, one report indicates nuclease activity of a Schiff base manganese complex $[Mn^{III}(salen)]^+$ when activated by magnesium monoperphthalate. Single-strand breaks are observed at micromolar concentrations of the complex (*163*).

3. Cobalt Complexes

Λ-Tris(4,7-diphenyl-1,10-phenanthroline)cobalt(III), a photoactivatable molecular probe for left-handed ds DNA (Z-DNA), cleaves the

genome of simian virus 40 at specific sites, in the enhancer and promoter blocks and in the region downstream of 3′ termini, suggesting local Z conformations in SV40 DNA (*164*). Binding constants of $[Co^{III}(phen)_3]^{3+}$ to calf thymus DNA were found to be $9.4 \times 10^3\ M^{-1}$ by voltammetric studies (*165*).

4. Nickel Complexes

Highly sequence-specific oxidative cleavage of ds DNA has been achieved with a synthetic 55-residue protein, containing the DNA binding domain of Hin recombinase and the tripeptide Gly-Gly-His at the terminal amine (*166*). Nickel(II) is strongly chelated by these three amino acid residues and, after activation by magnesium monoperphthalate, DNA is cleaved at a single deoxyribose position on one strand of each binding site.

Simple square planar Ni(II) complexes of tetraazamacrocycles such as Schiff bases or cyclams are active as DNA cleavers in the presence of peroxides (potassium monopersulfate or magnesium monoperphthalate) (*167*, *168*). G bases are oxidized by the active form of these nickel complexes because of their preferential binding onto N-7 of guanines. One particular complex (**3**, Fig. 5), because of its steric hindrance, is able to promote the oxidation only of highly accessible guanine residues: terminal G, G mismatch, G bulge, or G in hairpin loops (*168*, *169*). The same complex has been used to probe accessible guanine N-7 positions in folded RNA structure (*170*).

5. Ruthenium Complexes

Barton *et al.* have developed the use of photoactivatable chiral ruthenium–phenanthroline complexes as probes to study DNA structures (*161*, *171*). The $[Ru^{II}(bpy)_3]^{2+}$ complexes are known to cleave DNA by photoactivation without (*172*) or in the presence of potassium peroxodisulfate (*173*, *174*). The Λ-tris(3,4,7,8-tetramethyl-1,10-phenanthroline)ruthenium(II) complex cleaves A forms of DNA helices under visible light irradiation (*171*).

The mode of interaction of such $[Ru^{II}(phen)_3]^{2+}$ derivatives with DNA has been a matter of some debate. Both intercalation and surface binding in the major groove were initially proposed for each of the enantiomers Δ and Λ, with intercalation as the predominant mode of interaction (*175*) (see also Ref. *176* for an interesting presentation of molecular recognition and chemical reactions in restricted spaces such as micelles, dendrimers, and DNA). However, viscosity data are against a classical intercalation interpretation (*177*). Additional results obtained by absorbance, fluorescence, and circular dichroism

have indicated that both stereoisomers of $[Ru^{II}(phen)_3]^{2+}$ have little selectivity for right-handed B-DNA and left-handed Z-DNA (*178*). Both enantiomers have the same affinity constant of $10^4\ M^{-1}$ for calf thymus DNA. Both NMR and circular dichroism (CD) studies of the binding of the same two enantiomers with the self-complementary oligonucleotide $d(CGCGATCGCG)_2$ suggest that the isomers bind to DNA in the minor groove at the central AT site, the observed AT specificity being more pronounced with the Δ than with the Λ enantiomer (*179*). The chiral discrimination was found to be higher when one phen ligand was replaced by a dipyrido[3,2-*a*:2′,3′-*c*] phenazine (dppz) ligand (*180a*). This latter ligand intercalates within DNA base pairs. Photocleavage of DNA by the excited state of $[Ru^{II}(bpy)_2(dppz)]^{2+}$ is not mediated by singlet oxygen, but by an electron transfer (*180b*).

Strekas *et al.* have reported the enantiospecific cleavage of DNA by Λ-$[Ru^{II}(bpy)_2(ppz)]^{2+}$, and not by the Δ enantiomer, in the presence of Cu(II), 3-mercaptopropionic acid, and hydrogen peroxide (ppz = 4′,7′-phenanthroline-5′,6′:5,6-pyrazine) (*181*). Copper binds to the second available phenanthroline site of the ppz ligand.

Thorp *et al.* have extensively studied the nuclease activity of ruthenium bipyridine-type complexes by generating Ru^{IV}–oxo entities by electrochemical methods (*182*, *183*). In the presence of DNA the reactive form $[Ru^{IV}{=}O(dppz)(tpy)]^{2+}$, prepared by electrochemical $2e^-$ oxidation of $[Ru^{II}(H_2O)(dppz)(tpy)]^{2+}$ (**4**, Fig. 5; see Ref. *184* for the X-ray structure), has been shown to decay within few seconds with concomitant DNA cleavage (*184–186*). Studies of DNA degradation products generated by $[Ru^{IV}{=}O(tpy)(bpy)_2]^{2+}$ indicate that this Ru^{IV}–oxo complex cleaves DNA by attacking H-1′ on deoxyribose units, as previously observed for the $Cu(phen)_2/H_2O_2$ (see Section II,B) and Mn-TMPyP/$KHSO_5$ systems (see Section II,E). The sugar degradation product 5-methylene-2(5*H*)-furanone (5-MF, Fig. 6) was identified (*187a*). The Ru^{IV}–oxo complex is also able to oxidize guanine residues to produce piperidine-labile cleavages. It should be noted that the corresponding ruthenium(III)–hydroxo complex $[Ru^{III}{-}OH(tpy)(bpy)_2]^{2+}$ is only able to oxidize G bases, and is unable to attack deoxyribose units. Covalent adducts are formed between CT DNA and ruthenium complexes, when the excited states of these complexes are able to oxidize guanine residues (*187b*).

6. *Rhodium Complexes*

The complexes $[Rh^{III}(phen)_2(phi)]^{3+}$ (**5**, Fig. 5) and $[Rh^{III}(phen)(phi)_2]^{3+}$ (phi = phenanthrenequinone diimine) cleave supercoiled

DNA on photoactivation in the region 310–360 nm, which corresponds to the ligand-to-metal charge transfer band (*188*). The complex **5** cleaves ds DNA at 5′-pyrimidine–purine steps such as 5′-CCAG-3′. The single-site cleavage patterns suggest the absence of diffusible species mediating the strand scission, and the asymmetry in cleavage pattern oriented to the 5′ side on each strand indicates that **5** attacks B-DNA from the major groove. NMR studies support the specific intercalation of the phi ligand of the Δ enantiomer of **5** (*189*). Intercalation of **5** through the major groove is also consistent with data on DNA cleavage products. This is also true when the phen ligand is replaced by a polyamine such as ethylenediamine: the corresponding $[Rh^{III}(polyamine)_2(phi)]^{3+}$ complex intercalates within a 5′-GC base pair in the major groove of B-DNA for the Δ enantiomer and within a 5′-AT base pair for the Λ isomer (*190*).

The initial DNA cleavage step involves H-3′ abstraction by the excited state of the phi ligand of **5**. Free nucleobases are released and 3′- and 5′-phosphate ends are detected, as well as base propenoic acids and 3′-phosphoglycaldehyde residues. These latter products are consistent with the reaction of dioxygen with the 3′-centered radical (*191a*). The formation of the 3′-phosphoglycaldehyde fragment is proportionally higher with two ethylenediamine ligands and one phi ligand (*191b*).

The three-dimensional folding of $tDNA^{Phe}$ was compared to native $tRNA^{Phe}$ by using **5** as a chemical probe (*192*). Both nucleic acids are cleaved at the same sites, suggesting that the global tertiary structure of $tDNA^{Phe}$ resembles that of $tRNA^{Phe}$ (for recent studies on DNA propeller twisting, sequence-specificity recognition of DNA, and recognition based on sequence-dependent twistability with enantiomers of **5**, see Refs. *193–195*, respectively).

7. *Platinum Complexes*

A platinum dimer $[Pt_2(P_2O_5H_2)_4]^{4+}$, containing diphosphonates as assembling ligands, cleaves supercoiled DNA when photoactivated (*196, 197*). The long-lived triplet state (9.5 μsec) of this platinum complex is probably responsible for its oxidative nuclease activity.

8. *Uranium Complexes*

Uranyl(III) salts such as $UO_2(OAc)_2$ or $UO_2(NO_3)_2$ have been used as photochemical agents for DNA cleavage and for probing of protein–DNA contacts (*198–199*). Single-strand DNA breaks are induced by uranyl acetate or uranyl nitrate under irradiation in the 420-nm region. The binding constant of the UO_2 dication is estimated to be of

the order of 10^{10} M^{-1} at pH 4 and preliminary data on DNA cleavage products suggest that the UO_2^{2+} chromophore binds in the minor groove by bridging phosphate groups of opposite strands. Photocleavage by UO_2^{2+} is not oxygen dependent and piperidine treatment does not significantly increase the number of DNA breaks, and free nucleobases are generated. All these data are in favor of H-1′ abstraction by the excited state of the uranyl salt, which is able to oxidize alcohols and olefins in aqueous medium (*199*).

E. Metalloporphyrin Complexes

The following discussion focuses on (1) the different ways of interaction of metalloporphyrins with DNA, (2) the two major modes of activation, by light or by oxidants, and the corresponding reactive species that are generated, and (3) the mechanism of DNA cleavage, which will be mainly detailed for the manganese derivative of the most extensively studied DNA-binding porphyrin, namely *meso*-tetrakis(4-*N*-methylpyridiniumyl)porphyrin (H_2TMPyP).

1. Interaction of Metalloporphyrins with DNA and Cleavage Activity

Since publication of the early works on the DNA intercalation and cleavage properties of some cationic porphyrin derivatives (*200–203*), a large variety of porphyrins and metalloporphyrins have retained the attention of researchers and generated a great number of works in the field of chemical and photochemical cleavage of DNA. The most frequently studied compounds in that family are natural products such as hemin [ferric protoporphyrin IX (*204–206*)], deuterohemin (*206*), coproporphyrin (*207*), or methylpyrroporphyrin (*208*, *209*), and also synthetic derivatives based on the porphyrin core bearing a large variety of hydrophobic, anionic, or cationic functional groups in the meso positions (*202*, *210–213*) (Fig. 7). All these ligands can take up various metals, such as Zn, Fe, Co, Mn, and Ni, which modulate the interaction and the reactivity with DNA. At least (see below), covalent attachment of the porphyrin ligand to a variety of suitable vectors opens the possibility to target their cleavage properties on selected sequences of DNA.

Binding mechanisms depend on the nature of the metal, its size, and its charge, and on the location of different substituents at the porphyrin periphery. In the absence of any X-ray crystallographic data on a porphyrin–DNA complex, our understanding of the nature of the binding process is based on the results of a variety of physicochemical studies: extensive NMR, equilibrium dialysis, flow dichro-

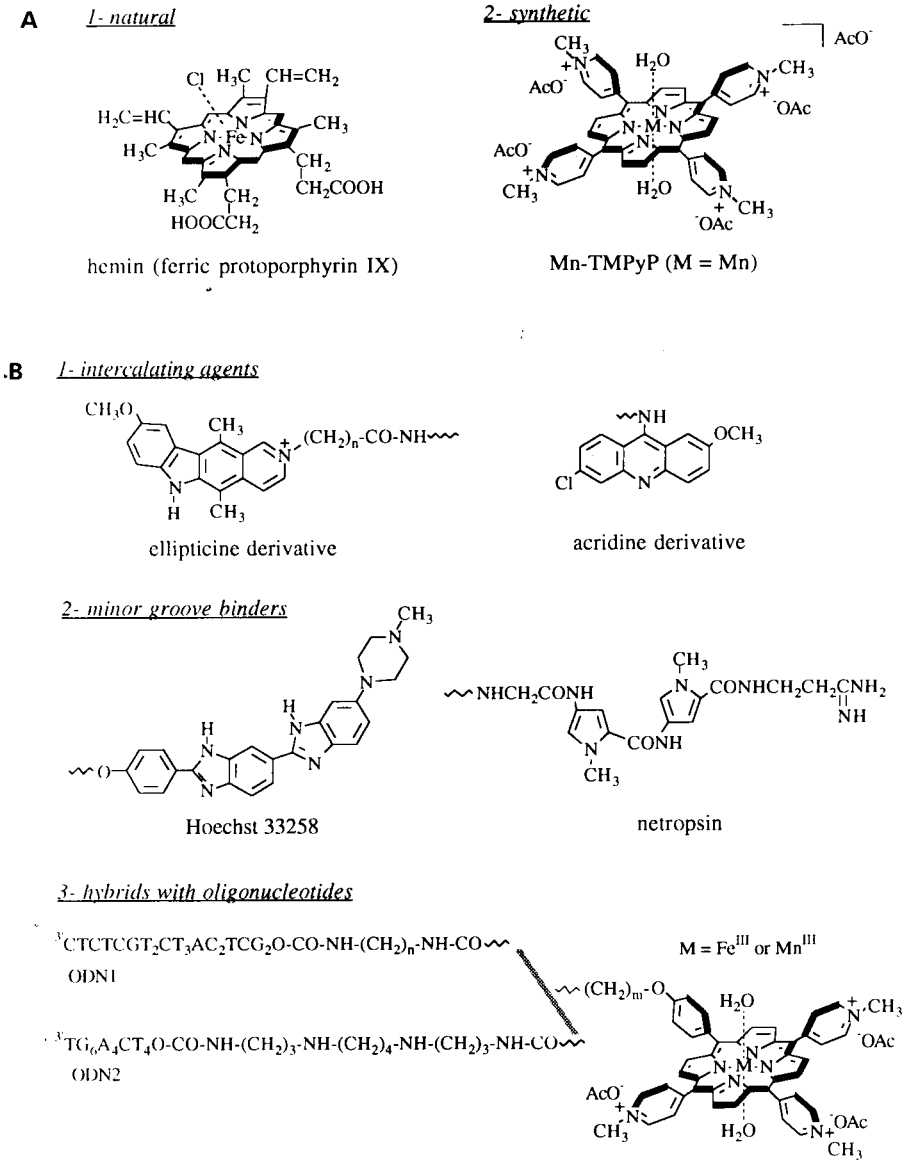

FIG. 7. (A) Examples of metalloporphyrins used in DNA cleavage. (B) Examples of vectors and hybrid molecules.

ism, and viscosimetry measurements (*214*, *215*). Some general features concerning cationic porphyrins can be pointed out, mainly deduced from the present knowledge on H_2TMPyP and its metallated derivatives:

1. The free ligand H_2TMPyP and its square planar complexes with Ni^{II} and Cu^{II} interact with poly(dG–dC)$_2$ and behave as intercalating molecules (*202*, *214*, *216*). H_2TMPyP is aligned perpendicular to the DNA helix axis (*217*, *218*). With poly(dA–dT)$_2$, these same nonaxially liganded molecules do not intercalate but bind externally, probably in the minor groove because of its higher electrostatic potential (*202*, *210*, *214*, *216*, *217*, *219–222*). The affinity constant of H_2TMPyP for calf thymus DNA is $7.7 \times 10^5\ M^{-1}$ (*210*, *223*).

2. Cationic complexes possessing (i) bulky substituents on the porphyrin framework or (ii) at least one axially bound ligand are too thick for intercalation into poly(dG–dC)$_2$, poly(dA–dT)$_2$, or DNA. As an example of the first category, due to a strong hindrance to the rotation of the ring substituents, porphyrins substituted with *ortho*-methylpyridiniumyl groups do not intercalate. In fact, only half of the porphyrin ring is necessary for DNA intercalation, and most of the porphyrins are capable of intercalative binding provided at least two *meso*-pyridiniumyl substituents in cis position can freely rotate and come in-plane with the porphyrin macrocycle (*210*). As an example of the second category, Zn-TMPyP, which is five-coordinated, does not intercalate, but lies at an angle of 62–67° relative to the helix axis and binds outside to AT sites (*202*, *224*, *225*). For the diaxially liganded complexes with Mn^{III}, Fe^{III}, or Co^{III}, intercalation is also precluded, consequently they bind in an outside fashion to DNA. The Co–TMPyP complex displays an orientation angle of roughly 45° relative to the helix axis and appears to bind to a partially melted region of DNA (*217*). These outside-binding porphyrins are believed to interact in the minor groove of DNA. A detailed study of the chemical reactivity of Mn–TMPyP (*226*, *227*) showed effectively that this metalloporphyrin cleaves DNA from the minor groove. The interaction is largely electrostatic in nature, because, as expected, it is sensitive to ionic strength. The exact nature of the ligand(s) occupying the axial site(s) of Mn–TMPyP under the conditions of most DNA binding studies is unknown. On the basis of recent X-ray studies analyses of Mn–TMPyP (*228*), axial ligand candidates are two water molecules that may serve as DNA donor/acceptor hydrogen bond sites with DNA.

Analyses of Mn–TMPyP–mediated strand scission on a restriction fragment (*224*), and on a series of short ds ODNs containing a tri-

nucleotide sequence consisting only of adenine and thymine bases (i.e., three contiguous AT base pairs, called the AT triplet) (*227*), have revealed that this AT triplet has to be considered as the minimal size of the metalloporphyrin-preferred binding site. Such cleavage selectivity is due to a tight interaction between this manganese porphyrin and AT-rich regions of DNA and is consistent with the relative affinity of Mn–TMPyP for poly[d(A–T)·d(A–T)] and poly[d(G–C)·d(G–C)] (12×10^4 and 0.2×10^4 M^{-1}, respectively) (*229*). It can be explained by electrostatic interactions of the cationic porphyrin, with the more negative potential in the minor groove of AT-rich polymers compared to GC polymers (*227*). When the AT sequence is longer than a triplet, cleavage not only affects adjacent GC or CG base pairs, but also base pairs inside the AT-rich sequence. A duplex that contains, for example, four overlapping triplets gives four consecutive cleavage sites (*230*).

Hydrophobic or anionic porphyrin derivatives do not exhibit any intrinsic affinity for DNA and so the only ways to induce DNA oxidative damage are to force them to stay close to DNA, either by linking to DNA vectors, by using dicationic metal salts in order to favor ternary associations of porphyrin/metallic cation/DNA, or by working at high concentrations with derivatives able to generate diffusing active species.

As pioneered by Dervan *et al.* (*123*, *231*), there is the possibility of targeting the activity of a DNA cleaver by attaching it to different vectors (see also Sections II,B,2, II,C,2, and II,C,3). We describe now work done in our laboratory on the different ways to recognize the cut specific sequences of DNA by linking tailored cationic manganese porphyrins to intercalators, minor-groove binders, or oligonucleotides as a rather well-documented example (see Fig. 7 for structures and Fig. 8 for DNA interaction modes).

The covalent attachment of a chelated redox-active transition metal to an intercalating agent is a way to mimic bleomycin (see Section II,2,A), as shown by Lown and Joshua, by attaching an iron(III) deuteroporphyrin IX to 9-chloroacridine via a polyamine linker (*232*). Shudo *et al.* have used a potent mutagen (resulting from glutamic acid pyrolysis) as an intercalator to be linked either to a derivative of Fe^{III}-[tris-*o*-tolyl(*p*-aminophenyl)]porphyrin, to a hydrophobic macrocycle complex, or to Fe^{III}–protoporphyrin IX (*233*). These molecules are able to cleave ds DNA in the presence of molecular oxygen and a reducing agent, but only using high amounts of probes relative to DNA. Recently, hemin was covalently connected to two 9-aminoacridines, giving a bisdentate compound

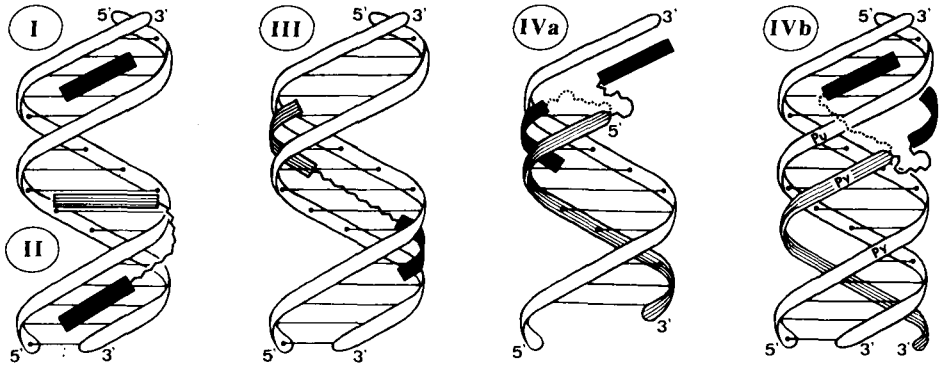

FIG. 8. Different ways to address the nuclease activity of cationic manganese porphyrins on selected sequences of DNA: free Mn–TMPyP (**I**) (*226, 227*); the vector strategy can be an intercalator (**II**) (*237, 238*), a minor-groove binder (**III**) (*240*), an ODN in antisense (**IVa**) (*246, 250*), or an antigene (**IVB**) (*247, 248, 289*). The solid black areas represent cationic manganese porphyrin; the striped areas are vector. Two possible ways of interaction of the manganese porphyrin moiety with DNA are represented by solid and dotted wavy lines.

with higher DNA binding affinity than that of the hemin (*234*). The first synthesized "metalloporphyrin–ellipticine" hybrid molecule was based on a tris(*p*-tolyl)porphyrin moiety (Fig. 7) (*235*). Because one key point in this strategy is to choose porphyrins having an intrinsic affinity for DNA, it was decided to use only cationic porphyrin precursors (*236–238*). The affinity of such cationic metalloporphyrin–ellipticin conjugates for a DNA duplex depends on the nature and the length of the linker and ranges from 2.9×10^8 to $8.2 \times 10^9\ M^{-1}$ for poly[d(A–T)] and from 1.0 to $7.0 \times 10^8\ M^{-1}$ for poly[d(G–C)] (*229, 238*). These hybrid molecules (iron or manganese complexes) are cytotoxic against L1210 cells in culture with ID_{50} values ranging from 0.7 to 1.6 μM, whereas the corresponding zinc or nickel hybrids are not cytotoxic. On the same cell line, the ID_{50} value of BLM is only 1.7 μM (*238*).

Recently, potential sequence-specific DNA cleavers have been prepared by attaching a cationic manganese porphyrin motif and minor-groove binders such as the antibiotic netropsin (*239*) or Hoechst 33258, a bisbenzimidazole dye having a strong preference for AT-rich regions (see Fig. 7 for structure) (*240a*). Preliminary results obtained with a Mn–cationic porphyrin/H33258 hybrid showed that the dye was directing the selectivity of cleavage (*240b*).

Several examples of sequence-selective cleavage of DNA by various cleaving agents covalently attached to oligonucleotides have been de-

scribed in the literature (see Sections II,B,2 and II,C,3). First, hybrid molecules based on metalloporphyrin-substituted ODNs were prepared with hydrophobic derivatives of methylpyrroporphyrin XXI tethered to $(dT)_7$ ODNs (*208*). The corresponding iron(III) compound activated by H_2O_2 induced, on the ss DNA target, direct breaks and cross-linked products; these latter lesions were partly transformed to DNA breaks after piperidine treatment. Damage appears to cover 10 bases around the position of the reactive moiety on the target sequence, but only limited yields of cleavage were attained (10–20%). In a similar approach, antisense ODNs linked to proto- and methylpyrroporphyrins and their zinc derivatives were shown to create cross-links on an RNA target at G bases located close to the photosensitizer in the hybrid complex (*209*). Iron(III)–hemin or deuterohemin conjugates, on activation with H_2O_2 or reductants, gave alkali-labile lesions and alkali-labile cross-links (*206*, *241*). Also described is a palladium–coproporphyrin I conjugate (*207*) that, by photochemical activation, leads to 30% of DNA cleavage over 10 bases on the target sequence. The iron(III) *meso*-tetra(4-carboxyphenyl)porphyrin–ODN hybrid in the presence of a reductant mediates an efficient direct DNA cleavage at low concentration, with a reagent:target ratio of 1:1 (*242*).

Cationic metalloporphyrins, due to their high intrinsic affinity for nucleic acids, appear as the most reasonable candidates to be coupled to ODNs. The metalloporphyrin moiety (bottom of Fig. 7) usually carries three cationic pyridiniumyl groups (*243*) but derivatives bearing four cationic substituents, as it is the case in the parent compound Mn–TMPyP, have recently been described (*244*, *245*). Such conjugates were used to target the initiation codon region of the *tat* gene of the HIV-1 genome in an antisense strategy (*246*) or to target one possible triple helix site in the *rev* and *pol* genes of HIV-1 in an antigene strategy (*247*, *248*) (Fig. 7, ODN1 or ODN2; for a review on the triple-helix strategy, see Ref. *249*). Development in this field presumes a careful design of the tether of the conjugate, depending on the cleaving agent and on what is known about its interaction with the target as well as chemical modifications to improve their stability (*206*, *208*, *229*, *241*, *245*, *248*, *250*).

Other hybrid molecules have been prepared wherein porphyrin is attached to the intercalating agent acridione (*251*), to a nucleoside (*252*), to chlorambucil (a DNA cross-linking agent) (*253*), or to dextran (a water-soluble polymer) (*254*). The synthesis of a bis(arginyl) tricationic porphyrin designed to target the major groove of DNA has been reported (*255*). The concept of hybrid porphyrin vector molecules has

been extended to pyropheophorbide–polyamine molecules (*256*), which are able to cleave DNA by electron transfer when activated at 690 nm, a suitable wavelength in phototherapy.

2. *Modes of Activation and Reactive Species*

Depending on their structure, porphyrin derivatives can be either chemically or photochemically activated to degrade biological molecules and especially to produce DNA breaks.

a. Photoactivatable Porphyrin Derivatives: Singlet Oxygen or Electron Transfer? Two different categories of photoactivatable porphyrin derivatives are currently under study as photosensitizers in the photodynamic therapy approach: (1) derivatives of hematoporphyrin, such as HpD, which is a modified protoporphyrin IX with two α-hydroxyethyl groups instead of two vinyl groups, and (2) fully synthetic porphyrin derivatives having a noticeable affinity for DNA.

The first category corresponds to porphyrin molecules having hydrophobic substituents at the periphery of the tetrapyrrole ring or substituents bearing hydroxy or carboxylic acid functions. Some of these HpD derivatives have been proposed for phototherapy of cancers in human clinical trials, including Photofrin, which is currently used in the treatment of superficial bladder cancer (*257–260*). The toxicity of these porphyrin derivatives on tumor cells is mainly due to their affinity for membranes (*257*) and may be explained, when they are activated with red light at 630 nm, by the generation of reactive singlet oxygen in a Type II photochemical reaction. Current efforts are focused on the preparation of new macrocyclic conjugated molecules having a strong absorption between 600 and 700 nm, in the region corresponding to the maximum of light penetration through tissues. Phthalocyanine or pyropheophorbide derivatives are potential new photosensitizers (*261–263*).

The second category of porphyrins that can be photoactivated corresponds to those molecules exhibiting a reasonable affinity for DNA or RNA, and as a result are potential DNA or RNA cleavers. The paradigm molecule in this domain is the *meso*-tetrakis(4-*N*-methylpyridiniumyl)porphyrin (H_2TMPyP, Fig. 7, M = H_2), which exhibits high quantum yields for formation of singlet oxygen (*264*). The photonuclease activity of H_2TMPyP was initially reported by Fiel *et al.* in 1981 (*265*). In further studies, it was confirmed that H_2TMPyP and Zn–TMPyP are able to photolyse supercoiled plasmid DNA to open circular and linear DNA by irradiation at 436 nm (*266, 267*). Single-stranded breaks are the main damage induced on ds DNA by

photoactivated H_2TMPyP, occurring mainly at guanine bases and also on thymines. Inhibition of cleavage by nitrogen bubbling (dioxygen removal) suggests that the Type II photoprocess (mediated by singlet oxygen) occurs with significantly higher yields compared to Type I reactions (electron transfer reactions between porphyrin excited states and DNA bases) and are responsible for the formation of alkali-labile sites in aerated systems (*268*).

With photoactivatable cationic zinc porphyrin–ellipticine conjugates (*269*), both the fluorescence yield and production of singlet oxygen are lower compared to those of Zn–TMPyP, the parent porphyrin molecule, due to the quenching of the singlet state of the porphyrin moiety by the attached ellipticine. Interestingly, these photochemical properties are dramatically enhanced in the presence of DNA as a result of a conformational change: the ellipticine moiety intercalates in ds DNA and so can not quench the zinc–porphyrin singlet state. On irradiation at 436 nm, the photocleavage of supercoiled ΦX174 DNA is 50-fold greater than that of HpD and involves singlet oxygen as a probable main species responsible for DNA cleavage (*270*).

It has been shown that phosphorus(V) tetraphenylporphyrin is also capable of inducing DNA cleavage via a photoreaction involving singlet oxygen, and an electron transfer from DNA to the short-lived singlet excited state of the phosphorus (*271*). Water-soluble sulfonated porphyrins such as H_2TPPS or Zn–TPPS are good photosensitizers, but very poor DNA cleavers, probably because of their weak interactions with DNA due to their anionic groups (*265*, *267*).

b. Activation by Oxidants and Reactive Species Involved: Diffusing Oxygenated Reactive Species or Nondiffusible Metal–Oxo Entities? The oxidative cleavage of DNA with a cationic water-soluble porphyrin was first demonstrated by Fiel *et al.* with Fe-TMPyP (Fig. 7, M = Fe) activated by a reducing agent in the presence of molecular oxygen (*200*). Then Dabrowiak *et al.* (*224*, *272*) showed that not only reducing agents such as ascorbate or superoxide anion in the presence of oxygen but also oxygen atom donors such as iodosylbenzene are able to activate the complex with an efficiency depending on the metal. Several other activating agents were subsequently investigated: potassium monopersulfate ($KHSO_5$) (*272–274*), magnesium monoperphthalate (MMPP) (*275*, *276*), and, more recently, peroxynitrite ($ONOO^-$) (*277*). Hydrogen peroxide appears 10^3- to 10^4-fold less efficient as cofactor compared to $KHSO_5$ for Mn–TMPyP activation (*230*, *274*). These single-oxygen-atom donors are expected to react directly with the metalloporphyrin in a one-step process to yield a cata-

lytically active species and it is thought, by analogy with cytochrome *P*-450 modeling studies (*36*), that the reactive species involved in DNA breaks is a high-valent oxo intermediate [Eq. (7)]. Under treatment with ascorbate in the presence of molecular oxygen, reductive activation of O_2 by manganese or iron porphyrins can also yield high-valent metal–oxo species [Eq. (8)]. Alternatively, H_2O_2 and peroxy radicals are possible intermediates, as suggested by the use of inhibitors and scavengers, but diffusible hydroxyl radicals can be excluded. However, hydroxyl radicals produced in close proximity to a DNA target might be involved [Eq. (9)] (*278*):

$$\text{Por–M}^{\text{III}} \xrightarrow[\text{MMPP, or } H_2O_2]{+\ \text{PhIO, KHSO}_5,} \text{Por–M}^{\text{V}}\text{=O}; \tag{7}$$

$$\text{Por–M}^{\text{III}} \xrightarrow{+\ e^-} \text{Por–M}^{\text{II}} \xrightarrow[-\ H_2O]{+\ O_2 + e^- + 2H^+} \text{Por–M}^{\text{V}}\text{=O}; \tag{8}$$

$$O_2 \xrightarrow{+\ \text{Por–M}^{\text{II}}} O_2^- \xrightarrow{+\ H^+} O_2 + H_2O_2 \xrightarrow{\text{Por–M}^{\text{II}}} + HO^- + HO\cdot; \tag{9}$$

$$\text{Por–M}^{\text{III}} \xrightarrow{H_2O_2} \text{Por–M}^{\text{IV}}\text{–OH} + HO\cdot. \tag{10}$$

For Mn–TMPyP activated by $KHSO_5$ (*272*, *273*), the quasi-absence of additional weaker bands close to the main fragments in PAGE analysis strongly supports a nondiffusible active species, namely, a high-valent manganese–oxo porphyrin complex similar to the iron–oxo intermediate involved in cytochrome *P*-450 chemistry [Eq. (7)]. An investigation using Mn–TMPyP/$KHSO_5$ in aqueous solution to oxidize carbamazepine, an analgesic and anticonvulsant drug, shows that, through a "redox tautomerism" mechanism involving a coordinated water molecule on the metalloporphyrin catalyst, the oxidizing entity can be localized on one or the other face of the activated metalloporphyrin (*279*). Subsequently it was reported that oxidation at C-1′ of DNA deoxyribose results from such a mechanism, supporting a Mn^V–oxo as the reactive species involved in a cytochrome *P*-450-type hydroxylation reaction during DNA cleavage (*280*). With hydrogen peroxide as cofactor, breaks are as well-defined, as in the case of $KHSO_5$, and probably result from the same chemistry (*230*), suggesting that H_2O_2 is able to generate Mn^V–oxo species via a heterolytic cleavage of the peroxidic O–O bond [Eq. (7)]. However, because the reaction is much less efficient, the question of a homolytic cleavage of H_2O_2 giving hydroxyl radicals and M^{IV}–OH species with an intrinsic lower reactivity [Eq. (10)] is still open in this particular case.

In similar conditions with $KHSO_5$, Fe-TMPyP is less active compared to the manganese derivative: such a difference is not fully understood at present. Electrochemical methods were also used to activate Mn^{III} and Fe^{III} complexes of TMPyP to bring about DNA cleavage (*281*).

Anionic porphyrins are usually much less reactive, as it has been reported for Fe–TPPS activated with DTT (*200*). Cleavage experiments with anionic manganese porphyrins activated by $KHSO_5$ failed, even in the presence of polycations (*274*). In the case of hemin (ferric protoporphyrin IX chloride), for which some of its effects on gene expression might be mediated by nicking of DNA, strand scissions require the presence of O_2, a reducing agent, and transition metals salts, e.g., Co^{II}, Zn^{II}, Ni^{II}, used to favor a ternary association, porphyrin/metallic cation/DNA (*204*, *205*). In another strategy, hemin or deuterohemin linked to ODNs showed unexpected selective cleavage (30 to 50% of the target) after activation by either H_2O_2 or reducing agents and subsequent piperidine treatment (*206*, *241*). Linked to intercalating agents, deuterohemin activated by molecular oxygen and reducing agents appears to be a weak DNA-cleaving agent. Because DNA cleavage was partially inhibited by catalase and superoxide dismutase, this suggests that these BLM models produce reduced oxygen species (superoxide, hydrogen peroxide, hydroxyl radicals) rather than metal–oxo entities.

3. Mechanism of DNA Cleavage

The mechanism of DNA damage may involve either diffusing oxygen-reactive species, implying that the damage spans over several bases, or a nondiffusible oxidative species coordinated onto metalloporphyrin, inducing then a more localized damage. Oxidation of bases or deoxyriboses can lead to direct breaks, to alkali-labile lesions, and also to the formation of cross-linked products that can be converted (partially or totally) to DNA breaks after alkali treatment. The mechanism of DNA cleavage is now well-known for the Mn–TMPyP/$KHSO_5$ system. Additional and partial information exists for few other porphyrin derivatives.

a. Deoxyriboses as Main Targets for the Mn^{III}–TMPy / $KHSO_5$ System. When produced in the proximity of DNA, one (at least) of the reactive species evoked above attacks deoxyribose moieties and produces oxidative lesions, leading to breaks of the sugar phosphate DNA backbone, according to the mechanism detailed below. Gel electrophoresis analyses of DNA binding and cleavage specificity indi-

cated that cationic manganese or iron porphyrins bind to the minor groove and cleave DNA at all four possible nucleotide positions, strongly suggesting that deoxyriboses are the primary sites of attack (*225*). Other preliminary data were obtained by reference to the mechanism of BLM: neither Mn^{III}, Fe^{III}, or Co^{III} complexes of H_2TMPyP activated by ascorbate, superoxide ion, or iodosylbenzene (*224*) nor Mn–TMPyP in the presence of $KHSO_5$ (*276*) produce base propenals, the main characteristic products of DNA damage induced by BLM. At least, these data suggest that, if H-4′ is the target for the high-valent manganese–oxo species as observed for metallo-BLM-mediated DNA breaks, then the oxygen-dependent route is not involved (see Fig. 4). Alternative targets accessible from the minor groove are the tertiary C–H bond at C-1′ and two secondary C–H bonds at C-2′ (pro-R H-2′) and C-5′ (pro-S H-5′) (see Ref. *7* for a discussion on the accessibility of sugar C–H bonds with respect to groove binding). Further studies evidenced two main mechanisms:

1. First, a simplified model of DNA, polydeoxyadenylic acid, was shown to be readily cleaved at neutral pH by Mn–TMPyP/$KHSO_5$ with spontaneous release of free adenine and, after heating, formation of a rather unstable sugar degradation product identified as 5-methylene-2(5*H*)-furanone, supporting a C-1′ oxidation pathway. The first β-elimination created a 5′-phosphate end and the second one was accompanied by 5-MF release. The two DNA strands were terminated by phosphate groups (Fig. 6, route A) (*282*).

2. On extension to other polydeoxynucleotides, ds copolymers, and calf thymus DNA (*226*, *276*) it was shown that (i) a preliminary amount of free bases was released at ambient temperature; (ii) after heating, two other products were detected and have been identified as 5-MF and furfural (FUR) by HPLC; (iii) the appearance of FUR was correlated with an enhanced release of the corresponding bases during the thermal step and provided evidence for a C-5′ oxidative pathway (Fig. 6, route B): hydroxylation at C-5′ gives a C-5′ aldehyde at one strand terminus and a 3′-phosphate at the other at ambient temperature. On heating, two β-eliminations result in the formation of FUR and in free base release, leaving a phosphate at the 5′ terminus (*227*, *230*, *283*). The α,β-unsaturated aldehyde intermediate produced by the first β-elimination was formally identified during the course of cleavage reaction on poly(dA)·poly(dT) (*284*). Both routes A and B gave rise to the same phosphate termini, but the sugar degradation products were different and the chronology of base release and DNA break was inverted. The two monophosphate esters (at 3′ and

5′ ends) on both sides of the cleavage site were characterized by ^{31}P NMR analysis (*285*).

The FUR:5-MF ratio is indicative of the relative reactivities of the activated Mn–TMPyP complex toward C-5′ and C-1′ for various DNA and DNA models. The C-1′ target is the main hydroxylation site for calf thymus DNA and GC polymers when selective attack at C-5′ is observed for AT polymers or AT-rich sequences in DNA, which suggests that the mechanism of DNA cleavage is highly sequence dependent. Hydroxylation at C-1′, which is located in the minor groove, also confirms that the cationic manganese porphyrin interacts with this groove. Subtle changes in the interactions of the cleaving reagent with DNA explain that reactivity changes from one target to the other: the largely opened single helix of ss polydeoxynucleotides or the widened minor groove of GC-rich ds polymers allows the more reactive tertiary C-1′ carbon to be oxidized. For AT-rich ds polymers, the narrow minor groove restricts the access to C-1′, deeply located in the groove, and then C-5′, which is located at the entrance of the groove, is preferred. Until now, oxidative chemistry at C-1′ of deoxyribose has been demonstrated only for $Cu^{I}(Phen)_2/H_2O_2$ (*7*, *83*, *286*), enediyne antibiotics such as neocarzinostatin in the presence of thiols (*7*, *287*), and more recently for ruthenium–oxo complexes (*187a*). Oxidative chemistry at C-5′, besides the case of Mn–TMPyP, represents the major mode of DNA cleavage by neocarzinostatin (*287*), but, because of the presence of reducing agents, the end-product FUR could never be observed (*7*).

b. Nucleobases as Possible Alternative Targets. In the case of hydrophobic or anionic metalloporphyrins linked to oligonucleotides, induced damage to the DNA target included chain scission, alkali-labile lesions, and cross-links that were partly transformed to DNA breaks (*206–208*, *241*). Hemin or deuterohemin conjugates show unexpected selective cleavage, at guanine positions in the close vicinity of the metalloporphyrin location on the target sequence (*206*, *241*). This guanine-selective DNA cleavage is due to complete transformation of cross-linked products on piperidine treatment, but nothing is known on the chemical nature of this base damage. In the case of cationic metalloporphyrins linked to oligonucleotides, an ODN–manganese porphyrin hybrid was shown to recognize and cut selectively the ss target sequence, even in the presence of a large excess of random DNA (*246*). The vectorized metalloporphyrin cleaved the labeled 35-mer target at 10 n*M*, a concentration two orders of magnitude order lower than the "free" metalloporphyrin Mn–TMPyP. Because the

cleavage pattern shows an intense smear near the junction of ss and ds regions of the duplex, the mechanism, in this case, must not be restricted to the specific 5′ or 1′ attack, as previously observed for Mn–TMPyP (*246*, *288*). On hot piperidine treatment, these smears are transformed into cleavage products at G residues, the intensity of the cleavage sites revealed by piperidine decreasing with the distance from the location of the metalloporphyrin moiety. The exact nature of the damage still remains to be elucidated, but it is clear that guanine damage strongly suggests that the active manganese–oxospecies is not acting only as a deoxyribose cleaver, as observed when the cationic manganese porphyrin is not tethered to an ODN (*245*, *250*, *289*).

III. Metal Ions and Nucleic Acid Hydrolysis

A. Role of Metal Ions in Enzyme-Catalyzed Nucleic Acid Hydrolysis

Nucleases are able to catalyze the hydrolysis of P–O bonds of phosphodiesters within a few seconds (*290*). This efficiency is impressive, because we know that the same noncatalyzed hydrolysis is a very slow reaction at ambient temperature (the half-life of a phosphodiester linkage of DNA being estimated to be 200 million years at pH 7), making very challenging the rational design of metallonuclease mimics.

During the past decade, many crystal structures of phosphate-hydrolyzing enzymes have been determined at high-level resolution, allowing a precise determination of metal ion binding sites. These ions, calcium, magnesium, zinc, iron, and manganese, play a key role in two catalytic events, in neutralizing the negative P–O charge by cation complexation and in assisting the nucleophilic attack of a coordinated H_2O/OH^- (or an amino acid residue) onto the tetragonal phosphorus atom of the phosphate to be cleaved.

The role of the divalent metal ions present in natural phosphodiesterases became clear in bovine pancreatic deoxyribonuclease I (DNase I), the first endonuclease structure determined by X-ray crystallography. The nucleophilic attack of a water molecule activated by a histidine residue is facilitated by the interaction of a calcium ion with the phosphate group to be cleaved (*291*). Glutamic and aspartic residues involved in magnesium binding have been identified in the crystal structure of four type II restriction enzymes: *Eco*RI (*292*), *Eco*RV (*293*), *Pvu*II (*294*), and *Bam*HI (*295*), as well as in that of the repair

enzyme *E. coli* exonuclease III (*296*). Recent studies on *Eco*RV report that the apparent affinity of the enzyme for magnesium(II) is much higher at the recognition site (GATATC) than at nonrecognition sites (*297*, *298*). Two metal ion binding sites have been identified in the structure of the exonuclease catalytic site of the Klenow fragment of DNA polymerase I of *E. coli:* one for zinc (two aspartic and one glutamic residues) and the second one for magnesium (two aspartic residues) (*299*). A similar spatial distribution of acidic amino acid residues was found in the structure of *E. coli* DNA topoisomerase I, an enzyme involved in DNA topology by breaking and religating ds DNA (*300*). Alkaline phosphatase (*301*), phospholipase C (*302*), the ribonuclease H domain of HIV-1 reverse transcriptase (*303*), and P1 nuclease (*304*) are additional examples of hydrolytic enzymes having at least two metal ions at their active site. The crystal structure of the kidney bean purple acid phosphatase has been determined (*305*). This enzyme catalyzes adenosine triphosphate hydrolysis and its active site contains a dinuclear Fe^{III}–Zn^{II} motif. In this case, a transition metal is involved in the active site of the enzyme and its role in the phosphate hydrolysis is still an open question. One possibility is that the phosphate ester coordinates at the more labile Zn^{II} and that Fe^{III}–OH is then involved in inducing hydrolysis at the phosphorous. With all the detailed crystal structures now available, it is possible to better understand the role of the metal ions acting as cofactors in DNA cleavage catalyzed by hydrolyzing enzymes.

When at least two metal centers are present, the mechanism of DNA cleavage is referred to as "the two-metal-ion assisted phosphoryl transfer." The pair of metal ions could serve as a Lewis acid, polarizing the P–O bonds of the substrate to make a better electrophile, orient the two reactants (the phosphorus center and the nucleophile), and stabilize the pentacoordinate transition state. One metal would activate an incoming nucleophile (e.g., a coordinated water molecule) by lowering its pK_a and facilitating its attack on the phosphorus atom, the other one would stabilize the leaving oxygen atom linked to the 3′-carbon of the sugar residue (Fig. 9). The phosphate ester to be cleaved is not always bridging two metals; it can bind to one metal only, as in P1 nuclease (*304*).

Because the metal center is usually chelated by several carboxylate residues that reduce the overall charge of the resulting complex, this might render deprotonation of a metal-bound water molecule less likely. Karlin has proposed that a water molecule or a hydroxo ligand bridging two metals could have a considerably lower pK_a and might be involved in the nucleophilic attack (*306*). Such a bridging hydroxo

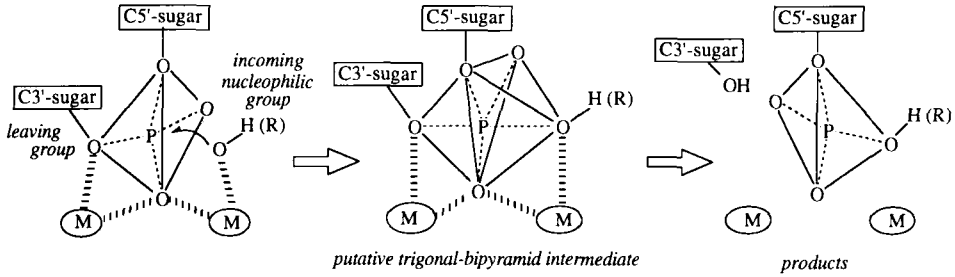

FIG. 9. Proposed DNA phosphate hydrolysis by enzymes containing dinuclear metal centers, via "two-metal-ion assisted phosphoryl transfer." Solid lines indicate the geometry around the central phosphorus atom. Charges on oxygen atoms and metals have been omitted.

ligand is present in the crystal structure of the kidney bean purple acid phosphatase (*305*), wherein the Fe^{III}–Zn^{III} distance is 3.1 Å. It is also proposed for *Penicillium citrinum* P1 nuclease, which shows two zinc ions separated by 3.2 Å but, apparently, this bridging hydroxo (in fact, the authors suggested a water molecule) is not directly involved in the described catalysis mechanism (*304*). Such nucleophilic bridging oxygen atoms are also proposed for hydrolysis of model compounds such as phosphate diesters (*307*) or monoesters (*308*).

An S_N2 phosphate nucleophilic displacement seems to prevail in biology (*309*). The concomitant approach of the nucleophile and the release of the leaving group take place at and from apical positions of a pentavalent phosphorus intermediate. The stereochemistry of the P–O bond hydrolysis is an inversion of configuration as evidenced for the first time for the 3′-exonuclease activity of DNA polymerase I (*310*). The nucleophile approaches on one face of the initial tetrahedral phosphate group and promotes the spatial rearrangement to the trigonal bipyramid transition state (pentavalent phosphorus intermediate), where the leaving group is opposite to the incoming nucleophile. The O–P–O angles must change from the initial tetrahedral value of 109° to 120° for equatorial groups and to 90° for the two apical groups with respect to the equatorial plane. A two-metal core can stabilize the pentavalent transition state or intermediate (Fig. 9).

B. Hydrolysis of RNA. The Case of Ribozymes

In RNA, the 2′-OH group on the ribose unit constitutes an intramolecular nucleophile, making the attack of the vicinal 3′-phosphodiester bridge much easier than that for DNA, which is deprived of such

a possibility. A first trans-esterification step involving the 2′-OH nucleophilic attack on the 3′-phosphate leads to a five-membered ring phosphate and so to fragments of RNA, ending with a 2′,3′-cyclic phosphate on one side and a 5′-OH function on the other side. Hydrolysis of the cyclic phosphodiester occurs readily, this second step being facilitated by the fact that the phosphodiester to be attacked by water is a cyclic strained phosphodiester (*311*). Nucleophilic attack of the 2′-OH is the key step in the alkaline hydrolysis of RNA.

Nonenzymatic hydrolysis of RNA assisted by metals (*312–316*) as well as by some ribozymes (*317, 318*) presumably follows the mechanism described above. Metals may be involved in the deprotonation of the 2′-OH group (*319*). Ribozymes, now recognized as metalloenzymes (*318, 320, 321*), correspond to selected sequences of RNA able to cleave the same strand (intramolecular process) or an RNA sequence on a different strand (intermolecular process). Metal ions are necessary to ribozymal activity (*318*). They promote the folding of the secondary structure of RNA into an active tertiary structure, and it is difficult to discriminate between their structural and/or catalytic role (*322, 323*).

The so-called hammerhead ribozymes belong to the category of ribozymes that involve the 2′-OH group of adjacent ribose as a nucleophile. Recent kinetic data suggest that two magnesium ions are involved in the cleavage step (*317*). One Mg^{II} is linked to the 2′-oxygen atom of the ribose ring at the cleavage site and the second one acts as a Lewis acid by coordinating the leaving 5′-oxygen atom. Despite a large value of 4.4 found for the apparent solvent isotope effect $k_{cleav}(H_2O)/k_{cleav}(D_2O)$, a proton transfer step is not involved in the rate-determining step of the RNA cleavage. Because the concentration of Mg^{II}–OD in D_2O is severalfold lower than that of Mg^{II}–OH in H_2O, a magnesium–hydroxo species is probably the key intermediate in the ribozyme-catalyzed reaction (*317*).

The mechanism of RNA cleavage does not always make use of the advantage of the adjacent 2′-OH nucleophile, because examples exist of enzymatic hydrolysis or cleavage by trans-esterification of RNA, for which the products of the reaction are 5′-phosphate and/or 3′-OH ending fragments. This latter mechanism, involving an external nucleophile, has been observed for RNase H (*304*) or RNase P (*324*) or group I and II introns (*318, 320, 321, 325*). Whatever is the attacking nucleophile (intramolecular or external), both mechanisms involve an in-line S_N2 nucleophilic substitution at the phosphorus center (*317, 328, 325*).

An important point is the flexibility of the scissile phosphodiester. In this respect, the double-stranded structure of DNA is too rigid, as

illustrated by the failure of metal complexes to cleave an RNA substrate when hybridized onto a complementary strand of DNA (*326*). Some bent phosphates are particularly prone to hydrolysis in looped RNA molecules in the presence of metals (*312*, *314–316*). Substrate flexibility is necessary to allow the RNA molecule to adopt a conformation favoring (1) either deprotonation of the 2′-OH group by a properly oriented basic species or nucleophilic attack by an exogenous nucleophile from the RNA (3′-OH of guanosine for group I and 2′-OH of adenosine for group II introns) and (2) potential straining of the scissile phosphodiester to make it more susceptible to cleavage. The complete understanding of all parameters involved in the cleavage step is important to improve the design of highly efficient ribozymes that might have a real future as modulators of gene expression and as potential drugs in inflammatory, neoplastic, and viral diseases (*327*).

C. Hydrolytic Cleavage of RNA, DNA, and Simple Phosphodiesters by Metal Complexes

Metals can facilitate the hydrolytic cleavage of phosphodiesters by (1) neutralization of the initial phosphate charge as well as the developing charge in the pentavalent intermediate, (2) stabilization of the transition state, and (3) lowering the pK_a of a bound water (or alcohol molecule), and stabilization of the leaving group on the phosphate (acid/base catalysis). One single metal is probably not sufficient to fulfill all these requirements (see Ref. *328* for a comprehensive review on how metals can help hydrolysis), because it may only accelerate the rate of phosphate hydrolysis by affecting some of the parameters described above. A metallic cation needs to be helped by surrounding components, as in DNase I (*291*) or in the Zn/imidazole system developed by Breslow *et al.* (*329*). As previously mentioned, from X-ray data on di- or trinuclear metal clusters of protein active sites, an emerging unified concept supports the necessity of a two-metal ion catalysis for the hydrolysis of phosphomono- or diesters, because it better fulfills all the requirements of an efficient catalytic process (Fig. 9).

In the following discussions, recent examples of metal-promoted phosphate hydrolysis will be described, whereby one or two metals have been shown to play a key role, and metal ion participation in the hydrolysis process will be assessed. Metal-promoted hydrolysis seems to be a more suitable term than metal-catalyzed hydrolysis, because up to now one cannot find any case of an efficient metal-catalyzed nucleic acid hydrolysis in the literature. In order to hydrolyze a phosphate ester with water, with a half-life of 1 hr, the

first-order reaction rate constant must be $\sim 2 \times 10^{-4}$ sec^{-1}, whereas a half-life of 1 min requires a constant of about 10^{-2} sec^{-1}. For comparison, the half-life of DNA or RNA phosphodiesters extrapolated in physiological conditions are estimated to be 200×10^6 and 800 years, respectively. Due to this tremendous difference, results are often expressed in terms of enhancement of the rate constant of the considered phosphate hydrolysis compared to that in the absence of metal ions. The order of magnitude of the rate constant acceleration of phosphate ester hydrolysis should be in the range of 12 to 14 in order to cleave the DNA phosphodiester bonds within hours or minutes under physiological conditions (*330*). Hydrolysis assays are carried out in general in pseudo-first-order (excess of metal complex over substrate) and sometimes in second-order conditions with activated phosphate ester, RNA, or DNA models. The activity described is not necessarily relevant to RNA and even less to DNA hydrolysis. Only some examples can be found whereby a few turnovers could be evidenced for the metal species involved in the hydrolysis reaction (*331–333*). Nevertheless, with regard to the real challenge that this reaction represents to chemists, the results are significant.

The cleavage of a P–O bond of phosphomono- or diesters results in a nucleophilic substitution on the scissile phosphate. This is a true hydrolysis if a water molecule is the attacking nucleophile, or a transesterification when the nucleophile is an alcohol. These two formally distinct reactions will be discussed in this section, which is devoted to hydrolytic cleavage of nucleic acids and models, in contrast to the oxidative cleavage described in Section II.

1. Cleavage of RNA by Mononuclear Copper Complexes

Apart from the well-documented oxidative DNA or RNA cleavage (see Section II,B), some copper complexes favor RNA hydrolysis. Among them are $[Cu^{II}(typ)(H_2O)]^{2+}$ and $[Cu^{II}(bpy)(H_2O)_2]^{2+}$, two copper complexes with a bipyridine or a terpyridine ligand (**6** and **7**, Fig. 10). The monoterpyridine complex of Cu^{II} was shown to be able to promote the hydrolysis of 2′,3′-cAMP (*332*). ApA (*334*), and poly(A_{12-18}), but not the corresponding deoxypolynucleotide substrate poly(dA_{12-18}) in similar conditions (*335*). The mechanism of phosphodiester cleavage involves, as a first step, a trans-esterification due to an intramolecular attack of the 2′-OH group of the RNA riboses on the phosphate, because 2′,3′-cAMP was found as a product of poly(A_{12-18}) cleavage (*335*). Hydrolysis of 2′,3′-cyclic phosphate diester was also metal promoted and led to a mixture of 2′-AMP and 3′-AMP (*332*). This complex was able to achieve almost complete hydrolysis of

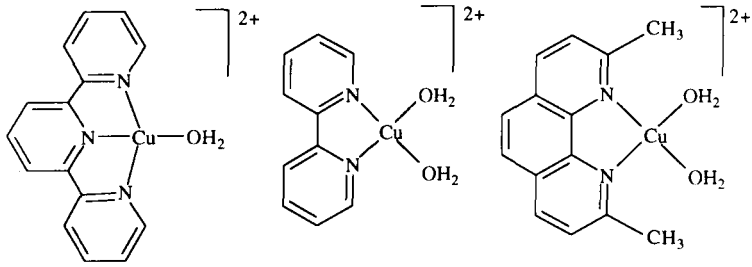

$[Cu^{II}(tpy)(H_2O)]^{2+}$ **6** $[Cu^{II}(bpy)(H_2O)_2]^{2+}$ **7** $[Cu^{II}(neocuproine)(H_2O)_2]^{2+}$ **8**

FIG. 10. Structure of terpyridyl (**6**), bipyridyl (**7**), and neocuproine (**8**) copper complexes.

poly(A_{12-18}) in 20 hr at neutral pH and 37°C [concentrations of poly (A_{12-18}) and Cu^{II} were 60 and 160 μM, respectively] (*335*). At a complex concentration of 60 μM, the pseudo-first-order rate constant was 1.6×10^{-5} sec^{-1} for the hydrolysis of poly(A_{12-18}). Cleavage of poly (A_{12-18}) by $[Cu^{II}(tpy)(H_2O)]^{2+}$ shows a bell-shaped rate constant versus pH dependence, with a maximum rate constant of cleavage (corresponding to the trans-esterification step) at pH 7.8, in agreement with a pK_a of 8 for the metal-bound water molecule. The order of the reaction with respect to the metal complex was one in the case of 2′,3′-cAMP as substrate (*332*).

The monobipyridine copper complex is less reactive than the terpyridine analogue in promoting the hydrolysis of poly(A_{12-18}) (*335*) or ApA (*334*), but this reaction involves also a transient 2′,3′-cAMP intermediate with an optimal reactivity at a pH value corresponding to the pK_a of the metal-bound water molecule (pK_a = 7.8). The yield from the cleavage is 60% for poly(A_{12-18}) at neutral pH and 37°C after 20 hr (*335*) [poly(A_{12-18}), 60 μM; complex, 160 μM], but the complex is almost inactive on ApA, which gives a half-life of 42 days in the presence of a large excess of metal complex (*334*).

The lower efficiency of the bipyridine complex compared to its terpyridine analogue was proposed to be due to its dimerization at neutral pH. A related complex that cannot dimerize, $[Cu^{II}$(neocuproine)$(H_2O)_2]^{2+}$ (**8**, Fig. 10), was proved to be much more efficient than both bpy and tpy complexes (*334*). The half-life of ApA with respect to the trans-esterification step was 3 min (ApA, 0.5 mM; complex, 10 mM) at neutral pH and 37°C. The reaction is first order with respect to the copper complex and, as in the two previous examples, a pH dependence of rate constants is observed (optimal reactivity at pH 7). The

neocuproine complex-promoted hydrolysis is calculated to proceed 1000-fold more rapidly than in the case of the bipyridine complex.

A catalysis through a "double Lewis acid" activation of the scissile phosphate (coordination of two oxygen atoms of the phosphate onto the copper instead of one oxygen atom for a single Lewis acid assistance) was proposed by Chin (*334*) to account for the higher reactivity of **8** compared to **6**. The mechanism proposed by Bashkin *et al.* for **6** is totally different and is based on the fact that the optimal rate of phosphate trans-esterification is at a pH value close to the pK_a value of the metal-bound water molecule (*332, 335*). Because monoaqua complexes as in **6** do not form stable four-membered ring phosphate coordinates, they may just behave as acid/base coreactants like histidine residues in ribonuclease A (*336*) or like imidazole buffer (*337*).

2. *Cleavage of Phosphodiesters by Mononuclear Cobalt Complexes*

cis-Diaqua cobalt complexes can provide up to 10 orders of magnitude rate acceleration for hydrolyzing phosphate diester models with good as well as poor leaving groups (*330, 338*). Chin studied $[Co^{III}(trpn)(H_2O)_2]^{3+}$ and $[Co^{III}(tren)(H_2O)_2]^{3+}$ complexes, with pK_a values for the two water-bound molecules of 5.6 and 8 (**9** and **10**, Fig. 11) (*290*). Both complexes exhibit the highest activity at pH 7, where only one coordinated water molecule is deprotonated, giving an aqua–hydroxo–cobalt complex. The mechanism of the reaction is supposed to involve coordination of the phosphate onto the metal followed by an intramolecular attack of the hydroxo ligand on the metal-bound ester, forming a four-membered ring intermediate (Fig. 12). Despite presenting the same water-bound pK_a values and the same affinity for phosphates, **9** was 300 times more efficient than **10**. This difference might be due to the easier stabilization of the four-membered ring of the chelated phosphate with the more flexible trpn ligand com-

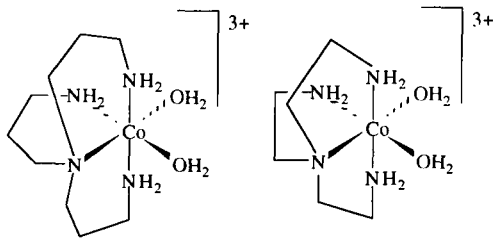

$[Co^{III}(trpn)(H_2O)_2]^{3+}$ **9** $[Co^{III}(tren)(H_2O)_2]^{3+}$ **10**

FIG. 11. Structures of $[Co^{III}(trpn)(H_2O)_2]^{3+}$ (**9**) and $[Co^{III}(tren)(H_2O)_2]^{3+}$ (**10**).

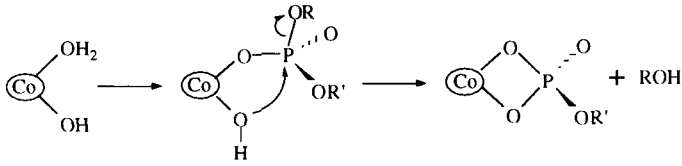

FIG. 12. Intramolecular metal-bound hydroxide nucleophilic attack.

pared to tren. These cobalt complexes are also efficient in the hydrolysis of 3′,5′-cAMP (*290*).

3. Cleavage of DNA by Cerium Salts

Cerium(III) salts under air or cerium(IV) salts in the absence of oxygen are able to mediate hydrolysis of DNA phosphodiester linkages. Single- and double-stranded oligodeoxyribonucleotides (*339*) as well as dideoxyribonucleotides (*340, 341*) are cleaved by $Ce^{III}Cl_3$. Under air Ce^{III} is oxidized to Ce^{IV} *in situ*, and this latter cerium salt is responsible for the cleaving activity. The pseudo-first-order rate constant was 5×10^{-5} sec^{-1} (half-life 3.6 hr) for the hydrolysis of TpT (100 μM) by $Ce(NH_4)_2(NO_3)_6$ (10 mM) at 50°C and neutral pH (*342*). Komiyama *et al.* proposed that a Ce^{IV}–hydroxo form intramolecularly attacks the phosphate of DNA, which is bound to the same cerium ion to promote hydrolysis (*342*). The reaction would also involve acid assistance by a metal-bound water molecule, also bound to the same cerium ion, and electrostatic interaction between the phosphate charge and the cerium(IV) ion.

Up to now, these mononuclear complexes do not fulfill the requirements for an efficient *in vitro* or *in vivo* DNA or RNA hydrolysis, especially because the rate constant acceleration is too slow to allow the cleavage of phosphodiester bonds of DNA within hours or minutes under physiological conditions. Efforts were made to enhance their cleavage efficiency by tethering them to antisense oligonucleotides (see Section III,C,6).

4. Cleavage of Phosphodiesters by Homodinuclear Complexes

A cooperative effect of two mononuclear complexes has been observed in the hydrolysis of phosphate mono- or diesters, the reaction order being then two with respect to the metal (*343–348*). Hydrolysis of methyl *para*-nitrophenylphosphate diester doubly coordinated to a dinuclear cobalt(III) complex was reported, and a crystalline compound of dimethylphosphate coordinated to the same cobalt complex was characterized $[Co_2^{III}(1,4,7\text{-triazacyclononane})_2\ (OH)_2\{O_2P(OCH_3)_2\}]^{3+}$

(*307*). Synergistic effects between two different metals could also promote the phosphate cleavage (*349–351*). All these data suggested that it was possible to prepare and to use dinuclear complexes to promote the hydrolysis of phosphodiester linkages (*308, 352–355*).

The effectiveness of the binuclear complex **11** (Fig. 13), with two mononuclear cyclen–cobalt(III) units linked together by an anthracenyl spacer (cyclen = 1,4,7,10-tetraazacyclododecane), was compared with the monomer in the hydrolysis of phosphate monoesters (*354*). The reaction assisted by this rigid binuclear complex, having a "phosphate-sized pocket," was 10 times faster than that promoted in the presence of two equivalents of the single cyclen–Co^{III} complex. In these experiments the substrate concentration was 25 μM and the total cobalt concentration was 2 mM at 25°C and neutral pH (*354*). No such cooperativity could be noted using a diester substrate because the pseudo-first-order rate constants were similar for both **11** and the mononuclear complex. With **11** as catalyst, an overall rate enhancement of 10^6 was achieved over the uncatalyzed hydrolysis of paranitrophenyl phosphate monoester as substrate.

Two different binuclear copper(II) complexes have been prepared recently, one with a bridging phenoxy ligand having two bis-benzimidazole arms (**12**, Fig. 14), and the second having a bis-cyclen–naphthalene ligand (**13**, Fig. 15) (*352, 353*). Both of them show bimetallic cooperativity for the hydrolysis of phosphate diesters, contrary to studies with the dinuclear cobalt complex (*354*). The pseudo-first-order rate constants for hydrolysis of the *para*-nitrophenylphosphate ester of propylene glycol by bis-benzimidazole-based copper complexes

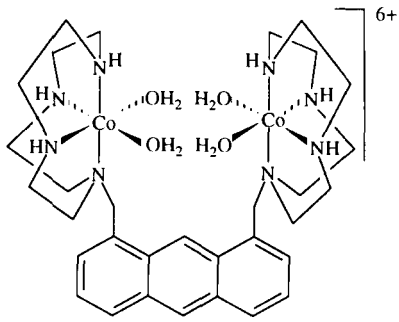

dinuclear Co^{III} complex **11**

FIG. 13. Structure of the covalent binuclear Co^{III} complex with a 1,4,7,10-tetraazacyclododecane ligand (**11**).

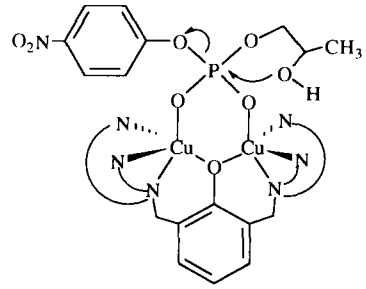

dinuclear Cu^{II} complex **12**

FIG. 14. Double-Lewis acid activation of phosphate diester proposed for the bis-benzimidazole binuclear Cu^{II} complex **12**. The Cu–Cu distance is 3.7 Å. Charges on oxygen atoms and metals have been omitted.

at 25°C and pH 7 are 4×10^{-5} and 2.1×10^{-3} sec^{-1} (half-lives of 5 hr and 5 min, respectively) for the mononuclear (containing only one bis-benzimidazole arm) and the dinuclear (**12**) compounds (*352*). The binuclear complex **12** is therefore 50 times more active than its mononuclear analogue. This factor constitutes a significant enhancement compared to the case of the corresponding binuclear versus mononuclear cobalt(III) complexes (only a 10-fold acceleration) (*354*). The

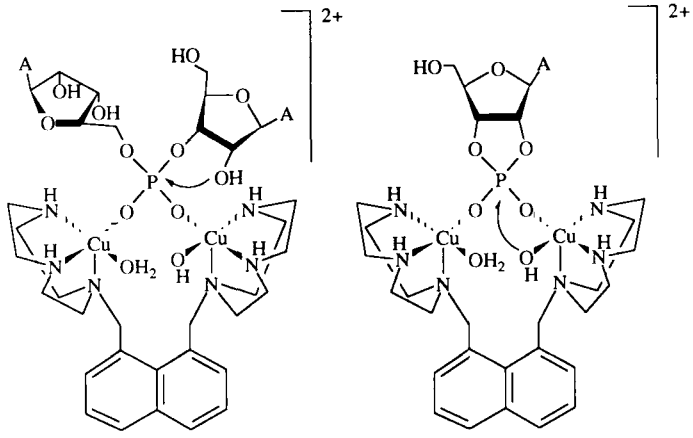

dinuclear Cu^{II} complex **13**

FIG. 15. Cooperativity of two Cu^{II} ions in the covalent binuclear complex **13** for cleaving RNA models.

double Lewis acid activation by the two metal centers was proposed to explain this higher reactivity (Fig. 14). The crystal structure of **12** with an inert dibenzylphosphate revealed a bridging phenolate (*352*). The 3.67-Å Cu–Cu distance is comparable to the distance between the two Zn centers in 3′-exonuclease (3.9 Å) (*299*). HIV RNase H (4 Å) (*303*), and alkaline phosphatase (3.94 Å) (*301*).

While complex **12** was inactive toward RNA cleavage (*352*), the complex **13** at 2 m*M* concentration cleaved the RNA models ApA and 2′,3′-cAMP (0.05 m*M*) with pseudo-first-order rate constants of 2.2×10^{-4} and 2.5×10^{-3} sec^{-1}, respectively (*353*). It therefore provides about 10^5 rate acceleration for cleavage of ApA, and 10^8 for hydrolyzing 2′,3′-cAMP over the background hydrolysis at pH 6. Bell-shaped pH–rate constant profiles, with a maximum at the pK_a value of the metal-bound water molecule, have been reported for these dinuclear copper complexes, suggesting that a metal–hydroxo species is involved in the reaction. The large difference in the rate acceleration for cleavage of ApA and 2′,3′-cAMP (10^5 and 10^8) was interpreted in terms of a better efficiency of the metal–hydroxo species when acting as nucleophile (as in the case of 2′,3′-cAMP) rather than as a base (as in the case of ApA) (Fig. 15).

Binuclear Zn^{II} complexes compared to mononuclear species were also shown to be more efficient by a factor of about 3 for hydrolyzing phosphate mono- and diesters (*308*). These complexes are based on dimers derived from 1,4,7-triazacyclododecane and 1,5,9-triazacyclotetradecane ligands (**14** and **15**, Fig. 16). A 10^3 rate enhancement over the noncatalyzed reaction was obtained. The distance between the metal binding sites influenced the reagent reactivity. Short spacers

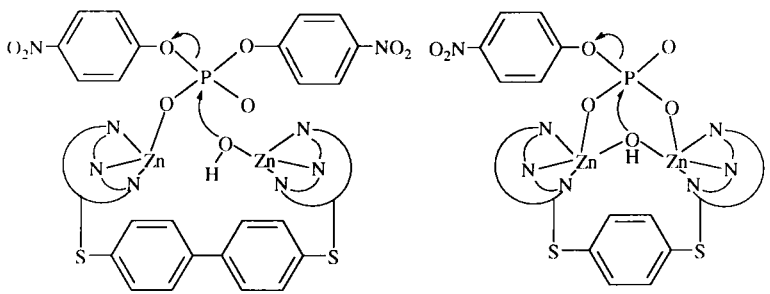

dinuclear Zn^{II} complex **14** dinuclear Zn^{II} complex **15**

FIG. 16. Mechanism of phosphomono- or diester hydrolysis promoted by the binuclear Zn^{II} complexes **14** and **15**. Charges on oxygen atoms and metals have been omitted.

(as in **15**) were better for hydrolyzing monophosphates, whereas longer spacers (as in **14**) favor hydrolysis of diesters. The tether between the two metal ligands must also be rigid. A single Lewis acid activation associated with a metal-bound hydroxide attack was proposed for the hydrolysis of phosphodiesters. For the hydrolysis of phosphomonoesters the mechanism was rather ascribed to double Lewis acid activation by coordination of phosphate on both metals and the nucleophile was proposed to be a bridging hydroxo between the two metals (Fig. 16).

Another dinuclear Zn^{II} complex with *N,N,N′,N′*-tetrakis[(2-pyridyl) methyl]-2-hydroxy-1,3-diaminopropane was shown to be able to achieve phosphodiester cleavage of diribonucleotide ApA at 50°C and neutral pH (*355*) (**16**, Fig. 17). The hydrolytic cleavage of ApA was significantly accelerated by the cooperation of two metals in the binuclear complex because the mononuclear complex was inactive in comparable experimental conditions. The pseudo-first-order rate constant is 1.9×10^{-5} sec^{-1} (half-life 10 hr) (ApA, 100 μM; $ZnCl_2$, 5 m*M*; ligand, 2.5 m*M*). Deprotonation of 2′-OH by a metal hydroxo would be involved in the mechanism of reaction because the products of cleavage were adenosine, adenosine 2′- or 3′-phosphate, and 2′,3′-cAMP.

5. *Cleavage of Phosphodiesters through Cooperation of Two Different Metal Ions*

Some homogeneous solutions of mixed hydroxo clusters of appropriate combinations of two metal ions have been prepared (by avoiding the precipitation of polymeric aggregates of metal–hydroxo species) (*349–351*). The two combined metals, in a 1 : 1 mixed cluster, were located close to each other and were shown to participate in a cooperative bimetallic mechanism of phosphate hydrolysis. The metal

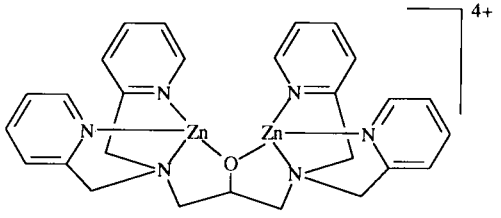

dinuclear Zn^{II} complex **16**

FIG. 17. Structure of the dinuclear Zn^{II} complex with *N,N,N′,N′*-tetrakis[(2-pyridyl)-methyl]-2-hydroxy-1,3-diaminopropane ligands (**16**).

pair could be a lanthanide ion with a nonlanthanide ion (La^{III}/Fe^{III}), or two nonlanthanide ions (Zn^{II}/Sn^{IV}) (**17** and **18**, Fig. 18). The La^{III}/Fe^{III} (**17**) or La^{III}/Sn^{IV} associations were shown to be efficient in RNA and, to a lesser extent, in DNA models of hydrolysis (*349, 351*), whereas Zn^{II}/Sn^{IV} (**18**) promoted hydrolysis only of RNA models (*350*). One of the metal ions of the association must have a metal-bound water molecule with a relatively high pK_a value (La^{III} or Zn^{II}) and the other metal center should be a strong Lewis acid (its metal-bound water has a low pK_a value) (Fe^{III} or Sn^{IV}) (Table I). The association of two strong acidic metals was inefficient (Fe^{III}/Sn^{IV} or Lu^{III}/Fe^{III}) (*351*). Associations between a lanthanide and a nonlanthanide ion (La^{III}/Fe^{III} or La^{III}/Sn^{IV}) were the most active on RNA and DNA simplified substrates (*349, 351*). The ions La^{III}, Eu^{III}, Ce^{IV}, and Lu^{III} were tested in association with Fe^{III} (*351*). Among them, only La^{III}, and to a lesser extent Eu^{III}, showed cooperativity with Fe^{III}.

The overall efficiency of these "nonmolecular" bimetallic sysems to promote phosphate ester hydrolysis was illustrated with ApA as RNA model (0.1 m*M*); hydrolysis occurred with a mixture of $LaCl_3$ and $FeCl_3$ (10 m*M* each) to more than 70% at 50°C and neutral pH in 5 min (*351*). The products of the reaction included adenosine and 2′- and 3′-monophosphate adenonsine, indicating that the mechanism involved a first trans-esterification step by the vicinal 2′-OH of ribose. With the same mixture of metal ions, the DNA model TpT (0.1 m*M*) (Fig. 18), left, B = thymine) was converted to thymidine and 3′- and 5′-monophosphate thymidine with 36% of conversion in 24 hr at 70°C at neutral pH. The important point is the notion of cooperativity between the two metals.

In the second example of cooperativity of two metal ions described by Komiyama *et al.*, the two nonlanthanide metals, the Zn^{II}/Sn^{IV} sys-

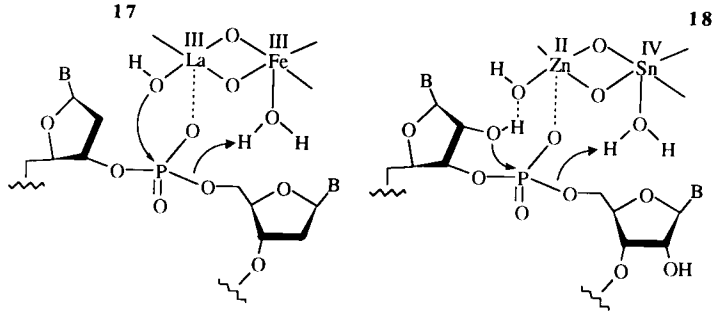

FIG. 18. Proposed mechanism of DNA or RNA hydrolysis mediated by La^{III}/Fe^{III} or Zn^{II}/Sn^{IV} systems (**17** and **18**).

TABLE I

VALUES OF pK_a FOR METAL-BOUND WATER MOLECULES

Molecule	pK_a
$Sn^{IV}(H_2O)$	-0.6^a
$Ce^{IV}(H_2O)$	0^b
$In^{III}(H_2O)$	$2.1–4.4^a$
$Fe^{III}(H_2O)$	$2.5–3.1^a$
$Al^{III}(H_2O)$	$4.3–5^a$
$La^{III}(H_2O)$	7.4^c
$Zn^{II}(H_2O)$	8^a

[a] From Ref. *350*.
[b] From Ref. *342*.
[c] From Ref. *349*.

tem (10 m*M* of each metal ion), the half-life of the RNA model ApA (50 m*M*) is 3 hr at 50°C and neutral pH (*350*). The products of the reaction are adenosine, 2′- and 3′-phosphate adenosine, and some 2′,3′-cyclic phosphate adenosine (Fig. 18, right, B = adenine). The authors showed that the best association with Zn^{II} is observed when the bound water molecule on the metal is most acidic. The order of decreasing cooperativity is $Sn^{IV} > In^{III} > Fe^{III} > Al^{III}$ (see Table I for respective pK_a values).

The mechanism of the phosphate hydrolysis promoted by these metal associations was proposed to involve the La^{III}– or Zn^{II}–hydroxo ligand as nucleophile attacking the scissile phosphate (for the TpT substrate), or as a Brønsted base able to deprotonate the 2′-OH of the ribose, respectively. The water molecules bound to Fe^{III} or Sn^{IV} are believed to act as a Brønsted acid (proton source) with respect to the 5′-oxygen atom of the leaving alcohol (Fig. 18).

6. *Cleavage of RNA by Oligonucleotides Modified with Metal Complexes*

Linking artificial RNases to oligodeoxynucleotides by a covalent tether has emerged as an important topic due to the lack of sequence-specific natural RNases and to the potential therapeutic issue of reactive antisense oligonucleotides (*327*). The promotion of RNA cleavage by such hydrolyzing reagents is attractive due to the easier hydrolysis of the RNA target compared to that of oligodeoxynucleotide carrier. This represents a considerable advantage for the strategy compared

to the "oligonucleotide–oxidative cleaver" approach, because the latter cleavers do not discriminate between the oxidaton of the nucleic acid target and the oligonucleotide carrier. However, this strategy is dependent on robust complexes that are inert to metal release and would be optimized if they could undergo several reaction turnovers. The first promising metal complex in this respect consisted of a hexadentate Schiff base ligand of lanthanide ions (*331*). Provided that special attention is given to mediate hydrolytic cleavage of RNA in the hybridized zone of the duplex ODN vector/RNA target, the conjugated ODN could behave as a catalyst. After the cleavage of a first RNA target, the melting of the nicked duplex would release two RNA fragments and a free conjugate, which would be available again to bind and cleave another RNA substrate. This would considerably lower the concentration of antisense conjugated ODN necessary for biological effects.

Covalent attachment of RNA-hydrolizing metal complexes to ODNs involved, up to now, essentially Eu^{III}, Lu^{III}, and Cu^{II} complexes. The *in vitro* sequence-specific hydrolytic cleavage of RNA by metal complexes conjugated to ODNs, at physiological pH, was reported (1) with a terpyridine–Cu^{II} entity (*356*) mediating 18–25% of target cleavage at 45°C within 72 hrs (2) with an iminodiacetate–Lu^{III} or –Eu^{III} entity (*357*) mediating 17% of target cleavage in 8 hr at 37°C, and (3), more interestingly, with a stable texaphyrin–Eu^{III} (*358*) or robust terpyridine-derived hexadentate–Eu^{III} entity (*359*). The latter achieves near quantitative cleavage of target RNA (88%) in 16 hr at 37°C, where the complex moiety is remarkably resistant toward decomposition. In general, cleavage of RNA occurs in the single-stranded zone of the RNA target in the vicinity of the metal complex.

Attempts to position the metal complex in the middle of the oligonucleotide vector have been reported (*360*). A mono-bpy–Cu^{II} complex was covalently bound to the uracil C-5 position of 2′-deoxyuridine nucleoside in order to incorporate this synthon into an ODN sequence. One of the various nucleoside–bipyridine synthesized conjugates was able to mediate 65% of cleavage of poly(A_{12-18}) in 24 hr, whereas the free mono-bpy-Cu^{II} complex degrades 78% of the same polymer in 48 hr [poly(A_{12-18}), 60 μM; complex, 160 μM; 37°C, pH 7.1]. In contrast to the Eu^{III}–ODN conjugates described previously, the Cu^{II} conjugates were inactivated by 0.5 m*M* EDTA and consequently are not relevant for an *in vitro* utilization.

Beside RNA targeting, a monoiminodiacetate–Ce^{IV} complex conjugated to an ODN has been reported to cleave sequence selectively a ss DNA target (60% yield after 12 hr) (*361*), but its reactivity toward RNA or ds DNA has not been described.

Although these ODNs conjugated to artificial hydrolyzing reagents do not show a reactivity comparable to that of their analogues coupled with oxidative reagents, improvement of their reactivity may be possible. They constitute an interesting alternative in nucleic acid cleavage that is worth pursuing. In order to be relevant as reactive antisense oligonucleotides in a cellular context, they should be able to promote the cleavage of RNA molecules more rapidly than the general turnover of mRNA molecules inside cells (20 min to 24 hr) (*362*).

IV. Conclusion

DNA and RNA cleavage, a very active field of research, has been developed in two main and complementary directions within the past decade: oxidative cleavage and hydrolysis. In some cases, these two different strategies are linked. This was the case of the pseudohydrolysis of DNA involving a selective oxidative step followed by a reduction (*363*). In general, the two different approaches are separated, but the same goals are involved. There is first the preparation of new chemical tools to study genomic DNA, because recognition sites of most of the restriction enzymes are too often limited to palindromic sequences, and it is useful to have artificial nucleases able to cleave DNA at any desired sequence. Second, the synthesis of compounds that cleave nucleic acids should help in the design of potential therapeutic agents for the treatment of cancer and viral diseases. The challenging development of new, efficient DNA and RNA cleavage agents will require a strong cooperation between chemists, biochemists, and molecular biologists.

V. Addendum

References listed below appeared in the literature after the submission of this manuscript. Devoted to the general topic of this review, three books must be mentioned (*364–366*). For work related to specific sections, see the following addenda:

Section II,A: From recent two-dimensional NMR studies on bleomycin analogs, a revisited structural model for specificity, binding, and double-strand cleavage was proposed (*367*). An investigation of the reaction of Fe^{III}–BLM with iodosylbenzene by ES–MS showed that neither hypervalent iron nor activated oxygen was involved but that hypervalent iodide I(III) was the oxidant (*368*).

Section II,B: The ss DNA region of the *lac*UV-5 promoter of *e. coli* RNA polymerase could be targeted by tetrahedral cuprous chelates of 1,10-phenanthroline, resulting in inhibition of transcription (*369*).

Section II,C: Iron–EDTA was covalently attached to pyrrole–imidazole polyamides for sequence-specific recognition and cleavage of ds DNA from within the minor groove (*370*).

Section III,A: The crystal structure of the NH_2-terminal fragment of T4 DNA polymerase was published and its complexes with metal ions and short deoxyoligonucleotides were compared to that of the 3′–5′ exonuclease domain of the Klenow fragment (*371*).

Section III,B: The molecular mechanism of the action of ribozymes was the subject of numerous papers (for some of them see Refs. *372–376*).

Section III,C: Selective recognition of phosphomonoesters and their P–O ester bond cleavage by new dinuclear Zn^{II}–cryptate was described (*377*). Cleavage of RNA by lanthanide complexes attached to oligonucleotides showed that it was possible to target the duplex region of the hybrid by creating a bulge site on the RNA target (*378*).

VI. List of Abbreviations and Definitions

A	Adenine
2′-AMP, 3′-AMP, 5′-AMP	2′-, 3′-, or 5′-Adenosine monophosphate
2′,3′-cAMP	2′,3′-cyclic adenosine monophosphate
ApA	Adenylyl-3′,5′-adenosine
BLM	Bleomycin
bpy	2,2′-Bipyridine
C	Cytosine
CD	Circular dichroism
Conjugate	A conjugate is a hybrid molecule made of two partners tethered by a covalent link, the biochemical or biological properties of one moiety being targeted toward biological macromolecules or cells, and with the second entity acting as vector
Cyclen	1,4,7,10-Tetraazacyclododecane
dG	Deoxyguanosine
dppz	Dipyrido[3,2-*a*:2′,3′-c]phenazine
ds	Double strand(ed)
DTT	Dithiothreitol
EDTA	Ethylenediaminetetraacetate
G	Guanine
HIV	Human immunodeficiency virus
HpD	Hematoporphyrin
5-MF	5-Methylene-2(5*H*)-furanone
MMPP	Magnesium monoperphthalate

PAGE	Polyacrylamide gel electrophoresis
ODN	Oligodeoxyribonucleotide (oligonucleotide for short)
phen	1,10-Phenanthroline (oP has also been used)
ss	Single strand(ed)
T	Thymine
TMPyP	Dianion of *meso*-tetrakis(4-*N*-methylpyridiniumyl) porphyrin
TPPS	Dianion of *meso*-tetrakis(4-sulfonatophenyl)porphyrin
TpT	Thymidylyl-3′,5′-thymidine
tpy	2,2′:6′,2″-Terpyridine
tren	Tris(2-aminoethyl)amine
trpn	Tris(3-aminopropyl)amine

Acknowledgments

The authors are indebted to all co-workers and collaborators whose names are listed in the references. We are also grateful to the Centre National de La Recherche Scientifique (CNRS), the Association pour la Recherche contre le Cancer (ARC, Villejuif), the Agence Nationale de Recherche sur le Sida (ANRS, Paris), and the Région Midi-Pyrénées for financial support.

References

1. Westheimer, F. H. *Science* **1987,** *235,* 1173.
2. Roberts, R. J.; Halford, S. E. In "Nucleases"; Linn, S. M., Lloyd, R. S., and Roberts, R. J., Eds.; Cold Spring Harbor Laboratory Press: New York, 1993, 2nd ed., p. 35.
3. Hecht, S. M. *Acc. Chem. Res.* **1986,** *19,* 383.
4. Stubbe, J.; Kozarich, J. W. *Chem. Rev.* **1987,** *87,* 1107.
5. Hecht, S. M. *Bioconjugate Chem.* **1994,** *5,* 513.
6. Petering, D. H.; Byrnes, R. W.; Antholine, W. E. *Chem. Biol. Interactions* **1990,** *73,* 133.
7. Pratviel, G.; Bernadou, J.; Meunier, B. *Angew. Chem., Int. Ed. Engl.* **1995,** *34,* 746.
8. Dumas, P.; Bergdoll, M.; Cagnon, C.; Masson, J. M. *EMBO J.* **1994,** *13,* 2483.
9. Bates, N. P.; Williams, M. V.; Besell, E. M.; Hudson, G. V.; Hudson, B. V. *J. Clin. Oncol.* **1994,** *12,* 288.
10. Murad, A. M.; Triginelli, S. A.; Ribalta, J. C. L. *J. Clin. Oncol.* **1994,** *12,* 55.
11. Espinoza-Jacobs, M. C.; Suntharalingam, M.; Eisenberger, M.; Sinibaldi, V.; Salazar, O. M. *Am. J. Clin. Oncol.* **1995,** *18,* 52.
12. Loehrer, P. J.; Johnson, D.; Elson, P.; Einhorn, L. H.; Trump, D. *J. Clin. Oncol.* **1995,** *13,* 470.
13. Bakker, P. J. M.; Danner, S. A.; ten Napel, C. H. H.; Kroon, F. P.; Sprenger, H. G.; van Leusen, R.; Meenhorst, P. L.; Muusers, A.; Veenhof, C. H. N. *Eur. J. Cancer* **1995,** *31A,* 188.
14. Sebti, S. M.; Mignano, J. E.; Jani, J. P.; Srimatkandada, S.; Lazo, J. S. *Biochemistry* **1989,** *28,* 6544.
15. Xu, E. H.; Johnston, S. A. *J. Biol. Chem.* **1994,** *269,* 21117.

16. Joshua-Tor, L.; Xu, E. H.; Johnston, S. A.; Rees, D. C. *Science* **1995,** *269,* 945.
17. Poddevin, B.; Orlowski, S.; Belehradek, J.; Mir, L. M. *Biochem. Pharmacol.* **1991,** *42,* 567.
18. Tounekti, O.; Pron, G.; Belehradek, J.; Mir, L. M. *Cancer Res.* **1993,** *53,* 5462.
19. Brown, S. J.; Mascharak, P. K.; Stephen, D. W. *J. Am. Chem. Soc.* **1988,** *110,* 1996.
20. Boger, D. L.; Coletti, S. L.; Honda, T.; Menezes, R. F. *J. Am. Chem. Soc.* **1994,** *116,* 5607.
21. Boger, D. L.; Honda, T. *J. Am. Chem. Soc.* **1994,** *116,* 5647.
22. Oshitari, T.; Kobayashi, S. *Tetrahedron Lett.* **1995,** *36,* 1089.
23. Kénani, A.; Bailly, C.; Houssin, R.; Hénichart, J. P. *Anti-Cancer Drugs* **1994,** *5,* 199.
24. Porvik, L. F.; Hogan, M.; Datagupta, N. *Biochemistry* **1979,** *18,* 96.
25. Kane, S. A.; Natrajan, A.; Hecht, S. M. *J. Biol. Chem.* **1994,** *269,* 10899.
26. Bailly, C.; Waring, M. J. *J. Am. Chem. Soc.* **1995,** *117,* 7311.
27. Mandeville, R. A.; Ellena, J. F.; Hecht, S. M. *J. Am. Chem. Soc.* **1994,** *116,* 10851.
28. Wu, W.; Vanderwall, D. E.; Stubbe, J.; Kozarich, J. W.; Turner, C. J. *J. Am. Chem. Soc.* **1994,** *116,* 10843.
29. Urata, H.; Ueda, Y.; Usami, Y.; Akagi, M. *J. Am. Chem. Soc.* **1993,** *115,* 7135.
30. Burger, R. M.; Peisach, J.; Horwitz, S. B. *J. Biol. Chem.* **1981,** *256,* 11636.
31. Burger, R. M.; Blanchard, J. S.; Horwitz, S. B.; Peisach, J. *J. Biol. Chem.* **1985,** *260,* 15405.
32. Ortiz De Montellano, P. R., Ed.; "Cytochrome P-450, Structure, Mechanism, and Biochemistry"; Plenum Press: New York, 1986.
33. Murugesan, N.; Hecht, S. M. *J. Am. Chem. Soc.* **1985,** *107,* 493.
34. Pratviel, G.; Bernadou, J.; Meunier, B. *Biochem. Pharmacol.* **1989,** *36,* 2599.
35. Girardet, M.; Meunier, B. *Tetrahedron Lett.* **1987,** *28,* 2955.
36. Meunier, B. *Chem. Rev.* **1992,** *92,* 1411.
37. Sam, J. W.; Tang, X. J.; Peisach, J. *J. Am. Chem. Soc.* ***1994,*** *116,* 5250.
38. Guajardo, R. J.; Chavez, F.; Farinas, E. T.; Mascharak, P. K. *J. Am. Chem. Soc.* **1995,** *117,* 3883.
39. Burger, R. M.; Tian, G.; Drlica, K. *J. Am. Chem. Soc.* **1995,** *117,* 1167.
40. Radtke, K.; Lornitzo, F. A.; Byrnes, R. W.; Antholine, W. E.; Petering, D. H. *Biochem. J.* **1994,** *302,* 655.
41. D'Andreas, A. D.; Haseltine, W. A. *Proc. Natl. Acad Sci. U.S.A.* **1978,** *75,* 3608.
42. Nightingale, K. P.; Fox, K. R. *Nucleic Acids Res.* **1993,** *21,* 2549.
43. Giloni, L.; Takeshita, M.; Johnson, F.; Iden, C.; Grollman, A. P. *J. Biol. Chem.* **1981,** *256,* 8608.
44. McGall, G. H.; Rabow, L. E.; Ashley, G. W.; Wu, S. H.; Kozarich, J. W.; Stubbe, J. *J. Am. Chem. Soc.* **1992,** *114,* 4958.
45. Kozarich, J. W.; Worth, Jr., L.; Frank, B. L.; Christner, D. F.; Vanderwall, D. E.; Stubbe, J. *Science* **1989,** *245,* 1396.
46. Worth, Jr., L.; Frank, B. L.; Christner, D. F.; Absalon, M. J.; Stubbe, J.; Kozarich, J. W. *Biochemistry* **1993,** *32,* 2601.
47. (a) Rabow, L. E.; McGall, G. H.; Stubbe, J.; Kozarich, J. W. *J. Am. Chem. Soc.* **1990,** *112,* 3203; (b) Burger, R. M.; Drlica, K.; Birdsall, B. *J. Biol. Chem.* **1994,** *269.* 25978.
48. Giese, B.; Beyrich-Graf, X,; Erdmann, P.; Giraud, L.; Imwinkelried, P.; Müller, S. N.; Schwitter, U. *J. Am. Chem. Soc.* **1995,** *117,* 6146.
49. Giese, B.; Beyrich-Graf, X.; Erdmann, P.; Petretta, M.; Schwitter, U. *Chem. Biol.* **1995,** *2,* 367.

50. Duff, R. J.; De Vroom, E.; Geluk, A.; Hecht, S. M. *J. Am. Chem. Soc.* **1993,** *115,* 3350.
51. Absalon, M. J.; Krishnamoorthy, C. R.; McGall, G.; Kozarich, J. W.; Stubbe, J. *Nucleic Acids Res.* **1992,** *20,* 4179.
52. Morgan, M. A.; Hecht, S. M. *Biochemistry* **1994,** *33,* 10286.
53. Povirk, L. F.; Han, Y. H.; Steighner, R. J. *Biochemistry* **1989,** *28,* 5808.
54. (a) Absalon, M. J.; Wu, W.; Kozarich, J. W.; Stubbe, J. *Biochemistry* **1995,** *34,* 2076. (b) Kane, S. A.; Hecht, S. M.; Sun, J. S.; Garestier, T.; Hélène, C. *Biochemistry* **1995,** *34,* 16715.
55. Gajewski, E.; Aruoma, O. I.; Dizdaroglu, M.; Halliwell, B. *Biochemistry* **1991,** *30,* 2444.
56. Kasamatsu, T.; Nakagawa, T.; Kohda, K. *Biol. Pharm. Bull.* **1994,** *17, 391.*
57. Suzuki, H.; Nagai, K.; Akutsu, E.; Yamaki, H.; Tanaka, N.; Umezawa, H. *J. Antibiot.* **1970,** *23,* 473.
58. Carter, B. J.; De Vroom, E.; Long, E.; Van der Marel, G. A.; Van Boom, J. H.; Hecht, S. M. *Proc. Natl. Acad. Sci. U.S.A.* **1990,** *87,* 9373.
59. Holmes, C. E.; Hecht, S. M. *J. Biol. Chem.* ***1995,*** *268,* 25909.
60. Keck, M. V.; Hecht, S. M. *Biochemistry* **1995,** *34,* 12029.
61. Shinozuka, K.; Morishita, H.; Yamazaki, T.; Sugiura, T.; Sawai, H. *Tetrahadron Lett.* **1991,** *32,* 6869.
62. Otsuka, M.; Satake, H.; Sugiura, Y.; Murakami, S.; Shibasaki, M.; Kobayashi, S. *Tetrahedron Lett.* **1993,** *34,* 8497.
63. Loeb, K. E.; Zaleski, J. M.; Westre, T. E.; Guajardo, R. J.; Masharak, P. K.; Hedman, B.; Hodgson, K. O.; Solomon, E. I. *J. Am. Chem. Soc.* **1995,** *117,* 4545.
64. Guajardo, R. J.; Hudson, S. E.; Brown, S. J.; Mascharak, P. K. *J. Am. Chem. Soc.* **1993,** *115,* 7971.
65. Guajardo, R. J.; Mascharak, P. K. *Inorg. Chem.* **1995,** *34,* 802.
66. Huang, L.; Quada, J. C.; Lown, J. W. *Bioconjugate Chem.* **1995,** *6,* 21.
67. Sergeev, D. S.; Zarytova, V. F.; Mamaev, S. V.; Godovikova, T. S.; Vlassov, V. V. *Antisense Res. Dev.* **1992,** *2,* 235.
68. (a) Zarytova, V. F.; Sergeyev, D. S.; Godovikova, T. S. *Bioconjugate Chem.* **1993,** *4,* 189. (b) Sergeyev, D. S.; Godovikova, T. S.; Zarytova, V. F. *Nucleic Acids Res.* **1995,** *23,* 4400.
69. Oakley, M. G.; Turnbull, K. D.; Dervan, P. B. *Bioconjugate Chem.* **1994,** *5,* 242.
70. Sigman, D. S.; Graham, D. R.; D'Aurora, V.; Stern, A. M. *J. Biol. Chem.* **1979,** *254,* 12269.
71. Sigman, D. S. *Acc. Chem. Res.* **1986,** *19,* 180.
72. Sigman, D. S. *Biochemistry* **1990,** *29, 9097.*
73. Marshall, L. E.; Graham, D. R.; Reich, K. A.; Sigman, D. S. *Biochemistry* **1981,** *20,* 244.
74. Pope, L. E.; Sigman, D. S. *Proc. Natl Acad. Sci. U.S.A.* **1991,** *81,* 3.
75. Veal, J. M.; Merchant, K.; Rill, R. L. *Nucleic Acids Res.* **1991,** *19,* 3383.
76. Alastair, G. R.; Nazhat, N. B. *J. Am. Chem. Soc.* **1987,** *109,* 1990.
77. Williams, L. D.; Thivierge, J.; Goldberg, I. H. *Nucleic Acids Res.* **1988,** *16,* 11607.
78. Dizdaroglu, M.; Aruoma, O. I.; Halliwell, B. *Biochemistry* **1990,** *29,* 8447.
79. Mayer, J. M. *Comments Inorg. Chem.* **1988,** *8,* 125.
80. Drew, H.; Travers, A. *Cell* **1984,** *37,* 491.
81. Yoon, C.; Kuwabara, M. D.; Spassky, A.; Sigman, D. S. *Biochemistry* **1990,** *29,* 2116.
82. Veal, J. M.; Rill, R. L. *Biochemistry* **1991,** *30,* 1132.

83. Goyne, T. E.; Sigman, D. S. *J. Am. Chem. Soc.* **1987,** *109,* 2846.
84. Sigman, D. S.; Chen, C. H. B. *Annu. Rev. Biochem.* **1990,** *59,* 207.
85. Spassky, A. *Biochemistry* **1992,** *31,* 10502.
86. Mazumder, A.; Perrin, D. M.; McMillin, D.; Sigman, D. S. *Biochemistry* **1994,** *33,* 2262.
87. Pearson, L.; Chen, C. H. B.; Gaynor, R. P.; Sigman, D. S. *Nucleic Acids Res.* **1994,** *22,* 2255.
88. Sigman, D. S.; Bruice, T. C.; Mazumder, A.; Sutton, C. L. *Acc. Chem. Res.* **1993,** *26,* 98.
89. Chen, C. B.; Sigman, D. S. *Proc. Natl. Acad. Sci. U.S.A.* **1986,** *83,* 7147.
90. François, J. C.; Saison-Behmoaras, T.; Barbier, C.; Chassignol, M.; Thuong, N. T.; Hélène, C. *Proc. Natl. Acad. Sci. U.S.A.* **1989,** *86,* 9702.
91. François, J. C.; Saison-Behmoaras, T.; Chassignol, M.; Thuong, N. T.; Sun, J. S.; Hélène, C. *J. Biol. Chem.* **1989,** *264,* 5891.
92. Chen, C. H. B.; Gorin, M. B.; Sigman, D. S. *Proc. Natl. Acad. Sci. U.S.A.* **1993,** *90,* 4206.
93. Bergstrom, D. E.; Gerry, N. P. *J. Am. Chem. Soc.* **1994,** *116,* 12067.
94. Sun, J. S.; François, J. C.; Lavery, R.; Saison-Behmoaras, T.; Montenay-Garestier, T.; Thuong, N. T.; Hélène, C. *Biochemistry* **1988,** *27,* 6039.
95. François, J. C.; Saison-Behmoaras, T.; Chassignol, M.; Thuong, N. T.; Sun, J. S.; Hélène, C. *Biochemistry* **1988,** *27,* 2272.
96. Shimidzu, M.; Inoue, H.; Ohtsuka, E. *Biochemistry* **1994,** *33,* 606.
97. Thuong, N. T.; Hélène, C. *Angew. Chem., Int. Ed. Engl.* **1993,** *32,* 666.
98. Perrin, D. M.; Mazumder, A.; Sadeghi, F.; Sigman, D. S. *Biochemistry* **1994,** *33,* 3848.
99. Chen, C. B.; Sigman, D. S. *Science* **1987,** *237,* 1197.
100. Sutton, C. L.; Mazumder, A.; Chen, C. H. B.; Sigman, D. S. *Biochemistry* **1993,** *32,* 4225.
101. Ebright, R. H.; Ebright, Y. W.; Pendergrast, P. S.; Gunasekera, A. *Proc. Natl. Acad. Sci. U.S.A.* **1990,** *87,* 2882.
102. Bruice, T. W.; Wise, J. G.; Rosser, D. S. E.; Sigman, D. S. *J. Am. Chem. Soc.* **1991,** *113,* 5446.
103. Pan, C. Q.; Feng, J. A.; Finkel, S. E.; Landgraf, R.; Sigman, D. S.; Johnson, R. C. *Proc. Natl. Acad. Sci. U.S.A.* **1994,** *91,* 1721.
104. Pendergrast, P. S.; Ebright, Y. W.; Ebright, R. H. *Science* **1994,** *265,* 959.
105. Pfau, J.; Arvidson, D. N.; Youderian, P.; Pearson, L. L.; Sigman, D. S. *Biochemistry* **1994,** *33,* 11391.
106. Chen, C. H. B.; Mazumder, A.; Constant, J. F.; Sigman, D. S. *Bioconjugate Chem.* **1993,** *4,* 69.
107. Floyd, R. A. *Biochem. Biophys. Res. Commun.* **1981,** *99,* 1209.
108. Fenton, H. J. H. *J. Chem. Soc.* **1864,** *65,* 899.
109. Walling, C. *Acc. Chem. Res.* **1975,** *8,* 125.
110. Demple, B.; Halbrook, J. *Nature* **1983,** *304,* 466.
111. Meunier, B.; Pratviel, G.; Bernadou, J. *Bull. Soc. Chim. Fr.* **1994,** *131,* 933.
112. Kennard, C. H. L. *Inorg. Chim. Acta* **1967,** *1,* 347.
113. Douglas, B. E.; Radanovic, D. J. *Coord. Chem. Rev.* **1993,** *128,* 139.
114. Tullius, T. D.; Dombroski, B. A. *Science* **1985,** *230,* 679.
115. Tullius, T. D.; Dombroski, B. A.; Churchill, M. E. A.; Kam, L. *Methods Enzymol.* **1987,** *155,* 537.
116. Tullius, T. D. *Nature* **1988,** *332,* 663.

117. Dixon, W. J.; Hayes, J. J.; Levin, J. R.; Weidner, M. F.; Dombroski, B. A.; Tullius, T. D. *Methods Enzymol.* **1991,** *208,* 380.
118. Burkhoff, A. M.; Tullius, T. D. *Cell* **1987,** *48,* 935.
119. Celander, D. W.; Cech, T. R. *Biochemistry* **1990,** *29,* 1355.
120. Imlay, J. A.; Chin, S. M.; Linn, S. *Science* **1988,** *240,* 640.
121. Pogozelski, W. K.; McNeese, T. J.; Tullius, T. D. *J. Am. Chem. Soc.* **1995,** *117,* 6428.
122. Tullius, T. D. *Trends Biochem. Sci.* **1987,** *12,* 297.
123. Hertzberg, R. P.; Dervan, P. B. *J. Am. Chem. Soc.* **1982,** *104,* 313.
124. Van Dyke, M. W.; Hertzberg, R. P.; Dervan, P. B. *Proc. Natl. Acad. Sci. U.S.A.* **1982,** *79,* 5470.
125. Hertzberg, R. P.; Dervan, P. B. *Biochemistry* **1984,** *23,* 3934.
126. Hertzberg, R. P.; Hecht, S. M.; Reynolds, V. L.; Molineux, I. J.; Hurley, L. H. *Biochemistry* **1986,** *25,* 1249.
127. Hurley, L. H.; Lee, C. S.; McGovern, J. P.; Warpehoski, M. A.; Mitchell, M. A.; Kelly, R. C.; Aristoff, P. A. *Biochemistry* **1988,** *27,* 3886.
128. Gunderson, S. I.; Chapman, K. A.; Burgess, R. R. *Biochemistry* **1987,** *26,* 1539.
129. Sawadogo, M.; Roeder, R. G. *Cell* **1985,** *43,* 165.
130. Han, H.; Schepartz, A.; Pellegrini, M.; Dervan, P. B. *Biochemistry* **1994,** *33,* 9831.
131. Vary, C. P. H.; Vournakis, J. N. *Proc. Natl. Acad. Sci. U.S.A.* **1984,** *81,* 6978.
132. Cartwright, I. L.; Hertzberg, R. P.; Dervan, P. B.; Elgin, S. C. *Proc. Natl. Acad. Sci. U.S.A.* **1983,** *80,* 3213.
133. Richard-Foy, H.; Hager, G. L. *EMBO J.* **1987,** *6,* 2321.
134. Jantzen, H. M.; Strähle, U.; Gloss, B.; Stewart, F.; Schmid, W.; Boshart, M.; Miksicek, R.; Schütz, G. *Cell* **1987,** *49,* 129.
135. Dervan, P. B. *Science* **1986,** *232,* 464.
136. Taylor, J. S.; Schultz, P.; Dervan, P. B. *Tetrahedron* **1984,** *40,* 457.
137. Youngquist, R. S.; Dervan, P. B. *J. Am. Chem. Soc.* **1985,** *107,* 5528.
138. Wade, W. S.; Dervan, P. B. *J. Am. Chem. Soc.* **1987,** *109,* 1574.
139. Griffin, J. H.; Dervan, P. B. *J. Am. Chem. Soc.* **1986,** *108,* 5008.
140. Youngquist, R. S.; Dervan, P. B. *Proc. Natl. Acad. Sci. U.S.A.* **1985,** *82,* 2565.
141. Sluka, J. P.; Horwath, S. J.; Bruist, M. F.; Simon, M. I.; Dervan, P. B. *Science* **1987,** *238,* 1129.
142. Youngquist, R. S.; Dervan, P. B. *J. Am. Chem. Soc.* **1987,** *109,* 7564.
143. Lin, S. B.; Blake, K. R.; Miller, P. S.; Ts'o, P. O. P. *Biochemistry* **1989,** *28,* 1054.
144. Boutorin, A. S.; Vlassov, V. V.; Kazakov, S. A.; Kutiavin, I. V.; Podyminogin, M. A. *FEBS Lett.* **1984,** *172,* 43.
145. Chu, B. C. F.; Orgel, L. E. *Proc. Natl. Acad. Sci. U.S.A.* **1985,** *82,* 963.
146. Dreyer, G. B.; Dervan, P. B. *Proc. Natl. Acad. Sci. U.S.A.* **1985,** *82,* 968.
147. Boidot-Forget, M.; Thuong, N. T.; Chassignol, M.; Hélène, C. *C. R. Acad. Sci. Paris Ser. 2* **1986,** *302,* 75.
148. Moser, H. E.; Dervan, P. B. *Science* **1987,** *238,* 645.
149. Strobel, S. A.; Moser, H. E.; Dervan, P. B. *J. Am. Chem. Soc.* **1988,** *110,* 7927.
150. Povsic, T. J.; Dervan, P. B. *J. Am. Chem. Soc.* **1989,** *111,* 3059.
151. Strobel, S. A.; Dervan, P. B. *J. Am. Chem. Soc.* **1989,** *111,* 7286.
152. Horne, D. A.; Dervan, P. B. *J. Am. Chem. Soc.* **1990,** *112,* 2435.
153. Strobel, S. A.; Dervan, P. B. *Science* **1990,** *249,* 73.
154. Griffin, L. C.; Kiessling, L. L.; Beal, P. A.; Gillespie, P.; Dervan, P. B. *J. Am. Chem. Soc.* **1992,** *114,* 7976.
155. Han, H.; Dervan, P. B. *Proc. Natl. Acad. Sci. U.S.A.* **1993,** *90,* 3806.
156. Han, H.; Dervan, P. B. *Proc. Natl. Acad. Sci. U.S.A.* **1994,** *91,* 4955.

157. Ermacora, M. R.; Ledman, D. W.; Hellinga, H. W.; Hsu, G. W.; Fox, R. O. *Biochemistry* **1994,** *33,* 13625.
158. Heilek, G. M.; Marusak, R.; Meares, C. F.; Noller, H. F. *Proc. Natl. Acad. Sci. U.S.A.* **1995,** *92,* 1113.
159. Iverson, B. L.; Shreder, K.; Morishima, T.; Rosingana, M.; Sesler, J. L. *J. Org. Chem.* **1995,** *60,* 6616.
160. Groves, J. T.; Kady, I. O. *Inorg. Chem.* **1993,** *32,* 3868.
161. Pyle, A. M.; Barton, J. K. *Prog. Inorg. Chem.* **1990,** *38,* 413.
162. Sugden, K. D.; Geer, R. D.; Rogers, S. J. *Biochemistry* **1992,** *31,* 11626.
163. Gravert, D. J.; Griffin, J. H. *J. Org. Chem.* **1993,** *58,* 820.
164. Müller, B. C.; Raphael, A. L.; Barton, J. K. *Proc. Natl. Acad. Sci. U.S.A.* **1987,** *84,* 1764.
165. Carter, M. T.; Rodriguez, M.; Bard, A. J. *J. Am. Chem. Soc.* **1989,** *111,* 8901.
166. Mack, D. P.; Dervan, P. B. *Biochemistry* **1992,** *31.* 9399.
167. Chen, X.; Rokita, S. E.; Burrows, C. J. *J. Am. Chem. Soc.* **1991,** *113,* 5884.
168. Burrows, C. J.; Rokita, S. E. *Acc. Chem. Res.* **1994,** *27,* 295.
169. Chen, X.; Rokita, S. E.; Burrows, C. J. *J. Am. Chem. Soc.* **1992,** *114,* 322.
170. Chen, X.; Woodson, S. A.; Burrows, C. J.; Rokita, S. E. *Biochemistry* **1993,** *32,* 7610.
171. Mei, H. Y.; Barton, J. K. *Proc. Natl. Acad. Sci. U.S.A.* **1988,** *85,* 1339.
172. Kelly, J. M.; McConnell, D. J.; OhUigin, C.; Tossi, A. B.; Kirsh-De Mesmaeker, A.; Masschelein, A.; Nasielski, J. *J. Chem. Soc., Chem. Commun.* **1987,** 1821.
173. Görner, H.; Stradowski, C.; Schulte-Frohlinde, D. *Photochem. Photobiol.* **1988,** *47,* 15.
174. Tossi, A. B.; Görner, H.; Schulte-Frohlinde, D. *Photochem. Photobiol.* **1989,** *50,* 585.
175. Long, E. C.; Barton, J. K. *Acc. Chem. Res.* **1990,** *23,* 273.
176. Turro, N. J.; Barton, J. K.; Tomalia, D. A. *Acc. Chem. Res.* **1991,** *24,* 332.
177. Satyanarayana, S.; Dabrowiak, J. C.; Chaires, J. B. *Biochemistry* **1992,** *31,* 9319.
178. Satyanarayana, S.; Dabrowiak, J. C.; Chaires, J. B. *Biochemistry* **1993,** *32,* 2573.
179. Eriksson, M.; Leijon, M.; Hiort, C.; Nordén, B.; Gräslund, A. *Biochemistry* **1994,** *33,* 5013.
180. (a) Hiort, C.; Lincoln, P.; Nordén, B. *J. Am. Chem. Soc.* **1993,** *115,* 3448; (b) Sentagne, C.; Chambron, J. C.; Sauvage, J. P.; Paillous, N. *J. Photochem. Photobiol. B: Biol.* **1994,** *26,* 165.
181. Baker, A. D.; Morgan, R. J.; Strekas, T. C. *J. Chem. Soc., Chem. Commun.* **1992,** 1099.
182. Grover, N.; Thorp, H. H. *J. Am. Chem. Soc.* **1991,** *113,* 7030.
183. Grover, N.; Gupta, N.; Singh, P.; Thorp, H. H. *Inorg. Chem.* **1992,** *31,* 2014.
184. Gupta, N.; Grover, N.; Neyhart, G. A.; Linag, W.; Singh, P.; Thorp, H. H. *Angew. Chem., Int. Ed. Engl.* **1992,** *31,* 1048.
185. Neyhart, G. A.; Grover, N.; Smith, S. R.; Kalsbeck, W. A.; Fairley, T. A.; Cory, M.; Thorp, H. H. *J. Am. Chem. Soc.* **1993,** *115,* 4423.
186. Gupta, N.; Grover, N.; Neyhart, G. A.; Singh, P.; Thorp, H. H. *Inorg. Chem.* **1993,** *32,* 310.
187. (a) Cheng, C. C.; Goll, J. G.; Neyhart, G. A.; Welch, T. W.; Singh, P.; Thorp, H. H. *J. Am. Chem. Soc.* **1995,** *117,* 2970; (b) Lecomte, J. P.; Kirsch-De Mesmaeker, A.; Feeney, M. M.; Kelly, J. M. *Inorg. Chem.* **1995,** *34,* 6481.
188. Pyle, A. M.; Long, E. C.; Barton, J. K. *J. Am. Chem. Soc.* **1989,** *111,* 4520.
189. David, S. S.; Barton, J. K. *J. Am. Chem. Soc.* **1993,** *115,* 2984.
190. Shields, T. P.; Barton, J. K. *Biochemistry* **1995,** *34,* 15049.

191. (a) Sitlani, A.; Long, E. C.; Pyle, A. M.; Barton, J. K. *J. Am. Chem. Soc.* **1992,** *114,* 2303; (b) Shields, T. P.; Barton, J. K. *Biochemistry* **1995,** *34,* 15037.
192. Lim, A. C.; Barton, J. K. *Biochemistry* **1993,** *32,* 11029.
193. Campisi, D.; Morii, T.; Barton, J. K. *Biochemistry* **1994,** *33,* 4130.
194. Sitlani, A.; Barton, J. K. *Biochemistry* **1994,** *33,* 12100.
195. Terbrueggen, R. H.; Barton, J. K. *Biochemistry* **1995,** *34,* 8227.
196. Kalsbeck, W. A.; Grover, N.; Thorp, H. H. *Angew. Chem., Int. Ed. Engl.* **1991,** *30,* 1517.
197. Kalsbeck, W. A.; Gingell, D. M.; Malinsky, J. E.; Thorp, H. H. *Inorg. Chem.* **1994,** *33,* 3313.
198. Nielsen, P. E.; Jeppesen, C.; Buchardt, O. *FEBS Lett.* **1988,** *235,* 122.
199. Nielsen, P. E.; Hiort, C.; Sönnichsen, S. H.; Buchardt, O.; Dahl, O; Nordèn, B. *J. Am. Chem. Soc.* **1992,** *114,* 4967.
200. Fiel, R. J.; Beerman, T. A.; Mark, E. H.; Datta-Gupta, N. *Biochem. Biophys. Res. Commun.* **1982,** *107,* 1067.
201. Banville, D. S.; Marzilli, L. G.; Wilson, W. D. *Biochem. Biophys. Res. Commun.* **1983,** *113,* 148.
202. Fiel, R. J. *J. Biomol. Struct. Dyn.* **1989,** *6,* 1259.
203. Pasternak, R. F.; Gibbs, E. J. In "Metal DNA Chemistry"; Tullius, T., Ed.; American Chemical Society: Washington, D.C., 1989, p. 59.
204. Aft, R. L.; Mueller, G. C. *J. Biol. Chem.* **1983,** *258,* 12069.
205. Sakurai, H.; Shibuya, M.; Shimizu, C.; Akimoto, S.; Maeda, M.; Kawasaki, K. *Biochem. Biophys. Res. Commun.* **1986,** *136,* 645.
206. Frolava, E. I.; Ivanova, E. M.; Zarytova, V. F.; Abramova, T. V.; Vlassov, V. V. *FEBS Lett.* **1990,** *269,* 101.
207. Fedorova, O. S.; Savitskii, A. P.; Shoikhet, K. G.; Ponomarev, G. V. *FEBS Lett.* **1990,** *259,* 335.
208. Le Doan, T.; Perrouault, L.; Hélène, C.; Chassignol, M.; Thuong, N. T. *Biochemistry* **1986,** *25,* 6736.
209. Mastruzzo, L.; Woisard, A.; Ma, D. D. F.; Rizarelli, E.; Favre, A.; Le Doan, T. *Photochem. Photobiol.* **1994,** *60,* 316.
210. Sari, M. A.; Battioni, J. P.; Dupré, D.; Mansuy, D.; Le Pecq, J. B. *Biochemistry* **1990,** *29,* 4205.
211. James, D. A.; Arnold, D. P.; Parsons, P. G. *Photochem. Photobiol.* **1994,** *59,* 441.
212. Iverson, B. L.; Shreder, K.; Kral, V.; Smith, D. A.; Smith, J.; Sessler, J. L. *Pure Appl. Chem.* **1994,** *66,* 845.
213. Meng, G. G.; James, B. R.; Skov, K. A.; Korbelik, M. *Can. J. Chem.* **1994,** *72,* 2447.
214. Marzilli, L. G. *New J. Chem.* **1990,** *14,* 409.
215. Strickland, J. A.; Marzilli, L. G.; Wilson, W. D. *Biopolymers* **1990,** *29,* 1307.
216. Gibbs, E. J.; Maurer, M. C.; Zhang, J. H.; Reiff, W. M.; Hill, D. T.; Malicka-Blaszkiewicz, M.; McKinnie, R. E.; Liu, H.-Q.; Pasternack, R. F. *J. Inorg. Biochem.* **1988,** *32,* 39.
217. Sehlstedt, U.; Kim, S. K.; Carter, P.; Goodisman, J.; Vollano, J. F.; Nordèn, B.; Dabrowiak, J. C. *Biochemistry* **1994,** *33,* 417.
218. Geacintov, N. E.; Ibanez, V.; Rougee, M.; Bemsasson, R. V. *Biochemistry* **1987,** *26,* 3087.
219. Marzilli, L. G.; Pethö, G.; Lin, M.; Kim, M. S.; Dixon, D. W. *J. Am. Chem. Soc.* **1992,** *114,* 7575.
220. Pasternack, R. F.; Bustamante, C.; Collings, P. J.; Gianetto, A.; Gibbs, E. J. *J. Am. Chem. Soc.* **1993,** *115,* 5393.

221. Hui, X.; Gresh, N.; Pullman, B. *Nucleic Acids Res.* **1990,** *18,* 1109.
222. Pasternack, R. F.; Gibbs, E. J.; Villafranca, J. J. *Biochemistry* **1983,** *22,* 5409.
223. Pasternack, R. F.; Gibbs, E. J.; Villafranca, J. J. *Biochemistry* **1983,** *22,* 2406.
224. Ward, B.; Skorobogaty, A.; Dabrowiak, J. C. *Biochemistry* **1986,** *25,* 6875.
225. Ward, B.; Skorobogaty, A.; Dabrowiak, J. C. *Biochemistry* **1986,** *25,* 7827.
226. Pratviel, G.; Pitié, M.; Bernadou, J.; Meunier, B. *Angew. Chem., Int. Ed. Engl.* **1991,** *30,* 702.
227. Pitié, M.; Pratviel, G.; Bernadou, J.; Meunier, B. *Proc. Natl. Acad. Sci. U.S.A.* **1992,** *89,* 3967.
228. Prince, S.; Körber, F.; Cooke, P. R.; Lindsay Smith, J. R.; Mazid, M. A. *Acta Crystallogr.* **1993,** *C49,* 1158.
229. Ding, L.;,Bernadou, J.; Meunier, B. *Bioconjugate Chem.* **1991,** *2,* 201.
230. Pitié, M.; Pratviel, G.; Bernadou, J.; Meunier, B. In "The Activation of Dioxygen and Homogeneous Catalytic Oxidation"; Barton, D. H. R., Martell, A. E., and Sawyer, D. T., Eds.; Plenum Press; New York, 1993, p. 333.
231. Cartwright, I. L.; Herzberg, R. P.; Dervan, P. B.; Elgin, S. C. R. *Proc. Natl. Acad. Sci. U.S.A.* **1983,** *80,* 3213.
232. Lowin, J. W.; Sondhi, S. M.; Ong, C.-W.; Skorobogaty, A.; Kishikawa, H.; Dabrowiak, J. C. *Biochemistry* **1986,** *25,* 5111.
233. Hashimoto, Y.; Iijima, H.; Nozaki, Y.; Shudo, K. *Biochemistry* **1986,** *25,* 5103.
234. Uno, T.; Sowa, N.; Shimabayashi, S. *Chem. Pharm. Bull.* **1994,** *42,* 988.
235. Etemad-Moghadam, G.; Ding, L.; Tadj, F.; Meunier, B. *Tetrahedron* **1989,** *45,* 2641.
236. Ding, L.; Etemad-Moghadam, G.; Cros, S.; Auclair, C.; Meunier, B. *J. Chem. Soc., Chem. Commun.* **1989,** 1711.
237. Ding, L.; Etemad-Moghadam, G.; Meunier, B. *Biochemistry* **1990,** *29,* 7868.
238. Ding, L.; Etemad-Moghadam, G.; Cros, S.; Auclair, C.; Meunier, B. *J. Med. Chem.* **1991,** *34,* 900.
239. Anneheim-Herbelin, G.; Perée-Fauvet, M.; Gaudemer, A.; Helissey, P.; Giorgi-Renault, S.; Gresh, N. *Tetrahedron Lett.* **1993,** *34,* 7263.
240. (a) Frau, S.; Bernadou, J.; Meunier, B.; Delaunay, J.-C.; Vercauteren, J. *New J. Chem.* **1995,** *19,* 873; (b) Frau, S.; Bernadou, J.; Meunier, B. *Bioconjugate Chem.* **1997,** *8,* 222.
241. Frolova, E. I.; Fedorova, O. S.; Knorre, D. G. *Biochimie* **1993,** *75,* 5.
242. Ramalho Ortigao, J. F.; Rück, A.; Gupta, K. C.; Rösch, R.; Steiner, R.; Seliger, H. *Biochimie* **1993,** *75,* 29.
243. Casas, C.; Lacey, C. J.; Meunier, M. *Bioconjugate Chem.* **1993,** *4,* 366.
244. Jakobs, A.; Bernadou, J.; Meunier, B. *J. Org. Chem.* **1997,** *62,* 3505.
245. Mestre, B.; Jakobs, A.; Pratviel, G.; Meunier, B. *Biochemistry* **1996,** *35,* 9140.
246. Pitié, M.; Casas, C.; Lacey, C. J.; Pratviel, G.; Bernadou, J.; Meunier, B. *Angew. Chem., Int. Ed. Engl.* **1993,** *32,* 557.
247. Bigey, P.; Pratviel, G.; Meunier, B. *J. Chem. Soc., Chem. Comm.* **1995,** *181.*
248. Bigey, P.; Pratviel, G.; Meunier, B. *Nucleic Acids Res.* **1995,** *23,* 3894.
249. Thuong, N. T.; Hélène, C. *Agnew. Chem., Int. Ed. Engl.* **1993,** *32,* 666.
250. Mestre, B.; Pratviel, G.; Meunier, B. *Bioconjugate Chem.* **1995,** *6,* 466.
251. Mehta, G.; Sambaiah, T.; Maiya, B. G.; Sirish, M.; Chatterjee, D. *J. Chem. Soc., Perkin Trans.* **1993,** *1,* 2667.
252. Li, H.; Czuchajowski, L. *Tetrahedron Lett.* **1994,** *35,* 1629.
253. Mehta, G.; Sambaiah, T.; Maiya, B. G.; Sirish, M.; Dattagupta, A. *Tetrahedron Lett.* **1994,** *35,* 4201.

254. Nakajima, O.; Mizoguchi, H.; Hashimoto, Y.; Iwasaki, S. *J. Am. Chem. Soc.* **1992,** *114,* 9203.
255. Perrée-Fauvet, M.; Gresh, N. *Tetrahedron Lett.* **1995,** *36,* 4227.
256. Mansouri, S.; Gossauer, A.; Meunier, B.; Paillous, N. *New J. Chem.* **1994,** *18,* 745.
257. Gomer, C. J.; Rucker, N.; Murphree, A. L. *Cancer Res.* **1988,** *48,* 4539.
258. "Photosensitizing Compounds: Their Chemistry, Biology and Clinical Use"; Ciba Foundation Symposium 146; J. Wiley: Chichester, 1989.
259. Ho, Y.-K.; Missert, J. R.; Dougherty, T. J. *Photochem. Photobiol.* **1991,** *54,* 83.
260. Dolphin, T. J. *Can. J. Chem.* **1994,** *72,* 1005.
261. Kvam, E.; Moan, J. *Photochem. Photobiol.* **1990,** *52,* 769.
262. Oleinick, N. L.; Antunez, A. R.; Clay, M. E.; Rihter, B. D.; Kenney, M. E. *Photochem. Photobiol.* **1993,** *57,* 242.
263. Bellnier, D. A.; Henderson, B. W.; Pandey, R. K.; Potter, W. R.; Dougherty, T. J. *J. Photochem. Photobiol. B: Biol.* **1993,** *20,* 55.
264. Verlhac, J. B.; Gaudemer, A.; Kraljic, I. *Nouv. J. Chim.* **1984,** *8,* 401.
265. Fiel, R. J.; Datta-Gupta, N.; Mark, E. H.; Howard, J. C. *Cancer. Res.* **1981,** *41,* 3543.
266. Kelly, J. M.; Murphy, M. J.; McConnell, D. J.; OhUigin, C. *Nucleic Acids Res.* **1985,** *13,* 167.
267. Praseuth, D.; Gaudemer, A.; Verlhac, J.-B.; Kraljic, I.; Sissoëff, I.; Guillé, E. *Photochem. Photobiol.* **1986,** *44,* 717.
268. Croke, D. T.; Perrouault, L.; Sari, M. A.; Battioni, J.-P.; Mansuy, D.; Helene, C.; Le Doan, T. *J. Photochem. Photobiol. B: Biol.* **1993,** *18,* 41.
269. Milder, S. J.; Ding, L.; Etemad-Moghadam, G.; Meunier, B.; Paillous, N. *J. Chem. Soc., Chem. Commun.* **1990,** 1131.
270. Sentagne, C.; Meunier, B.; Paillous, N. *J. Photochem. Photobiol. B: Biol.* **1992,** *16,* 47.
271. Saito, T.; Kitamura, M.; Tanaka, M.; Morimoto, M.; Segawa,H.; Shimidzu, T. *Nucleosides Nucleotides* **1994,** *13,* 1607.
272. Dabrowiak, J. C.; Ward, B.; Goodisman, J. *Biochemistry* **1989,** *28,* 3314.
273. Fouquet, E.; Pratviel, G.; Bernadou, J.; Meunier, B. *J. Chem. Soc., Chem. Commun.* **1987,** 1169.
274. Bernadou, J.; Pratviel, G.; Bennis, F.; Girardet, M.; Meunier, B. *Biochemistry* **1989,** *28,* 7268.
275. Pratviel, G.; Bernadou, J.; Ricci, M.; Meunier, B. *Biochem. Biophys. Res. Commun.* **1989,** *160,* 1212.
276. Pratviel, G.; Pitié, M.; Bernadou, J.; Meunier, B. *Nucleic Acids Res.* **1991,** *19,* 6283.
277. Groves, J. T.; Marla, S. S. *J. Am. Chem. Soc.* **1995,** *117,* 9578.
278. Byrnes, R. W.; Fiel, R. J.; Datta-Gupta, N. *Chem.-Biol. Interactions* **1988,** *67,* 225.
279. Bernadou, J.; Fabiano, A.-S.; Robert, A.; Meunier, B. *J. Am. Chem. Soc.* **1994,** *116,* 9375.
280. Pitié, M.; Bernadou, J.; Meunier, B. *J. Am. Chem. Soc.* **1995,** *117,* 2935.
281. Rodriguez, M.; Kodadek, T.; Torres, M.; Bard, A. *Bioconjugate Chem.* **1990,** *1,* 123.
282. Bernadou, J.; Lauretta, B.; Pratviel, G.; Meunier, B. *C. R. Acad. Sci. Paris* **1989,** *309III,* 409.
283. Van Atta, R. B.; Bernadou, J.; Meunier, B.; Hecht, S. M. *Biochemistry* **1990,** *29,* 4783.
284. Pratviel, G.; Pitié, P.; Périgaud, C.; Gosselin, G.; Bernadou, J.; Meunier, B. *J. Chem. Soc., Chem. Commun.* **1993,** 149.

285. Gasmi, G.; Pasdeloup, M.; Pratviel, G.; Pitié, M.; Bernadou, J.; Meunier, B. *Nucleic Acids Res.* **1991,** *19,* 2835.
286. Kappen, L. S.; Goldberg, I. H. *Biochemistry* **1989,** *28,* 1027.
287. Goldberg, I. H. *Acc. Chem. Res.* **1991,** *24,* 191.
288. Pratviel, G.; Bigey, P.; Bernadou, J.; Meunier, B. In "Genetic Response to Metals"; Sarkar, B., Ed.; Marcel Dekker: New York, 1995, p. 153.
289. Pitié, M.; Meunier, B. *J. Biol. Inorg. Chem.* **1996,** *1,* 239.
290. Chin, J. *Acc. Chem. Res.* **1991,** *24,* 145.
291. Suck, D.; Lahm, A.; Oefner, C. *Nature* **1988,** *321,* 620.
292. Rosenberg, J. M. *Curr. Opin. Struct. Biol.* **1991,** *1,* 104.
293. Winkler, F. K.; Banner, D. W.; Oefner, C.; Tsernoglou, D.; Brown, R. S.; Heathman, S. P.; Bryan, R. K.; Martin, P. D.; Petratos, K.; Wilson, K. S. *EMBO J.* **1993,** *12,* 1781.
294. Cheng, X.; Balendiran, K.; Schildkraut, I.; Anderson, J. E. *EMBO J.* **1994,** *13,* 3927.
295. Newman, M.; Strzelecka, T.; Dorner, L. F.; Schildkraut, I.; Aggarwal, A. K. *Science* **1995,** *269,* 656.
296. Mol, C. D.; Kuo, C.; Thayer, M. M.; Cunningham, R. P.; Tainer, J. A. *Nature* **1995,** *374,* 381.
297. Kostrewa, D.; Winkler, F. K. *Biochemistry* **1995.** *34,* 683.
298. Vipond, I. B.; Baldwin, G. S.; Halford, S. E. *Biochemistry* **1995,** *34,* 697.
299. Beese, L. S.; Steitz, T. A. *EMBO J.* **1991,** *10,* 25.
300. Lima, C. D.; Wang, J. C.; Mondragin, A. *Nature* **1994,** *367,* 138.
301. Kim, E. E.; Wycoff, H. W. *J. Mol. Biol.* **1991,** *218,* 449.
302. Hough, E.; Hansen, L. K.; Birknes, B.; Junge, K.; Hansen, S.; Hordvik, A.; Little, C.; Dodson, E.; Derewenda Z. *Nature* **1989,** *338,* 357.
303. Davies II, J. F.; Hostomska, Z.; Hostomsky, Z.; Jordan, S. R.; Matthews, D. A. *Science* **1991,** *252,* 88.
304. Volbeda, A.; Lahm, A.; Sakiyama, F.; Suck, D. *EMBO J.* **1991,** *10,* 1607.
305. Sträter, N.; Klabunde, T.; Tucker, P.; Witzel, H.; Krebs, B. *Science* **1995,** *268,* 1489.
306. Karlin, K. D. *Science* **1993,** *261,* 701.
307. Wahnon, D.; Lebuis, A.-M.; Chin, J. *Angew. Chem., Int. Ed. Engl.* **1995,** *34,* 2412.
308. Chapman, Jr., W. H.; Breslow, R. *J. Am. Chem. Soc.* **1995,** *117,* 5462.
309. Knowles J. R. *Annu. Rev. Biochem.* **1980,** *49,* 877.
310. Gupta, A. P.; Benkovic, S. J. *Biochemistry* **1984,** *23,* 5874.
311. Westheimer, F. H. *Acc. Chem. Res.* **1968,** *1,* 70.
312. Brown, R. S.; Dewan, J. C.; Klug, A. *Biochemistry* **1985,** *24,* 4785.
313. Breslow, R.; Huang, D.-L. *Proc. Natl. Acad. Sci. U.S.A.* **1991,** *88,* 4080.
314. Ciesiolka, J.; Marciniec, T.; Krzyzosiak, W. J. *Eur. J. Biochem.* **1989,** *182,* 445.
315. Dange, V.; Van Atta, R. B.; Hecht, S. M. *Science* **1990,** *248,* 585.
316. Kazakov, S.; Altman, S. *Proc. Natl. Acad. Sci. U.S.A.* **1992,** *89,* 7939.
317. Sawata, S.; Komiyama, M.; Taira, K. *J. Am. Chem. Soc.* **1995,** *117,* 2357.
318. Pyle, A. M. *Science* **1993,** *261,* 709.
319. Dham, S. C.; Derrick, W. B.; Uhlenbeck, O. C. *Biochemistry* **1993,** *32,* 13040.
320. Cech, T. R. *Angew. Chem., Int. Ed. Engl.* **1990,** *29,* 759.
321. Piccirilli, J. A.; Vyle, J. S.; Caruthers, M. H.; Cech, T. R. *Nature* **1993,** *361,* 85.
322. Dahm, S. C.; Uhlenbeck, O. C. *Biochemistry* **1991,** *30,* 9464.
323. Celander, D. W.; Cech, T. R. *Science* **1991,** *25,* 401.
324. Altman, S. *Angew. Chem., Int. Ed. Engl.* **1990,** *29,* 749.
325. McSwiggen, J. A.; Cech, T. R. *Science* **1989,** *244,* 679.

326. Kolasa, K. A.; Morrow, J.; Sharma, A. P. *Inorg. Chem.* **1993,** *32,* 3983.
327. Stull, R. A.; Szoka, F. C. *Pharmaceut. Sci.* **1995,** *12,* 465.
328. Bashkin J. K.; Jenkins, L. A. *Comments Inorg. Chem.* **1994,** *16,* 77.
329. Breslow, R.; Huang, D.-L.; Anslyn, E. *Proc. Natl. Acad. Sci. U.S.A.* **1989,** *86,* 1746.
330. Chin, J.; Banaszczyk, M.; Jubian, V.; Zou, X. *J. Am. Chem. Soc.* **1989,** *111,* 186.
331. Morrow, J. R.; Buttrey, L. A.; Shelton, V. M.; Berback, K. A. *J. Am. Chem. Soc.* **1992,** *114,* 1903.
332. Bashkin, J. K.; Jenkins, L. A. *J. Chem. Soc., Dalton Trans.* **1993,** 3631.
333. Schneider, H.-J.; Rammo, J.; Hettich, R. *Angew. Chem., Int. Ed. Engl.* **1993,** *32,* 1716.
334. Linkletter, B.; Chin, J. *Angew. Chem., Int. Ed. Engl.* **1995,** *34,* 472.
335. Stern, M. K.; Bashkin, J. K.; Sall, E. D. *J. Am. Chem. Soc.* **1990,** *112,* 5357.
336. Suck, D.; Oefner, C. *Nature* **1986,** *321,* 620.
337. Breslow, R. *Acc. Chem. Res.* **1991,** *24,* 317.
338. Kim, J. K.; Chin, J. *J. Am. Chem. Soc.* **1992,** *114,* 9792.
339. Komiyama, M.; Matsumoto, Y.; Hayashi, N.; Matsumara, K.; Takeda, N.; Watanabe, K. *Polymer J.* **1993,** *25,* 1211.
340. Takasaki, B. K.; Chin, J. *J. Am. Chem. Soc.* **1994,** *116,* 1121.
341. Komiyama, M.; Matsumara, K.; Yonezawa, K.; Matsumoto, Y. *Chem. Express* **1993,** *8,* 85.
342. Komiyama, M.; Takeda, N.; Takahashi, Y.; Uchida, H.; Shiiba, T.; Kodama, T.; Yashiro, M. *J. Chem. Soc., Perkin Trans.* **1995,** 269.
343. Wahnon, D.; Hynes, R.; Chin, J. *J. Chem. Soc., Chem. Commun.* **1994,** 1441.
344. Chin, J.; Banaszczyk, M. *J. Am. Chem. Soc.* **1989,** *111,* 4103.
345. Connolly, J. A.; Banaszczyk, M.; Hynes, R. C.; Chin, J. *Inorg. Chem.* **1994,** *33,* 665.
346. Takasaki, B. K.; Chin, J. *J. Am. Chem. Soc.* **1993,** *115,* 9337.
347. Takasaki, B. K.; Chin, J. *J. Am. Chem. Soc.* **1995,** *117,* 8582.
348. Tsubouchi, A.; Bruice, T. C. *J. Am. Chem. Soc.* **1994,** *116,* 11614.
349. Takeda, N.; Irisawa, M.; Komiyama, M. *J. Chem. Soc., Chem. Commun.* **1994,** 2773.
350. Irisawa, M.; Takeda, N.; Komiyama, M. *J. Chem. Soc., Chem. Commun.* **1995,** 1221.
351. Irisawa, M.; Komiyama, M. *J. Biochem.* **1995,** *117,* 465.
352. Wall, M.; Hynes, R. C.; Chin, J. *Angew. Chem., Int. Ed. Engl.* **1993,** *32,* 1633.
353. Young, M. J.; Chin, J. *J. Am. Chem. Soc.* **1995,** *117,* 10577.
354. Vance, D. H.; Czarnik, A. W. *J. Am. Chem. Soc.* **1993,** *115,* 12165.
355. Yashiro, M.; Ishikubo, A.; Komiyama, M. *J. Chem. Soc., Chem. Commun.* **1995,** 1793.
356. Bashkin, J. K.; Frolova, E. I.; Sampath, U. *J. Am. Chem. Soc.* **1994,** *116,* 5981.
357. Matsumara, K.; Endo, M.; Komiyama, M. *J. Chem. Soc., Chem. Commun.* **1994,** 2019.
358. Magda, D.; Miller, R. A.; Sessler, J. L.; Iverson, B. L. *J. Am. Chem. Soc.* **1994,** *116,* 7439.
359. Hall, J.; Hüsken, D.; Pieles, U.; Moser, H. E.; Häner, R. *Chem. Biol.* **1994,** *1,* 185.
360. Modak, A. S.; Gard, J. K.; Merriman, M. C.; Winkeler, K. A.; Bashkin, J. K.; Stern, M. K. *J. Am. Chem. Soc.* **1991,** *113,* 283.
361. Komiyama, M.; Shiiba, T.; Takahashi, Y.; Takeda, N.; Matsumara, K.; Kodama, T. *Supramol. Chem.* **1995,** *4,* 31.
362. Sachs, A. B. *Cell* **1993,** *74,* 413.
363. Pratviel, G.; Duarte, V.; Bernadou, J.; Meunier, B. *J. Am. Chem. Soc.* **1993,** *115,* 7939.
364. "Metal Ions in Biological Systems. Interaction of Metal Ions with Nucleotides,

Nucleic Acids and their Constituants."; Sigel, A., and Sigel, H., Eds.; Marcel Dekker: New York, 1996, Vol. 32.
365. "Metal ions in Biological systems. Probing of nucleic acids by metal ion complexes of small molecules."; Sigel, A., and Sigel, H., Eds.; Marcel Dekker: New York, 1996, Vol. 33.
366. "DNA and RNA Cleavers and Chemotherapy of Cancer and Viral Diseases"; Meunier, B., Ed.; Kluger Academic Publishers: Dordrecht/Boston/London, 1996, Series C, p. 479.
367. Stubbe, J.; Kozarich, J. W.; Wu, W.; Vanderwall, D. *Acc. Chem. Res.* **1996,** *29,* 322.
368. Sam, J. W.; Tang, X.-J.; Magliozzo, R. S.; Peisach, J. *J. Am. Chem. Soc.* **1995,** *117,* 1012.
369. Perrin, D. M.; Hoang, V. M.; Mazumder, A.; Sigman, D. S. *Biochemistry* **1996,** *35,* 5318.
370. Swalley, S. E.; Baird, E. E.; Dervan, P. B. *J. Am. Chem. Soc.* **1996,** *118,* 8198.
371. Wang, J.; Yu, P.; Lin, T. C.; Konigsberg, W. H.; Steitz, T. A. *Biochemistry* **1996,** *35,* 8110.
372. Kuimelis, R. G.; McLaughlin, L. W. *Biochemistry* **1996,** *35,* 5308.
373. Zhou, D.-M.; Usman, N.; Wincott, F. E.; Matulic-Ademic, J.; Orita, M.; Zhang, L.-H.; Komiyama, M.; Kumar, P. K. R.; Taira, K. *J. Am. Chem. Soc.* **1996,** *118,* 5862.
374. Abramovitz, D. L.; Friedman, R. A.; Pyle, A. M. *Science* **1996,** *271,* 1410.
375. Amontov, S. V.; Taira, K. *J. Am. Chem. Soc.* **1996,** *118,* 1624.
376. Zhou, D.-M.; Kumar, P. K. R.; Zhang, L.-H.; Taira, K. *J. Am. Chem. Soc.* **1996,** *118,* 8969.
377. Koike, T.; Inoue, M.; Kimura, E.; Shiro, M. *J. Am. Chem. Soc.* **1996,** *118,* 3091.
378. Hall, J.; Hüsken, D.; Häner, R. *Nucleic Acids Res.* **1996,** *24,* 3522.

ADVANCES IN INORGANIC CHEMISTRY, VOL. 45

STRUCTURE–FUNCTION CORRELATIONS IN HIGH-POTENTIAL IRON PROTEINS

J. A. COWAN and SIU MAN LUI

Evans Laboratory of Chemistry, The Ohio State University, Columbus, Ohio 43210

I. Scope of the Review

High-potential iron proteins (HiPIPs) comprise a subset of the 4Fe–4S cluster family of metalloproteins that are characterized by a positive reduction potential, E_m, in the range of +50 to +450 mV. This class is differentiated from the 4Fe–4S centers in low-potential ferredoxins, which show a negative E_m, typically varying between −100 and −650 mV. The origin of these distinct redox properties has been rationalized in terms of the three-state hypothesis of Carter (*1*), summarized in Scheme 1, and can be attributed to the stability of the common $[Fe_4S_4(SR)_4]^{2-}$ state.

The physical biochemistry of these two classes of 4Fe–4S proteins has been extensively studied and reviewed, especially with regard to redox and electron transfer chemistry (*2–22*), whereas the magnetic properties of the cluster have been probed by electron paramagnetic resonance (EPR) (*23–34*), nuclear magnetic resonance (NMR) (*24*, *25*, *35–54*), and susceptibility measurements (*56–61*). Mössbauer spec-

0898-8838/98 $25.00

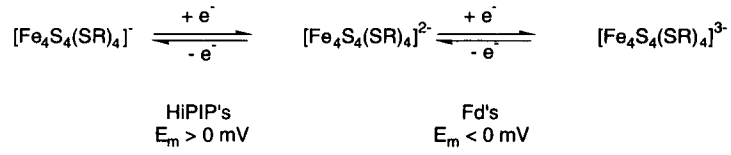

Scheme 1

troscopy has also been used extensively to investigate the distribution of valence states over the four iron centers (*24*, *27*, *32*, *33*, *62–68*).

This review will not dwell on the aforementioned "classical" areas of investigation, nor on more recent theoretical developments in magnetic coupling schemes that advance understanding of the electronic and magnetic properties of such centers. These topics have received extensive coverage elsewhere (*45*, *56*, *58*, *69–74*), including a series of concise commentaries in Ref. *55*, and interested readers are directed to this literature. Rather, this article will focus on more recent developments in understanding structure–function relationships for these proteins; including natural *in vivo* function, recent structural advances through X-ray and NMR solution studies, and new insights on the functional roles of amino acid residues in the control of cluster stability and redox chemistry. Although model complexes will not be a focus of this review, per se, reference will be made to results obtained from such investigations when they complement, and lend additional insight into, data from protein studies. The literature on synthetic cluster chemistry has also been the subject of review (*75–78*).

II. Source and Function of HiPIPs

The 4Fe–4S cluster proteins have now been identified in a large number of functional contexts, varying from a structural or sensory role in RNA- and DNA-binding and repair proteins or enzymes (*79–84*), and metabolic enzymes (*85*), including catalysis of hydrolyase isomerization reactions (*86*, *87*). In the facultative anaerobe *Escherichia coli* the transcription factor FNR (fumarate nitrate reduction) regulates gene expression in response to oxygen deprivation (*88–90*). The loss of the Fe–S cluster by exposure to oxygen is accompanied by conversion to the monomeric form of the protein and decreased DNA binding, suggesting that oxygen regulates the activity of wild-type FNR through the lability of the Fe–S cluster to oxygen (*90*). A plausible mechanism for such lability is discussed in Section IV,A,1. Clearly, these functional activities are distinct from traditional elec-

tron transfer reactions (*6*, *7*, *9*, *11*, *19*, *21*, *43*, *48*, *51*, *71*, *73*, *91–97*). Table I provides a summary listing of proteins with no electron transfer role, and their functional characteristics. For those proteins where a structural role in a DNA-binding protein is suggested, the cluster appears to be nonredox active, and so it is difficult to define the cluster as a high- or low-potential center. In other cases, oxidation of the cluster is accompanied by loss of a labile Fe to generate a 3Fe–4S center (*28*, *83*, *84*, *98–101*). The factors underlying the stability of oxidized $[Fe_4S_4(SR)_4]^-$ clusters will be discussed later.

Table II summarizes the sources and key properties of isolated HiPIPs, almost all of which have been isolated from photosynthetic organisms, and there has been extensive speculation on their involvement in respiratory electron transport chains (*18*, *21*, *91–93*, *95*, *96*, *102–105*). Evidence in support of such a hypothesis has recently emerged from studies of a partially reconstructed reaction center (RC) complex from *Rhodoferax fermentans* (*93*, *95*). The kinetics of photoinduced electron transfer from HiPIP to the reaction center suggested the formation of a HiPIP–RC complex with a dissociation constant of 2.5 μM. *In vivo* and *in vitro* studies by Schoepp *et al.* (*94*) similarly have demonstrated that the only high-redox-potential electron transfer component in the soluble fraction of *Rhodocyclus gelatinosus* TG-9 that could serve as the immediate electron transfer donor to the reaction-center-bound cytochrome was a HiPIP. *In vitro* experiments have shown HiPIP to be an electron donor to the *Chromatium* reaction center (*106*). Fukumori and Yamanaka (*107*) also reported that *Chromatium vinosum* HiPIP is an efficient electron acceptor for a thiosulfate-oxidizing enzyme isolated from that organism.

TABLE I

CLASSES OF 4FE–4S-CONTAINING PROTEINS WITH NONREDOX ROLES[a]

Protein	Protein function	Cluster function
Aconitase (*28*, *100*)	Isomerase	Catalytic
Lysine 2,3-amino mutase (*86*)	Enzyme	Catalytic
Glutamine phosphoribosyl pyrophosphate amidotransferase (*85*)	Enzyme	Structural
Endonuclease III (*81*)	DNA repair	Structural
Transcription factor FNR (fumarate nitrate reduction) (*90*)	Transcriptional regulation	Sensory
Iron-response protein (IRP) (*83*, *84*)	Translational regulation	Sensory
Mut Y (*79*)	DNA repair	Structural

[a] Some data is from Ref. *80*.

TABLE II

SOURCES AND KEY PROPERTIES OF HiPIPs[a]

Source	E_m (mV)	No. of residues	Net charge[b]
Chromatiaceae			
Chromatium purpuratum (*91*)	+390	—[c] (dimeric?)	—[c]
Chromatium tepidum (*123*)	+323	83	−4
Thiocapsa roseopersicina (*103, 105, 173, 174*)	+346 or +325	85	−6
Chromatium warmingii (*175*)	+355	85	−4
Chromatium vinosum (*138*)	+356	85	−5
Chromatium gracile (*39, 173*)	+350	83	−7
Thiocapsa pfennigii (176)	+352	81	−9
Ectothiorhodospiraceae			
Ectothiorhodospira halophila (*11, 161, 177*)	+120 (iso I)	71	−12
Ectothiorhodospira vacuolata (*161, 172*)	+260 (iso I)	72	−5
	+ 150 (iso II)	71	−8
Ectothiorhodospira shaposhnikovii (*172*)	+270 (iso I)	72	−6
	+155 (iso II)	71	−8
Rhodospirillaceae			
Rhodoferax fermentans (*21, 93, 95*)	+351	—[c]	—[c]
Rhodopila globiformis (*159, 161*)	+450	57	−3
Rhodospirillum salinarum (*17, 172*)	+265 (iso I)	57	−5
	—[c] (iso II)	54 (hexameric)	−1
Rhodopseudomonas marina (*96*)	+345	53	+5
Rhodocyclus tenuis (*114, 159, 172*)	+300	62	+2
Rhodomicrobium vannielii (*172*)	—[c]	53	+4
Rhodocyclus gelatinosus (*35, 94, 161*)	+332	74	+3
Denitrifying bacteria			
Paracoccus halodenitricans (*178*)	+282	71	−13
Aerobic sulfur bacteria			
Thiobacillus ferrooxidans (*26, 159, 179, 180*)	+380	53 (tetramer)	+1

[a] Data from Ref. *172*.

[b] Net charge of the peptide chain assuming His to be protonated and the Cys to be ionized. The charge on the cluster is omitted.

[c] Not determined.

III. X-Ray and Solution Structures

A. AVAILABLE STRUCTURAL DATA

Most high-potential iron proteins have been isolated from purple photosynthetic bacteria and vary in size from 6 to 10 kDa; the tertiary structures of many have been determined in the crystalline and/or solution states, including HiPIPs from *C. vinosum* (*1, 49, 52, 108–110*), *Ectothiorhodospira halophila* I (*48, 102, 111, 112*), *Ectothiorhodospira*

vacuolata II (*113*), and *Rhodocyclus tenuis* (*114*). The availability of high-resolution structural data allows identification of common structural traits that may be of functional significance for cluster chemistry, and that may also be subsequently investigated by site-directed mutagenesis. Such experiments have allowed the various contributing factors to cluster chemistry to be disentangled and their relative importance gauged (Section IV). A similar use of recombinant DNA techniques has also been made in studies of the coordination environment of iron–sulfur centers in low-potential ferredoxins (*115*).

Table III summarizes the sources of available X-ray and solution structural data on HiPIPs. In general there appears to be no significant variation between the solid state and solution structures. Bertini and co-workers have provided the solution structures of both reduced and oxidized HiPIPs (*48*, *112*, *116*), advancing the standard NMR methodologies to paramagnetic proteins (*53*). In agreement with the X-ray studies, they found structural similarities between the two states at different oxidation levels (*117–119*), consistent with the general design concept of electron transfer proteins.

B. Structure–Function Correlations

1. Primary Structure

The structures of the 4Fe–4S clusters in HiPIPs and low-potential ferredoxins (Fds) are very similar; however, there are major differ-

TABLE III

High-Resolution Structures of HiPIPs

Source of HiPIP	X-Ray or NMR	Resolution (Å)
Chromatium vinosum (C77S mutant) (*108*)	NMR_{red}	RMSD, 0.62 ± 0.9 (backbone) 1.09 ± 0.11 (heavy atoms)
Ectothiorhodospira halophila I (*48*)	NMR_{ox}	RMSD, 0.67 ± 0.46 (backbone) 1.23 ± 1.06 (heavy atoms)
Chromatium vinosum (*49*)	NMR_{ox}	RMSD, 0.57 ± 0.14 (backbone) 1.08 ± 0.16 (heavy atoms)
Chromatium vinosum (*52*)	NMR_{red}	RMSD, 0.62 ± 0.12 (backbone) 1.19 ± 0.18 (heavy atoms)
Ectothiorhodospira vacuolata II (*113*)	$X\text{-}Ray_{ox}$	1.8 (*R* factor, 16.3%)
Rhodocyclus tenuis (*114*)	$X\text{-}Ray_{red}$	1.5 (*R* factor, 17.3%)
Ectothiorhodospira halophila I (*102*)	$X\text{-}Ray_{red}$	2.5 (*R* factor, 18.4%)
Chromatium vinosum (*109*)	$X\text{-}Ray_{ox}$	2.0 (*R* factor, 24%)
Chromatium vinosum (*1, 110*)	$X\text{-}Ray_{red}$	2.5 (*R* factor, 24.7%)

ences in the local environment of the clusters in these two types of proteins. The sequences and folding patterns, the locations of the cysteine residues, and the positions of the hydrogen bonds are very different (*120–122*). For example, the amino acid sequence motif $-CX_2CX_2C \cdot \cdot \cdot X_n \cdot \cdot \cdot C-$ for Fds differs from that of HiPIPs, typically $-CX_2CX_{16}CX_{13}C-$, which in turn differs from the sequence motif for novel cluster-containing proteins such as endonuclease III, with the compact sequence $-CX_6CX_2CX_5C-$. Reviews of protein folding patterns around clusters, and issues related to the evolution of such proteins, have appeared in the literature (*120*, *122*).

2. Secondary and Tertiary Structure

Carter has reviewed the comparative crystallography of oxidized and reduced *C. vinosum* HiPIP (*1*), and the dimensional changes of the iron–sulfur cube following oxidation or reduction have also been extensively tabulated and discussed for both model complexes and protein-bound clusters (*118*). In spite of the low sequence homology in HiPIPs, there is a remarkable similarity in tertiary structure, especially around the cluster (*114*). No significant secondary structure is observed in the HiPIPs, with only two short α-helical segments, three strands of antiparallel β-pleated sheet, and one small helix near the N terminus (Fig. 1). The 4Fe–4S cluster is buried in the protein interior and is inaccessible to solvent (Fig. 2). This feature has been pro-

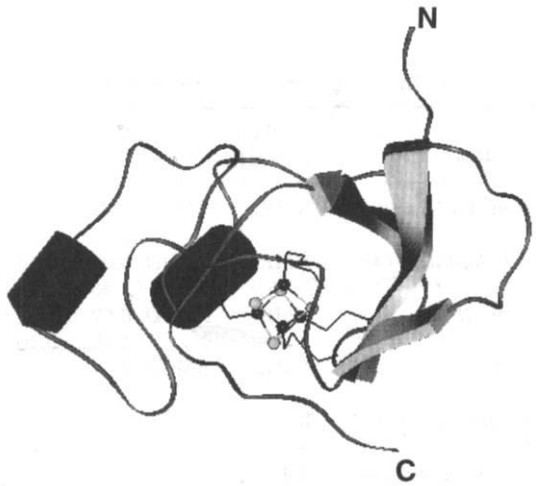

FIG. 1. Secondary and tertiary structural elements of *Chromatium vinosum* HiPIP.

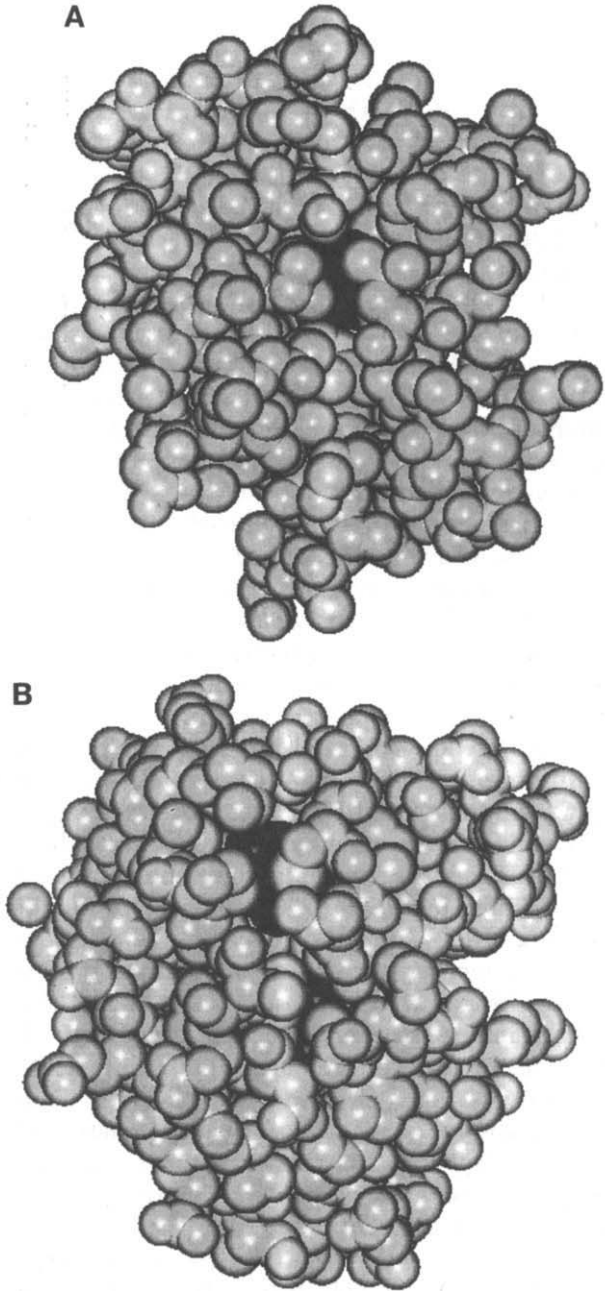

FIG. 2. Exposure of the 4Fe–4S cluster illustrated for high- and low-potential ferredoxins. (A) *Chromatium vinosum* HiPIP; (B) *Azotobacter vinelandii* Fd (the 4Fe–4S cluster is more exposed than the 3Fe–4S center).

posed to account for the stability of the $[Fe_4S_4(SR)_4]^{-/2-}$ oxidation states and the positive reduction potential, relative to the low-potential ferredoxins (*119*). Note, however, from the images in Fig. 2, that it is predominantly the depth of penetration required of solvent, rather than the "exposed" area of the cluster, that is the critical distinction between these protein classes. Finally, the coordinated sulfur atoms in *C. vinosum* HiPIP are involved in five (conserved) H-bond interactions with peptide NH protons, which are maintained in both oxidation states.

Benning *et al.* (*113*) have reported the molecular structure of the oxidized HiPIP (isoform II) from *E. vacuolata*, which shows close similarity to that of other HiPIPs, that is, a series of reverse turns wrapping around an iron–sulfur cluster to form a hydrophobic pocket. These researchers also pointed out that the structure of *E. vacuolata* II HiPIP [net charge = −8 (reduced); E_m, +150 mV] is intermediate between *C. vinosum* [net charge = −4 (reduced); E_m, + 352 mV) and *E. halophila* I [net charge = −11 (reduced); E_m, +120 mV) HiPIPs, based on the pattern of insertions and deletions, overall structural identity, and the percentage amino acid sequence identity, suggesting that neither the overall net charge of the protein nor minor structural changes underlie the difference in redox potentials.

A common theme among the high- and low-potential Fds is the relatively large number of hydrophobic aromatic residues that surround the cluster. However, low-potential Fds typically position the cluster closer to the protein surface, with a greater likelihood of solvent influence (Fig. 2), whereas for HiPIPs the cluster is completely inaccessible to water and is surrounded by hydrophobic residues (*8*, *20*). The importance of this fact for understanding the relative E_m values of Fds has been debated (*8*, *20*, *119*). In this regard, Moulis *et al.* (*123*) have studied the HiPIP from the thermophilic purple sulfur bacterium *Chromatium tepidum*, which shows optimal growth at 50°C. It was found that HiPIP from *C. vinosum* shares 74 of the 83 residues composing the primary structure of *C. tepidum* HiPIP. The most significant difference involves a stretch of eight amino acids that acts as a link between two strands of a twisted β-sheet that coordinates the 4Fe–4S cluster, and an area of extensive interaction of the cluster with the solvent. Regardless of this structural difference, these two HiPIPs show identical absorption and electron paramagnetic resonance spectra and redox potential.

Further variations in local environment can be demonstrated by the fact that Phe-83 and Phe-66 in both the *E. halophila* and the *C. vinosum* proteins are conserved; however, their side chains adopt

quite different conformations. Breiter *et al.* (*102*) proposed that the difference in side chain conformation of the above Phe may be one of many subtle factors in modulating oxidation–reduction potentials. However, the structurally similar Phe-54 in *E. vacuolata* II HiPIP did not show a conformation similar to that of the corresponding residue in *E. halophila*, and so another possible link between conformation and E_m appears unsubstantiated (*113*).

3. *Hydrogen Bonding*

Differences in the numbers of hydrogen bonds from backbone amides to cysteine and sulfide ligands have long been believed to play a significant role in the differentiation of high- and low-potential Fds. In the case of the low-potential Fds, eight hydrogen bonds per cluster are identified between amide N–H and sulfur ligands, whereas in structurally characterized HiPIPs there are only five. The NH–S bonds are speculated to stabilize the more negatively charged reduced states (*4*, *20*, *124*). However, the comparative study of Rayment *et al.* (*114*) clearly demonstrates that such a correlation (summarized in Table IV) cannot fully explain the wide variation of E_m values for this class of center. Perhaps the number of H-bond contacts better reflects other structural constraints around the cluster binding pocket, but does not influence E_m strongly, per se. This conclusion is further supported by experimental solution studies. In particular, Sweeney and

TABLE IV

INFLUENCE OF HYDROGEN-BOND CONTACTS ON 4Fe–4S CLUSTER E_m[a]

Protein	E_m (mV)	H-bond contacts[b]
Ectothiorhodospira halophila I HiPIP	+120	5
Ectothiorhodspira vacuolata II HiPIP	+150	5
Chromatium vinosum HiPIP	+360	5
Rhodocyclus tenuis HiPIP	+330	5
Clostridium pasteurianum Fd[c]	−403	—[d]
Bacillus thermoproteolyticus Fd[e]	−280	8
Peptococcus aerogenes Fd[f]	−430	8
Azotobacter vinelandii Fd I[g]	−650	8

[a] From Refs. *102*, *113*, *114*, *181*, and *182*.
[b] Number of H-bond contacts per 4Fe–4S center.
[c] Contains 2× 4Fe–S centers.
[d] Not evaluated.
[e] Contains 1× 4Fe–4S center.
[f] Contains 2× 4Fe–4S centers.
[g] Contains 1× 4Fe–4S center and 1× 3Fe–4S center.

Magliozzo (*125*) have examined the effect of deuterium substitution of exchangeable hydrogen atoms on the E_m of *C. pasteurianum* Fd. Deuteration of the slowly exchangeable H atoms yielded essentially no shift in E_m, and so the NH–S bonds are apparently not important in the modulation of cluster reduction potential in this protein.

C. Intermolecular Aggregation

Most HiPIPs have been assumed to function as monomers. However, the HiPIP from *Rhodospirillum salinarum* has been shown to exist as a tetramer or hexamer (*17*). Other evidence points to aggregation as a common phenomenon for HiPIPs, with possible functional implications. Dunham *et al.* interpreted EPR features observed in concentrated solutions of *C. vinosum* HiPIP as arising from dimerization (*27*), whereas *E. halophila*, *E. vacuolota*, and *R. tenuis* HiPIPs crystallize as dimers (*113*). Although the same general face is involved in this dimerization, it was noted that the orientations of protein units were distinct for each. Nevertheless, it is possible that this hydrophobic face may be involved in physiological interactions with redox partners.

IV. Functional Roles of Residues

The preceding discussion paints a rather confusing picture of the critical factors that control cluster chemistry. Only recently, with the power of site-directed mutagenesis, have some of the functional roles of specific residues that form the cluster binding pocket been resolved. Figures 1 and 3 show that in *C. vinosum* HiPIP the iron–sulfur cluster is enclosed by several hydrophobic aromatic side chains from the C-terminal domain (residues 43–80) and a short portion of the N-terminal domain (residues 17–20) (*110*). This N-terminal sequence adopts an α-helical conformation and accommodates a conserved tyrosine residue that lies in close proximity (3.75 Å) to the reduced cluster (Figs. 3 and 4) (*2*, *113*). The importance of these residues in mediating electron transfer and controlling cluster redox potentials has been a subject of speculation (*2*, *3*, *110*, *126*, *127*), but had not been tested. To address these questions, two groups have synthesized and expressed genes for the high-potential iron proteins from *C. vinosum* and *E. halophila* I behind the T7 *lac* promoter in a pET-21(d)(+) expression vector in *E. coli* (*128*, *129*). Such expression systems yield ~35 mg of HiPIP per liter of cell culture, while mutagenesis and iso-

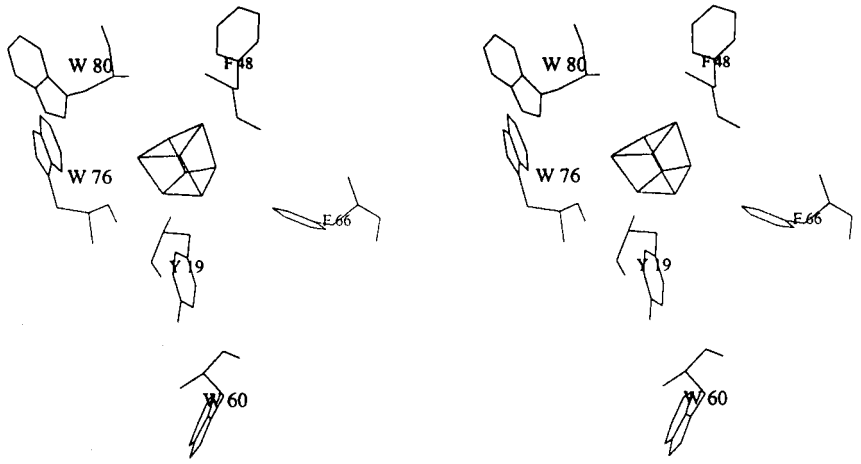

FIG. 3. Stereoview of the aromatic residues forming the hydrophobic pocket for the 4Fe–4S cluster in *Chromatium vinosum* HiPIP.

topic labeling is facile. The availability of recombinant proteins has allowed a critical assessment of the functional role of individual residues in iron–sulfur proteins by use of site-directed mutagenesis (*13*, *130–134*). Furthermore, incorporation of isotopic labels (^{15}N, ^{13}C) and ^{19}F-labeled amino acids allows the use of advanced NMR techniques (*42*, *43*, *48*, *49*, *135–137*) to explore the chemistry of the 4Fe–4S prosthetic site. These studies have contributed to the many recent advances in this area of cluster chemistry, although in some cases the

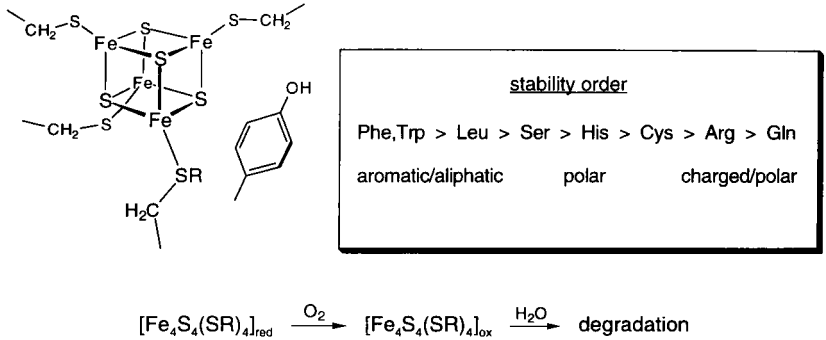

FIG. 4. Stability order for the 4Fe–4S cluster in *Chromatium vinosum* HiPIP following oxidation. A likely mechanism for the oxidative instability of the reduced protein in an aerobic environment is shown.

results have sharply contrasted with prior proposals and expectations. Subsequent discussions herein explore the chemistry of residues in the inner core as they relate to cluster stability, solvent accessibility, and redox chemistry. Unless otherwise stated, residue numbering will correspond to *C. vinosum.*

A. Cluster Stability

1. Tyrosine 19

The N-terminal sequence adopts an α-helical conformation and accommodates a conserved tyrosine residue that lies in close proximity to the reduced cluster (Fig. 3), and has been implicated in defining the cluster potential and electron transfer pathways. In fact, excluding four cysteines, only two residues, Tyr-19 and Gly-75, are structurally conserved over the series *C. vinosum*, *E. vacuolata*, *E. halophila*, and *R. tenuis*. The conserved Gly is possibly to satisfy the steric requirements of the Tyr, which abutts the cluster. To evaluate the functional role of this key residue, a large number of mutants (Tyr-19Ser, Cys, Phe, Trp, Leu, Ile, Ala, Gln, Arg, and His) have been stably expressed in *E. coli* as holoproteins and found to be stable in the reduced form (*131*, *134*), but exhibited varying degrees of oxidative instability in the presence of dioxygen as quantitatively evaluated by direct monitoring of the change in cluster absorbance accompanying degradation (*131*). Minimal changes are observed in E_m for these mutants, and this topic is addressed in more detail in Section IV,C.

a. Oxidative Degradation of Mutants. It has been observed that oxidized native HiPIP is unstable relative to the reduced form (although over a much longer time scale) (*138*). These mutants show the same sensitivity, but in an accelerated time frame. The relative stability of each mutant was found to vary significantly, with the aromatic Phe and Trp mutants being the most stable, and the polar Ser and Arg mutants being the least stable (Fig. 4, Table V). With the exception of the Phe and Trp mutants, oxidation by atmospheric oxygen resulted in rapid decomposition of the iron–sulfur cluster, as evidenced by the decrease in absorbance at 388 nm. Because ferricyanide oxidation also resulted in rapid cluster degradation, the oxidative instability of the cluster appears to originate from the intrinsic oxidation state of the cluster in the modified protein environment, rather than attack by reactive oxygen-derived radicals following cluster oxidation by molecular oxygen. Exclusion of dioxygen was observed to improve the stability of the mutant proteins. The aromatic residue at

TABLE V

DECAY OF FERRICYANIDE-OXIDIZED HiPIPs IN AN ANAEROBIC ENVIRONMENT[a]

Protein	k (min^{-1})[b]	$t_{1/2}$ (min)
Native	—[c]	—
Tyr-19Phe,Trp	—[c]	—
Tyr-19Leu	$2.0 \pm 1.0 \times 10^{-2}$	34
Tyr-19Ser	$3.7 \pm 1.2 \times 10^{-2}$	19
Tyr-19His	$4.4 \pm 0.8 \times 10^{-2}$	16
Tyr-19Cys	$5.1 \pm 1.2 \times 10^{-2}$	14
Tyr-19Arg	$8.8 \pm 2.1 \times 10^{-2}$	8
Tyr-19Gln	$54 \pm 6.3 \times 10^{-2}$	1.3

[a] Data from Ref. *131*.

[b] Measurements made at ambient temperature in 10 m*M* Tris buffer (pH 7.0).

[c] Stable on this time scale.

position 19 is therefore essential for oxidative stability of the 4Fe–4S cluster, with a minimal influence on E_m.

b. Mechanism of Cluster Degradation. Tyr-19 mutant proteins demonstrate, to varying extents, increased solvent access to the cluster pocket. This is quantitated by the determination of rate constants for H_2O/D_2O exchange, measured by NMR experiments, which reflect the ability of water molecules to exchange with backbone amide protons and Trp NHs in the cluster binding pocket. (NMR methods for elucidating solvent accessibility to the cluster are described in Section IV,B.) These observations are consistent with a model in which Tyr-19 plays a critical role in preserving the structural rigidity of the polypeptide backbone through H-bonding from the phenolic OH, which lies 3.0 Å from the amide of Asn-72, and 2.7 Å from a conserved solvent molecule (*114*), to maintain a hydrophobic barrier for exclusion of water from the cluster cavity. It has been proposed that in the absence of the aromatic ring at position 19, solvent accessibility results in facile oxidation of the cluster by dissolved oxygen, with subsequent rapid hydrolysis of the $[Fe_4S_4(SR)_4]^-$ core. Such a decrease in cluster stability in the absence of a polar solvent is consistent with previous studies of model complexes that demonstrate sensitivity of the oxidized $[Fe_4S_4(SR_4]^-$ core to hydrolytic decomposition (*139–143*). The stability of such clusters is significantly improved in solvents of low polarity. Similarly, sterically encumbered, hydrophobic thiolate ligands are found to stabilize the $[Fe_4S_4(SR)_4]^-$ core (*141*, *144*).

The chemistry developed from Tyr-19 mutants is summarized in Fig. 4, and the main conclusions are as follows: (1) Tyr-19 excludes H_2O from the cluster binding pocket; (2) degradation is not mediated by reactive oxygen species; and (3) cluster degradation arises through hydrolysis of the oxidized cluster. The influence of the charged residues or increased solvent access on the E_m of the cluster is discussed in Section IV,C.

c. Calorimetric Investigation of Protein Stability. Similar trends have been observed in the stability of the homologous Tyr-12 mutants of *E. halophila* 1 HiPIP (*134*). For this protein the relative stabilities of native and mutant HiPIPs have been quantitatively evaluated by differential scanning calorimetry. The data was best fit by a three-step model (Scheme 2) that included the reversible endothermic unfolding of the polypeptide (step 1), the exothermic release of the 4Fe–4S cluster (step 2), and an irreversible transition to the final state at high temperatures (step 3).

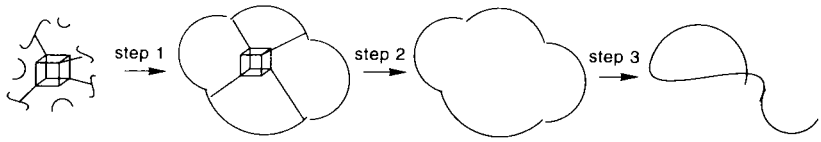

Scheme 2

Assuming that release of the cluster is a constant, and that the exothermic response from each of the mutants and native protein is independent of pH, the apparent destabilization energies ($\Delta\Delta H_D^{app}$) were estimated for the mutants relative to native HiPIP. Table VI summarizes pertinent data. Both changes to the side chain at position 12, and pH variations, result in destabilization of the protein. Because the packing volumes for Tyr and Phe are similar (*145*), the ΔT_m of -12.9°C relative to native at pH 7 reflects the importance of the hydrogen bonds, formed between the hydroxyl of Tyr-12 and both the amide side chain of Asn-14 and the backbone amide of Lys-59, to the overall structural stability of the protein. Because H bonds are estimated to contribute from 0.5 to 1.5 kcal mol^{-1} to protein stability, the $\Delta\Delta G_D^{app}$ of 2.3 kcal mol^{-1} for Tyr-19Phe at pH 7 is consistent with loss of two H bonds. Interestingly, the largest loss in stability was found with the Trp mutants, most likely as a result of the structural perturbations required to accommodate the larger Trp side chain.

It should be noted that the stability trend in Table VI, measured

TABLE VI

DIFFERENTIAL SCANNING CALORIMETRY DATA FOR Tyr-12 MUTANTS OF *Ectothiorhodospira halophila* I HiPIP[a]

Protein	pH	T_m (°C)	$\Delta\Delta H_D^{app}$ (kcal mol^{-1})[b]	$\Delta\Delta G_D^{app}$ (kcal mol^{-1})[b]
Native	7.0	67.7	−21.7	−12.9
	9.0	66.4	−23.0	−12.0
	10.0	66.5	−22.9	−12.3
	10.8	56.7	−33.4	−19.6
	11.0	50.3	−40.3	—
Tyr-12Phe	7.0	54.8	−21.2	—
	9.0	54.4	−20.7	—
	10.0	54.2	−24.2	—
	10.8	37.1	−29.2	—
Tyr-12Trp	7.0	37.4	−23.7	−30.3
Tyr-12His	7.0	42.2	−33.3	−25.5
	9.0	39.0	−53.3	−27.4

[a] Data from Ref. *134*.
[b] 1 kcal ≡ 4.2 kJ.

by relative $\Delta\Delta H_D^{app}$ values, is different from that reported in Fig. 4 for Tyr-19 mutants of HiPIP; however, in each case different properties were being measured, namely, the stability of the tertiary structure in the former and the stability of the cluster in the latter case. This is, at first, surprising because there is a strong structural homology between *C. vinosum* and *E. halophila* HiPIP, and similar stabilities might be expected. The abrupt change in $\Delta\Delta H_D^{app}$ between pH 10 and 11 most likely reflects a change in ionization state of a titratable residue. On the basis of pK_a values, solvent accessibility, and structural contacts with other residues, Lys-59 is a likely candidate because this has a pK_a of 10.4 and forms a salt bridge to Gln-61.

2. *Phenylalanines 48 and 66*

A number of point mutations of the conserved aromatic residues, phenylalanines 48 and 66 (Phe-48His,Arg and Phe-66Tyr,Asn,Cys,-Ser), in *C. vinosum* high-potential iron–sulfur protein have been examined with the aim of understanding the functional role of these residues (*130*, *146*). Both Phe-48 and Phe-66 lie in the cluster binding pocket, and Phe-66 possibly π-complexes with the cluster. Nonconservative replacements with polar residues have a minimal effect on the midpoint potential of the $[Fe_4S_4(SR)_4]^{-/2-}$ cluster, typically less than +25 mV, with a maximum change of +40 mV for Phe-66Asn (dis-

cussed more fully in Section IV,C). With the exception of the Phe-66Tyr mutant, the oxidized state is found to be unstable relative to the recombinant oxidized native protein, with regeneration of the reduced state. A likely pathway for this transformation is summarized in Scheme 3 and appears to involve degradation of the cluster in a fraction of the sample, which provides the reducing equivalents required to bring about reduction of the remainder of the sample. Some experimental observations that support this model include the observation of a transient $[Fe_3S_4(SR)_3]^{2-}$ EPR signal that is generated and then decays (but maximally constitutes only ~13% of the total sample) and the fact that >20% of the sample degrades to apoprotein, depending on the excess concentration of oxidant used.

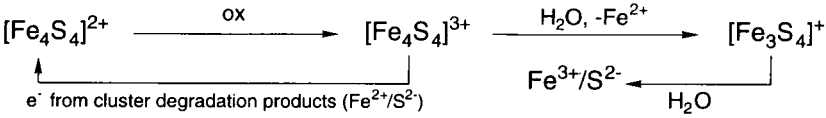

Scheme 3

This degradative reaction appears to proceed through an $[Fe_3S_4(SR)_3]^{2-}$ intermediate that is characterized by a typical EPR signature (Fig. 5) and power saturation behavior (Fig. 6), and is prompted by the increased solvent accessibility of the cluster core in the nonconservative Phe-66 mutants as evidenced by $^1H-^{15}N$ heteronuclear single quantum coherence (HSQC) NMR experiments, to be described in Section IV,B (*130*). These results are consistent with a model where, again, an important role of the aromatic residues (Fig. 3) is to protect the cluster from hydrolytic degradation in the oxidized state. In the case of Tyr-19 mutants, auto-reduction is not usually observed because the mutants are less stable and the cluster rapidly degrades as a result of increased solvent accessibility.

3. *Cysteine 77*

The influence of oxygen ligation on 4Fe–4S cluster properties has been examined in the Cys-77Ser mutant of *C. vinosum* HiPIP (*108*, *147*, *148*). In the reduced state there is evidence for only minor perturbations to the electronic structure of the cluster, as indicated by the similar pattern of NMR chemical shifts relative to native HiPIP. In contrast, there appears to be a stronger electronic interaction between the hard O donor of the Ser ligand and the oxidized cluster; consequently the oxidized Cys-77Ser mutant shows rather dramatic

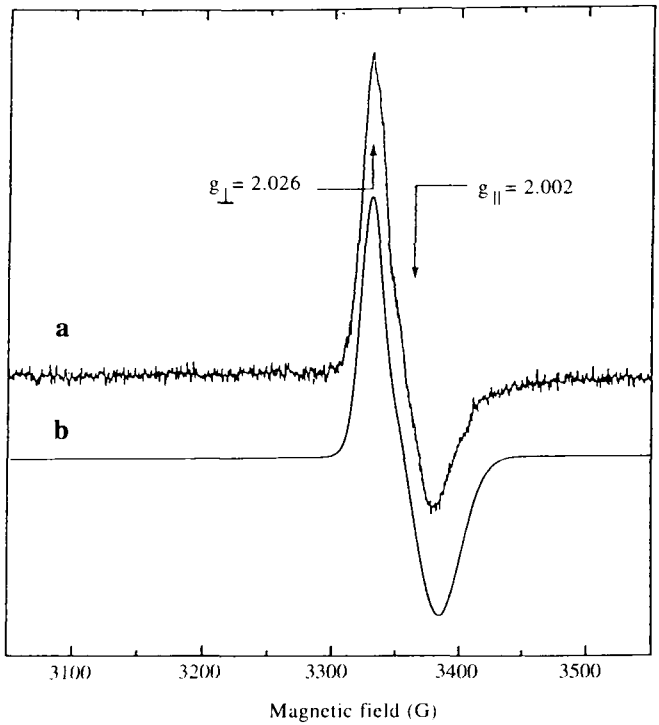

FIG. 5. (a) EPR spectrum of the intermediate formed during oxidative degradation of Phe-66Cys HiPIP. (b) Computer simulation of the spectrum. The EPR spectrum was obtained with a microwave frequency of 9.456 GHz, a modulation frequency of 100 kHz, a modulation amplitude of 1 G, a microwave power of 1.2 mW, and a temperature of 15 K (*130*).

changes in the NMR spectra, which reflect a change in electron localization on the cluster (*147*). In particular, there is a change in the pair of iron centers ascribed to the mixed-valent pair (Fig. 7). Substitution of a sulfur thiolate by an oxygen ligand does not, however, significantly perturb the E_m for the $[Fe_4S_4(SR)_4]^{-/2-}$ couple; the reduction potential of Cys-77Ser decreases by only ~30 mV relative to native protein, consistent with the change from sulfur to oxygen ligation.

Most of the Cys-77Ala,Asp,Tyr mutants tested did not yield stable proteins because the ligands were either electronically or sterically incapable of binding to the vacant coordination site on iron; only the Cys-77Ser mutant resulted in formation of a stable cluster, thus we conclude that the iron center must be ligated to achieve a stable as-

	oxidized native		$[Fe_3S_4]^+$ intermediate	
	g_1	g_4	g_1	g_4
$P_{1/2}$ (mW)	7	20	0.1	0.05

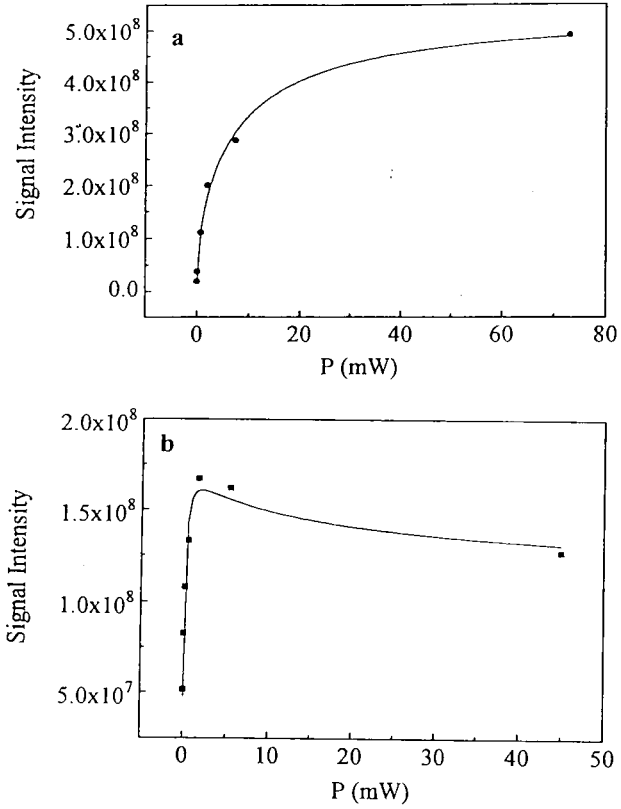

FIG. 6. Power saturation profile of (a) native and (b) $[Fe_3S_4(SR)_3]^{2-}$ intermediate forms (*130*). Saturation powers are summarized at the top of the figure.

sembly. The selection of Cys rather than Ser as a cluster ligand would appear to result more from the intrinsic stability of thiolate coordination, rather than modulation of the reduction potential.

4. Lessons from Model Complexes

The general trend observed following mutation of hydrophobic residues in the cluster pocket is an increase in solvent accessibility, re-

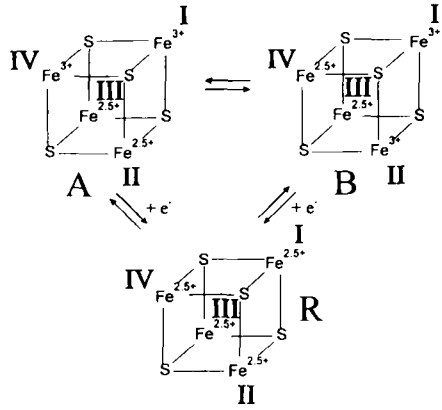

FIG. 7. Change in charge distribution over the $[Fe_4S_4(SR)_4]^-$ cluster following mutation of Cys-77 to Ser (*147*). In the reduced cluster **R**, each iron has a formal +2.5 charge. In the oxidized form the cluster equilibrates between the two states **A** and **B**. Residue 77 coordinates to iron ion IV. State **A** is favored when the harder ligand Ser binds in the Cys-77Ser mutant. (Reprinted with permission from Ref. *147*: Babini, E.; Bertini, I.; Borsari, M.; Capozzi, F.; Dikiy, A.; Eltis, L. D.; Luchinat, C. *J. Am. Chem. Soc.* **1996,** *118,* 75. Copyright 1996 American Chemical Society.)

sulting in facile oxidation of the cluster by atmospheric oxygen and subsequent rapid breakdown of the $[Fe_4S_4(SR)_4]^-$ core by water. Such a decrease in cluster stability in the presence of a polar solvent is consistent with previous studies of model complexes that demonstrate sensitivity of the oxidized $[Fe_4S_4(SR)_4]^-$ core to solvolytic decomposition (*139–143*). Cluster degradation appears to proceed by way of an $[Fe_3S_4(SR)_3]^{2-}$ center, both in the case of proteins and model complexes. There is, in fact, extensive evidence from model studies for oxidative conversion of an $[Fe_4S_4(SR)_4]^-$ core to an $[Fe_3S_4(SR)_3]^{2-}$ center, and subsequent degradation in nucleophilic solvents (*142*). In enzyme systems, oxidative conversion to an $[Fe_3S_4(SR)_3]^{2-}$ center was first reported for mammalian aconitase (*28, 83, 84, 100, 101*).

In the case of aconitase and other proteins carrying a 3Fe–4S cluster, the absence of a Cys ligand is in part responsible for the lability of the fourth iron center. Of relevance here is a modeling study by Tanaka and co-workers (*144*), who have shown that the adamantanethiolate-ligated cluster, $[Fe_4S_4(SAd)_4]^-$, exhibits extreme lability in H_2O/DMF (3 vol%), but found that the presence of free AdSH in H_2O/DMF (23 vol%) significantly enhanced its stability. The authors proposed that the hydrolysis of $[Fe_4S_4(SAd)_4]^-$ results from dissociation of the terminal ligand, followed by coordination of H_2O to the cluster core; suggesting that the oxidation state of the synthetic 4Fe–4S clus-

ter can be stabilized by inhibiting dissociation of the terminal thiolate ligands from the cluster core. Strong association of the bound Cys is undoubtedly a requirement for the stability of solvent-exposed clusters.

B. Solvent Accessibility

Solvent accessibility of native and mutant HiPIPs has been determined by multinuclear NMR methods, in particular, by use of the $^1H/^2H$ exchange rates of backbone amide protons, evaluated by $^1H-^{15}N$ HSQC experiments, and from the isotopic perturbation of ^{19}F chemical shifts of labeled native and mutant HiPIPs (*43*, *149*).

1. $^1H-^{15}N$ HSQC to Probe Backbone Amide Proton Exchange and Solvent Accessibility

Because $^1H-^{15}N$ coupling is over one bond, the intensity of cross-peaks in a $^1H-^{15}N$ HSQC experiment does not depend on backbone conformation. This contrasts with the intensity of cross-peaks (and the magnitude of coupling constants) in the fingerprint region of a homonuclear $^1H,^1H$ correlated spectroscopy (COSY) experiment, which results from a three-bond (H–N–C^α–H), or higher (in the case of a total correlated spectroscopy (TOCSY) experiment), correlation that will vary with a change of backbone dihedral angles (*150*). The rate of change of the intensities of $^1H-^{15}N$ cross-peaks for a lyophilized sample dissolved in D_2O provides a direct measure of the accessibility of solvent to the backbone amides (*149*, *150*), and permits an evaluation of $^1H/^2H$ exchange rate constants. Such experiments are illustrated in Fig. 8 and the resulting data may be presented in a color-coded representation of the exchange regimes, as described in Ref. *149*. Experiments such as these clearly demonstrate that there is no significant difference in the $^1H/^2H$ exchange regimes observed for the reduced relative to the oxidized form of recombinant native HiPIP, and that the four cluster-binding cysteines and their neighboring residues lie in the very slow exchange region. However, the backbone amides of Tyr-19 and neighboring residues are found to lie in the slow exchange regime in the native protein, but switch to the moderate or very fast exchange regimes in the Tyr-19Leu and Tyr-19His mutant HiPIPs. This trend is consistent with the stability order indicated in Fig. 4.

2. ^{19}F NMR Parameters as a Probe of Solvent Accessibility

Because fluorine-19 NMR resonances exhibit a strong environmental dependence, they provide a probe of redox-dependent conforma-

tional change in electron transfer proteins, and structural characterization of mutants, whereas evaluation of H_2O/D_2O solvent isotope effects on ^{19}F chemical shifts reflects solvent accessibility to various protein domains. These experiments provide a useful complement to the ^1H–^2H exchange experiments described above (*151*, *152*). Both the chemical shift and the T_1 relaxation time are sensitive to interaction with the solvent. When ^{19}F is solvent exposed the T_1 relaxation times become longer and the ^{19}F resonance frequency shows an isotopic shift when the aqueous solvent is changed from H_2O to D_2O (*153*, *154*). This solvent shift should be greater than 0.1 ppm to be of significance. In general, T_1 measurements are less reliable than the isotopic effect as a probe of solvent accessibility for proteins that contain paramagnetic cofactors, because the paramagnetic relaxation mechanism may also reduce the relaxation time.

Fluorine-labeled analogues of *C. vinosum* high-potential iron protein have been investigated by ^{19}F NMR spectroscopy. By incorporation of specific fluorine-labeled amino acid residues, one can insert unique probes at well-defined locations within the protein core. The synthesis and purification of 2-, 3-, and 4-fluorophenylalanine (abbreviated 2-F-, 3-F-, and 4-F-Phe, respectively), 3-fluorotyrosine (3-F-Tyr), and 5-fluorotryptophan (5-F-Trp) derivatives of *C. vinosum* HiPIP, the assignment of ^{19}F NMR resonances, the measurement of longitudinal relaxation times, and the temperature dependence of ^{19}F and ^1H resonances have all been reported (*42*, *43*, *136*). These measurements were used to examine structural perturbations of mutants, the dynamics of interaction of residues with the cluster, and solvent accessibility, and as a test of the relative contribution of cross-relaxation to magnetization decay.

C. Overview of Factors Influencing Redox Properties

1. Key Parameters

Many factors have been proposed to influence cluster redox potentials and electron transfer pathways, including solvent exposure, hydrophobic effects, hydrogen bonding, electric fields from backbone amide dipoles, neighboring charges, and bonding contacts mediated by π complexation. The ability of nature to tune the redox chemistry of biological redox cofactors is indeed well illustrated by the 4Fe–4S-cluster proteins (−650 to +450 mV) and *c*-type cytochromes (−400 to +400 mV), and has been the subject of recent reports (*155*, *156*). Even within the HiPIP family the redox potentials are tuned over a large range, from +50 to +450 mV (Table II).

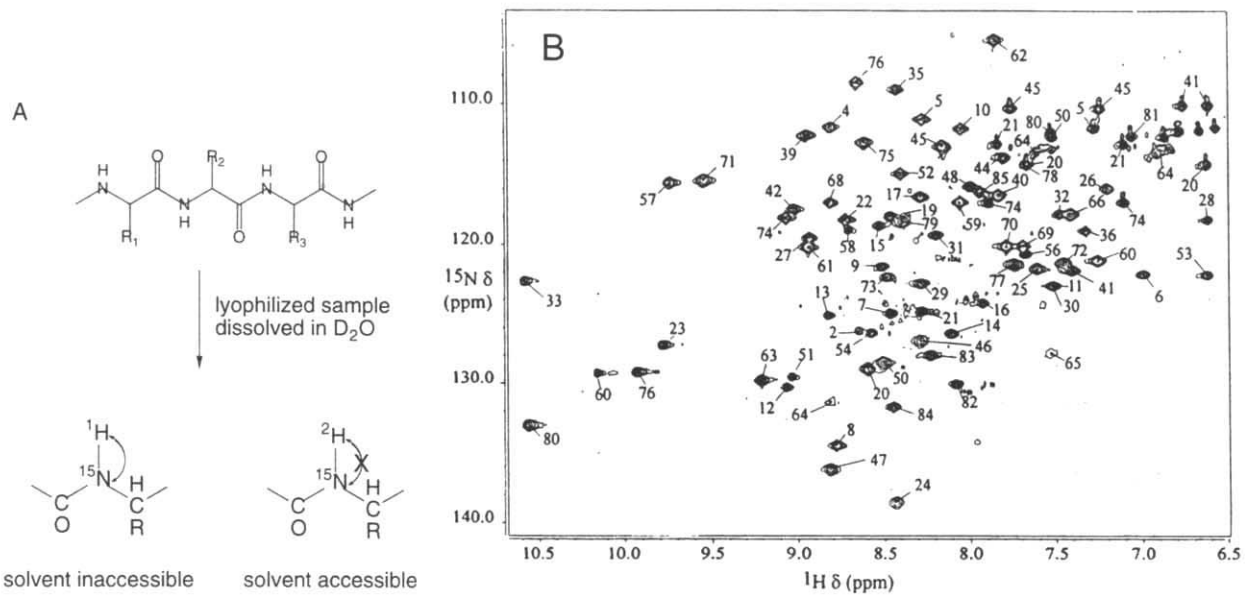

FIG. 8. Deuterium exchange of backbone amides (A) results in loss of the cross-peak intensity in $^{1}H-^{15}N$ HSQC spectra (B) and provides a probe of solvent accessibility (*149*). (C) Time course of $^{1}H-^{15}N$ HSQC spectra obtained after dissolving a lyophilized sample of *C. vinosum* HiPIP in D_2O (*149*). The time (in minutes) for each spectrum is indicated in the corner of each plot. Cross-peaks disappear more rapidly for the Tyr-19Leu mutant relative to reduced native HiPIP.

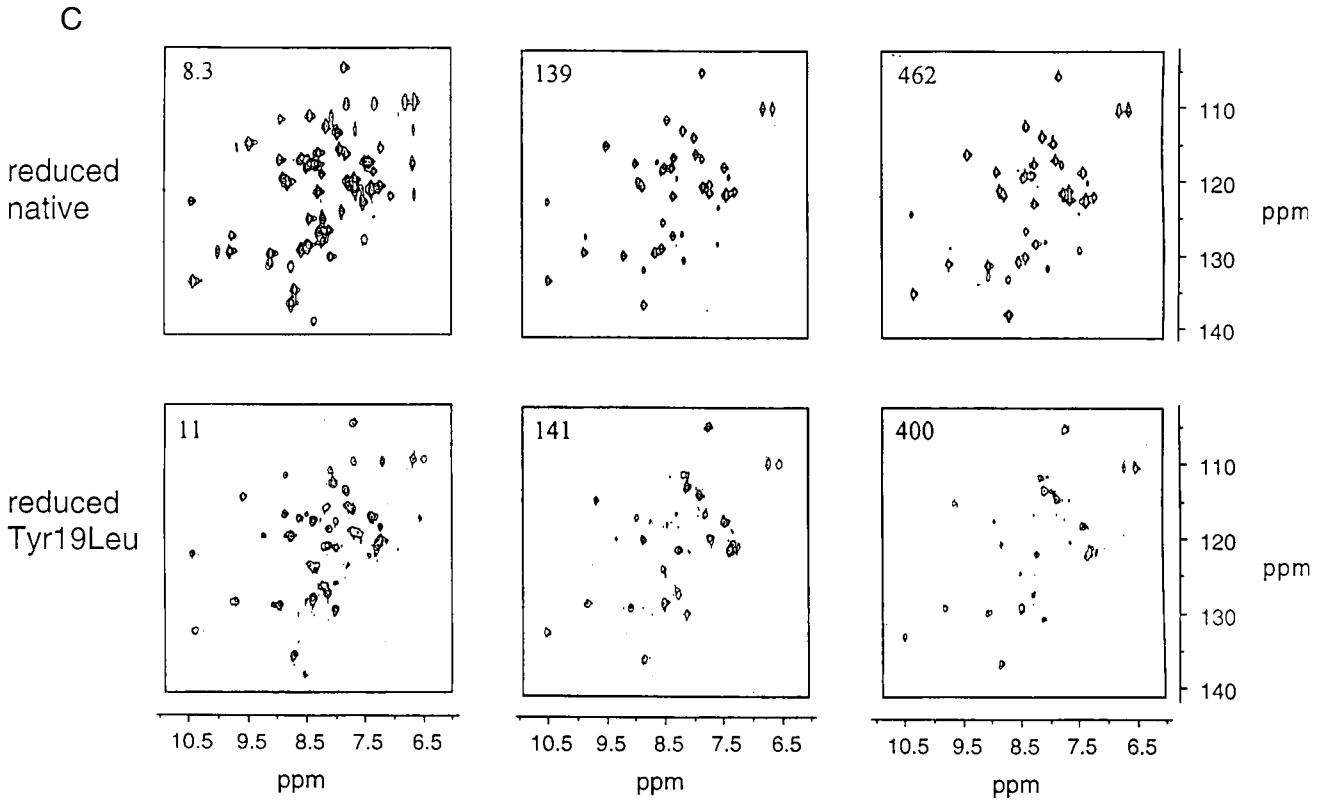

FIG. 8. *Continued*

In this section our attention is focused on the question of what factors control the relative stabilities of the $[Fe_4S_4(SR)_4]^{-/2-/3-}$ cluster states, that is, the factors underlying the three-state hypothesis of Carter (*1*), depicted earlier in Scheme 1. The cluster oxidation levels used are −1, −2, and −3; each differs by one electron and represents the net charge of the cluster, including the cysteinyl sulfur charge contributions. In terms of formal iron valences only, the −1, −2, and −3 states correspond to $[Fe_3^{3+}Fe^{2+}]$, $[Fe_2^{3+}Fe_2^{2+}]$, and $[Fe^{3+}Fe_3^{2+}]$, respectively (*61*). However, Mössbauer and NMR experiments show that the oxidized HiPIP from *E. halophila* has two iron(III) ions and one mixed-valence pair (*61*, *63*, *64*, *66*, *157*). On the basis of Mössbauer spectroscopy of *C. vinosum* (*63*, *66*, *67*) and *E. halophila* (iso II) HiPIPs (*62*), the presence of an iron(III) pair and a mixed-valence pair in the cluster is increasingly seen as a general feature of all oxidized HiPIPs, although it is unknown whether this electronic distribution is relevant for the function of the proteins. After reduction, the ferric center is localized at one site.

HiPIP can be reduced to the normally unobtainable $[Fe_4S_4(SR)_4]^{3-}$ oxidation level (superreduction), either by pulse radiolysis (*97*) or by dithionite after partial unfolding in 80% Me_2SO (*158*). The structural features of the protein that underlie the thermodynamic barrier for superreduction of native HiPIP remain uncertain. Nevertheless, it has been suggested that exposure of the cluster to solvent may stabilize the reduced $[Fe_4S_4(SR)_4]^{3-}$ state. Similarly, Kamen and co-workers (*159*) reported the amino acid sequence of a HiPIP with the highest known redox potential (+450 mV) from *Rhodopila globiformis.* Based on sequence alignment with other known HiPIPs, they suggested that the very positive potential might be attributed to a more hydrophobic environment for the 4Fe–4S cluster in this protein (*159*).

2. *Electrostatic Influence*

Bertini and co-workers (*160*) have tried to rationalize the reduction potentials within the series of HiPIPs by quantitatively assessing the electrostatic contributions from surface-charged residues, dipolar contributions from polar residues, and solvent dipoles and polarizabilities, to the energy of the cluster. A correlation with reduction potential was found only for the net charge of the protein in the absence of other factors; however, this work does not explain the significant change in E_m when comparing high- and low-potential Fds.

Backes *et al.* (*20*) and Krishnamoorthi *et al.* (*44*) suggested that the polarity of cluster environment and ability to delocalize electrons by the amino acid residues around the cluster also contribute to the posi-

tive potentials of HiPIPs. The influence of surface charges on redox potentials of HiPIPs from *R. globiformis*, *C. vinosum*, *R. gelatinosus*, *E. vacuolata* (I and II), and *E. halophila* (I and II) has been evaluated by Luchinat *et al.* using differential pulse voltammetry (*161*). The authors proposed that the peptide charge, ranging from −13 to +5, controls the redox potentials (*161*), whereas a decrease in reduction potential with pH was observed in the pH range where deprotonation of the imidazolium nitrogen of histidine residues occurs. It was suggested that surface charges may be capable of influencing the cluster potential in spite of the known quenching of electrostatic interaction by solvents.

Heering *et al.* (*162*) have used direct electrochemical measurements to study HiPIPs from various sources (*E. vacuolata* I and II, *C. vinosum*, *R. gelatinosus*, *R. tenuis*, *R. globiformis*, and *R. salinarum*). In contrast to Luchinat *et al.* (*161*), these researchers found no significant pH dependence of E_m for most HiPIPs, with the exception of *C. vinosum* and *R. gelatinosus* HiPIPs (maximum slopes of −20 mV/pH unit). These researchers also divided the HiPIPs into two groups based on sequence alignment, optical spectra, overall charges, and the redox thermodynamics. First, *Chromatium*-like HiPIPs with redox potentials between 300 and 350 mV were proposed to be dominated by solvent effects; however, this is not substantiated by studies of mutant HiPIPs (*155*). Second, *Ectothiorhodospira*-like HiPIPs with potentials between 50 and 450 mV were proposed to depend on both the overall charge of the peptide and solvation; however, the evidence for this generalization is weak.

Clearly there has been substantial confusion on this issue, with many hypotheses concerning the factors that control cluster redox properties (*113*, *160*, *163*, *164*). It is only since the availability of expression systems, which allow analysis by site-directed mutagenesis, that these ideas have been open to experimental testing. In particular, the roles of key aromatic core residues in regulating the reduction potential, the enthalpy and entropy of reduction for the prosthetic $[Fe_4S_4(SR)_4]^{-/2-}$ cluster, and the self-exchange rate constants for electron transfer reactions of *C. vinosum* high-potential iron protein (HiPIP) have been directly addressed by a combination of site-directed mutagenesis, high-field NMR (EXSY) experiments, and variable-temperature spectrochemical redox titration measurements (*155*). The results of mutagenesis experiments have thus far emphasized that most of the factors previously speculated to control cluster chemistry actually play a negligible role in defining the reduction potential of the 4Fe–4S center (*134*, *155*). Surface charge may play a

minor role in defining the midpoint potential (E_m) (*161*); however, the ability to delocalize charge over amino acid residues, and the polarity of the cluster environment, appear to be of lesser importance (*113*, *155*). These issues are of general relevance for understanding the mechanisms employed by proteins for modulating the chemistry of protein-bound redox cofactors.

3. *Comparison of Thermodynamic Parameters*

Because the enthalpies and entropies of metalloprotein electron transfer processes are influenced by changes in protein conformation and solvation, as well as by other structural and medium effects (*5*, *165*, *166*), comparison of these parameters over a range of HiPIPs differing by single-point mutations affords considerable insight into the factors underlying cluster redox chemistry.

Few reports of the temperature dependence of 4Fe–4S cluster potentials have appeared in the literature. With the exception of a small number of *c*-type cytochromes, the enthalpic component is typically found to be negative for the available data on heme proteins and 4Fe–4S proteins, reflecting favorable bonding changes on reduction. For HiPIPs, the ΔH values typically lie within 4 to 5 kcal mol^{-1} of each other (Table VII), which is consistent with their similar E_m values and the importance of the enthalpy term in defining the free en-

TABLE VII

SUMMARY OF 4Fe–4S CLUSTER REDOX PARAMETERS FOR SELECTED MUTANT *Chromatium vinosum* HiPIPs[a]

Protein	E_m (mV)	ΔH (kcal mol^{-1})	ΔS (cal K^{-1} mol^{-1})	k_{ex} ($\times 10^{-3}$ M^{-1} sec^{-1})
Native	345	−32.2	−81.4	14.5
Cys-77Ser	315	−19.4	−40.7	—
Tyr-19Trp	372	−30.4	−73.2	—
Tyr-19Leu	370	−25.0	−55.4	24.5
Tyr-19His	348	−26.4	−61.8	—
Phe-66Tyr	356	−25.0	−56.2	—
Phe-66Cys	361	−27.1	−63.1	—
Phe-66Ser	368	−25.4	−56.6	13.3
Phe-66Asn	392	−25.1	−54.0	—
Phe-48His	360	−25.3	−57.1	10.0
Phe-48Arg	368	−26.0	−59.3	5.0

[a] Data from Ref. *155*. All measurements are at 25°C; standard deviations are as follows: $E_m \pm 7$ mV; $\Delta H \pm 2$ kcal mol^{-1}; $\Delta S \pm 5$ cal K^{-1} mol^{-1}. Errors in these measured rate constants (k_{ex}) are on the order of ±20%.

ergy for reduction. The enthalpy changes are usually more negative for the $[Fe_4S_4(SR)_4]^{-/2-}$ couple than for the $Fe^{3+/2+}$ heme couple in cytochromes (*156*), presumably as a result of favorable interactions between the cluster and the polypeptide, including coordination from four cysteine residues and favorable interactions with aromatic rings.

As an exception to the above-noted trend, the reduction enthalpies and entropies for Cys-77Ser differ markedly from native (Table VII), although the ΔG values are similar. Such an isoequilibrium relationship implies that the mutant differs from the native only with regard to the electronic properties of the cluster, with no significant structural perturbation of the surrounding peptide.

Native HiPIP shows the most negative enthalpy and entropy change. Mutants that result in either increased solvent access to the cluster, or a change from sulfur to oxygen donor ligands (such as Cys-77Ser), show enthalpy and entropy changes that are less negative relative to recombinant native HiPIP (Table VII) (*155*). These proteins do not show a substantive change in E_m because the favorable entropy change is offset by a less favorable change in the reaction enthalpy. This is analogous to the situation observed for cytochromes with positive E_m values as described by Bertrand *et al.* (*156*).

Asso *et al.* (*23*) have reported on the redox characteristics of ferredoxins I and II from *Desulfovibrio vulgaris* Miyazaki. For the $[Fe_4S_4(SR)_4]^{2-/3-}$ couple in Fd II, $\Delta H = +2.3$ kcal mol^{-1} (+9.65 kJ mol^{-1}) and $\Delta S = -24.6$ cal K^{-1} mol^{-1} (-103 J K^{-1} mol^{-1}), which demonstrates that the 760-mV difference in potential for these two clusters arises from enthalpic effects. Low-potential clusters in Fds tend to lie closer to the protein surface and are more solvent exposed; however, the available results on HiPIP mutants suggest that the difference in ΔH terms observed for the Fd may not arise from either solvent exposure or a local variation in side chain identity. However, the role of solvent may be different for HiPIPs and Fds, which employ different redox couples.

4. *Influence of Solvent on E_m*

The influence of varying solvent dielectric on the reduction potentials has been examined by Blonk *et al.* (*143*) for the cluster series $[Fe_4S_4(SR)_4]$. When R = Ph a minimal variation in E_m was observed for both the high- and low-potential couples. For example, in nitrobenzene ($\varepsilon = 35.7$) $E_m = -0.33$ V, but in dichloromethane ($\varepsilon = 9.1$) $E_m = -0.32$ V for the high-potential couple. Also, when R = ^{t}Bu, $E_m = -0.65$ V in dichloromethane and -0.70 V in *N*,*N*-dimethylformamide ($\varepsilon = 37.6$). Similar minimal variations in E_m values were observed for

the low-potential redox couple. This is consistent with the observations made for the mutant HiPIPs, and seems to indicate that the lack of sensitivity of the 4Fe–4S cluster potentials to solvent is an effect that is neither limited to, nor a result of, the presence of a protein matrix.

Heering *et al.* (*162*) have argued that HiPIPs may be considered to fall into two classes, one with an E_m that is independent of the total charge and centered around 336 mV, and one with an E_m that is dependent on the total charge. After subtraction of the contribution from the overall charge it was proposed that the remaining part of the potential reflected variations of polarity and solvation in the local cluster environment. However, the results of studies on mutant proteins indicate no clear role for changes in the polarity of residues neighboring the cluster, and provide a clear indication that solvation is not a critical factor for HiPIPs. The results of mutational studies do not support any significant role in the definition of cluster potential (*147*, *148*, *155*). Rather, these residues appear to inhibit solvent access to the cluster pocket that can result in hydrolytic degradation of the $[Fe_4S_4(SR)_4]^-$ center.

5. *Self-Exchange Rates for Native and Mutant HiPIP*

The electron self-exchange transfer rate constants for native and mutant HiPIPs have been estimated using ^1H 2D EXSY methods (Fig. 9) (*155*). Although the net charge of the peptide chain is -3 at pH 7.0 (*126*, *167*), it has been previously noted that the redox kinetics of *C. vinosum* HiPIP do not depend on the ionic strength of the solvent, most likely reflecting the self-aggregation of HiPIPs through a hydrophobic face, in a manner consistent with other crystallographically defined HiPIP dimers (*113*). However, an increase in self-exchange rate constants with decreasing pH has previously been observed for *C. vinosum* HiPIP (*126*), and so it is likely that neutralization of charged residues at the binding interface is required for electrostatic stabilization.

Aromatic side chains surrounding the cluster have long been believed to mediate electron transfer reactions, both self-exchange reactions and electron transfer with other redox partners. On the basis of crystallographic results, Carter *et al.* (*1*) have suggested that Tyr-19 is a critical residue for mediating electron transfer, whereas Bertini *et al.* (*73*) have proposed Phe-48 as a mediator of electron transfer in the self-exchange reaction of the HiPIP from *E. vacuolata.* In early studies of oxidation–reduction chemistry of HiPIP with nonphysiological reactants, Mizrahi and co-workers (*126*) proposed several charge-

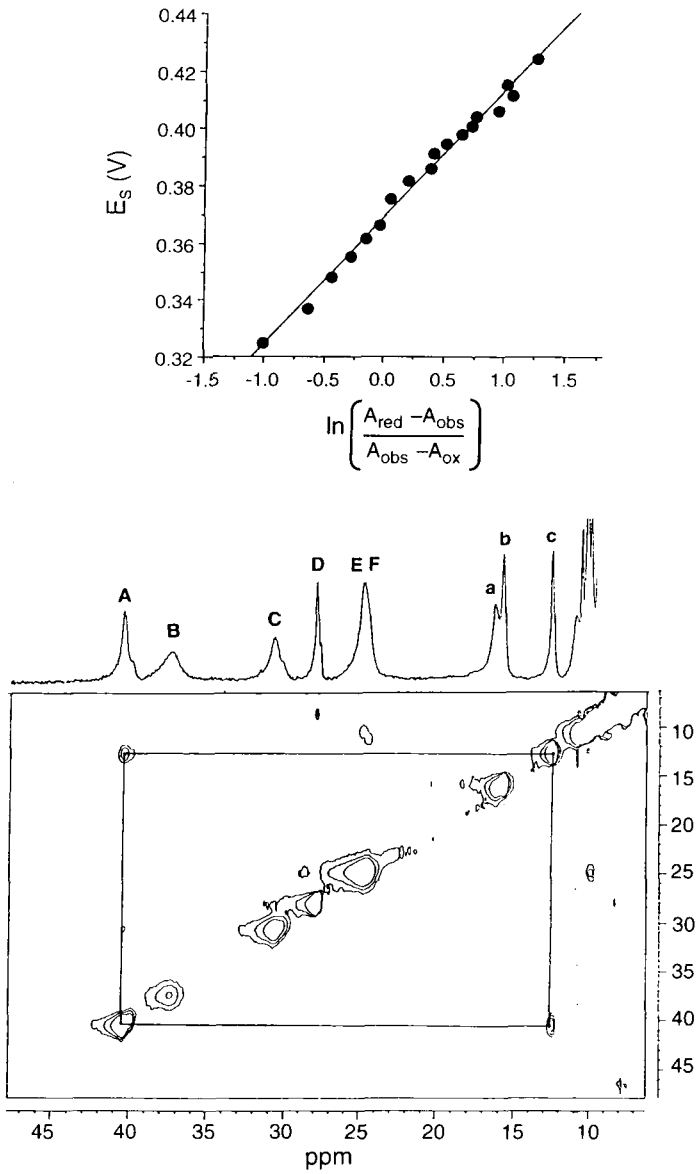

FIG. 9. (Top) Evaluation of midpoint potentials by spectrochemical titration experiments. E_S is the solution potential and the A values refer to the absorbances of the species. (Bottom) EXSY spectrum to evaluate electron-exchange rates. Uppercase letters denote resonances for the oxidized HiPIP, and lowercase letters indicate the reduced protein. Cross-peaks derive from the exchange of magnetization between the same proton as it switches between the oxidized and reduced protein states.

relay pathways involving Phe-48, Phe-66, and Trp-76 residues. In fact, all of these aromatic residues are widely conserved in the HiPIP family (Table VIII). However, experimental results demonstrate that, relative to native HiPIP, the exchange rates for the mutant proteins differ by no more than a factor of two. These observations are consistent with the pathway approach of Beratan *et al.* that tends to emphasize σ-bonding pathways in mediating electron transfer through a protein framework (*168*). A critical appraisal of the available experimental data, particularly for mutant proteins, suggests that the role of aromatic core residues is to prevent solvent access that might compromise the stability of the oxidized cluster, rather than to mediate cluster redox potentials or electron transfer (*119*).

The conclusion from these studies is that neither specific aromatic amino acid side chains nor solvent accessibility appear to play a major role in defining the reduction potentials or electron transfer properties of the cluster in high-potential iron proteins. The role of the aromatic core is to maintain a hydrophobic barrier to solvent water and inhibit oxidation and hydrolytic degradation of the cluster.

6. *Dipole Contributions to E_m*

Warshel and collaborators (*4*, *169*) have investigated the control mechanism for the redox potential of an Fe–S cluster by its protein

TABLE VIII

CONSERVED RESIDUES AROUND THE 4Fe–4S CORE IN SEVERAL HiPIPs

HiPIP[a]	17	19	48	49	60	65	66	68	71	75	76	80
Chromatium vinosum	Leu	Tyr	Phe	Met	Trp	Leu	Phe	Gly	Ile	Gly	Trp	Trp
Thiocapsa pfennigii	Leu	Tyr	Phe	Ile	Trp	Leu	Tyr	Gly	Val	Gly	Trp	Trp
Rhodocyclus gelatinosus	Leu	Tyr	Leu	Phe	—	Leu	Phe	Gly	Val	Gly	Trp	Trp
Rhodocyclus tenuis	Phe	Tyr	Gln	Phe	Ala	Val	Ile	Gly	Ile	Gly	Tyr	Phe
Ectothiorhodospira halophila I	His	Tyr	Phe	Trp	Trp	Val	His	Asp	Val	Gly	Trp	Tyr
Ectothiorhodospira halophila II	His	Tyr	Phe	Trp	Trp	Val	His	Asp	Val	Gly	Trp	Tyr
Ectothiorhodospira vacuolata I	Leu	Tyr	Leu	Trp	Trp	Val	Phe	Asn	Val	Gly	Trp	Tyr
Ectothiorhodospira vacuolata II	Leu	Tyr	Leu	Trp	Trp	Val	Phe	Gly	Val	Gly	Trp	Trp

[a] Numbering refers to *C. vinosum*.

environment, by examining the variation in the midpoint potential of the 4Fe–4S clusters of several structurally well-characterized proteins, *Azotobacter vinelandii* ferredoxin (AvFd I), *Peptococcus aerogenes* ferredoxin (PaFd), *Bacillus thermoproteolyticus* ferredoxin (BtFd), and *C. vinosum* HiPIP (CvHiPIP). By using the "protein dipoles Langevin dipoles" (PDLD) approach (*170, 171*), these researchers were able to model the protein control of the 4Fe–4S cluster redox potentials (Figs. 10 and 11). This microscopic electrostatic model includes both protein and solvent water. Langen *et al.* (*4*) have reported that the total differential solvation energies are substantially reduced in BtFd, PaFd, and AvFd I; in contrast, in *C. vinosum* HiPIP very little change occurs. These calculations demonstrated a critical role for the orientation of amide groups in the neighborhood of a cluster in tuning its reduction potential. These amides are not necessarily those involved in H-bonding to the cluster. The large differences between the potentials of the 4Fe–4S clusters of PaFd, AvFd I, and CvHiPIP were modeled and attributed principally to the different con-

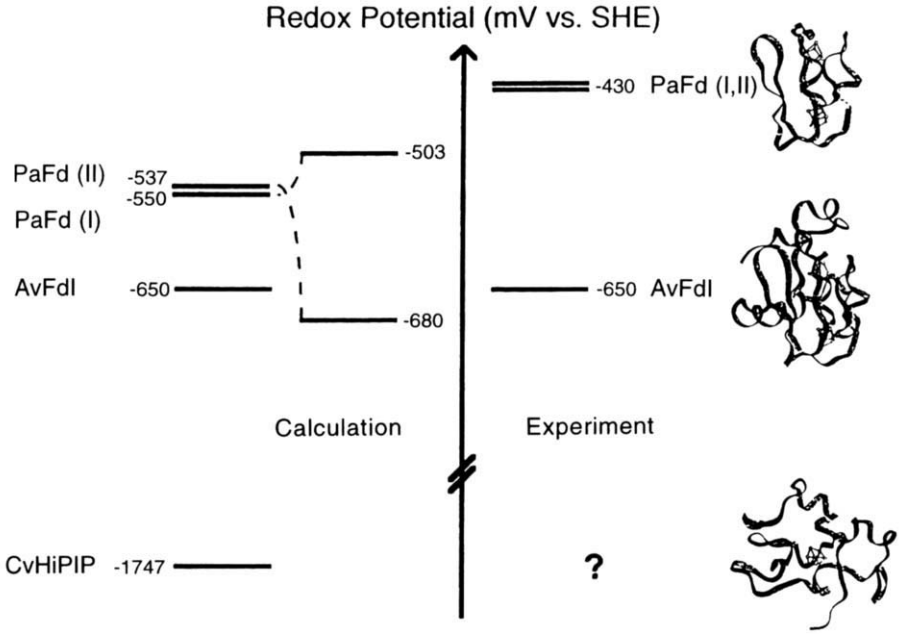

FIG. 10. Theoretical calculation of E_m for the $[Fe_4S_4(SR)_4]^{2-/3-}$ redox couple in representative high- and low-potential ferredoxins. (Reprinted with permission from Ref. *169.* Jensen, G. M.; Warshel, A.; Stephens, P. J. *Biochemistry* **1994,** *33,* 10911. Copyright 1994 American Chemical Society.)

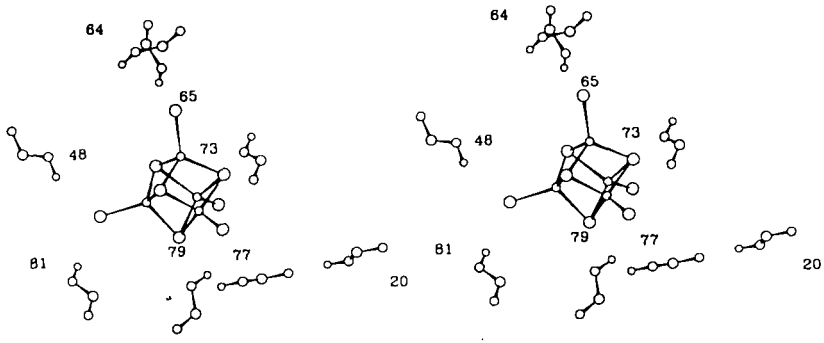

FIG. 11. Stereoview showing the orientations of amide dipoles around the cluster in *Chromatium vinosum* HiPIP. (Reproduced with permission from Ref. *169*: Jensen, G. M.; Warshel, A.; Stephens, P. J. *Biochemistry* **1994,** *33,* 10911. Copyright 1994 American Chemical Society.)

figurations of main-chain amide groups near the clusters. Also, for the two Fds, the water contribution to the redox potentials of AvFd I and PaFd, which show strong structural homology, the solvent plays an important role in establishing the trend in redox potentials. In fact, these two proteins appear to have significantly different extents of water penetration to the cluster, and solvent dipoles close to the cluster in PaFd are an important contribution to its higher potential.

In general, the differences in the oxidation levels used by the HiPIPs, in contrast to the low-potential ferredoxins, are thought to be principally due to differences in local amide dipoles, the more hydrophobic environment of the 4Fe–4S cluster, and fewer hydrogen bonds (*20*).

V. Final Comments and Perspectives

It is clear that there have been many recent and significant advances in the understanding of iron–sulfur cluster biochemistry, and HiPIPs in particular. Many issues relating to function and the role of residues in defining E_m and k_{ex} have been resolved. It seems likely that future research on these proteins will focus on the still unresolved issues of cluster assembly *in vivo*, and the chemistry of nontraditional iron–sulfur proteins such as those described in Table I. In particular, the issue of how a protein environment defines the chemical role of the cluster will become increasingly clear as a result of the growing number of recombinant proteins that are accessible to analysis following site-directed mutagenesis.

References

1. Carter, C. W. *in* "Iron-Sulfur Proteins"; Lovenberg, W., Ed.; Academic Press: NY, 1977; Vol. 3, pp. 157–204.
2. Przysieck, C. T.; Meyer, T. E.; Cusanovich, M. A. *Biochemistry* **1985,** *24,* 2524.
3. Packer, E. L.; Sternlicht, H.; Rabinowitz, J. C. *Proc. Natl. Acad. Sci. U.S.A.* **1972,** *69,* 3278.
4. Langen, R.; Jensen, G. M.; Jacob, U.; Stephens, P. J.; Warshel, A. *J. Biol. Chem.* **1992,** *267,* 25625.
5. Taniguchi, V. T.; Sailasuta-Scott, N.; Anson, F. C.; Grey, H. B. *Pure Appl. Chem.* **1980,** *52,* 2275.
6. Adzamli, I. K.; Davies, D. M.; Stanley, C. S.; Sykes, A. G. *J. Am. Chem. Soc.* **1981,** *103,* 5543.
7. Cusanovich, M. A. *Int. Symp. Interact. Iron Proteins Oxygen Electron Transp.* **1982,** 365.
8. Orme-Johnson, N. R.; Mims, W. B.; Orme-Johnson, W. H.; Bartsch, R. G.; Cusanovich, M. A.; Peisach, J. *Biochim. Biophys. Acta* **1983,** *748,* 68.
9. Augustin, M. A.; Chapman, S. K.; Davies, D. M.; Watson, A. D.; Sykes, A. G. *J. Inorg. Chem.* **1984,** *20,* 281.
10. Przysiecki, C. T.; Meyer, T. E.; Cusanovich, M. A. *Biochemistry* **1985,** *24,* 2542.
11. Bhattacharyya, A. K.; Meyer, T. E.; Cusanovich, M. A.; Tollin, G. *Biochemistry* **1987,** *26,* 758.
12. Ueyama, N.; Terakawa, T.; Sugawara, T.; Fuji, M.; Nakamura, A. *Chem. Lett.* **1984,** *8,* 1287.
13. Iismaa, S.E.; Vazquez, A. E.; Jensen, G. M.; Stephens, P. J.; Butt, J. N.; Armstrong, F. A.; Burgess, B. K. *J. Biol. Chem.* **1991,** *266,* 21563.
14. Ueyama, N.; Terakawa, T.; Nakata, N.; Nakamura, A. *J. Am. Chem. Soc.* **1983,** *105,* 7098.
15. Hartshorn, R. T.; Lim, M. C.; Sykes, A. G. *Inorg. Chem.* **1988,** *27,* 4603.
16. Ohno, R.; Ueyama, N.; Nakamura, A. *Inorg. Chim. Acta* **1990,** *169,* 253.
17. Meyer, T. E. F. J.; Bartsch, R. G.; Tollin, D.; Cusanovich, M. A. *Biochim. Biophys. Acta* **1990,** *1017,* 118.
18. Kuznetsov, B. A.; Shumakovich, G. P.; Mutuskin, A. A.; Mazhorova, L. E. *Dokl. Akad. Nauk SSSR* **1990,** *312,* 1244.
19. Jackman, M. P.; Lim, M. C.; Sykes, A. G.; Salmon, G. A. *J. Chem. Soc., Dalton Trans* **1988,** *11,* 2843.
20. Backes, G.; Mino, Y.; Loehr, T. M.; Meyer, T. E.; Cusanovich, M. A.; Sweeney, W. V.; Adman, E. T.; Sanders-Loehr, J. *J. Am. Chem. Soc.* **1991,** *113,* 2055.
21. Hochkoeppler, A.; Zannoni, D.; Ciurli, S.; Meyer, T. E.; Cusanovich, M. A.; Tollin, G. *Proc. Natl. Acad. Sci. U.S.A.* **1996,** *93,* 6998.
22. Loehr, T. M. *J. Raman Spectrosc.* **1992,** *23,* 531.
23. Asso, M.; Mbarki, O.; Guigliarelli, B.; Yagi, T.; Bertrand, B. *Biochem. Biophys. Res. Commun.* **1995,** *211,* 198.
24. Banci, L.; Bertini, I.; Ferretti, S.; Luchinat, C.; Piccioli, M. *J. Mol. Struct.* **1993,** *292,* 207.
25. Bertini, I.; Ciurli, S.; Dikiy, A.; Luchinat, C. *J. Am. Chem. Soc.* **1993,** *115,* 12020.
26. Cavazza, C.; Guigliarelli, B.; Bertrand, P.; Bruschi, M. *FEMS Microbiol. Lett.* **1995,** *130,* 193.
27. Dunham, W. R.; Hagen, W. R.; Fee, J. A.; Sands, R. H.; Dunbar, J. B.; Humblet, C. *Biochim. Biophys. Acta* **1991,** *1079,* 253.
28. Emptage, M. H.; Kent, T. A.; Kennedy, M. C.; Beinert, H.; Munck, E. *Proc. Natl. Acad. Sci. U.S.A.* **1988,** *80,* 4674.

29. Gayda, J. P.; Bertrand, P.; More, C.; Le Gall, J.; Cammack, R. C. *Biochem. Biophys. Res. Commun.* **1981,** *99,* 1265.
30. Gloux, J.; Gloux, P.; Lamotte, B.; Mouesca, J.-M.; Rius, G. *J. Am. Chem. Soc.* **1994,** *116,* 1953.
31. Heering, H. A.; Bulsink, Y. B. M.; Hagen, W. R.; Meyer, T. E. *Eur. J. Biochem.* **1995,** *232,* 811.
32. Hu, Z.; Jollie, D.; Burgess, B. K.; Stephens, P. J.; Munck, E. *Biochemistry* **1994,** *33,* 14475.
33. Papaefthymiou, V.; Millar, M. M.; Muenck, E. *Inorg. Chem.* **1986,** *25,* 3010.
34. Peisach, J.; Beinert, H.; Emptage, M. H.; Mims, W. B.; Fee, J. A.; Orme-Johnson, W. H.; Redina, A. R.; Orme-Johnson, N. B. *J. Biol. Chem.* **1983,** *258,* 13014.
35. Banci, L.; Bertini, I.; Briganti, F.; Luchinat, C.; Scozzafava, A.; Oliver, M. V. *Inorg. Chem.* **1991,** *30,* 4517.
36. Banci, L.; Bertini, I.; Carloni, P.; Luchinat, C.; Orioli, P. L. *J. Am. Chem. Soc.* **1992,** *114,* 10684.
37. Banci, L.; Bertini, I.; Carloni, P.; Luchinat, C.; Orioli, P. L. *J. Am. Chem. Soc.* **1992,** *114,* 10683.
38. Banci, L.; Pieratelli, R. *NATO ASI, Ser. C* **1995,** *457,* 281.
39. Sola, M.; Cowan, J. A.; Gray, H. B. *Biochemistry* **1989,** *28-12,* 5261.
40. Sola, M.; Cowan, J. A.; Gray, H. B. *J. Am. Chem. Soc.* **1989,** *111,* 6627.
41. Rueterjans, H.; Messori, L.; Ohlenschlaeger, O.; Briganti, F.; Bertini, I. *Appl. Magn. Reson.* **1993,** *4,* 477.
42. Li, D.; Soriano, A.; Cowan, J. A. *Inorg. Chem.* **1996,** *35,* 1980.
43. Li, D.; Agarwal, A.; Cowan, J. A. *Book of Abstracts, 210th ACS National Meeting* **1995,** *Issue Pt. 1,* INOR-674.
44. Krichnamoorthi, R.; Cusanovich, M. A; Meyer, T. E.; Przysiecki, C. T. *Eur. J. Biochem.* **1989,** *181,* 81.
45. Ciurli, S.; Cremonini, A.; Kofod, P.; Luchinat, C. *Eur. J. Biochem.* **1996,** *236,* 405.
46. Ciurli, S.; Luchinat, C.; Scozzafava, A. *Top. Mol. Organ. Eng.* **1994,** *11,* 143.
47. Cheng, H.; Markley, J. L. *Annu. Rev. Biophys. Biomol. Struct.* **1995,** *24,* 209.
48. Bertini, I.; Eltis, L. D.; Felli, I. C.; Kastrau, D. H. W.; Luchinat, C.; Piccioli, M. *Chem Eur. J.* **1996,** *1,* 598.
49. Bertini, I.; Dikiy, A.; Kastrau, D. H. W.; Luchinat, C.; Sompornpisut, P. *Biochemistry* **1995,** *34,* 9851.
50. Bertini, I.; Capozzi, F.; Luchinat, C.; Piccioli, M.; Vicens Oliver, M. *Inorg. Chim. Acta* **1992,** *198-200,* 483.
51. Bertini, I.; Capozzi, F.; Ciurli, S.; Luchinat, C.; Messori, L.; Piccioli, M. *J. Am. Chem. Soc.* **1992,** *114,* 3332.
52. Banci, L.; Bertini, I.; Dikiy, A.; Kastrau, D. H. W.; Luchinat, C.; Sompornpisut, P. *Biochemistry* **1995,** *34,* 206.
53. Banci, L.; Bertini, I.; Luchinat, C.; Messori, L.; Torano, P. *Appl. Magn. Reson.* **1993,** *4,* 461.
54. Bertini, I.; Capozzi, F.; Luchinat, C.; Piccioli, M. *Eur. J. Biochem.* **1993,** *212,* 69.
55. (a) Blondin, G.; Girerd, J.-J. *J. Biol. Inorg. Chem.* **1996,** *1,* 170; (b) Krockel, M.; Grodzicki, M.; Papaefthymiou, M.; Trautwein, A. X.; Kostikas, A. *ibid.* 173; (c) Noodleman, L.; Case, D. A.; Mouesca, J.-M.; Lamotte, B. *ibid.* 177; (d) Bertini, I.; Luchinnat, C. *ibid.* 183; (e) Belinsky, M. I. *ibid.* 186.
56. Aizman, A.; Case, D. A. *J. Am. Chem. Soc.* **1982,** *104,* 3269.
57. Mouesca, J.-M.; Noodleman, L.; Case, D. A. *J. Quant. Chem., Quant. Biol. Symp.* **1995,** *22,* 95.

58. Noodleman, L. *Inorg. Chem.* **1988,** *27,* 3677.
59. Antanaitis, B. C.; Moss, T. H. *Biochim. Biophys. Acta* **1975,** *405,* 262.
60. Cerdonio, M.; Wang, R.-H.; Rawlings, J.; Gray, H. B. *J. Am. Chem. Soc.* **1974,** *96,* 6534.
61. Herskovitz, T.; Averill, B. A.; Holm, R. H.; Ibers, J. A.; Phillips, W. D.; Weiher, J. F. *Proc. Natl. Acad. Sci. U.S.A.* **1972,** *69,* 2437.
62. Bertini, I.; Campos, A. P.; Luchinat, C.; Teixeira, M. *J. Inorg. Biochem.* **1993,** *52,* 227.
63. Dickson, D. P. E.; Johnson, C. E.; Cammack, R.; Evans, M. C. W.; Hall, D. O.; Rao, K. K. *Biochem. J.* **1974,** *139,* 105.
64. Middleton, P.; Dickson, D. P. E.; Johnson, C. E.; Rush, J. D. *Eur. J. Biochem.* **1980,** *104,* 289.
65. Dickson, D. P. E.; Johnson, C. E.; Middleton, P.; Rush, J. D.; Cammack, R.; Hall, D. O.; Mullinger, R. N.; Rao, K. K. *J. Phys. (Paris), Colloq.* **1976,** 171.
66. Dickson, D. P. E.; Cammack, R. *Biochem. J.* **1974,** *143,* 763.
67. Moss, T. H.; Bearden, A. J.; Bartsch, R. G.; Cusanovich, M. A.; San Pietro, A. *Biochemistry* **1968,** *7,* 1591.
68. Evans, M. C. W.; Hall, D. O.; Johnson, C. E. *Biochem. J.* **1970,** *119,* 289.
69. Belinski, M.; Bertini, I.; Galas, O.; Luchinat, C. *Z. Naturforsch., A: Phys. Sci.* **1995,** *50,* 75.
70. Bominaar, E. L.; Borshch, S. A.; Girerd, J.-J. *J. Am. Chem. Soc.* **1994,** *116,* 7957.
71. Bominaar, E. L.; Borshch, S. A.; Girerd, J.-J. *J. Am. Chem. Soc.* **1994,** *116,* 5362.
72. Palii, A. V.; Ostrovsky, S. M.; Klokishner, S. I.; Tsukerblat, B. S. *Phys. Lett. A* **1994,** *185,* 480.
73. Bertini, I.; Gaudemer, A.; Luchinat, C.; Piccioli, M. *Biochemistry* **1993,** *32,* 12887.
74. Belinskii, M. *Chem. Phys.* **1993,** *176,* 15.
75. Ueyama, N.; Nakamura, A. *Kikan Kagaku Sosetsu* **1995,** *24,* 44.
76. Tomohiro, T.; Uoto, K.; Kodaka, M.; Shimura, T.; Kubota, Y.; Okada, T.; Okuno, H. *Kagaku Gijutsu Kenkyusho Hokoku* **1992,** *87,* 187.
77. Spiro, T. G.; Hare, J.; Yachandra, V.; Gewirth, A.; Johnson, M. K.; Remsen, E. *Met. Ions Biol.* **1982,** *4,* 407.
78. Noodleman, L.; Peng, C. Y.; Case, D. A.; Mouesca, J.-M. *Coord. Chem. Rev.* **1995,** *144,* 199.
79. Michaels, M. L.; Pham, L.; Nghiem, Y.; Cruz, C.; Miller, J. H. *Nucleic Acids Res.* **1990,** *18,* 3841.
80. Prince, R. C.; Grossman, M. J. *Trends Biochem. Sci.* **1993,** *18,* 153.
81. Cunningham, R. P.; Asahara, H.; Bank, J. F.; Scholes, C. P.; Salerno, J. C.; Surerus, K.; Munk, E.; McCracken, J.; Peisach, J.; Emptage, M. H. *Biochemistry* **1989,** *28,* 4450.
82. Haile, D. J.; Roualt, T. A.; Harford, J. B.; Kennedy, M. C.; Blondin, G. A.; Beinert, H.; Klausner, R. D. *Proc. Natl. Acad. Sci. U.S.A.* **1992,** *89,* 11735.
83. Kennedy, M. C.; Mende-Mueller, L.; Blondin, G. A.; Beinert, H. *Proc. Natl. Acad. Sci. U.S.A.* **1992,** *89,* 11730.
84. Roualt, T. A.; Stout, C. D.; Kaptain, S.; Harford, J. B.; Klausner, R. D. *Cell* **1991,** *64,* 881.
85. Switzer, R. L. *Biofactors* **1989,** *2,* 77.
86. Chang, C. H.; Ballinger, M. D.; Reed, G. H. *Biochemistry* **1996,** *35,* 11081.
87. Emptage, M. H. *in* "Metal Clusters in Proteins"; Que, L., Ed.; ACS: Washington, 1988; Vol. 372, pp. 343–371.

88. Khoroshilova, N.; Beinert, H.; Kiley, P. J. *Proc. Natl. Acad. Sci. U.S.A.* **1995,** *92,* 2499.
89. Beinert, H.; Kiley, P. *FEBS Lett.* **1996,** *382,* 218.
90. Lazazzera, B. A.; Beinert, H.; Khoroshilova, N.; Kennedy, M. C.; Kiley, P. J. *J. Biol. Chem.* **1996,** *271,* 2762.
91. Kerfeld, C. A.; Chan, C.; Hirasawa, M.; Kleis-SanFrancisco, S.; Yeates, T. O.; Knaff, D. B. *Biochemistry* **1996,** *35,* 7812.
92. Hochkoeppler, A.; Kofod, P.; Zannoni, D. *FEBS Lett.* **1995,** *375,* 197.
93. Hochkoeppler, A.; Kofod, P.; Ferro, G.; Ciurli, S. *Arch. Biochem. Biophys.* **1995,** *322,* 313.
94. Schoepp, B.; Parot, P.; Menin, L.; Gaillard, J.; Richaud, P.; Vermeglio, A. *Biochemistry* **1995,** *34,* 11736.
95. Hochkoeppler, A.; Ciurli, S.; Venturoli, G.; Zannoni, D. *FEBS Lett.* **1995,** *357,* 70.
96. Meyer, T. E.; Cannac, V.; Fitch, J.; Bartsch, R. G.; Tollin, D.; Tollin, G.; Cusanovich, M. A. *Biochim. Biophys. Acta* **1990,** *1017,* 125.
97. Butler, J.; Sykes, A.; Buxton, G. V.; Harrington, P. C.; Wilkins, R. G. *Biochem. J.* **1980,** *189,* 641.
98. Burbaev, D. S.; Solozhenkin, I. P.; Zvyagil'skaya, R. A.; Blyumenfel'd, L. A. *Biofizika* **1981,** *26,* 447.
99. Castro, L.; Rodriguez, M.; Radi, R. *J. Biol. Chem.* **1994,** *269,* 29409.
100. Faridoon, K. Y.; Zhuang, H.-Y.; Sykes, A. G. *Inorg. Chem.* **1994,** *33,* 2209.
101. Ramsay, R. R.; Singer, T. P. *Biochemistry* **1984,** *221,* 489.
102. Breiter, D. R.; Meyer, T. E.; Rayment, I.; Holden, H. M. *J. Biol. Chem.* **1991,** *266,* 18660.
103. Ciszewska, H.; Bagyinka, C.; Tigyi, G.; Kovacs, K. L. *Acta Biochim. Biophys. Hung.* **1989,** *24,* 361.
104. Zannoni, D.; Ingledew, W. J. *Arch. Microbiol.* **1983,** *135,* 176.
105. Zorin, N. A.; Gogotov, I. N. *Biokhimiya(Moscow)* **1983,** *48,* 1181.
106. Kennel, S. J.; Bartsch, R. G.; Kamen, M. D. *Biophys. J.* **1972,** *12,* 882.
107. Fukumori, Y.; Yamanaka, T. *Curr. Microbiol.* **1979,** *3,* 117.
108. Bentrop, D.; Bertini, I.; Capozzi, F.; Dikiy, A.; Eltis, L.; Luchinat, C. *Biochemistry* **1996,** *35,* 5928.
109. Carter, C. W.; Kraut, J.; Freer, S. T.; Xuong, N. H.; Alden, R. A.; Bartsch, R. G. *J. Biol. Chem.* **1974,** *249, 4212.*
110. Carter, C. W.; Kraut, J.; Freer, S. T.; Xuong, N. H.; Alden, R. A. *J. Biol. Chem.* **1974,** *249,* 6339.
111. Breiter, D. R. *Diss. Abstr. Int. B 1992* ***1991,*** *53,* 1383.
112. Banci, L.; Bertini, I.; Eltis, L. D.; Felli, I.; Kastrau, D. H. W.; Luchinat, C.; Piccioli, M.; Pierattelli, R.; Smith, M. *Eur. J. Biochem.* **1994,** *225,* 715.
113. Benning, M. M.; Meyer, T. E.; Rayment, I.; Holden, H. M. *Biochemistry* **1994,** *33,* 2476.
114. Rayment, I.; Wesenberg, G.; Meyer, T. E.; Cusanovich, M. A.; Holden, H. M. *J. Mol. Biol.* **1992,** *228,* 672.
115. Moulis, J.-M.; Davasse, V.; Golinelli, M.-P.; Quinkal, I. *J. Biol. Inorg. Chem.* **1996,** *1,* 2.
116. Banci, L.; Bertini, I.; Dikiy, A.; Kastrau, D. H.; Luchinat, C.; Sompornpisut, P. *Biochemistry* **1995,** *34,* 206.
117. Cowan, J. A. "Inorganic Biochemistry: An Introduction"; Cowan, J. A., Ed.; VCH: New York, 1993; Chap. 5.

118. Berg, J. M.; Holm, R. H. *in* "Metal Ions in Biology"; Spiro, T. G., Ed.; Wiley Interscience: New York, 1982; Vol. 4, pp. 1–66.
119. Stout, C. D., *in* "Metal Ions in Biology"; Spiro, T. G., Ed.; John Wiley and Sons: New York, 1982; Vol. 4, pp. 97–146.
120. Cammack, R. *Adv. Inorg. Chem.* **1992,** *38,* 281.
121. Beinert, H. *FASEB J.* **1990,** 42483.
122. Matsubara, H.; Saeki, K. *Adv. Inorg. Chem.* **1992,** *38,* 223.
123. Moulis, J. M.; Scherrer, N.; Gagnon, J.; Forest, E.; Petillot, Y.; Garcia, D. *Arch. Biochem. Biophys.* **1993,** *305,* 186.
124. Adman, E.; Watenpaugh, K. D.; Jensen, L. H. *Proc. Natl. Acad. Sci. U.S.A.* **1975,** *72,* 4854.
125. Sweeney, W. V.; Magliozzo, R. S. *Biopolymers* **1980,** *19,* 2133.
126. Mizrahi, I. A.; Meyer, T. E.; Cusanovich, M. A. *Biochemistry* **1980,** *19,* 4727.
127. Bertini, I.; Gaudemer, A.; Luchinat, C.; Piccioli, M. *Biochemistry* **1993,** *32,* 12887.
128. Agarwal, A.; Tan, J.; Eren, M.; Tevelev, A.; Lui, S. M.; Cowan, J. A. *Biochem. Biophys. Res. Commun.* **1993,** *197,* 1357.
129. Eltis, L. D.; Iwagami, S. G.; Smith, M. *Protein Eng.* **1994,** *7,* 1145.
130. Bian, S.; Hille, C. R.; Hemman, C.; Cowan, J. A. *Biochemistry* **1996,** *35,* 14544.
131. Agarwal, A.; Li, D.; Cowan, J. A. *Proc. Natl. Acad. Sci. U.S.A.* **1995,** *92,* 9440.
132. Shen, B.; Jollie, D. R.; Diller, T. C.; Stout, C. D.; Stephens, P. J.; Burgess, B. K. *Proc. Natl. Acad. Sci. U.S.A.* **1995,** *92,* 10064.
133. Kowal, A. T.; Werth, M. T.; Manodori, A.; Cecchini, G.; Schroeder, I.; Gunsalus, R. P.; Johnson, M. K. *Biochemistry* **1995,** *34,* 12284.
134. Iwagami, S. G.; Creagh, A. L.; Haynes, C. A.; Borsari, M.; Felli, I. C.; Piccioli, M.; Eltis, L. D. *Can. Protein Sci.* **1995,** *4,* 2562.
135. Li, D.; Cottrell, C. E.; Cowan, J. A. *J. Protein Chem.* **1995,** *14,* 115.
136. Lui, S. M.; Cowan, J. A. *J. Am. Chem. Soc.* **1994,** *116,* 4483.
137. Bertini, I.; Felli, I.; Kastrau, D. H. W.; Luchinat, C.; Piccioli, M.; Viezzoli, M. S. *Eur. J. Biochem.* **1994,** *225,* 703.
138. Bartsch, R. G. *Methods Enzymol.* **1978,** *53,* 329.
139. Maskiewicz, R.; Bruice, T. C. *Proc. Natl. Acad. Sci. U.S.A.* **1977,** *74,* 5321.
140. Nakamoto, M.; Tanaka, K.; Tanaka, T. *J. Chem. Soc., Chem. Commun.* **1988,** *21,* 1422.
141. O'Sullivan, T.; Millar, M. M. *J. Am. Chem. Soc.* **1985,** *107,* 4096.
142. Roth, E. K. H.; Jordanov, J. *Inorg. Chem.* **1992,** *31,* 240.
143. Blonk, H. L.; Kievit, O.; Roth, E. K.-H.; Jordanov, J.; van der Linden, J. G. M.; Steggerda, J. J. *Inorg. Chem.* **1991,** *30,* 3231.
144. Kambayashi, H.; Nagao, H.; Tanaka, K.; Nakamoto, M.; Peng, S.-M. *Inorg. Chim. Acta* **1993,** *209,* 143.
145. Chothia, C. *Nature* **1975,** *254,* 304.
146. Soriano, A.; Cowan, J. A. *Inorg. Chim. Acta* **1996,** *251,* 285.
147. Babini, E.; Bertini, I.; Borsari, M.; Capozzi, F.; Dikiy, A.; Eltis, L. D.; Luchinat, C. *J. Am. Chem. Soc.* **1996,** *118,* 75.
148. Agarwal, A.; Li, D.; Cowan, J. A. *J. Am. Chem. Soc.* **1996,** *118,* 927.
149. Li, D.; Agarwal, A.; Cowan, J. A. *Inorg. Chem.* **1996,** *35,* 1121.
150. Bertini, I.; Luchinat, C. "NMR of Paramagnetic Substances"; Bertini, I., and Luchinat, C., Eds.; Elsevier: New York, 1996; Vol. 150, pp. 185–220.
151. Gerig, J. T. *Methods Enzymol.* **1986,** *177,* 3.
152. Gerig, J. T. *Prog. Nucl. Magn. Reson.* **1994,** *26,* 293.
153. Gerig, J. T. *Bio. Magn. Reson.* **1978,** *1,* 139.

154. Hansen, P. E.; Dettman, H. D.; Sykes, B. D. *J. Magn. Reson.* **1985,** *62,* 487.
155. Soriano, A.; Li, D.; Bian, S.; Agarwal, A.; Cowan, J. A. *Biochemistry* **1996,** *35,* 12479.
156. Bertrand, P.; Mbarki, O.; Blanchard, L.; Guerlesquin, F.; Tegoni, M. *Biochemistry* **1995,** *34,* 11071.
157. Bertini, I.; Briganti, F.; Luchinat, C.; Scozzafava, A.; Sola, M. *J. Am. Chem. Soc.* **1991,** *113,* 1237.
158. Cammack, R. *Biochem. Biophys. Res. Commun.* **1973,** *54,* 548.
159. Ambler, R. P.; Meyer, T. E.; Kamen, M. D. *Arch. Biochem. Biophys.* **1993,** *306,* 215.
160. Banci, L.; Bertini, I.; Ciurli, S.; Luchinat, C.; Pierattelli, R. *Inorg. Chim. Acta* **1995,** *240,* 251.
161. Luchinat, C.; Capozzi, F.; Borsari, M.; Battistuzzi, G.; Sola, M. *Biochem. Biophys. Res. Commun.* **1994,** *203,* 436.
162. Heering, H. A.; Bulsink, Y. B. M.; Hagen, W. R.; Meyer, T. E. *Biochemistry* **1995,** *34,* 14675.
163. Carter, C. W. J. *J. Biol. Chem.* **1977,** *252,* 7802.
164. Kassner, R. J.; Yang, W. *J. Am. Chem. Soc.* **1977,** *99,* 4351.
165. Taniguchi, V. T.; Malmstrom, B. G.; Anson, F. C.; Gray, H. B. *Proc. Natl. Acad. Sci. U.S.A.* **1982,** *79,* 3387.
166. Taniguchi, V. T.; Ellis, W. R. J.; Cammarata, V.; Webb, J.; Anson, F. C.; Gray, H. B.; "Electrochemical and Spectrochemical Studies of Biological Redox Components"; Amer. Chem. Soc.: Washington, D.C., 1982; p. 51.
167. Mizrahi, I. A.; Cusanovich, M. A. *Biochemistry* **1980,** *19,* 4733.
168. Beratan, D. N.; Betts, J. N.; Onuchic, J. N. *Science* **1991,** *252,* 1285.
169. Jensen, G. M.; Warshel, A.; Stephens, P. J. *Biochemistry* **1994,** *33,* 10911.
170. Churg, A. K.; Warshel, A. *Biochemistry* **1986,** *25,* 1675.
171. Warshel, A.; Russell, S. T. *Q. Rev. Biophys.* **1984,** *17,* 283.
172. Meyer, T. E. *Methods Enzymol.* **1994,** *243,* 435.
173. Tedro, S. M.; Meyer, T. E.; Bartsch, R. G.; Kamen, M. D. *J. Biol. Chem.* **1981,** *256,* 731.
174. Ciszewska, H.; Bagyinka, C.; Kovacs, K. L. *Biokonvers. Soln. Energ., Mater. Mezhdunar. Simp.* **1984,** 330.
175. Wermter, U.; Fischer, U. *Bioscience* **1983,** 38C, 986.
176. Tedro, S. M.; Meyer, T. E.; Kamen, M D. *J. Biol. Chem.* **1974,** *249,* 1182.
177. Tedro, S. M.; Meyer, T. E.; Kamen, M. D. *Arch. Biochem. Biophys.* **1985,** *241,* 656.
178. Tedro, S. M.; Meyer, T. E.; Kamen, M. D. *J. Biol. Chem.* **1977,** *252,* 7826.
179. Kusano, T.; Takeshima, T.; Sugawara, K.; Inoue, C.; Shiratori, T.; Yano, T.; Fukumori, Y.; Yamanaka, T. *J. Biol. Chem.* **1992,** *267,* 11242.
180. Kusano, T.; Takeshima, T.; Sugawara, K.; Inoue, C.; Shiratori, T.; Yano, T.; Fukumori, Y.; Yamanaka, T. *Biohydrometall. Technol., Proc. Int. Biohydrometall. Symp.* **1993,** *2,* 725.
181. Stombaugh, N. A.; Sundquist, J. E.; Burris, R. H.; Orme-Johnson, W. H. *Biochemistry* **1976,** *15,* 2633.
182. Fukuyama, K.; Matsubara, H.; Tsukihara, T.; Katsube, Y. *J. Mol. Biol.* **1989,** *210,* 383.

ADVANCES IN INORGANIC CHEMISTRY, VOL. 45

THE METHYLAMINE DEHYDROGENASE ELECTRON TRANSFER CHAIN

C. DENNISON,*[,1] G. W. CANTERS,* S. DE VRIES,† E. VIJGENBOOM,* and R. J. VAN SPANNING‡

*Leiden Institute of Chemistry, Gorlaeus Laboratories, Leiden University, 2300 RA Leiden, The Netherlands
†Laboratory for Microbiology and Enzymology, Technical University of Delft, 2628 BC Delft, The Netherlands
‡Biological Laboratory, Free University of Amsterdam, 1007 MC Amsterdam, The Netherlands

I. Introduction

Textbook coverage of cellular respiration is often based on the mitochondrial paradigm. Mitochondiral respiration is attractive because of its relatively uncomplicated organization. The respiratory chain consists of a single sequence of redox proteins with only two possible substrates and a single terminal electron acceptor. The simplicity of the mitochondrial respiratory apparatus belies its evolutionary origin.

[1] Present address: Department of Chemistry, University College Dublin, Belfield, Dublin 4, Ireland.

0898-8838/98 $25.00

According to the endosymbiontic hypothesis mitochondria derive from ancestors that are closely related to modern purple bacteria, for example, *Pseudomonas, Rhodobacter,* and *Paracoccus*. Although mitochondria are embedded in a cellular environment with narrowly controlled conditions regarding pH, redox balance, and substrate availability, bacteria may encounter a variety of environmental conditions. A repertoire of respiratory chains and regulatory mechanisms as opposed to a single electron transfer chain allows them to cope with a variety of environments.

During respiration cellular redox free energy is converted into chemic-osmotic and chemical energy. The conversion is mediated by the flow of electrons, which, in an oxidizing environment, run from low to high potential. In mitochondria the reducing equivalents flow via NADH and ubiquinone to the terminal electron acceptor, molecular oxygen. In bacteria the reducing equivalents may be derived from a variety of sources, such as sulfur or nitrogen in low oxidation states (S, S^{2-}, NH_3), molecular hydrogen, or even ferrous ions. Terminal electron acceptors may by provided by molecular oxygen, or by sulfur and nitrogen in high oxidation states, e.g., SO_4^{2-}, NO_2^-, and NO_3^-. A bacterium has a collection of respiratory routes at its disposal, thus unraveling the respiratory machinery is a complicated task requiring not only identification of branches of the various electron transport chains and their composition, but also the elucidation of their genetic organization and the mechanisms that control selective gene activation and expression.

This review focuses on the electron transfer chain that is employed by the organism *Paracoccus versutus* [formerly *Thiobacillus versutus* (*1*)] when it is provided with methylamine as its sole source of nitrogen and energy. The chain is similar to the methylamine dehydrogenase chain of *Paracoccus denitrificans*, and the results of the *P. versutus* studies will be compared with the *P. denitrificans* data where appropriate. One of the attractive features of this chain is that it consists of only four redox components: methylamine dehydrogenase (MADH), amicyanin (ami), cytochrome c_{550}, and cytochrome *c* oxidase (COX). Only MADH contains an organic prosthetic group, tryptophan-tryptophyl quinone (TTQ); the other three proteins contain metals (Fe and Cu) as their prosthetic group. MADH converts methylamine to formaldehyde and ammonia, which then enter the metabolic cycles of the cell, while the electrons that are liberated in the conversion step are fed into amicyanin and, subsequently via cyt c_{550}, into COX, where they are used for the reduction of the terminal electron acceptor, molecular oxygen, to water.

In Section II the composition and organisation of the respiratory chains of *P. versutus* and *P. denitrificans* will be reviewed. The gene organization and composition, and their possible control elements, will also be discussed. Section III will deal with the structure and function of the four components of the MADH redox chain. Structures determined by X-ray diffraction (XRD) and nuclear magnetic resonance (NMR) techniques are available for the members of the MADH chain or for closely related analogues. Finally, the enzymology and reaction kinetics of the chain will be reviewed.

II. Composition and Organization of Respiratory Chains

A. The Respiratory Network of *Paracoccus versutus* and *Paracoccus denitrificans*

1. Introduction

Paracoccus versutus and *P. denitrificans* (*2*) are phylogenetically closely related species; together with *Rhodobacter* and *Rhizobium* species they belong to the α-cluster of purple bacteria (*3*, *4*). These gram-negative eubacteria are unable to ferment availabe growth substrates, and are therefore completely dependent on respiration-linked oxidative phosphorylation for their (free) energy requirements. Usually, these organisms are found in soil, sewage, or sludge, environments where the availability of suitable carbon and energy sources as well as of terminal electron acceptors is subject to ever-fluctuating conditions. The ability of the cells to survive in these variable environments depends on the properties of their respiratory network as well as on their readiness to adapt to environmental changes.

One of the best studied organisms in this respect is *P. denitrificans* (*5*, *6*, *7*, *8*). This bacterium has a great nutritional adaptability: it can grow chemolithoautotrophically with hydrogen or thiosulfate as sole energy source; autotrophically with methanol, formaldehyde, formate, or methylamine as sole energy source; or heterotrophically with a variety of sugars, organic and amino acids, and alcohols (*9*). Apart from oxygen, *N*-oxides such as nitrate, nitrite, nitric oxide, or nitrous oxide can serve as electron acceptors of the respiratory process (*10*, *11*). This versatility in utilization of electron donors and acceptors is the consequence of the ability of the bacterium to redirect electron fluxes to alternative branches within its respiratory network (short-term adaptation) as well as to change the makeup of the respiratory network

(long-term adaptation) in response to environmental changes (*7*, *8*, *12–16*).

Elucidation of the composition of the network at different growth conditions and the role of each component within it have been facilitated by biochemical and physiological analyses of respiratory mutants that were created by means of targeted gene exchange techniques (*17*, *18*). As a result of these approaches, strains that have a mutation in the chromosomal gene encoding one of the redox enzymes are generated. These mutations may be either marked or unmarked, in which case the target gene is interrupted by an antibiotic resistance gene or (partly) deleted, respectively. Because the number of antibiotic resistance markers that may be used in *P. denitrificans* is limited, the advantage of the latter approach is that more than one mutation in different target genes can be created in the same strain. This technique has been extremely useful in the attempt to unravel the many respiratory branches that operate in parallel in *P. denitrificans*. At present, a number of the genes and gene clusters encoding its respiratory enzymes have been cloned (*8*), and, by using the above approach, a comprehensive set of respiratory mutants with single or multiple mutations in either of these genes, and in different combinations, has become available for detailed analyses. On the basis of these analyses, the elucidation of the organization of the network under different growth conditions has been achieved (*8*, *19*).

2. *The Makeup and Bioenergetics of the Respiratory Network*

a. Aerobic Growth. The constitutive part of the respiratory network consists of nicotinamide adenine dinucleotide (NADH) dehydrogenase, succinate dehydrogenase, ubiquinone-10, the cytochrome bc_1 complex, and cytochromes c_{550} (located in the periplasm), and c_{552} (anchored in the membrane). NADH dehydrogenase and cytochrome bc_1 are membrane-bound protein complexes by which the free energy made available by the electron transfer reactions is used for the generation of a proton gradient across the membrane. Depending on the availability of suitable carbon and energy sources as well as on terminal electron acceptors, additional components and/or branches are expressed and linked to the constitutive part of the network. When the bacterium experiences relatively high (for instance, atmospheric) oxygen concentrations it synthesizes an aa_3-type cytochrome *c* oxidase. This terminal four-subunit complex spans the membrane and catalyzes the four-electron reduction of dioxygen to water with the concomitant generation of an electrochemical potential across the membrane. The resulting electron transfer chain thus comprises three

sites of energy conservation (NADH dehydrogenase, the cytochrome bc_1 complex, and the aa_3-type oxidase), by which means the bacterium is able to generate ATP per electron very efficiently. With respect to the organization and function, the aerobic respiratory network resembles the one that is operating in mitochondria (*20*, *21*), organelles of eukaryotic cells that are optimized for energy production (Fig. 1). In *P. denitrificans*, the concentration of the aa_3-type cytochrome *c* oxidase decreases with decreasing oxygen concentrations, and the protein is virtually absent during anaerobiosis (*22*, *23*). In addition, the expression of this oxidase is twofold increased in cells grown on methanol or methylamine as compared with heterotrophically grown cells (*24–26*). Oxidases of this type are found in a wide variety of cells. Apart from their presence in eukaryotic cells, aa_3-type cytochrome *c* oxidases have been encountered in many eubacterial (both gram negative and positive), and archaebacterial (*Sulfolobus acidocaldarius*) species (*27*, *28*).

In addition to the aa_3-type oxidase, *P. denitrificans* has the genetic potential to express two other types of terminal oxidases: the bb_3-type quinol oxidase and the cbb_3-type cytochrome *c* oxidase (*7*, *12*). The three types of oxidases share common biochemical properties and architectural features (*7*, *29*). The most pronounced homology is found between the respective subunits I of the enzymes, which harbor the metal centers involved in electron transport and catalysis of oxygen

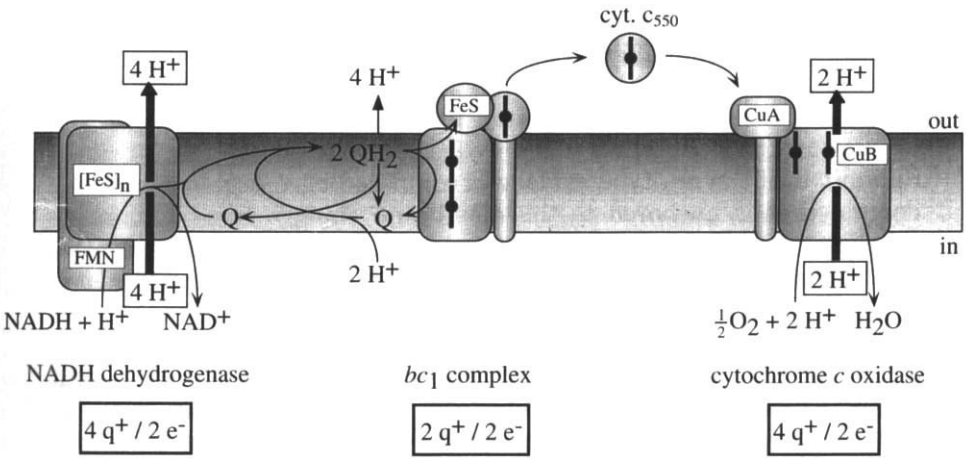

FIG. 1. Scheme of the mitochondrial respiratory chain: NADH dehydrogenase, ubiquinone (Q), the bc_1 complex, cytochrome c_{550}, and the aa_3-type cytochrome *c* oxidase. Not included is succinate dehydrogenase. Pumped protons (H^+) are boxed, scalar protons are not. Charge separation ($q/2e^-$) sites are indicated.

reduction. The subunits I all have 12 transmembrane α-helices with a total of six invariant histidine residues located in helices 2, 6, 7, and 10. These histidines are the ligands for the low- and high-spin hemes (*a* and a_3 in the aa_3-type oxidase, and *b* and b_3 in the bb_3- and cbb_3-type oxidases, respectively), and a copper ion, Cu_B, the latter two of which form the binuclear reaction center (*30*, *31*). On the basis of this resemblance, it has been postulated that the three different types of oxidases are all members of a superfamily of heme–copper oxidases sharing a common ancestor (*7*, *29*). Amino acid residues implied in the pathway of pumped protons and chemical protons are conserved in aa_3-type cytochrome *c* and bb_3-type quinol oxidases (*31*, *32*). Evidence for the suggested pathways has recently been obtained from studies on the three-dimensional structure of the aa_3-type oxidase, which was determined from X-ray analysis of the crystallized protein complex (*33*, *34*). These pathways are apparently not present in cbb_3-type oxidases, because they lack the conserved amino acid sequences at the corresponding positions of the sequence (*7*, *35*). Nevertheless, all three types of oxidases have proton pumping capacities and contribute to the generation of the electrochemical gradient (*35*). From the viewpoint that such a fundamentally important feature should be conserved among all members of the oxidase family, it may thus be that the mechanism of proton efflux is not yet understood properly. Alternatively, the proton channel in the cbb_3-type oxidases may be composed of residues different from those of the other types.

The most striking difference between these types of oxidase consists in the nature of the other subunits, which are involved in binding their dedicated electron donors and in enhancing the stability of the enzyme complex. Here, we will only focus on the electron entry sites. Subunit II of the aa_3-type oxidase is composed of a large periplasmic domain that is anchored to the membrane via two transmembrane α-helices (*33*). The soluble domain contains a binuclear Cu_A center that mediates the electron transfer between cytochrome *c* and heme *a* (*33*, *36*, *37*). With respect to its primary amino acid sequence as well as its geometry, its counterpart in the bb_3-type quinol oxidase is very similar (*28*, *38*). The most pronounced difference is the lack of a Cu_A center, which makes it unsuited to react with cytochromes *c*. Instead, it receives electrons directly from quinol. The electron entry pathway in the cbb_3-type oxidase is poorly understood. Apart from subunit I (CcoN), the oxidase consists of two membrane-anchored subunits, one of which has a single heme *c* (CcoO), whereas the other one has two hemes *c* (CcoP) (*35*, *39*, *40*). Mutant studies have revealed that cyto-

chrome bc_1, or cytochrome c_{550}, but not cytochrome c_{552}, can act as electron donor for this oxidase (*8*). Perhaps the two hemes in CcoP make up an electron transfer pathway between the cytochrome bc_1 complex and the oxidase, whereas CcoO is responsible for electron transfer between the soluble cytochrome and the oxidase.

It is not only on the basis of electron entry sites that these types of oxidases are different. As compared with the aa_3- and bb_3-type cytochrome *c* oxidases, the cbb_3-type oxidase has a ~10-fold higher affinity for oxygen (*41*). Not surprisingly, therefore, expression of the latter oxidase increases at decreasing oxygen concentrations (*6*, *42*). Oxidases of the cbb_3-type or their allocated gene clusters have thus far been characterized in *P. denitrificans* (*35*), *Rhodobacter capsulatus, Azotobacter vinelandii, Agrobacterium tumefaciens, Pseudomonas aeruginosa* (*40*), and *Rhodobacter sphaeroides* (*27*), and in several members of the Rhizobiaceae (*39*, *42*, *43*). The latter organisms are able to fix atmospheric nitrogen in symbiosis with a legume host plant, during which interaction the bacteria are lodged in the plant nodules. The oxygen concentration in these specific plant compartments is extremely low to prevent irreversible oxidation of nitrogenase, the enzyme responsible for nitrogen fixation. In order to keep the electron fluxes through the respiratory network going the bacteria rely almost exclusively on the high-affinity cbb_3-type oxidase.

The bb_3-type quinol oxidase of *P. denitrificans* is the counterpart of the well-known *Escherichia coli* bo_3-type quinol oxidase (*12*, *44*). This type of oxidase is common in all genera of eubacteria (*28*). Because these redox enzymes couple the oxidation of quinol directly to the reduction of oxygen, this electron transfer route is less efficient with respect to free energy transduction than those involving the energy-generating cytochrome bc_1 complex. Little is known as to whether and how the expression of the quinol oxidase is fine-tuned in response to environmental changes. A model for electron transfer during heterotrophic growth is shown in Fig. 2A.

b. Anaerobic Growth. In the absence of molecular oxygen, electron flow is dependent on the availability of *N*-oxides that may serve as alternative electron acceptors (*8*, *10*, *44*, *45*, *46*). At the shift from oxygen limitation to anaerobiosis, the makeup of the respiratory network drastically changes. The expression of nitrate, nitrite, nitric oxide, and nitrous oxide reductases as well as of the blue copper-containing electron carrier pseudoazurin is established, and in a concerted action these terminal oxidoreductases couple the removal of electrons from the respiratory network to the reduction of the corresponding

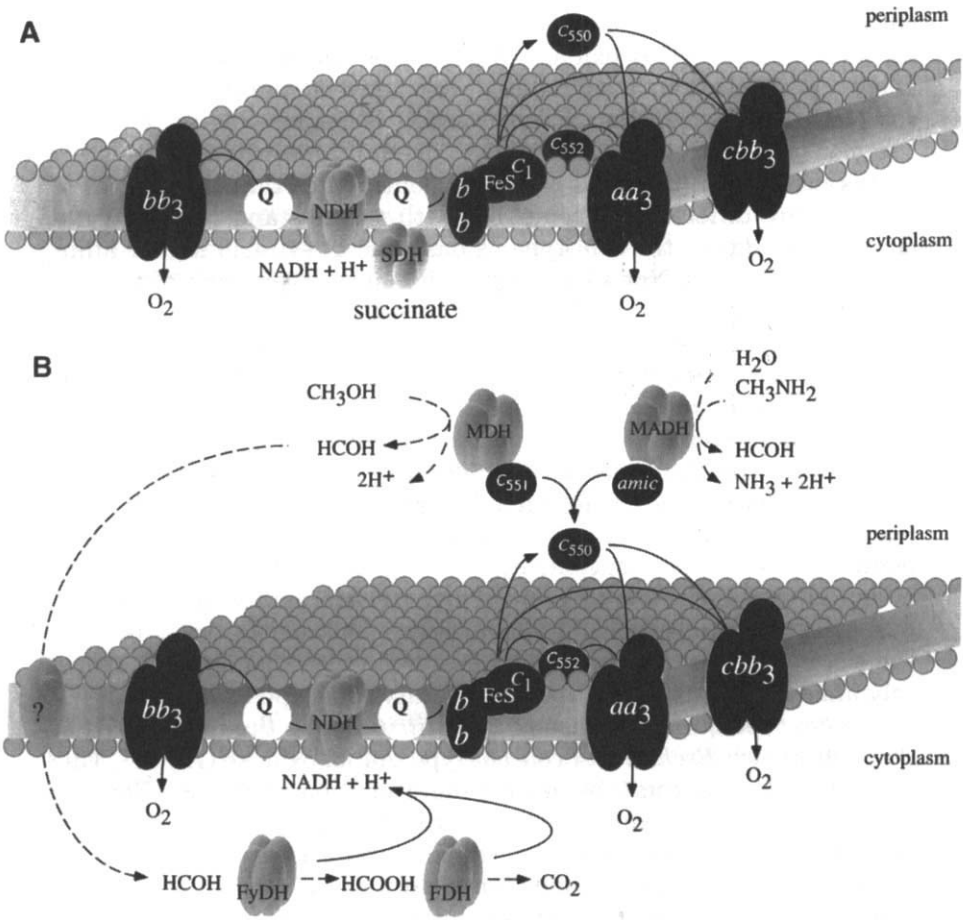

FIG. 2. The respiratory network of *P. denitrificans* during (A) aerobic heterotrophic growth and (B) methylotrophic growth. Common components of the two networks: NADH dehydrogenase (NDH), ubiquinone (Q), the cytochrome bc_1 complex (bb, FeS, c_1), cytochromes c_{550} and c_{552}, and the three oxidases: the aa_3-type cytochrome c oxidase (aa_3), the cbb_3-type cytochrome c oxidase (cbb_3), and the bb_3-type quinol oxidase (bb_3). Succinate dehydrogenase (SDH) is relevant during aerobic heterotrophic growth. Methanol dehydrogenase (MDH), methylamine dehydrogenase (MADH), amicyanin (amic), cytochrome c_{551i} (c_{551}), formaldehyde dehydrogenase (FyDH), formate dehydrogenase (FDH), and a putative formaldehyde carrier (?) are induced during methylotrophic growth. Solid arrows indicate the pathways of electron transfer; dashed arrows indicate molecule conversion and transfer.

N-oxides, ultimately yielding molecular nitrogen (denitrification). With respect to free energy transduction, these pathways are less efficient as compared to aerobic respiration because either they bypass the cytochrome bc_1 complex (route to nitrate reductase), or the branches terminate in non-energy-conserving enzymes (routes to the nitrite, nitric oxide, and nitrous oxide reductases). In addition, growth under this condition brings the bacterium in the apparent paradox of maintaining high electron fluxes to support competitive growth on the one hand, and of preventing the accumulation of the toxic intermediates nitrite and nitric oxide on the other hand. It may be anticipated that global and local regulatory pathways controlling the expression and/or activity of these oxidoreductases are optimally integrated to solve this paradox. Indeed, it has been determined that a number of regulatory proteins, among which are two members of the fumarate nitrate reductase (FNR) family of transcription activators (*8*, *47*), are involved in regulation of gene expression during the aerobic–anaerobic shift.

c. Autotrophic Growth. In the situation that *P. denitrificans* experiences a shortage of heterotrophic substrates, it can switch to autotrophic growth, during which hydrogen or thiosulfate are oxidized by hydrogenase or a thiosulfate-oxidizing enzyme, respectively (*48–50*). Carbon supply is accomplished by the fixation of atmospheric carbon dioxide via the Calvin cycle under this growth condition. The bacterium is also able to grow on C_1 substrates such as methanol or methylamine (*19*), a process considered as autotrophic growth too, because these carbon sources are oxidized merely with the purpose to gain energy (*26*).

In the presence of methanol as the sole source of energy, *P. denitrificans* induces the expression of the *mxa* gene cluster encoding methanol dehydrogenase (MDH) and its dedicated electron acceptor cytochrome c_{551i} (*14*, *51*). Both proteins are located in the periplasm and in subsequent redox steps they connect the oxidation of methanol to the reduction of cytochromes c_{550} and c_{552}. MDH consists of a large subunit (66 kDa; α-MDH) and a small subunit (9 kDa; β-MDH) that are complexed together in an α_2–β_2 tetrameric configuration (*52*, *53*). The large subunit has eight topologically identical antiparallel β-sheets arranged in a superbarrel structure with radial symmetry. The center of this structure makes up the active site pocket where the cofactor of the enzyme, pyrroloquinoline quinone (PQQ), is noncovalently incorporated in the protein structure, and in close contact with a Ca^{2+} ion. Methanol-oxidizing branches are found in a wide variety of methylotrophic bacteria (*54*). Apart from *P. denitrificans*, much of

the current knowledge on the physiology and molecular genetics of this system has been obtained from studies on the facultative methylotrophic bacteria *Methylobacterium extorquens* AM1, *Methylo bacterium organophilum* XX, and *Methylobacterium organophilum* DSM 760 (reviewed in Ref. *55*). Like in *P. denitrificans*, the methanol-oxidizing branch of these bacteria is composed of MDH, a dedicated cytochrome *c*L, a cytochrome *c*H (L and H refer to low and high isoelectric points, respectively), and a cytochrome *c* oxidase. The work of Lidstrom *et al.* (*55*) further revealed that the synthesis of a fully active methanol-oxidizing branch requires a total of at least 32 genes, among which are the *pqq* genes involved in cofactor biosynthesis, and a comprehensive set of so-called *mxa, mxb, mxc,* and *mxd* genes, some of which encode the structural enzymes, others of which encode enzymes involved in calcium insertion, and proteins involved in regulation of gene expression and protein activity (*55*).

Growth on methylamine is accompanied by the appearance in the periplasm of methylamine dehydrogenase and its electron acceptor amicyanin, both of which are encoded by the *mau* gene cluster (*15, 56–58*). Like MDH, MADH has an α_2–β_2 configuration made up by a small (16 kDa; β-MADH) and a large (47 kDa; α-MADH) subunit, which is also shaped like a superbarrel with radial symmetry (*59, 60*). The active site, however, is found in the small subunit (*61*). This site is created after the cross-linking and modification of two tryptophan residues of the peptide chain, resulting in the formation of the prosthetic group tryptophan-tryptophyl quinone. Electrons derived from the oxidation of methylamine are transferred via the blue copper protein amicyanin to the electron transport network at the level of cytochrome *c* (cyt c_{550}) (*62, 63*). Methylamine-oxidizing branches similar to that of *P. denitrificans* have also been identified in *P. versutus*, and *M. extorquens* AM1. Obligate (*Methylobacillus flagellatum* KT) and restricted facultative (*Methylophilus methylotrophus* W3A1) methylotrophic bacteria use similar branches for the oxidation of methylamine, but the dedicated electron acceptor of MADH in these bacteria appears to be either another type of blue copper protein, azurin (*64*), or a cytochrome *c* (*65, 66*), respectively, rather than amicyanin. The presence or absence of the latter redox carrier correlates with the presence or absence of its allocated gene, *mauC*, in the *mau* gene clusters of the different species.

In addition to the proteins expressed specifically during and involved in the oxidation of methanol and methylamine, a cytochrome c_{553i} is expressed during growth on these C_1 substrates (*5, 67*). The gene encoding this cytochrome (*cycB*) has been cloned and shown to

be part of the *xox* gene cluster (*68*). Surprisingly, the products of the genes located upstream and downstream of *cycB* (*xoxF* and *xoxJ*, respectively) have a large degree of similarity with α-MDH and MxaJ, respectively. The role of this putative oxidizing branch still remains obscure, because mutational analysis of this gene cluster did not reveal a clear function of the proteins (*68*).

The oxidation product of both methanol and methylamine is formaldehyde, which crosses the membrane into the cytoplasm. This transport process has been suggested to involve a specific formaldehyde carrier (*69*). In the cytoplasm, formaldehyde is further oxidized to formate via two consecutive reactions. In the first reaction, an NAD-linked glutathione-dependent formaldehyde dehydrogenase (FlhA) catalyzes the oxidation of formaldehyde into *S*-formylglutathione (*70*). In the second reaction, the latter molecule is converted into formate by *S*-formylglutathione hydrolase, which is a human esterase D homologue (*71*). The *flhA* gene cluster of *P. denitrificans* encoding the two enzymes has recently been identified upstream of the *xox* gene cluster (*72*). Finally, formate is oxidized to carbon dioxide predominantly by an NAD-dependent formate dehydrogenase (*54*). It has been reported, however, that *P. denitrificans* can synthesize isoenzymes of the formaldehyde and formate dehydrogenases that are NAD independent (*73*). A schematic view of the respiratory network that operates during C_1 metabolism is presented in Fig. 2B.

The free energy yield from the six-electron oxidation of methanol or methylamine to carbon dioxide may vary from 12 to 24 charge separations (q) per mole of substrate, depending on the types of oxidases and dehydrogenases that contribute to the electron transfer reactions. Two of the electrons that are released during the first step of oxidation of these sources are transferred to either of the two cytochrome *c* oxidases, via cytochrome *c* or amicyanin, yielding 4 q/mol substrate. In the case that the formaldehyde and formate dehydrogenases are both NAD dependent, transfer of the remaining four electrons may yield an additional 16 to 20 q/mol substrate, depending on the partitioning of electrons among the quinol oxidase on the one hand and the cytochrome bc_1 complex and the cytochrome *c* oxidases, on the other hand, at the level of the *Q* pool. In case the NAD-independent formaldehyde or formate dehydrogenases also contribute to the catabolic reactions, these values drop to 8 to 12 q/mol substrate because the energy-conserving NADH dehydrogenase complex is bypassed.

Counterparts of many redox enzymes of *P. denitrificans* are also present in *P. versutus*. Moreover, the DNA sequences of the genes and gene clusters encoding cytochrome c_{550} (*cycA*), the aa_3-type oxidase (*cta*

gene clusters), and the methylamine-oxidizing branch (*mau* gene cluster) have been shown to be strongly similar to their counterparts in *P. denitrificans* (*73a*). These findings indicate that the organization and function of the respiratory networks in both organisms resemble each other to a great extent. This resemblance is in agreement with the physiology of *P. versutus*, which has strong similarities to that of *P. denitrificans*. One of the differences appears to be that the former organism is unable to use methanol as source of energy.

B. Respiratory Genes and Their Expression

1. Control of Expression of Respiratory Genes

The expression of the components of the methanol- and methylamine-oxidizing branches is subject to complex regulatory cascades that have to orchestrate the optimal composition of the respiratory network under these growth conditions in order to maintain respiratory electron flows at competitive rates, on the one hand, yet to prevent the accumulation of the toxic intermediate formaldehyde on the other. Moreover, parts of these signal transduction systems coordinate gene expression according to an energetic hierarchy, ensuring that the C_1-oxidizing branches are expressed only when the cell is unable to metabolize energetically more favorable substrates (*19*). This view is corroborated by extensive physiological and biochemical studies on this type of metabolism. MADH and amicyanin are synthesized only when the cell uses methylamine (and to a lesser extent other alkylamines) as sole source of energy (*15*, *74*). MDH and XDH and their dedicated cytochromes, on the other hand, are expressed not only during growth on methanol but also during growth on methylamine or choline. Because the oxidation of all these carbon sources yields formaldehyde, it has been postulated that the latter molecule is an important trigger in the regulation of expression of their allocated gene clusters (*73*). The synthesis of all enzymes involved in the oxidation of methanol or methylamine is blocked when heterotrophic growth substrates are available next to these C_1 substrates (*14*, *15*). Growth during C_1 metabolism also affects the regulation of expression of the other components of the branches, cytochrome c_{550} and the cytochrome *c* oxidases. The amount of these components increases two- to fivefold as compared to heterotrophic growth (*24*). Apparently, this increased supply meets the demands on increased velocities of electron transfer within this part of the respiratory network. A number of different regulatory proteins that control

the expression of the *flh, xox, mxa*, and *mau* gene clusters (*75*), as well as that of the *cco* and *qox* gene clusters, have been identified (*8*).

a. mxa Gene Cluster. Expression of the *mxa* genes is controlled by the gene products of the *mxaXYZ* genes, which are located upstream of the structural *mxa* gene cluster (*14*). MxaY and MxaX are a protein histidine kinase and a DNA-binding response regulator, respectively, a set of proteins that belongs to the family of two-component regulators. As suggested above, the effector molecule for the sensor domain of MxaY is probably formaldehyde. The general principle for signal transduction via two-component regulatory systems is that binding of the effector molecule triggers the autophosphorylation of the kinase, after which the phosphate group is transferred to the response regulator. Once phosphorylated, the latter may bind to the promoter region of its target gene in order to facilitate transcription by the RNA polymerase (*76*). Surprisingly, however, MxaY was shown to be dispensable in this cascade, suggesting that an alternative kinase takes over its role (*77*). The role of MxaZ in this cascade is still unclear. The MxaYX regulatory system appears to be specifically dedicated to the regulation of expression of the *mxa* genes; *mxaX* mutants showed an unimpaired expression of the *mau*, *flhA*, and *xox* genes (*14*, *75*). A two-component system, MxcQE, with a function similar to that of MxaYX, has now also been identified in *M. organophilum* XX. Its allocated gene cluster, however, is separated more than 40 kb from its target *mxa* gene cluster (*78*).

b. mau Gene Cluster. The *mau* gene cluster of *P. denitrificans* consists of 11 genes. Of these, 10 encode the structural proteins and proteins involved in cofactor biosynthesis and are transcribed in one direction; the 11th one is located upstream and is divergently transcribed (*15*, *57*, *58*). It encodes MauR, which is a transcription activator that belongs to the family of one-component LysR-type regulators. The spatial organization of the functional domains involved in DNA binding, signal perception, and dimerization in the members of this family is conserved (*79*). Usually the target locus of this type of regulator codes for a set of proteins that oxidize a particular substrate. The substrate molecule in turn serves as the trigger for the activation of the LysR regulator. This characteristic would be in agreement with the suggestion that methylamine is the molecule that triggers the expression of the *mau* gene cluster. The current view with respect to the mode of action of LysR-type regulators is that signal perception (i.e., binding of the activator molecule) induces dimerization of the regulator followed by binding to a target site up-

stream of the promoter. As a result, the dimer may come into contact with RNA polymerase, after which transcription is initiated. In agreement with this view is the observation that MauR binds to the *mau* promoter region in a band-shift assay (*80a*). The target site for LysR-type activators is usually a conserved T-N11-A motif that harbors small palindromic sequences at its ends. Such a motif, however, has not been recognized in the *mau* promoter region, indicating that the target site of MauR is slightly different from the conserved one. The target site for CatR, another member of the family of the LysR-type activators, is G-N11-A (*80b*), suggesting that small deviations of the target sequence indeed occur. Promoter probe studies have further shown that *mau* gene expression increases almost 1600-fold during growth on methylamine as compared to heterotrophic growth. This increase was not observed in the MauR mutant, which confirms that MauR is responsible for the increase in gene expression in the wild type (*80a*). The expression of the *mauR* gene is more or less constant, and independent of the growth condition or the concentration of MauR. Apparently, its expression is not autoregulated, a feature different from that of most other *lysR*-type genes. A counterpart of *mauR* has also been described in *P. versutus,* although the orientation of it is opposite to that of the *P. denitrificans* gene (*81*). Analysis of the corresponding region upstream of the *mau* gene cluster from *M. extorquens* AM1 did not reveal sequences with similarity to *mauR* (*56*).

c. Hierarchical Control. Apart from regulation by their cognate activators, the regulation of the expression of both *mxa* and *mau* gene clusters is subject to some kind of hierarchical control that suppresses transcription during heterotrophic growth. Indeed, it has been shown that the expression of the *mau* genes is virtually blocked in the situation that the bacterium grows in the simultaneous presence of succinate and methylamine. Further, both MADH and MDH are absent once succinate is added to the growth medium in addition to their corresponding substrates (*19*). The view that a global transcription activator is responsible for these phenomena has recently been corroborated by the analysis of a mutant disturbed in many aspects of C_1 metabolism (*75*). This mutant was unable to grow on methanol, methylamine, or choline. Moreover, the expression of the *flhA, mxa, mau,* and *xox* genes was completely blocked. These pleiotropic effects were explained by assuming that the mutated gene in this strain encodes a regulator that affects the expression of all these C_1 genes and gene clusters. Apparently, this regulator is not a repressor protein

because in the mutant in which the regulator gene has been knocked out one would expect constitutive expression rather than repression. Therefore, it has been suggested that this protein acts as a second activator in synergism with either of the two dedicated activators of *mxa* and *mau* gene expression. If this view is correct, one may expect that the presence and/or activity of this second activator is suppressed during heterotrophic growth. The identification of its allocated gene has been facilitated by the isolation of a genomic locus that fully complements the mutation. A scheme of the regulatory pathways that control gene expression during C_1 metabolism is shown in Fig. 3.

d. Redox Control. The expression of *cycA* and the *cta* and *cco* gene clusters, encoding cytochrome c_{550} and the aa_3-type and cbb_3-type cytochrome *c* oxidases, respectively, is also controlled by regulatory pathways that respond to the switch from heterotrophic growth to C_1 me-

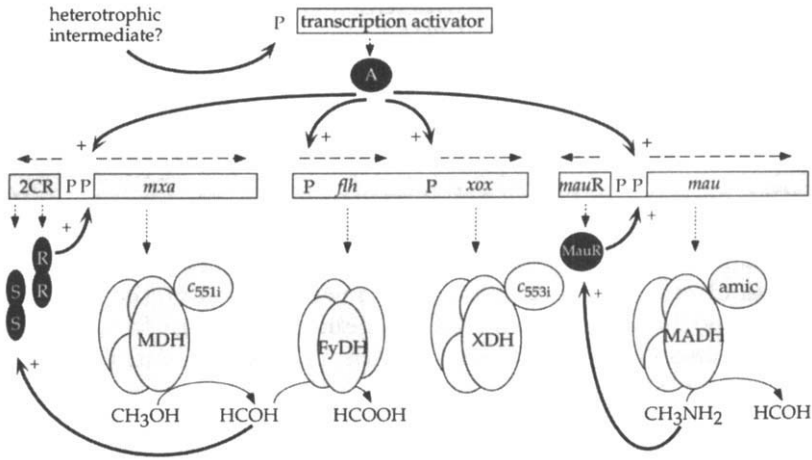

FIG. 3. Model of regulatory pathways involved in C_1 metabolism in *P. denitrificans*. Genes and gene clusters are boxed; promoter regions (P) are designated. Structural proteins are methanol dehydrogenase (MDH), methylamine dehydrogenase (MADH), formaldehyde dehydrogenase (FyDH), the product of the *xox* genes (XDH), the cytochromes c_{551i} (c_{551i}) and c_{553i} (c_{553i}), and amicyanin (amic). Regulatory proteins (shaded) are the proposed formaldehyde sensor MxaY (S, dimer), and its allocated regulator MxaX (R, dimer) encoded by their corresponding *mxa* two-component regulatory genes (2CR), the LysR-type activator of *mau* gene expression (MauR), and the proposed global activator (A). Dotted arrows represent the transcription–translation process. Dashed arrows indicate the direction of transcription. Thin solid lines indicate substrate conversion. Thick solid lines indicate the processes involved in signal transduction and regulation (+, positive; −, negative).

tabolism. The cbb_3-type oxidase is hardly detectable in cells grown heterotrophically at relatively high (atmospheric) oxygen concentrations, but its synthesis increases when the cell experiences a shortage of oxygen or when it grows on C_1 compounds (*6*, *22*). In the former situation the electron output rate is limiting, whereas in the latter one the electron input rate increases, thus one might expect that the components in the respiratory network become more reduced under these growth conditions. The suggestion that a change of the redox potential of one of these components is the trigger for increased expression of the *cco* gene cluster has recently been corroborated by the finding of a homologue of the *E. coli* FNR protein in *P. denitrificans*, designated FnrP (*35*). FNR in *E. coli* dictates the extent of expression of a number of genes involved in the aerobic–anaerobic switch (*82*, *83*). The protein has a redox-sensitive [4Fe–4S] cluster that is supposed to either sense the oxygen concentration or the redox state of one of the components of the respiratory network. Reduction of the cluster triggers a conformational change, on which the protein dimerizes and binds to its target site, a so-called FNR-box (*82*, *84*). This box harbors a conserved TTGAT–ATCAA sequence motif, which is usually located directly upstream of the RNA polymerase binding site. This organization makes sure that the FNR dimer and RNA polymerase bind next to each other on the DNA, thereby allowing physical contact between these two protein complexes. Once this occurs transcription starts. The functional domains of FNR are also present in FnrP from *P. denitrificans* (*47*). A knock-out of its allocated gene resulted in a number of effects on gene expression, among which was a decrease of *cco* gene expression to a residual 25% of the wild-type level, and a threefold increase of *qox* gene expression. In agreement with this observation was the finding of an FNR-box within the promoter regions of the *cco* and *qox* gene clusters. The mutation did not affect the expression of cytochrome c_{550} or the aa_3-type oxidase. Moreover, the promoter regions of their allocated genes do not contain an FNR-box. Analyses of strains with promoter–reporter gene fusions have revealed that the expression of the *cycA* gene increases 10- to 20-fold in cells grown on methanol or methylamine as compared to succinate-grown cells (*85*). Further, the authors came across two different *cycA* promoters. Perhaps one of these promoters is switched on for elevated gene expression during C_1 metabolism. The amount of aa_3-type oxidase increases twofold during C_1 metabolism. As yet, virtually nothing is known about the nature and mode of action of the transcription regulators controlling their expression in response to

the growth condition. Whether one of the regulatory proteins identified in the C_1 signal transduction network is required for the observed boost in induction of gene expression during growth on C_1 substrates is a matter of speculation.

III. Structure and Function of the MADH Redox Chain Components

A. Structure and Function of Amicyanin and Cytochrome c_{550}

1. *Amicyanin*

a. Structure. Amicyanin (AmCu) is a member of the type 1 blue (cupredoxin) family of copper proteins. The protein functions as the obligate electron acceptor for the enzyme methylamine dehydrogenase in the methylamine-utilizing redox chain of *P. versutus* and *P. denitrificans* (*86*). The primary structures of amicyanin from these two sources (*86*, *87*) are compared in Table I. It is clear that the homology between the two amicyanins is high, with 63% identity of amino acid residues. The three-dimensional structure of the oxidized AmCu(II) form of the protein from *P. versutus* has been solved by X-ray crystallography (*88*), and the NMR-derived solution structure of the diamagnetic reduced protein is also available (*89*). Amicyanin from *P. denitrificans* has also been studied crystallographically in its Cu(II) state (*90*, *91*) with the structure obtained showing very high similarity to that of the *P. versutus* protein (*vide infra*). By far the most interesting aspect of the crystallographic studies on *P. denitrificans* amicyanin is the availability of the structure of its binary complex with MADH (*92*) and also that of a ternary complex with MADH and cytochrome c_{551i} (*93*, *94*). These studies will be discussed in more detail in a later section of this review.

The structural studies on amicyanin from *P. versutus* show that the protein consists of nine β-strands that form into two antiparallel β-sheets, giving the molecule an overall structural motif known as a β-sandwich (see Fig. 4). This overall topology is very similar to that of other structurally characterized cupredoxins, with the homology to plastocyanin being greatest (*87*). The only notable difference between amicyanin and most other cupredoxin structures is the presence of a 21-residue N-tereminal extension that forms an extra β-strand in the structure. The recently published structural studies (*95*, *96*) on the type 1 blue copper protein rusticyanin show that it, too, possesses an

TABLE I

COMPLETE AMINO ACID SEQUENCES OF AMICYANINS FROM *Paracoccus versutus* AND *Parococcus denitrificans*[a]

P. versutus	Gln	Asp	Lys	Ile	Thr	Val	Thr	Ser	Glu	Lys	Pro	Val	Ala	Ala	Ala	15
P. denitrificans		Asp	Lys	Ala	Thr	Ile	Pro	Ser	Glu	Ser	Pro	Phe	Ala	Ala	Ala	
P. versutus	Asp	Val	Pro	Ala	Asp	Ala	Val	Val	Val	Gly	Ile	Glu	Lys	Met	Lys	30
P. denitrificans	Glu	Val	Ala	Asp	Gly	Ala	Ile	Val	Val	Asp	Ile	Ala	Lys	Met	Lys	
P. versutus	Tyr	Leu	Thr	Pro	Glu	Val	Thr	Ile	Lys	Ala	Gly	Glu	Thr	Val	Tyr	45
P. denitrificans	Tyr	Glu	Thr	Pro	Glu	Leu	His	Val	Lys	Val	Gly	Asp	Thr	Val	Tyr	
P. versutus	Trp	Val	Asn	Gly	Glu	Val	Met	Pro	His	Asn	Val	Ala	Phe	Lys	Lys	60
P. denitrificans	Trp	Ile	Asn	Arg	Glu	Ala	Met	Pro	His	Asn	Val	His	Phe	Val	Ala	

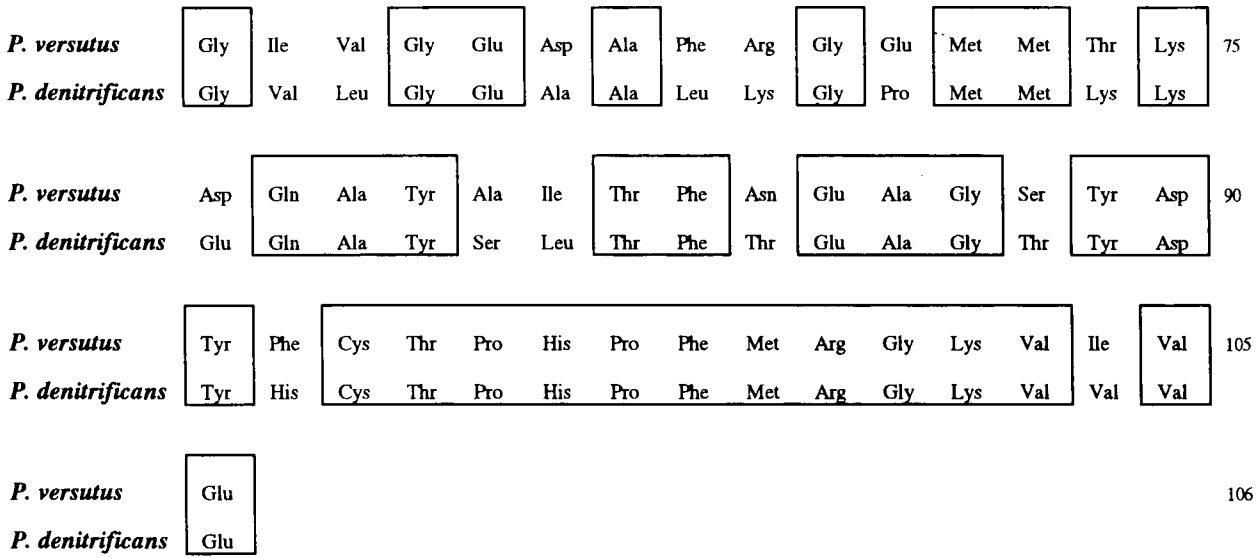

[a] Data for *P. versutus* from Ref. *73a*; data for *P. denitrificans* from Ref. *63*. Identical residues are boxed.

FIG. 4. Representation of the three-dimensional structure of *P. versutus* amicyanin.

N-terminal extension, but in this case it is 35 residues long and is involved in three β-strands that contribute to both β-sheets of the protein.

The single copper atom that makes up the active site of amicyanin is found at one end of the β-sandwich (Fig. 4). The metal is strongly coordinated by the S of a cysteine (Cys-93) and the N^{δ} atoms of two histidine ligands (His-54 and His-96). The copper atom is displaced by 0.4 Å from the plane of these three equatorial ligands in the direction of a distant axial methionine ligand. The active site of oxidized amicyanin from *P. versutus* is shown in Fig. 5 and the bond lengths and angles found for this protein and that from *P. denitrificans* are listed in Table II. From the numbering of the amino acids in Fig. 5 it is clear that one of the histidine ligands (His-54, *P. versutus* numbering) is found at some distance in the primary structure from the three other coordinating residues, which are found close together on a single loop. The C-terminal ligand-containing loop is a common feature of all the cupredoxins and the length of this loop in amicyanin is the shortest of all the type 1 blue copper proteins.

Another feature of amicyanin that is common to all structurally investigated cupredoxins is the presence of a hydrophobic patch on the protein surface, which surrounds the exposed imidazole ring of

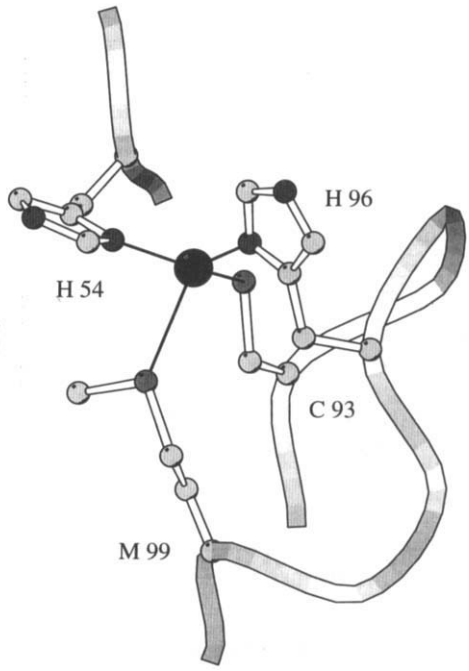

FIG. 5. Representation of the Cu site of *P. versutus* amicyanin, highlighting the loop that contains the three copper ligands Cys-93, His-96, and Met-99. The copper atom is indicated by the dark sphere in the center of the figure.

the C-terminal histidine ligand (His-96 in the case of amicyanin). This patch has been proposed as the main port of entry and exit of electrons into and out of the active sites of cupredoxins.

b. Spectroscopy. Spectroscopically, oxidized amicyanin from *P. versutus* is typical of a type 1 blue copper protein, with a main visible absorption band at 596 nm, due to a $p\pi S(Cys) \rightarrow d_{x^2-y^2}$ Cu(II) charge transfer transition (*97–99*) and a hyperfine coupling constant of 5.3 mT in its EPR spectrum. It is known that although the cupredoxins are classified together on the basis of spectroscopic similarities, the fine details of these features differ from one member of the family to another. Two distinct classes of cupredoxins have been identified on the basis of specific spectroscopic features. These are the type 1 axial sites in which the g_x and g_y values are close together and which have little absorption at around 460 nm in their visible spectra [this second electronic transition has been assigned as a $\sigma S(Cys) \rightarrow d_{x^2-y^2}$ Cu(II)

TABLE II

BOND DISTANCES AND ANGLES AT THE ACTIVE SITE OF AMICYANIN FROM *P. versutus* AND *P. denitrificans*

Parameter	AmCu(II) *P. versutus*	AmCu(II) *P. denitrificans*
Resolution (Å)	2.15	1.31
Bond lengths (Å)		
Cu–$N^{\delta 1}$ (His-54)[a]	2.04	1.95
Cu–S^{γ} (Cys-93)	2.13	2.11
Cu–$N^{\delta 1}$ (His-96)	2.13	2.03
Cu–S^{δ} (Met-99)	2.84	2.90
Bond angles at copper atom (degrees)		
$N^{\delta 1}$ (His-54)–Cu–S^{γ} (Cys-93)	132	136
$N^{\delta 1}$ (His-54)–Cu–$N^{\delta 1}$ (His-96)	104	104
$N^{\delta 1}$ (His-54)–Cu–S^{δ} (Met-99)	84	84
S^{γ} (Cys-93)–Cu–$N^{\delta 1}$ (His-96)	111	112
S^{γ} (Cys-93)–Cu–S^{δ} (Met-99)	117	110
$N^{\delta 1}$ (His-96)–Cu–S^{δ} (Met-99)	101	100

[a] *Paracoccus versutus* numbering.

charge transfer transition (*98*, *99*)]. The second class of cupredoxin active sites has more rhombic EPR spectra features accompanied by an increased absorption at 460 nm (*97–99*). The amicyanins from *P. versutus* (*100*) and *P. denitrificans* (*62*, *101*) both have type 1 axial sites, which is thought to be consistent with a relatively long Cu–S (Met) axial bond length [crystallographic studies have shown that in type 1 rhombic sites the Cu–S(Met) bond is significantly shorter (*95*, *96*, *102–105*)]. The relationship between the spectroscopy and active site structure of these two classes of type 1 copper center is supported by resonance Raman studies (*106*, *107*) showing that the more rhombic sites have a longer Cu–S(Cys) bond length.

Recently an additional spectroscopic technique has been utilized to quantify the extent of the axial interaction at the active sites of cupredoxins. This involves the observation and interpretation of the paramagnetically shifted signals in the ^1H NMR spectrum of the oxidized protein, and the pioneering work has been carried out on amicyanin (*108*). It has been possible for the first time to observe shifted ligand proton (resonances and assign them using exchange spectroscopy on 50:50 mixtures of oxidized and reduced samples, so as to correlate the paramagnetic resonances with their assigned diamagnetic counterparts. The paramagnetic ^1H NMR spectra of wild-type amicyanin, two amicyanin mutants (*vide infra*), and type 1 blue cop-

per protein azurin are shown in Fig. 6. On comparing the spectra for amicyanin and azurin it is clear that in the latter the $C^{\gamma}H$ resonances of the axial Met ligand are not shifted outside of the diamagnetic envelope, whereas in amicyanin they are found at ~11–12 ppm. Because the observed shifts are mainly due to Fermi-contact contributions (i.e., delocalization via covalent bonds) this demonstrates the presence of covalency of the Cu–S(Met) interaction in amicyanin and not in azurin. This is also consistent with the shorter reported Cu–S (Met) distance in amicyanin (2.8 Å) as compared to azurin (3.1 Å). One of the amicyanin mutants has a rhombic type 1 site (*vide infra*) and consistent with this the shift of the $C^{\gamma}H$ Met resonances is much larger (see Fig. 6C).

c. pH Switch. A distinctive feature of amicyanin is that, in the reduced form, the ligand His-96 protonates with a pK_a of 6.7. This behavior was originally observed in NMR studies (*109*, *110*) and later in extended X-ray absorption fine structure (EXAFS) (*111*), kinetic (*112*), and electrochemical (*113*) experiments. The protonation of His-96 results in a trigonal geometry at the Cu(I) center. Because such a coordination environment is favorable for Cu(I), as compared to the cupric form of the protein, an increase in the reduction potential, on protonation, is observed (Fig. 7). This behavior of amicyanin is another feature that strengthens the analogy to plastocyanin (PCu), which also undergoes a similar active site protonation (*114–118*). In the case of PCu(I), crystallographic studies have been carried out at various pH values (*117*). In these investigations structural details of the protonation processes are obtained and these are illustrated qualitatively in Fig. 8. The presence of a second conformation of the protonated histidine, as depicted in Fig. 8, is evident in NMR studies on both amicyanin (*110*) and plastocyanin (*118*). An intriguing difference between PCu(I) and AmCu(I) lies in the pK_a value for the protonatable histidine ligand. In PCu(I), a value of ~5 is found whereas the pK_a in AmCu(I) is almost 2 pH units higher. The possible physiological role that the active site protonation plays in the case of amicyanin will be addressed later in this review. However, at this stage it is interesting to note that plastocyanin functions in the inner thylakoid of the chloroplast, where the pH is known, under illumination, to be quite acidic, whereas amicyanin is thought to function physiologically at more neutral pH values. The type 1 blue copper protein pseudoazurin also undergoes an active site protonation, in its reduced state, with a pK_a value similar to that of plastocyanin (*119–121*).

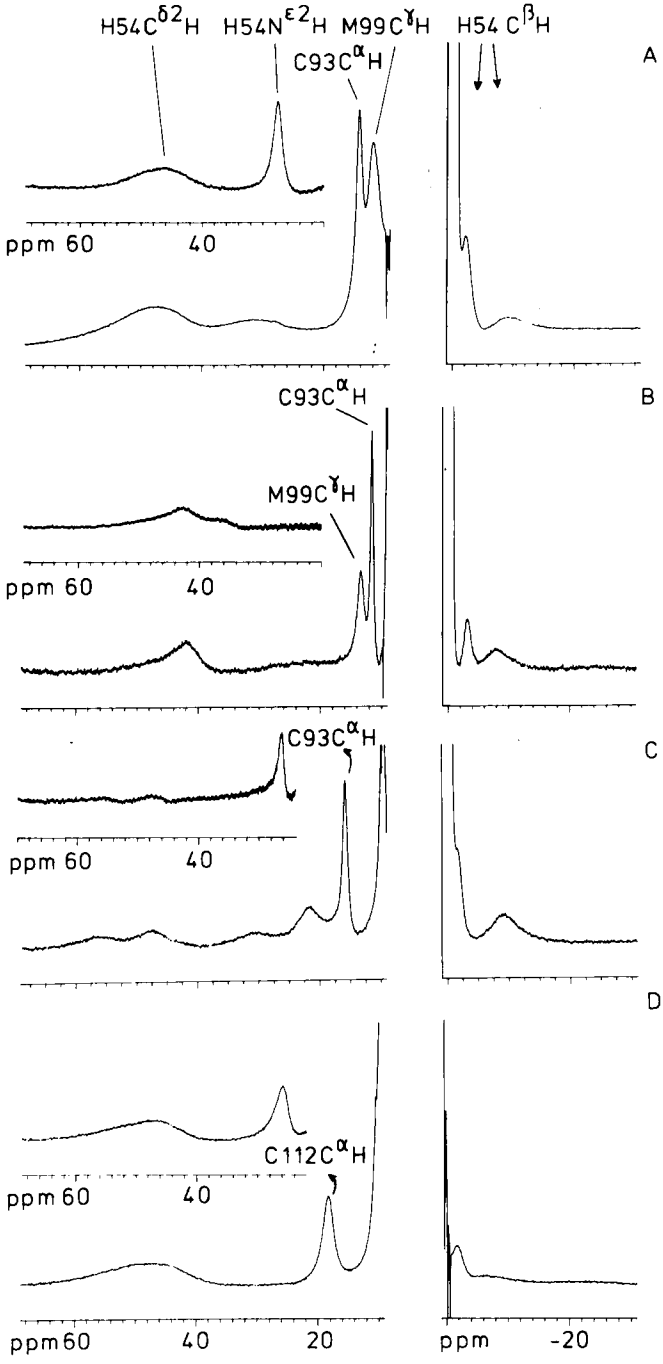
H54C$^{\delta 2}$H
H54N$^{\epsilon 2}$H
M99C$^{\gamma}$H
C93C$^{\alpha}$H
H54 C$^{\beta}$H
A
ppm 60
40
C93C$^{\alpha}$H
B
M99C$^{\gamma}$H
ppm 60
40
C93C$^{\alpha}$H
C
ppm 60
40
D
C112C$^{\alpha}$H
ppm 60
40
ppm60
40
20
ppm
-20

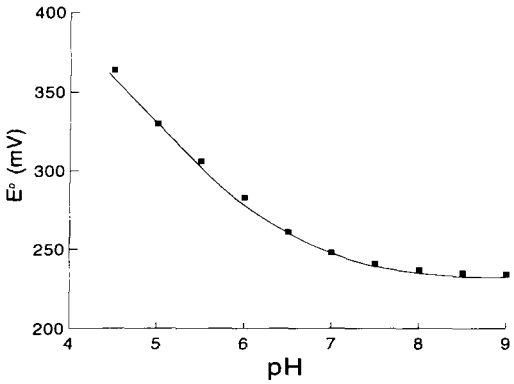

FIG. 7. Variation of the reduction potential ($E°$) of wild-type amicyanin with pH (I = 0.10 M, NaCl). The values are obtained from cyclic voltammetry and are all referenced to the NHE at 22°C. The line shown is the fit to the following equation (*113*): $E°$ (pH) = $E°$ (high pH) + (RT/nF) ln(1 + [H^+]/K_a^{red}).

d. Electron Self-Exchange. Amicyanin functions as an electron transfer protein. A basic property of all redox couples is the process of electron self-exchange, whereby the two oxidation states involved interconvert according to the following equation:

$$\text{AmCu(I)} + \text{AmCu(II)} \rightleftharpoons \text{AmCu(II)} + \text{AmCu(I)}.$$

The study of electron self-exchange rates are therefore facilitated by the fact that the process has no driving force. The self-exchange rate constant provides an intrinsic measure of the electron transfer capabilities of a redox metalloprotein. Reported self-exchange rate constants for cupredoxins range from 10^3 to 10^6 M^{-1} sec^{-1} (*122*). In all cases it is believed that type 1 blue copper proteins self-exchange via their hydrophobic patches and that electron transfer occurs through the exposed histidine ligand. However, this has only been proved in the case of the cupredoxin azurin (*123–125*). The observed self-exchange rate constant (25°C) of 1.2 × 10^5 M^{-1} sec^{-1} for amicyanin at

FIG. 6. One-dimensional water eliminated Fourier transform spectroscopy (WEFT) spectra of (A) wild-type amicyanin; (B) the amicyanin mutant H96D; (C) the amicyanin mutant H^{96}PFM → H^{96}QGAGM; (D) wild-type *Pseudomonas aeruginosa* azurin. The diamagnetic region from 9 to 1 ppm has been omitted from the centers of the spectra. The insets show the spectra in H_2O, where an additional peak from an exchangeable proton appears. Peak assignments for wild-type amicyanin are given at the top of panel A. All spectra were collected at 32°C on samples containing 50 mM phosphate, pH 7.0.

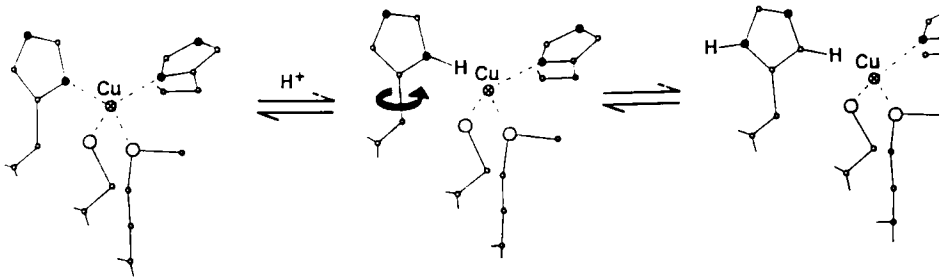

FIG. 8. The H^+-induced dissociation of the Cu(I)—N(His-96) bond of amicyanin, and the existence of two conformers of the protonated form.

pH 8.2, which is almost independent of ionic strength (*110*), is intermediate in the range of values reported for cupredoxins (10^3 to 10^6 M^{-1} sec^{-1}). Plastocyanins from higher plants and green algae have self-exchange rate constants of $\sim 10^3$ M^{-1} sec^{-1} (*126*). These small rate constants are thought to be due to the presence of a large acidic patch on the protein surface, resulting in a large electrostatic repulsion during the self-exchange process. The cupredoxin with the largest self-exchange rate constant is azurin (*127*), which does not have any areas of localized charge on its surface and hence protein–protein association is thought to be facilitated. The intermediate value for amicyanin may reflect the presence of a number of basic residues around the periphery of the hydrophobic patch. The self-exchange rate constant of amicyanin is diminished at lower pH values due to the protonation of His-96 (*110*). This leads to an increased reorganization barrier on going from three-coordinate Cu(I) to four-coordinate Cu(II) and hence the rate of electron transfer is lowered.

e. Mutants. The use of mutagenesis in the study of amicyanin has focused on the active site, with two types of changes made. The first of these involves single mutations of ligating amino acids, whereas the second type has focused on changing a whole ligand-containing loop ("loop-directed mutagenesis"). The axial ligand Met-99 has been replaced with a glutamine (*128*). The identical mutation of the axial Met-121 ligand of azurin has previously been carried out. However, subtle differences exist at the active sites of these two cupredoxins, making the comparison of the effect of the same mutation in the two proteins intriguing. The mutation has a very similar effect in both amicyanin and azurin, with the only difference being a less rhombic EPR spectrum in the former. Both the M99Q

and M121Q mutants of amicyanin and azurin, respectively, are good models for the active site of stellacyanin, which naturally has an axial glutamine ligand.

The replacement of the equatorial ligand His-96 by an aspartate has also been carried out in amicyanin (*129*). The mutant binds Cu(II) to give a variant that is spectroscopically and probably structurally similar to the wild-type protein. The electron self-exchange rate constant of both the M99Q and the H96D amicyanin mutants is considerably diminished, by approximately two orders of magnitude, when compared to the wild-type value of $1.2 \times 10^5\ M^{-1}\ sec^{-1}$. In the case of the H96D mutant it is possible that the efficient electron transfer pathway, involving His-96, has been destroyed. This is further highlighted by the fact that wild-type amicyanin gives a good electrochemical response at a bare glassy carbon electrode but that the H96D mutant does not. An alternative argument could be that in both the H96D and M99Q variants the reorganization energy of the site has been increased by the mutations made.

As mentioned earlier in this section, three of the four active site ligands in cupredoxins are situated close together on a single loop (see Fig. 5). In Table III the loops found in this area of three different cupredoxins are shown. To investigate the role the length and composition of this loop have on the active site properties of amicyanin the corresponding loops from plastocyanin (*113*) and azurin (*130*) have been introduced. The properties of these mutants are compared to wild-type protein in Table IV. In both cases a novel site that is produced does not resemble, spectroscopically, wild-type amicyanin or

TABLE III

C-TERMINAL LIGAND-CONTAINING LOOP OF *Paracoccus versutus* AMICYANIN, POPLAR PLASTOCYANIN, *Alcaligenes faecalis* S-6 PSEUDOAZURIN, AND *Pseudomonas aeruginosa* AZURIN

Protein		Partial C-terminal amino acid sequences													
Amicyanin	93	Cys	Thr	—	Pro	—	His	Pro	—	—	Phe	Met			
Plastocyanin	84	Cys	Ser	—	Pro	—	His	Gln	Gly	Ala	Gly	Met			
Pseudoazurin	78	Cys	Thr	—	Pro	—	His	Tyr	Ala	Met	Gly	Met			
Azurin	112	Cys	Thr	Phe	Pro	Gly	His	Pro	—	Ala	Leu	Met			

TABLE IV

COMPARISON OF THE PROPERTIES OF WILD-TYPE AMICYANIN AND THE PLASTOCYANIN AND AZURIN LOOP MUTANTS

Properties	Wild type	Plastocyanin loop	Azurin loop
Main visible absorption (nm)	596	593	608
$A_{\sim 450}/A_{\sim 600}$	0.10	0.26	0.19
EPR	Axial	Rhombic	Rhombic
Reduction potential (pH 7.0, mV)	234	301	n.d.[a]
Active site pK_a	6.7	5.6	<5.7

[a] n.d., Not determined.

the protein whose active-site loop was introduced. It is also interesting to note that in both cases the pK_a for His-96 is >1 pH unit lower and that the rate of electron self-exchange is diminished.

A final loop-directed mutagenesis experiment carried out on amicyanin involved the introduction of a dinuclear Cu_A center, such as that found in subunit II of CCO (Fig. 9) (*131*). This was achieved by replacing the wild-type loop between Cys-93 and Met-99 with the sequence AEICGPGHSG containing an additional cysteine. The Cu_A variant has spectroscopic properties very similar to those of native Cu_A cen-

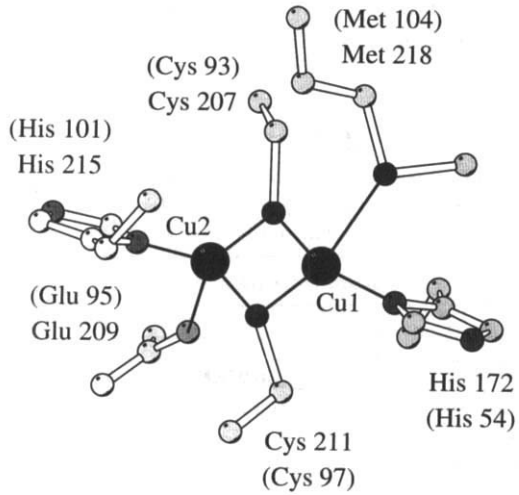

FIG. 9. Representation of the engineered Cu_A site in the soluble domain of subunit II of the bo_3 quinol oxidase from *E. coli* (*37*).

ters (Fig. 10). The paramagnetic form of this mutant has been studied using proton NMR. In this case, as compared to that of wild-type amicyanin (Fig. 11), much sharper isotropically shifted ^1H NMR resonances are observed (*132*), due to much faster electronic spin relaxation. The Fermi-contact shifts have been used to provide detailed information concerning the spin density distribution on the Cu_A ligands. The amount of spin density on the ligands is approximately the same in the Cu_A center as in the mononuclear type 1 site. However, in the former this involves two cysteine and two histidine ligands. The two weak axial interactions at the Cu_A site carry less than 1% spin density and probably have very little covalency. A comparison to the spectrum of the soluble Cu_A domains of the CCOs from *B. subtilis* (*133*) and *P. versutus* (*134*) confirm the similarity of the electronic structure of the Cu_A amicyanin mutant to those of native sites.

2. *Cytochrome c_{550}*

a. Structure. The cytochrome *c* (cyt *c*) component of the MADH redox chain is the monoheme type I cyt c_{550} (also known as cyt c_2). The amino acid sequences of the cyt c_{550}s from *P. versutus* (*135*) and *P. denitrificans* (*136*) are shown in Table V. From this comparison it is clear that there is a strong similarity (84%) between the proteins from these two sources. Cytochrome c_{550} is one of the larger of the bacterial members of this class of metalloproteins and exhibits the highest similarity to the mitochondrial cyt *c* (*137*). A major difference between the bacterial cyt c_{550}s and the mitochondrial cyt *c*s is the presence of a C-terminal 13- to 16-amino-acid-long tail in the former.

The three-dimensional structure of cyt c_{550} from *P. versutus* is not currently available, although NMR studies have provided details of the secondary structure elements plus the dynamic properties of the protein (*138*). The crystal structure of cyt c_{550} from *P. denitrificans* has been reported (*139*) at 1.7 Å resolution (see Fig. 12). The structure shows that the heme group is surrounded by five helices. The protoporphyrin IX ring is covalently attached to the protein via thioether linkages between its vinyl groups and two N-terminal cysteine residues of the protein. Typically, the cysteines are found in the consensus sequence CXXCH. The iron component of the heme is further attached to the protein via two axial ligands: the $N^{\varepsilon 2}$ of His-19 and the S^{δ} of Met-100. The complex environment of the heme in *P. denitrificans* cyt c_{550} also consists of a number of hydrogen bonding interactions involving six water molecules, the side chains of Thr-35, Arg-45, Tyr-55, Trp-71, and Tyr-79, plus a number of protein backbone groups.

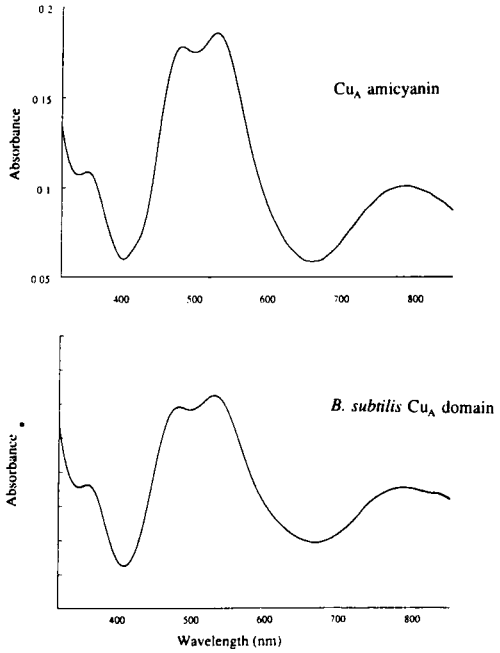
Cu$_A$ amicyanin
Absorbance
0.2
0.15
0.1
0.05
400
500
600
700
800
B. subtilis Cu$_A$ domain
Absorbance
Wavelength (nm)

A

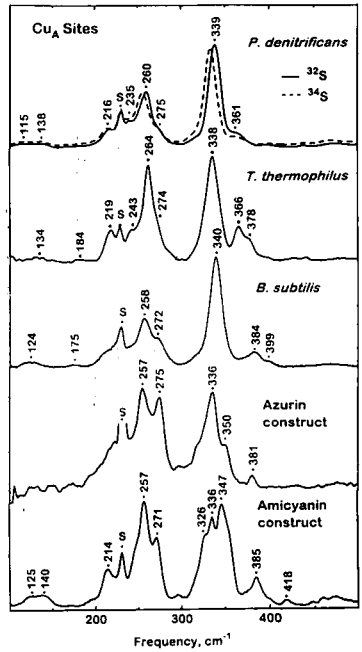
Cu$_A$ Sites
P. denitrificans
^{32}S
^{34}S
115
138
216
235
260
275
339
361
338
264
T. thermophilus
134
184
219
243
274
340
366
378
B. subtilis
124
175
258
272
384
399
Azurin construct
257
275
336
350
361
Amicyanin construct
214
257
271
326
336
347
385
418
125
140
200
300
400
Frequency, cm^{-1}

C

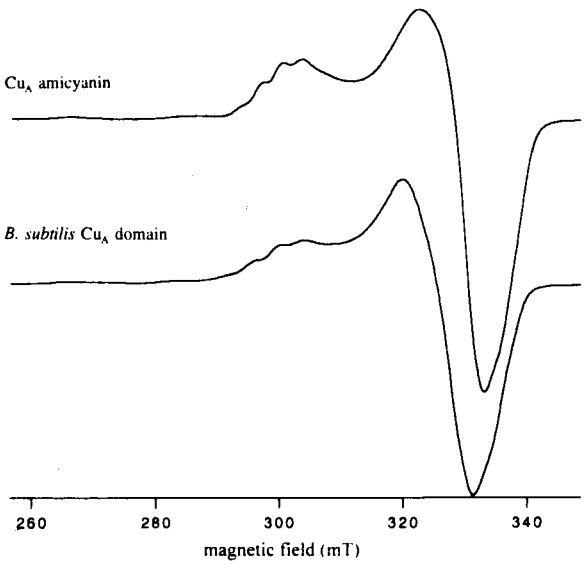
Cu$_A$ amicyanin
B. subtilis Cu$_A$ domain
260
280
300
320
340
magnetic field (mT)

B

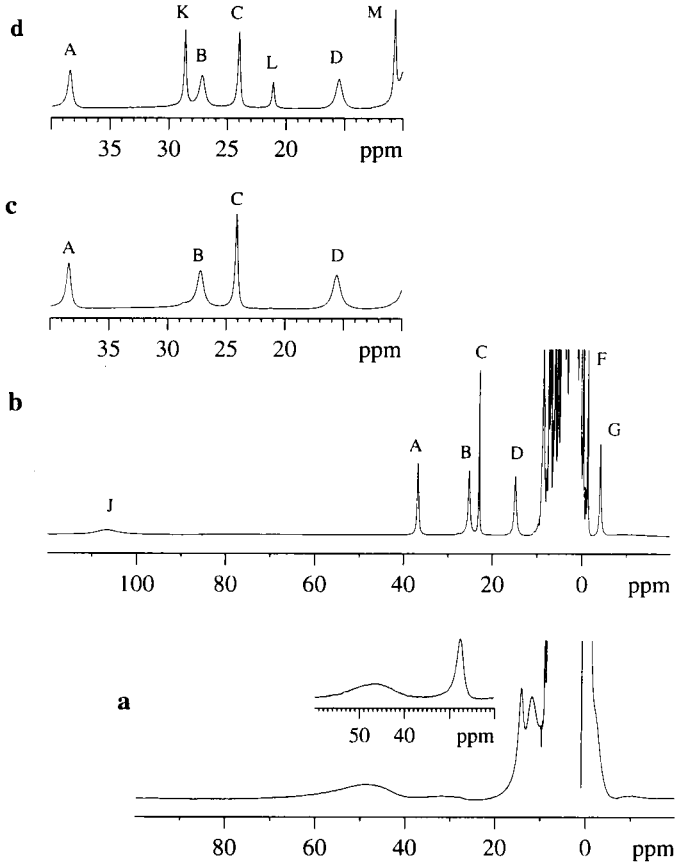

FIG. 11. WEFT spectra of (a) wild-type amicyanin in ^2H_2O at 32°C, with the inset showing the spectrum in H_2O, (b) Cu_A amicyanin in ^2H_2O at 25°C, (c) the region between 40 and 10 ppm in the spectrum of Cu_A amicyanin in ^2H_2O at 7°C, and (d) the same portion of the spectrum of Cu_A amicyanin in H_2O at 7°C.

FIG. 10. Visible spectra of the Cu_A amicyanin variant and the Cu_A domain of COX from *B. subtilis*. (A) The Cu_A amicyanin sample was in HEPES buffer at pH 7.0 whereas the Cu_A domain was in Tris buffer at pH 8.0. (B) The EPR spectra were obtained with the samples at 23 K, with glycereol added as a cryoprotectant. (C) The resonance Raman spectra of Cu_A sites on 488-nm (~150-mW) excitation at 15 K. CCO fragments from *P. denitrificans* (2.0 m*M* in Cu_A), *T. thermophilus* (1.8 m*M* in Cu_A), *B. subtilis* (1.5 m*M* in Cu_A), Cu_A construct in *P. aeruginosa* azurin (~0.4 m*M* in Cu_A), and Cu_A construct in *P. versutus* amicyanin (1.7 m*M* in Cu_A).

TABLE V

COMPARISON OF AMINO ACID SEQUENCES OF CYTOCHROME c_{550} FROM *Paracoccus versutus* AND *Paracoccus denitrificans*[a]

```
Tv    1 MKISIYATLAALSLALPAVA/QEGDAAKGEKEFNKCKACHMVQAPDGTDIV 50
        ***********  ***** * * ****************** ********
Pd    1 MKISIYATLAAITLALPAAA/QDGDAAKGEKEFNKCKACHMIQAPDGTDII 50

Tv   51 KGGKTGPNLYGVVGRKIASVEGFKYGDGILEVAEKNPDMVWSEADLIEYV 100
        ******************** ****** ********** * ********
Pd   51 KGGKTGPNLYGVVGRKIASEEGFKYGEGILEVAEKNPDLTWTEADLIEYV 100

Tv  101 TDPKPWLVEKTGDSAAKTKMTFKLGKNQADVVAFLAQHSPDAGAEA-APA 149
        ********  * *  ******** ************* *****    * *
Pd  101 TDPKPWLVKMTDDKGAKTKMTFKMGKNQADVVAFLAQNSPDAGGDGEAAA 150

Tv  150 EGAAN 154
        **  *
Pd  151 EGESN 155
```

[a] Identical residues are indicated; Tv, *P. versutus* (formerly *Thiobacillus versutus*); Pd, *P. denitrificans*.

Although *P. denitrificans* cyt c_{550} consists of 135 amino acid residues (134 in *P. versutus*), only 122 of these were observed in the crystallographic studies. It has been suggested that this observation is consistent with proteolytic cleavage of the C terminus of the protein, which has also been observed in mass spectroscopic studies on the *P. versutus* protein (*138*). Recent NMR studies on *P. versutus* cyt c_{550} have clearly shown that, in solution, the C terminus of the protein is unstructured and highly mobile, thus making it more prone to proteolysis (*138*).

A common feature of most *c*-type cytochromes is the presence of a ring of basic residues surrounding the exposed heme edge. The center of this ring has a more hydrophobic nature with a conserved phenylalanine residue being found here. Cytochrome c_{550} is no different from the other members of this family in this respect and the role of this surface patch on the electron transfer reactions of the protein will be discussed in subsequent sections of this review.

Cytochrome c_{550} possesses a low-spin iron center (except at extremes of pH values) due to the presence of the axial histidine and methionine ligands (*140*). Therefore, the oxidized form of the protein (Fe^{3+}, d^5) is paramagnetic and the reduced form (Fe^{2+}, d^6) is diamagnetic.

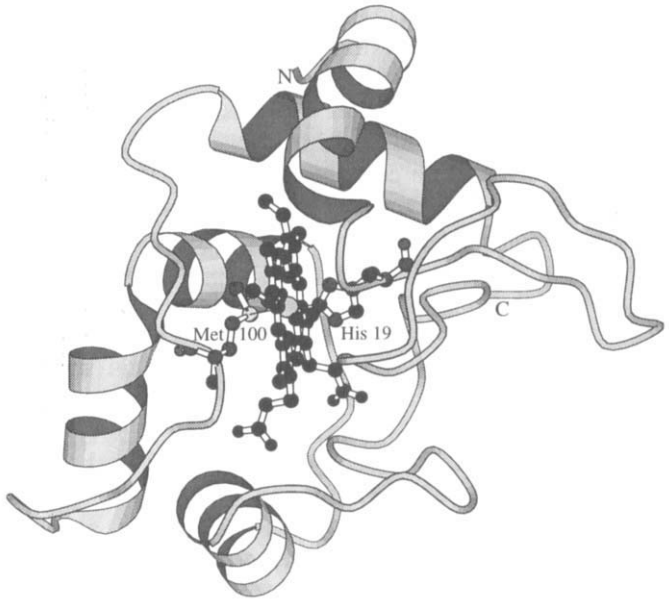

FIG. 12. Ribbon representation of a model of *P. versutus* cyt c_{550} based on the structure of the *P. denitrificans* protein. The heme, axial ligating residues, and His-118 are in ball-and-stick representation. N and C indicate the N and C termini, respectively.

The visible spectrum of the reduced protein is typical of that of a *c*-type cytochrome. The α-band is found at 550 nm, which is utilized in the classification of the protein. On oxidation the α- and β-bands broaden and the intense Soret transition shifts from 416 to 410 nm and its molar absorptivity lowers. An interesting feature of the visible spectrum of the oxidized protein is a weak transition at 696 nm thought to be due to the presence of an axial methionine ligand. The EPR spectrum is typical of a *c*-type cytochrome with values of 1.08, 1.91, and 3.35 for g_x, g_y, and g_z, respectively.

b. pH Effects. At high pH the oxidized form of cyt c_{550} undergoes a number of spectroscopic changes. This is thought to be the result of deprotonation of a lysine residue, which, in its neutral form, replaces the methionine as the axial ligand to the iron (*141*). This conclusion is consistent with the observations that the 696-nm visible absorption band disappears at high pH, and with a decrease in the isotropic shift of the $C^{\varepsilon}H_3$ resonance of the methionine ligand in the ^1H NMR spectrum. In cyt c_{550} the alkaline transition occurs with a pK_a of around 11, whereas in mitochondrial cyt *c* the pK_a is lower, with a value between 9 and 10 typically found (*142*).

A number of mutations have been introduced in *P. versutus* cyt c_{550} in order to investigate the alkaline transition in this protein. The residue Lys-14, which is found in the ring of basic residues surrounding the exposed heme edge, has been replaced with a glutamine and a glutamate (*143*). The rationale behind these changes came from work on horse cyt *c* in which the corresponding Lys-13, which is involved in a salt bridge with Glu-90, was chemically modified with a neutral and a negative group. In both cases a lowering of the pK_a for the alkaline transition of 1 pH unit was observed and was ascribed to the breaking of the salt bridge (*144*). The Lys-14Glu and Lys-14Gln mutants of cyt c_{550} have pK_a values, for the alkaline transition, that are almost identical to that of wild-type protein. This shows that salt bridges made by this residue are not important in maintaining the high pK_a of the alkaline transition in cyt c_{550}.

Various studies on mitochondrial cyt *c* have led to the proposal that two different lysine residues can coordinate to the metal atom, in place of the axial methionine, at alkaline pH values, and site-directed mutagenesis experiments have shown that Lys-79 is one of these (*145*). The corresponding lysine of cyt c_{550} from *P. versutus* (Lys-99) has been replaced with a glutamine (*146*). The effect on the pK_a of the alkaline transition is minimal; the value has lowered by 0.4 pH units to 10.8 in the Lys-99Glu variant. This indicates that the role of this residue in the alkaline transition is not so prominent as in the case of the mitochondrial protein.

A more direct investigation of the alkaline transition of *c*-type cytochromes involved the replacement of the axial Met-100 ligand by a lysine in cyt c_{550}. This produces a variant in which Lys-100 is thought to be the axial ligand and which exhibits spectroscopic properties similar to the alkaline form of cyt *c* (*147*). These spectral features are independent of pH up to a value of 12. Interestingly, the Met-100Lys mutant of cyt c_{550} exhibits certain spectroscopic properties similar to cyt *f*, in which the N terminus of Tyr-1 is known to be one of the axial ligands (*148*).

c. Redox Potential. The reduction potential of cyt c_{550} is typical for this class of heme-containing proteins, and a value of 252 mV in 50 m*M* cacodylate buffer at pH 7 (and at room temperature) has been reported (*147*). The reduction potential of cyt c_{550} is independent of ionic strength but is affected by pH, as shown in Fig. 13. This dependence of the reduction potential on pH is thought to be mainly due to protonation/deprotonation of the heme propionates. Of the mutations made in cyt c_{550}, those at positions 14 and 99 have very little effect on the reduction potential. However, the replacement of the axial methionine ligand with a lysine leads to a drop of approximately 330 mV

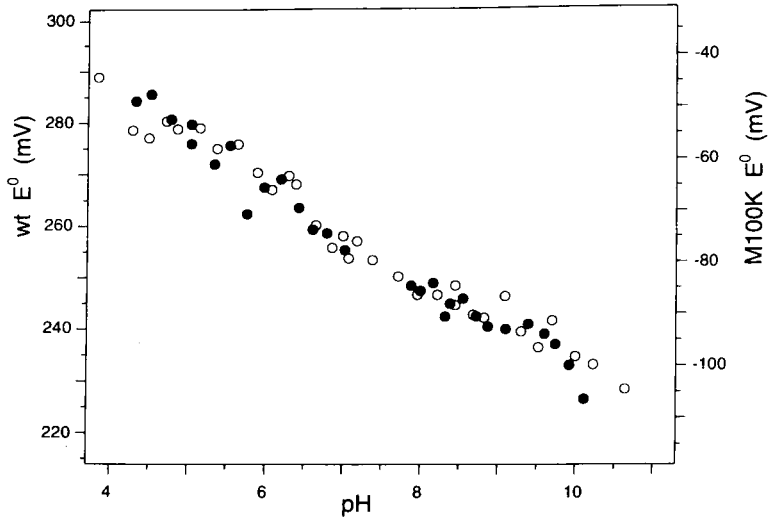

FIG. 13. Midpoint potential (E°) as a function of pH. Data points (±3 mV) were obtained with cyclic voltammetry. Protein concentration was 0.10–0.15 m*M* in 50 m*M* cacodylate/NaOH or HEPES/NaOH buffer. The solid circles and the left *y* axis refer to wild-type cyt c_{550}, whereas the open circles and the right *y* axis are for the M100K cytochrome c_{550} variant.

in the reduction potential. Again, a pH dependence of the reduction potential similar to that in the wild-type protein (Fig. 13) is seen. The drastic effect of the Met-100Lys mutation on the reduction potential of cyt c_{550} is not unexpected, because it gives a potential very similar to that observed for the alkaline form of cyt *c*. Cytochrome *f* has a much higher reduction potential of 365 mV, which is thought to be due to the more buried nature of the heme in this protein (*148*).

d. Electron Self-Exchange. Numerous studies have been made of the self-exchange reactivity of class I *c*-type cytochromes (*149–156*). In most of these it is found that the protein has a low self-exchange rate constant at low ionic strength, which increases as the ionic strength is increased. This behavior is thought to be due to the basic residues that surround the exposed heme edge and prevent efficient protein–protein association. The small (80 amino acid residues) cyt c_{551}s are known to behave differently with respect to self-exchange reactivity. These bacterial proteins have ionic-strength-independent self-exchange rate constants of 10^7 M^{-1} sec^{-1} (*152*). This has been attributed to the smaller number of basic residues around the exposed heme edge of these proteins and to the presence of a larger hydrophobic patch in this area.

Cytochrome c_{550} from *P. versutus* has a self-exchange rate constant (40°C) of $2 \times 10^2\ M^{-1}\ sec^{-1}$ at zero ionic strength and a pH of 6.0 (*143*). The self-exchange rate constant increases by almost three orders of magnitude to $1 \times 10^5\ M^{-1}\ sec^{-1}$ at an ionic strength of 0.55 *M*. The *P. denitrificans* protein appears to be more efficient at self-exchanging, with a reported (*151*) rate constant (25°C) of $1.6 \times 10^4\ M^{-1}\ sec^{-1}$ ($I = 0.1\ M$ and pH 7.5), which compares with a value (40°C) of $4 \times 10^3\ M^{-1}\ sec^{-1}$ for the *P. versutus* protein under similar conditions ($I = 0.1\ M$, pH 6.0). These differences are thought to be due to small structural variations among the two proteins, especially regarding the surface charge properties.

The two mutations at positions 14 of cyt c_{550} from *P. versutus* both have an effect on the self-exchange rate constants (40°C), with values at zero ionic strength of 7×10^3 and $1.2 \times 10^4\ M^{-1}\ sec^{-1}$ reported for the Lys-14Gln and Lys-14Glu variants, respectively (pH 6.0) (*143*). This observation proves the role of the positive area around the heme edge as the recognition site involved in the self-exchange process. It also shows that the removal of a single positive charge in this area favors the formation of an encounter complex and results in a higher second-order self-exchange rate constant.

B. Structure and Function of Methylamine Dehydrogenase and Cytochrome *c* Oxidase

1. *Methylamine Dehydrogenase*

a. Structural Aspects of Methylamine Dehydrogenase. MADH from *P. versutus* is an $\alpha_2\beta_2$ heterotetramer with subunit molecular masses of 47.5 and 12.9 kDa, respectively. The small subunit contains the prosthetic group tryptophan-tryptophyl quinone, which is formed by a 2′–4 covalent cross-link of two tryptophan residues (Trp-57 and Trp-108; see Fig. 14) (*157*). Trp-57 is further modified at positions C-6 and C-7 to yield an orthoquinone structure with E_{m_7} = 90–100 mV (*158*).

The three-dimensional structures of MADH from *P. versutus* and *P. denitrificans* have been determined in the presence and absence of amicyanin, and in the presence of amicyanin and cytochrome c_{551i} (*57*, *59–61*, *92*, *159*). The architecture of the tetramer is best described as consisting of two $\alpha\beta$ catalytic units (Fig. 15). Each α-subunit interacts with the β-subunit in the $\alpha\beta$ catalytic units and with the α-subunit of the other $\alpha\beta$ catalytic unit, but there are no interactions between the two β-subunits of the tetramer. The large subunit consists of seven

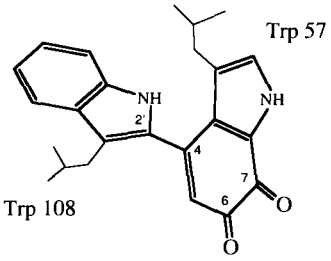

FIG. 14. Structure of the tryptophan-derived TTQ cofactor of MADH. The covalent attachment to the protein through the C^{β} atoms of the modified tryptophans is also shown.

four-stranded antiparallel β-sheets arranged in a circle with a quasi-sevenfold axis. The right-handed twist of these antiparallel β-sheets gives this subunit the appearance of a propeller. The small subunit consists of a central three-stranded β-sheet and some smaller β structures. These β-sheets are connected by long loops and extended regions. The small subunit contains 12 cysteine residues, all of which are involved in disulfide bridge formation, and this extensive cross-linking provides the small subunit with a very rigid structure.

The angle between the planes formed by the indole rings of the TTQ cofactor is approximately 40°, a value similar to that observed by NMR for a TTQ model compound (*161*) and also similar to what has been calculated (*162*). This calculation-based structure suggests that the protein is not a strong determinant of the TTQ conformation. Although the TTQ cofactor, especially the Trp-108 moiety, is located close to the surface of the protein, it interacts via hydrogen bonding with many surrounding residues, all of which (except Phe-64) are derived from the β-subunit (Fig. 16). In fact, all potential H-bond donors and acceptors of the TTQ cofactor participate in H bonding. There is a small pocket near the orthoquinone moiety of Trp-57—involving only C-6 and O-6 and not C-7 and O-7—where substrate and/or ammonia (or water) can bind. Atoms C-5′ and C-6′ of Trp-108 are accessible to solvent but are covered by amicyanin in the MADH–amicyanin complex (at least in *P. denitrificans*) and close to the Cu site. The distance between C-6′ of Trp-108 and the Cu of amicyanin is 9.3 Å; the distance between C-6′ and His-95 of amicyanin only 5.4 Å.

b. Factors Affecting the Structure and Activity of MADH. The pH profile of the reaction catalyzed by MADH is strongly dependent on the type of electron acceptor. Using artificial dyes as electron acceptors, a pH optimum around pH 7.5 occurs, whereas with amicya-

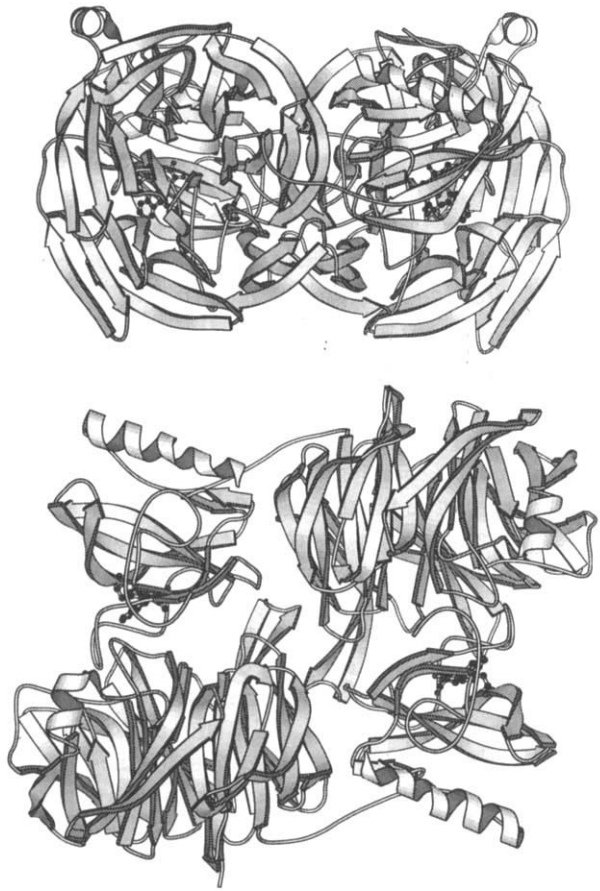

FIG. 15. Representation of the structure of methylamine dehydrogenase based on the crystal structure (*60*, *159*). The secondary structure elements, β-sheets and α-helices, are indicated as plates. The cofactor TTQ is presented in a ball-and-stick form. (Top) This representation shows clearly the small and large subunits, with the extended arm of the large subunit embracing the small subunit. (Bottom) The molecule is turned 90° with respect to the orientation in the top drawing, along the sevenfold symmetry present in the large subunit. A remarkable feature is that the cofactor is located on the extension of this sevenfold axis.

nin no pH optimum is observed (*163*). Furthermore, the absolute turnover number obtained with the natural electron acceptor is much higher (under optimal conditions at 20°C, k_{cat} = 55 electrons/sec) than is obtained with the dyes. As may be expected from products formed in the reaction, both [H^+] and [NH_4^+] have a strong effect on the vari-

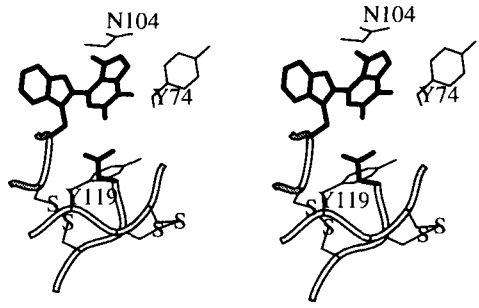

FIG. 16. Stereoview of the TTQ cofactor and surrounding residues. In bold, Trp-108, Trp-59, and Asp-74; disulfide bridges are shown between Cys-109 and Cys-78 (left) and between Cys-77 and Cys-121 (right).

ous steps of the overall reaction. However, other monovalent cations can have similar effects.

The optical spectrum of MADH is largely due to the optical properties of the cofactor TTQ (Fig. 17). Ammonia but also other monovalent cations such as Cs^+, Rb^+, K^+, Na^+, and Li^+, or substrate analogues such as trimethyl- or tetramethylammonia, have a profound effect on the optical spectrum of $MADH_{ox}$, $MADH_{semi}$, and $MADH_{red}$, and also on the activity of the enzyme (*163–165*). To interpret the different effects on the optical spectrum and on the rate of various intermediate steps, it is appropriate to distinguish two types of binding sites for monovalent cations, type I and type II. In the presence of cations such as trimethylammonium and tetramethylammonium, a red shift in the optical spectrum is observed (type I), whereas others (K^+ and Na^+) change the optical spectrum in a manner as observed for reduc-

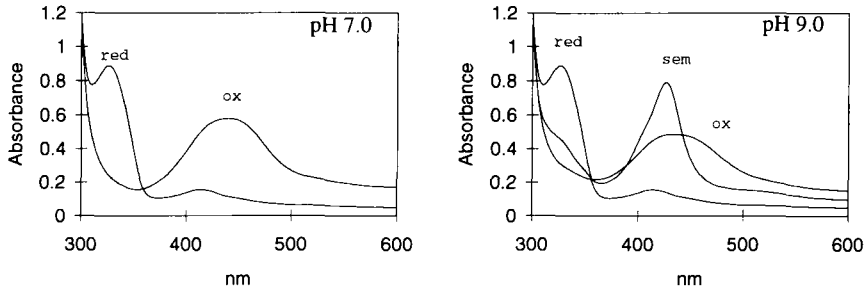

FIG. 17. Left: Absorption spectra of $MADH_{ox}$ and $MADH_{red}$ (obtained with methylamine addition) at pH 7.0. Right: Absorption spectra of the three redox forms of MADH at pH 9.0, the reduced forms being obtained by dithionite addition. The enzyme concentration in both panels is 30 μM.

tion (type II). Cations such as Li^+, Rb^+, Cs^+, and NH_4^+ may bind to both the type I and type II binding sites because they show both optical effects dependent on pH and concentration. Cations binding to the type I binding site compete with the substrate methylamine for binding; binding constants calculated for $MADH_{ox}$ using either an equilibrium binding method or the stopped-flow approach yield the same value. A type I optical spectrum is transiently formed on binding of the substrate.

Resonance Raman spectroscopy suggests a strong electrostatic interaction between type I monovalent cations and the TTQ, but a covalent bond is not formed between the cation and the cofactor (*166*). In particular, an electrostatic interaction with the C-6 carbonyl oxygen atom has been postulated. EPR experiments clearly show strong magnetic coupling between the ^{14}N or ^{15}N nucleus of added NH_4^+ and the electron spin in "dithionite-generated" TTQ_{semi}, but also between the Cs nucleus and TTQ_{semi} (*167*, *168*). Because Cs^+ does not bind covalently to TTQ_{semi}, covalent binding of ammonium or formation of an iminosemiquinone is not a prerequisite to interpret the EPR experiments. In agreement with this is the occurrence of the C-6 oxygen vibration in the resonance Raman spectrum of the dithionite-generated TTQ_{semi} in the presence of added ammonium. In other words, the C-6 oxygen atom is not displaced by NH_4^+ and binding of the cation close to the TTQ_{semi} may be sufficient to elicit the broadening effects seen in EPR.

This latter interpretation is apparently in contradiction to the interpretation given of the electron spin echo envelope modulation (ESEEM) experiments in which TTQ_{semi} had been generated with ^{14}N- or ^{15}N-labeled methylamine (*169*). Like the EPR spectrum, the ESEEM spectrum showed magnetic interaction between the electron spin and the substrate nitrogen. However, the magnitude of the ^{14}N isotropic coupling was proposed to indicate covalent attachment of the substrate nitrogen to the TTQ_{semi}, i.e., the iminosemiquinone had been generated. Recent ESEEM expeiments on the dithionite-generated TTQ_{semi} indicate that this radical is mainly in the anionic form, with the C-6 oxygen forming a hydrogen bond, and further that the angle between the indole ring planes is $48° \pm 11°$ (*170*).

The location of the type II binding site is more difficult to establish. The binding affinity is lower and less specific than for the type I binding site, but in view of the strong negative cooperativity observed between type I and type II cations and the large optical effects displayed, the type II binding site is expected to be close to the TTQ. The monovalent cations not only bind to $MADH_{ox}$ but also to $MADH_{red}$ and

$MADH_{semi}$, as is clear from both optical and EPR spectroscopy. In the presence of Cs^+, Na^+, and NH_4^+, the amount of TTQ semiquinone increases, thus this state is selectively stabilized by these cations. In contrast, trimethylamine binds most strongly to $MADH_{ox}$, does not bind to $MADH_{red}$, and slightly decreases the amount of TTQ_{semi}.

Although k_{cat} and the rate of reduction of TTQ_{ox} by substrate methylamine are practically independent of pH, the rates of other steps show a clear pH dependence and generally increase with increasing pH. For example, the rate of association of methylamine and the specificity constant k_{cat}/K_m for amicyanin are strongly pH dependent. The rate of association of methylamine shows an apparent pK of 8.7 that may be ascribed to the presence of a protonatable group on MADH; methylamine (pK_a = 10.7) is, in this interpretation, assumed to bind as the protonated cation. The pH dependence of the specificity constant for amicyanin can be explained by assuming the presence of two protonatable groups with pK_a values of 6.7 and 8.2. The pK_a value of 6.7 may correspond to the histidine residue, which, when protonated, is responsible for the low rate of the self-exchange reaction of amicyanin. The pK_a of 8.2 may be due to deprotonation of the cation binding site (possibly Asp-76) on the enzyme, similar to what has been concluded on the basis of the optical effects seen for MADH from *P. denitrificans*.

Because TTQ is a two-electron donor and amicyanin is a one-electron acceptor, one can in principle observe two different TTQ-associated oxidation phases, namely, from $TTQ_{red} \rightarrow$ amicyanin and from $TTQ_{semi} \rightarrow$ amicyanin. This is borne out experimentally. The first reaction, $TTQ_{red} \rightarrow$ amicyanin, is much slower than the second, because the TTQ_{semi} form is not normally observed. However, in the presence of monovalent cations the first oxidation step is accelerated much more than the second, consistent with the accumulation of the TTQ_{semi} under these conditions. The monovalent cations do not influence the affinity of amicyanin for MADH but directly affect the rate of electron transfer from the TTQ to the copper site. A semiquantitative analysis suggests that monovalent cations specifically lower the reorganizational barrier (by lowering the value of the reorganization parameter λ (2.2 eV) (cf. *171*) for the first oxidation step somewhat more than for the second, whereas the change in redox midpoint potentials has only a minor effect on the rates.

2. *Cytochrome c Oxidase*

The DNA-derived protein sequence of cytochrome *c* oxidase from *P. versutus* is very similar to that of *P. denitrificans* (*172*). The enzyme

is present in the cytoplasmic membrane of the bacterium and detergents are required for its isolation. To purify the enzyme, the membranes are first preextracted with sodium deoxycholate, which removes loosely bound proteins and the less hydrophobic proteins. Triton X-100 is further used to solubilize the enzyme from *P. versutus*, followed by chromatography on diethylaminoethyl (DEAE) and Q-sepharose columns; a pure enzyme preparation is obtained only after two additional chromatography runs on Mono-Q.

The enzyme purified in Triton X-100 consists of two subunits with apparent molecular masses of 33 and 50 kDa. Its optical spectrum shows features characteristic for cytochrome aa_3: a γ band maximum at 426 nm and an α band maximum at 603 nm for the oxidized enzyme; these values shift to 444 and 605 nm, respectively, for the dithionite-reduced enzyme. The low-temperature EPR spectrum of the oxidized enzyme shows signals originating from low-spin heme *a* ($g_{z,y,x}$ = 2.94, 2.29, 1.39) and from Cu_A (g_z = 2.18 and $g_{x,y} \sim 2.01$). EPR signals from cytochrome a_3 and Cu_B are absent, perhaps due to the antiferromagnetic coupling between these redox centers. The reduced enzyme shows no EPR signals. All these structural and spectroscopic properties are similar to those obtained for the cytochrome aa_3 oxidase from *P. denitrificans* and mitochondrial cytochrome aa_3 oxidases (*173*, *174*).

Optimal activity of the purified enzyme solubilized in Triton X-100 is obtained in the presence of excess phospholipids. The pH optimum of the steady-state reaction with horse heart ferrocytochrome *c* occurs at pH 6, yielding a turnover of about 80 electrons/sec, similar to the value obtained for the enzyme from *P. denitrificans*. Remarkably, a purified membrane-bound *c* cytochrome, identified by its N-terminal sequence as cytochrome c_1 from the bc_1 complex, stimulates the rate of electron transfer between horse heart cytochrome *c* and the cytochrome *c* oxidase by about a factor of two. The *in vitro* enzyme assay with purified cytochrome oxidase and reduced amicyanin showed no activity; only after the addition of endogenous cytochrome c_{550} (or horse heart cytochrome *c*) did oxidation of amicyanin occur, in agreement with the sequence of electron transfer; ami $\rightarrow$ cyt $c_{550} \rightarrow$ CCO.

IV. Electron Transfer Kinetics and Enzymology

A. The Catalytic Cycle of MADH

By analogy with the copper–topaquinone-containing amine oxidase, the catalytic cycle of MADH can be viewed as comprising a reductive

part and an oxidative part (*175*). As discussed above, spectroscopic techniques such as EPR, ESEEM, and resonance Raman spectroscopy indicate that the substrate, or more specifically the ammonium group of the substrate, binds in close vicinity to the TTQ cofactor. Because Cs^+, for example, produces effects in the EPR spectrum of TTQ_{semi} similar to those of ammonia, i.e., hyperfine coupling to the electron spin, the conclusion that these monovalent cations interact electrostatically with TTQ seems justified. However, recent studies have indicated that an iminosemiquinone is probably formed (*177*, *178*). Both alternatives have been incorporated in the scheme of the catalytic cycle depicted in Fig. 18.

As a first step, an electrostatic Michaelis complex is formed (see Fig. 18A) between protonated methylamine and MADH (perhaps involving Asp-76), as evidenced by the transient red shift observed in stopped-flow experiments (*163*). Hereafter, a nucleophilic attack by the amine nitrogen of the substrate takes place at position C-6 of the TTQ cofactor (*159*). The carbinolamine thus formed expells water, leading to the formation of the substrate imine. The expelled water molecule may remain closely bound to the cofactor. The next step is α-proton abstraction (by Asp-76) from the substrate and simultaneous reduction of TTQ, yielding the so-called product imine. Evidence in agreement with proton abstraction (although hydrogen or hydride transfer cannot be ruled out) may come from the large deuterium isotope effect associated with this step (*179–181*). Next is the release of the product formaldehyde; its oxygen atom is proposed to be derived from the enzyme-bound water molecule. At this stage the reductive phase, leading to the formation of the aminophenol intermediate, is completed.

The oxidative phase (see Fig. 18B) consists of two sequential one-electron oxidation reactions with two different amicyanin molecules. On the basis of experiments with apoamicyanin and Zn^{2+}- or Ag^+-substituted amicyanin, one can conclude that oxidized amicyanin has a much higher affinity for MADH than does reduced amicyanin, and further that reduced amicyanin rapidly dissociates from the enzyme (*vide infra*) (*182*). The presence of ammonia or another monovalent cation in the active site promotes rapid oxidation by amicyanin; in particular, the rate of the step from the fully reduced cofactor to the semiquinone state is enhanced (*176*, *183*). It was further observed that the rate of oxidation by amicyanin of the hydroquinone form of TTQ in the absence of NH_4^+ is about 20- to 30-fold lower than the rate of oxidation of the aminophenol (*176*). Nevertheless, whether oxidation of the aminophenol to the iminosemiquinone occurs in the cata-

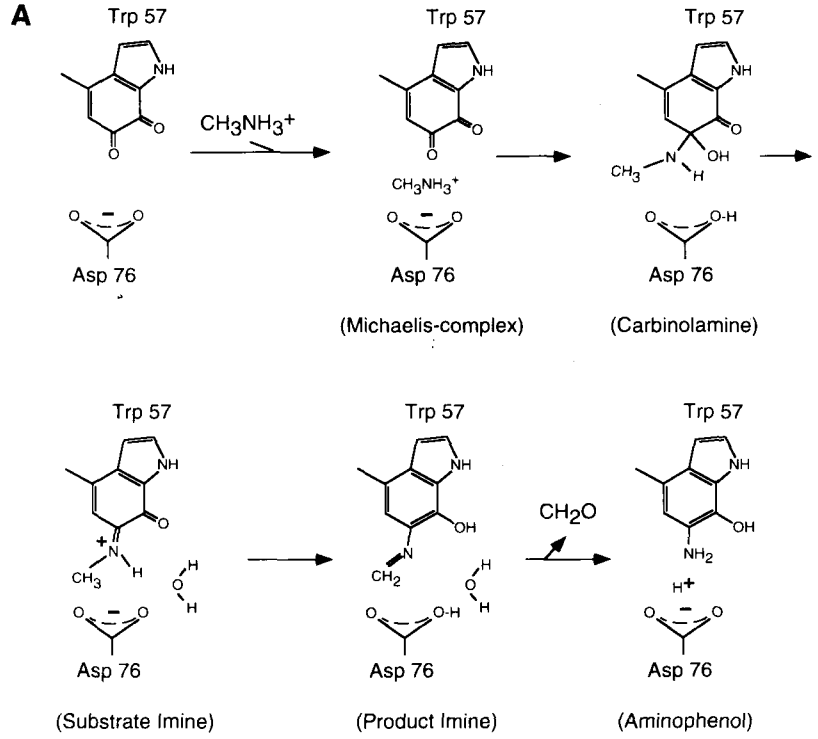

FIG. 18. Catalytic cycle of methylamine dehydrogenase. Both the reductive phase (A) and the oxidative phase (B) are shown; Ami, amicyanin. See text for details.

lytic cycle or during hydration to the hydroquinone form, followed by oxidation to the anionic semiquinone (Fig. 18B), cannot be decided on basis of these latter observations. It is also possible that both reactions may occur. After this step either semiquinone intermediate, or both, may be further oxidized by a second molecule of amicyanin, yielding TTQ_{ox}. In this last step, the monovalent cation NH_4^+ dissociates from MADH, either by itself or as a result of the binding of a substrate molecule, initiating the next catalytic cycle.

B. Reactions between Partners of the MADH Redox Chain

Electron transfer reactions have been investigated only for the first three members of the MADH redox chain from *P. versutus*. In the case of the *P. denitrificans* system extensive studies have been carried out on the reaction between amicyanin and the enzyme MADH (*160*, *171*,

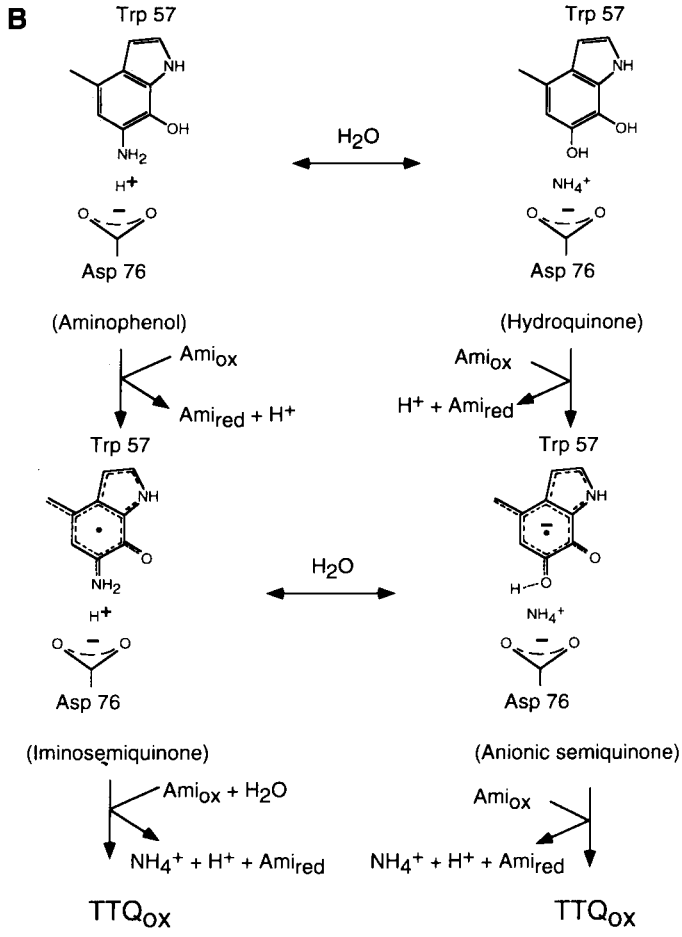

FIG. 18. *Continued*

176, *177*, *184*). The availability of the crystal structure of the binary complex of these two proteins (*92*) adds to the impact of these studies, and provides a model to which current electron transfer theories can be applied. The theoretical results can then be compared with kinetic studies of electron transfer within the complex. Additional studies (*185*, *186*) have focused on the electron transfer reaction between MADH, amicyanin, and cytochrome c_{55li} from *P. denitrificans* (as pointed out in Section II, MADH and amicyanin are induced by growth on methylamine, and cytochrome c_{55li} is induced by growth on methanol). Again, a crystal structure is available for the complex of

these three proteins (*89*, *90*). Studies have also been published on the reaction between cytochrome c_{550} and the Cu_A domain of subunit II of cytochrome *c* oxidase, both from *P. denitrificans* (*187*).

Studies of the *P. versutus* system have concentrated on the nonphysiological electron transfer reaction between MADH and cytochrome c_{550} (*182*). The effects of the Lys-14Gln and Lys-14Glu mutations, at the exposed heme edge of cytochrome c_{550}, on this reaction have been evaluated. Removal of the positive charge at position 14 results in a 20-fold lowering of the second-order rate constant for the reduction of cytochrome c_{550} by MADH. The introduction of a negative charge at this position results in a much larger decrease in the observed rate constant (500-fold). These large effects are not due to alterations in the driving force for the different reactions because the reduction potentials of the two cytochrome c_{550} variants are almost the same as the wild-type value (*vide supra*). Additionally, the two variants both have self-exchange rate constants larger than the wild-type value, and from simple Marcus theory an increase in the rate constant for the cross-reaction with MADH would be expected. These results clearly indicate that the positive charge around the heme edge of cytochrome c_{550} is important for association with a negatively charged region on MADH. Consistent with this observation, the second-order rate constant for the reduction of wild-type cytochrome c_{550} by MADH decreases as the ionic strength is increased.

An extension of the above studies provides a very interesting insight into the interaction between MADH and amicyanin (*182*). Experiments were carried out using redox-inert analogues of oxidized and reduced amicyanin to block the reaction between MADH and cytochrome c_{550}. Zn(II)- and Ag(I)-substituted amicyanin were utilized, and the results of these experiments are shown in Fig. 19. The much greater effect of the Zn(II)–amicyanin on the reaction indicates that the oxidized cupredoxin has a much greater affinity for MADH than does its reduced counterpart. This makes perfect sense in that physiologically oxidized amicyanin needs to associate more strongly with MADH, so that electron transfer can occur. Once the electron has been passed to the copper site the decreased affinity of the reduced protein would facilitate dissociation. Involvement of the protonatable His-96 ligand of amicyanin, which is found in a central position of the interface between the two proteins (see Fig. 20; *vide infra*), is an intriguing option. It has been proposed that once electron transfer from MADH to amicyanin has occurred the histidine ligand will protonate [the pK_a of His-96 in Cu(I) amicyanin is approximately 7; *vide supra*] and thus will aid dissociation (*182*).

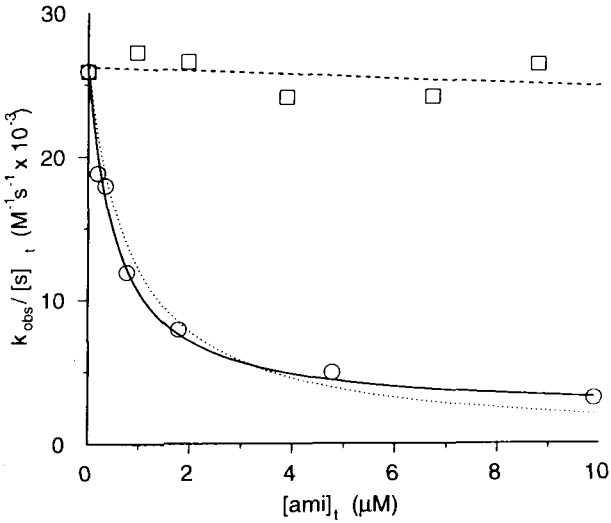

FIG. 19. Inhibition with redox-inactive amicyanins of the oxidation of MADH by cytochrome c_{550}. The circles show the effect of Zn(II)–amicyanin; the squares represent data obtained using Ag(I)–amicyanin (*182*).

The electron transfer reaction between amicyanin and cytochrome c_{550} of *P. versutus* has also been studied (*182a,b*). The effects on this reaction, of the surface mutations to cytochrome c_{550} (K14Q and K14E) and of altering the ionic strength, have been investigated. The results show that oppositely charged surfaces on the two proteins are not utilized in this reaction. This suggests that the basic patch of cytochrome c_{550} is used along with the hydrophobic patch of amicyanin.

Before reviewing the details of the reactions between proteins from *P. denitrificans* it is important to first discuss the available structural information. The proteins MADH and amicyanin are known to associate quite strongly in solution (*188*). A binary complex has been crystallized and the structure (*92*) of part of the interface between the two proteins is shown in Fig. 20. The hydrophobic patch of amicyanin, which surrounds the exposed imidazole ring of the ligand His-96, is found associating with a mainly hydrophobic region on the L subunit of MADH. There are also interactions between amicyanin and the larger H subunit of MADH. The two proteins interact in such a way that the TTQ cofactor of MADH and the copper of amicyanin are approximately 9 Å apart.

A crystal structure is also available for a ternary complex of MADH, amicyanin, and cytochrome c_{551i} (*89*, *90*). The latter protein

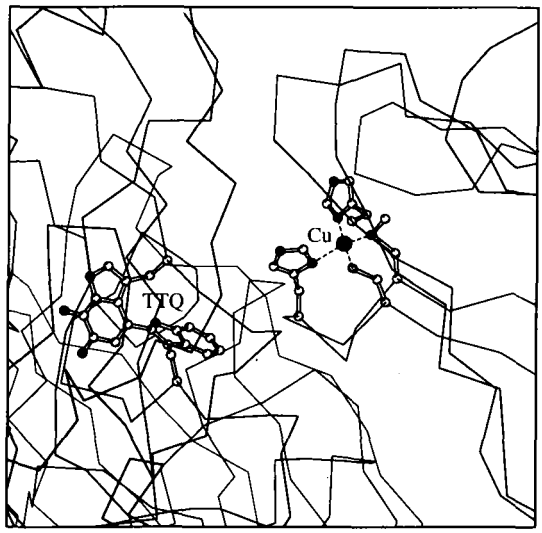

FIG. 20. Position of the TTQ cofactor of MADH and the copper of amicyanin in the crystal structure of the binary complex of the two proteins. The distance from the edge of the TTQ cofactor to the Cu atom is 9.3 Å. The side chain of His-96 is positioned between the Cu and the TTQ. The interface between the two proteins in the complex is formed by the hydrophobic patch of amicyanin and a similar hydrophobic surface of MADH, surrounding the exposed edge of the TTQ cofactor.

is, in fact, the dedicated electron acceptor of the enzyme methanol dehydrogenase (*18*) and the physiological relevance of this complex is at present a matter of debate (see also Section II,A,2). In the ternary complex, MADH and amicyanin associate in almost the same manner as in the binary complex structure. The amicyanin–cytochrome c_{551i} interface in the ternary complex is a lot more polar than that involving MADH and amicyanin. However, the association does not involve oppositely charged surfaces on the two proteins.

Initial studies of the electron transfer reaction between MADH and amicyanin, from *P. denitrificans,* utilized dithionite-reduced MADH (as opposed to the substrate-reduced enzyme). A study of the temperature and driving force dependence of the rate resulted in relatively large calculated values for the reorganization energy (λ) and electronic coupling (H_{AB}) of 2.3 eV and 11.7 cm^{-1}, respectively, for this reaction (*160, 171*). The authors concluded that the electron transfer reaction is coupled to protein rearrangements, and so the observed rate constants contain a contribution from the equilibrium constant for the rearrangement process. It is claimed that the calculated elec-

tronic coupling value is consistent with the distance between the redox cofactors in the binary complex of the proteins. This implies that the crystallographic complex is very similar to that formed in solution. A direct distance of 7.8 Å was derived using a β (electronic decay factor) value of 1.4 $Å^{-1}$, whereas a through-bond path length of 12.4 Å was predicted using a β value of 0.7 $Å^{-1}$. The direct distance between the TTQ cofactor of MADH and the copper of amicyanin is 9.4 Å, whereas a pathway analysis provided a route of 14 Å, including a 3.6-Å through-space jump.

As explained in detail above, the reduction of MADH by its physiological substrate (methylamine) is believed to result in the formation of an aminophenol form of the TTQ cofactor. Subsequent one-electron oxidation of MADH leads to the formation of an aminosemiquinone TTQ intermediate, and finally, following a second electron transfer step, to the quinone TTQ resting state of the enzyme (*176–178*). The temperature dependence of the rate constants observed for the oxidation of methylamine-reduced MADH by amicyanin provides values of λ (3.53 eV) and H_{AB} (22,850 cm^{-1}) that are physically meaningless. This indicates that the reaction is gated, i.e., the observed rate constant does not describe electron transfer. To further investigate the cause of gating, the oxidation of both dithionite- and methylamine-reduced MADH, by amicyanin, was studied in deuterated solvent (*176*). The observation of a large solvent (D_2O/H_2O) kinetic isotope effect for the reaction involving methylamine-reduced MADH, and not for the dithionite-reduced protein, clearly indicates that the adiabatic process that gates electron transfer involves the transfer of an exchangeable proton.

The question of the physiological significance of the crystal structure of the ternary complex of MADH, amicyanin, and the cytochrome c_{551i} from *P. denitrificans* has already been mentioned. The argument used in favor of this structure being physiologically relevant is that, *in vitro,* cytochrome c_{551i} is the most efficient electron acceptor for the MADH–amicyanin complex, of three *c*-type cytochromes found in *P. denitrificans* (*63*). However, the fact that cytochrome c_{551i} is the dedicated electron acceptor of the enzyme methanol dehydrogenase (*18*) would, intuitively, argue against this proposal. Additionally, a mutant strain of *P. denitrificans* in which the cytochrome c_{551i} gene has been knocked out exhibited growth characteristics, on methylamine, identical to the wild-type strain. A different mutant strain, with the cytochrome c_{550} gene knocked out, showed a decrease in the maximum specific growth rate on methylamine. Nevertheless, the Davidson group has carried out extensive studies on the electron

transfer reactions between MADH, amicyanin, and cytochrome c_{551i}. Polarized absorption spectroscopy has been utilized (*189*) to demonstrate that the crystallographic complexes (binary and ternary) are both capable of methylamine oxidation. In the ternary complex the subsequent reduction of the heme of cytochrome c_{551i} occurs in about 35 min at pH 9.0. Interestingly, the reduction of heme still occurs in crystals containing apoamicyanin, but in that case takes approximately 4 days (at pH 7.5). It should be noted that in all cases a pH dependence of the rate of electron transfer from MADH is observed, with faster rates obtained at the more alkaline pH values. This has been attributed either to the protonation of the His-95 ligand of amicyanin at lower pH values (*vide supra*) and/or to the stabilization of the TTQ aminosemiquinone at high pH.

Studies in solution of the reaction between the MADH–amicyanin complex and cytochrome c_{551i} have been interpreted in the following way. It is believed that the association of amicyanin with MADH leads to a lowering of the reduction potential of the amicyanin by 73 mV, to a value of 221 mV (at pH 7.5) (*184*) (this assumption was also made in the analysis of the MADH–amicyanin kinetics). This makes electron transfer to cytochrome c_{551i}, which has a reduction potential of 190 mV (*190*), more favorable. This proposal has been questioned (*182a*), and it has been suggested that the observed differences between the reduction potential of free amicyanin and amicyanin complexed to MADH reflect nothing more than the different affinities of oxidized and reduced amicyanin for MADH, which was not taken into account in the interpretation of the spectroelectrochemical data (*184*). Another assumption that has been made in the interpretation of the kinetics of this reaction is that amicyanin complexed to MADH is solely responsible for the observed reduction of cytochrome c_{551i}. The reduction of cytochrome c_{551i} by free amicyanin, although thermodynamically unfavorable, occurs too quickly to be monitored by the technique used (*184*). This indicates that the interaction of free amicyanin and cytochrome c_{551i} allows the two proteins to associate in a way that enhances the electronic coupling between the two metal centers. Alternatively, the faster reaction could be due to an enhanced association constant for the two proteins in the absence of MADH.

More detailed electron transfer studies indicate that cytochrome c_{551i} and the MADH–amicyanin complex associate in solution (*186*). The temperature dependence of the rate constant for electron transfer from copper to iron, within this ternary complex, provides estimates of λ and H_{AB} of 1.1 eV and 0.3 cm^{-1}, respectively. These results are consistent with electron transfer over distances of 13–23 Å, de-

pending on the β value used. This appears to agree with a direct copper-to-iron distance of 24.7 Å (the copper-to-heme edge distance is 22.7 Å) in the ternary complex. Again these results are used to imply that the arrangement of the proteins seen in the crystallographic studies is also relevant in solution.

Extensive mutagenesis studies have been used to investigate the interaction between cytochrome c_{550} and the soluble Cu_A domain of subunit II of cytochrome *c* oxidase (both proteins from *P. denitrificans*) (*187*). Removal of acidic residues on the surface of the Cu_A domain, close to the metal site, results in a decrease in the second-order rate constant for the oxidation of cytochrome c_{551i}. This indicates that the acidic patch on the Cu_A domain of cytochrome *c* oxidase is used for association with the basic patch of cytochrome c_{550}. Similar studies have also been carried out on the complete oxidase from *P. denitrificans* utilizing, in this case, horse heart cytochrome *c* as the electron donor (*191*). Again the importance of the acidic residues of subunit II of the oxidase, for this interaction, was demonstrated.

ACKNOWLEDGMENTS

The authors thank Petra van Bastelaere, Ilaria Ciabatti, and Gertrüd Warmerdam for providing information on the protein chemistry of cytochrome oxidase of *P. versutus* and the DNA sequence of the COX-encoding gene of *P. versutus*. Thanks to Rutger Diederix, Lars Jeuken, and Aldo J. Jongejan for help with producing the figures. Parts of the work were supported by the European Community under the HCMP network (CHRX-CT93-0189) and by the foundation for chemical research (SON) under the auspices of the Netherlands Science Organization (NWO).

REFERENCES

1. Katayama, Y.; Hiraishi, A.; Kuraishi, H. *Microbiology* **1995,** *141,* 1469.
2. Beijerinck, M.; Minkman, D. C. J. *Zentralbl. Bakteriol. Parasitenik. Abt. II* **1910,** *25,* 30.
3. Goodhew, C. F.; Pettigrew, G. W.; de Vreese, B.; van Beeumen, J.; van Spanning, R. J. M.; Baker, S. C.; Saunders, N.; Ferguson, S. J.; Thompson, I. P. *FEMS Microbiol. Lett.* **1996,** *137,* 95.
4. Woese, C. R. *Microbiol. Rev.* **1987,** *51,* 221.
5. Bosma, G.; Braster, M.; Stouthamer, A. H.; van Verseveld, H. W. *Eur. J. Biochem.* **1987,** *165,* 665.
6. Bosma, G.; Braster, M.; Stouthamer, A. H.; van Verseveld, H. W. *Eur. J. Biochem.* **1987,** *165,* 657.
7. van der Oost, J.; de Boer, A. P. N.; de Gier, J.-W. L.; Zumft, W. G.; Stouthamer, A. H.; van Spanning, R. J. M. *FEMS Microbiol. Lett.* **1994,** *121,* 1.

8. van Spanning, R. J. M.; de Boer, A. P. N.; Reijnders, W. N. M.; de Gier, J. W. L.; Delorme, C. O.; Stouthamer, A. H.; Westerhoff, H. V.; Harms, N.; van der Oost, J. *J. Bioenerg. Biomembr.* **1995,** *27,* 499.
9. van Verseveld, H. W.; Stouthamer, A. H. "The Genus *Paracoccus*"; The Prokaryotes, 2nd Ed.; Balows, Trupes, Dworkin, Hardev, and Scleifer, Eds.; Springer-Verlag, New York, 1991; pp. 2321–2334.
10. Stouthamer, A. H. *J. Bioenerg. Biomembr.* **1991,** *23,* 163.
11. Stouthamer, A. H. *Anton Leeuwenhoek Int. J. Gen. Microbiol.* **1992,** *61,* 1.
12. de Gier, J. W. L.; Lubben, M.; Reijnders, W. N. M.; Tipker, C. A.; Slotboom, D. J.; van Spanning, R. J. M.; Stouthamer, A. H.; van der Oost. J. *Mol. Microbiol.* **1994,** *13,* 183.
13. de Gier, J. W. L.; van der Oost, J.; Harms, N.; Stouthamer, A. H.; van Spanning, R. J. M. *Eur. J. Biochem.* **1995,** *229,* 148.
14. Harms, N.; Reijnders, W. N. M.; Anazawa, H.; van der Palen, C. J. N. M.; van Spanning, R. J. M.; Oltmann, L. F.; Stouthamer, A. H. *Mol. Microbiol.* **1993,** *8,* 457.
15. van Spanning, R. J. M.; van der Palen, C. J. N. M.; Slotboom, D. J.; Reijnders, W. N. M.; Stouthamer, A. H.; Duine, J. A. *Eur. J. Biochem.* **1994,** *226,* 201.
16. van Spanning, R. J. M.; de Boer, A. P. N.; Reijnders, W. N. M.; Spiro, S.; Westerhoff, H. V.; Stouthamer, A. H.; van der Oost, J. *FEBS Lett.* **1995,** *360,* 151.
17. van Spanning, R. J. M.; Wansell, C. W.; Harms, N.; Oltmann, L. F.; Stouthamer, A. H. *J. Bacteriol.* **1990,** *172,* 986.
18. van Spanning, R. J. M.; Wansell, C. W.; Reijnders, W. N. M.; Harms, N.; Ras, J.; Oltmann, L. F.; Stouthamer, A. H. *J. Bacteriol.* **1991,** *173,* 6962.
19. Harms, N.; van Spanning, R. J. M. *J. Bioenerg. Biomembr.* **1991,** *23,* 187.
20. Albracht, S. P. J.; van Verseveld, H. W.; Hagen, R. H.; Kalkman, M. L. *Biochim. Biophys. Acta.* **1980,** *593,* 173.
21. John, P.; Whatley, F. R. *Nature* **1975,** *254,* 495.
22. Bosma, G. Ph.D. thesis, 1989; Vrije Universiteit, Amsterdam.
23. van Verseveld, H. W.; Braster, M.; Boogerd, F. C.; Chance, B.; Stouthamer, A. H. *Arch. Microbiol.* **1983,** *135,* 229.
24. van Spanning, R. J. M. Ph.D. thesis, Vrÿe Universiteit, Amsterdam, The Netherlands, 1991.
25. van Verseveld, H. W.; Stouthamer, A. H. *Arch. Microbiol.* **1978,** *118,* 13.
26. van Verseveld, H. W. Stouthamer, A. H. *Arch. Microbiol.* **1978,** *118,* 21.
27. Garciahorsman, J. A.; Berry, E.; Shapleigh, J. P.; Alben, J. O.; Gennis, R. B. *Biochemistry* **1994,** *33,* 3113; Garciahorsman, J. A.; Barquera, B.; Rumbley, J.; Ma, J. X.; Gennis, R. B. *J. Bacteriol.* **1994,** *176,* 5587.
28. Castresana, J.; Lubben, M.; Saraste, M. *J. Mol. Biol.* **1995,** *250,* 202.
29. Saraste, M.; Castresana, J. *FEBS Lett.* **1994,** *341,* 1.
30. Brown, S.; Moody, A. J.; Mitchell, R.; Rich, P. R. *FEBS Lett.* **1993,** *316,* 216.
31. Hosler, J. P.; Fergusonmiller, S.; Calhoun, M. W.; Thomas, J. W.; Hill, J.; Lemieux, L.; Ma, J. X.; Georgiou, C.; Fetter, J.; Shapleigh, J.; Tecklenburg, M. M. J.; Babcock, G. T.; Gennis, R. B. *J. Bioenerg. Biomembr.* **1993,** *25,* 121.
32. Babcock, G. T.; Wikstrom, M. *Nature* **1992,** *356,* 301.
33. Iwata, S.; Ostermeier, C.; Ludwig, B.; Michel, H. *Nature* **1995,** *376,* 660.
34. Kleymann, G.; Ostermeier, C.; Ludwig, B.; Skerra, A.; Michel, H. *Biotechnology* **1995,** *13,* 155.
35. de Gier, J. W. L.; Schepper, M.; Reijnders, W. N. M.; van Dyck, S. J.; Slotboom, D. J.; Warne, A.; Saraste, M.; Krab, K.; Finel, M.; Stouthamer, A. H.; van Spanning, R. J. M.; van der Oost, J. *Mol. Microbiol.* **1996,** *20,* 1247.

36. Hill, B. C. *J. Bioenerg. Biomembr.* **1993,** *25,* 115.
37. Wilmanns, M.; Lappalainen, P.; Kelly, M.; Sauereriksson, E.; Saraste, M. *Proc. Natl. Acad. Sci. U.S.A.* **1995,** *92,* 11955.
38. Chepuri, V.; Lemieux, L.; Au, D. C.-T.; Gennis, R. B. *J. Biol. Chem.* **1990,** *265,* 11185.
39. Mandon, K.; Kaminski, P. A.; Elmerich, C. *J. Bacteriol.* **1994,** *176,* 2560.
40. Thonymeyer, L.; Beck, C.; Preisig, O.; Hennecke, H. *Mol. Microbiol.* **1994,** *14,* 705.
41. Preisig, O.; Zufferey, R.; Thonymeyer, L.; Appleby, C. A.; Hennecke, H. *J. Bacteriol.* **1996,** *178,* 1532.
42. Preisig, O.; Anthamattan, D.; Hennecke, H. *Proc. Natl. Acad. Sci. U.S.A.* **1993,** *90,* 3309.
43. Kahn, D.; Batut, J.; Daveran, M.-L.; Fourment, J. In "New Horizons in Nitrogen Fixation"; Palacios, R. J., Mora, W. E., and Newton, W. E., Eds.; Kluwer Academic: Dordrecht, The Netherlands, 1993; p. 474.
44. Richter, O. M. H.; Tao, J. S.; Turba, A.; Ludwig, B. *J. Biol. Chem.* **1994,** *269,* 23079.
45. Berks, B. C.; Ferguson, S. J.; Moir, J. W. B.; Richardson, D. J. *Biochim. Biophys. Acta Bioenergetics* **1995,** *1232,* 97.
46. Ferguson, S. J. *Anton Leeuwenhoek Int. J. Gen. Microbiol.* **1994,** *66,* 89.
47. van Spanning, R. J. M.; de Boer, A. P. N.; Reijnders, W. N. M.; Stouthamer, A. H.; Westerhoff, H. V.; van der Oost, J. *Molec. Microbiol.* **1996,** *23,* 893.
48. Friedrich, C. G.; Mitrenga, G. *FEMS Microbiol. Lett.* **1981,** *10,* 209.
49. Wodara, C.; Kostka, S.; Egert, M.; Kelly, D. P.; Friedrich, C. G. *J. Bacteriol.* **1994,** *176,* 6188.
50. John, P.; Whatley, F. R. *Biochim. Biophys. Acta* **1977,** *463,* 129.
51. van Spanning, R. J. M.; Wansell, C. W.; de Boer, T.; Hazelaar, M. J.; Anazawa, H.; Harms, N.; Oltmann, L. F.; Stouthamer, A. H. *J. Bacteriol.* **1991,** *173,* 6948.
52. Anthony, C.; Ghosh, M.; Blake, C. C. F. *Biochem. J.* **1994,** *304,* 665.
53. Blake, C. C. F.; Ghosh, M.; Harlos, K.; Avezoux, A.; Anthony, C. *Nature Struct. Biol.* **1994,** *1,* 102.
54. Anthony, C. *Adv. Microb. Physiol.* **1986,** *27,* 113.
55. Lidstrom, M. E.; Anthony, C.; Biville, F.; Gasser, F.; Goodwin, P.; Hanson, R. S.; Harms, N. *FEMS Microbiol. Lett.* **1994,** *117,* 103.
56. Chistoserdov, A. Y.; Chistoserdova, L. V.; Mcintire, W. S.; Lidstrom, M. E. *J. Bacteriol.* **1994,** *176,* 4052.
57. Chistoserdov, A. Y.; Boyd, J.; Mathews, F. S.; Lidstrom, M. E. *Biochem. Biophys. Res. Commun.* **1992,** *184,* 1226.
58. van der Palen, C. J. N. M.; Slotboom, D. J.; Jongejan, L.; Reijnders, W. N. M.; Harms, N.; Duine, J. A.; van Spanning, R. J. M. *Eur. J. Biochem.* **1995,** *230,* 860.
59. Chen, L.; Mathews, F. S.; Davidson, V. L.; Huizinga, E. G.; Vellieux, F. M. D.; Hol, W. G. J. *Proteins: Struct. Funct. Genet.* **1992,** *14,* 288.
60. Vellieux, F. M. D.; Huitema, F.; Groendijk, H.; Kalk, K. H.; Frank, J.; Jongejan, J.; Duine, J. A.; Petratos, K.; Drenth, J.; Hol, W. G. J. *EMBO J.* **1989,** *8,* 2171.
61. Chen, L.; Mathews, F. S.; Davidson, V. L.; Huizinga, E. G.; Vellieux, F. M. D.; Duine, J. A.; Hol, W. G. J. *FEBS Lett.* **1991,** *287,* 163.
62. Husain, M.; Davidson, V. L. *J. Biol. Chem.* **1985,** *260,* 14626.
63. van Spanning, R. J. M.; Wansell, C. W.; Reijnders, W. N. M.; Oltmann, L. F.; Stouthamer, A. H. *FEBS Lett.* **1990,** *275,* 217.
64. Gak, E. R.; Chistoserdov, A. Y.; Lidstrom, M. E. *J. Bacteriol.* **1995,** *177,* 4575.
65. Burton, S. M.; Byrom, D.; Carver, M.; Jones, G. D. D.; Jones, C. W. *FEMS Microbiol. Lett.* **1983,** *17,* 185.

66. Chandrasekar, R.; Klapper, M. H. *J. Biol. Chem.* **1986,** *261,* 3616.
67. Husain, M.; Davidson, V. L. *J. Biol. Chem.* **1986,** *261,* 8577.
68. Ras, J.; Reijnders, W. N. M.; van Spanning, R. J. M.; Harms, N.; Oltmann, L. F.; Stouthamer, A. H. *J. Bacteriol.* **1991,** *173,* 6971.
69. Kostler, M.; Kleiner, D. *FEMS Microbiol. Lett* **1989,** *65,* 1.
70. van Ophem, P. W.; Duine, J. A. *FEMS Microbiol. Lett.* **1994,** *116,* 87.
71. Harms, N.; Ras, J.; Reijnders, W. N. M.; van Spanning, R. J. M.; Stouthamer, A. H. *J. Bacteriol.* **1996,** *178,* 6296.
72. Ras, J.; van Ophem, P. W.; Reijnders, W. N. M.; van Spanning, R. J. M.; Duine, J. A.; Stouthamer, A. H.; Harms, N. *J. Bacteriol.* **1995,** *177,* 247.
73. Harms, N. Ph.D. Thesis, Vrije Universiteit, Amsterdam, The Netherlands, 1988.
73a. Ubbink, M.; van Kleef, M. A. G.; Kleinjan, D.-J.; Hoitink, C. W. G.; Huitema, F.; Beintema, J. J.; Duine, J. A.; Canters, G. W. *Eur. J. Biochem.* **1991,** *202,* 1003.
74. Husain, M.; Davidson, V. L. *J. Bacteriol.* **1987,** *169,* 1712.
75. Harms, N.; Ras, J.; Koning, S.; Reijnders, W. N. M.; Stouthamer, A. H.; van Spanning, R. J. M. In "Microbial Growth on C1 Compounds"; Lidstrom, M. E., and Tabita, F. R., Eds.; Kluwer Academic: Dordrecht, The Netherlands, 1995; pp. 126–132.
76. Parkinson, J. S. *Cell* **1993,** *73,* 857.
77. Yang, H.; Reijnders, W. N. M.; van Spanning, R. J. M.; Stouthamer, A. H.; Harms, N. *Microbiology* **1995,** *141,* 825.
78. Xu, H. H.; Janka, J. J.; Viebahn, M.; Hanson, R. S. *Microbiology* **1995,** *141,* 2543.
79. Schell, M. A. *Annu. Rev. Microbiol.* **1993,** *47,* 597.
80. (a) Delorme, C.; Huisman, T. T.; Reijnders, W. N. M.; Chan, Y.-L.; Harms, N.; Stouthamer, A. H.; van Spanning, R. J. M. *Microbiology* **1997,** *143,* 793; (b) Parsek, M. R.; Ye, R. W.; Pun, P.; Chakrabarty, A. M. *J. Biol. Chem.* **1994,** *269,* 11279.
81. Huitema, F.; van Beeumen, J.; van Driessche, G.; Duine, J. A.; Canters, G. W. *J. Bacteriol.* **1993,** *175,* 6254.
82. Gunsalus, R. P.; Park, S. J. *Res. Microbiol.* **1994,** *145,* 437.
83. Spiro, S. *Anton Leeuwenhoek Int. J. Gen. Microbiol.* **1994,** *66,* 23.
84. Khoroshilova, N.; Beinert, H.; Kiley, P. J. *Proc. Natl. Acad. Sci. U.S.A.* **1995,** *92,* 2499.
85. Stoll, R.; Page, M. D.; Sambongi, Y.; Ferguson, S. J. *Microbiology* **1996,** *142,* 2577.
86. van Spanning, R. J. M.; Wansell, C. W.; Reijnders, W. N. M.; Oltmann, L. F.; Stouthamer, A. H. *FEBS Lett.* **1990,** *275,* 217.
87. van Beeumen, J.; van Bun, S.; Canters, G. W.; Lommen, A.; Chothia, C. *J. Biol. Chem.* **1991,** *266,* 4869.
88. Romero, A.; Nar, H.; Messerschmidt, A.; Kalverda, A. P.; Canters, G. W.; Durley, R.; Mathews, F. S. *J. Mol. Biol.* **1994,** *236,* 1196.
89. Kalverda, A. P.; Wymenga, S. S.; Lommen, A.; van de Ven, F. J. M.; Hilbers, C. W.; Canters, G. W. *J. Mol. Biol.* **1994,** *240,* 358.
90. Durley, R.; Chen, L.; Lim, L. W.; Mathews, F. S. *Protein Sci.* **1993,** *2,* 739.
91. Cunane, L. M.; Chen, Z.; Durley, R. C. E.; Mathews, F. S. *Acta Crystallogr.* **1996,** *D52,* 676.
92. Chen, L.; Durley, R.; Poliks, B. J.; Hamada, K.; Chen, Z.; Mathews, F. S.; Davidson, V. L.; Satow, Y.; Huizinga, E.; Vellieux, F. M. D.; Hol, W. G. J. *Biochemistry* **1992,** *31,* 4959.
93. Chen, L.; Mathews, F. S.; Davidson, V. L.; Tegoni, M.; Rivetti, C.; Rossi, G. L. *Protein Sci.* **1993,** *2,* 147.
94. Chen, L.; Durley, R. C. E.; Mathews, F. S.; Davidson, V. L. *Science* **1994,** *264,* 86.

95. Walter, R. L.; Ealick, S. E.; Friedman, A. M.; Blake, R. C.; Proctor, P.; Shoham, M. *J. Mol. Biol.* **1996,** *263,* 730.
96. Botuyan, M. V.; Toy-Palmer, A.; Chung, J.; Blake, R. C.; Beroza, P.; Case, D.; Dyson, H. *J. Mol. Biol.* **1996,** *263,* 752.
97. Han, J.; Loehr, T. M.; Lu, Y.; Valentine, J. S.; Averill, B. A.; Sanders-Loehr, J. *J. Am. Chem. Soc.* **1993,** *115,* 4256.
98. Canters, G. W.; Gilardi, G. *FEBS Lett.* **1993,** *325,* 39.
99. LaCroix, L. B.; Shadle, S. E.; Wang, Y.; Averill, B. A.; Hedman, B.; Hodgson, K. O.; Solomon, E. I. *J. Am. Chem. Soc.* **1996,** *118,* 7755.
100. van Houwelingen, T.; Canters, G. W.; Stobbelaar, G.; Duine, J. A.; Frank, J.; Tsugita, A. *Eur. J. Biochem.* **1985,** *153,* 75.
101. Husain, M.; Davidson, V. L.; Smith, A. J. *Biochemistry* **1986,** *25,* 2431.
102. Adman, E. T.; Godden, J. W.; Turley, S. J. *J. Biol. Chem.* **1995,** *270,* 27458.
103. Guss, J. M.; Merritt, E. A.; Phizackerley, R. P.; Freeman, H. C. *J. Mol. Biol.* **1996,** *262,* 686.
104. Petratos, K.; Dauter, Z.; Wilson, K. S. *Acta Crystallogr.* **1988,** *B44,* 628.
105. Adman, E. T.; Turley, S.; Bramson, R.; Petratos, K.; Banner, D.; Tsneroglou, D.; Beppu, T.; Watanabe, H. *J. Biol. Chem.* **1989,** *264,* 87.
106. Andrew, C. R.; Yeom, H.; Valentine, J. S.; Karlsson, B. G.; Bonander, N.; van Pouderoyen, G.; Canters, G. W.; Loehr, T. M.; Sanders-Loehr, J. *J. Am. Chem. Soc.* **1994,** *116,* 11489.
107. Andrew, C. R.; Sanders-Loehr, J. *Acc. Chem. Res.* **1996,** *29,* 365.
108. Kalverda, A. P.; Salgado, J.; Dennison, C.; Canters, G. W. *Biochemistry* **1996,** *35,* 3085.
109. Lommen, A.; Canters, G. W.; van Beeuman, J. *Eur. J. Biochem.* **1988,** *176,* 213.
110. Lommen, A.; Canters, G. W. *J. Biol. Chem.* **1990,** *265,* 2768.
111. Lommen, A.; Pandya, K. I.; Koningsberger, D. C.; Canters, G. W. *Biochim. Biophys. Acta* **1991,** *1076,* 439.
112. Kyritsis, P.; Dennison, C.; Kalverda, A. P.; Canters, G. W.; Sykes, A. G. *J. Chem. Soc., Dalton Trans.* **1994,** *3017.*
113. Dennison, C.; Vijgenboom, E.; Hagen, W. R.; Canters, G. W. *J. Am. Chem. Soc.* **1996,** *118,* 7406.
114. Segal, M. G.; Sykes, A. G. *J. Am. Chem. Soc.* **1978,** *100,* 4584.
115. Sykes, A. G. *Chem. Soc. Rev.* **1985,** *14,* 283.
116. Sykes, A. G. *Adv. Inorg. Chem.* **1991,** *36,* 377.
117. Guss, J. M.; Harrowell, P. R.; Murata, M.; Norris, V. A.; Freeman, H. C. *J. Mol. Biol.* **1986,** *192,* 361.
118. Kojiro, C. L.; Markley, J. L. *FEBS Lett.* **1983,** *162,* 52.
119. Dennison, C.; Kohzuma, T.; McFarlane, W.; Suzuki, S.; Sykes, A. G. *J. Chem. Soc., Chem. Commun.* **1994,** 581.
120. Dennison, C.; Kohzuma, T.; McFarlane, W.; Suzuki, S.; Sykes, A. G. *Inorg. Chem.* **1994,** *33,* 3299.
121. Vakoufari, E.; Wilson, K. S.; Petratos, K. *FEBS Lett.* **1994,** *347,* 203.
122. Kyritsis, P.; Dennison, C.; Ingledew, W. J.; McFarlane, W.; Sykes, A. G. *Inorg. Chem.* **1995,** *34,* 5370.
123. van de Kamp, M.; Floris, R.; Hali, F. C.; Canters, G. W. *J. Am. Chem. Soc.* **1990,** *112,* 907.
124. van de Kamp, M.; Canters, G. W.; Andrew, C. R.; Sanders-Loehr, J.; Bender, C. J.; Peisach, J. *Eur. J. Biochem.* **1993,** *218,* 229.

125. van Pouderoyen, G.; Mazumdar, S.; Hunt, N. I.; Hill, H. A. O.; Canters, G. W. *Eur. J. Biochemistry* **1994,** *222,* 583.
126. Armstrong, F. A.; Driscoll, D. C.; Hill, H. A. O. *FEBS Lett.* **1985,** *190,* 242.
127. Groeneveld, C. M.; Canters, G. W. *J. Biol. Chem.* **1988,** *263,* 167.
128. Diederix, R. E. M.; Dennison, C.; Canters, G. W. In preparation.
129. Dennison, C.; Canters, G. W. In preparation.
130. Dennison, C.; Bunning, C.; Comba, P.; Canters, G. W. Unpublished results.
131. Dennison, C.; Vijgenboom, E.; de Vries, S.; van der Oost, J.; Canters, G. W. *FEBS Lett.* **1995,** *365,* 92.
132. Dennison, C.; Berg, A.; Canters, G. W. *Biochemistry* **1997,** *36,* 3262.
133. Dennison, C.; Berg, A.; de Vries, S.; Canters, G. W. *FEBS Lett.* **1996,** *394,* 340.
134. Salgado, J.; Canters, G. W. Unpublished results.
135. Ubbink, M.; van Beeumen, J.; Canters, G. W. *J. Bacteriol.* **1992,** *174,* 3707.
136. van Spanning, R. J. M.; Wansell, C. W.; Harms, N.; Oltmann, L. F.; Stouthamer, A. H. *J. Bacteriol.* **1990,** *172,* 986.
137. Margoliash, E.; Smith, E. L.; Kriel, G.; Tuppy, H. *Nature* **1961,** *192,* 1121.
138. Ubbink, M.; Pfuhl, M.; van der Oost, J.; Berg, A.; Canters, G. W. *Protein Sci.* **1996,** *5,* 2494.
139. Benning, M. M.; Meyer, T. E.; Holden, H. M. *Arch. Biochem. Biophys.* **1994,** *310,* 460.
140. Moore, G. R.; Pettigrew, G. W. "Cytochromes *c*, Evolutionary, Structural and Physicochemical Aspects"; Springer-Verlag: Berlin, 1990.
141. Lommen, A.; Ratsma, A.; Bijlsma, N.; Canters, G. W.; van Wielink, J. E.; Frank, J.; van Beeuman, J. *Eur. J. Biochem.* **1990,** 192, 653.
142. Davis, L. A.; Schejter, A.; Hess, G. P. *J. Biol. Chem.* **1974,** *249,* 2624.
143. Ubbink, M.; Canters, G. W. *Biochemistry* **1993,** *32,* 13893.
144. Osheroff, N.; Borden, D.; Koppenol, W. H.; Margoliash, E. *J. Biol. Chem.* **1980,** *255,* 1689.
145. Ferrer, J. C.; Guillemette, J. G.; Bogumil, R.; Inglis, S. C.; Smith, M.; Mauk, A. G. *J. Am. Chem. Soc.* **1993,** *115,* 7507.
146. Ubbink, M.; Warmerdam, G. C. M.; Campos, A. P.; Teixeira, M.; Canters, G. W. *FEBS Lett.* **1994,** *351,* 100.
147. Ubbink, M.; Campos, A. P.; Teixeira, M.; Hunt, N.; Hill, H. A. O.; Canters, G. W. *Biochemistry* **1994,** *33,* 10051.
148. Martinez, S. E.; Huang, D.; Szczepaniak, A.; Cramer, W. A.; Smith, J. L. *Structure* **1994,** *2,* 95.
149. Dixon, D. W.; Hong, X.; Woehler, S. E.; Mauk, A. G.; Sishta, B. P. *J. Am. Chem. Soc.* **1990,** *112,* 1082.
150. Dixon, D. W.; Hong, X.; Woehler, S. E. *Biophys. J.* **1989,** *56,* 339.
151. Timkovich, R.; Cork, M. S.; Taylor, P. V. *Biochemistry* **1984,** *23,* 3526.
152. Timkovich, R.; Cai, M. L.; Dixon, D. W. *Biochem. Biophys. Res. Commun.* **1988,** *150,* 1044.
153. Gupta, R. K.; Koening, S. H.; Redfield, A. G. *J. Magn. Reson.* **1972,** *7,* 66.
154. Gupta, R. K. *Biochim. Biophys. Acta* **1983,** *292,* 291.
155. Senn, H.; Engster, A.; Wüthrich, K. *Biochem. Biophys. Acta* **1983,** *743,* 58.
156. Keller, R. M.; Wüthrich, K.; Pecht, I. *FEBS Lett.* **1976,** *70,* 180.
157. McIntire, W. S.; Wemmer, D. E.; Chistoserdov, A. E.; Lidstrom, M. E. *Science* **1991,** *252,* 817.
158. McIntire, W. S. *Methods Enzymol.* **1995,** *258,* 149.

159. Huizinga, E. G.; van Zanten, B. A. M.; Duine, J. A.; Jongejan, J. A.; Huitema, F.; Wilson, K. S.; Hol, W. G. J. *Biochemistry* **1992,** *31,* 9789.
160. Brooks, H. B.; Davidson, V. L. *Biochemistry* **1994,** *33,* 5696.
161. Itoh, S.; Ongino, M.; Komatsu, M.; Oshiro, Y. *J. Am. Chem. Soc.* **1992,** *114,* 7294.
162. Itoh, S.; Oshiro, Y. *Methods Enzymol.* **1995,** *258,* 164.
163. Gorren, A. C. F.; Duine, J. A. *Biochemistry* **1994,** *33,* 12202.
164. Kuusk, V.; McIntire, W. S. *J. Biol. Chem.* **1994,** *269,* 26136.
165. Gorren, A. C. F.; Moenne-Loccoz, P.; Backes, G.; de Vries, S.; Sanders-Loehr J.; Duine, J. A. *Biochemistry* **1995,** *34,* 12926.
166. Moenne-Loccoz, P.; Nakamura, N.; Itoh, S.; Fukuzumi, S.; Gorren, A. C. F.; Duine, J. A.; Sanders-Loehr J. *Biochemistry* **1996,** *35,* 4713.
167. Kenney, W. C.; McIntire, W. S. *Biochemistry* **1983,** *22,* 3858.
168. Gorren, A. C. F.; de Vries, S.; Duine, J. A. *Biochemistry* **1995,** *34,* 9748.
169. Warncke, K.; Brooks, H. B.; Babcock, G. T.; Davidson, V. L.; McCracken; J. *J. Am. Chem. Soc.* **1993,** *115,* 6464.
170. Warncke, K.; Brooks, H. B.; Lee, H.; McCracken, J.; Davidson, V. L.; Babcock; G. T. *J. Am. Chem. Soc.* **1995,** *117,* 10063.
171. Brooks, H. B.; Davidson, V. L. *J. Am. Chem. Soc.* **1994,** *116,* 11201.
172. Steinrucke, P.; Steffen, G. C.; Panskus, G.; Buse, G.; Ludwig, B. *Eur. J. Biochem.* **1987,** *167,* 431; Ciabatti, I.; Warmerdam, G. C. M.; Vijgenboom, E.; Canters, G. W. Unpublished results.
173. Ludwig, B.; Schatz, G. *Proc. Natl. Acad. Sci. U.S.A.* **1980,** *77,* 196.
174. Buse, G.; Steffens, G. C. M. *J. Bioenerg. Biomembr.* **1991,** *23,* 269.
175. Hartmann, C.; Klinman, J. P. *J. Biol. Chem.* **1987,** *262,* 962.
176. Bishop, G. R.; Davidson, V. L. *Biochemistry* **1995,** *34,* 12082.
177. Bishop, G. R.; Brooks, H. B.; Davidson, V. L. *Biochemistry* **1996,** *35,* 8948.
178. Bishop, G. R.; Valente, E. J.; Whitehead, T. L.; Brown, K. L.; Hicks, R. P.; Davidson, V. L. *J. Am. Chem. Soc.* **1996,** *118,* 12868.
179. Brooks, H. B.; Jones, L. H.; Davidson, V. L. *Biochemistry* **1993,** *32,* 2725.
180. Davidson, V. L.; Jones, L. H.; Graichen, M. E. *Biochemistry* **1992,** *31,* 3385.
181. Hyun, Y.-L.; Davidson, V. L. *Biochim. Biophys. Acta* **1995,** *1251,* 198.
182. (a) Ubbink, M.; Hunt, N. I.; Hill, H. A. O.; Canters, G. W. *Eur. J. Biochem.* **1994,** *222,* 561; (b) Kyritsis, P.; Kohzuma, T.; Sykes, A. G. *Biochim. Biophys. Acta* **1996,** *1295,* 245.
183. Gorren, A. C. F.; van der Palen, C. J. N. M.; van Spanning, R. J. M.; Duine, J. A. In "Microbial Growth on C1 Compounds"; Lidstrom, M. E., and Tabita, F. R., Eds.; Kluwer Academic: Dordrecht, The Netherlands, 1996; pp. 197–204.
184. Gray, K. A.; Davidson, V. L.; Knaff, D. B. *J. Biol. Chem.* **1988,** *263,* 13987.
185. Davidson, V. L.; Jones, L. H. *J. Biol. Chem.* **1995,** *270,* 23941.
186. Davidson, V. L.; Jones, L. H. *Biochemistry* **1996,** *35,* 8120.
187. Lappalainen, P.; Watmough, N. J.; Greenwood, C.; Saraste, M. *Biochemistry* **1995,** *34,* 5824.
188. Davidson, V. L.; Graichen, M. E.; Jones, L. H. *Biochim. Biophys. Acta* **1993,** *1144,* 39.
189. Merli, A.; Brodersen, D. E.; Morini, B.; Chen, Z.; Durley, R. C. E.; Mathews, F. S.; Davidson, V. L.; Rossi, G. L. *J. Biol. Chem.* **1996,** *271,* 9177.
190. Gray, K. A.; Knaff, D. B.; Husain, M.; Davidson, V. L. *FEBS Lett.* **1986,** *207,* 239.
191. Witt, H.; Zichermann, V.; Ludwig, B. *Biochim. Biophys. Acta* **1995,** *1230,* 74.

Index

D

E

F

N

O

P

R

S